Universidad Politécnica de Madrid

Escuela Técnica Superior de

Ingenieros de Caminos, Canales y Puertos

Polyolefin fibre-reinforced concrete: from material behaviour to numerical and design considerations

Tesis Doctoral

Marcos García Alberti

Ingeniero de Caminos, Canales y Puertos

Madrid, 2015

Marcos García Alberti

Madrid, 2015

I.S.B.N.: 978-84-606-9210-2

Departamento de Ingeniería Civil: Construcción
Escuela Técnica Superior de
Ingenieros de Caminos, Canales y Puertos
Universidad Politécnica de Madrid

Polyolefin fibre-reinforced concrete: from material behaviour to numerical and design considerations

Tesis Doctoral

Marcos García Alberti
Ingeniero de Caminos, Canales y Puertos

Directores de la Tesis:

Jaime C. Gálvez Ruiz
Doctor Ingeniero de
Caminos, Canales y Puertos

Alejandro Enfedaque Díaz
Doctor Ingeniero de
Caminos, Canales y Puertos

Madrid, 2015

Tesis Doctoral

Polyolefin fibre-reinforced concrete: from material behaviour to numerical and design considerations

Tribunal nombrado por el Mgfco. y Excmo. Sr. Rector de la Universidad Politécnica de Madrid, el día ..... de ..... de 2015.

Presidente D. .....

Vocal D. .....

Vocal D. .....

Vocal D. .....

Secretario D. .....

Suplente D. .....

Suplente D. .....

Realizado el acto de defensa y lectura de la Tesis el día ..... de ..... de 2015 en la E.T.S. de Ingenieros de Caminos, Canales y Puertos de la U.P.M.

Calificación: .....

EL PRESIDENTE LOS VOCALES

EL SECRETARIO

A mis padres y hermano

A mi mujer, Sierra, y mi hijo Marcos

"*Given the faults of human nature, coupled with the complexity of the design of everything, from lectures to bridges, it behoves us to beware of the lure of success and to listen to the lessons of failure*." (Petroski, 2006)

Agradecimientos

Quiero expresar mi más sincero agradecimiento a Jaime Gálvez, director de esta Tesis, por haberme permitido dar mis primeros pasos en la investigación científica. Además, por la dedicación, apoyo y comprensión y por haberme transmitido los mejores valores académicos durante el proceso de realización de este trabajo. Quiero agradecer igualmente a Alejandro Enfedaque, también director de esta Tesis, su esfuerzo, paciencia y ayuda en muchas horas de laboratorio y discusiones, y haberme acompañado en todo mi proceso de aprendizaje con cercanía y empatía. A ambos, mi más sincero agradecimiento por su labor docente y por haberme hecho sentir parte de su equipo desde el primer día.

Deseo extender mi agradecimiento a Sika, cuya financiación ha hecho posible el desarrollo de esta Tesis. De forma personal, a Alberto Rey, por sus continuas aportaciones y su apoyo durante todo este periodo. A Ángel González Lucas, por el interés y apoyo constante a la investigación. También a Ramón Martínez y Ramiro García, así como a Carsten Rieger y Gustav Bracher por su acogida en Suiza en mi visita a Hagerbach.

Al Prof. Ildefonso Lucea, por su conversación diaria, y a los profesores Amparo Moragues, Manuel Fernández Cánovas, Jaime Fernández, Encarnación Reyes, Mª Jesús Casati, Miguel Ángel Sanjuán, Jose Mª Goicolea, Juan Carlos Mosquera y Francisco Gálvez que por diversas razones han facilitado mi labor investigadora. Al Dpto. de Ingeniería Civil: Construcción de la Escuela de Ingenieros de Caminos, Canales y Puertos de la Universidad Politécnica de Madrid. También al Dpto. de Ciencia de Materiales de la misma escuela, que ha compartido sus equipos y utillajes cuando ha sido necesario. A Iván Rodríguez Osorio por haber colaborado conmigo en las fases de laboratorio. A Vikas Agrawal por su colaboración durante el conteo de fibras, a Alejandro Ferreras por la ayuda con los ensayos de p*ull-out* y a Luis Pinillos y Acciona por su aportación en el estudio del caso práctico. A Alfredo Casero y Miguel Ángel de Felipe, cuya ayuda en el laboratorio también ha sido esencial. Y por supuesto, a todos con los que he compartido el Laboratorio de Materiales de Construcción y Química en estos años: Juan Antonio Alonso, Jose Juan Conchillo, Fernando Suárez, David Galé, Rebeca Antón, Héctor Romero, Cristina Argiz, Néstor León, Silvia Monteagudo, Jesús Bernal, Daniel Alonso, Michiel Fenaux y Arancha Hueso.

A mis compañeros de doctorado, especialmente a Julio César López, Teresa Ancochea y Maricely de Abreu. También a Andrew Selby y a todos los compañeros de los jueves, cuyo poso también se nota en esta Tesis. A todos mis excompañeros de trabajo en Ferrovial, Telvent-Abengoa, Tableros y Puentes, en los departamentos de Ordenación y de Tecnologías del Tráfico del Ayuntamiento de Madrid y en el Dpto. de Ingeniería Civil de la Universidad de Alicante. Singularmente, a mis compañeros y amigos de Pacadar, de los que he sentido su apoyo durante todo este tiempo. A mis amigos de siempre, que no hace falta que nombre porque siempre están ahí.

Por último y en especial, quiero agradecer a Sierra su paciencia y comprensión durante este tiempo en el que, además, hemos tenido a Marcos. A mi padre, sobre todo por haberme transmitido la mejor y más valiosa ética del trabajo, tanto en el ámbito de la ingeniería como en el de la investigación y la docencia. A Yago, Luis, Sonia y Clemen, por esa contribución anímica intangible. Gracias a mi madre y a mi abuela. Finalmente, al resto de mi familia y amigos de Madrid, Alicante, Navia de Suarna y Villarrubia de los Ojos.

Resumen

La presente Tesis proporciona una gran cantidad de información con respecto al uso de un nuevo y avanzado material polimérico (con base de poliolefina) especialmente adecuada para ser usada en forma de fibras como adición en el hormigón.

Se han empleado fibras de aproximadamente 1 mm de diámetro, longitudes entre 48 y 60 mm y una superficie corrugada. Las prometedoras propiedades de este material (baja densidad, bajo coste, buen comportamiento resistente y gran estabilidad química) justifican el interés en desarrollar el esfuerzo de investigación requerido para demostrar las ventajas de su uso en aplicaciones prácticas.

La mayor parte de la investigación se ha realizado usando hormigón autocompactante como matriz, ya que este material es óptimo para el relleno de los encofrados del hormigón, aunque también se ha empleado hormigón normal vibrado con el fin de comparar algunas propiedades. Además, el importante desarrollo del hormigón reforzado con fibras en los últimos años, tanto en investigación como en aplicaciones prácticas, también es muestra del gran interés que los resultados y consideraciones de diseño que esta Tesis pueden tener.

El material compuesto resultante, Hormigón Reforzado con Fibras de Poliolefina (HRFP o PFRC por sus siglas inglesas) ha sido exhaustivamente ensayado y estudiado en muchos aspectos. Los resultados permiten establecer cómo conseguidos los objetivos buscados:

- Se han cuantificado las propiedades mecánicas del PFRC con el fin de demostrar su buen comportamiento en la fase fisurada de elementos estructurales sometidos a tensiones de tracción.
- Contrastar los resultados obtenidos con las bases propuestas en la normativa existente y evaluar las posibilidades para el uso del PFRC con fin estructural para sustituir el armado tradicional con barras de acero corrugado para determinadas aplicaciones.
- Se han desarrollado herramientas de cálculo con el fin de evaluar la capacidad del PFRC para sustituir al hormigón armado con las barras habituales de acero.
- En base a la gran cantidad de ensayos experimentales y a alguna aplicación real en la construcción, se han podido establecer recomendaciones y consejos de diseño para que elementos de este material puedan ser proyectados y construidos con total fiabilidad.

Se presentan, además, resultados prometedores en una nueva línea de trabajo en el campo del hormigón reforzado con fibras combinando dos tipologías de fibras. Se combinaron fibras de poliolefina con fibras de acero como refuerzo del mismo hormigón autocompactante detectándose sinergias que podrían ser la base del uso futuro de esta tecnología de hormigón.

Abstract

This thesis provides a significant amount of information on the use of a new advanced polymer (polyolefin-based) especially suitable in the form of fibres to be added to concrete. At the time of writing, there is a noteworthy lack of research and knowledge about use as a randomly distributed element to reinforce concrete.

Fibres with an approximate 1 mm diameter, length of 48-60 mm, an embossed surface and improved mechanical properties are employed. The promising properties of the polyolefin material (low density, inexpensive, and with good strength behaviour and high chemical stability) justify the research effort involved and demonstrate the advantages for practical purposes.

While most of the research has used self-compacting concrete, given that this type of matrix material is optimum in filling the concrete formwork, for comparison purposes standard vibration compacted mixes have also been used. In addition, the interest in fibre-reinforced concrete technology, in both research and application, support the significant interest in the results and considerations provided by the thesis.

The resulting composite material, polyolefin fibre reinforced concrete (PFRC) has been extensively tested and studied. The results have allowed the following objectives to be met:

- Assessment of the mechanical properties of PFRC in order to demonstrate the good performance in the post-cracking strength for structural elements subjected to tensile stresses.
- Assessment of the results in contrast with the existing structural codes, regulations and test methods. The evaluation of the potential of PFRC to meet the requirements and replace traditional steel-bar reinforcement applications.
- Development of numerical tools designed to evaluate the capability of PFRC to substitute, either partially or totally, standard steel reinforcing bars either alone or in conjunction with steel fibres.
- Provision, based on the large amount of experimental work and real applications, of a series of guidelines and recommendations for the practical and reliable design and use of PFRC.

Furthermore, the thesis also reports promising results about an innovative line in the field of fibre-reinforced concrete: the design of a fibre cocktail to reinforce the concrete by using two types of fibres simultaneously. Polyolefin fibres were combined with steel fibres in self-compacting concrete, identifying synergies that could serve as the base in the future use of fibre-reinforced concrete technology.

Content

List of figures

Page

List of tables

List of symbols and acronyms

Latin letter symbols

Symbol	Definition
a	Cracks
a_0	Notch length
A	Cross section of the sample
A_f	Cross section of one fibre
B	Brittleness number
B	Depth of the beam
$c.v.$	Coefficient of variation
$c.d.$	Coefficient of distribution
D	Height of the beam
$d_{ag,max}$	Maximum aggregate size
d_e	Equivalent diameter
d_f	Mean diameter in the slump flow test
E	Elasticity modulus
f_{ck}	Characteristic compressive strength of concrete
$f_{ck,7d}$	Compressive strength 7 days
$f_{ck,\ 28d}$	Compressive strength 28 days
f_{cm}	Medium compressive strength of concrete
f_{ct}	Concrete tensile strength
f_{LOP}	Strength corresponding to the limit of proportionality
f_{MIN}	Minimum post-cracking strength
f_{REM}	Maximum post-cracking remaining strength
f_{PEAK}	Maximum strength
f_t	Indirect tensile strength
f_{Rj}	Residual flexural strength corresponding to a crack opening j in three-point bending tests
f_{R1}	Residual flexural strength corresponding to a crack opening 0.5 mm in three-point bending tests
f_{R2}	Residual flexural strength corresponding to a crack opening 1.5 mm in three-point bending tests
f_{R3}	Residual flexural strength corresponding to a crack opening 2.5 mm in three-point bending tests
f_{R4}	Residual flexural strength corresponding to a crack opening 3.5 mm in three-point bending tests
F_j	Load at each j crack mouth opening displacement
G_F	Specific Fracture energy
h	Specimen height
h_{SP}	Ligament height
K	Stress intensity factor
l_c	Critical length
l_{ch}	Characteristic length

Symbol	Definition
l_{cs}	Reference length
l_f	Fibre length
L	Span of the test
L_{PEAK}	Peak load
L_{LOP}	Load corresponding to the limit of proportionality
L_{MIN}	Minimum post-cracking load
L_{REM}	Maximum post-cracking remaining load
L_{Ri}	Load corresponding o a crack opening i in three-point bending tests
$l_{frictional}$	Load with only frictional adhesion
$l_{debonding}$	Load which debonding took place
l_f	Fibre length
l_{fr}	Cord of the circumference
n	Number of fibres
P	Load
P_u	Ultimate load
s_m	Mean distance between cracks
th	Theoretical number of fibres
T_v	Flow time
T_{500}	Time the patty lasts to reach diameter 500 mm in the slump flow test
u	Distance to a second wall
v_{cf}	Average shear stress
V	Volume
V_f	Fibre volumetric fraction
w	Crack opening
w_c	Critical crack opening
W	Size
W	Work of fracture
W_f	Dosage of fibres for a volume of concrete
y	distance between neutral axis and tensile side of the cross section

Greek letter symbols

Symbol	Definition
β	Angle
β_{ch}	Material empirical parameter
δ	Deflection
ε	Strain
ε_u	Ultimate Strain
γ	Shear strain rate
μ	Plastic viscosity
σ	Stress transferred through cohesive crack
σ_{Nu}	Ultimate stress
ρ	Density of the fibres
τ	Shear stress
τ_0	Shear yield stress
υ	Poisson's ratio
θ	Orientation factor
φ	Angle

Acronyms

Acronym	Definition
AR	Alkali resistant
CDZ	Compressive Damage Zone
CEN	European Committee for Standardization
CMOD	Crack mouth opening displacement
CT	Computed tomography
DIC	Digital image correlation
FPZ	Fracture process zone
FR-SCC	Fibre-reinforced self-compacting concrete
FRC	Fibre-reinforced concrete
GRC	Glass fibre reinforced concrete
HSC	High strength concrete
ITZ	Interfacial transition zone
LEFM	Linear elastic fracture mechanics
LP	Limestone powder
LVDT	Linear variable differential transformer
NLFM	Non-linear fracture mechanics
PF	Polyolefin fibre
PFR-SCC	Polyolefin fibre-reinforced self-compacting concrete
PFRC	Polyolefin fibre-reinforced concrete
RC	Steel-bar Reinforced Concrete
SCC	Self-compacting concrete
SEM	Scanning electron microscopy
SIFCON	Slurry infiltrated fibre concrete
SIMCON	Slurry infiltrated mat concrete
SF	Steel fibre
SFR-SCC	Steel fibre-reinforced self-compacting concrete
SFRC	Steel fibre-reinforced concrete
SFRS	Steel fibre reinforced shotcrete
PFRS	Macro-synthetic fibre reinforced shotcrete
SLS	Service Limit State
SP	Superplasticizer
TBM	Tunnel boring machine
UHPFRC	Ultra high-performance fibre reinforced concrete
ULS	Ultimate Limit State
VCC	Vibrated conventional concrete
VMA	Viscosity-modifying agents
WWF	Welded-wire-fabric

Chapter 1

Introduction

The development of concrete technologies that provides some additional performance has enabled to adapt such an excellent material to new perspectives and requirements. Since concrete is the foremost construction material, those technologies have been the centre of both research and applications. Nowadays, the requirements to which a structural piece of concrete are subjected, encompass a varied number of possibilities. The most relevant issues are related to mechanical responses including flexural or tensile stresses and not excluding impact loadings, fatigue, fire resistance, seismic design situations, durability issues or toughness and ductility. The field of concrete knowledge has therefore become opened to special types of concrete that can meet certain specific requirements in what has been denominated high-performance concrete. The most relevant advances that have been applied are probably high strength concrete (HSC), self-compacting concrete (SCC) and fibre reinforced concrete (FRC), among others.

FRC is especially well suited under such a variation of structural demands to the material because it could be considered as a generic term for a huge quantity of concrete types, each of them with precise technologies and characteristics. Variations on shapes, materials, mix designs or placing conditions can provide singular concrete types that adapt to a certain purpose. If the main reason to introduce fibres in concrete could be considered that it enhances the tensile behaviour, the target design situation can mark the type of fibre to be used if the technology is known. However, some fibres provide some other characteristics as avoiding fire spalling or providing electrical resistivity to the concrete piece.

Nonetheless, the most challenging issue in the field of FRC is to provide residual tensile strengths in the crack openings for which concrete work on structural pieces that may allow the substitution of the traditional steel-bar reinforcement. That is to say, that in the case certain requirements are met, it is possible to produce a concrete with randomly distributed fibres in the mix that can meet the structural demands of the design even (and especially) if tension stresses are present. Furthermore, the combination of different modern technologies derives in new possibilities as FRC-SCC that has shown to enhance the flexural performance of FRC under certain situations.

Steel fibre reinforced concrete (SFRC) has shown to be adequate for such structural uses though having some of the well-known drawbacks of steel as are its weight, cost or durability among others. The development of macro-synthetic polyolefin-based fibres that provided residual strengths to concrete analogous to steel fibres has opened the door to a new field of FRC that is the centre of this thesis. The core aim of this work is to characterize the material behaviour of polyolefin fibre reinforced concrete (PFRC) to enable the use of polyolefin fibres as the only reinforcement of concrete pieces. If FRC concrete is a tailor-made type of concrete (Grünewald, 2004), the better understanding of this new type of concrete may be useful to fit PFRC in the effective design situations that can optimise and exploit its benefits.

1.1 Scope of the research

The increasing number of FRC structural applications in practice and the considerable amount of published research of the last four decades in the field support some of the initial possibilities to be explored with the abovementioned polyolefin fibres. In such a sense, standardised methodologies and tests as well as recommendations and codes provided remarkably important tools to face the research tasks. The most relevant structural codes for FRC have appeared in recent years (ACI Committee 544, Reapproved 2009; CNR-DT 204, 2006; DBV, 1992; EHE-08, 2008; FIB, 2010). Accordingly, normalization of test methods were also approved very close in time (ASTM C 1609/C 1690M-07, 2007; EN 14845-1, 2006; EN 14845-2, 2006; EN 14651:2007+A1, 2007; RILEM TC162-TDF, 2002). In the case of the production of polymer fibres for concrete, European Standard 14889-2 (EN 14889-2, 2008) was approved with specifications and definitions for the fibres. Additionally, reports about structural applications of FRC have been published using in most of the cases SFRC (Serna, et al., 2009; Laranjeira, 2010; Lopez, et al., 2014).

The scope of the research can be summarized in the title of the thesis being focussed on the performance of PFRC with the existing techniques and tests and deriving design considerations and tools. The aim was to provide practical knowledge for future applications of PFRC, such as mechanical properties, fracture behaviour, fibre positioning, constitutive models or discussing analytical models to assess the orientation of the fibres. If the reliability of the use of PFRC is proportional to the knowledge about it, the reduction of the degrees of scatter in the post-cracking response by means of operational and manufacture procedures was found to be also possible.

Hence, the main objectives of this research can be summarized as follows:

- Characterize the mechanical behaviour of polyolefin fibre reinforced concrete.
- Perform numerical tools for the design of PFRC elements with polyolefin fibres as the only reinforcement of the concrete.
- Reaching experimental and design conclusions that permit a reliable use of PFRC.

Some specific objectives are expressed below:

- Assess fresh properties of PFR-SCC and design a mix able to preserve the self-compacting properties with high polyolefin fibre dosages
- Obtain comparative results with steel fibre reinforced concrete and plain concrete.
- Design a vibrated conventional concrete (VCC) with analogous fracture properties and perform a similar campaign as the performed for FRC-SCC with the same fibre dosages.
- Evaluate the mechanical properties and the fracture behaviour of PFR-SCC and PFR-VCC with progressively increasing of fibre dosage in the range 3-10 kg/m³ and compare the results.
- Use a fibre combination of polyolefin and steel fibres, assess their mechanical properties, and fracture behaviour.
- Test the improvements obtained using a new chemical additive with the aim of improving adhesion between the fibre and the concrete.
- Design and perform tests to analyse the pull-out behaviour of the polyolefin fibres.
- Explore with scanning electron microscopy (SEM) the interface fibre-matrix.
- Study the influence of pouring and compaction methods.
- Study the influence of fibre length with the two most commonly used lengths: 48 and 60 mm.
- Analyse the influence of orientation factor and the variations in structural-size elements and in the fracture properties.
- Propose a model to predict the final positioning of the polyolefin fibres.
- Propose constitutive models to predict the post-cracking tensile behaviour of PFRC.
- Verify the proposed models with the experimental results.

1.2 Research strategy

In order to meet the objectives two parallel methodological lines have been followed: the experimental and the modelling works. The experimental works have been performed in four steps that could be summarized in mix design, mechanical and fracture testing, influence of the placing conditions and counting exercises and pull-out tests. The modelling works have dealt with two main issues: the orientation factor and FEM simulations of three-point bending tests.

The research was initially defined with the aim of obtaining fresh, mechanical and fracture properties of a combination of PFRC with SCC. The fracture results of the standard test methods showed that beyond the material properties and the typical scatter of the material, some other considerations should be studied. Accordingly, the influence of setting stages, fibre length or specimen sizes were assessed. Moreover, since the fracture results for important deformations outperformed the results of SFR-SCC, it was considered adequate to combine long polyolefin fibres with short steel-hooked fibres to improve the post-cracking strength for small deformations. Fibre counting exercises were performed and several sizes, pouring methods and compactions procedures were assessed too.

Hence, the first part of the research sought to define the material properties of PFRC. The following chapters were performed with the aim of evaluating PFRC behaviour in structural-size elements and some other important parameters as placing conditions and the influence fibre length. Once the main properties were known from laboratory tests, a numerical part of the thesis is presented to provide tools to assess the use of PFRC in real structures. Additionally, a final work was performed. The quality control of a real application of PFRC has been described to provide sound conclusion on the reliability of the material.

1.3 Outline of the thesis

In the present document, the referred subjects were divided into six parts in addition to the present chapter:

Part I: State of the art, describes the actual knowledge, discusses the concepts that are used in the document and motivates the significance of the thesis.

Part II: Experimental characterization of PFRC, supplies the procedures and results used to assess the behaviour of the material and the main material parameters.

Part III: Fibre positioning: experimental assessment, studies the influence of fresh concrete properties, compaction procedures, framework geometry and fibre on the mechanical performance and the orientation and distribution of fibres using PFRC.

Part IV: Material modelling provides an analytical model for the assessment of the orientation factor and constitutive models obtained from inverse analysis. It also shows the fitting with the previously discussed experimental data.

Part VI: Application focuses on the quality control of a Case Study.

Part VI: Concluding remarks, summarizes the conclusion obtained and the design considerations made notwithstanding the proposal of future works.

In a relatively short time-period, the works have been performed and the present document written. The document has been split according to the described parts. The structure of the document is shown in Figure 1-1 in which the number of the chapters related with the description is indicated in parenthesis.

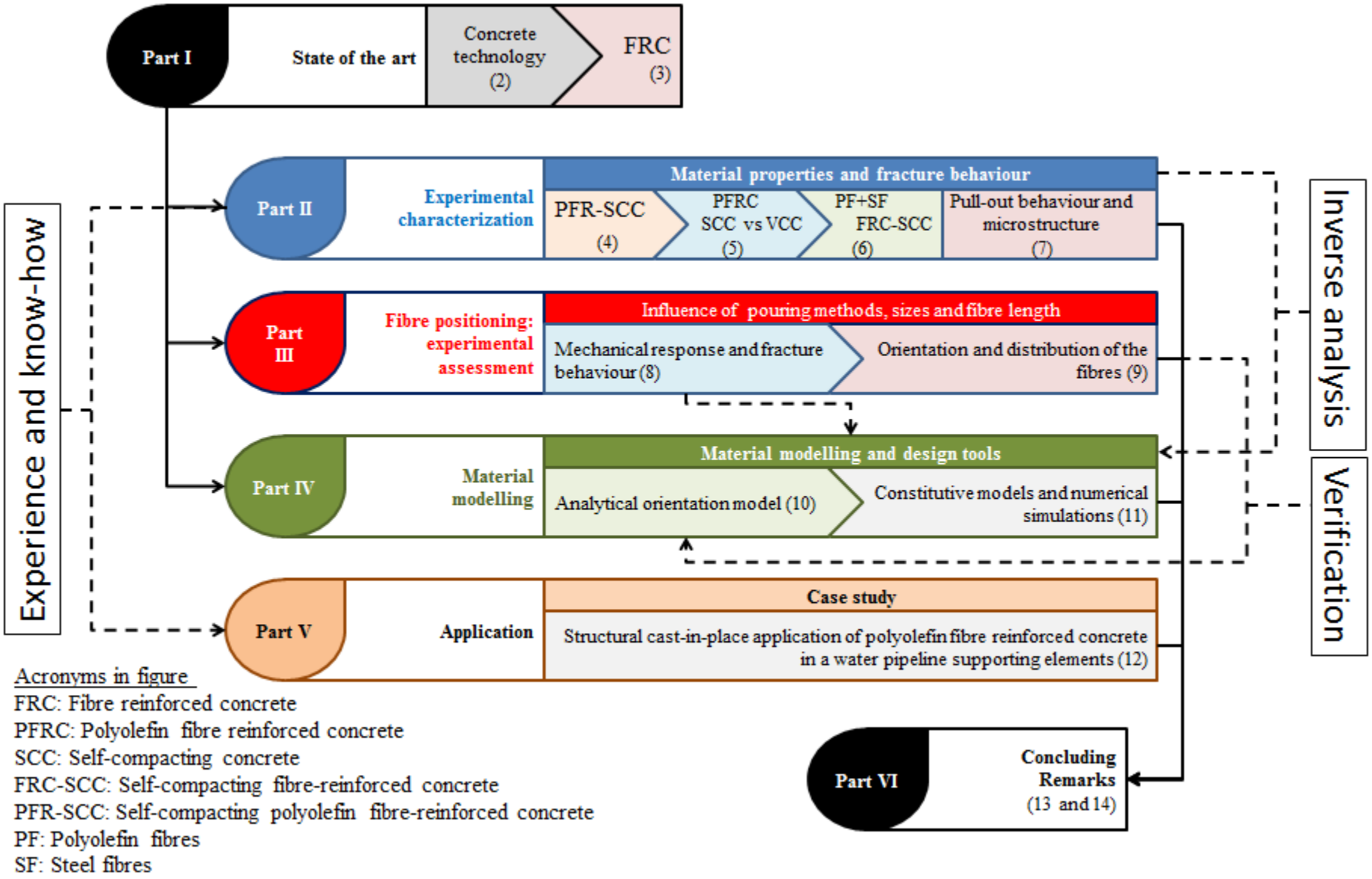

Figure 1-1: Outline of the thesis

PART I: STATE OF THE ART

Chapter 2

Concrete: the composite brittle material

Concrete is a composite material made with widespread available constituent materials, which perform at the end such an excellent material in its hardened state. Moreover, the initial fresh state in which it is produced confers the concrete a magnificent versatility and adaptability to the increasingly higher requirements of nowadays structural design. Since such properties involve also economic advantages, concrete is the foremost construction material. That is to say, on the one hand, that it is possible to design the material for a particular project and using locally available materials but also with the fresh and hardened properties desired. On the other hand, the final product supplies a uniform, durable and high-quality material. In such a sense, some of the most important developments of concrete technology were studied with the aim of improving its properties or to combining them with other construction materials. That would be the case of Self-Compacting Concrete (SCC) or Fibre-Reinforced Concrete (FRC) stemmed from conventional concrete due to the more challenging designing procedures being also combined for this research and so being essential for its conclusions. That does not exclude that it would also be the case of the most widely known steel bar reinforcing of concrete. With its development, technologies and supremacy in construction, concrete plays a key-role in our modern societies and it could be said that scarcely any aspect of our daily lives depend indirectly o directly on concrete (Mindess, et al., 2003).

Not only research focussed on concrete made with Portland cement, modern admixtures and other supplementary cementing materials have provided empirical relationships that have approach its behaviour, but also chemical and physical principles governing the behaviour of concrete have been the centre of fruitful research. In such a way, a large variety of properties and methods might deserve to be described not being the scope of the present document. Having said that, it should be noted that it has only been summarized in the present chapter those underlying concepts used ahead and that may be worthwhile for a more comprehensive reading of the document. The deep knowledge of the material is essential for the practical use of it, as Professor Torroja stated:

"Each material has a distinct specific personality and each form imposes a different stress configuration" (Torroja Miret, 1956)

2.1 Brief comments on SCC design

Since the first applications of SCC in the 1980s, this material has experienced a great development throughout the entire world. The main reasons for such success are the ease of its production and the high performance of the final hardened product (Okamura, 1999; Liu, 2010). As reviewed by Almeida (Almeida Filho, et al., 2010), the SCC advantages have been reported in a large amount of research and publications. Numerous practical applications have also been reported being an early example the use in the Akashi-Kaikyo suspension bridge, in service since April 1998. As reported by Ozawa (Ozawa, et al., 1999) the use of high performance SCC allowed the application of a new construction system in the bridge. The unusually fast increase in the use of SCC in the construction industry is the result of a series of advantages and achievements such as the improvements of production methods, the reduction of the structural element final cost, the correct filling of highly congested reinforcement areas, the excellent mechanical properties, the good durability and the uniformity of the hardened material (Domone, 2006; Burón, 2006). Nevertheless in order to obtain adequate properties of SCC in fresh state it is often required the use of high cement content and special admixtures (Sedran & De Larrard, 1999; Petersson & Billberg, 1999; Malhotra & Mehta, 2005) which increase the risk of initial shrinkage cracking and also penalizes the production cost (Rozière, et al., 2007). The high dosage of cement yields to the required fresh-state high flowability but it also increases the tendency of early age increase (Bissonnette, et al., 1999). Recent improvements in the production technology developed by precast factories (Navarro Ferrer & Estaban García, 2003) and in situ applicators have led to important reduction of cement content and superplasticizer (Sonebi, 2004) and consequently made SCC a more cost competitive material. There is large amount of research focused on high-performance SCC, but there is still a lack of studies seeking medium strength SCC to be used in more conventional requirements such as traditional building structures (Bermejo Nuñez, 2009).

Regarding the materials used to produce SCC, there are no relevant differences but a more special care on the knowledge of the aggregates and their regularity in order to assure the fresh properties characteristic of SCC. The distribution of aggregates sizes is decisive in the fresh-state behaviour. The finest particles contribute to maintain the cohesion of the mix preventing the segregation of the heavier elements when moving inside the mass. The maximum aggregate size is also critical, above all, when passing ability is required because of high density steel bar reinforcement. SCC usually contains additionally filler composed by particles passing through 0.063 mm sieve, which is defined in standard (UNE EN 12620, 2003). In the Spanish structural concrete code (EHE-08, 2008) the maximum quantity of particles passing 0.063 mm sieve are limited to 250 kg/m³ because higher amounts of limestone filler could modify and accelerate hydration processes in some cases and also

affect the durability. There are no special requests for cement but for evaluating the compatibility with the indispensable use of superplasticizer (SP). Summarizing, SCC is produced with the same basic constituent materials compared with vibrated conventional concrete (VCC), but for the mix proportioning and the needing of admixtures.

Chemical admixtures permit the reduction of water. The development of SP based on poly-carboxylates has been the keystone and has gone forward hand to hand with the evolution of SCC technology (Spiratos, et al., 2003). In many cases, high flowing ability is attained by using SP while stability against segregation is achieved by a large quantity of fine materials or by using viscosity-modifying agents (VMA) which increase the cost of the mix. That is why in the present research, the use of VMA has been avoided but it could be useful when it is desired to diminish the cement content of the mix (Viacava, et al., 2012). The theoretical basis of the action of SP is based on the tendency to flocculate of anhydrous cement particles when brought into contact with water. By means of adding admixtures with dispersing effect of the cement particles, it is possible to avoid the adverse impact of flocculation and increase the percentage of hydration of the cement. The dispersing effect caused by the SP molecules is due to their adsorption into the cement particle and to their orientation forming ionized groups with positive charge coinciding with cement electrical charge and so provoking that cement particles repel instead of flocculate (Mas, 2012). The limits of the use of the SP should be tested, being in the common range of use between 0.5% and 2% in percentage of the cement weight. With the same water/cement ratio more cement would hydrate what would lead to slight increases of compressive strength. However, excessive dosages may not produce the desired effects and may even decrease some mechanical properties (Dubey, et al., 2012).

Concerning the referred changes on the mix proportioning, several design methods have been proposed. It has to be highlighted that it is required to start the mix design with a carefully studied theoretical mix proportioning that may allow the reduction of the unavoidable empirical adjustments. Additionally, in the first step it should be taken into account both, the fresh-state and the hardened performance desired, marking the design challenges for fresh-state empirical tests. Such results permit the evaluation of the degree of self-compactability achieved by means of standardized fresh-state tests and have been incorporated to the existing design codes (EHE-08, 2008; ACI, 2007; EFNARC, 2002; Fédération Internationale du Béton fib/International Federation for Structural Concrete, 2010). Since the so-called Rational Mixed design method purposed by Okamura and Ozawa in 1999 and the purposed method by the *Laboratoire Central des ponts et Chaussées* (Sedran, 1996; De Larrard, 1997; De Larrard, et al., 1998; Zerbino, et al., 2006), several authors and institutions have developed, enhanced and purposed a variety of methods. Some of them include the use of rheometers or viscometers, although it should be highlighted that all of them include a final last step with an empirical adjustment based on empirical tests. The most relevant ones are one proposed by the Swedish Cement and Concrete Institute (Petersson, et al., 1996; Gettu, et al., 2004; Gettu, et al., 2004) , the method purposed by Domone et al. in 1999 at University College London and the one proposed by *Universidad Politécnica de Cataluña* (Gomes, 2001). The latter two take into account the voids left among the aggregates to be filled by the paste. In a general overview of the methods, the paste and the aggregate skeleton were purposed to be optimized separately. In the present study, the optimum distribution of the aggregates was taken as the maximum dry packing density obtained according to the ASTM C29/29M-09 (ASTM International, 2009). The paste was optimized in the empirical adjustment tests with the objective of achieving a mixture with moderate cement content able to reach the self-compacting fresh properties required even with the addition of the two types of fibres and

without VMA. A more detailed and useful overview of the SCC mix proportioning methods and some informative proportions used in the technical bibliography can be found in (ACHE, 2008; Alberti, 2013).

2.2 The fresh state of VCC and SCC

Concrete evolves from a fluid fresh-workable mass to a significantly steady solid strength with time. The reaction named hydration is an exothermal reaction of Portland cement with water which leads to a hardening of the cementitious material. In the very initial stages when the concrete is poured in the formwork, a period of rapid evolution of heat occurs. This stage has been reported to last about 15 minutes and to be followed by 2 or 4 hours of relative inactivity (Habel, 2004). After this second stage, an acceleration period determines the final set and a rate of initial hardening (Mindess, et al., 2003). There are some other relatively important time-dependent effects as swelling, shrinkage, or viscoelastic that affect the evolution of the mechanical properties beyond the first 24 hours of settings, though the first hours determine the workability of the concrete. Accordingly, the fresh properties play an important role for the concrete being short-term requirements equally important than long-term properties usually referred to strength and durability.

On the one hand, as it was denoted in the introduction, fresh-state behaviour of concrete is not only one of its main advantages but also normally one of the major requirements. On the other hand, some of the fresh properties may also affect the hardened properties of the final product.

Traditionally, fresh concrete has been poured in layers and compacted by means of vibration tools. The fresh-state behaviour of such vibrated conventional concrete (VCC) has traditionally been classified carrying out slump tests (EN 12350-2, 2002). The test measures the shear resistance of concrete to flowing by its own weight and relates the consistency of concrete with the descent of the mass using such empirical results to classify the workability of the material. The test is not associated to the energy required to compact concrete or to other factors that influence workability as could be water/cement ratio, aggregates or mix properties. However it has been widely used and has become the reference measurement in the standards to evaluate the VCC consistencies.

The developments of chemical admixtures that affect this initial state have given rise to a large amount of new possibilities such as the aforementioned SCC. Its flowing capacity assures the complete filling of narrow sections or through high densely reinforced areas and in absence of any vibration method. It consolidate under its own weight and also enhancing the finishing without segregation or bleeding.

From a material point of view, the main differences between SCC and VCC in the fresh-state behaviour could be estimated by rheological models that deal with deformation and flow under stress and which have provided interesting tools. Concerning conventional concrete, it has shown that it is reasonable to approximate the concrete flow behaviour using a Bingham model (Níelsson, et al., 2003; Grünewald, et al., 2003). While a Newtonian liquid would follow expression (2-1), Bingham model describes a fluid that needs to exceed some initial yield stress (τ_0) before flow can occur as a result of expression (2-2). The slope of the lines of Figure 2-1(a) is commonly known as plastic viscosity (μ). In such a sense, the Bingham model reduces to Newtonian model in case yield value is zero (ACHE, 2008). Unlike conventional concrete, SCC is characterized by a very low shear yield stress. In Figure 2-1(b), it can be seen the typical response of different kinds of concrete: conventional (VCC), high strength (HSC) and self-compacting (SCC).

$$\tau = \mu\gamma \qquad (2-1)$$

$$\tau = \tau_0 + \mu\gamma \qquad (2-2)$$

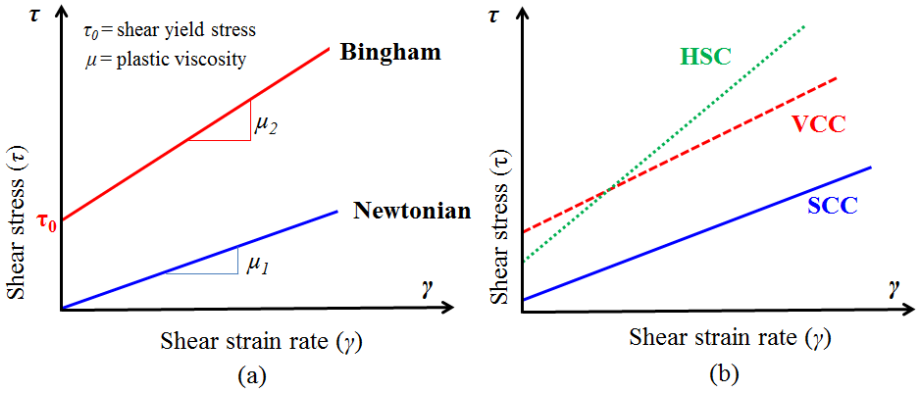

Figure 2-1: Rheological models.

However, most of the referred research has been focussed on the relation of τ_0 and μ with the empirical results that have been profusely used to characterize SCC in fresh state (Wallevik, 2003; Níelsson & Wallevik, 2003; Zerbino, et al., 2006). The most common way to characterize the fresh-state behaviour of plain SCC has been foremost slump flow test (EN 12350-8, 2010), though there are some other remarkably interesting tests. The characterisation of fresh state of SCC is assessed to determine the distinctive features of SCC as compared with VCC. The main ones are shown ahead, not being discussed in this thesis some additional fresh state differential characteristics such as pump-ability, finish-ability, washout and resistance or risk of blocking. The latter is usually measured by L-box test (UNE-EN 12350-10, 2011) and it has not been reported in the present document due to the presence of long fibres that would undervalue the passing ability of the FRC-SCC (Ferrara, et al., 2007). Having said that, the two test considered more adequate to characterize the fresh-state behaviour of the SCC and FRC-SCC were the slump flow test (EN 12350-8, 2010) and the V-funnel test (EN 12350-9, 2010). The referred tests were consequently performed for each SCC produced in this research. In the case of VCC, the slump test was carried out. The test methods are succinctly described below after the definition of the main properties measured.

Filling ability: In the absence of any external compaction methods, SCC has the ability to fully fill the formwork not keeping air trapped and flowing horizontally and vertically by the only action of its own weight and the casting energy. This property can be measured by slump flow test and V-funnel test.

Segregation resistance: This property is closely related with the uniformity of the aggregate distribution and can be measured by observing the homogeneity of the distribution of the aggregates in the patty obtained in the sump flow test. It can additionally be observed in the absence of paste segregation in the edge of the spread. The opposition of the SCC components to separate taking in account the dynamic effects of flow could also be estimated by the V-funnel test.

Passing ability: The concrete mass should pass through obstacles keeping the homogeneous distribution of the components being decisive the maximum aggregate size as well as the distance among obstacles. It can be measured by slump flow tests and V-funnel test. The J-Ring test and L-box test are also very adequate to evaluate this property (ACHE, 2008).

With the characteristic values of each test, it is possible to characterize the fresh-state behaviour of a given SCC. It could be done by the classification methods of the existing codes and guides (EHE-08, 2008; EFNARC, 2002) but some very useful rules, practical for design purpose, have been developed as the one shown in Figure 2-2 proposed in reference (Walraven, 2003).

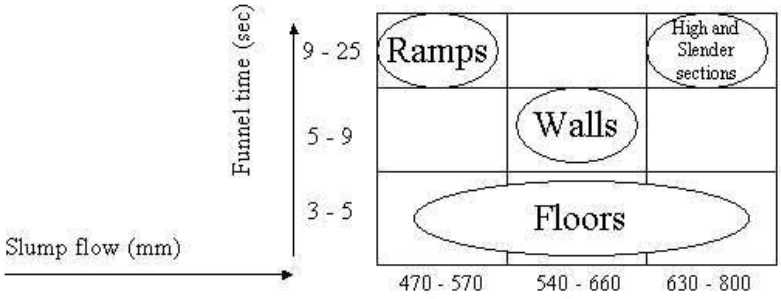

Figure 2-2: Application areas in relation to SCC properties [from: (Walraven, 2003)].

2.2.1 Slump flow test

The slump flow test is framed in EN 12350-8 and has become the referential value for designing SCC. It is used to assess flowability and flow rate. The cone and the procedure are similar to slump test (EN 12350-2, 2002), but SCC spreads forming a patty and the cone should be placed on a steel plate. On the plate, circumferences of diameter 210 mm and 500 mm diameter are marked. Once concrete is poured in the cone without compaction, the cone is vertically lifted within 30 seconds. The elapsed time from start to when the mass first reaches the 500 mm diameter is registered (T_{500}). Once the advance of the patty has finished, the largest diameter and its perpendicular diameter are measured, being the result the average of both measurements (d_f). It is important to check for any signs of segregation. It could be observed either in paste/mortar frequently in the edge or in coarse aggregate typically remaining in the centre of the patty. The scheme of the test is depicted in Figure 2-3. Domone concluded that being the slump flow test results adequate and the procedure simpler it was the more convenient test to be preferred (Domone, 1998). Despite their inherent limitations, being this test remarkably simple and a single-point workability test, it is especially adequate to be used for the specification and quality control of SCC and therefore slump flow test has probably become the reference test to characterize the fresh-state properties of SCC.

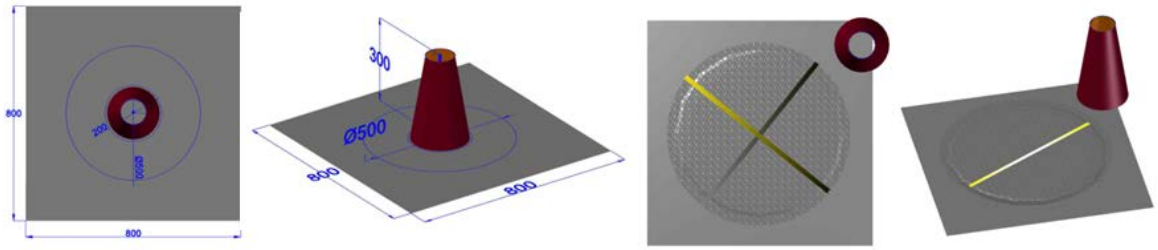

Figure 2-3: Scheme of the slump flow test.

2.2.2 V-funnel test

The V-funnel test described in EN 12350-9 is used to assess the viscosity and filling ability of self-compacting concrete. The V-funnel of dimensions shown in Figure 2-4 is filled and after around 10 seconds of resting, the gate is opened and the flow time (T_v) is registered until it is possible to see through the gate.

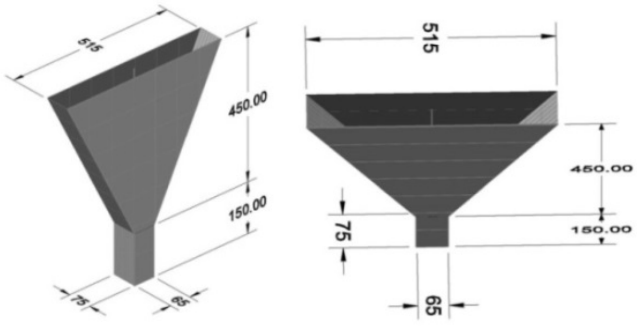

Figure 2-4: V-funnel dimensions.

2.3 Mechanical properties: strength and brittleness

The most important mechanical properties of concrete, compressive strength, tensile strength and modulus of elasticity of each type of concrete are discussed in this study. Standardized tests encompass the European standards for testing hardened concrete EN 12390 (EN 12390-3, 2009; EN 12390-6, 2009; EN 12390-13, 2013). The tensile strength is assessed by an indirect tensile strength tests also known as Brazilian test (Rocco, et al., 1999). The response of concrete to stress in the elastic branch of compression can be measured by the referred standard obtaining the secant modulus of elasticity. Direct tensile strength and flexural strength are discussed in sections dealing with fracture due to the significance of such tests in this report and in FRC. Indeed, the residual post-cracking strengths are the keystone to understand FRC behaviour.

The pre-eminence of compressive strength to characterize the mechanical behaviour of concrete is not only due to its good performance in compression as compared with its weakness in tension. Other factors are the easy and inexpensive tests and so the large amount of results in research and practice, the structural design primarily based on compressive strength which at the end has made it to be the reference parameter in structural codes (Fédération Internationale du Béton fib/International Federation for Structural Concrete, 2010; EHE-08, 2008) and finally the existing correlations with many other features of concrete. It is worth mentioning that compressive failure in plain concrete is also a brittle failure and it is produced by the combination of compressive and shear stresses. Pure compressive strength cannot itself cause compression failure but a secondary tensile stress produced due to the compressive force (Mindess, et al., 2003). These secondary effects are described in more detail in subsection 3.4 of the present document.

Concerning the differences between VCC and SCC, several considerations can be made. First all, water/cement ratio plays such an important role in compressive strength and SCC typically presents some other additional singularities. Moreover, better compaction is obtained in SCC during the setting. In such a way, with same water/cement ratio, the compressive strength of SCC would be higher (Bermejo Nuñez, 2009). Domone (Domone, 2007) compared results of 70 studies and found that very similar mechanical properties were obtained when comparing VCC with SCC except for the modulus of elasticity which was found to be significantly lower in SCC (40% lower for low strength and only 5% at high strengths). The contribution of limestone powder to the 28-day strength was highlighted. The reduction of the elasticity modulus is explained by the higher volume of paste and so the lower contribution of aggregates which modulus of elasticity is higher compared with the paste (Chopin, et al., 2003; Leemann & Gasser P. & Holzer, 2006; Georgiadis, et al., 2007; Pons, et al., 2003; Vieira & Bettencourt, 2003). Some other authors

have found that cementitious paste with limestone fines creates lower porosity and finer microstructure and so the modulus of elasticity of the paste is higher in SCC, concluding that at the end, that modulus of elasticity of SCC tends to be around 2% lower than in VCC (Parra, et al., 2011). In the same research, results showed that the splitting tensile strength of SCC, made with limestone filler, was on average 15% lower than that of VCC. Nevertheless, some authors have concluded that there is an increase of the indirect tensile strength in SCC made with fly ash (Klug, et al., 2003; Dinakar, et al., 2007).

2.4 Fracture behaviour of concrete

The main mechanical disadvantage of concrete is its small tensile strength and ductility, being usually considered to be zero in some designing procedures. The failure of concrete under tension is associated with micro-cracking in the interface between cement and aggregates and the ease of cracks to propagate under tensile loads explain its weakness (Mindess, et al., 2003). Moreover, as it was aforementioned, even failure under compression is finally caused by secondary tensile stresses. That is why fracture properties of concrete are reported as a detailed tensile behaviour after the first crack has occurred. The crack formation and propagation or the behaviour of different size specimens under uni-axial or bending tests have been the centre of a large amount of research (Bazant, et al., 1997; Bazant, et al., 1983; Cendón, et al., 2000; Elices, et al., 2002; Elices, et al., 1996; Hillerborg, et al., 1976; RILEM TC-187-SOC, 2007). Analysing the typical macroscopic behaviour under tension schematized in Figure 2-5 by a stress-strain curve, it can be seen that two main processes take place: one ascending branch until the maximum load is reached and a post-cracking branch, known for quasi-brittle materials as “softening curve”. Nevertheless, as described by Habel (Habel, 2004) with the help of Figure 2-5, in the end of the first branch of the curve micro-cracks have already been activated (point A) and the propagation of the cracks occurs at a stress level of 70-90% of the tensile strength (point B). When the maximum load is reached (point C), the micro-cracks interconnect in a network forming the fracture process zone (FPZ). The following fracture processes follow the softening curve localizing FPZ until the formation of larger cracks (that become visible at some point D) and concluding with the collapse of the piece when no bridging stresses between the crack faces are possible.

2.4.1 Fracture mechanics overview

In contrast to most of the other typical construction materials, such as homogenous brittle materials as glass or typical structural metals, concrete structures stand full of cracks. In such sense, failure of concrete structures involves the evolution of stable large cracking to form large fractures (Bazant, et al., 1997). That made that linear elastic fracture mechanics (LEFM) were not applied to concrete until recent times. Nowadays, some nonlinear fracture models such as cohesive crack approach have been used to explain the fracture processes of concrete. Fracture processes are essential in FRC and that is why a brief summary of concepts needed ahead in the present document has been placed in this chapter. LEFM models are only applicable when fracture process zone is small compared to the specimen size and so considering that fracture processes occur at the tip of a sharp crack. Moreover, when crack length is small compared with the fully developed FPZ it is essential to have detailed information in all FPZ and not only in the tip as LEFM (Bazant, et al., 1997). The appropriate description of what is taking place in FPZ is even more decisive in order to understand the fracture mechanisms when a proper design of some reinforcements or modifications is desired. Two simplified approaches can describe with detail the fracture process in the direction of the crack: cohesive crack models (Hillerborg, et al., 1976) and smeared crack models (Bazant, et al., 1983).

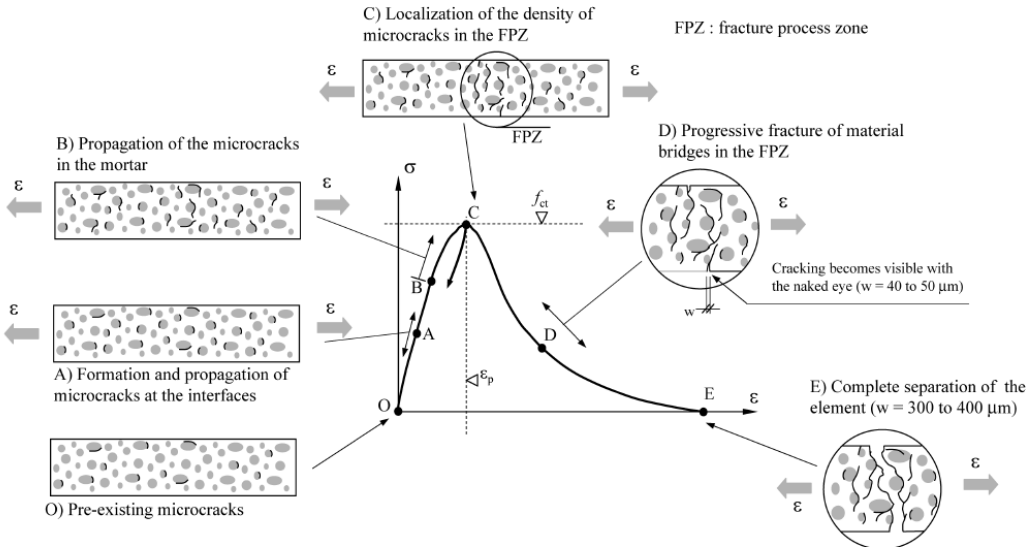

Figure 2-5: Conceptual illustration of the quasi-static concrete behaviour under tension and of crack formation and propagation [from: (Habel, 2004)].

The cohesive crack model has often been used to represent the bridging action of fibres being more extensively detailed in (Bazant, et al., 1997). The referred model is based on the assumption of the crack line as a fictitious crack able to transfer stress from one face to the other including the nonlinearity in the boundary conditions of the cracked line. That is why it is also known as fictitious crack model or crack with bridging stresses model. Hillerborg settled that the stress transferred through the cohesive crack was a function of the crack opening and gave rise to the concept of softening function with the expression (2-3).

$$\sigma = f(w) \qquad (2-3)$$

The softening function is considered as a material property. The corresponding softening curve starts at the maximum stress and the area below the curve is named cohesive fracture energy and is computed by expression (2-4) being w_c the critical crack opening where cohesive stress becomes zero (Elices, et al., 2002). A schematic view of the shape of the softening function for concrete and cementitious materials is presented in Figure 2-6.

$$G_F = \int_0^{w_c} f(w)dw \qquad (2-4)$$

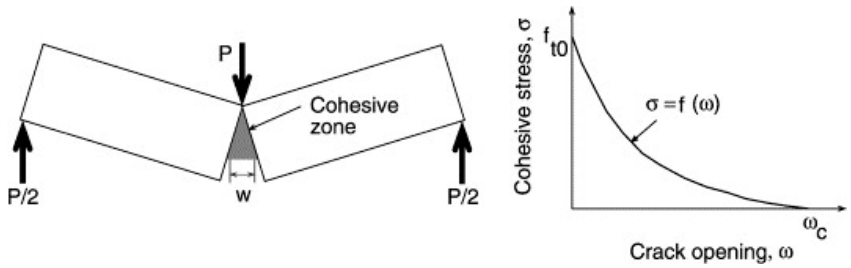

Figure 2-6: Cohesive crack and softening curve for Mode I fracture of concrete [from: (Gálvez, et al., 2002)].

The bulk material is idealized as an isotropic linear elastic material with elasticity modulus (E) and Poisson´s ratio (υ) (Elices, et al., 1996). That is to say that the energy supplied to break the specimen would be G_F times the broken surface in such ideal case (Bazant, et al.,

1997). One more assumption is worth noting: the crack is supposed to form when the maximum stress is equal to tensile strength (f_{ct}) forming expression (2-5) and one of the possible is as shown in Figure 2-7.

$$f(0) = f_{ct} \qquad (2-5)$$

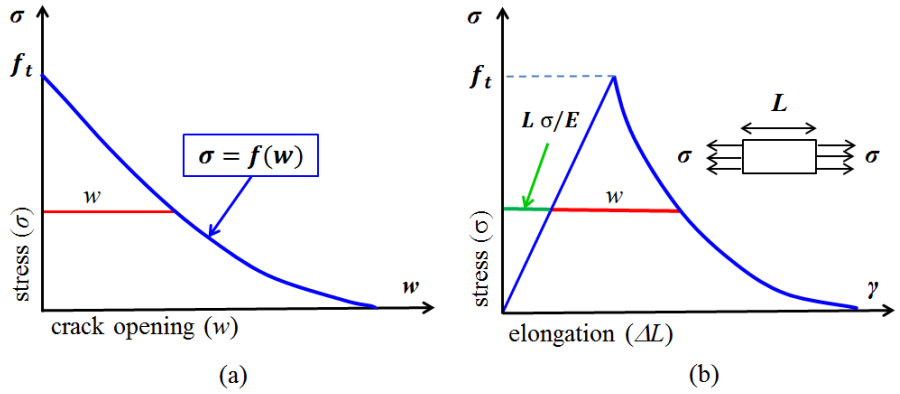

Figure 2-7: Resulting stress-elongation curve when the bulk material is supposed to behave elastically [Adapted from (Bazant, et al., 1997)].

The softening curve has been proposed to be linear (Hillerborg, et al., 1976), bilinear (Roelfstra, et al., 1986; Kooiman, et al., 2000; Guinea, et al., 1994) or exponential, as the expression (2-6) extracted from the reference (Bazant, et al., 1997). Figure 2-8 overviews some of the possibilities. The most widely used for modelling is the use of bilinear $\sigma - w$ relation and the so called inverse analysis adjusting experimental response of a notched specimen by trial-and-error optimization using finite elements methods (De Oliveira e Sousa, et al., 2006).

$$\sigma = f_{ct}.e^{\left(-\frac{f_t \omega}{G_F}\right)} \qquad (2-6)$$

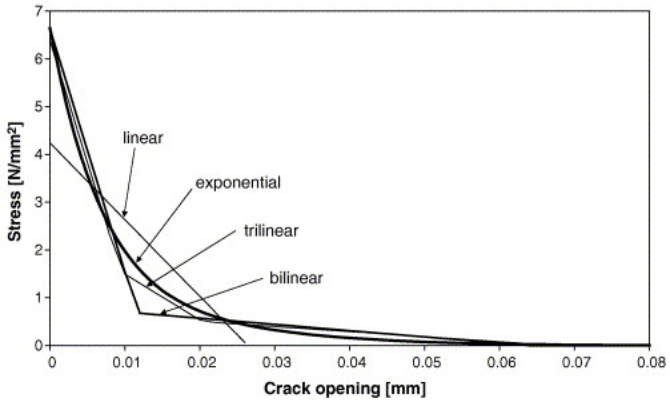

Figure 2-8: Example of various types of functions used for obtaining softening curves (Slowik, et al., 2006).

Subsequently, with a couple of material parameters obtained empirically, specific fracture energy (G_F), and the tensile strength (f_{ct}), the softening curve can be computed. The initial slope is marked by an opening value w_1 as if the linear softening stated by Hillerborg (Hillerborg, et al., 1976) is considered. That initial slope can be computed as f_{ct}/w_1 as shown in Figure 2-9 and it has shown to be accurate when large softening is not taking place (Bazant, et al., 1997).

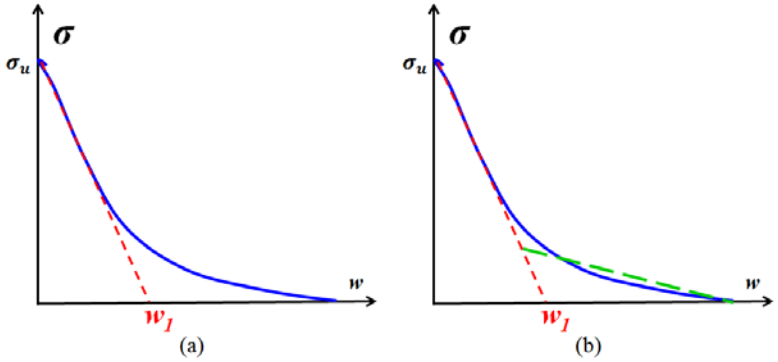

Figure 2-9: (a) Initial linear approximation of the softening curve and (b) its bilinear approximation [adapted from: (Planas, et al., 2003)].

Two more fracture parameters were defined in the model and extracted from the material properties. Hillerborg assumed that the behaviour of the beams depends on a critical length (l_{ch}) obtained by expression (2-7) and which is usually named as "characteristic length". Planas and Elices defined in 1992 (Planas, et al., 1992) a resembling parameter, known as "linear equivalent length" and shown in expression (2-8). The more brittle the fracture the steeper of the initial slope would be and so being closely related with the brittleness of the material. That is why l_{ch} can be used as an index of brittleness or by means of the denominated brittleness number defined by Hillerborg that can be computed by expression (2-9).

$$l_{ch} = \frac{E \cdot G_f}{{f_t}^2} \qquad (2-7)$$

$$l_1 = \frac{E \cdot w_1}{2 f_t} \qquad (2-8)$$

$$\beta_{ch} = \frac{D}{l_{ch}} \qquad (2-9)$$

2.4.2 Size effect in concrete structures

The size effect could be defined as the deviation on the structural strength of the actual load bearing capacity predicted by plastic limit analysis or any other classical strength theory based on critical stresses or strains (Bazant, et al., 1997). The load bearing capacity predicted by plastic limit analysis or any classical deterministic strength theory, such as elasticity, plasticity or viscosity, gives relevant information about the maximum load independent on the structure size for a given geometry. In order to assess the bearing capacity of a certain real structure, the understanding of size effect of quasi-brittle materials, fracture mechanics provide design engineers tools to take it into account. Moreover, the use of linear elastic fracture mechanics (LEFM) as a failure criterion seems especially adequate being the structure made of concrete, providing information not only about the size (W) but also about the cracks (a) using formulations as the expression (2-10) in which both concepts are related with the stress intensity factor. Nevertheless most of the structures in the reality are designed to fall in the non-linear fracture zone (NLFM) and the failure with classical LEFM does not agree either with fracture tests (Polanco-Loria, 1997).

$$K = \sigma_{applied}\sqrt{\pi a} \cdot f\left(\frac{a}{W}\right) \qquad (2-10)$$

That is to say that, according to the strength criterion or any limit strength, the failures are assumed to occur under an ultimate load (P_u) or stress (σ_{Nu}) where such limit stress remains constant, for a given geometry, independent of the structure size, notched or not. The most comprehensive example is that applying plastic and elastic formulations to beams in bending shear and torsion, the resulting formulas are basically the same but for a multiplicative factor, resulting in a plot log (σ_{Nu}) versus log(D) an horizontal line. Conversely, failures governed by LEFM exhibit a strong size effect with an inclined line of slope -1/2 that can be better understood by observing Figure 2-10 adapted from references (Bazant, et al., 1994) and justified in reference (Bazant, et al., 1997). As the authors explain in the mentioned reference, the reality of structures is a transitional behaviour from the horizontal straight line describing strength criterion to the inclined straight line of LEFM. Such transitional behaviour is described by a curve (NLFM) that approaches the behaviour for very small sizes to the strength criterion and the behaviour of very large sizes to LEFM. That behaviour was derived by Bazant (Bazant, 1984) and expressed in terms of a "Size effect law" by means of expression (2-11), where B and β_{ch} are at the end material empirical parameters, and that has been verified by a large amount of experimental evidence in notched and unnotched structures (Bazant, et al., 1994; Bazant, et al., 1997).

$$\sigma_{Nu} = \frac{B \cdot f_t}{\sqrt{1 + \beta_{ch}}} \qquad (2-11)$$

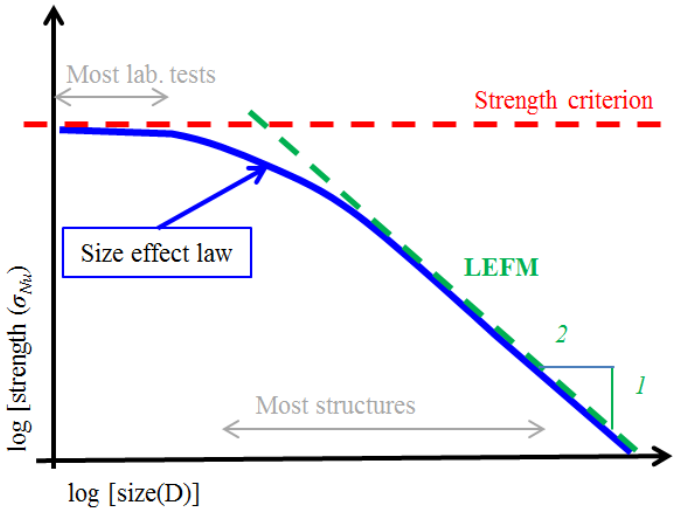

Figure 2-10: Size effect law proposed by Bazant [adapted from: (Bazant, 1984)].

2.4.3 Characterisation of fracture behaviour

In order to characterize the fracture behaviour of concrete, it is needed to perform fracture tests that stress the specimen under tension up to failure. The tests usually performed are flexural tensile strength tests because stable tensile test are difficult to perform with keeping parallel faces that not allow the appearance of asymmetric failure modes (Elices, et al., 1996). The three-point bending tests on notched specimens allow the estimation of the specific fracture energy (G_F) by means of expression (2-12) purposed in the recommendation (RILEM TC-187-SOC, 2007). Such expression relates the work of fracture W defined as the area under the curve load versus load-point displacement ($P - \delta$) and the ligament area $B(D - a_0)$; being B the depth of the beam, D its height and a_0 the notch length. The specific fracture energy is considered as the reference material property of concrete in fracture mechanics field. The tensile strength (f_{ct}) is also needed to characterize its fracture behaviour being assessed by indirect tests as aforementioned.

$$G_F = \frac{\int P d\delta}{B \cdot (D - a_0)} = \frac{W}{B \cdot (D - a_0)} \qquad (2-12)$$

Regarding the differences in fracture behaviour between VCC and SCC, it should be noted that both concrete types have a remarkably similar behaviour based on previous research (Fava, et al., 2003). It should be highlighted that in the reference, the brittleness of both concretes were close when characteristic lengths were compared as well as fracture energies and softening functions simulated by a cohesive crack model. SCC composed with filler had remarkably similar values of w_c, but also had higher results of G_F and l_{ch} even though its f_{ct} and E were lower compared with a conventional concrete.

Chapter 3

Fibre-reinforced concrete

In the beginning of the 1960s decade, the modern concept of disperse reinforcement of concrete was first proposed by adding steel fibres to the fresh mix (Habel, 2004; Kawashima, et al., 2011). Since then, the concept has been widely developed and numerous types of fibres are nowadays successfully employed in practical for a large variety of functional purposes. In the past decades various constituent materials such as steel, glass, carbon and synthetic polymers along with different fibre shapes and surface textures have been studied and tested, focused on achieving diverse purposes on the resulting composite material (Cavalaro, et al., 2014). It should not surprise that the inherent brittle nature of concrete, which is at the end a composite material, has been tried to be improved by the addition of randomly distributed elements of similar sizes compared with its constituent materials but much superior tensile capacities. Concrete has been traditionally reinforced with continuous steel-bar reinforcing placed in the tensile zone of structural members such as beams, slabs or columns. The combination of steel corrugated bars and concrete has been the most successful composite material in construction. The section forces can be equilibrated in structural members by taking advantage of the best performance of each material: compression by concrete and tensile stresses by steel. Nonetheless, the developing of micro-cracks and macro-cracks by the sole use of continuous reinforcing cannot still be even slowed (Nawy, 2008). Having steel-bar Reinforced Concrete (RC) become the par excellence solution for construction structures in the last century, the possibility of partial or even total substitution of steel-bars by steel fibres would not only allow to lessen the final cost of the structure but also provide some other improved properties. Once such

substitution has been accepted as viable, it has boosted industrial developments and research on fibres appearing new types of fibres, with varied shapes and possibilities.

The production of Steel Fibre-Reinforced concrete (SFRC) requires the use of materials, admixtures and special operational technology that inevitably increase the cost of the composite material. This is the reason why SFRC is only profitable when special structural requirements are demanded. Some applications like pavements and tunnelling often need special requirements that can be achieved using SFRC, although it has been also employed to meet other structural demands (Cavalaro, et al., 2014; Serna, 2007). As SFRC has become more popular in building and civil construction, some constitutive models, design approaches and tests have been developed (Köksal, et al., 2008; Chung, 2003; Banthia & Gupta, 2006; ACI Committee 544, 2008; CNR-DT 204, 2006; RILEM TC 162-TDF, 2000; RILEM TC-162-TDF, 2002; Liu, et al., 2008; EHE-08, 2008; fib Model Code, 2010).

The good performance of steel combined with concrete is widely known but also its drawbacks. Steel is highly corrosive in nature in addition to expensive for purchase and for storing and handling. Durability issues about SFRC concerned engineers and industry and the development of plastic industry allowed the production of fibres chemically stable (Ramakrinshnan, 1999). In the last years, the efforts of plastic industry focused on achieving a new generation of polyolefin based synthetic macro-fibres not only inert in alkaline environment and with structural benefits (Ugbolue, 2009). Polyolefin Fibre-Reinforced Concrete (PFRC) has considerable residual tensile strengths but it is still needed to extend research for a better comprehension of the possibilities of such composite material.

The intention of this chapter is to discuss the influencing parameters of the behaviour of FRC and in particular of PFRC. This thesis was steered with the aim of making contributions that may approach to structural macro-level uses of PFRC. One unavoidable methodology is to take advantage of the SFRC knowledge which advances and uses are broader studied. Such literature approach also seeks to enhance the understanding of the composite material in order to address properly the experimental research and further discussion. Considering the influence of fibres in the structural design possibilities of FRC, fresh and hardened properties of FRC in the meso-scale have been reviewed too. The mechanics of fibre reinforcement and the fracture behaviour are discussed in more detail due to its significance on the structural behaviour of FRC. The micro level was considered with a brief overview of the hydration processes and pull-out behaviour of FRC.

The same day Pharaoh commanded the taskmasters of the people and their foremen,

"You shall no longer give the people straw to make bricks, as in the past; let them go and gather straw for themselves" (Exodus 5:6-7).

3.1 FRC overview

3.1.1 Historical evolution and applications of FRC

Straws to reinforce bricks or horsehair to reinforce plaster are the oldest examples of reinforcing brittle matrixes. It is such an intuitive technique which was already used by ancient peoples as Mesopotamians or Egyptians. The Exodus is probably the oldest cite and there exist some old examples as the construction of the *ziggurats* of *Aqaf Quf* (Newman, et al., 2003). In 1874 Bérard patented in California (USA) what he named "Improvement in artificial stone" (see Figure 3-1) in which he purposed to add waste iron small pieces to a concrete. At the beginning of 20th century asbestos fibres were used to reinforce cement mortars. Such asbestos fibres were discarded due to environmental and healthy affection but it may be considered as the first applications of modern FRC. Between the years 1912 and 1927, several patents of cement mixes reinforced with glass or steel fibres were developed in France, Germany and the United States (ACHE, 2000).

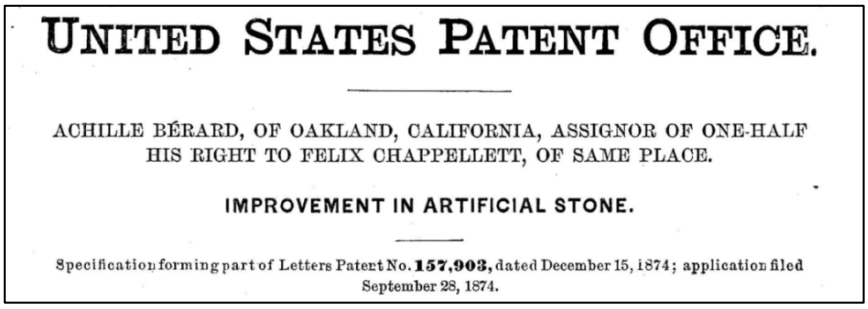

UNITED STATES PATENT OFFICE.

ACHILLE BÉRARD, OF OAKLAND, CALIFORNIA, ASSIGNOR OF ONE-HALF HIS RIGHT TO FELIX CHAPPELLETT, OF SAME PLACE.

IMPROVEMENT IN ARTIFICIAL STONE.

Specification forming part of Letters Patent No. **157,903**, dated December 15, 1874; application filed September 28, 1874.

Figure 3-1: Bérard patent dating 1874.

It was in the 1950s when the first studies on composite materials (more precisely when the works of Romualdi with Batson and Mandel in 1963 and 1964) had higher impact and boosted new research. At the same time-period, Biryukovski in 1964 and Majudar with Ryder in 1968 developed the first glass fibres dating also in that decade the first applications of fibre reinforced concrete in Civil Engineering. Even though the wide range of benefits and possibilities of FRC had not been still explored, it gave rise to the most spread application of steel fibres for pavements requiring high-abrasion resistance. Moreover, and also during the 1960s, the first experiments using plastic fibres with and without steel reinforcement were conducted (Goldfein, 1963). However, since the pioneering works in synthetic fibres (Zonsveld, 1975; Krenchel, et al., 1986) the main disadvantages of micro-polymer fibres were the low modulus of elasticity and the poor bonding. Such short and low-modulus polypropylene fibres became the first widely used plastic fibres. Those micro fibres, 6 to 20 mm long and tens of microns of diameter, did not have structural capacity but were very effective for passive fire-protection, anti-spalling or cracking control of initial shrinkage.

It was not until the decade of the 1990s when the first promising macro-synthetic fibres offered structural benefits to concrete having similar sizes as steel fibres though being chemically stable and with lower weight. The macro-fibres are manufactured using a variety of materials, having had the polyolefin based fibres the best results.

That is to say that, even if it is curtailed the structural applications in civil engineering to the modern concept of fibre reinforcing, it would already deal with a practical experience of more than 40 years. The approximate annual consumption of structural fibres for concrete in Spain was around 38.000 t in 2007 (Aguado, et al., 2007; Serna, et al., 2009). Some of

the more representative applications are shown in Figure 3-2. It was close to an equal distribution between mining and tunnelling (projected concrete, precast elements and segments) and pavements (industrial, ports, airports or roads). Common applications of FRC comprises also overlays in bridge decks, thin shell elements, seismic and explosion-resisting structures and many others, being a versatile and practical technology with a wide range of uses.

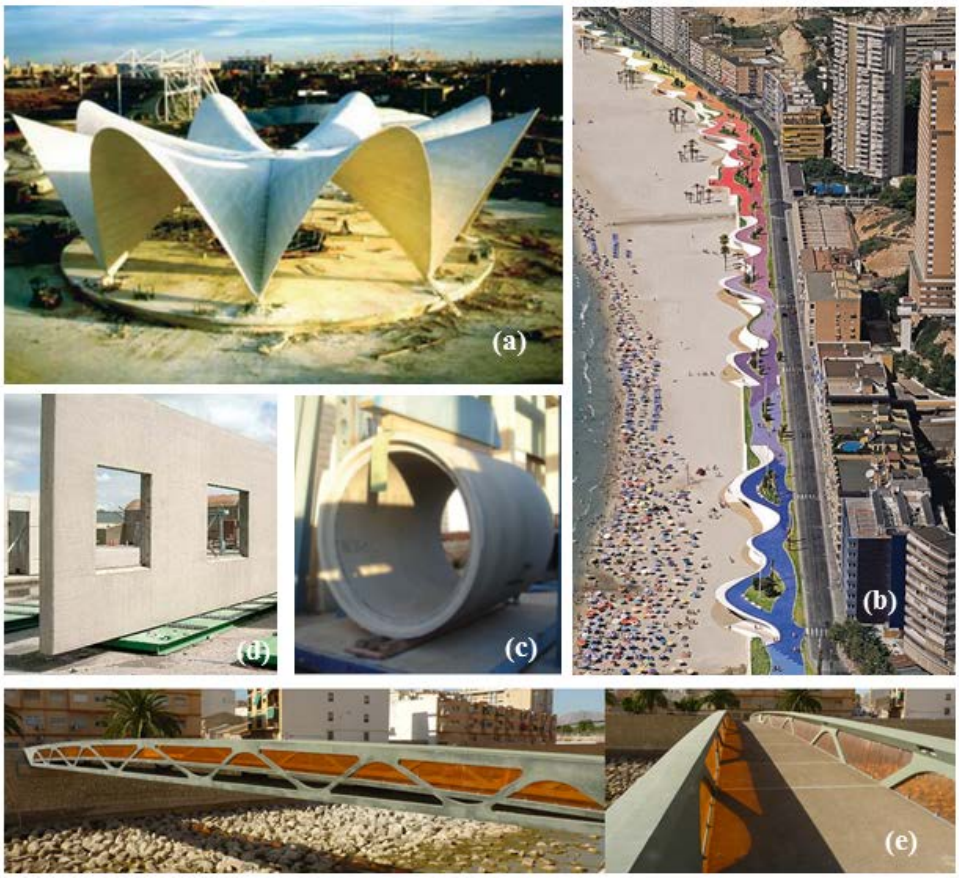

Figure 3-2: Applications of FRC: (a) shell of the submarine restaurant in Parque Oceanográfico de Valencia; (b) wall of the promenade Paseo Marítimo in Benidorm; (c) prefabricated SFRC panels for precast houses in Belgium; (d) sanitation pipes; (e) the UHPFRC Footbridge over the Ovejas ravine in Alicante (López, et al., 2014).

Concerning structural FRC, it should be noted that the possibility of a total substitution of the continuous steel-bar reinforcement in isostatic structures under uni-axial bending is still pending and remarkably complex. Nevertheless, the addition of fibres encompasses successfully the substitution of steel bars in elements with significantly variable stress distributions or pieces working in two or three dimensions. In some other structures with relatively low reliability level such as slabs-on-grade, foundations or walls, total substitutions of steel-bars is possible and in some other load carrying structures RC and FRC can be profitable to be combined (Døssland, 2008). Other more specific applications of FRC are those in which, due to the structural configuration of loads, only compressive stresses are expected such as double curvature shells. The composite material resists material the minor bending that occur during the life of a real structure as in the thin shell of the of the submarine restaurant in *Parque Oceanográfico* site in Valencia (Domingo, et al., 2003) and shown in Figure 3-2 (a).

Replacement for conventional steel mesh in industrial ground-floor slabs is the most spread use being nearly 65% of the fibre produced worldwide used in floors, road-pavements or

other types of slabs-on-ground (Newman, et al., 2003). By adding steel or synthetic structural fibres, research has shown to be possible to reduce the minimum required ground supported slab thickness (Soutsos, et al., 2012). The two main requirements for slab designing are shrinkage control and post-cracking strength in which plastic macro-fibres are very adequate. Furthermore, Polyolefin fibres have in such applications additional advantages as the absence of corrosion, the safe-handling, low pump-wear or lightweight in transport and storing.

Figure 3-3: Temporary load stages of a segment (De la Fuente, et al., 2014): (a) demoulding; (b) stocking; (c) transportation; (d) thrust of the jacks.

Projected concrete in tunnelling as well as the tunnel precast FRC segments for Tunnel Boring Machine (TBM) have also been extensively used as can be seen for example in references (Bakhshi, et al., 2014; De la Fuente, et al., 2014; Meda, et al., 2014; Mobasher, 2014; Serna, 2007). Their potential for production, improved handling robustness and long-term durability benefits are probably the main reasons. Structural situations should include transitional load cases as demoulding, storage, transportation and handling as well as construction load cases of TBM thrust jack forces and grouting pressure (see Figure 3-3); the use of FRC may allow the elimination or at least a significant reduction of the steel-bar reinforcement which leads to a significant cost reduction. The use of polyolefin based structural macro-fibres for FRC has confirmed in recent research to improve durability and serviceability of the concrete lining of water tunnels compared with steel fibres (Behfarnia, et al., 2014). By the same token, macro-synthetic fibres have been used in tunnelling or under extreme conditions in several applications in Norway, United Kingdom or Australia (Wimpenny, et al., 2009).

More than 20 bridges including motorway-bridges have been constructed using ultra high strength FRC in Japan. The *Sakata Mirai* footbridge shown in Figure 3-4 was the first one, constructed in 2002 and it was located in a saline environment not being detected deterioration (*"other than some spots of corrosion stains on the concrete surface and chloride ion ingress limited to a thin surface layer"*) 10 years after its construction (Uchida, et al., 2014).

Figure 3-4: Sakata Mirai footbridge (Uchida, et al., 2014).

The construction industry and precast companies are exploring some other special applications of FRC with new requirements. That is the case, for example, of the FRC wind towers. The trend of such towers is to require taller towers up to 140 m. Concrete towers have higher self-frequency than similar steel towers, but also around three times more mass and 5 times more damping and so reducing the dynamic effects. Precast FRC is especially suitable for wind towers due its fast execution, extended linear response, improved fatigue performance and cost efficiency (Lancha, 2014). The design was reported for a wind turbine generator tower made of precast prestressed high strength fibre reinforced concrete as shown in Figure 3-5.

Two main reasons were the keystone for selecting FRC: the anisotropy of stresses in the shell and the good performance under fatigue (Lee, et al., 2004) which plays a key role in the design. In addition, the total substitution of passive reinforcement allowed the reduction of the thickness of the shell from a minimum of 150 mm to 80 mm due to the lower durability cover requirements. Furthermore, FRC allowed reductions of anchorage length of passive an active reinforcement and enhances the performance of the joints (Baran, et al., 2012).

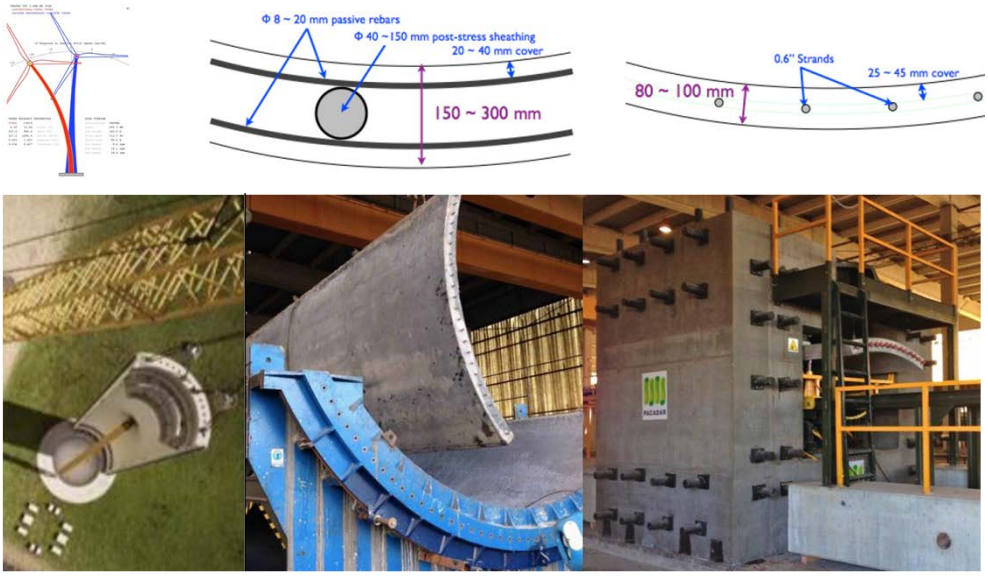

Figure 3-5: FRC wind towers: design considerations and tests of the shells (Lancha, 2014).

One other field with interesting future prospects for structural FRC, whether itself or in combination with other concrete technologies is rehabilitation of structures. One possible concept is to use a high performance FRC only in the areas of the structure where such improvement could be exploited. For example, durability requirements in zones exposed to severe environmental conditions or strengthening the areas where concentrated forces might be applied or impact might take place (Denarié, et al., 2003; Habel, et al., 2006; Brühwiler, et al., 2013). Macro-synthetic structural fibres have also been used for such types of tasks. Since structural-efficient polymer fibres are chemically stable and with

structural load-bearing capacity, such fibres are especially adequate for its use in the rehabilitation of singular buildings. That is the case of the high performance PFR-SCC designed, for the reconstruction of the Cathedral of La Laguna in Canary Island in Spain thanks also to the high surface-finish quality required (Stähli, et al., 2007; Carballosa de Miguel & Pacios Alvarez, 2011).

Moreover, some recent events as Fukushima nuclear accident or the attack on the Twin Towers have evidenced the need of structural designs providing some added response under seismic situations or impact loadings. Many structures are vital for emergency response and post-earthquake recovery as hospitals. In such accidental situations, bridges are critical for the transportation networks and are required to have a high degree of functionality even after a seismic event in Spanish earthquake resistant code (NCSP-07 , 2007). Structural integrity of some other buildings such as nuclear power plants or high-rise buildings is essential. FRC is especially well-suited among innovative construction materials to enhance the structural response under such type of loadings due to their substantial strain capacity and crack control capability. The benefits under impact have been reported for example in reference (Ferrara, 2007). FRC does not only absorb part of the impact energy but also allows larger deformations avoiding the collapse of the structure.

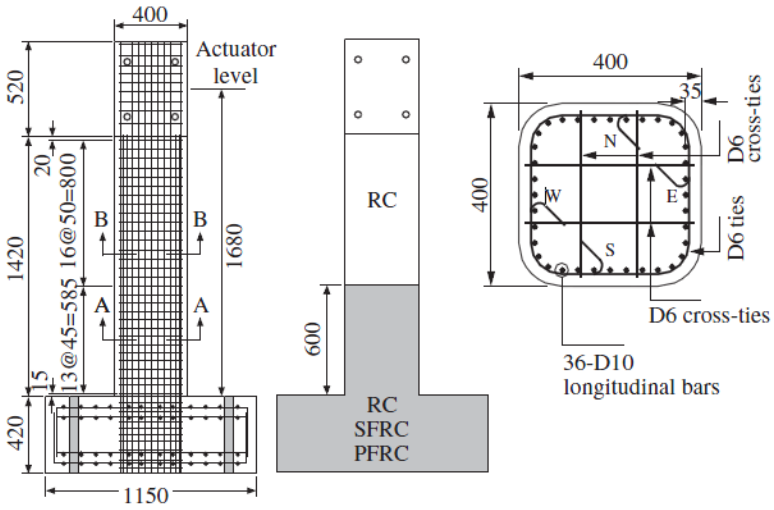

Figure 3-6: Specimen configuration of the scaled columns (Kawashima, et al., 2011).

Seismic response is based in the same properties and has been the centre of a recent work carried out in Japan (Kawashima, et al., 2011). Three scaled models of a cantilever prototype column were studied. The bridge abutments were 7.5 m tall and with squared section size 1.8 m with the design considerations of current Japan Specifications of Highway Bridges (Japan Road Association, 2002). Shear-span ratio was chosen to ensure flexural failure. The three prototypes were identical except for the material used in the potential plastic hinge region and the footing which was poured using concrete, SFRC and micro-polypropylene fibre reinforced cement composite (see Figure 3-6). The FRC columns lessened damage of cover and core of concrete at the column plastic hinge. Polymer FRC showed superior performance due to tis higher deformation capacity. Future prospects of the polyolefin fibre reinforced concrete in these special structures are especially adequate providing deformation capacity, post-cracking strength and chemical stability altogether.

3.1.2 Fibres: one more constituent element of the composite

Cracking in concrete is a consequence of tension that may occur either due to external forces or to other deformation effects such as shrinkage in the initial stages of its loading history. In such a way, the possible reinforcement of the fibres depends on the cause of the cracking process considered. That is why there exist a wide range of fibre types intending to prevent cracking propagation with numerous and different origins (TRB, 2006) and using wide-ranging constituent materials, shapes and sizes. The most typical ones and their mechanical properties are shown in Table 3-1. Material properties of the fibres compared with the concrete matrix are critical (Naaman, 2003), particularly their modulus of elasticity because the stiffer elements of the composite sections would theoretically absorb more proportion of the stress in the section. As a general rule, the higher modulus of elasticity, the better anchorage and friction with matrix and the higher slenderness of the fibres, the better mechanical performance (Fanella, et al., 1985; Köksal, et al., 2008).

Table 3-1: Typical properties of fibres [from: (Nawy, 2008; Bentur, et al., 2006)].

Type of Fibre	*Diameter (mm)*	*Specific gravity*	*Tensile strength (GPa)*	*Modulus of elasticity (GPa)*	*Ultimate elongation (%)*
Acrylic	0.02-0.35	1.1	0.2-0.4	2	1.1
Asbestos	0.0015-0.02	3.2	0.6-1.0	83-138	1-2
Cotton	0.2-0.6	1.5	0.4-0.7	4.8	3-10
Glass	0.005-0.15	2.5	1.0-2.6	70-80	1.5-3.5
Graphite	0.008-0.009	1.9	1.0-2.6	230-415	0.5-1.0
Kevlar	0.010	1.45	3.5-3.6	65-133	2.1-4.0
Nylon (high tenacity)	0.02-0.40	1.1	0.76-0.82	4.1	16-20
Carbon PAN	0.007-0.009	1.7	2.5-4.0	230-390	0.5-1.5
Carbon Pitch	0.009-0.018	1.6	0.5-3.1	30-32	0.5-2.4
Polyester (high tenacity)	0.02-0.40	1.4	0.72-0.86	8.3	11-13
Polypropylene	0.02-0.40	0.95	0.55-0.76	3.5	15-25
Rayon (high tenacity)	0.02-0.38	1.5	0.4-0.6	6.9	10-25
Rock wool	0.01-0.8	2.7	0.5-0.76	---	0.5-0.7
Sisal	0.01-0.10	1.5	0.8	---	3.0
Steel	0.1-1.0	7.85	0.3-2.0	200	0.5-3.5
Polyolefin	**0.15-0.635**	**0.91**	**0.2-1.1**	**2.7-20.5**	**7 - 15**
Concrete matrix	---	1.5-2.5	0.003-0.007	10-45	0.02

Spanish structural code (EHE-08, 2008) considered three typologies of fibres: steel, synthetic and glass fibres while the American Concrete Institute (ACI Committee 544, 2008) added to them a group of natural fibres. In 2006 European standards EN 14889 and EN 14845, regarding fibres for concrete, were approved. The standards included only steel and polymer fibres. That classification and comments are discussed in subsection 3.1.4 due to its significance for the present research.

At this part of the document it is clear that steel fibres have been the most frequently used in structural FRC being the centre of a large amount of research (Kooiman, et al., 2000; Martinie & Roussel, 2011; Soroushian, et al., 1992; Døssland, 2008; Maya, 2011; Zerbino, et al., 2006) and in combination with traditional steel-bar reinforcement (Habel, 2004). Furthermore, the so called Ultra High-Performance Fibre Reinforced Concrete (UHPFRC) combining several advanced technologies of concrete such as FRC, high strength concrete (HSC) and SCC have shown to be possible and economical in some applications as in the Footbridge over the Ovejas ravine, shown in Figure 3-2(a) (López, et al., 2014). Moreover, SFRC performance has been reported under a wide range of mechanical requests: flexural (Ravindrarajah, et al., 1984; Barros, et al., 1999), shear in prestressed beams (Narayanan, et al., 1987), under biaxial compression (Tan, et al., 1994; Bencardino, et al., 2008), fatigue (Nanni, 1991), fracture (Barros, 2001; Kazemi, et al., 2008), or tension-stiffening (Bischoff, 2003). Recent research has also used steel fibres from waste tyres which disposition is a relevant problem to be solved in the EU states and could become an alternative to tyre-recycling (Aiello, et al., 2009). Such fibres and the most common shapes of the used steel fibres have been gathered in Figure 3-7.

Figure 3-7: Several shapes and types of steel fibres (Banthia & Sappakittipakorn, 2007; Aiello, et al., 2009).

Glass fibre reinforced concrete (GRC) has been mainly used in exterior building façade panels and as architectural precast concrete due to the good performance in the short-term periods. One of those uses has been, for example in the access towers of Santiago Bernabeu Stadium located in Madrid. Some image of it is shown in Figure 3-8 besides some typical glass fibres. However they have important drawbacks regarding durability. Glass fibres loss their properties inside the cementitious matrix with time due to a variety of factors that are still under study (Enfedaque, et al., 2012; Purnell, et al., 1998; Purnell, et al., 1999; Purnell, et al., 2000; Purnell, et al., 2005). Chemical corrosion of the AR glass fibres seems to be the main responsible for the strength loss (Enfedaque, 2008).

Figure 3-8: Glass fibres.

Low-modulus polypropylene micro-fibres are used in small proportions for cracking control of the initial shrinkage because in the first hours of setting, both concrete and fibres modulus of elasticity is similar (Banthia, et al., 2006; Melián, et al., 2010). Such short Polypropylene fibres may be also employed in walls of buildings because they have sound performance in case of fire and also help to prevent explosive spalling (Liu, et al., 2008). In Figure 3-9, the visual aspect of the fibres and also the aspect of a concrete surface after spalling and water dots left by the fibres after fire resistance tests are shown. The mechanical properties of FRC with this type of fibres have been carefully studied and have shown that compressive strength remains stable while small improvements in its toughness was found (Elser, et al., 1996). Recent research has also deepened on its fracture behaviour and future possibilities (Cifuentes, 2010).

Figure 3-9: Typical micro-polypropylene fibres, fire spalling and water dots in concrete under fire resistance tests (Gálvez, et al., 2014).

Polyolefin based macro-fibres are in some cases made with or partially composed by polypropylene but should not be confused with the abovementioned polypropylene micro-fibres. Polyolefin fibres have been designed to approximate the post-cracking behaviour of a PFRC to a SFRC but with lower fibre contents in terms of weight. Polyolefin fibres are chemically stable and possess improved mechanical properties and a surface treatment to boost the interfacial bond between fibre and matrix. The typical shapes and outlook of polyolefin fibres can be seen in Figure 3-10. Polyolefin based macro-synthetic structural fibres have similar sizes as steel fibres, between 30 and 65 mm. Although some research (Pujadas, 2013) and several applications (De la Fuente, et al., 2013) have been performed since the first developments, there is still a substantial lack of knowledge being this type of fibres especially well-suited for future FRC developments and are the centre of this thesis.

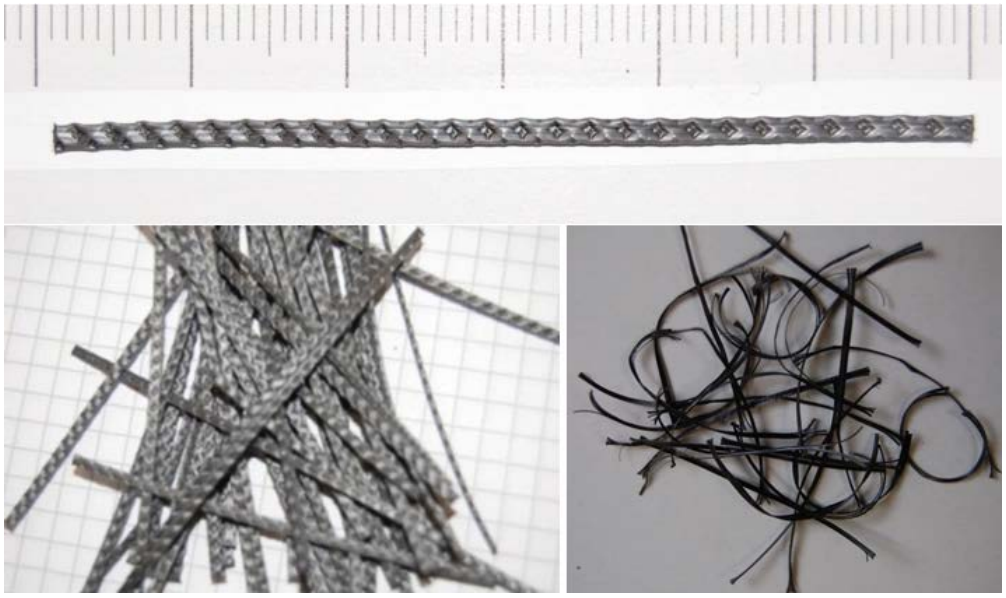

Figure 3-10: Polyolefin fibres visual aspect: typical shapes and surfaces.

At the beginning of the 1970s, Ali (Ali, et al., 1972) carried out researches using carbon fibres and so completing the range of fibres used to reinforce concrete. Carbon fibres are synthetic high-modulus fibres inert to most chemicals what makes them adequate to perform in the alkaline cement environment (Bentur, et al., 2006). There have been found two main production processes with two different starting materials: poly-acrylonitrile and petroleum. The first ones make up the known as PAN carbon fibres. The petroleum-pitch based carbon fibres have recently been developed for use as reinforcement of cement-based composites (Nawy, 2008). It should be noted that PAN fibres are of higher quality and properties being its main drawback their high-cost. The pitch carbon fibres have a much lower modulus of elasticity but significantly close to the typical concrete values. Their lower price and the better properties compared with other synthetic fibres have made them more attractive for cementitious matrixes (Zheng, et al., 1995). The diameter of the filaments is the same order of magnitude of a cement particle and they can be uniformly distributed and randomly oriented inside the matrix volume. The function of the typical carbon fibres is similar to that of steel fibres acting to sew the cracks. However, the presence of carbon fibres, does not only improve the mechanical properties of concrete but it also converts it into an electrically conductive material (Ivorra, et al., 2010). Concrete is a poor electrical conductor. Such electrical conductivity opens a new broad field on multifunctional-concrete applications as anti-static flooring, heating due to its resistivity, preventing freezing of bridge decks (Yehia, et al., 1999), walling of electromagnetic shield rooms (Wu, et al., 2005), cathodic protection of steel-bars in concrete (Chen, et al., 1995; Bertolini, et al., 2004) or electrochemical extraction of chlorides from reinforced concrete using conductive cement paste as an anode (Pérez, et al., 2010). In such sense, research on the percolation threshold (Chung, 2003; Chen, et al., 2004; Chiarello, 2005) and the possible applications of this multifunctional material have been carried out (Garcés, et al., 2010; Baeza, 2011). Some studies have also been focused on the possibility of acting the concrete as a self-deformation strain-sensor (Wen, et al., 2003). In any event, due to its remarkably higher cost compared with polymeric fibres, carbon fibres have limited potential only to singular applications.

Natural fibres added to concrete are only used in developing regions. Their mechanical properties are very limited and usually have durability problems (Filho, et al., 2000; Li, et al., 2000; Silva, et al., 2010).

Although all the fibres have proven to enhance in some way the response of the composite, the present chapter encompasses more deeply the properties of the so called structural fibres in which polyolefin fibres would be enclosed. Structural fibres are defined as the types of fibres that allow partial or total substitution of the steel-bar reinforcement and as a consequence which mechanical contributions can be taken into account for the structural design.

3.1.3 How many fibres are effective?

The following added variable to be considered is the quantity, usually reported in volume fraction of fibres added to the mix (V_f) and computed by expression (3-1) or directly in kg/m³ of the mix proportioning. Fibre content may affect the production technology beyond their material properties and has to be taken into account for pouring and compaction methods in order to assure a good quality of the final product.

From the point of view of structural fibres, steel and macro-synthetic fibres, the deformation capacity in tension is improved even with the addition of very small proportions of fibres (Kooiman, 2000). In bending, the post-cracking load-bearing capacity can be increased at low volume fractions but for structural uses the amount of fibres has to be increased up to moderate values (depending on the fibre type) in order to achieve post-cracking structural tensile strengths. The higher volume fraction the better structural response due to the more fibres placed in the cracks up to some quantity that jeopardise the workability and final compaction (Yazici, et al., 2007). Nevertheless, the increasing of fibre volume hardly provides compressive strength improvements.

$$V_f(\%) = \frac{W_f}{\rho \cdot V} * 100 \qquad (3-1)$$

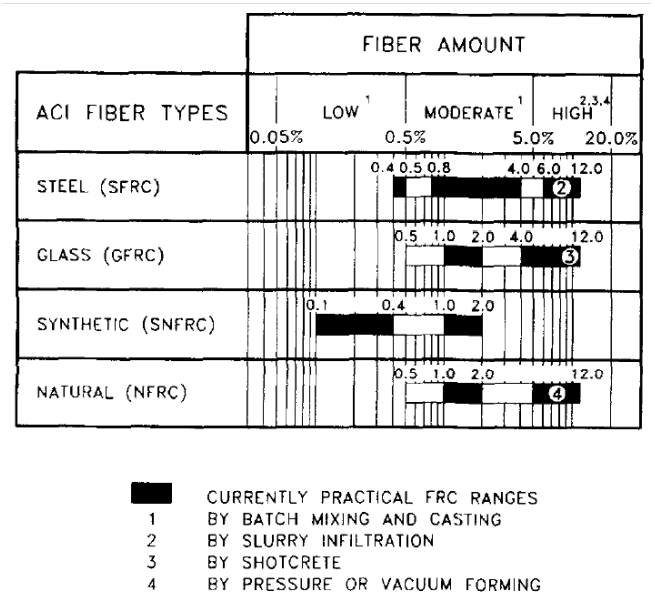

Figure 3-11: Fibre types and amount used by volume per cent of matrix (Zollo, 1996).

However, since the orientation and distribution of fibres through a cross section is not homogeneous, it is not possible to achieve with reliability the same area of reinforcing with fibres as compared with conventional bars. For normal fibre contents, concrete exhibits a softening response (Døssland, 2008). In the case of structural macro-fibres the common maximum volume fraction considered for the production of FRC is about 1.5%. For ultra-high-performance FRC in which strain-hardening and multiple cracking characteristics are sought, it has been reported that with a proper design, the critical V_f would be 2% (Naaman, 2003). In such sense, Spanish structural concrete code (EHE-08, 2008) limits fibre-contain up to 1.5%. Applications out of the scope of this FRC review reach higher volumes as are shotcrete and spray techniques (3-7%) or SIFCON (slurry infiltrated fibre concrete) and SIMCON (slurry infiltrated mat concrete) (7-15%). The latter can be found, for example in reference (Bentur, et al., 2006). Classifications and range of uses are nowadays reported in the most common fibres and some other factors as pull-out energy, micro-structural formations, positioning or durability are assessed by experimental research and analytical approaches. In 1996, Zollo completed an overview on 30 years of FRC research and summarized the typical volume fraction used for each type of fibres as shown in Figure 3-11.

3.1.4 Classification of fibres following European standards

At this point of the present thesis, it has been clearly denoted that the most relevant fibres for reinforcing concrete are steel and polymer fibres. That is why European Committee for Standardization (CEN) approved in 2006 the European Standard 14889 comprising two parts: the first one dealing with steel fibres and the second one regarding polymer fibres. In such standards not all the characteristics that may be relevant to the performance of FRC were addressed. It was focussed on standardized testing methods, specifications and fibre classification. It did not include effects on the early age of concrete, creep or chemical attacks because of the lack of meaningful and standardized test methods. The code defines the possible geometrical shapes and physical parameters of the fibres and settles the procedures for the measurements of the fibre mechanical properties such as tensile strength or modulus of elasticity. The polymer fibres are divided into two groups: non-structural micro-fibres and structural macro-fibres separated by the diameter of 0.30 mm. Figure 3-12 is a scheme of the classification of the fibres made by reference (EN 14889-2, 2008).

It should be highlighted that EN 14889 requires the manufacturer to declare the volume of fibres in kg/m³ which provides a flexural post-cracking tensile strength of 1.5 MPa in a value of crack mouth opening displacement (CMOD) of 0.5 mm and having at least 1 MPa of residual strength for CMOD of 3.5 mm. Those values should be measured with the standardized test EN 14651 (EN 14651:2007+A1, 2007) which will be explained in detail in subsection 3.7. It is worth noting that those two residual strengths are the main values to fulfil the most common requirements in order to consider the fibres as structural fibres. In the case of EN 14889, those two requirements are made with a reference concrete enclosed in EN 14845 (EN 14845-1, 2006; EN 14845-2, 2006) and with the referred fixed values of residual strength. Model Code, however, defined the same requirements as a percentage of the maximum strength obtained in the test (EHE-08, 2008; fib Model Code, 2010). That has been justified with the aim of avoiding brittleness (Di Prisco, et al., 2013). As an example of the requirements, the subsequent CE marking of the polyolefin fibres that have been used in the core of this thesis has been placed in Appendix A.

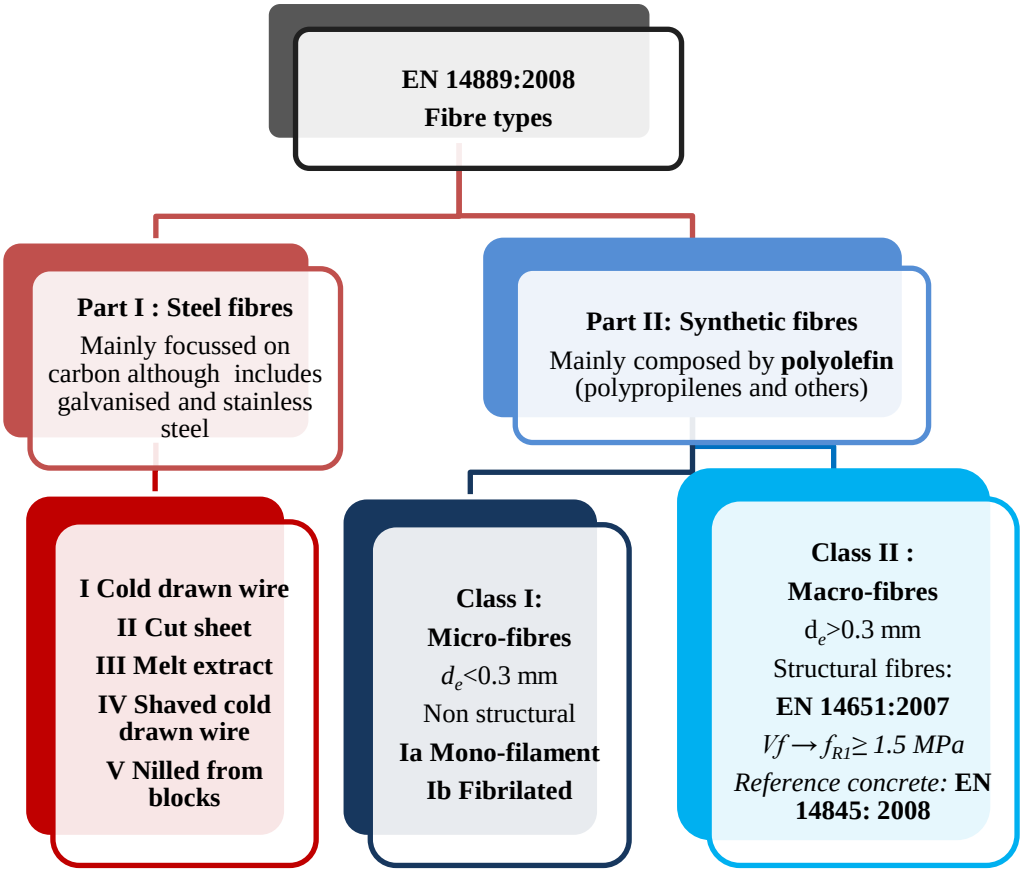

Figure 3-12: Fibre classification following EN-14889.

3.2 Polyolefin fibres to reinforce concrete

Polyolefin fibres with surface bulges and grooves along the fibres surface are produced from homo-polymeric resin into a mono-filament form (Bentur, et al., 2006). There is not a broad amount of publications on polyolefin fibres until recent times. The development of polyolefin based structural fibres with the mechanical properties shown in Table 3-1 has extended the use of plastic fibres beyond shrinkage cracking control. The fibres used in the present thesis are novel and with improved properties compared with the existing bibliography. The increasingly interest in macro-fibres as a reinforcement has led to some research and applications but there is still a needing of knowledge and comprehension of its behaviour.

3.2.1 Why polyolefin fibres?

It is not the scope of this report to discuss the advances made in polymer science, chemical composition or engineering that has led to the strong importance of polyolefins. Polyethylene and polypropylene are widespread polyolefins and the fastest growing polymer family thanks to the lower cost of production compared with other plastics and materials they replace (Ugbolue, 2009). Hygienic applications as diapers or food packaging but also automotive parts, geotextiles, upholstery fabrics, surgical masks, filters and many other applications as fibres and films. Polyolefin fibres encompass a broad spectrum of uses in modern societies. Their low cost, good resistances to chemicals and high strength and toughness have also encouraged its use.

Table 3-2: Commercial advantages and disadvantages of polyolefin fibres (McIntyre, 2004).

Advantages	Disadvantages
Low density (0.90–0.96 g/cm³)	Low melting point (120–125 °C for PE;
Good tensile properties	160–165 °C for PP)
Good abrasion resistance	Prone to photolytic degradation
Excellent resistance to chemicals	Inferior shrink resistance above
Excellent resistance to mildew,	100 °C
micro-organisms and insects	Poor dye-ability
Almost negligible moisture regain	High flammability
Good wicking action	Inferior resilience
High insulation	Creep
Comfortable to the skin	

The first polyolefin fibres were extruded in 1930s and by the 1990s polyolefin industries were consolidated after two decades of significant growths that led to a total world-production of about to six million tons (McIntyre, 2004). Polyolefin fibres are manufactured fibres composed of at least 85% of polyolefin units. A typical polyolefin fibre density is ranging from 0.90 to 0.96 g/cm³ and it is extremely low moisture regain. Their commercial advantages and disadvantages have been placed in Table 3-2 although not all of them are applicable to the case of reinforcing concrete. Polyolefin fibres in general have good tensile properties, good abrasion resistance and excellent resistance to chemicals what added to the low cost placed them as an excellent alternative to corrosive steel fibres.

3.2.2 Polyolefin fibres literature review

One of the reasons of the good performance of the polyolefin fibres is the good bond with concrete matrix due to their rough surface. However, some of the first references on polyolefin fibres found were performed using cylindrical and smooth surface fibres (Yan, et al., 1998). The study concluded that the interface fibre-matrix was roughening due to the damage of the fibre surface produced during the mixing process. Such roughening formed a mechanical interlock opposing to the relative movement of fibres after cracks initiated. Wang, Backer and Li made studies on several synthetic types of fibres trying to improve the materials and surface treatments, bundling effects and pull-out resistance, encouraged by the sophistication of the synthetic fibre industry (Wang, et al., 1987; Li, et al., 1990).

Very close in time, Ramakrishnan at the end of the 1990, published studies on polyolefin fibres used in barriers, pavements and also for a bridge deck overlay. The amount of fibres reached 14.8 kg/m³ (1.66%) reporting a considerable increase of toughness and ductility, but also a great increase in the impact and fatigue resistance of the concrete. Each project was additionally inspected for durability and the authors concluded that polyolefin fibres combined structural benefits of steel fibres with the benefits of a synthetic material. Moreover, when polyolefin and steel fibres were compared, he concluded that there was less chance for balling, segregation, bleeding or any construction problems. In addition, the author underlined the use of non-corrosive, non-hazardous, non-metallic, non-magnetic fibres and the finishing surface protrusions were nor hazardous (Ramakrishnan, et al., 1997; Ramakrinshnan, 1999).

In a further research, Ramakrishnan and Sivakumar (Ramakrishnan, et al., 1999) studied PFRC under cycling loading with the aim of avoiding the use of metallic fibres in offshore

structures and bridges, parts of high-rise buildings or crane-girders in industrial buildings typically subjected to cyclic and dynamic loading. They already considered the advantages of FRC in case of a seismic event due to the ability of the material to undergo increasing deformations beyond yield stresses while still sustaining gravity and other loads. Six different polyolefin FRC mixes were subjected to flexural fatigue reaching an endurance limit at about two million cycles. Not only dynamic effects but also fracture results showed important improvements using polyolefin fibres. Even though the higher volume fractions the better results, also the higher scatter was obtained (Lamanna, et al., 2002). In 1998, Mindess and Wang (Mindess, et al., 1998) studied polyolefin fibre reinforced concrete with three volume fractions 0.5%, 1.0% and 1.5% under impact loading. They found that specimens containing 1.5% by volume of polyolefin fibres performed almost identically with the steel-bar reinforced specimens in terms of both maximum loads and fracture energies, under impact loading. Several types and shapes were also tested under dynamic loadings. Yan, Jenkins and Pendleton used polyolefin fibres with diameters 25, 15 and 6 μm (all of them with smooth surface) using both straight and crimped fibres (Yan, et al., 2000). They verified that the more diameter fibres and the crimped ones had higher damping ratios of the FRC. In a second part of the report, two damping mechanisms in polyolefin FRC were suggested: interfacial debonding and friction. With the straight fibres, both debonding and interfacial friction took place. Using the crimped fibres, the interface was subjected to a significant relative displacement that caused debonding (Yan, et al., 2000).

It has been in the last 15 years when more advances have been achieved thanks to the development of plastic industry and to the increasing interest on FRC. Trottier and Mahoney (Trottier, et al., 2001; Trottier, et al., 2002) made a comparative analysis of slabs-on-ground behaviour with four types of reinforcement: welded-wire-fabric (WWF), deformed steel fibres, low-denier fibrillated synthetic fibres and monofilament synthetic fibres. The WWF reinforcement was the lightest available for shrinkage or temperature cracking control and the fibres were added in medium volumes. In fresh state they concluded that the concrete turned out to be very workable with the macro-synthetic fibres. In hardened state they did not esteem significant changes on compressive strength. The most relevant results were found for round panel and flexural tests. They concluded that monofilament macro-synthetic fibres outperformed, at all deflections, all other reinforcing options evaluated with moderate fibre volumes. In the same time-period, Cengiz and Turangli (Cengiz, et al., 2004) compared steel mesh with both steel fibre reinforced shotcrete (SFRS) and macro-synthetic fibre reinforced shotcrete (PFRS) in panel tests. SFRS increased ductility, toughness, shear and punching strength. Concerning advantageous use for shotcrete of the polymer fibres, they concluded that there was a remarkable reduction of loss of fibres due to rebound with important cost implications (the fibres are the most expensive component of a conventional shotcrete). In such tests, they also settled that 7 kg/m³ was close to the optimum macro-synthetic fibre-dosage since a very slight additional increase in toughness and a decrease in first-peak load were obtained with 10 kg/m³ of fibres. They also mentioned that there is an optimum point for the use of synthetic fibres as a substitution of steel fibres and that using both types of fibres together some synergy effects in fibre system were observed.

Regarding one of the main advantages of PFRC, Bernard in 2004 (Bernard, 2004) tried to evaluate the durability performance of macro-synthetic fibres on pre-cracked specimens under inland and coastal environments for 7 and 24 months. He compared the residual energy absorption with plain and SFRS specimens. When compared with the prior exposure tested specimens steel fibres loss of strength was substantial even after only 7 months of

exposure. Conversely, durability of PFRS was found to be excellent in both inland and coastal environments.

Tunnelling and mining have probably been the pioneering uses of polyolefin fibre with structural possibilities. In 2009, after 10 years of experience, Bernard also reported macro-synthetic fibres excel with regard to corrosion resistance and embrittlement (Bernard, 2009). The author concluded that the same advantages that have led to the wide-spread adoption of macro-synthetic fibres for fibre reinforced shotcrete in the underground mining industry would be eminently applicable to civil construction.

The optimum macro-synthetic fibre geometry has also been sought. Indeed, some of the previous references tested several shapes and bond mechanisms were evaluated (Trottier, et al., 2002). Nevertheless, the works carried out by Won, Lim and Park were focussed on this and linked pull-out results with flexural results in several shapes (Won, et al., 2006). The main basis was to fully exploit matrix anchorage without fracturing the fibres and reaching the maximum pull-out resistance. In terms of bond, the crimped ones were the best ones among eight shapes of deformed synthetic structural fibres which are shown in Figure 3-13. Then, they tried various crimped geometries on fibres. Finally, they carried out flexural tests with the considered optimum fibre. The fibres that they used still had very low elasticity modulus (3-5 GPa) and thus the reduction of the flexural load was high after the initial crack was formed. They concluded that additional study on this subject would be required for structural use of macro-synthetic fibres.

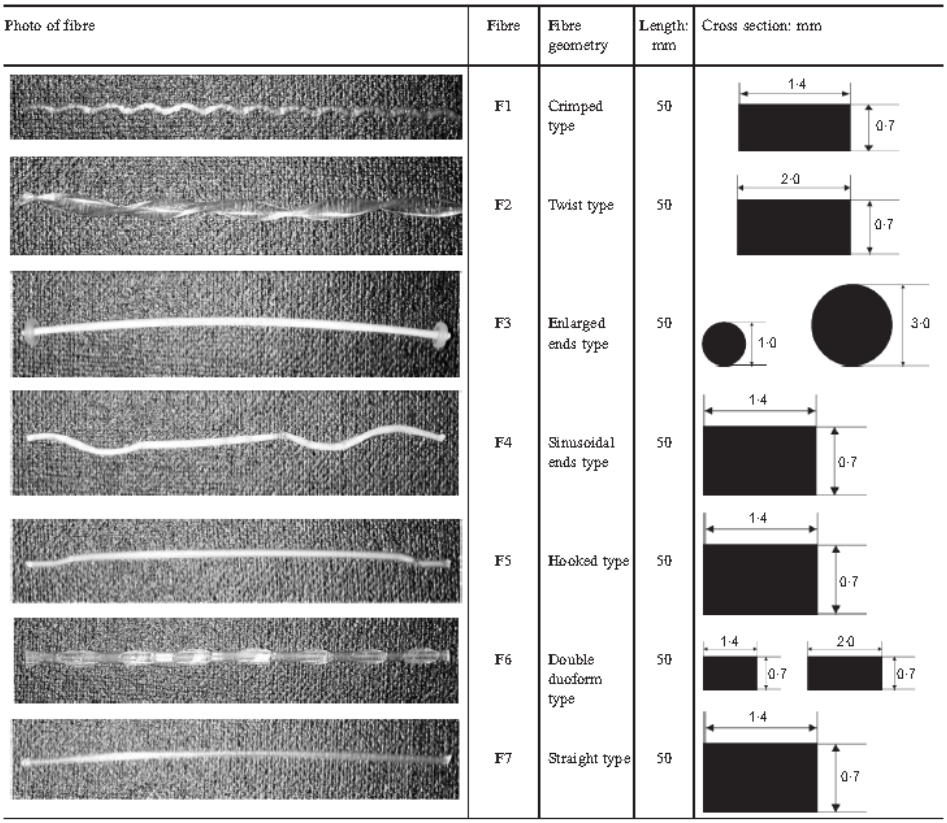

Figure 3-13: Geometry of the structural synthetic fibres tests by (Won, et al., 2006).

Seeking the enhancement of modulus of elasticity of polyolefin fibres, some special procedures have been reported. The interest of the industry led to the use of some novel fibre technologies for the production of bi-component polyolefin fibres (Akers, et al., 2009; Kaufmann, et al., 2007). The bi-component strategy was to combine two polymers: a core

of high-modulus with a sheath of low modulus. For that purpose they combined high density polyethylene and polypropylene fibres in varied diameters.

Concerning mechanical properties of PFRC research barely exists. Some improvements in compressive strength, tensile strength, permeability and resistivity have been reported, though with high amounts of fibres up to 14.5 kg/m³ and with fibre properties much lower than the ones this research had available (Han, et al., 2012).

In recent years, the behaviour of PFRC has been compared with SFRC in various references (Buratti, et al., 2011; Soutsos, et al., 2012). Nonetheless, in 2012, the first use of polyolefin based macro-synthetic fibres reporting post-cracking strength that comply the requirements of Spanish structural code (EHE-08, 2008) were used in the reconstruction of the La Laguna cathedral in Canary Islands. The requirements were achieved in combination with self-compacting concrete and they even made a prototype due to the use of such a new material (Pacios, et al., 2011; Pacios Alvarez, et al., 2012). In order to achieve the proper mix design they used fibres of 44 and 50 mm long and fibres dosages of 7 kg/m³ (Carballosa de Miguel, et al., 2011). They also made durability tests and proved the good performance of the combination of macro-polymer fibres with SCC.

Recently, Pujadas (Pujadas, 2013; Pujadas, et al., 2014) concluded that although SFRC is the main source of the existing design codes and constitutive models, it was possible to fit on them the PFRC behaviour. The conclusions obtained on tested slab-elements with a total substitution of the reinforcement showed the viability of PFRC under hyper-static configurations. However, they concluded that the models of the standards overestimate its performance. The referred total substitution achievability using PFRC (as the sole reinforcement) was also concluded for concrete pipes (De la Fuente, et al., 2013). Regarding its use in concrete lining of water tunnels (Behfarnia, et al., 2014) the results reported the high performance of PFRC having the concrete better characteristics in flexural toughness, permeability and resistance to chloride penetration than SFRC.

The discussed results of the last few years have questioned the existing design codes. The existing code for Concrete Industrial Ground Floors TR34 says that synthetic fibres provide significantly lower performance than steel fibres and the work of Alani questioned the validity of such statement (Alani, et al., 2013). The authors of the report built a large scale slab with PFRC and compared it with a slab made of SFRC tested earlier. The tests showed comparable results and the conclusions were strong: “the use of 7 kg/m³ compares favourably with steel hook ended at a dose of 40 kg/m³”. That is to say that those sentences, as the commented one in TR34, are being reviewed since PFRC has shown its good performance. Not only advantages have been reported. The paper conclusions also observed that the melting point of the fibres was around 150 ºC what may be cause of concern to floor construction purposes. It has to be mentioned that the research was carried out with polyolefin based macro-synthetic fibres with analogous properties to the ones used in this research. The same problem of outdated codes, occurs in Spain with the recommendations for harbour paving (ROM 4.1-94 , 1994) still taking in account only steel fibres to reinforce the concrete pavements.

In this subsection, the evolution of polyolefin based fibres has been reviewed. Moreover, it is clear that more research is needed to seek their best performance for structural applications and in order to improve their reliability. In addition, it has been clearly reported that economic and social benefits are possible to be achieved and that some adjustments might be needed in the existing codes to provide the engineers some simple and safe tools to design PFRC. Though not only the good perspectives are based on the

inevitable comparison with steel fibres, it is also clear that construction industry has accepted with interest the PFRC possibilities.

3.2.3 Polyolefin fibres versus steel and micro-synthetic fibres

Steel and synthetic fibres are the most commonly used in FRC and their mechanical properties have become very important for their applications. However, not only its mechanical properties but also its fresh state, reliability and durability performance have shown differences. In such a sense, the overall cost of the materials and the works are decisive for the election of a final design of the concrete. In such a list of possibilities, it is also assumed the alternative of using, at the same time, several concrete modern technologies what would also imply more research. Further discussions will show that one more option is using combinations of various types of fibres whereas it is a complete field of future possibilities to be performed. However, the present state of the art is only wide regarding steel fibres and micro-polymer fibres. In order to enrich PFRC research, the comparison with SFRC and micro-fibres is still needed. Therefore, it was unavoidable to make use of such bibliography to perform a schematic comparison chart comprising the general performance of the three typologies of fibres presented on Table 3-3 adapted from the reference (Wimpenny, et al., 2009).

It was already clear that the progress in knowledge of PFRC is needed when reading previous subsection 3.2.2. Most of the research was done comparing structural polyolefin fibres with steel-hooked fibres in several types of concrete or mechanical tests. Nevertheless, it was also noted that the main advantages of polymer fibres were both price and durability. Another factor that should not be overlooked is the rise in steel prices in the last decade which, if they continue, could increase the price of the more regular SFRC (Jerrett, et al., 2008) leaving it out of the market.

At this point of the review, it is not possible to continue without making few comments about corrosion of steel fibres which their major drawback. It is well-known that steel is protected of corrosion in the alkaline environment of cementitious mixes (Fernández Cánovas, 2007). It is also clear at this point of this report that polymeric fibres are chemically stable and have high durability performance. Steel fibres may corrode and if in RC structures this effect harms the structural integrity, for SFRC that is not so obvious. What is logical is to assure that since the fibres are randomly distributed, some fibres are not with enough cover concrete to be protected and they will corrode. Some research in the last decades has settled that the small size of the fibres allows a safe thinner cover. That means that more chloride ions are required to produce the steel fibre depassivation and therefore the corrosion as the one shown in (Mangat, et al., 1988; Janotka, et al., 1992; Granju, et al., 2005). In some recent works, it was concluded that in order to avoid corrosion of steel fibres located in the more external parts of the elements it was needed to use water/cement ratios lower than 0.5 and guarantee to have at least 2 mm of cover concrete (Balouch, et al., 2010). In any event, the oxidation of any steel fibre may occur also in storing or handling of the fibres. Additionally, it may take place due to carbonation process of the concrete that lessens the pH of the concrete. Design life considerations of concrete structures have been traditionally achieved by means of cover depth requirements. With the use of steel fibres randomly distributed, it is not possible to assure such regular requirement in the structural codes as (EHE-08, 2008). Additionally, design life of structures trend is to be stricter in the following years what makes durability performance even more important.

Table 3-3: Comparison of steel and micro-synthetic fibres with polyolefin based macro-fibres adapted from (Wimpenny, et al., 2009).

Characteristic	Steel Fibres	Synthetic micro- fibres	Polyolefin based macro-fibres
Shape/Texture	Cold drawn hooked ends	Straight smooth	Continuously embossed
Collation	Glued bundles	Fibrillated	Uncollated
Length (mm)	35-60	12-20	48-60
Diameter (mm)	0.75	0.02-0.03	0.5-1
Tensile Strength (MPa)	1050	30	550
Elastic Modulus (GPa)	>200	2	10
Dosage (kg/m^3)	25-35	1-2	6-12
Melting point (°C)	>800	150	150
Base material	Carbon steel	Polypropylene	Polyolefin
Workability	Reduced	Slightly reduced	Slightly reduced
Plastic shrinkage cracking	Unaffected	Reduced	Slightly reduced
Early-age thermal cracking	Reduced	Unaffected	Reduced
Long-term shrinkage cracking	Reduced	Unaffected	No data
Stray current corrosion	Reduced	Unaffected*	Eliminated
Durability in chloride exposure*	Increased	Unaffected*	Greatly Increased
Fire spalling resistance	Slightly Increased	Greatly Increased	Increased
Compressive strength	Unaffected	Unaffected	Unaffected
Residual flexural strength	Increased	Unaffected	Increased
Impact strength	Greatly Increased	Unaffected	Increased
Flexural toughness	Increased	Unaffected	Increased
Abrasion resistance	Increased	Slightly increased	Slightly increased
Freeze-thaw resistance	Slightly increased	Increased	Increased
Flexural energy absorption	Greatly Increased	Unaffected	Greatly Increased
Concrete permeability	Slightly increased	Slightly increased	Slightly increased
Pump wear	Increased	Reduced	Reduced
Safety*	Hazard from handling and protruding fibres	Increased	Increased
Finishing	Extra care during floating	Exposed fibres soon abrade	Fibres may float and protrude in poorly designed

Comparison with plain concrete except where indicated by* done with RC

3.3 Mix proportioning, fresh state and fabrication of FRC

Macro-fibre volumes that are currently used in practise range from 0.3% to 1.5%. With such volume fractions, the procedure for mix proportioning can be essentially the same as the one used for plain concrete (Mindess, et al., 2003). The addition of fibres does not affect the nature of the components of the mix but it does affect the mix workability. This can be compensated with slight variations of the aggregate distribution and fine content or addition of admixtures and using trial mixes to achieve the final proportions. FRC can be manufactured, in general, with the same equipment and similar procedures just carefully studying the best mixing sequence to ensure a good uniform dispersion of each type of fibres avoiding segregations and balling of the fibres.

The cement content and the water/cement ratio are decisive as in plain concrete and no additional-restriction on the cement type has been reported for FRC in the bibliography. Regarding cement content for SFRC, an increment of 10% of cement weight compared with plain concrete could be recommended (Kooiman, 2000). Steel fibres are more rigid, stiffer and heavier than the mass of concrete. Moreover, during the mixing and pouring they do not bend and so affect directly the workability. Polyolefin fibres can fold in such processes and so affect in a minor extent to the fresh properties thanks to their lower density.

Concerning the aggregates, not only an increase of fines/total aggregates is typically adequate but also a limited maximum aggregate size ($d_{ag,max}$). For SFRC it usually accepted that $d_{ag,max}$ should not surpass 2/3 of the fibre length and it is frequent the use of fibres 2-5 times longer than the maximum aggregate size (Johnston, 1996; Grünewald, 2004). The limitation of $d_{ag,max}$ not only enhances workability but it also affects the effectiveness in the hardened state because it determines its distribution. Additionally, the risk of fibre balling decreases with lower $d_{ag,max}$ and increasing the percentage of fine aggregates as shown in Figure 3-14. Placing conditions can also play an important role in the design of the mix. For example, it has been recommended to reduce 10% of coarse aggregates for pumping (Grünewald, 2004).

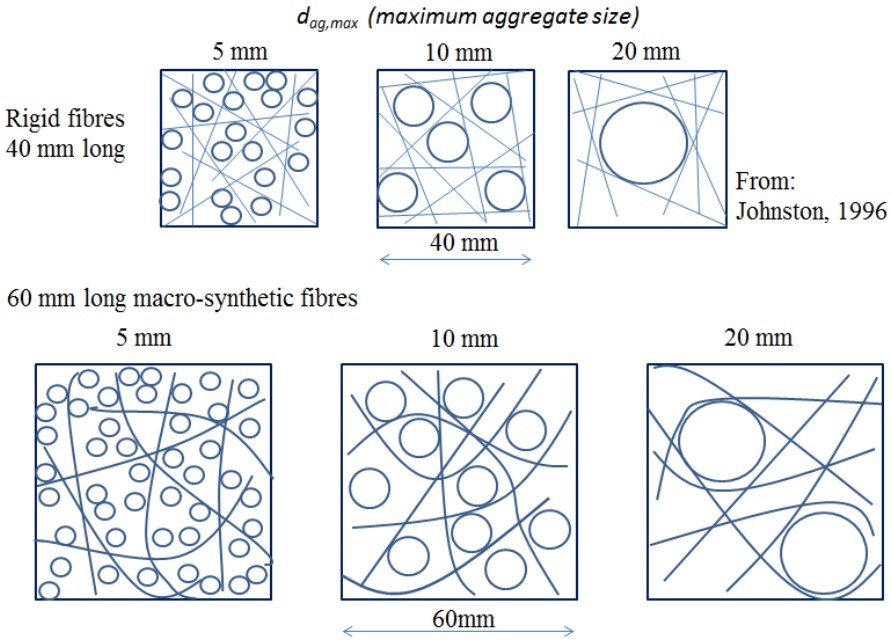

Figure 3-14: Effect of the aggregate size on the fibre distribution.

It should be noted that the coarse aggregate content might limit the maximum fibre dosage. An example obtained in research (Swamy, et al., 1974) for straight steel fibres 25 mm long, and with d_e and $d_{ag,max}$ of 0.25 mm and 10 mm respectively is shown in Figure 3-15. The maximum fibre content was settled as the critical fibre content from which compactability drastically decreases and may vary for each given type of fibres.

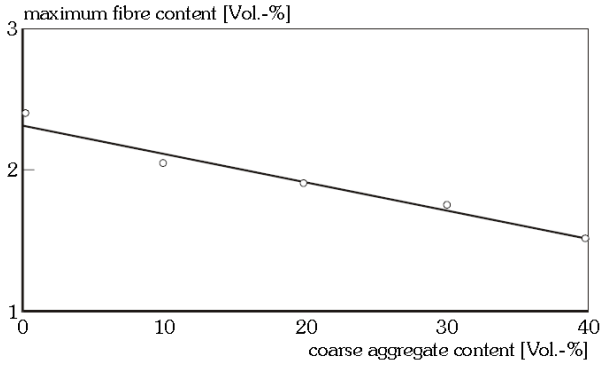

Figure 3-15: Effect of the coarse aggregate content on the maximum content of SF [from: (Grünewald, 2004), after: (Swamy, et al., 1974)].

Aspect ratio (l_f/d_e) is also related with compactability or with the so called packing density. At a given diameter and fibre dosage, compactability has shown to be linearly related with the aspect ratio of the fibres (Grünewald, 2004). The aspect ratio of most modern fibres is in the range of 50 to 150, mainly due to workability and dispersion motives. The packing density is improved for lower aspect ratios but also for higher fine aggregate content, which in normal fibre dosages is optimum with a percentage of fine aggregate over the total aggregates in the gap of 40-60%. The existing bibliography about steel fibres reports possible effects as the shown in Figure 3-16(a) that might not be possible for synthetic fibre because they would not oppose to bend. The possibility of folding allows a final location of a fibre as shown in Figure 3-17. In any event, such recommendations must be taken into account for the mix proportioning and are in the ranges indicated in Figure 3-16(b) for fibre contents below 2%. Higher fibre contents are not considered in this document. Such high fibre contents would decrease not only workability but also compactability and would hamper the homogeneous distribution of the fibres harming at the end the final quality of the concrete obtained. However, it is possible to produce SCC even with important amounts of fibres. That is to say that, if the mix is properly designed, it can be placed by external vibration, pumped, projected or even compacted under its own-weight (in the case of SCC) passing through obstacles and with a good performance in hardened state.

Compaction of FRC might be more difficult to achieve with high fibre-content and coarse aggregate can greatly decrease the compactability. In VCC, it is recommended to achieve at least a descent of 9 cm in the slump test (EHE-08, 2008). Some research arguments have settled that SFRC appears stiffer than a plain concrete using static slump tests. However, with dynamic tests using vibration SFRC and plain concrete show the same workability (Grünewald, 2004). That is why EN-14845 (EN 14845-2, 2006) requires measuring the consistence of concrete with and without fibres by means of the Vebe test (EN 12350-3, 2009). Workability plays a key-role at the end and can strongly influence several stages of the production process as shown for example in reference (Kooiman, 2000). On another note, the placing conditions and the formwork geometries clearly affect the final properties of the hardened FRC because they influence the final positioning of the fibres (Torrijos, et al., 2010) and, subsequently, this topic discussed in a deeper slant ahead in subsection 3.5.

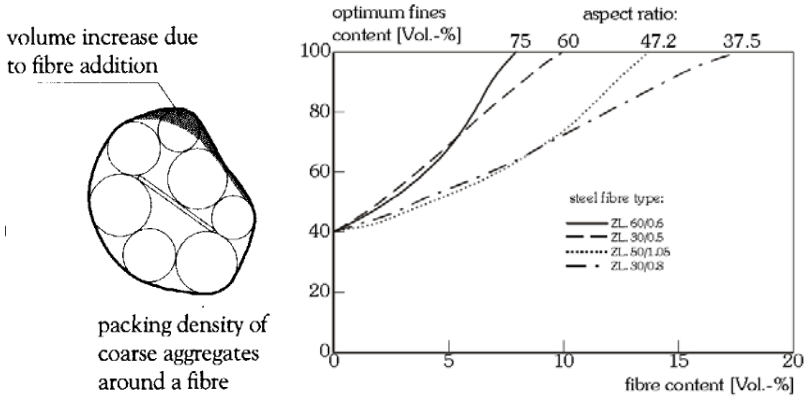

(a) (b)

Figure 3-16: (a) Effect of steel fibre addition on the packing density [from: (Kooiman, 2000)];(b) theoretical effect of the type and the content of SF on the optimum sand content [from: (Grünewald, 2004), after: (Hoy, 1998)].

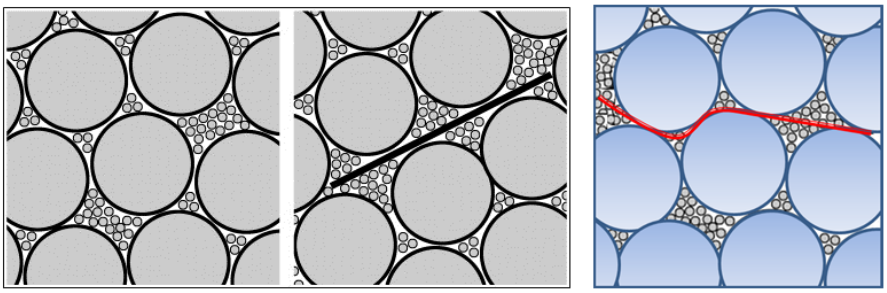

(a) (b)

Figure 3-17: Effect of packing of gravel and sand mixtures: (a) without fibre and with a rigid straight fibre [from: (Martinie, et al., 2010)]; (b) scheme of a macro-synthetic fibre.

In the case of SCC, the slump flow decreases with the addition of fibres depending on the type of fibre and its geometry. Design criteria purposed by Grünewald and Walraven in 2001 include a target slump flow diameter of 600 mm, with a recommended reference mixtures about 700 mm of diameter of the patty. The achievement of the desired fresh properties in the slump flow (EN 12350-8, 2010) test and V-funnel test (EN 12350-9, 2010) are closely related with the same properties discussed for plain SCC in Chapter 2 and can be assessed by using rheology measurements. The addition of fibres, depending on its surface area and length, alters the results on the tests which can provide information of the maximum content of a certain type of fibre that can be added without losing the concrete self-compactability properties. Some of the problems that may occur are represented in Figure 3-18. Rheological properties of the self-compacting concrete have been the centre of some research. Relations among yield stress and plastic viscosity with fibre volume fractions, geometrical characteristics or slump flow and V-funnel tests have been reported for various types of steel fibres and are available in the technical bibliography, for example, in references (Fanella & Naaman, 1985; Zollo, 1996; Martinie, et al., 2010; Ponikiewski, 2010). Some research based on short micro-polypropylene fibres has been also reported (Szwabowski, et al., 2002; Grünewald, et al., 2000). There is still a lack of knowledge about the influence of the polyolefin-based macro-fibres on the fresh properties. The lower density and their ease to bend inside the mass may change their behaviour when compared with rigid steel fibres.

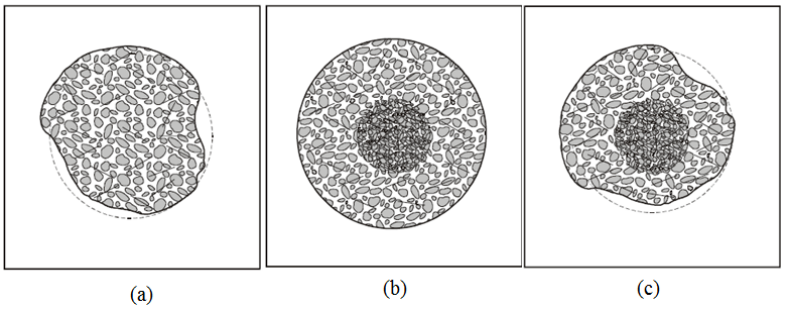

Figure 3-18: Flow patterns indicating that maximum fibre content of SCC was surpassed (Grünewald, et al., 2001): (a) obstruction of the flow; (b) clustering of fibres and/or aggregates which barely affects the slump flow; (c) clustering and obstruction of the flow.

Due to the significant variations that the pouring procedures can provide, it is important to highlight that VCC and SCC moulds are not usually filled with FRC in the same manner. As it will be discussed ahead, the final positioning of fibres is closely related with the workability of the concrete because it is decisive for the compaction procedures and the pouring methods and the formworks. In such a sense, VCC and SCC would imply several changes in every stage of the concrete production. Mixing schedules may be analogous if there are not big changes in the mix design and material properties. Nevertheless, in the placing stage SCC has shown to improve the positioning of fibres in the pouring direction. Conversely, external vibration tends to align the fibres perpendicular to the direction of vibration. In the finishing stage, the final levelling may help to align the fibres, especially when using rigid and heavy fibres. In order to avoid some of the differences that may produce such manufacturing stages, test recommendations EN 14651:2007+A1 and RILEM TC 162-TDF (RILEM TC 162-TDF, 2002) have fixed the procedure for casting the specimens and filling the moulds. This is of relevance because it may affect the reliability of the laboratory samples and it has to be taken into account to extrapolate from specimen results to structural members. It is required to put in the middle of the mould twice the volume put in both ends and filled in one layer up to approximately 90% of the height of the test specimen. The mould shall be topped up and levelled off while being compacted. Compaction shall be carried out by external vibration. Additionally, the standards say that, in the case of self-compacting concrete, the mould shall be filled in a single pour and levelled off without any compaction. The capacity of SCC to level itself makes it adequate to fill the mould from one end to the opposite. This technique has been commonly used for SFR-SCC and it has provided good and reliable results (Døssland, 2008; Grünewald, et al., 2012). However, there is no recommendation against pouring the concrete from the centre of the mould. A scheme of both procedures is shown in Figure 3-19.

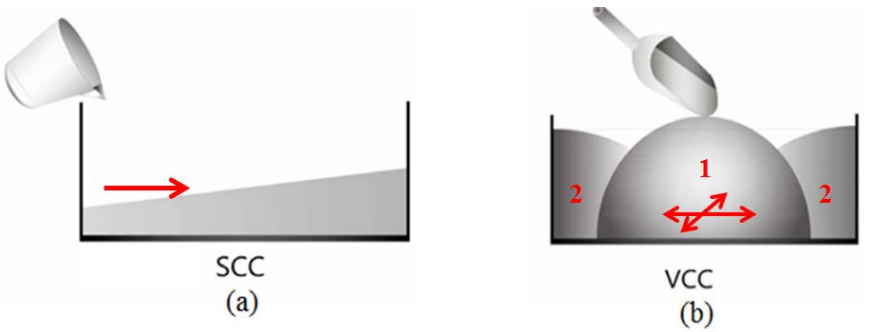

Figure 3-19: Filling methods for FRC: (a) flow method for SCC; (b) RILEM and EN-14651 Vibrated Concrete [after: (Grünewald, 2004)].

Therefore, it is clear that VCC and SCC differ on pouring methods. In addition, the fresh-state evaluations, compaction and finishing stages have notable changes. Such procedures affect at the end the positioning of the fibres and hence the scatter and performance in the hardened state. From a general point of view (there are some exceptions made on purpose in this research), Figure 3-20 shows a general diagram of the production methods of both types of concrete. The reliability of all the test methods is increased by assuring the production methods and storing of specimens. Some other factors are not only related to the manufacturing procedures but also to the relative size of the fibre and the formwork. For example, the fibre tends to place in a certain position when pouring a cylindrical sample which is not the same in a prismatic one. All these factors that affect the final positioning of the fibres are discussed together in subsection 3.6 due to their significant influence. There is still a lack of knowledge on how polyolefin based structural macro-fibres behave while varying the production methods.

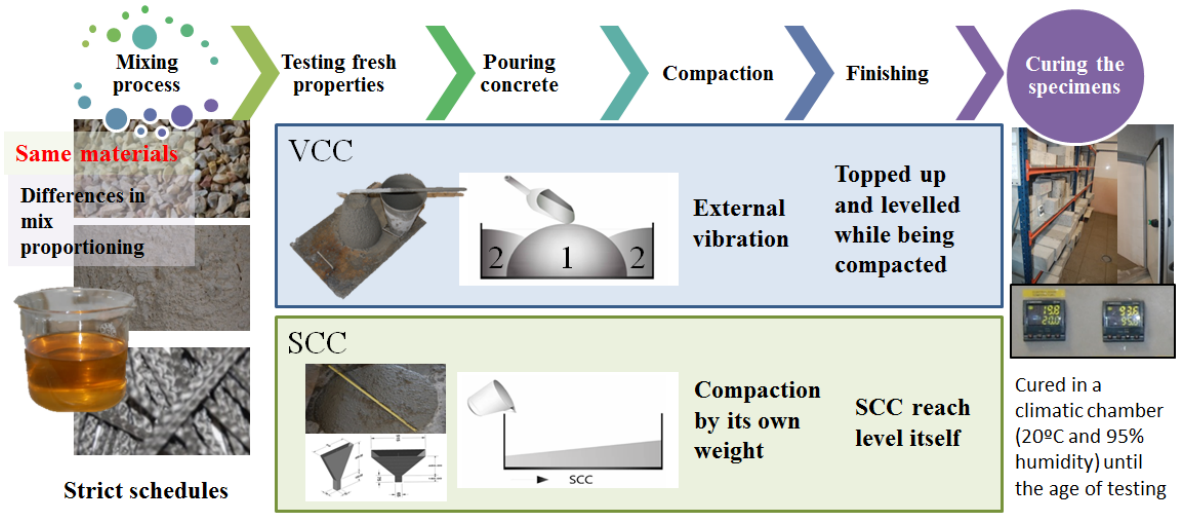

Figure 3-20: Typical concrete production procedures for VCC and SCC.

Conversely, distribution of fibres when discharging batches from ready-mix trucks has been assessed by comparing hooked-steel fibres and polyolefin fibres with similar characteristics to the ones of this thesis. The initial hypothesis was that steel fibres would have a tendency to sink causing that initial discharge samples to contain fewer steel fibres than later samples. On the contrary, synthetic fibres were supposed to float towards the top having more fibres per unit volume in the beginning of the discharge. In the mix, 25 kg/m³ of steel fibres and 7 kg/m³ of polyolefin fibres were used and caused no problems regarding casting in place or compaction (Sorensen, et al., 2014). Nevertheless, a certain percentage of truckloads did not meet the proposed limits of fibres contents in steel fibre batches. Therefore, the authors concluded that a code concerning steel fibre content would be desirable. In the case of the polyolefin fibres, the entire test complied the minimum amount of fibres placed in 90% of specified fibres. The upper limit of 115% was only surpassed by only one truck.

3.4 Effect of fibres on the mechanical properties

Compressive and tensile strength of fibre-reinforced concrete have been thoroughly studied in the last decades in both types of fibres, steel (Wafa, et al., 1992; Song, et al., 2005) and synthetic fibres (Song, et al., 2005). Since it has been explained in previous discussions, fibres typically enhance the tensile properties of the plain concrete. However, their

influences on other mechanical properties are varied depending on the type and shapes of the fibres. This subsection is focussed on the variations that fibres have shown in modifying the main mechanical properties: compressive, tensile and shear strengths and elasticity modulus of the composite material. It should be clarified that in this subsection tensile properties are referred to initial tensile strength assessed by tensile splitting tests. The residual post-cracking tensile strength is the key-stone of the use of structural fibres and deserves a special subsection focussed on fracture behaviour in tension or under tensile flexural tests.

Having noted that, compressive strength is still used to characterize concrete and it provides essential information. The test is performed in a similar way compared with plain concrete (EN 12390-3, 2009) and with the regular amounts of fibres, the strength results are not significantly affected. Though varying the amounts of fibres modest increases of compressive strength may occur it has to be highlighted that it is not the role of the fibres. Nevertheless, the failure is usually less brittle as it can be deduced from a typical curve of compressive strength and axial strain as the shown in Figure 3-21 extracted from (Boulekbache, et al., 2010). Ductility and toughness are considerably enhanced as a function of the increase in volume fractions and aspect ratios of the fibres used (Nawy, 2008).

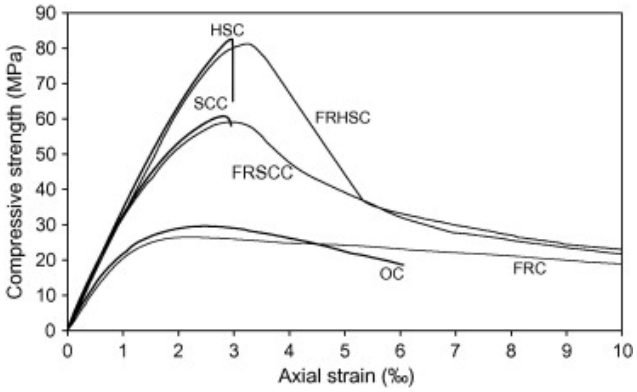

Figure 3-21: Stress–strain curves in compression for plain concrete and FRC (Boulekbache, et al., 2010).

The pre-peak behaviour in compression is similar to that of plain concrete. On the contrary, the presence of fibres greatly improves the post-peak behaviour and reduces substantially the descending slope of the stress–strain curve by softening the material when approaching failure. Although any increase on the compressive strength due to the addition of fibre is debatable, the abovementioned enhance of ductility in the compressive failure mode and the small loss of mass takes place even with small volume fractions of fibres. Those characteristics are especially well-suited for tunnelling, façades, or military applications where scaling or spalling should be prevented (Liu, et al., 2008). Some of the existing references for SFRC have varied shapes keeping the volume fraction constant (Fanella, et al., 1985) and some other authors have tried to study aspect ratios and volume fraction coupled (Yazici, et al., 2007). The conclusions were analogous in both cases: the increase of volume fraction and aspect ratio provides higher compressive strength, first cracking load and toughness. In any event, all the improvements were small and it seemed to be a threshold of volume fractions from which compressive strength falls even down to values smaller than those of plain concrete. This has been explained due to a worsening of workability and compaction. When the amount of fibres is increased, the presence of fibres reduced slightly the compression strength but the amount and the slope of the relation depend on the fibre type as shown in Figure 3-22 extracted from (Li, 1992). Although some

other parameters may have influence on the results, the graphic provide a comprehensive view and enables to evaluate that, except from Dramix HM-50, the maximum values obtained were in the range of 0.5 – 1.5 % of volume fraction.

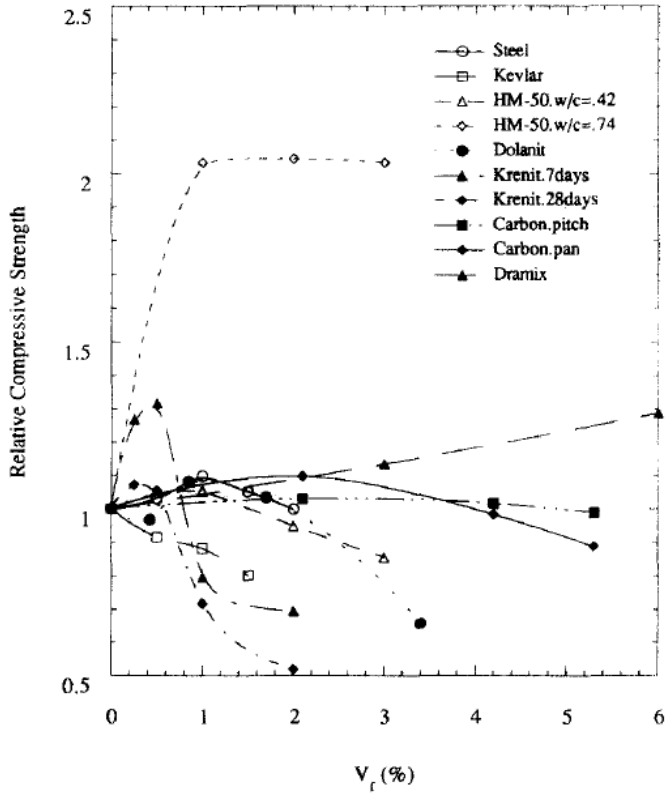

Figure 3-22: Relation between compressive strength and volume fraction on several types of fibres (Li, 1992).

Some existing fracture mechanics models of Compressive Damage Zone (CDZ) have been adapted for SFRC. The model purposed by Markeset (Markeset, 1993) provides a visual explanation of the failure process as can be seen in Figure 3-23. The model is based on longitudinal cracking occurring in a certain part of the specimen after the elastic initial response. Such longitudinal cracking initiates at stresses around 75% of peak stress. A second mode of failure takes place within the longitudinal tensile cracks forms a shear band as the adjoining parts start sliding relative to each other. The presence of fibres has been supposed to prevent this lateral deformations using SFRC providing the aforementioned ductile response (Kooiman, 2000; Schumacher, 2006).

Recent research has concluded that the ductility in compression increases with active confinement, and/or with fibre volume fraction being its benefits evident, in terms of strength and ductility, for fibre contents higher than 0.45% (Fantilli, et al., 2011). This conclusion could be applied to RC columns made with FR-SCC. The beneficial effect of fibres can be comparable with that of a confining pressure applied along the column.

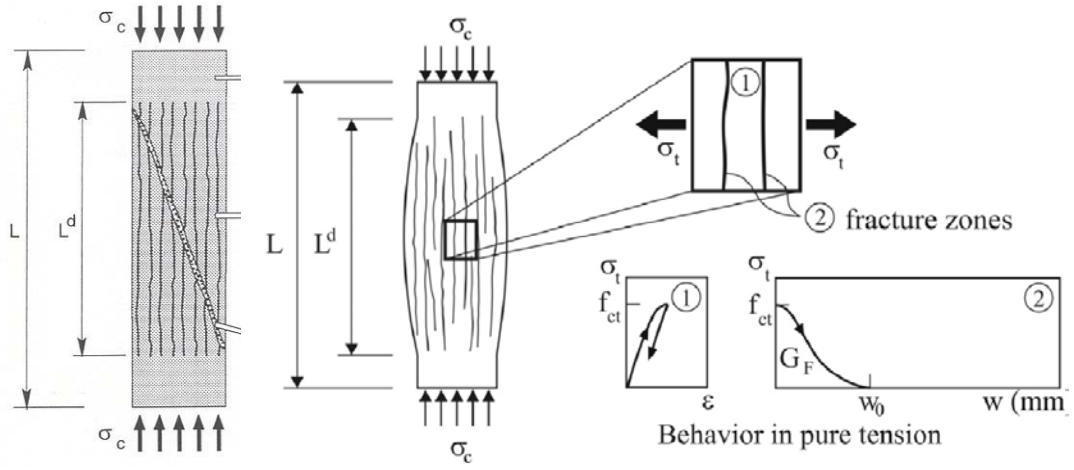

Figure 3-23: Illustration of the Compressive Damage Zone model for plain concrete (Markeset, 1993; Schumacher, 2006).

In order to assess the tensile strength, likewise it is accepted for plain concrete assessments, the splitting tests also named Brazilian tests (Fernando Carneiro, a Brazilian first proposed it) can be carried out. As it is described in Figure 3-24, the test is an indirect method applying tension in the form of splitting. In the test, a concrete cylinder similar to the type used for compression tests is placed with its axis horizontal between the platens of a testing machine, and the load is increased until failure by splitting along the vertical diameter. This is based on a theoretical distribution of stresses in the classical elasticity (Pastoriza, et al., 1970). When the load is evenly applied along a generatrix, the vertical diameter of the cylinder is subjected to a compressive strength that can be computed by expression (3-2). Expression (3-3) allows obtaining the horizontal tensile stress. This implies that only in the vicinity under the load compressive strength occurs and that a nearly constant tensile stress occurs in the central part of the vertical stress. The test methods (EN 12390-6, 2009) can be carried out by a simple press. Narrow strips of a packing material as plywood are interposed between the cylinder and the platens, which should not be allowed to rotate, and keeping constant the rate of application of stress placed in the standards. The tests and the procedures are quite adequate and easy to perform in order to measure the indirect tensile strength in terms of a peak load of plain concrete with brittle behaviour. It is possible to use a closed-loop system with the aim of processing the post-cracking behaviour of the specimen even though it is quite difficult to assure the boundary conditions. Additionally, a second mode of failure may take place after cracking has taken place due to splitting because the specimen splits in two parts being each half eccentrically loaded and thus subjected to bending. Processing the test results into uni-axial relationship seems therefore to be quite difficult (Kooiman, 2000).

$$\sigma_y = \frac{2P}{\pi LD}\left[\frac{D^2}{r \cdot (D-r)} - 1\right] \qquad (3-2)$$

$$\sigma_x = f_{ct,m\,(EN\ 12390-6)} = \frac{2P}{\pi LD} \qquad (3-3)$$

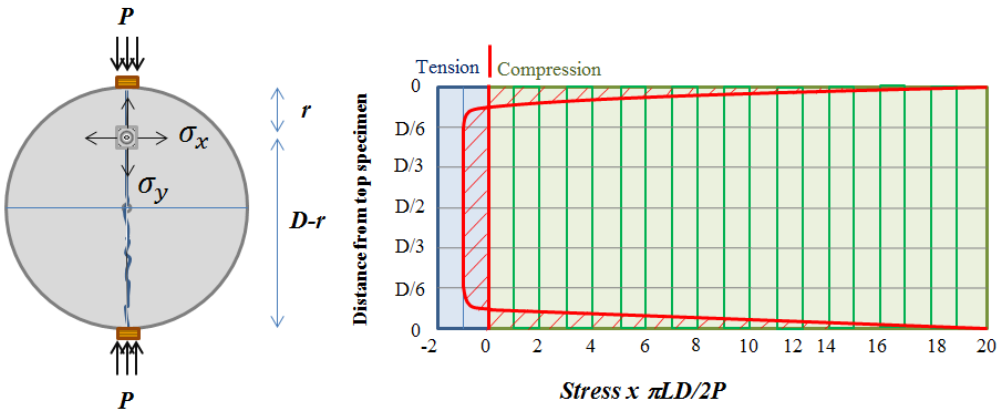

Figure 3-24: The Brazilian splitting test [after: (Neville, 1981; Pastoriza, et al., 1970)].

The existence of a post-cracking branch of the curve is itself a sign of the deformation capacity of FRC as shown in Figure 3-25. Even though the abovementioned second order effects do not enable accurate residual strength values, these indirect tests provide interesting values for the initial tensile strength. Some types of fibres may provide important improvements, especially for crimped or hooked steel fibres which are mechanically mobilized since the very initial deformations. In such a sense, fibres provide tensile strength to the composite material due to their capacity to transfer stress trough the crack and this test method may be adequate to be used as a quality control test. An increment of the fibre dosage would also enhance those residual strength values as shown in the references (Thomas, et al., 2007; El-Dieb, 2009). Furthermore, some relationships of this splitting tensile strength with compressive strength of concrete have been proposed. Such relationships are placed on the structural codes, being for conventional concrete the most common one that placed in Model Code (fib Model Code, 2010) and Spanish structural concrete code (EHE-08, 2008) related by the expression (3-4). The accuracy of those correlations is not clear even for the first crack being highly dependent on the type of fibres and the volume fraction. In a recent research, some correlations have been purposed for deformed and hooked steel macro-fibres (Xu, et al., 2009) but there is still a lack of data in what concerns to macro-synthetic structural fibres.

$$f_{ct} = 0.3 \cdot (f_{cm})^{\frac{2}{3}} \qquad (3-4)$$

Regarding the modulus of elasticity (*E)* of the composite material, the rule of mixtures in a parallel model (the rule of mixtures would take the fibres in account as spheres without the orientation and distribution variations) may provide values for an initial approach. It may be more accurate to use the expression (3-5) which takes into account the effects of fibre length and fibre orientation, by means of some experimental factors that should be estimated, $\eta_\theta \; and \; \eta_l$respectively (Bentur, et al., 2006).

$$E_{composite} = E_{matrix} \cdot (1 - V_f) + \eta_\theta \cdot \eta_l \cdot E_{fibres} \cdot V_f \qquad (3-5)$$

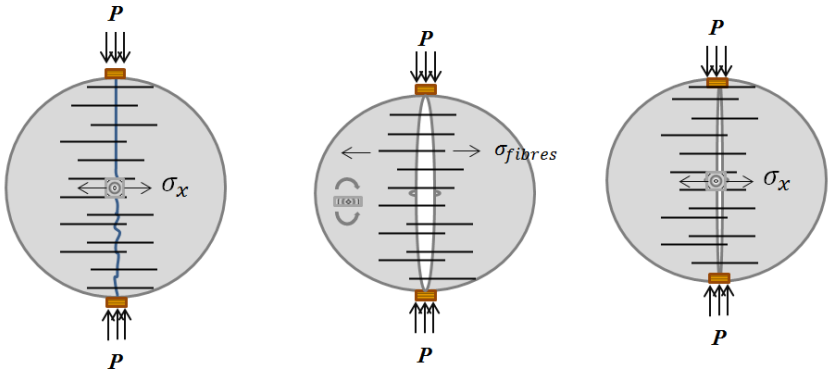

Figure 3-25: Second order effects during indirect tensile strength tests with FRC.

Nevertheless, in the scientific literature, there are contradictory results. Some authors have obtained modulus of elasticity of the composite material lessened by the addition fibres that had higher modulus of elasticity compared with the matrix (Thomas, et al., 2007; Altun, et al., 2007). In order to assess the evolution of the mechanical properties of SFRC, it can be define the so called steel fibre index which is the product of the volume fraction and the aspect ratio. Such index allowed a discussion in reference (Jo, et al., 2001) using previous results. In Figure 3-26, it can be seen that the relation of the modulus of elasticity in several references reaches a maximum and beyond that point the values descended again. Some other research has shown that for volume fractions lower than 1.5% of steel-hooked fibres, with aspect ratios of 50 and 71, both parameters improved the elasticity modulus (Gul, et al., 2014).

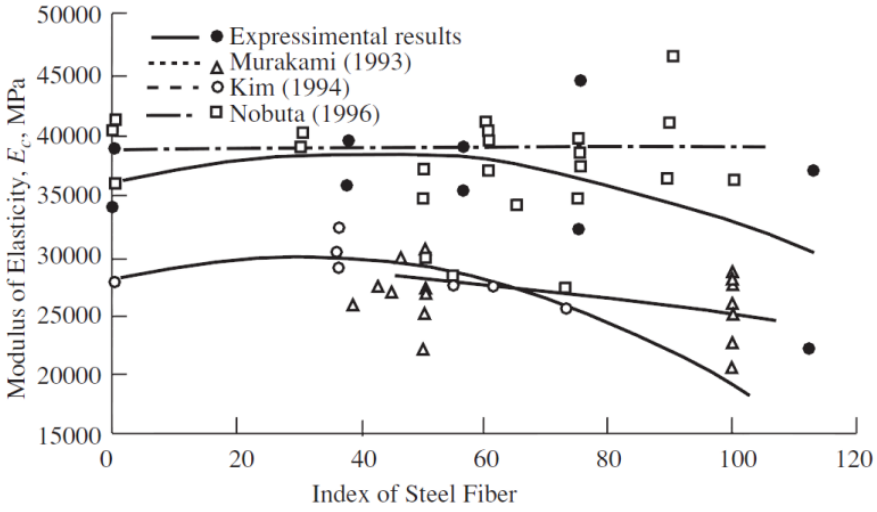

Figure 3-26: Modulus of elasticity versus index of steel fibres (Jo, et al., 2001).

Shear strength has also been related with tensile splitting strength by means of the expression (3-6) where v_{cf} is the average shear stress and which was proposed by Shamaran (Sharama, 1986) based on tests of SFRC. In general, as shear span/depth ratio (*a/d*) decreases and the fibre volume increases, the shear strength increases proportionally (Nawy, 2008). Steel fibres improve ductility of concrete under all modes of failure, even though there is little data about torsional and shear strength even for SFRC. The increase in strength of SFRC in pure shear has been shown to depend on the shear testing technique and the consequent degree of alignment of the fibres in the shear failure (ACI Committee 544, 2008).

$$v_{cf} = \frac{2}{3} f_{ct} \left(\frac{d}{a}\right)^{\frac{1}{4}} \qquad (3-6)$$

The ultimate shear strength of longitudinally reinforced concrete beams without stirrups have been tested under centre-point bending (Li, et al., 1992) . They used both, synthetic and steel fibres. Cracking processes developed in similar patterns as compared with plain concrete (reinforced with longitudinal bars). They found that shear strength increased due to fibre reinforcement with 1% of volume fraction of all the types of fibres in the range of 100 to 200 percent. They obtained such significant increases on ultimate strength of the beam and also a delay on the initial flexural and shear cracking. The research showed that FRC increased dowel capacity in the reinforcing bars due to a greater resistance to propagating dowel cracks across the steel, and increased capacity to resist tensile forces across the diagonal crack.

3.5 Bridging cracks

3.5.1 Mechanics of fibre reinforcement

Since it is well-defined that the contribution of fibres in the post-cracking strength of the composite is linked with its material properties, the interaction matrix-fibre is equally important. In such a sense, mechanical anchorage, surface treatments have also been reported being responsible for improvements on its behaviour. Figure 3-27 schematizes the potential fracture processes taking place when crack opening is growing. It is clear that fibres are randomly distributed in the concrete and if the interactions fibre-matrix allow it, it is possible to control crack propagation and so absorbing energy during the cracking process (Banthia, et al., 1996).

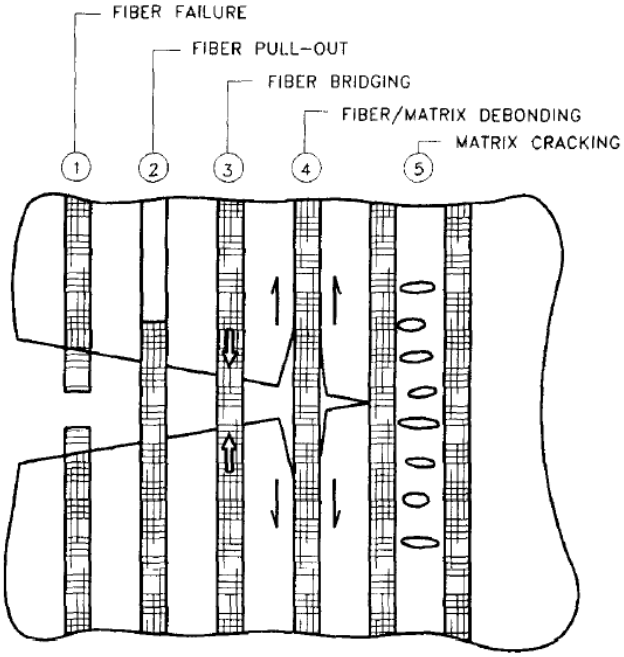

Figure 3-27: Energy absorbing fibre matrix mechanisms (Zollo, 1996).

At the optimum situation, the crack opening is controlled by the named “fibre bridging” having a portion of fibre on each side of the crack with enough embedded length allowing

fibres to work at 100% without any slipping (#3 in Figure 3-27). In such perfect situation, if crack growing process continued, it is possible to exploit the fully potential of the fibre up to its failure. On the contrary, if fibres slip during the opening processes the debonding process may occur and the fibre may be pulled-out. Finally, if one fibre is mobilised by friction shear stresses, it is possible that it provokes the matrix cracking. Those mechanisms are keystone of the fracture post-cracking capacities and the main influencing parameters of these processes have to be studied by SEM microscopies. Pull-out tests also clarify its relation with variations of orientation and distribution of fibres.

3.5.2 Fibre-matrix interactions

Fibre-matrix system is effective if fibres are capable of inducing an increase in strength to the cementitious reinforced matrix. Research suggests that the reinforcement is effective in concrete when tensile strength of the fibre is significantly higher than that of concrete (two or three times) but also when fibre-matrix bond strength is in the same order of magnitude of the tensile strength of the matrix and fibre modulus of elasticity in tension is significantly higher than that of the concrete (Naaman, 2003). Concerning the Poisson´s ratio and the thermal expansion coefficients it is preferable to be of the same order so non-detrimental debonding may take place under tensile loads. In spite of this, with the variation of the shapes or using deformed surfaces, it is possible to improve the stress transfer between the fibre and the matrix and overcoming such problems. In order to encompass the problem in all its complexity, the following types of interactions are particularly important to assess its effectiveness: physical and chemical adhesion, friction and mechanical anchorage induced by an overall complex geometry or by deformations on the fibre surface. The nature of the fibre-cement interface may change with time. In a properly designed FRC, the primary mode of failure should be that which consumes more energy during the process. In a general rule, fibre pull-out processes consumes more energy than that needed to split the fibres in two parts (Mindess, et al., 2003) although for polyolefin fibres it is not clear and the process of rupture might involve significant deformations. Moreover, many other aspects are influencing the process and a combination of adhesion, friction and some mechanical interlocks have reported the best results for structural macro-fibres. A range of competing processes needs to be considered, having significant contribution the interface morphologies, the shape and orientation of the fibres, etc. All these elements will be discussed in this chapter besides the pull-out behaviour which is the main way to measure the effectiveness of the system. Nevertheless, one new concept is worth to be defined at this point: the so called critical length (l_c). One perpendicular fibre in a certain matrix has a critical embedded length that allows mobilizing all its tensile stress without debonding or being pulled-out. It could be defined as the length above which the fibre will fracture rather than pull-out when a crack intersects the fibre at its midpoint (Mindess, et al., 2003). We need to define some useful additional parameters as the equivalent diameter (d_e) which is the diameter of circle having the same cross-sectional area of the fibre. The aspect ratio is the relation of the fibre length (l_f) and d_e. Then, if the ultimate strength (σ_u) and the maximum frictional shear stress were known, l_c could be computed by means of expression (3-7) as the scheme shown in Figure 3-28.

$$l_c = \frac{(\sigma_u \cdot d_e)}{2 \cdot \tau_u} \qquad (3-7)$$

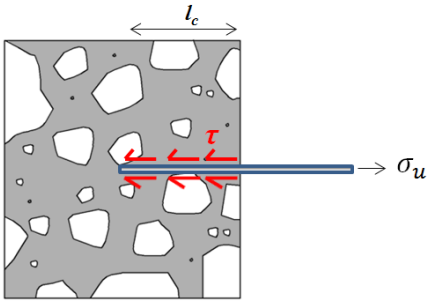

Figure 3-28: Equilibrium with critical embedded length of an ideal fibre.

3.5.3 Hydration and micro-structure brief considerations

Portland cement consists of four main phases which main compounds and abbreviations are: tricalcium silicate (C_3S), bicalcium silicate (C_2S), tricalcium aluminate (C_3A) and tetracalcium aluminoferrite (C_4AF) that react with water leading in the hardening of the cementitious material (Neville, 1981). The main products obtained from the hydration are calcium silicate hydrate, usually named as CSH-gel, and calcium hydroxide CH-crystals. In addition, in hardened cement paste, anhydrous cement, pores, water and other minor components can be found. Aggregates are considered as inert. However, concrete cannot just be described as a composite of coarse and fine aggregate in a matrix of cement paste because the microstructure of the paste close to the aggregate differs from that of cement paste bulk. An interfacial zone of increased porosity and presumably lower strength has been noticed (Taylor, 1990). Such Interfacial Transition Zone (ITZ) is especially important because bond between aggregates and paste is decisive for the strength of the final product. The micro-structural characteristics of the ITZ have been studied by Scanning Electron Micrographies (SEM) for example by (Diamond, et al., 2001). The aspect of the hydration products and the interface paste/aggregate with SEM technologies is shown in Figure 3-29. ITZ is characterized by a significantly higher water/cement ratio than the bulk paste what increases porosity as well the amount of CH-crystals, lessening strength (Monteagudo, 2014). The same concept has been applied to the interface fibre-matrix (Wei, et al., 1986). Test results of the micro-hardness of concrete and steel fibre indicated that the width of the ITZ was about 40-70 μm as shown in Figure 3-30. When a fibre is introduced into the concrete, it disturbs the distribution of the aggregates and the sand and leads to a mix around the fibres with slightly different composition having more cement paste around the fibres to fill the spaces (Dupont, 2003). Another factor disturbing the homogeneity of the concrete around fibres (or large aggregates assumed impermeable) is that hydration products can only infiltrate from one side resulting in a water cement/ratio significantly different (Li, et al., 1997). All these qualitative assumptions have not been proved yet in polyolefin based macro-fibres.

In such a case of polyolefin fibres, some of the first researches were made focussed in understanding the bond mechanism between polyolefin fibres and cement paste even though such first polyolefin fibres had smooth surface and cylindrical shape. Polyolefin fibres in concrete had shown to have good toughness or tensile strength but also a much higher impact/static strength ratio and toughness factor than do steel fibres. All of them being interesting parameter for projected concrete and that might be the reason for its use in one of the oldest reference of polyolefin fibres. A dock in the Port of Montreal was repaired using two types of projected concrete: one with polyolefin fibres and another with steel fibres. Flexural tests after 7 days with 11.4 kg/m³ of polyolefin fibres showed results similar to those obtained for the same reinforced concrete, but with 60 kg/m³ of steel fibres.

Nevertheless, at 28 days, polyolefin fibres present a lower toughness than do steel fibre, although it became equal again at 180 days (Khayat, et al., 1996). With the aim of understanding the evolution of bond mechanisms between polyolefin fibres and cement paste and the microstructural and morphological structure of fibre surfaces was characterized using scanning electron microscopy (SEM) in 2005 (Tagnit-Hamou, et al., 2005). They concluded that the low superficial hardness of polyolefin fibres, compared with steel fibres, allows it to change its morphology and increase bond with the paste and coinciding in that hydrate infiltration in the superficial layer of the fibre increases the bond between paste and fibre. This increase of superficial roughness was the consequence of impact between grains and fibres during mixing, which mechanically damaged the surface of the fibre. Moreover, penetration of hydrates into the fibre and so bond quality increases according to hydration time.

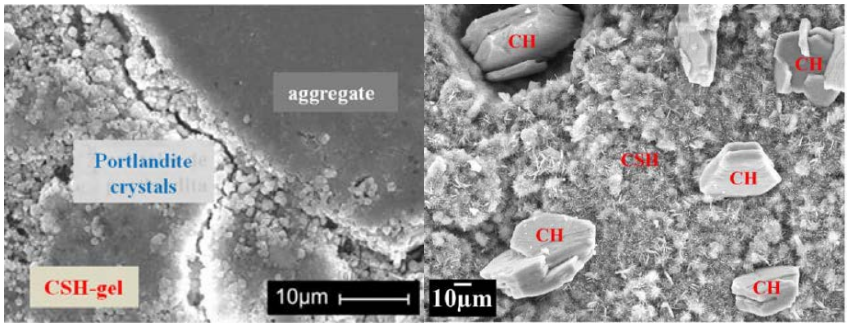

Figure 3-29: Visual aspect of the hydration products by SEM [From: (Monteagudo, 2014)].

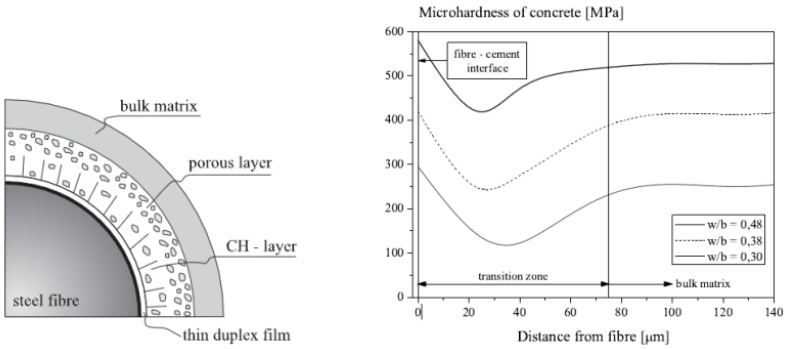

Figure 3-30: Interface transition zone [from: (Cunha Victor, et al., 2007)].

3.5.4 Pull-out behaviour

As stated above, the behaviour under tension of the fibre-matrix system is decisive in the post-cracking behaviour. Henceforth, the measurement of the pull-out resistance might permit to characterize the behaviour of the FRC under tension stress. The residual strength would be then directly related with the fibre pull-out response. The fibre-matrix interactions are logically the main mechanisms of the pull-out processes. That is to say that, in order to extract the fibre, the following interactions oppose to it (see also Figure 3-31):

- Bond adhesion at the fibre-matrix interface
- Interfacial shear stress along the fibre-matrix interface
- Mechanical anchorage in localised transfer points due to geometrical modifications or interface properties

However, the energy needed to overcome each of them varies with numerous factors. The most important ones are probably the material constituent of the fibre and its relation with

the cementitious matrix itself, the smooth or deformed surface, the existence of micro-fillers and the geometries of the fibres such as crimped or hooked. That is not all; the fibres behave in a different way when their embedded length changes and the energy absorbed during a pull-out test is a function of the inclining angle of the fibres which induces a different fracture response depending on the final orientation of the fibres. Furthermore, the boundary conditions of the test also affect the final result of the test. Even though analytical models have provided some adequate results, such models still need to be treated by empirical factors from pull-out tests.

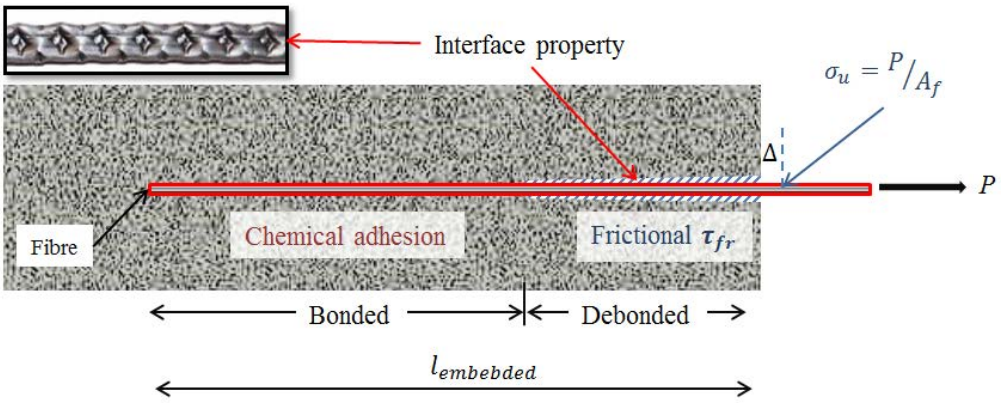

Figure 3-31: Pull-out mechanisms.

An extensive literature review on straight and hooked steel fibres pull-out response can be found in references (Laranjeira, et al., 2010a; Cunha Victor, et al., 2007; Laranjeira, et al., 2010b). While the fibre/matrix debonding and frictional sliding are the two main mechanisms controlling the pull-out of straight fibres, additional mechanisms due to fibre straightening during pull-out must be taken into account for mechanically deformed fibres, which introduces additional complexity on the pull-out response (Zīle, et al., 2013).

In order to assess the effectiveness of the fibre-matrix system, several methods of pull-out tests have been used in both single fibres or in groups of fibres. A pull-out test on single straight fibres embedded in cementitious matrix are performed to determine the fibre/matrix interface characteristics and it is mainly governed by the debonding process of the fibre and the friction between the fibre and matrix. From these types of tests, maximum pull-out force, bond shear stress at maximum load, frictional resistance and total pull-out work (area under the pull-out curve) can be calculated. The typical shape of a load-displacement curve obtained in a single straight and smooth surface fibre pull-out test is shown in Figure 3-32(a).

In the last part of the test, C-D branch, the fibre is fully debonded and the only forces opposing to the extraction of the fibre are the frictional forces between the fibre and the matrix. Such opposing forces (τ) reduce in the curve due to the decreasing of the embedded length and so the surface in contact. If the embedded length was kept constant and no deformation of the interface occurred, such τ would be a constant and so would be the load needed to produce the extraction at a constant rate. The initial branch (0-A) is almost linear with some non-linearity close to the peak where a turning point takes place. After such peak-load, the loads descend probably due to the growing of crack in the interface up to the total debonding of the fibre. If during the debonding phase, load attains the force corresponding to fibre ultimate tensile strength without exceeding the matrix shear strength, the fibre would break (Cunha Victor, et al., 2007).

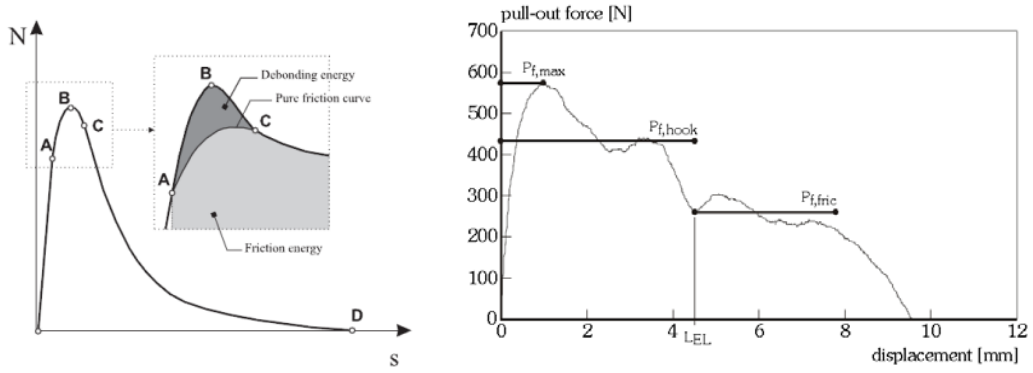

(a) (b)

Figure 3-32: Typical pull-out curve of: (a) straight Steel fibre with smooth surface (Cunha Victor, et al., 2007) ; (b) hooked-steel fibre (Grünewald, 2004).

It should be noted that this would lead to an abrupt decreasing of FRC toughness and it has, at the end, limited energy dissipated by this failure mode. However, it should be highlighted that one more mechanism is related with these effect which is the mode of tensile failure of the fibre itself and such comment was based in steel fibres. Steel fibres with mechanical anchorages have been improved by changing its shapes, as the case of the hooked-steel fibres which energy improvements can be seen in Figure 3-32(b). Some of the energy is needed to extract and rectify the hook (see Figure 3-33) of the fibres but after the process has taken place, the drop of toughness would also be noticeable (Laranjeira, et al., 2010b).

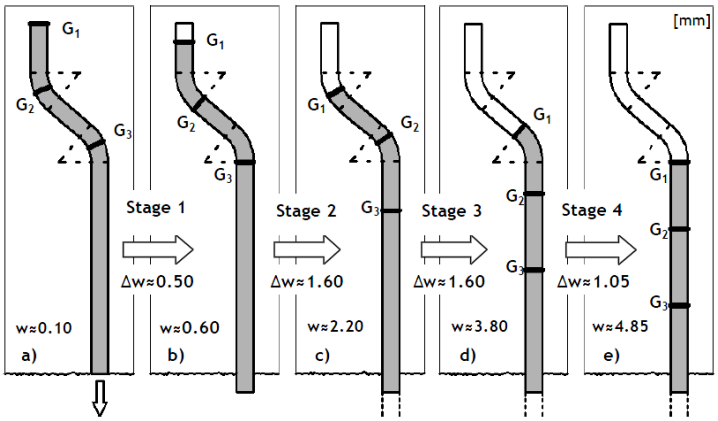

Figure 3-33: Main stages of the rectifying process of a hooked-steel fibre (Laranjeira, 2010).

In the case of synthetic fibres it is worth noting that the most effective modifications in the shapes in order to enhance the pull-out response have been by roughening the geometry of the fibre surface. Research about pull-out of polyolefin based fibres can be barely found. Nevertheless, the aspect of the pull-out test embedded 24 mm with quite similar characteristics compared with the ones used for this thesis has the shape shown in Figure 3-34(a). That shape seems to be reasonable because during pull-out processes the embossed surface probably deforms gradually along the fibre, as can be seen in Figure 3-34(b). The embossed surface would then cause the pull-out load to increase and decrease several times.

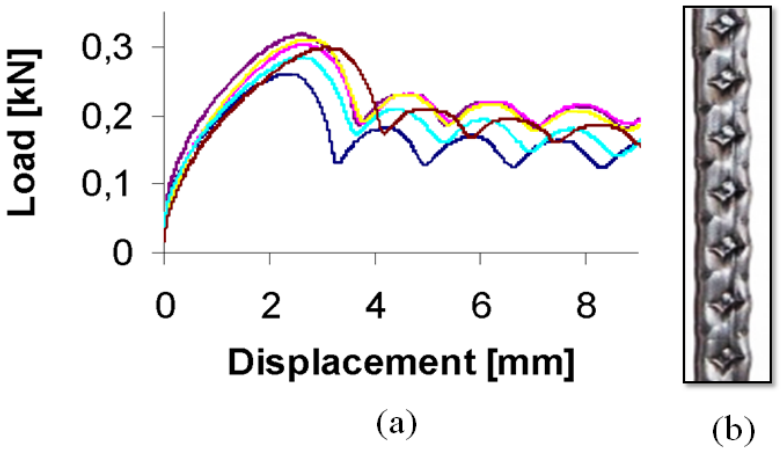

Figure 3-34: (a) Pull-out test of a polyolefin based macro-fibre made by (Døssland, 2008); (b) typical embossed surface of a Polyolefin fibre.

It is important to highlight that for steel fibres and in order to avoid brittle failure is desirable to ensure that the dominating mechanism of failure after cracking is the fibre pull-out. This assertion may be also applicable for steel-hooked fibres which increase the energy by the mechanical interlock but slip after the fibre has been rectified in its ends. Nevertheless, the modes of failure of polyolefin based macro-fibres has not been tested yet but it is known that allow higher deformations before breaking and it is not clear that the most advantageous mode of failure is to assure that they are mostly pull-out. That might be one of the main differences that could be found by means of pull-out tests. Nonetheless, there is still a lack of knowledge about the pull-out response of polyolefin based macro-fibres with deformed and treated surface.

Even though the tests are usually performed with relatively intuitive procedures, results are usually of difficult interpretation as it was previously introduced. First of all, the test seeks to measure how the fibres bridge the crack while it opens. That is to say that those fibres are sewing both parts of the element and in order to do so, fibres have to be connected with the matrix to bear loads and oppose to the opening of the crack. Therefore, it is possible to assess the stress transfer between the fibre and the matrix by means of pull-out tests (Naaman, et al., 1991) though such tests should represent the real manner in which a given type of fibre works. Geometrical aspects as fibre embedded length and orientation have to be taken into account but also some micro-scale aspects as the inter-action between fibres, modulus of elasticity of the matrix that may open the discussion to more variables. In the initial works, the problem was assumed as a perfectly elastic link with negligible Poisson´s effect and reducing the problem to a one dimension (Lawrence, 1972). Afterwards, the problem was studied performing a test with both sides of the fibre embedded in the matrix and it was observed that the distribution of the stress was not constant along the embedded length of the fibre as it is shown if Figure 3-35(a) (Wang, et al., 1988). The same authors in 1990 carried out tests with only one part of the fibre inside the matrix and the inclination of the fibre from 0º to 75º as it can be seen the scheme they published in reference (Li, et al., 1990) shown in Figure 3-35(c). They concluded that for the optimal use of FRC with one-dimensional fibre distribution, the optimal fibre length should be twice the critical length.

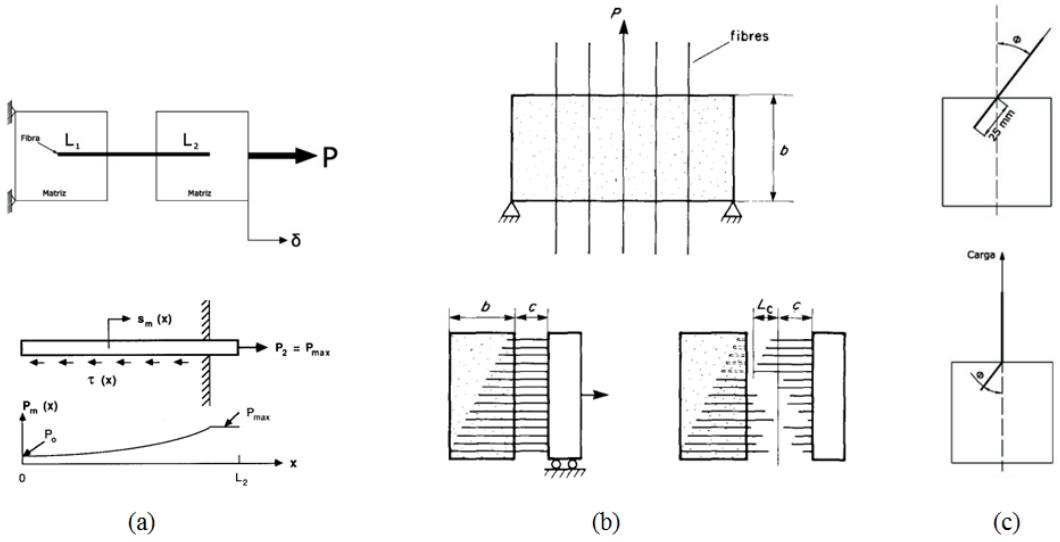

Figure 3-35: Pull-out tests: (a) schematic illustration of a pull-out specimen configuration (Wang, et al., 1988);(b) bond Strength measurement by direct pull-out and determination of fibre critical length (Li, et al., 1990);(c) specimen and test schematic for experiments of fibre pull-out at an angle (Li, et al., 1990).

Conversely, they stated that for a randomly three-dimensional fibre distribution, the fibre length should be close to the critical length in account for the increase when the fibres are pulled-out at angles. Figure 3-35(b) shows the proposed test that they made for measuring the bond strength from a direct pull-out (upper scheme) and for the determination of the critical length. The pull-out response of inclined fibres is different from those verified on aligned fibres. The process is governed besides fibre debonding and friction along the interface by additional mechanisms such as fibre bending, matrix spalling and local friction effects (Laranjeira, et al., 2010b). Hence, research continued with variations that included more realistic assumptions as the deformation of the matrix and matrix spalling during the pull-out of inclined fibres (Leung, et al., 1991; Leung, et al., 1992). They concluded that not only spalling but some other effects as shear and bending of inclined fibres should be taken into account for the interpretation of the pull-out results (see Figure 3-36). Banthia and Trottier in 1992 designed a test with the aim of understanding the sensitivity of steel fibre pull-out resistance to stress-rate and temperature (Banthia, et al., 1992). They concluded that deformed steel fibres embedded in cementitious matrices in general support a higher load under impact than under static pull-out.

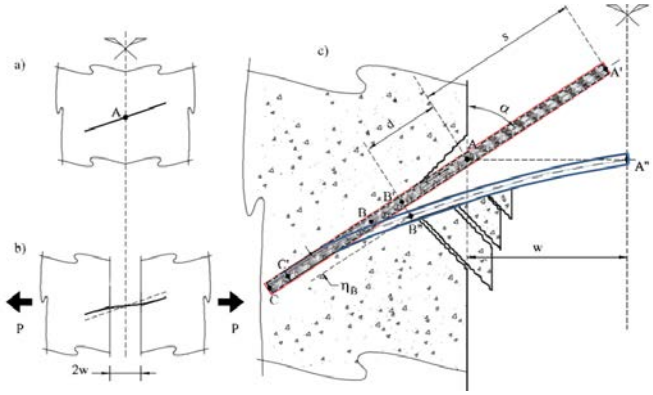

Figure 3-36: Pull-out of an inclined fibre: (a) undeformed state; (b) deformed state; (c) position of the fibre at a given displacement [adapted from: (Fantilli, et al., 2007)].

In addition to the matrix and fibre mechanical properties, interface property characterisation plays key-role in the system fibre-matrix behaviour as it has been widely mentioned. Composite material would increase substantially its mechanical capacities, durability and reliability if bond and frictional behaviour could be enhanced and guaranteed. That is why in the last decades, not only the mechanical properties of the fibres have been sought but also a large variety of shapes and surface treatments. In the review made by Li and Stang in 1997 about the interface property characterization and strengthening mechanisms in fibre reinforced cement based composites, the authors studied some of the most relevant treatments of scientific literature that were summarized in Table 3-4.

The three classes of strengthening mechanisms, fibre deformation, interface densification and fibre surface modification can lead to substantial improvements in the behaviour of the system fibre-matrix. The highest increase appeared by fibre deformation though it should be qualified that in the case of the hooked end of steel fibres would depend also on the matrix strength to withstand the anchorage stress of the hooked end. In such a case of the hooked-steel fibres, the pull-out strength can be even be higher for a shorter embedded length because almost all the energy is absorbed by the plastic deformation of the hooked end and the surrounding matrix (Cunha Victor, et al., 2007). Two distinctive pull-out modes of steel hooked fibres were observed by Robins et al.: slip after the hooked end is rectified or fibre fracture after reaching its tensile capacity (Robins, et al., 2002). When the hooked-end was straightened, due to the smooth surface the fibre is pulled out. Fibre fracture was most likely to occur with fibre embedment lengths larger than 5 mm in combination inclining angles surpassing 20 degrees. The mechanical anchorage appeared to be mobilised at greater crack-width and increasing fibre orientation. The details of this discussion can thus be belter understood seeing the graphics placed in Figure 3-37. In the case of polymer fibres, the technique of fibre deformation is highly available for macro-fibre thanks to the deformable and relatively large diameters. Fibre deformation techniques contribution is limited to certain composite properties that relate inversely to fibre diameter (Li, et al., 1997).

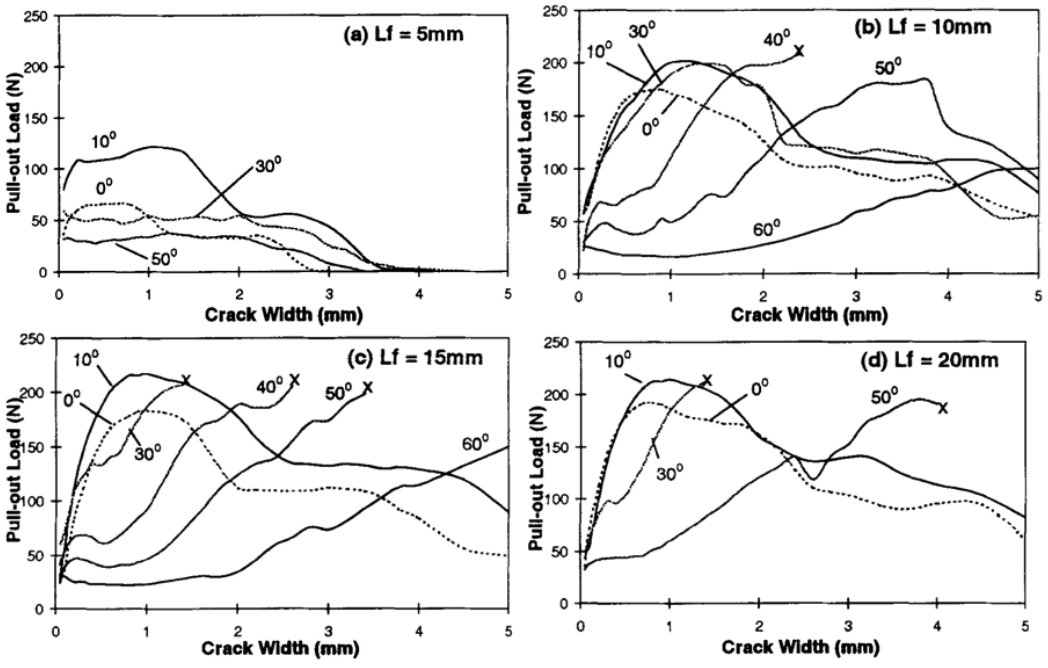

Figure 3-37: Influence of fibre orientation on the pull-out modes of hooked steel fibres (Robins, et al., 2002).

Table 3-4: Strengthening mechanism and effect on interface property (Li, et al., 1997).

Fibre type		Strengthening mechanism	Effect on interface properties	Reference
Polypropylene	Fibre deformation	Fibre fibrillation	Bond increase by factor 3	[Krenchel, 1986]
Polypropylene		Fibre twisting	Bond increase by factor 7	[Naaman, Shah 1984]
Nylon		Fibre crimping	Bond increase by factor of more than 6	[Li, Wang, Baker 1990]
Steel		Fibre crimping	Effective bond increase by factor of 1.4-10.5 depending on matrix type	[Banthia, 1990]
Steel		Fibre hooked end	Effective bond increase by factor of 2.8-27.6 depending on matrix type	[Banthia, 1990]
Steel		Fibre hooked end	Slip hardening	[Li, Stang, 1997]
Brass	Interface densification	Interface densification	Bond increase by 185 in microsilica matrix with low w/c ratio	[Chan, 1997]
Steel		Interface densification	Post-peak slip-dependence reduced	[Chan, 1997]
Steel		Interface densification	Bond increase by factor 2 using an Densit matrix	[Nielsen, 1995]
Steel		Interface densification	Bond increase by factor 2 using an DSP matrix	[Shannag, 1995]
Carbon		Interface densification	Bond increase by 95% using microsilica matrix with low w/c ratio	[Katz, Li, Kazmer, 1995]
Steel		Interface densification	Bond increase by 60%-80% by addition of 1.4% by weight of PVA	[Najm, Naaman, Chu, 1994]
Steel		Interface densification	Bond increase by factor 4 by addition of 15% by weight of acrylic polymer particles	[Wei, Mandel, Said, 1986]
Polyethylene	Surface modification	Plasma treatment	Bond increase by 50%-100%; factor of six increase demonstrated	[Li, Wu, Chan, 1996]
Polypropylene		Plasma treatment	Slip-hardening	[Li, Wang, Baker, 1988]

In addition to all these variables, the test has to be representative of the final behaviour of a fibre inside the concrete. In the case of smooth surface and straight fibres, the pull-out mechanisms are more easily interpreted. Hooked-steel fibres have also been the centre of most of the research. Whereas not many studies describe the active mechanisms during pull-out of fibres with embossed surfaces treatments probably because of the difficulty of observing the processes taking place within the matrix. Seeking the interpretation of the results, several techniques have also been used to achieve reliable results that may localize effects as the initial elastic deformation of the fibres or frictional sliding after debonding. Raman spectroscopy showed to be a powerful tool in order to localize the propagation of fibre debonding, interfacial shear strength or the non-linear variations of the maximum pull-

out force with embedded length (Bannister, et al., 1995). With photo-elastic birefringence, the fibre debonding and pull-out sequence and it was seen that it was not appropriate to report pull-out maximum load as the value associated with fibre debonding from the matrix (DiFrancia, et al., 1996). Some other techniques have used transparent matrices with the additional problem of the substantially different behaviour compared with cementitious brittle matrices (Gerstle, et al., 1991; Gent, et al., 1992). In such a sense, Video-Photography is especially well-suited and it has previously shown its capacities in straight and bent steel fibres removed from a cement matrix allowing catching the stages of the process: debonding, plastic deformation of the fibres, frictional sliding and the reduction of frictional resistance due to the fibre partially exiting the sample (Pompo, et al., 1996). It should be highlighted that some of those processes are significantly higher for polymer fibres due to their large deformations and lower modulus of elasticity and digital image techniques could provide very useful information. Some other authors have used micrographies to observe the duct and the matrix surface before and after the pull-out test for a better understanding of the process (Bentur, et al., 1985). In the theoretical debonding curves, the experimental data showed that models accurately reproduced the debonding process except for a decrease in interfacial sliding friction due to the wear of matrix asperities at the interface (Easley, et al., 1999). That decrease caused difficulties to the proposed models when steel fibres were used.

In the search of a test that relates all this variations, several configurations have been used. The test should avoid unrealistic stress concentrations and put both the matrix and the fibre in tension. They also have to allow variations in embedded lengths and inclining angles and the accurate measurement of the most important micro-mechanical processes. In such a sense, two main groups of pull-out tests have been used: single-sided and double-sided configurations (see Figure 3-38).

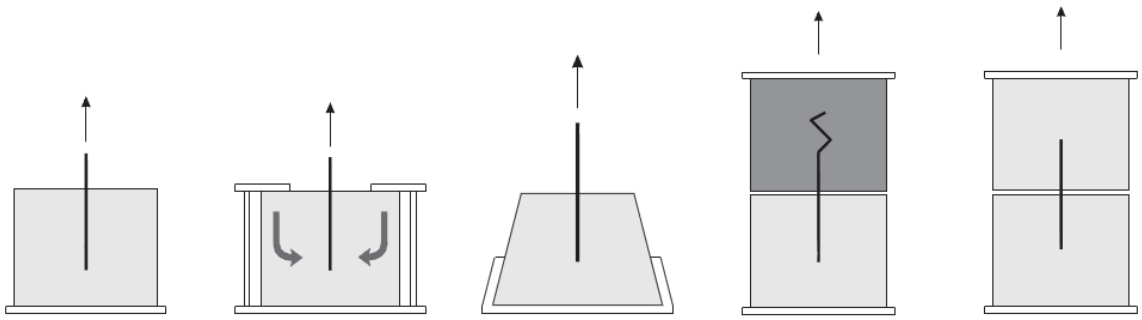

Figure 3-38: Examples of pull-out test configurations: single-sided and double-sided specimens (Cunha Victor, et al., 2007).

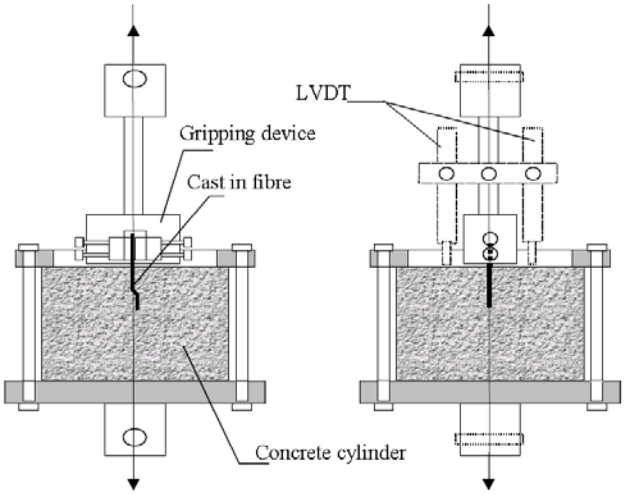

Figure 3-39: Pull-out test set up (Døssland, 2008).

Both types of tests have their drawbacks what makes important to notice their main problems to choose properly and design the adequate test for each fibre/matrix system. The double-side test, pull-out processes have to occur in only one side for a good interpretation of the results. This can be achieved by means of a mechanical anchorage in one of the halves or by a significantly larger embedded length or matrix strength in one of the halves. Nevertheless it is hardly possible to assure that the pull-out process really occurs only in one of the halves. In a theoretical setup, it could be possible to place a fibre perfectly centred and symmetrically embedded and tested and having equal slips in both sides. However, this is highly improbable and at the end the test has very difficult interpretation. That is why most of the literature found has used single-sided tests similar to the ones described in Figure 3-39 (Døssland, 2008; Cunha Victor, et al., 2007; Cunha, et al., 2010; Beckert, et al., 1998; Markovich, et al., 2001; Groth, 2000; Breitenbücher, et al., 2014; Soetens, et al., 2013). Several considerations should also be noticed in order to perform an effective test. The first one is related with the free fibre length needed in order to assure that non-relative slips take place. In addition, the boundary conditions imposed have to be carefully chosen avoiding lateral confinements that would produce improvements in the fibre resistance to be pulled out of the matrix.

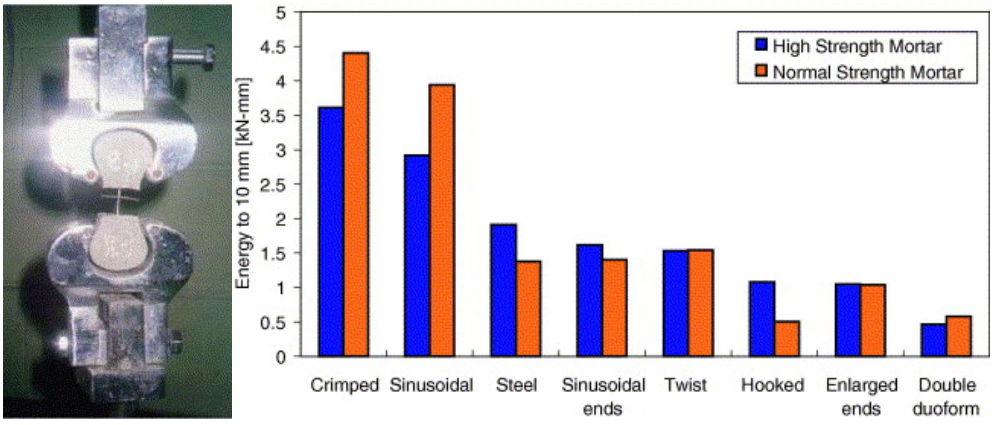

Figure 3-40: Comparison of absorbed energies from pull-out tests for various fibre types (Oh, et al., 2007).

Even with all the drawbacks and difficulties that have been previously detailed, it is also significant that those pull-out tests were easily carried out. That means that with a properly designed test, it is easy to compare the behaviour of several types of fibres or matrices and making a wide range of geometrical dispositions. Although the interpretation of the test in order to extract physical parameters is still under discussion and no test have been standardised, the correct performance of a repetitive test allows the assessment of many important parameters and models. One practical possibility is to measure the pull-out energy of several geometries of the fibres with the same test setup for example in reference (Banthia, et al., 1992). The same concept was exploited to evaluate the optimum among several shapes of synthetic fibres shown in Figure 3-40 (Oh, et al., 2007). In such a use, pull-out tests have shown to be a very useful tool.

Concerning the modelling of the pull-out behaviour, extensive studies have been carried out and some of them have related fibre bridging stress with the crack-opening relation. Analytical and numerical models for straight fibre pull-out response have been developed in both senses: predicting pull-out curves from an assumed bond-slip relationship and, the inverse problem, obtaining the bond-slip relationship by means of pull-out tests (Banholzer, et al., 2005; Banholzer, et al., 2006). Nonetheless, the fibres in the FRC are randomly oriented and the pull-out response is significantly sensitive to the fibre incidence-angle. Therefore, the predicting of inclined fibres is especially important when the models aim to relate pull-out behaviour with tensile strength. Classical approaches assumed perfect bond until the interface failure occurs. Researches have assessed the problem by fracture mechanics characterizing the interface in terms of specific fracture energy (Stang, et al., 1986), energy failure criteria (Shah, et al., 1991), cohesive interface models (Fantilli, et al., 2007) or by simulating the fibre as a beam bending on an elastic matrix (Li, et al., 1990). Despite the good agreement with experimental results, only the maximum pull-out load could be obtained and its applicability was questionable for large inclination angles. In order to overcome such limitations, the embedded part of the fibre was treated as a beam resting on an elastic and heterogeneous foundation whose stiffness was computed by means of a finite-element model. Considering the effects of mechanical anchorage such hooked-steel fibres, some semi-analytical models have been proposed (Laranjeira, et al., 2010b; Soetens, et al., 2013). The former considered the effect of the hook obtained from experimental results with a straight fibre pull-pout and the latter uses experimental and virtual work principles to describe the load-slip relation. By means of finite element simulations, several research have approached using interfacial friction laws as the basis for the solutions to the equilibrium and compatibility equations (Breitenbücher, et al., 2014; Zhao, et al., 2014; Zhan, et al., 2014) or assessed the size effect of in the fibre pull-out test (Yang, et al., 2003). In any event, modelling the pull-out response of inclined fibre seems to remain a topic open to discussion (Laranjeira, et al., 2010a). That is why most of the models linking the pull-out response to tensile behaviour make use of significant empirical and experimental parameters related with orientation. In such a sense, the constitutive relations are usually affected by orientation factors that are described in more detail in subsection 3.6 and chapters 9 and 10. Subsequently, constitutive relations obtained from pull-out are described subsection 3.7 taking in account such affecting factors to the bridging stress of a real piece with randomly distributed fibres.

3.6 Fibre orientation and distribution

Fibre orientation of composite materials is essential for its mechanical properties and therefore decisive to predict its behaviour. Deviations due to manufacturing operations can cause unexpected behaviour that should be taken into account and measured for modelling

its behaviour with reliability (Blanc, et al., 2006; Hine, et al., 1995; Fu, et al., 1996). Consequently, models and distribution functions have been used to reproduce the final disposition of the fibres and several techniques as image analysis used to validate the functions (Mlekusch, 1999). In the case of concrete, not only the manufacturing operations affect the orientation, but also the rheological properties of the fresh concrete, the formwork, the placing conditions and their influences can vary significantly with each type of fibre and matrix. The efficiency of an individual fibre in a certain matrix may be measured by pull-out tests. Nonetheless, the fibre bridging stress in a localized crack inside a specimen depends on the number, relative position and rotation to the principal stress direction as has been previously explained. Fibre reinforced concrete has randomly distributed and oriented fibres in the fresh mass that will take a final disposition in correlation to how all the setting processes affect that type of fibre inside that specific concrete and formwork boundary conditions.

3.6.1 Orientation factor

In order to measure the number of fibres placed on the cracked surface, research have widely used the so called orientation factor first proposed by Krenchel in 1975 (Krenchel, 1975) and placed in expression (3-8) where *n w*as the number of fibres in the cross section, *A* the cross section of the sample and A_f the section of one fibre. That is to say that being *th* the theoretical number of fibres that should be crossing the cross section, the orientation factor (θ) represents the real number of fibres that cross the referred surface. Various models assessed the theoretical values of the orientation factor. The models are reviewed in more detail in Chapter 9. In any event, it has been a very useful tool in order to assess the variations and scatter obtained in experimental results whether comparing the real number of fibres counted or by predictive models that have fit experimental results regarding rigid (steel) fibres. The orientation numbers can be considered (in concrete material science) sufficiently accurate values but some assumptions have to be accepted. The most relevant is that fibres were supposed to be rigid and the hooked end negligible in terms of orientation factor. This makes a big difference with polymer fibres because they can easily bend.

$$\theta = \frac{n}{th} = n\frac{A_f}{V_f A} \qquad (3-8)$$

Laboratory specimens are usually prismatic and notched what makes especially adequate to evaluate the distribution of the fibre in rectangular sections. Dupont and Vandewalle divided the cross section of a beam into three different orientation zones as shown in Figure 3-41(a). The bulk zone in the centre of a beam is considered as isotropic. In the proximity of the wall of the mould, the orientation factor increases as shown in Figure 3-41(b). The top surface of the section (free surface while filling the mould) was assumed to have the same boundary conditions as the sides of the mould because such surface is smoothened after casting and there are no fibres sticking out. The authors did not consider that the topping or levelling methods could affect the number of fibres placed on this area. Having said that, the values of the orientation factor at the corners of the rectangular section were taken as shown in Figure 3-41(c), being in the proper corner equal to one as the one-dimensional case was supposed. Those numbers simplify a much more complex behaviour in the transition zone from the bulk to nearby a wall. It has been assessed by heavy and slow convergent numerical integrations in the referred works (Dupont, et al., 2005; Kooiman, 2000). Laranjeira proposed an analytical approach and bilinear models to address the problem but still with a complex and limited functionality (Laranjeira, 2010). In this regard, many other factors may vary the final positioning of the fibre with major influences that are also difficult to assess. First of all, the presence of a boundary induces a positioning

of the fibre. If the gravity point of a rigid fibre is placed at a distance lower than half of the length of the fibre, it is geometrically impossible to become located perpendicular to the wall (Martinie, et al., 2011) even in a steady situation (see Figure 3-41(d)). In such a sense, the models have been applied by using diverse assumptions. In the present thesis, Chapter 9 presents a new model to assess the orientation factor.

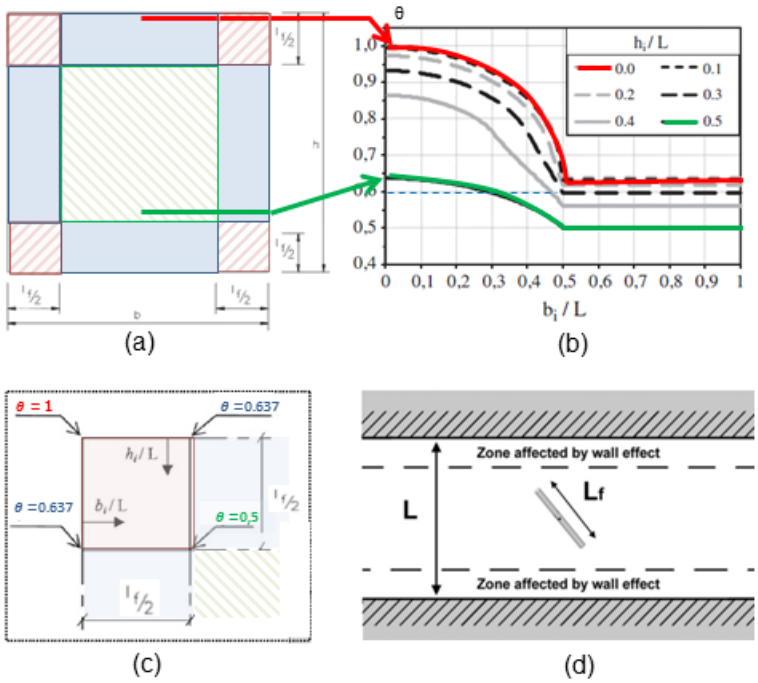

Figure 3-41: Wall effect: (a) orientation zones of a cross section of a rectangular beam by (Dupont, et al., 2005); (b) variation of the orientation factor at different distances of the wall by (Laranjeira, 2010);(c) detail of the corner by (Laranjeira, et al., 2012);(d) wall effect for a fibre length l_f in a structural element of thickness L (Martinie, et al., 2011).

The interest of modelling the flow of SCC with or without fibres has led to 3D computational models that have reproduced the slump flow test or L-box test. The models have been able to capture the flow behaviour of SCC and providing insight into the distribution of large aggregates and fibres and their orientations during the flow (Deeb, et al., 2014a; Deeb, et al., 2014b). The lengthy computational time might be its major drawback and some results have been placed summarizing the result in Figure 3-42.

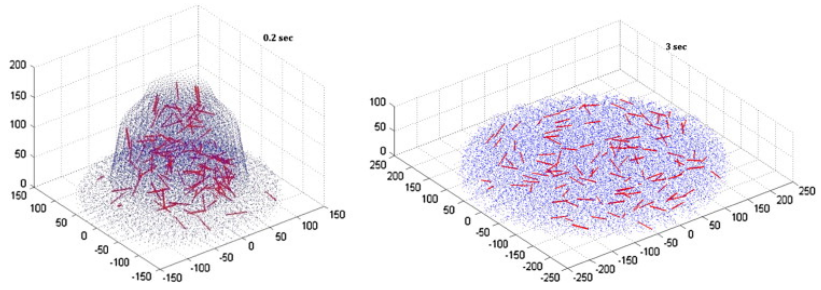

Figure 3-42: 3-D modelling of the slump flow test wit SFRC (Deeb, et al., 2014c).

In a recent paper, the authors settled that in practise it might not be practicable to perform the full three-dimensional simulation of the flow of FRC-SCC into the formwork. They proposed to determine the angle of inclination of fibres from the elliptical section as shown Figure 3-43 and by means of the expression (3-9) placed in reference (Deeb, et al., 2014c)

and that has been used for the analysis of fibre orientation in FRC (Ferrara, et al., 2011) and dealing with polymer composites (Hine, et al., 2014). They obtained sound conclusions about the orientation factor because it does not reflect the actual inclination of the fibres. In addition, the results of the orientation factor exceeded the exact number of fibres by the geometric probability of Buffon problem after ten seconds. In such a sense, by means of optical methods such as image analysis scan of the surface, it is possible to obtain a preferred orientation with accuracy. Nonetheless, the method was compared with computed tomographies (CT) and the results had non-negligible differences applied to a transverse section because of the low accuracy of an optical method in measuring the orientation of fibres almost perpendicular to the observed surface (Bernasconi, et al., 2012). Although micro-CT method is a non-destructive method, it requires expensive experimental facilities.

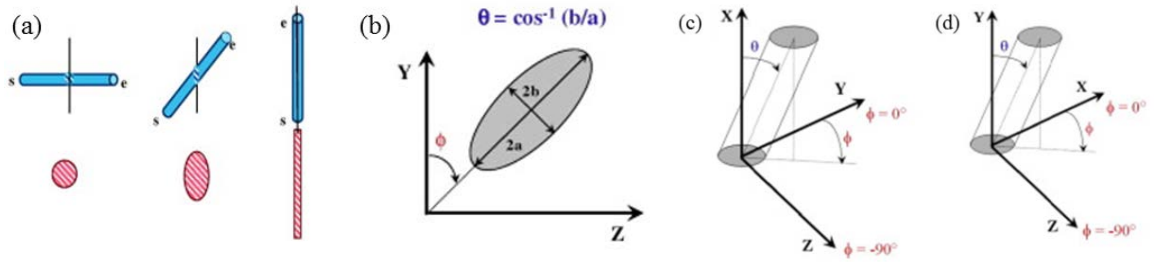

Figure 3-43: (a) Possible cross-sections of a fibre cut by a vertical plane (Deeb, et al., 2014c); (b) definition of the angle Φ (Bernasconi, et al., 2012); (c) definition of the angle θ for the XY plane (Bernasconi, et al., 2012); (d) definition of the angle Φ for the plane XZ (Bernasconi, et al., 2012).

$$\bar{\eta} = \frac{1}{n}\sum_{i=1}^{n}\cos\theta_i \qquad (3-9)$$

3.6.2 Estimating fibre orientation and distribution

Given the significant interest in developing techniques that enable the identification of the final orientation and distribution of the fibres inside a hardened concrete piece, many advanced technologies have been used. From expensive equipment to cumbersome procedures and from destructive to post-test methodologies, a wide range of options has enable to measure the positioning of fibres. The most intuitive technique to measure the orientation factor is counting the fibres on cuts. After the specimen is cured and even tested, a grid can be assumed on the surface sawn and the number of fibres can be recorded. It seemed to be a satisfactory method used to evaluate the distribution and orientation of fibres (Gettu, et al., 2005). One additional possibility is to cut the specimens in the three principal directions as shown in Figure 3-44. It allows also evaluating the quality of the manufacturing process and reveals any concentration of fibres due to excessive vibration or fibre segregations. In addition, cut surfaces may be treated with advanced digital image tools and provide even more information. Moreover, it allows an easy comparison with the orientation factor previously defined.

An additional possibility is to count the fibres on three sections perpendicular to each other and combined the results. This was suggested by (Døssland, 2008) and it is based on is based on the theory of that all orientations can be described as a combination of the three ideal orientations the author illustrated in the adapted Figure 3-45 (Thorenfeldt, 2003).

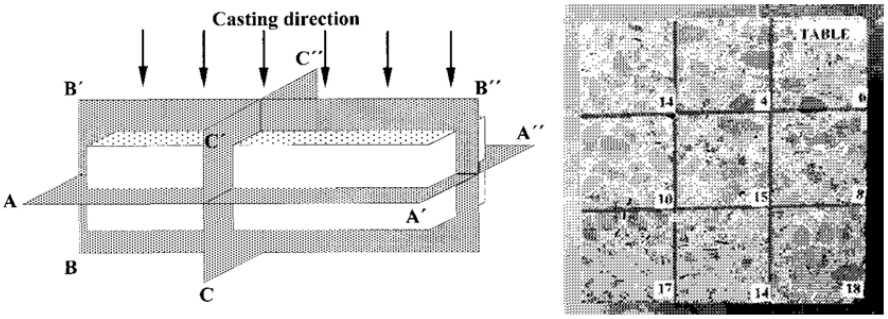

Figure 3-44: Examples of a counting exercise on cut surfaces proposed by (Gettu, et al., 2005).

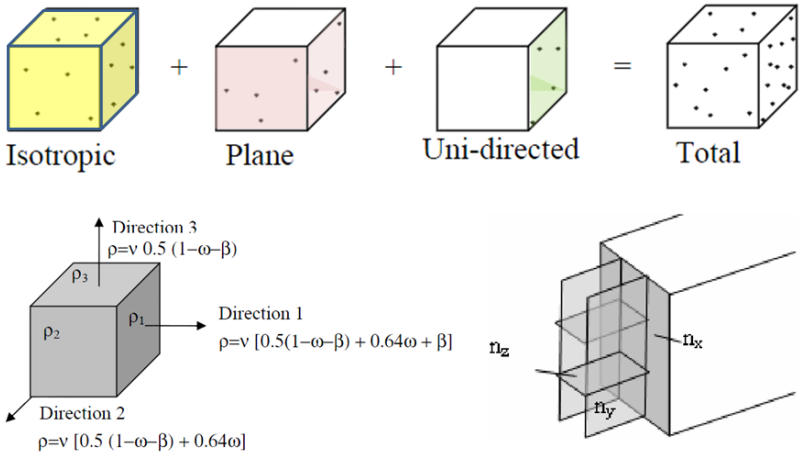

Figure 3-45: Share of fibres on each direction under the assumption that every orientation situation can be described by a combination of undirected fibres (β), plane oriented (ω) and isotropic (1-ω-β)[adapted from: (Døssland, 2008)].

One additional possibility that has been explored is the use of a translucent fluid and rheological models for the prediction of fibre distribution and orientation (Boulekbache, et al., 2010). It was concluded that fibre orientation was significantly sensitive to yield stress of the fluid and the conditions of flow confinement. That is to say that a flow profile develops from the frictional restraint of walls (see Figure 3-46). The authors established that with a low yield stress, the fibres were well oriented with the fluid flow and that the orientation factor governs the response of the material and improving flexural strength compared to a less workable concrete of high yield stress. They reported that the value of the orientation factor (θ) reached 0.57.

As it was previously referred and commented, techniques such as computed tomography (CT-scans) can be used for this purpose providing very accurate measurements of the fibre positioning. Such direct measurements by means of CT-scans have been used to detect steel fibres in concrete (Stähli, et al., 2007). It has also been successfully applied on concrete with polyolefin based macro-fibres to assess their distribution and orientation in a prismatic core. It provided an estimation of the fibre content close to the theoretical one (Pujadas, et al., 2014). A very dense tomography with spacing of 0.20 mm slices was performed to compensate for the lower energy absorption of the polypropylene fibres. Using the image analysis system the total volume, pore size distribution and fibre orientation could be calculated (see Figure 3-47). This technique had also been used for macro-synthetic fibres

to assess the rebound and orientation of fibres in wet sprayed concrete applications (Kaufmann, et al., 2013).

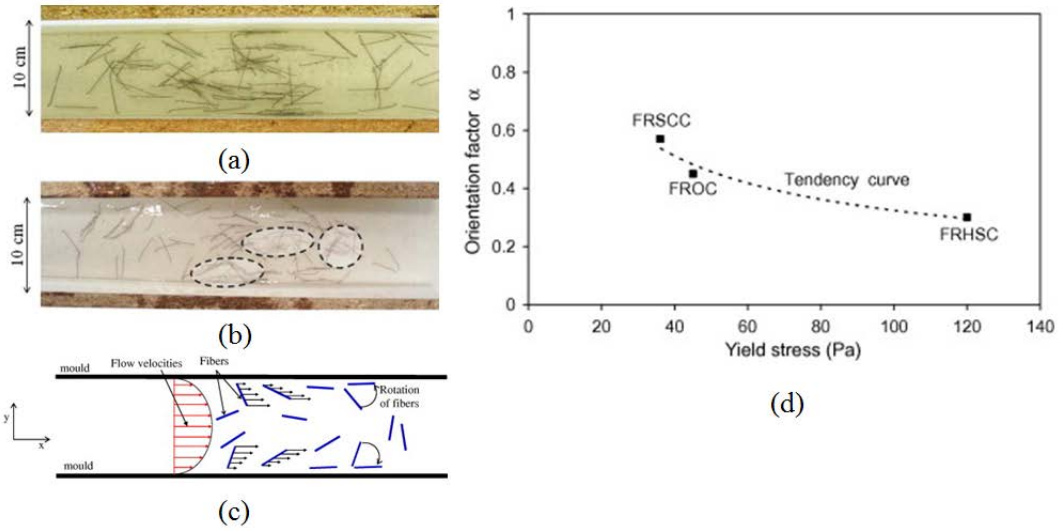

Figure 3-46: Channel flow in a Carbopol with yield stress (τ_0): (a) τ_0 = 25 Pa; (b) τ_0 = 70 Pa; (c) explanation of the fibre orientation in the channel; (d) orientation factor as a function of the yield stress [(Boulekbache, et al., 2010)].

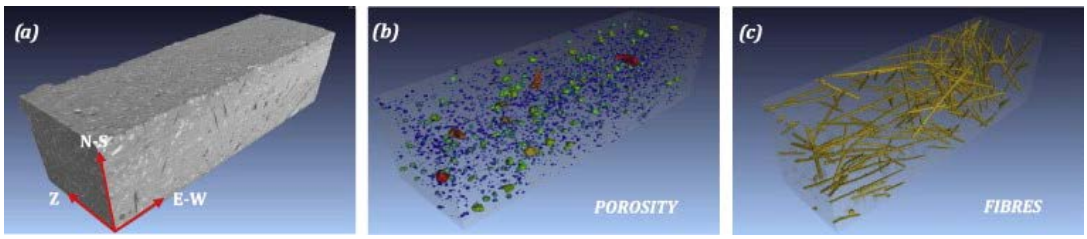

Figure 3-47: CT-Scan of a piece of PFRC: (a) total volume; (b) pore size distribution; (c) fibre orientation (Pujadas, et al., 2014).

Based on the electrical properties of concrete reinforced using steel fibres, several methods have been developed in order to assess the orientation and distribution of the fibres. The properties of SFRC allows to evaluate the presence of fibres by measuring its electrical resistivity (Lataste, et al., 2008), magnetic properties (Ferrara, et al., 2012; Faifer, et al., 2011) or inductivity (Torrents, et al., 2012; Cavalaro, et al., 2014). Other non-destructive measurements on fibre orientation can be obtained by techniques such as image analysis (Grünewald, 2004) or X-ray methods (Robins, et al., 2003). Blanco (Blanco, 2013) made a brief summary of the type of measurements in the literature and it has been extended with the references used for this work and is presented on Table 3-5.

In any event, manual counting has proved to be a remarkable and rather easy method of macro-fibres with the average aspect ratios that are employed as a reinforcement of concrete. In addition, it enables to refine the existing predictive models and with non-expensive equipment. It is also quite easy to take pictures of the sawn surfaces and to correlate with experimental results by means of a counting exercise on the resulting fracture surfaces of the tested sample. It should be highlighted that achieving predictive tools for fibre positioning is not only useful with the aim of improving the mechanical response of the material but also to improve its reliability which is commonly the reason why designers avoid the use of FRC.

Table 3-5: Methods to determine fibre orientation [Extended from: (Blanco, 2013)].

Method type		Technique	References
Destructive	Indirect	Manual counting + theoretical expression (2-8) by (Krenchel, 1975)	(Soroushian, et al., 1990) (Gettu, et al., 2005) (Dupont, et al., 2005) (Michels, et al., 2012) (Døssland, 2008)
		Mechanical testing	(Kooiman, 2000) (Barragán, 2002) (Grünewald, 2004) (Stähli, et al., 2007) (Ferrara, et al., 2011) (Zerbino, et al., 2012) (Torrijos, et al., 2010) (Abrishambaf, et al., 2013) (Kang, et al., 2011) (Di Prisco, et al., 2013)
	Direct	Image analysis	(Grünewald, 2004) (Lappa, 2007) (Stroeven, 1986) (Zandi, et al., 2011) (Sebaibi, 2014) (Kang, et al., 2011)
		X-ray method	(Van Gysel, 2000) (Robins, et al., 2003) (Ferrara, et al., 2006) (Vandewalle, et al., 2008) (Stroeven, et al., 1978) (Døssland, 2008)
		Computerized tomography	(Stähli, et al., 2008) (Trainor, et al., 2013) (Pujadas, 2013) (Kaufmann, et al., 2013) (Deeb, et al., 2014c) (Ponikiewski, et al., 2014)
Non-destructive	Direct	Alternating current-impedance spectroscopy (AC-IS)	(Ozyurt, et al., 2006) (Ferrara, et al., 2008)
		Translucent fluid	(Boulekbache, et al., 2010)
		Open coaxial transmission line	(Torrents, et al., 2009)
		Dielectric waveguide antennas	(Roqueta, et al., 2011)
		Electrical resistivity methods	(Lataste, et al., 2008)
		Magnetic monitoring	(Faifer, et al., 2011) (Ferrara, et al., 2012)
		Electromagnetic and inductive methods	(Torrents, et al., 2012) (Al-Mattarneh, 2014)

3.6.3 Causes and effects of changes in fibre positioning

Concrete is at the end poured on a formwork with a certain shape. Those formworks in the case of research are usually prismatic standardised moulds while in real structures are varied from thin slabs to beams, columns or any other shape. In addition, not only the geometry but also the casting method, dynamic effects such as the flow or the vibration may play an important role in the final positioning of the fibres (Laranjeira, 2010). As it was already mentioned in subsection 3.3, casting methods have to be considered in the structural design of structural elements because they can produce remarkable differences on fibre orientation as shown in references (Torrijos, et al., 2010; Martinie & Roussel, 2011; Stähli, et al., 2007). The main factors affecting fibre orientation proposed by (Laranjeira, 2010) are schematized in Figure 3-48. Some other uneven distributions can be produced by the presence of obstacles such as the reinforcing bars. In such a sense, it has been recommended for SFRC a bar spacing of at least three times the fibre length (Groth, 2000). This has not been assessed with macro-polymer fibres that are not stiff.

Compaction of VCC on a vibration table tends to produce a planar random orientation perpendicular to the direction of the vibration (Kooiman, 2000; Barragán, 2002). Just a quick note to mention that immersion vibrator for compaction is not recommended since there would be a lack of fibres where the vibrator is placed into the concrete (Døssland, 2008). Some authors have also reported that vibration has not big influence on fibre orientation if the specimen is vibrated for a short time (Dupont, 2003; Gettu, et al., 2005). In any event, according to experimental evidence (Laranjeira, et al., 2012), external vibration has a direct influence on the orientation of the fibres along its gravity axis. However, this effect is not clear yet with fibres with low density as the polyolefin ones that suggest that what may occur is the ascension of the fibres.

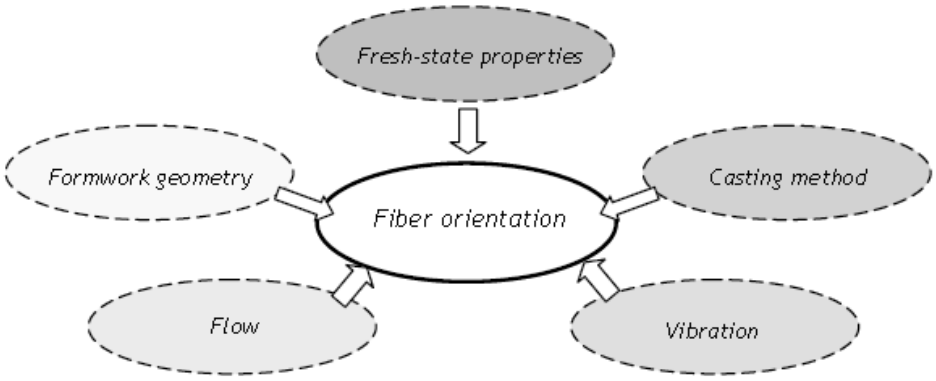

Figure 3-48: Main factors affecting fibre orientation (Laranjeira, 2010).

It is clear at this point that SCC-flow properties in the fresh state have shown to provide stronger alignment of the fibres (Stähli, et al., 2008; Boulekbache, et al., 2010) and therefore improved results in fracture as shown in Figure 3-49 (Grünewald, 2004). If the mass of concrete is assumed to flow in layers, the fibres crossing their borderlines would be forced to align with them. With the assumption of layers with thickness of the fibre length, Laranjeira corrected the value for isotropic conditions for an SCC-FRC. The proposed value for SCC in the bulk takes the value of 0.6 in the horizontal plane instead of 0.5 previously explained for VCC. That SCC value for the bulk coincides with the value of the average orientation factor in bulk of thickness equal to half the fibre length (Martinie, et al., 2011).

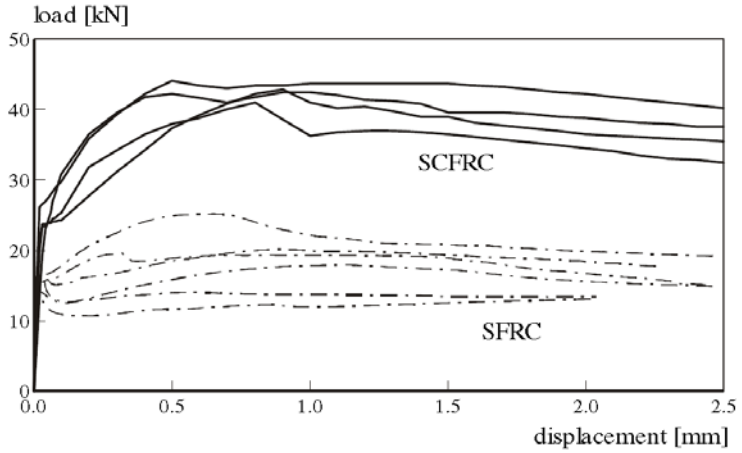

Figure 3-49: Comparison of results of three-point flexural tests of conventional steel fibre reinforced concrete (SFRC) and self-compacting fibre reinforced concrete (SCFRC) load (Grünewald, et al., 2012).

The fibre density may also produce some differences among the varied fibre types and their final positioning inside the concrete. It has been another line to study fibre distribution and another possible source of anisotropy (Stähli, et al., 2007; Ferrara, et al., 2007). The two main sources of non-homogenous distributions are then fibre behaviour inside the flux and wall effects. Inside a flux dominated by shear stresses, the fibre tends to place in the position of minimum energy and minimum torque which is at the end aligned with the flux. However, such position was described as unstable and the fibre moves at regular intervals rotating until it is again aligned (Martinie, et al., 2011). In the typical shapes of the construction industry, shear induced fibre orientation dominates wall effects and that it is almost instantaneous at the time scale of a typical casting process. This was emphasized by the authors for the case of fluid materials such as SCC.

Some other influences on the final orientation and distribution of the fibres have been assessed by changing the formworks. Using three types of hooked-end steel fibres and varying the length of the fibres (36, 50 and 60 mm long), beams 1800 mm long (what is three times the standardised moulds for laboratory specimens) were produced (Vandewalle, et al., 2008). By means of X-Ray detection and manual counting, the fibre orientation was analysed and significant conclusions were obtained in addition to the expected founding that a better fibre alignment leads to a higher post-cracking strength and that self-compacting concrete aligns the fibres along the flow. They concluded that beyond a certain distance, the fibre alignment did not change anymore and that the influence of fibre length was negligible on the fibre alignment. Once again, these effects were observed for the case of steel fibres that are heavier and stiffer.

The influence of the placing conditions was assessed for steel fibres but also for polymeric fibres 54 mm long and low dosage of 2.5 kg/m³ (Torrijos, et al., 2010). Standardised moulds of dimensions 150x150x600 mm³ were poured by three different methods: standard pouring method from the centre (C), in a vertical position of the mould and poured from the top (V) and after the FR-SCC had flowed along an inclined tube 5 m long (T). The authors counted the fibres in the three main perpendicular plains and performed fracture tests on notched specimens following standard EN 14651 and the results shown in Figure 3-50**.** They found that both steel and polymer fibres had a preferential planar orientation and that the casting procedure can significantly affect the fibre distribution and therefore should be taken into account for structural elements in service. The vertically poured elements, simulating a column (finally tested horizontally) had less efficient fibre reinforcement. The

tube was designed to act as pumping pipeline and improved the results for the long steel fibres but not in the case of the polymer fibres.

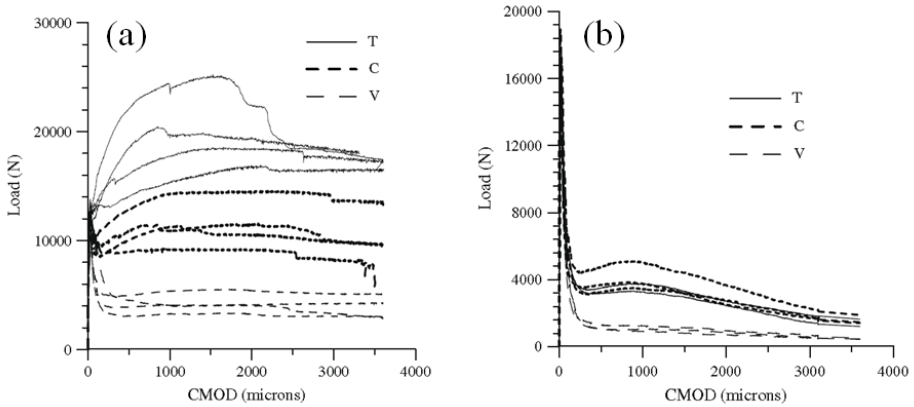

Figure 3-50: Load-CMOD curves from fracture tests poured from the centre (C), vertically poured (V) and poured after flowing in a inclined 5 m long tube (T) : (a) FR-SCC with the long steel fibres; (b) FR-SCC with 2.5 kg/m³ of 54 mm long polymer fibres (Torrijos, et al., 2010).

Concerning slabs, it has been found an exponentially decreasing relation between orientation factor and specimen thickness or height (Michels, et al., 2012). In the same sense, for structural thin elements, the residual mechanical properties can be quite different when diverse zones and directions were considered (Zerbino, et al., 2012). The authors used steel fibres 35 mm long and synthetic macro-fibres in low proportions (3 kg/m³) and concluded that although the fibre type influences the distribution and orientation of the fibres, the geometry of the structural elements seemed to be the main factor to be considered. Based on CT-scan results, some patterns of fibre orientation have been simulated and it was also found that the formwork surface plays a significant role among other factors in the final orientation of the fibres immersed on the concrete as shown in Figure 3-51 (Švec, et al., 2014). Rough surfaces reduced the rate of fluid shearing and thus the tendency of the fibres to orient to the flow direction. Subsequently, the flexural tests extracted from the cast slabs showed that the formwork surface can also have a strong influence on the resulting mechanical response, especially for structural elements with depth not large relative to their size.

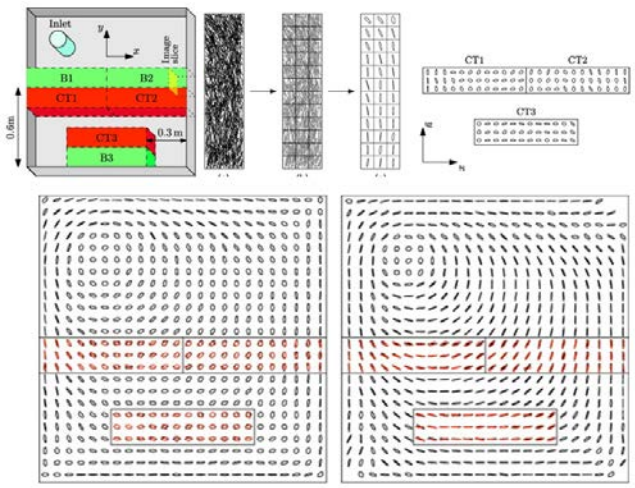

Figure 3-51: Scheme of the possibilities of CT-Scan combined with simulated fibre orientations (Švec, et al., 2014).

The increasing of the knowhow of manufacturing and processes as well as the better understanding of the material properties of FRC has boasted its use. The analysis of the causes and effects of non-homogeneous distributions of the fibres are framed in this relatively fast development of FRC because of the high scatter reported in flexural strength (Di Prisco, et al., 2009; Laranjeira, et al., 2011). Conversely, similar orientation states do not guarantee similar mechanical properties and therefore testing samples which mimic real components is still important for design of fibre-reinforced concrete structures (Şanal, et al., 2013). That is to say that predicting fibre orientation factor is not yet sufficient for the design of FRC. Moreover, most of the reported conclusions are questionable for macro-synthetic fibres that can fold and are low density compared with concrete.

3.7 FRC characterization as a structural material

It is clear at this point of this report that the behaviour of a structural FRC is not only governed by its constituent materials but also by the interface fibre/matrix properties, the reliability of the estimation of the actual positioning of fibres and their relative position to the stress and crack directions. All this features, that are additionally quite sensitive to a varied range of factors, may produce significant changes in the performance of FRC. Yet, it is also clear that the structural contribution of the fibres is always related to their load-bearing capacity. That is to say, that the so-called structural role of the fibres is related to their tensile post-cracking strength, their stiffness after crack growth initiates and hence the improving of the overall structural integrity. Other enhancements in the composite performance that are not mechanical (or clearly related with carrying loads) are also structural requirements out of the scope of this thesis. Seeking reliability and the correct translation of material behaviour from tests to a real structure, the effectiveness of the fibre reinforcement due to the orientation and distribution considering the formwork and the placing conditions have been explained in previous subsections.

The aim of this chapter is to discuss about the material response and its translation to constitutive relations from test results. Some of them included in the existing codes for the design of the FRC elements, and some other are related to classical approaches or further possibilities. In such a sense, some considerations related with typology of the test and the constitutive models, experimental coefficients or specific comments applied to polyolefin based fibre-reinforced concrete were also under consideration in this subsection.

3.7.1 The constitutive relations

The description of the fracture behaviour of plain concrete, assessed in subsection 2.4 of the previous chapter, have significant differences due to the fibre-reinforcement nature, first and foremost, in what regards to the post-cracking area. Since fibre volume fraction remains very small, the behaviour before cracking occurs is analogous to that of plain concrete (Dupont, 2003). After the crack has formed, the stress transfer across the crack that fibres provide avoids the concrete from collapse. Analytical, cross-sectional or FEM-based models by means of cohesive or smeared crack approaches are available for computing and designing FRC structures. In most models, such designing tools are achieved by indirect analysis procedures to characterize the material response by experimental results. Empirical parameters and significant material safety factors are derived from the usual scattering and the reliability of the testing procedures and the overall variations in concrete production. The main issues are referred to flexural tensile response of the material although there exists a model that accounts for the shear capacity of SFRC

or other that even being fracture in mode I, correctly capture the localized shear failure mechanism (Foster, et al., 2006; Voo, et al., 2010).

In a direct approach, the constitutive relations are attained by splitting the composite material into its two major components: matrix and fibres. Ideally, treating the fibres as discrete entities and including the response of the micro-scale fibre-matrix system from pull-out models, constitutive relations can be built (Radtke, et al., 2010). Some authors have used such direct approaches in which the input parameters are basically the material properties of the fibres and the matrix and the behaviour of the system is provided by means of pull-out models, mainly attained from experimental data. Yet, the response of the composite is traditionally characterized by testing specimens in the mesoscale under direct or flexural tensile stresses. In such a sense, the so-called inverse analysis approach entails the procedure in which the experimental results are simulated by iterative fitting the parameters of an assumed shape of the constitutive diagram (Laranjeira, 2010).

A constitutive relation could be built by taking in account the main effects already discussed and with a scheme similar to the shown in Figure 3-52. One of the main models to address the problem is the so-called stress-crack width approach (σ-w relation) in which the behaviour in tension of FRC is split into two different stages: an initial linear elastic branch expressed in terms of σ-ε and the σ-w relationship for the post-cracking branch after the limit of proportionality. Such model is based on the Fictitious Crack Model posed by Hillerborg in 1976 (Hillerborg, et al., 1976; Hillerborg, 1980). The other non-linear approach has the advantage of a single σ-ε diagram representing the stress-strain relation from compressive maximum deformation of the concrete to the maximum tensile strain assumed for FRC in the same manner it is done for conventional steel-bar reinforcement. Among the simplified diagrams, a scheme of FRC constitutive law is shown in Figure 3-53.

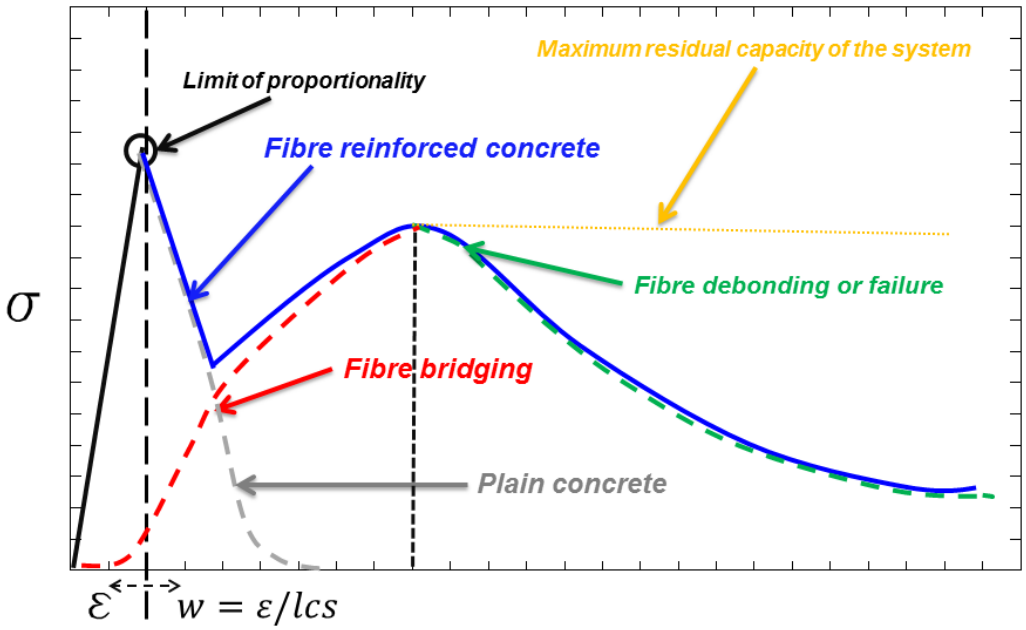

Figure 3-52: Conceptual bases of the discrete entities contribution to FRC constitutive relation.

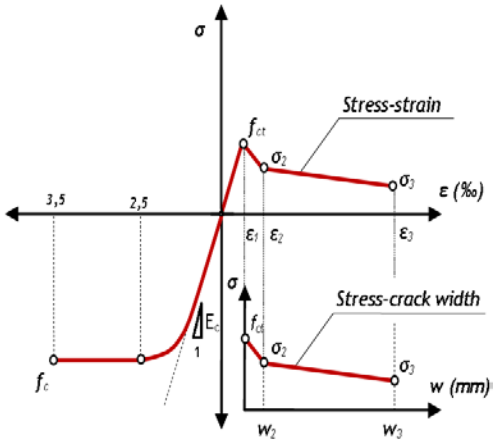

Figure 3-53: Simplified diagrams: scheme of FRC constitutive relation (Laranjeira, et al., 2010a).

3.7.2 Evaluation of post-cracking properties: testing methods

In order to develop a design tool that can reliably and accurately describe the behaviour of the fracture post-cracking stress softening in FRC materials, the definition of a stress-crack opening (σ-w) diagram such as in Figure 3-52 has proved to be a very practical solution. A huge amount of research effort, spanning for more than 50 years, have been devoted to develop testing methods to assess the parameters needed for the σ-w curve definition. This effort has produced a series of testing regulations in different countries and international institutions. The main testing types are briefly described below.

The uni-axial tension test as described in (RILEM TC 162-TDF, 2001) can be used to determine the tensile strength and the softening parameters defining the σ-w curve in FRC. The test uses a notched cylindrical specimen with both ends fixed with respect to rotation. It is conducted under controlled tensile displacements. The test set-up, as sketched in

Figure 3-54(a) is rather complex and demands highly trained and experienced personnel. Therefore, the uni-axial tension test is quite expensive and time consuming, and are not considered an appropriate method for practical material testing and only adequate for research purposes in specialised laboratories.

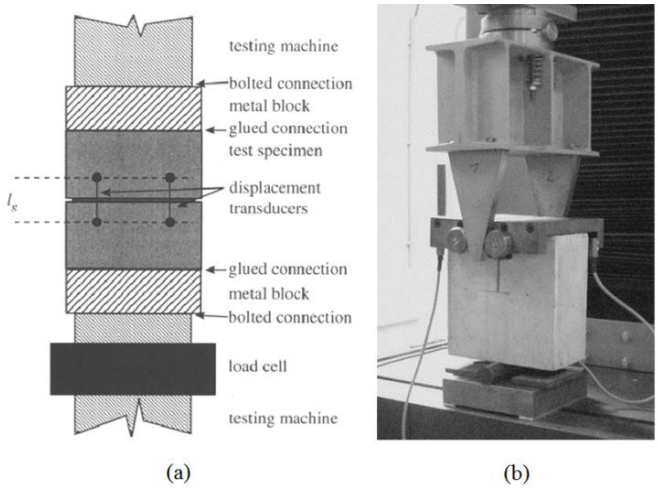

Figure 3-54: (a) An example of uni-axial tension testing for concrete (RILEM TC 162-TDF, 2001); (b) Wedge splitting test (Slowik, et al., 2006).

A somewhat simpler test is the wedge splitting test. In this test a prismatic specimen is split by means of a steel wedge pressed between roller bearings inserted on both sides of the specimen notch as a can be seen in Figure 3-54(b). The applied load on the wedge and the CMOD are measured as the test is performed.

The most economical and practical tests to determine the post-crack behaviour and assessing the influence of different conditions such as fibre types and dosage without compromise the reliability of the model are the bending tests. The three-point bending test as per (RILEM TC-162-TDF, 2002) uses beams of 150 x 150 mm cross section in a 500 mm span loaded in the middle of the upper face. A transverse notch of standard dimensions is made in the middle of the lower specimen face, in the same cross section where the load is applied. This set-up, as in Figure 3-55, ensures that the crack is formed in this predefined position, making simpler the crack control than in un-notched beams. This is the test recommended and defined in rules UNE-EN 14651 (EN 14651:2007+A1, 2007).

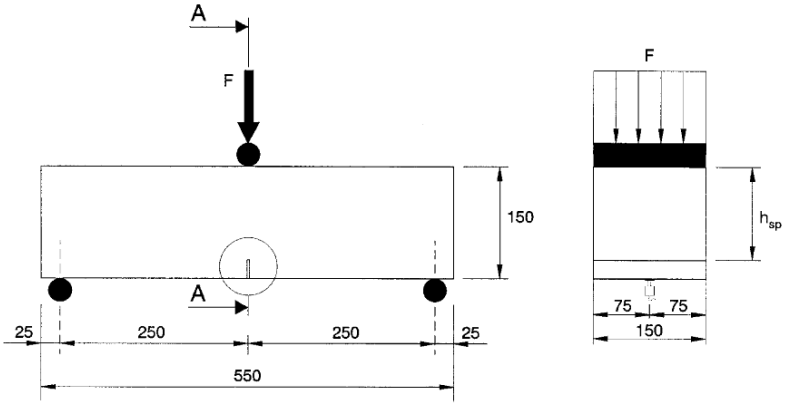

Figure 3-55: Test setup in (EN 14651:2007+A1, 2007).

Four point bending tests have also been adopted by some country national recommendations. The 150 x 150 mm cross section is loaded with two equal loads applied in both sides of the middle third of the span. The beam span is now 300 mm , un-notched, as per the present version of German Rules NBN B 15-238 (DBV, 1992) or as per Italian Rules UNI 11039 (CNR-DT 204, 2006). A typical set-up is shown in Figure 3-56. The advantage of the four point un-notched test is that the first crack will appear at the weakest section, therefore providing for the effect of variation of material strength. The disadvantage is that the measuring of the crack opening is harder because the crack position cannot be predicted.

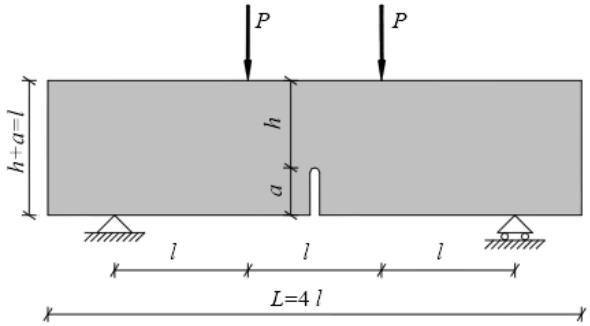

Figure 3-56 : Four-point bending test in UNI 11039 (CNR-DT 204, 2006).

The use of fibres in concrete has also a beneficial effect on the shear strength of sections. Many research reports indicate that the addition of steel or synthetic fibres significantly increases and shifts the failure mode from brittle to more ductile (Foster, et al., 2006). Nevertheless, the shear behaviour of FRC is still a challenge task due to the large amount of parameters involved. The post-crack shear resistance can be assessed based on either uni-axial tensile tests (Casanova & Rossi, 1997) or post-crack flexural strength from standard beam tests (RILEM TC 162-TDF, 2003). Specific laboratory specimens and tests can also be seen in (Barragán, 2002).

A close look at the behaviour of the fibre-bridged crack opening in the micro-scale fibre-matrix approach indicates that the fibres transmit tensile stress over the crack into the surrounding concrete. The fibre fracture would produce an undesirable brittle behaviour. Therefore, a good ductile performance should be based on keeping the fibre adhesive force to concrete to facilitate a pull-out mechanism in the crack opening. A number of parameters determine such ductile behaviour and avoid fibre failure such as fibre strength, matrix strength, number of fibres crossing the section, length of fibres, fibre geometry and surface, and fibre inclination angle to the crack plane. Figure 3-39 showed a typical set-up for a pull-out test. Pull-out tests results are used by some research teams to develop FRC constitutive relations by means of a direct analysis method (Naaman, 2003; Thorenfeldt, 2003).

3.7.3 On the tensile constitutive relations: codes and guidelines

In the specialised technical literature regarding the behaviour of FRC under tension stress, a number of different constitutive models can be found. Some of the models define the behaviour by relating applied stress to the specimen strain and produce some σ-ε diagrams. Other models prefer to define the behaviour of the FRC specimen under tension stress focusing on the post-cracking range and propos a stress- crack opening (σ-w) diagram. The initial use of fibres in concrete was only intended to control cracking and improve steel bar reinforcement durability. No consideration was given to the contribution of fibres to the post-cracking resistance. Although the experimental research on the use of steel fibres for concrete reinforcement started in the 1960's, it was not until the final year of the past century that the first codes and guidelines appeared.

In 1992, the German Code (DBV, 1992) proposed a σ-ε relationship for the structural design of tunnel linings using steel fibres in concrete. In addition, ACI Committee 544 produced some design considerations in 1966 regarding the reinforcement of concrete by adding steel fibres to the mix. In the last 15 years USA, Japan and many European countries have published codes and guidelines that allow the practical design of structures considering fracture mechanics concepts to take into account the post-cracking residual strength under tension stress. Responding to their own internal demand European countries like Germany (DBV , 2001) or Spain (EHE-08, 2008) have produced and even revised their codes and design guidelines. A complete review of the European codes can be seen in (Blanco, et al., 2013).

At present FRC appears in the new CEB-FIB Model Code 2010, MC2010 (fib Model Code, 2010) and it is considered a reference for newer revisions of Eurocode 2 and national European guidelines. Some of the main features of Model Code 2010 are listed below.

1) In the post-cracking range, a material can be considered either hardening or softening. The hardening condition means that the material shows increasing tensile strength up to an ultimate value of strain ε_u = 1%. One of the reasons for including this distinction is that in some cases the hardening behaviour shown in one direction is related to softening behaviour in the orthogonal direction.

2) It establishes a material classification based on two post-cracking residual strengths at certain CMOD values which define the Serviceability Limit State, SLS, (CMOD = 0.5 mm) and Ultimate Limit State, ULS, (CMOD = 2.5 mm). The CMOD curves are to be assessed by three-point bending tests as per UNE EN 14651.

3) It defines two simplified σ-w constitutive diagrams in bending test results. A rigid plastic model and a linear post-cracking model each of them for hardening and softening materials as shown in Figure 3-57.

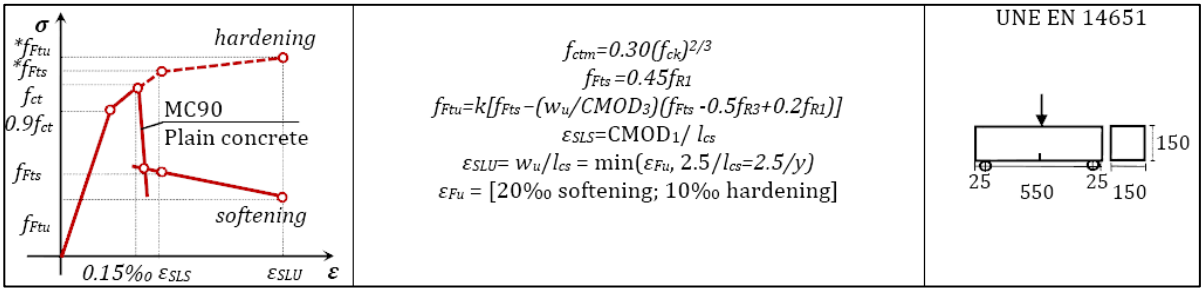

Figure 3-57: Constitutive models and tests of MC2010 [from: (Blanco, et al., 2013)].

4) Considering that continuum mechanics is governed by stress-strain (σ-ε) constitutive relationships while fracture mechanics is governed by a stress-crack opening (σ-w) law, the Code introduces the concept of the structural characteristic length, l_{cs}, for the structural element. This concept, initially proposed by Hillerborg (Hillerborg, et al., 1976), represents a "bridge" connecting continuous and fracture behaviours by defining the strain as w/l_{cs} . The values of l_{cs} have proposed by different authors as can be seen in Table 3-6 being h the height of the concrete element. The proposed general formulation to obtain this parameter can be seen in expression (3-10).

$$\varepsilon\,(y) = \varepsilon_u + \varepsilon_w = \frac{\sigma_u}{E_c} + \frac{w}{l_{cs}} \qquad (3-10)$$

5) It defines a simplified model to compute the ultimate residual tensile strength in uni-axial tension by means of the residual nominal bending strength as per Figure 3-58**.**

6) It distinguishes between structural and non-structural types of fibres, similarly to the Spanish Code (EHE-08, 2008). Fibres can be considered as structural if they have a high elastic modulus and if used in a certain dosages provide the FRC with a minimum performance in terms of toughness. This important distinction implies a significant change in FRC design since it extends the range of fibres that can be used for structural purposes and allowing partial or even total substitution of standard reinforcing bars by structural fibres.

Table 3-6: Proposed values for the reference length (De Montaignac, et al., 2012)

Reinforcement type	*lcs*	Reference
SFRC	*h*/2	(Ulfkjær, et al., 1995; Pedersen, 1996; Iyengar, et al., 1998; RILEM TC-162-TDF, 2002; Massicotte, 2004)
	2*h*/3	(AFGC-SETRA, 2002)
	h	(CNR-DT 204, 2006; fib Model Code, 2010)
	2*h*	(Strack, 2008; De Montaignac, et al., 2012)
SFRC and reinforcing bars	Min [s_m; *h*/2]*	(Massicotte, 2004)
	Min [s_m; *y*]*	(CNR-DT 204, 2006; fib Model Code, 2010)
	Min [s_m; *h*]*	(De Montaignac, et al., 2012)

*s_m was estimated with the Eurocode -2 (European Committee for Standardization, 2004)

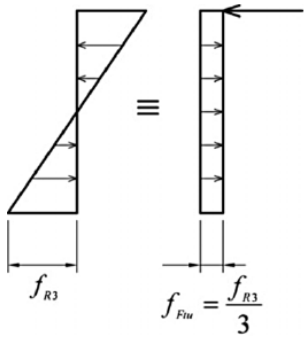

Figure 3-58: Simplified model adopted to compute the ultimate residual tensile (Di Prisco, et al., 2013)

PART II: EXPERIMENTAL CHARACTERIZATION OF THE MATERIAL

Chapter 4

Mechanical properties and fracture behaviour of polyolefin fibre-reinforced self-compacting concrete

4.1 Introduction

Although the characteristics of the fibres added to concrete are decisive for the composite material mechanical properties, there are other parameters that should be taken into account, such as the fibre content or the alignment of the fibres with the stress distribution (Zerbino, et al., 2012). The combination of SCC and FRC may permit a changing of fibre orientation and distribution by means of the flow properties of SCC, as has been already shown in SFR-SCC (Stähli, et al., 2008). Bond strength has also revealed some improvements for reinforced and prestressing steel and is a possible additional contribution of SCC to fibre reinforcing. However, the effect of the SCC flow has not yet been studied with polyolefin macro fibres. Even though this could be a good reason to develop a self-compacting concrete reinforced with polyolefin fibres, there are some other additional advantages such as a possible reduction of conventional reinforcement and uniformity, and hence excellent quality of the material obtained, that might merit consideration. Another factor that should not be overlooked is the rise in steel prices in the last decade which, if they continue, could increase the price of the more common SFRC (Jerrett & Cuddington, 2008) leaving it out of the market.

In order to broaden the application field of the synthetic fibre-reinforced concrete and of SCC at a reasonable cost, the possibility of producing it with moderate cement and admixture contents and reinforced with polyolefin fibres is studied in this chapter. This research is performed through adding several amounts of polyolefin fibres, ranging from

three to 10 kg/m³, to a reference SCC becoming a concrete named polyolefin fibre-reinforced self-compacting concrete (PFR-SCC). In addition to these mixtures, two concretes with 10 kg/m³ of polyolefin fibres were produced with a slight change in the skeleton of the aggregate that enhanced its fresh-state properties, with one having an adhesion improver admixture to test its influence on the concrete. As the compressive strength and tensile strength of fibre-reinforced concrete have been thoroughly studied in the last decades in both types of fibres, steel (Song & Hwang, 2004; Wafa & Ashour, 1992) and synthetic fibres (Song, et al., 2005), the fracture mechanisms and fracture energy of synthetic fibres-reinforced concrete is still a matter of interest. Furthermore, it is in fracture processes where the fibres absorb energy and provide ductility and toughness to the composite material with a brittle matrix.

Therefore, the fresh-state behaviour, hardened and fracture properties, and the flexural and toughness improvements that the polyolefin fibres provide to the control SCC are assessed. Furthermore, to evaluate the possibility of replacing SFRC for PFRC, a conventional SFR-SCC was manufactured using the same SCC mix. The influence of the fibres in the fresh state, mechanical properties, fracture fibre mechanisms and fibre-matrix interactions of PFR-SCC and SFR-SCC were compared in this research.

4.2 Materials and methods

4.2.1 Materials

A Portland cement type EN 197-1 CEM I 52.5 R-SR 5 was used in this study. A mineral admixture of limestone powder as micro-aggregate was employed with specific gravity and Blaine surface of 2700 kg/m³ and 400-450 m²/kg respectively. The calcium carbonate content of the limestone powder was higher than 98% and less than 0.05% was retained in the 45 µm sieve.

Concrete mixtures were manufactured with siliceous aggregates composed of two types of gravel 4-8 mm and 4-12 mm and sand of 0-2 mm. The grading of the aggregates and their physical properties are shown in Table 4-1 and the grading curve are shown in Figure 4-1. The maximum aggregate size was 12.7 mm. The proportion for dry maximum packing density of the aggregates was obtained based on the ASTM C29/29M-09 with the result for the optimum aggregate skeleton shown in Table 4-2.

To achieve the desired self-compacting properties an admixture named Sika Viscocrete 5720, which is a polycarboxylate based superplasticizer with a solid content of 36% and 1090 kg/m³, density was employed. The bond improver admixture Sikatell 250 was used in one of the concrete mixtures.

The polyolefin fibres on which behaviour the research was focused were 60 mm long, with a surface treatment and rough texture shown in Figure 4-2. The mechanical and physical properties of these fibres and the characteristics of the regular steel fibres added to the control SFRC are included in Table 4-3.

Table 4-1: Properties of coarse aggregate and sand.

Grading curve	% passing		
	Coarse		Fine
Sieve diameter (mm)	Gravel	Grit	Sand
16	100	100	100
12.7	99.86	100	100
8	6.24	94.65	100
4	0	17.35	99.83
2	0	1.98	97.67
1	0	1.12	82.82
0.5	0	0.90	39.03
0.25	0	0.54	12.53
0.125	0	0	2.58
0.063	0	0	1.54
Bottom	0	0	0
Surface-dry particle density (kg/m³)	2602	2622	2558
Saturated surface-dry particle density (kg/m³)	2615	2626	2584
Water absorption (%)	0.5	0.17	1.01

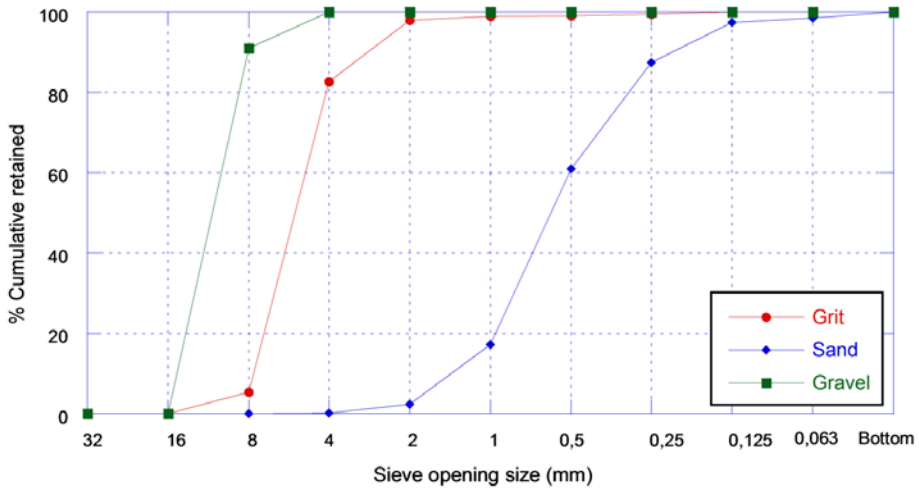

Figure 4-1: Grading curves of the aggregates.

Table 4-2: Proportion of aggregates for dry maximum packing density.

Aggregate	Value (%)
Gravel	24
Grit	16
Sand	60

Table 4-3: The physical and mechanical properties of fibres.

Fibre type	Density (g/cm³)	Length (mm)	Eq. Diameter (mm)	Tensile strength (MPa)	Modulus of elasticity (GPa)	Fibres per kg	Surface structure	Anchorage
Polyolefin fibre	0.910	60	0.903	>500	> 9	27000	Rough	Bond
Steel-hooked fibre	7.850	35	0.550	1100	210	14500	Smooth	Hooked

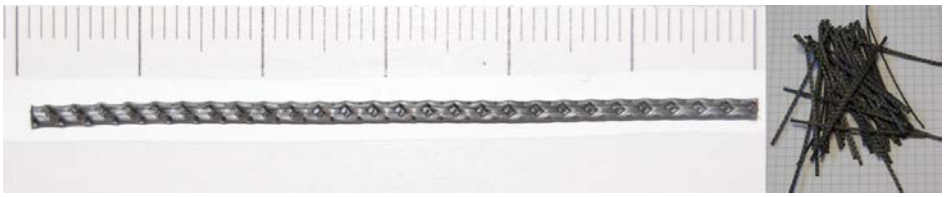

Figure 4-2: Polyolefin fibres (scale in mm).

4.2.2 Mix proportioning

The SCC used was developed and previously tested to fit with the initial requirements of achieving a medium-strength concrete that maintains the self-compactability properties even after the incorporation of fibres. In order to do so, some initial trial mixtures were performed to obtain a concrete mix design with as low a cement and admixture content as possible but without harming its self-compacting properties when fibres were added. In these trial mixtures, up to 6 kg/m³ of polyolefin fibres were added to the mix.

For the paste design, the cement required was at least 375 kg/m³ with a 1.25% of cement weight of Sika Viscocrete-5720 admixture and a water-to-powder ratio of 0.50. The limestone powder addition remained 200 kg/m³, with the paste representing 38% of the total concrete volume. The proportions of the aggregates were those obtained for the maximum dry packing density, shown in Table 4-2, and represented 25.5% of voids. The humidity of the aggregates was corrected before the manufacture of the concretes and the time schedule followed is shown in Table 4-4 and the sketch of the procedure in Figure 4-3.

Table 4-4: Mixing procedure.

Process	Duration of mixing process (s)
1. Homogenization of aggregates	60
2. Add 1/3 of fibres and mix	30
3. Add cement and limestone powder	30
4. Add 1/3 of fibres and mix	30
5. Add 75% of the mixing water and mix	30
6. Add 1/3 of the fibres and mix	30
6. Add 25% of the water with superplasticizer	240
7. Rest (superplasticizer acting period)	150
8. Final mix	120

Concrete mixtures were divided in three groups: control mixtures, moderate-fibre and high-fibre content mixtures.

The first control mixture was designed as a plain self-compacting concrete with no fibre addition (C0). The second control concrete was defined based on the same self-compacting concrete but adding 26 kg/m³ of hooked steel fibres (S26).

Three PFR-SCC with moderate fibre contents were designed by adding three (P3), four and a half (P4.5) and six (P6) kg/m³ of polyolefin fibre, respectively, to the same mix proportions used for the reference plain SCC (C0).

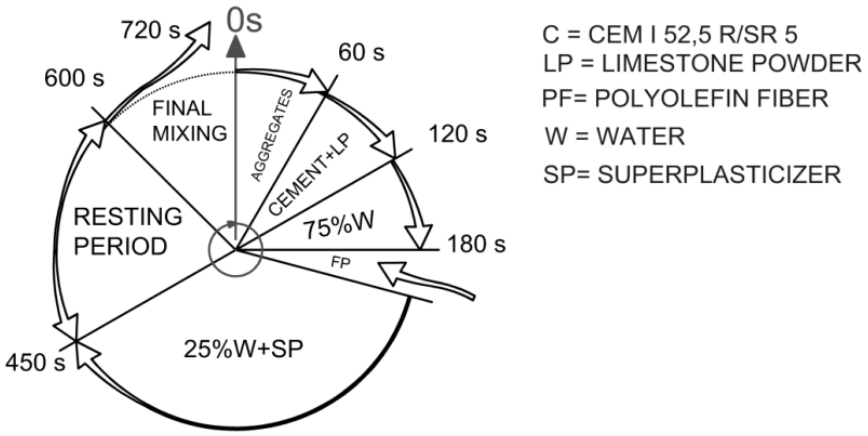

Figure 4-3: Mixing sequence.

Table 4-5: Concrete mix proportions.

	Control		Medium-fibre content			High-fibre content		
Material	C0	SC	P3	P4.5	P6	P10a	P10b	P10M
Cement (kg/m^3)	375	375	375	375	375	375	375	375
Limestone powder (LP) (kg/m^3)	200	200	200	200	200	200	200	200
Water (kg/m^3)	187.5	187.5	187.5	187.5	187.5	187.5	187.5	187.5
Sand (kg/m^3)	918	918	918	918	918	918	991	991
Grit (kg/m^3)	245	245	245	245	245	245	213	213
Gravel (kg/m^3)	367	367	367	367	367	367	320	320
w/c	0.50	0.50	0.50	0.50	0.50	0.50	0.50	0.50
Steel fibres (kg/m^3)	-	26	-	-	-	-	-	-
Polyolefin fibres (kg/m^3)	-	-	3	4.5	6	10	10	10
Superplasticizer (kg/m³)	4.7	4.7	4.7	4.7	4.7	4.7	4.7	5.6
% cement weight	1.25	1.25	1.25	1.25	1.25	1.25	1.50	1.50
Bond improver admixture (kg/m³)	-	-	-	-	-	-	-	7.5
% cement weight	-	-	-	-	-	-	-	2.00

When higher fibre content was added to the mix, 10 kg/m³, two different aggregate proportions were used. On the one hand, the same proportions were used for the C0 mixture so that direct comparison could be made (P10a). On the other hand, another mixture was produced in which the proportion of sand was increased up to 65% of the total content of

the aggregate to ease a better and more uniform distribution of fibres in the slump-flow test (P10b). For this mixture, the gravel and grit proportions were readjusted to 14% and 21% and the superplasticizer slightly increased to 1.50% of cement weight. The composition P10b was also used for one mixture where the adhesion improver was added (P10M). The composition of each concrete performed can be seen in Table 4-5.

4.2.3 Experimental program and test methods

For every concrete type, nine cylindrical specimens and four prismatic specimens of dimensions 150 x 300 mm² (diameter-height) and 430 x 100 x 100 mm³ (length-height-width) respectively were cast. All specimens were cured in a climatic chamber (20ºC and 95% humidity) until the age of testing. The characterization of the fresh-state properties was estimated on each mixture by means of the slump-flow test and V-funnel test following the standards EN 12350-8 (EN 12350-8, 2010) and EN 12350-9 (EN 12350-9, 2010). In order to produce the volume of concrete needed two batches of each type of concrete were produced.

Properties of the hardened concrete were measured by using the cylindrical samples. Compressive strength was obtained according to the standard EN 12390-3 (EN 12390-3, 2009) with an age of seven and 28 days. For the tensile strength, the tensile splitting test was carried out following the EN 12390-6 (EN 12390-6, 2009) standard. The Young's modulus was also estimated according to the ASTM C469-02e1 standard (ASTM C469-02e1, 2006).

The fracture behaviour tests were carried out in accordance with RILEM TC-187 SOC (RILEM TC-187-SOC, 2007) using three prismatic specimens. The setup of the three-point bending test, according to the standard noted above, was made in accordance with the depth of the beam. A span-to-depth ratio of 3.0 and a notch in the centre of the span of 1/3 of the depth were chosen with the loading cylinder above the notch. The test geometry setup is shown in Figure 4-4.

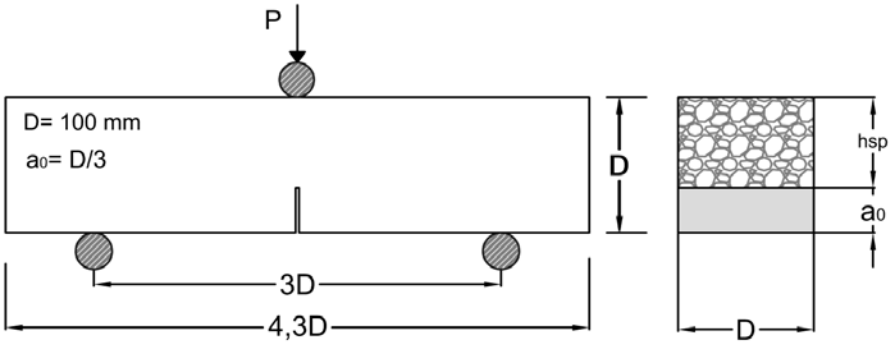

Figure 4-4: Three point bending test setup.

The test was performed with crack mouth opening displacement control (CMOD) by using a clip-on gauge device. Two more extensometers, linear variable differential transformer (LVDT) devices, were also placed on each side of the sample to measure the deflection. During the test, time, load, deflection, CMOD and also the machine actuator position were recorded. In the case of the FRC, the fibres absorbed energy and controlled the crack growth during the fracture process (Zollo, 1997). Regardless of it being due to fibre rupture, fibre bridging, fibre pull-out, fibre debonding or matrix cracking, these mechanisms prompted much higher deformations than regular concrete and the upper bound of the CMOD device was exceeded. In order to continue with the test, when the upper bound of

the referred device was reached, the control of the fracture test was changed to the machine actuator position. With the latter, it was possible to obtain deflection values up to 15 mm. Nonetheless, all the tests were stopped without reaching the collapse of the sample.

4.3 Results

4.3.1 Characterization in fresh state

Table 4-6 summarizes the fresh-state test results for all the concrete mixtures. All the results were within the most common standards, which set a slump-flow spread from 550 mm to 850 mm, a time for the slump-flow patty to reach 500 mm of diameter lower than 8 s, and an emptying time of the V-funnel between four and 20 seconds. It should be pointed out that before the bond improver admixture was incorporated into the mix in the P10M production process, a partial sample of the mix was extracted and a slump-flow test performed with a result of 580 mm. However, after adding the admixture the result was 535 mm.

Table 4-6: Test results for assessment of fresh concrete and mechanical properties.

		Control		Medium-fibre content			High-fibre content		
Test	Parameter	C0	SC26	P3	P4.5	P6	P10a	P10b	P10M
Slump-flow test	T_{500} (s)	3.5	3.5	3	3.5	4	6	4	7
	d_f (mm)	655	570	642	600	590	570	580	580(535)
V-funnel test	T_V (s)	8	14	12	11	16	20	16.5	15.5
Compressive strength	$f_{ck,7d}$ (MPa)	34.9	34.2	35.1	34.4	36.7	32.9	32.6	30.3
	c.v.	(0.02)	(0.06)	(0.03)	(0.06)	(0.02)	(0.02)	(0.02)	(0.01)
Compressive strength	$f_{ck,28d}$ (MPa)	39.3	41.7	39.3	38.5	41.4	36.9	37.0	35.5
	c.v.	(0.01)	(0.01)	(0.01)	(0.06)	(0.01)	(0.02)	(0.02)	(0.01)
Elasticity Modulus	E (GPa)	35.8	33.7	36.5	31.2	31.6	36.1	30.9	31.2
	c.v.	(0.03)	(0.01)	(0.02)	(0.01)	(0.02)	(0.02)	(0.01)	(0.01)
Indirect tensile strength	f_{ct} (MPa)	3.78	5.32	4.38	4.18	4.09	4.33	4.95	4.78
	c.v.	(0.14)	(0.15)	(0.09)	(0.20)	(0.03)	(0.09)	(0.03)	(0.05)

4.3.2 Mechanical properties

The most representative mechanical properties, compressive strength (EN 12390-3, 2009), indirect tensile strength (EN 12390-6, 2009) and elasticity modulus (ASTM C469-02e1, 2006) were measured in the cylindrical specimens. Compressive strength was obtained at seven days with one sample of each mixture and the 28- day test carried out with three specimens of each mixture. Tensile strength was assessed through splitting tests on two specimens of each mixture at 28 days. The elastic modulus was obtained through performing the test at 28 days. The results are shown in Table 4-6 as well as their coefficient of variation (c.v.).

4.3.3 Fracture results

With the data registered during the tests, the curve load versus CMOD and the curve load versus deflection were plotted. Due to the limited reading obtained with the CMOD device, the load-CMOD curves were represented only up to an opening crack mouth displacement of 4 mm. The load-deflection curves were recorded up to greater deflection, as previously commented. Given that the RILEM TC-187 SOC followed was performed for plain concrete, quasi-brittle failure was expected. However, as no FRC specimens collapsed the limit of the test was set at 8 mm deflection in order to obtain the fracture energy. The peak load (L_{PEAK}) was the maximum value before cracking and may be seen with the total fracture energy in Table 4-7 as well as their standard deviation.

Table 4-7: Mean values of the fracture energy and the peak load.

	Control		Medium-fibre content			High-fibre content		
	C0	SC26	P3	P4.5	P6	P10a	P10b	P10M
L_{PEAK} (N)	4970	5975	5674	5655	5994	5182	5316	5413
	(0.04)	(0.06)	(0.03)	(0.01)	(0.01)	(0.05)	(0.16)	(0.01)
G_F (N/m)	130	2621	835	1825	2781	3271	2865	4330
	(0.05)	(0.05)	(0.07)	(0.42)	(0.24)	(0.20)	(0.26)	(0.10)

Reference SCC fracture results (C0)

The curves resulting from fracture tests of the reference SCC (C0) are plotted in Figure 4-5. Observation of the curves reveals that the fracture behaviour of the three specimens tested showed the characteristic softening post-cracking curve of concrete (Elices & Planas, 1996). Such quasi-brittle cracking behaviour fitted the behaviour expected for conventional concrete and was comparable with the regular concrete softening curves (Fava, et al., 2003). As the material had hardly any capacity to bear any load after the peak load no other values, aside from G_F and L_{PEAK} could be analysed. It should be pointed out that the results showed very low dispersion.

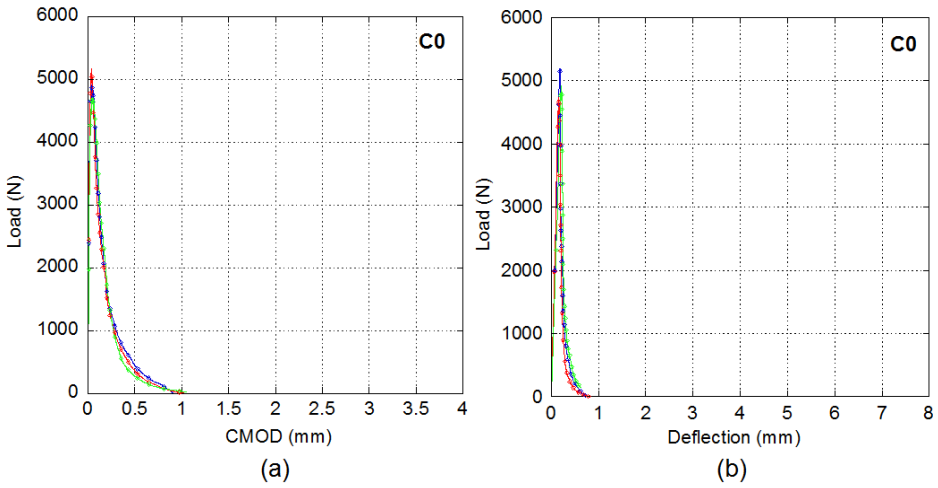

Figure 4-5: Fracture curves for three specimens of C0: (a) Load - CMOD curve; (b) Load - Deflection curve.

SFR-SCC fracture results (SC26)

The fracture curves for the concrete reinforced with steel-hooked fibres are shown in Figure 4-6. The shape of these curves, load-CMOD and load-deflection, showed a post-cracking short softening stage down to values around 60% of the peak load where the curve stayed almost steady up to an approximate CMOD value of 1.8 mm. The first unloading process caused, whether due to the failure of the fibre anchorage or to the failure of the fibre itself, was pronounced and followed by a small load recovery. Indeed, a staggered curve took place. The three tested specimens behaved similarly and there was almost no dispersion among them, as may be seen in Figure 4-6.

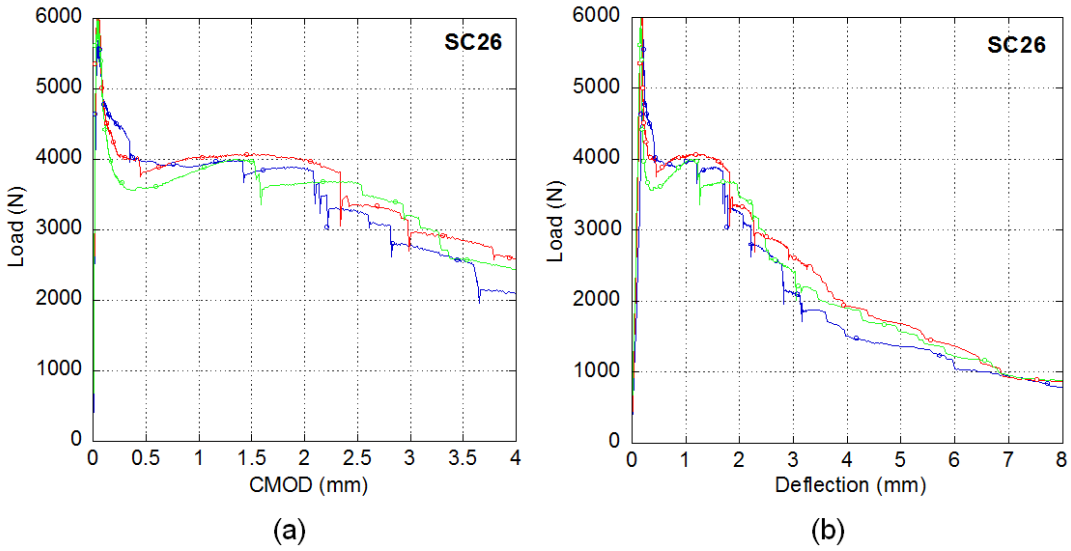

Figure 4-6: Fracture curves for three specimens of SC26: (a) Load - CMOD curve; (b) Load - Deflection curve.

PFR-SCC with moderate fibre content (P3, P4.5, P6) fracture test results

The fracture curves obtained in the different concrete types with moderate amounts of polyolefin fibres P3, P4.5 and P6 were meaningfully smoother than those obtained for SC26. The curves shown in Figure 4-7, Figure 4-8 and Figure 4-9 could be divided in three distinct trends that start or begin at three remarkable turning points. These were defined for the changing of trends that took place for the peak load, a minimum post-cracking value after a softening stage and the maximum post-cracking load. Once the minimum post-cracking value was reached, part of the energy released in the process of fracture was absorbed by the fibres and the load values increased again. Subsequently, the specimen began loading again due to the fibre capacity to absorb this energy. This trend continued up to values of deflection of around 4.5 mm with a maximum remaining load value. From that point on, the second unloading process took place. This process can only be seen in the load deflection curves due to the previous saturation of the CMOD device.

The contribution of 3 kg/m³ of polyolefin fibres seemed to be the lowest threshold capable of preventing the collapse of the specimen. Even with this small quantity, fibres were able to absorb the energy released in the fracture process and increase the load bearing capacity. This implies an increment in ductility when compared with the reference concrete without fibres (C0). The load values for the minimum post-cracking turning point were around 10% of the peak load and the remaining load was slightly higher at up to around 16% of the peak

load. The dispersion was small with analogous results for the three samples, as may be observed in Figure 4-7.

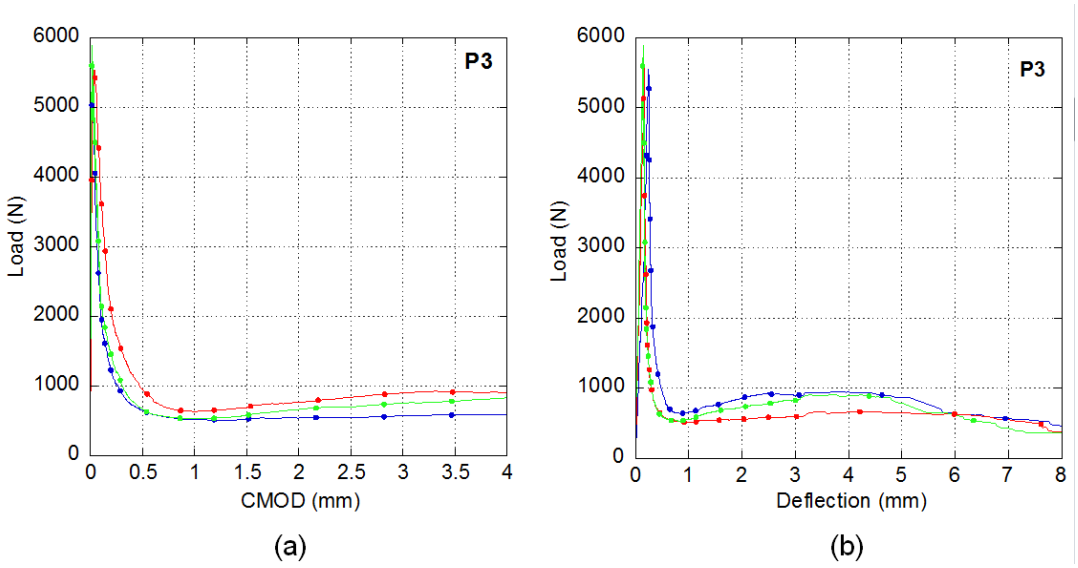

Figure 4-7: Fracture curves for three specimens of P3: (a) Load - CMOD curve; (b) Load - Deflection curve.

When the polyolefin fibre content was increased up to 4.5 kg/m³ the results showed higher dispersions, as may be seen in Figure 4-8. The previously mentioned behaviour for the P3 mixture was more pronounced due to the higher values of the minimum of post-cracking load (up to 20% of the peak load) and the remaining post-cracking load which reached values close to 40% of the peak load. It is interesting to highlight that the values of deflection and CMOD were analogous to those found in P3 for the turning points pointed above. The higher dispersion may have been caused by the lack of uniform distribution of fibre. This phenomenon might have occurred either because of the behaviour of the fibre on the concrete flow when filling the moulds or by the wall effect (Torrijos, et al., 2010).

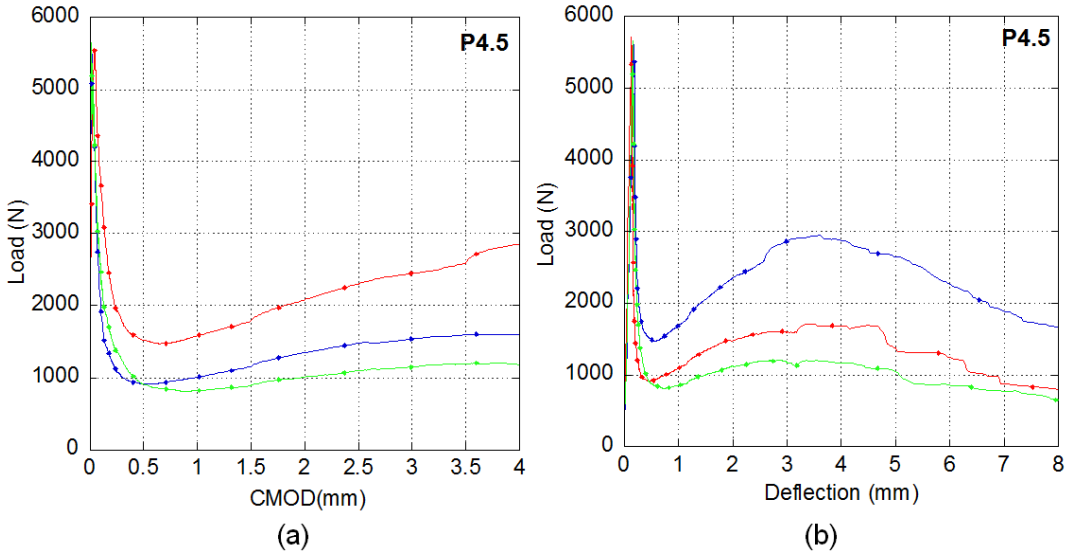

Figure 4-8: Fracture curves for three specimens of P4.5: (a) Load-CMOD curve; (b) Load - Deflection curve.

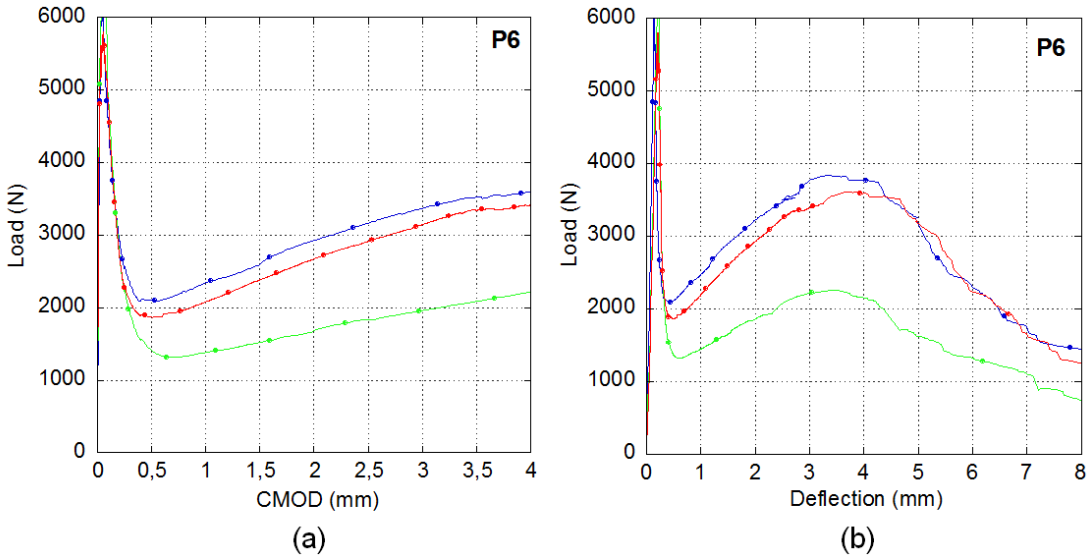

Figure 4-9: Fracture curves for three specimens of P6: (a) Load-CMOD curve; (b) Load - Deflection curve.

This tendency continued when 6 kg/m³ of fibres were added to the SCC mix It can be noticed not only in the greater values of the turning points previously mentioned but also in the dispersion of the results obtained. In Figure 4-9 the fracture curves of P6 mixture were analysed in a similar way to that performed in concretes P3 and P4.5. The first unloading softening process led to a minimum post-cracking load around 30% of the peak load. Afterwards the load increasing trend after this point reached even 50% of the peak load. It should be noted that both CMOD and deflection values corresponding to those turning points also remained in comparable values with the previously analysed P3 and P4.5 mixtures.

Self-compacting concrete with high polyolefin fibre content (P10a, P10b, P10M) fracture test results

The aim of developing a campaign with high polyolefin fibre content (10 kg/m³) was to reach improved mean values in the fracture curves that could be close to those found for SC26. Furthermore, as the number and distribution of fibres may be decisive in the test result dispersion, a greater degree of uniformity was expected in the results.

In Figure 4-10, the results for the mixture with 10 kg/m³ of fibres and with no change in the proportions of the aggregate (P10a) are shown. The curves were analogous to the P6 mixture with the three trends previously mentioned. In the load-CMOD curve, the turning point after the first softening post-cracking branch took values of load around 40% of the peak load and CMOD values close to 0.5 mm (which is similar to the previous results of P3, P4.5 and P6). Through observation of the load-deflection curve, it may be seen that one of the specimens remaining load was close to the peak load. There is a sharp rising of load at that point, noticeable in Figure 4-10 (b), and it is therefore necessary to clarify that it occurred when the test control changed from CMOD control to actuator position control. Leaving aside that top value, the remaining load reached around 90% of the peak load before it began the descending branch. Once again, these aforementioned deflection values corresponding to the remaining load were close to 4.5 mm. Even for the specimen with the lowest mean value, the minimum post-cracking load was around 2000 N. In this sample, the

reloading slope was not as steep as in the other two specimens tested. Dispersion, consequently, was still significant on the remaining post-cracking load recorded.

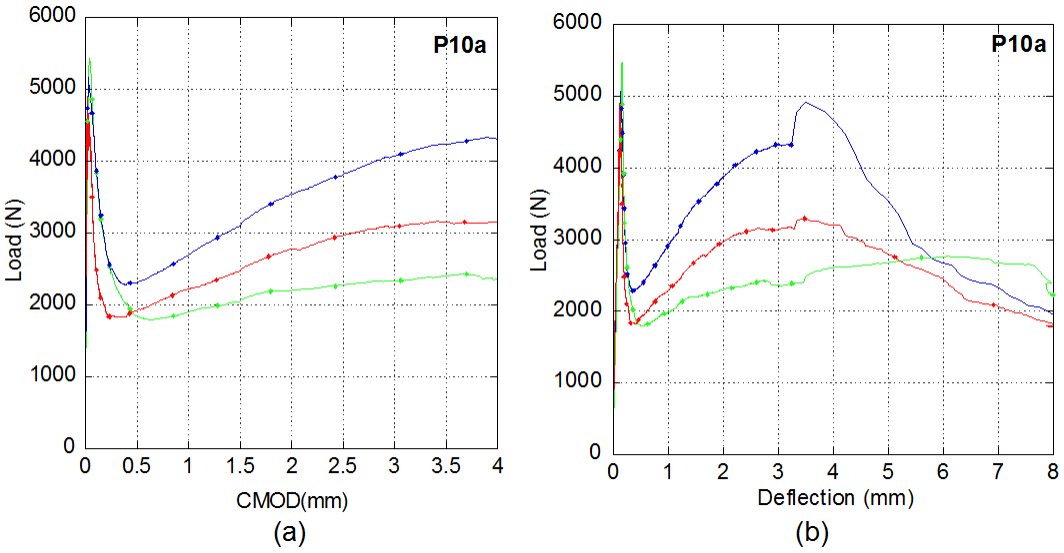

Figure 4-10: Fracture curves for three specimens of P10a: (a) Load - CMOD curve; (b) Load - Deflection curve.

For the mixture P10b, as the amount of sand was increased it had less coarse aggregate which meant that the self-compacting ability of the concrete was improved. As may be observed in Figure 4-11, the results were very similar to those obtained with P10a although the load values were slightly lower. The values of the minimum post-cracking loads were around 2000 N and the values of the remaining load stayed within the gap 2300-4200 N, showing analogous dispersion on the remaining post-cracking load.

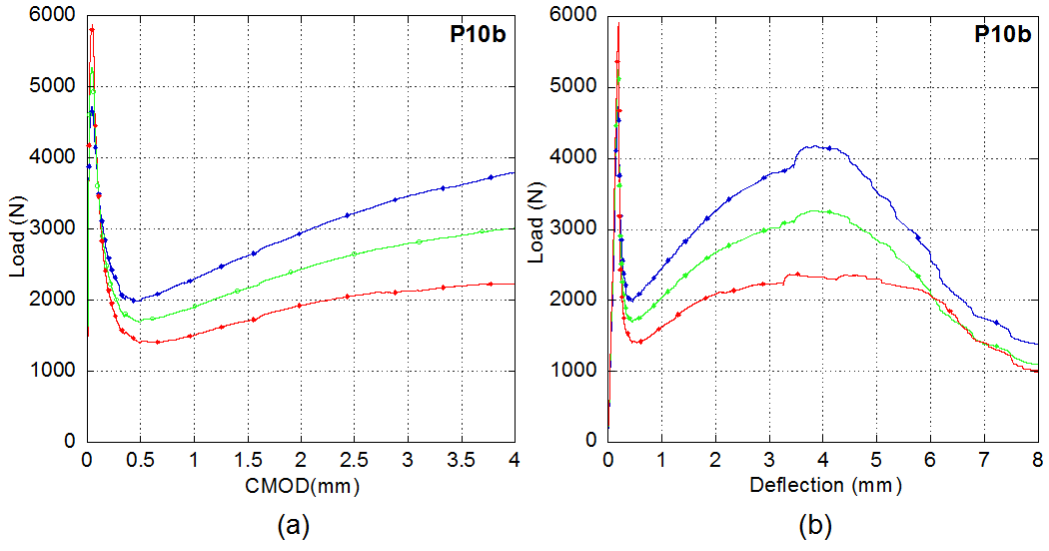

Figure 4-11: Fracture curves for three specimens of P10b: (a) Load - CMOD curve; (b) Load - Deflection curve.

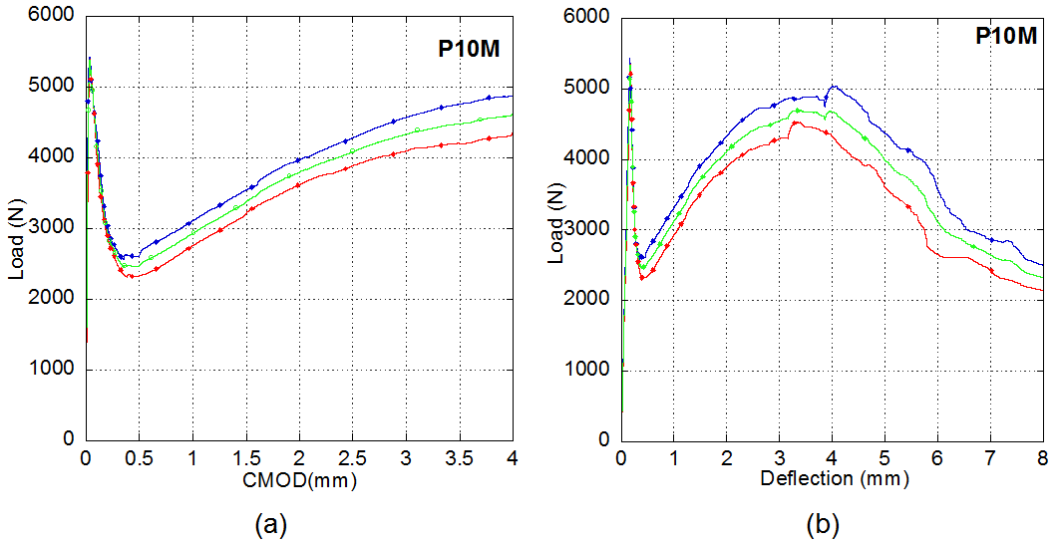

Figure 4-12: Fracture curves for three specimens of P10M: (a) Load - CMOD curve; (b) Load - Deflection curve.

In Figure 4-12, the fracture curves obtained from the test results of the mixture P10M are plotted. The tests showed a noteworthy small dispersion on the results. The minimum post-cracking load after the first unloading process reached approximate values of 2500 N which is 45% of the peak load with CMOD values being close to 0.5 mm. The remaining load before the final unloading process was higher than 85% of the peak load, being the CMOD value close to 4.5 mm as in the rest of the mixtures tested. It is also noticeable that for higher displacements, even 8 mm, the fibres still bore load values similar to the minimum post-cracking load.

4.4 Discussion

4.4.1 Fresh-state behaviour

All the concretes showed a good self-compacting behaviour across the tests performed. However, the reduction of the slump-flow spread was higher as the amount of fibres added grew. The results on the slump-flow test showed that medium contents of polyolefin fibres had less influence on the self-compacting properties of concretes than steel fibres.

As may be seen in Figure 4-13(a), for medium polyolefin fibre content (P3, P4.5 and P6), the results were homogeneous with no segregation signs. However, if Figure 4-13(b) is observed, when 10 kg/m³ of polyolefin fibre was added to the same mix proportioning, some non-homogeneous distribution of the fibres could be noticed. To obtain an improvement in the results of the slump-flow-spread and also T_{500} the mixture P10b was developed. The distribution of the fibres in P10b may be seen in Figure 4-13(b). When the slump-flow test was carried out for the P10M mixture after adding the bond improver admixture Sikatell 250, the distribution of fibres and aggregates was uniform with no segregation signs.

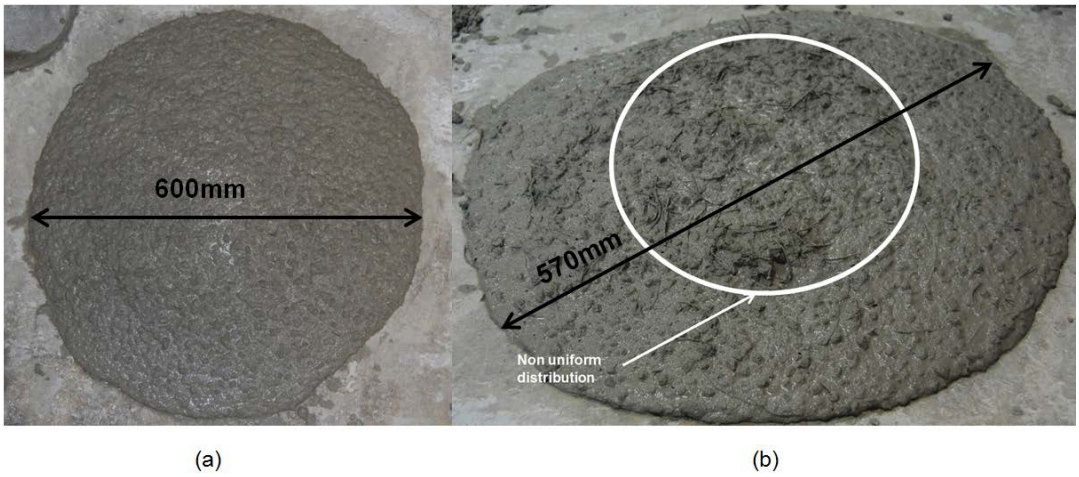

Figure 4-13: Slump-flow spread: (a) mixture P4.5; (b) mixture P10a.

As regards of the V-funnel test results, an increment in the emptying times as the fibre content grew was observed, with it being noticeably higher than those registered in the reference SCC (C0). The change in the skeleton of the aggregate in P10b and P10M mixtures enabled emptying times of the V-funnel close to the results of P6. Also, the results of P10b and P10M were analogous to those obtained in S26, even though the volume fraction of these PFR-SCC was three times higher.

Mechanical properties discussion

The compressive strength obtained for the moderate polyolefin fibre content specimens (P3, P4.5 and P6) was within the values of the two control mixtures, C0 and SC26, and close to a mean characteristic compressive strength of 40 MPa. No noticeable dispersion was found in any of the concrete mixtures.

However, when 10 kg/m³ of polyolefin fibres were added to the mix (as in the P10a, P10b and P10M mixtures) the compressive strength decreased to 37 MPa and even lower, down to 35.5 MPa, for the mixture with bond improving admixture. This phenomenon might have been caused by a lesser degree of compaction caused both by the high amount of fibres and by mechanical properties of fibres.

There was a change in the failure mode of the specimens when polyolefin fibres were added. The C0 specimens failed with the typical cones and brittle fracture abrupt mode while all the specimens with fibres showed a very smooth fracture without any mass loss.

With regard to elasticity modulus, the results showed no clear trend, though some minor differences were obtained probably due to a worse compaction. These small differences cannot be attributable to the properties of fibres itself since all of the results were in the gap of the logical experimental dispersion and in agreement with previous results found in literature (Altun, et al., 2007; Thomas & Ramaswamy, 2007).

The tensile strength of all the fibre-added concretes was higher than C0, as shown in Table 4-6. When comparing the control concrete with steel fibres (SC26), results for the medium-fibre content (P3, P4.5 and P6) were lower even though both were 10% higher than C0. The tensile strength of the high polyolefin fibre content concrete (P10a, P10b and P10M mixtures) was close to 5 MPa and similar to SC26. There was not a perfect trend that showed a relation between a greater amount of fibres and a greater tensile strength.

4.4.2 Fracture tests discussion

The fracture tests showed a significant increment of the fracture energy and toughness for all the polyolefin fibre-reinforced concrete mixtures when compared with the control concrete (C0). The results obtained for P6 are similar to SC26. Achievement of a proper comparison among the mixtures, which could provide conclusions about the polyolefin fibre influence on the fracture processes with fibre amount increment, would require extraction of additional data.

Through analysing the peak load values previously shown in Table 4-7, it was observed that the mean values increased with the amount of polyolefin fibres but not as much as with the steel-hooked fibres. This is in concordance with the indirect tensile strength results obtained, given that the peak load was directly related with the cracking process produced at the tip of the notch (Di Prisco, et al., 2009). However, the peak loads for all the high polyolefin fibre content concretes were higher than in C0 but lower than those registered in the medium fibre content concrete mixtures and did not agree with the tensile tests results. Additionally, it should be noted that the dispersion obtained in the tensile tests suggested that the fibre distribution was not uniform.

It was also observed that the contribution of the fibres should not only be compared with the peak load which value is on a branch almost fully elastic, but also with two noticeable post-cracking parameters: the minimum post-cracking load and the remaining maximum post-cracking load. Moreover, since the two types of fibres used have such different features and types of anchoring mechanisms, the results expected may show their contrast in those post-cracking parameters previously mentioned. In that regard, the comparison of some additional parameters may provide more useful information, especially for long strain results.

According to that explained above, it was appropriate to perform a fracture surface analysis in addition to the comparison of the mean values for the different mixtures and the analysis of the reference values of the standard EN 14651 (EN 14651:2007+A1, 2007) and the recommendation RILEM TC162 TDF (RILEM TC-162-TDF, 2002).

Mean fracture values comparison

To compare the fracture energy at reduced deformations of the self-compacting concrete with polyolefin fibres with the two control concretes C0 and SC26, fracture energy with a deflection of 1 mm was obtained. In order to compare results among the different amounts of fibre added, the fracture energy up to 5 mm of deflection was obtained. This deflection corresponds to the beginning of the second unloading process within 4 and 5 mm for all PFR-SCC. Additionally, if Figure 4-5 is observed 1 mm of deflection permits analysis of the entire tests for C0. Furthermore, as shown in Figure 4-6, it is possible to compare the differences on the influence between steel and polyolefin fibres in the fairest gap for the steel fibre. In Figure 4-14, fracture energy mean values for 1 and 5 mm deflection are summarized.

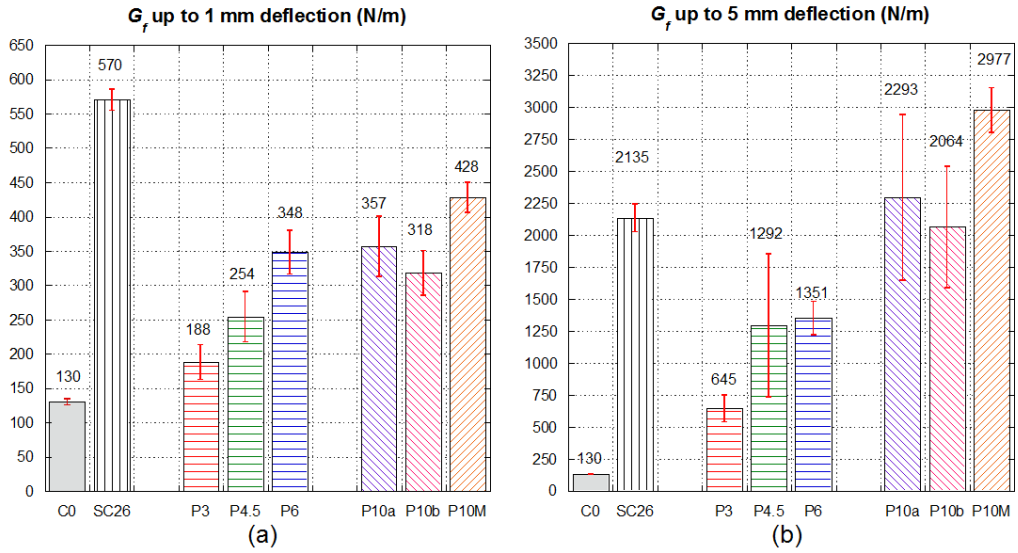

Figure 4-14: Fracture energy: (a) G_F up to 1 mm; (b) G_F up to 5 mm.

Figure 4-14 (a) shows the improvement of fracture energy in the first millimetre of deflection. The reference SFRC showed a high performance behaviour for the very initial deformations. Medium PFRC mixtures increased their values proportionally to the fibre content, reaching 33%, 45% and 60% approximate values for the P3, P4.5 and P6 mixtures compared with SC26. The high-fibre content remained at values of around 60% in the same comparison, though the mixture P10M reached a remarkable mean value of 75% even in these initial deformations.

However, when a comparison of fracture energy was made up to deflection values of 5 mm the fracture energy of the mixtures with high-fibre polyolefin content was 40% greater than SC26. Figure 4-14(b) shows the improvements ductility and toughness of all the polyolefin fibre-reinforced mixtures. It may also be observed that the mixtures P10a and P10b had similar values when compared with SC26 and the difference with P3, P4.5 and P6 became more evident when fracture energy up to 5 mm deflection was compared.

The shapes of the characteristic curves shown in Figure 4-5 fixed three significant turning points that were extracted for an improved data analysis. As the peak load had already been obtained, the values of the minimum load after cracking (L_{MIN}), and the remaining load registered (L_{REM}) as the maximum load after L_{MIN} are summarized on Figure 4-15. While L_{MIN} was much smaller for the polyolefin fibre-reinforced mixtures than for the control SC26 (even the value for P10M mixture is around 65%), for L_{REM} the value of P10M is higher. L_{REM} for the mixtures P6, P10a and P10b were close to 80% of L_{REM} of SC26, though it should be pointed out that these results were obtained with deformations close to 4.5 mm of deflection in which the load for SC26 was lower than 2000 N. The value shown in Figure 4-15(b) for SC26 was registered with a deflection between 1 and 2 mm, less than a half of the obtained for PFR-SCC.

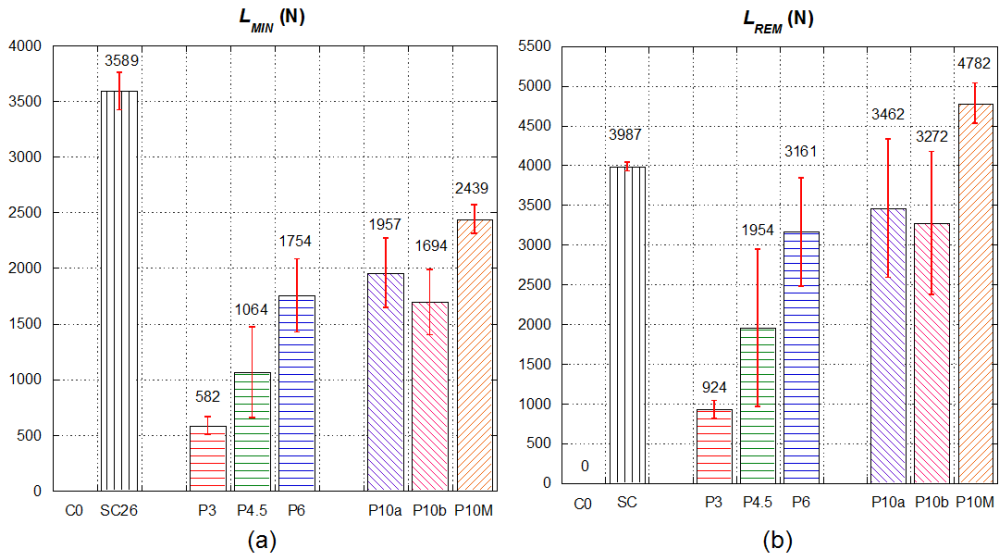

Figure 4-15: Mean values for turning points of the fracture curves: (a) L_{MIN}; (b) L_{REM}.

In order to obtain a better comparison between fracture behaviours, Figure 4-16 and Figure 4-17 were plotted. As the figures denote, polyolefin fibre-reinforced concrete with high content of fibres had very good behaviour for large deformations and even at deflection values of 8 mm load remained at similar values to L_{MIN}. However, for the initial post-cracking deformations, steel-hooked fibre showed a better behaviour and retained a higher load. This can be explained due to the better mechanical properties of the steel and to the anchorage of the hooked end of the fibres.

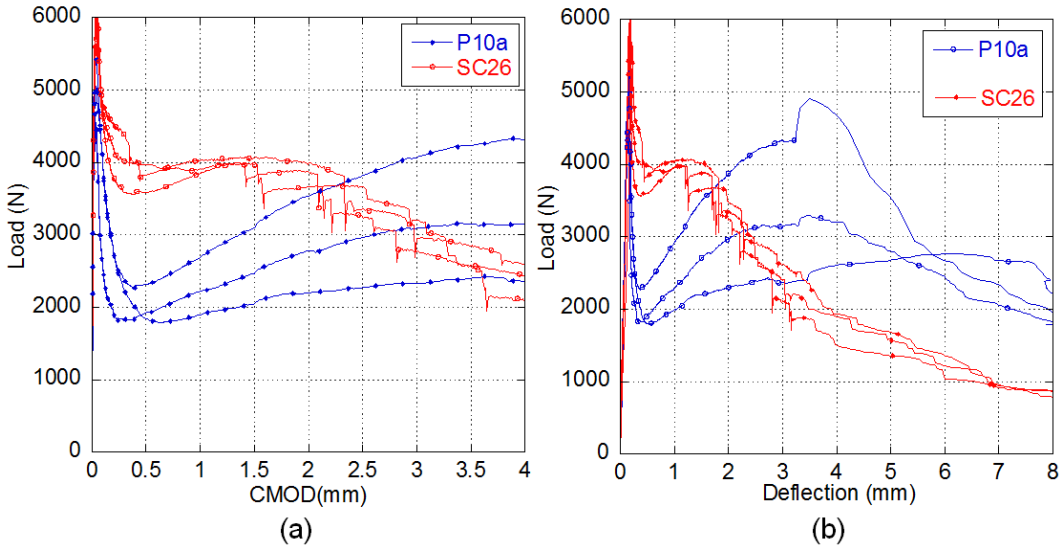

Figure 4-16: Load-CMOD and Load-Deflection curves of the SC26 and P10a beams.

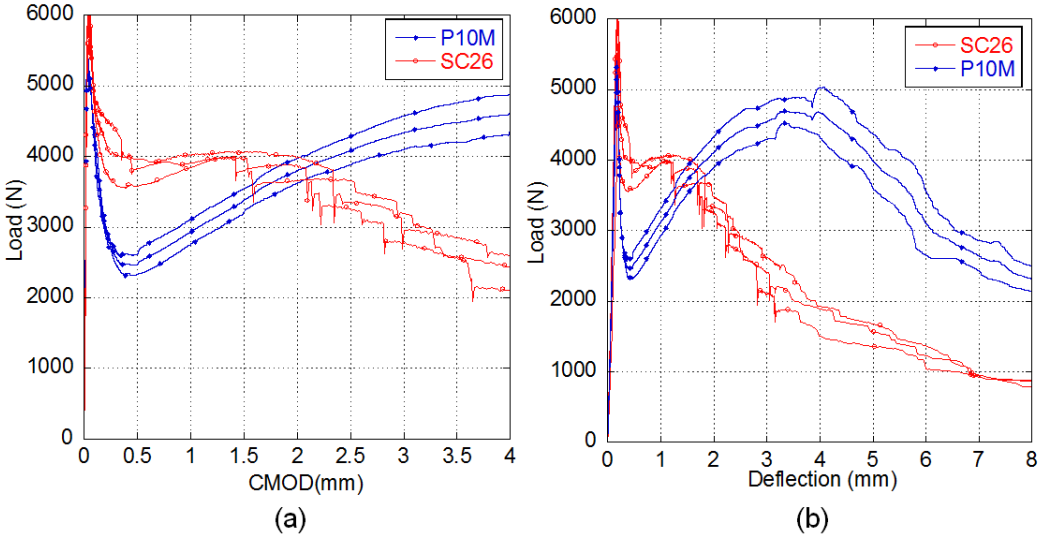

Figure 4-17: Load-CMOD and Load-Deflection curves of the SC26 and P10M beams.

Fracture surface analyses

The residual load-bearing capacity of a notched specimen is strongly related to the number of fibres and their distribution in the fracture surface. In the first branch of the post-cracking softening curve, the influence of the fibres is negligible until a certain opening of the crack is reached. From this point onwards the fibres are capable of absorbing the energy released in the fracture process and the specimen can bear higher loads again. As can be explained with a simple cross sectional analysis under flexural stresses, the contribution of fibres placed in the tensioned part of the section is more important than the rest of fibres. This corresponds to the central third of the whole section. The distribution of the fibres is a result of the casting procedure, certain wall effects or behaviour of the fibre along the flow of the fresh concrete. Finding a relation between the number of fibres in the tensioned part of the fracture surface with the value of L_{MIN}, may be of interest for small deformations which are commonly used for service limit states (SLS) design (Di Prisco, et al., 2009; Di Prisco, et al., 2013).

For high deformations almost the whole cross section is in tension and, similar to concrete, which is a quasi-brittle material, under tensile stresses it would already be almost fully cracked. Therefore, the total number of fibres would bear the final load obtained in the tests. Consequently, the total number of fibres could be correlated with both values, L_{MIN} and L_{REM}. These high deformations would correspond to ultimate limit state design (ULS).

An analysis of the fracture surface could not only explain the dispersion of the results but also measure the influence of the relative position of the fibres on the fracture behaviour of the materials.

The fracture surface of every specimen was analysed. All sections were pointedly flat. The total number of fibres, as well as the number of fibres placed on the central third of the section, were counted. In the case of the steel-hooked fibres, many were only on one side of the fracture surfaces generated and showed an anchorage failure. However, most of polyolefin fibres were broken with one fragment of fibre on each side of the fractured piece. Only a few were debonded.

Figure 4-18(a) shows one specimen of the P4.5 mixture with an effective distribution of fibres, in contrast with Figure 4-18(b) which shows one specimen of the P6 mixture with a

poor distribution. This non-uniformity of the positioning of fibres on the fracture surface suggested that for intermediate dosages it was not reliable to speak only about fibre dosage or fibre density but also about the amount of fibres in an effective position. This explains why the results of a P4.5 sample matched better with the P6 specimens and one of the results of a P6 sample was comparable with the P4.5 specimens. In addition, if Figure 4-7, Figure 4-8 and Figure 4-9 are compared, the dispersion obtained leads to a P4.5 result that would have a better fit with the P3 results. As is shown in Figure 4-18, one specimen with a theoretically smaller fibre quantity may provide better results for the fracture values and explain the high dispersion of these intermediate mixtures.

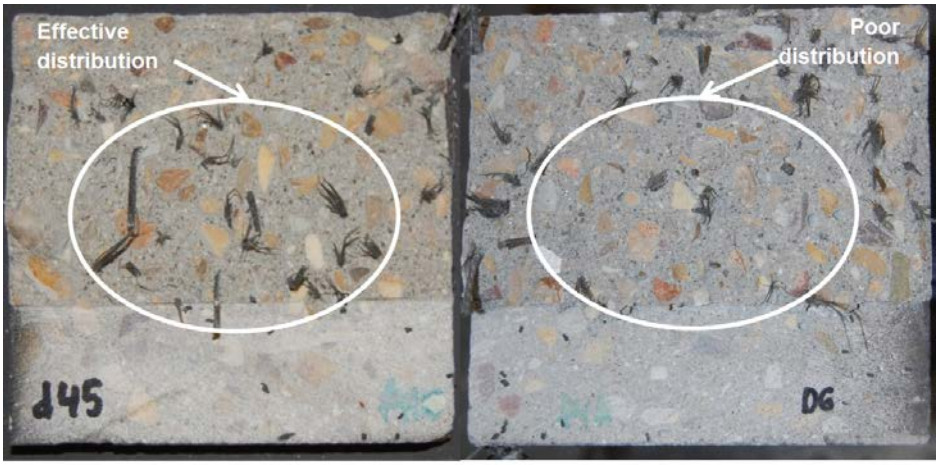

Figure 4-18: Fibre distribution on fracture surface: (a) fracture surface of a P4.5 specimen; (b) fracture surface of a P6 specimen.

In Figure 4-19 one specimen of the P3 mixture and one of a P10a mixture are portrayed. In the P3 sample the presence of only eight fibres were able to prevent the collapse. In the P10a fracture surface there is an even distribution of fibres. Therefore, these constant distributions of fibres, along with the reduced deviation of the fracture results, make these mixtures appealing for use in structural applications.

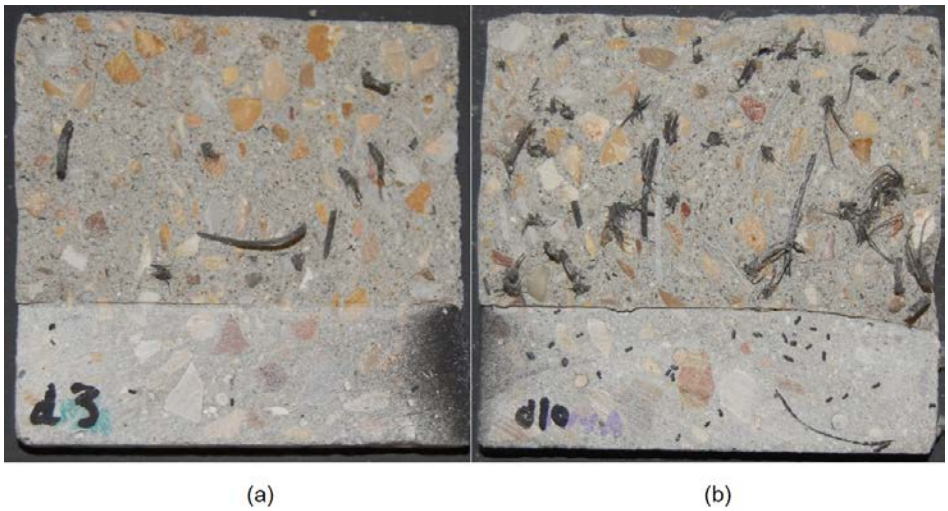

Figure 4-19: Extreme dosage fibre distribution: (a) fracture surface of a P3 specimen; (b) fracture surface of a P10a specimen.

Figure 4-20 analyses the influence of the number and position of fibres in the fracture behaviour of concrete. It was observed that for the number of fibres placed on the central third of the fracture surface, there seemed to be a very good linear fit with L_{MIN}. It was also observed that for the mixture with the bond improver (P10M) the slope was higher. In the case of the steel fibres, a higher and more uniform count of the distribution of the fibres was noted. This was logical, as a dosage of 26 kg/m³ of the steel fibres implies around 40% more fibres when compared with 10 kg/m³ of polyolefin fibres.

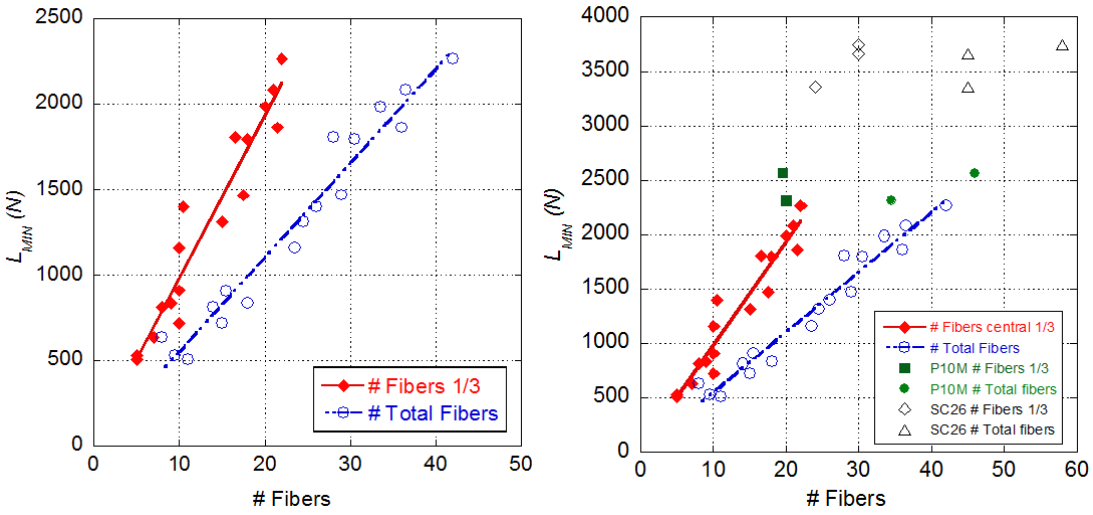

Figure 4-20: Minimum post-cracking load versus number of fibres.

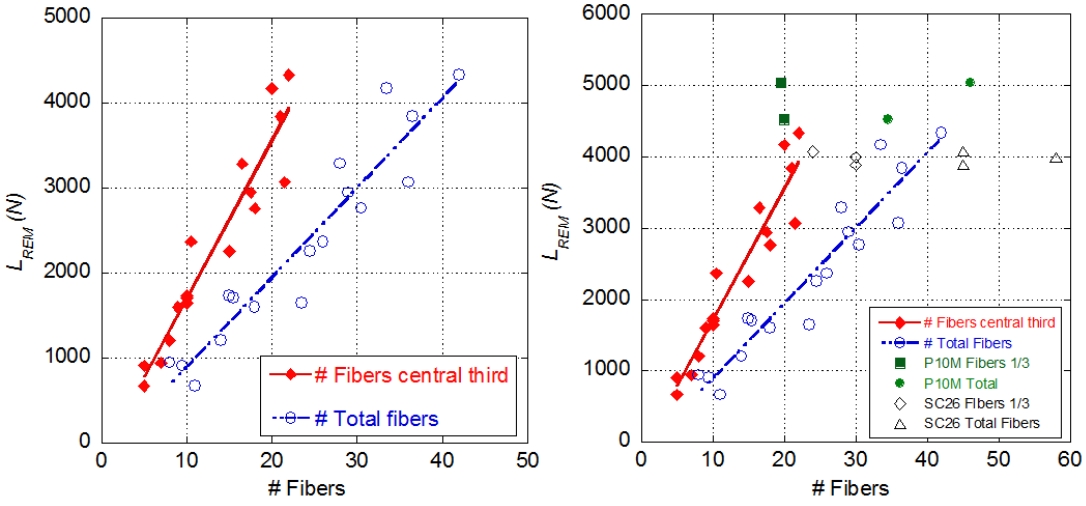

Figure 4-21: Remaining post-cracking load versus number of fibres.

Analysis of the reference values of standards and recommendations

As previously mentioned, some codes, standards and recommendations were performed to take into account FRC, even though such documents were mostly focused on SFRC (as is the case of the standard EN-14651 (EN 14651:2007+A1, 2007) and the RILEM TC-162 TDF (RILEM- TC 162-TDF, 2000) (RILEM TC-162-TDF, 2002). In order to address the possible fitting of the polyolefin fibre-reinforced concrete to the referred documents, the mean values were extracted from the fracture tests and the same assumptions considered.

The linear stress distribution assumed makes it possible to determine the stress in the limit of proportionality (f_{LOP}), as well as the stress in the CMOD values of 0.5 mm (f_{R1}), 1.5 mm (f_{R2}), 2.5 mm (f_{R3}) and 3.5 mm (f_{R4}). It should be noted that the specimen established dimensions for the fracture tests included in the standards are 550 x 150 x 150 mm (length-height-width), while the dimensions of the specimens tested in this chapter are 430 x 100 x 100 mm. The previously mentioned stress values corresponding to crack mouth opening displacements of 0.5, 1.5, 2.5 and 3.5 mm represent greater deformations in a smaller specimen (as shown in Figure 4-22). The geometric relation for the same rotation angle of the cracked cross section is linked to the values of height. Consequently, the value of CMOD 0.5 mm in a specimen with a height of 150 mm would correspond to a value of 0.333 mm in one with a 100 mm height if the same deformation were compared. However, for polyolefin FRC, the load values at a CMOD equal to 0.5 mm were close to the lowest values for all the tests. This was analysed in section 4.3.2, which showed the value L_{MIN} as the weakest point of the polyolefin FRC. In reality, when the values of stress for CMOD 0.333 mm were extracted (f_{R0}) the values obtained were higher than those obtained for 0.5 mm, as shown in Table 4-8. Given that such stress values, corresponding to CMOD 0.5 mm, are commonly used for SLS calculations the CMOD 0.5 mm was chosen. For greater deformations no correction was made in the CMOD, given that stress increased up to significantly higher deformations above the standards requirements.

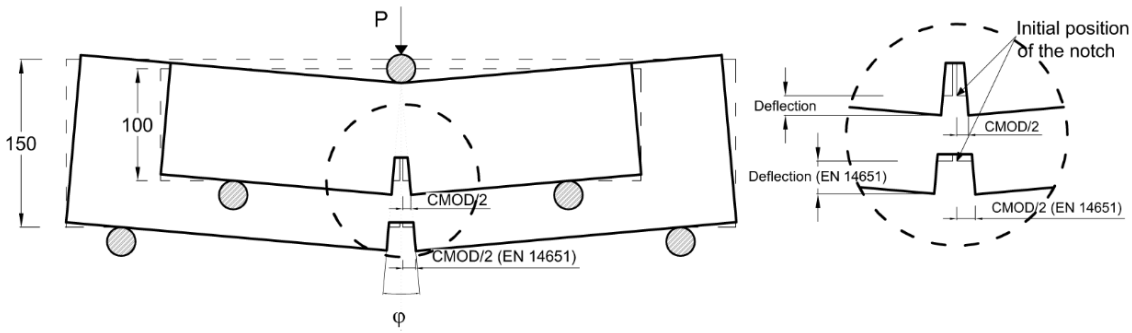

Figure 4-22: Crack mouth opening displacement relationship for the same rotation angle with two different heights of specimen.

The results extracted are shown in Table 4-8, as well as their standard deviation. In order to obtain the stresses through using the load values obtained in the tests, the following expression (4-1) in the standard and RILEM was employed. In this formula, L is the distance between the supporting cylinders and F is the force registered by the load cell, b is the width of the specimen and h_{sp} the length of the ligament. In this case, L=3D; h_{sp} =D-1/3D and b = D.

$$f_{ct,j} = \frac{3}{2}\frac{F_j \cdot L}{b \cdot h_{sp}^2} \qquad (4-1)$$

Post-cracking strength obtained from the fracture tests and the evolution of the strength with crack opening are represented for the four values of stress (f_{R1}, f_{R2}, f_{R3} and f_{R4}) that may be seen in Table 4-8. Limitation of at least two values of deformation to correlate with SLS and ULS verifications is commonly accepted. Some authors and national codes (EHE-08, 2008; Di Prisco, et al., 2009; FIB, 2010) have associated f_{R1} and f_{R3} respectively with them. In this connection, it is proposed that FRC may be used as substitute for conventional steel reinforcement if the relation f_{R1}/ f_{R3} is higher to 0.5 to relate with ULS behaviour and if f_{R1}/f_{LOP} ratio is higher to 0.4. As f_{R1} is 63% of f_{LOP} higher to 40% and f_{R3} is 57% of f_{LOP}

higher to 20% of f_{LOP}, the structural use of SC26 would be allowed. If the shapes of the SFRC fracture curves were analysed, the use of stress values related with CMOD 2.5 mm would be critical, and therefore should be related with deformations in ULS. Except for the P3 mixture, the rest of the PFRC mixtures had values higher to 20% of the peak load, which would mean that for deformations related to ULS would be suitable for structural use. The weak point of the polyolefin fibre-reinforced concrete was associated with reaching values of 40% of the peak load for smaller deformations in CMOD values of 0.5 mm (f_{R1}). While the high-fibre content mixtures without bond improver (P10a, P10b) were close to fulfil the standard requirements, P10M specimens did so. Consequently, the P10M would be adequate for structural use in the existing codes (EHE-08, 2008) or research recommendations (Di Prisco, et al., 2009). Mixtures P3, P4.5 and especially P6 showed a high performance ductility and toughness even though the results were not suitable with the existing standards.

Table 4-8: Bending test results: residual flexural strength.

Residual flexural tensile strength and coefficient of variation (MPa)

	f_{LOP}	f_{R0}	f_{R1}	$\%f_L$	f_{R2}	$\%f_L$	f_{R3}	$\%f_L$	f_{R4}	$\%f_L$
CMOD(mm)	<0.05	0.33	0.50		1.50		2.50		3.50	
SC26	6,05 (0.06)	4.00 (0.36)	3.84 (0.19)	63	3.99 (0.13)	66	3.46 (0.21)	57	2.70 (0.16)	45
P3	5.75 (0.04)	1.06 (0.30)	0.76 (0.17)	13	0.64 (0.10)	11	0.66 (0.09)	11	0.81 (0.14)	14
P4.5	5.73 (0.01)	1.29 (0.37)	1.13 (0.35)	20	1.30 (0.47)	23	1.64 (0.62)	29	1.82 (0.73)	32
P6	6.20 (0.01)	2.03 (0.22)	1.82 (0.35)	29	2.19 (0.58)	35	2.67 (0.72)	43	3.06 (0.73)	49
P10a	5.25 (0.05)	2.13 (0.26)	2.05 (0.26)	39	2.59 (0.54)	49	3.05 (0.78)	58	3.30 (0.93)	63
P10b	5.38 (0.15)	1.83 (0.35)	1.72 (0.42)	32	2.20 (0.66)	41	2.68 (0.83)	50	2.95 (1.02)	55
P10M	5.48 (0.01)	2.52 (0.15)	2.50 (0.20)	46	3.43 (0.23)	63	4.14 (0.28)	76	4.53 (0.41)	83

Some other existing guidelines, such as the Italian code CNR-DT 204/2006 (CNR-DT 204, 2006) limit the structural use of FRC with the softening behaviour in concrete where f_{R1} should be at least 20% of f_{LOP}. The proposed constitutive models of the code are obtained from uni-axial tension tests or four-point bending tests and also based on the SFRC research. Nonetheless, the fracture curves obtained would fit the shape of the constitutive models proposed. With this assumption it would even be possible to satisfy the requirements from the Italian code for both SLS and ULS with amounts of polyolefin fibres from 6 kg/m³ and higher.

The fracture curves of PFRC had a softening post-cracking branch that was significantly longer than the SFRC which led to smaller loading on CMOD of 0.5 mm. However, the SFRC curve was a decreasingly staggered fracture curve from that point on and the polyolefin fibre-reinforced concrete showed a hardening branch in the gap for CMOD between 0.5 and 5 mm.

4.5 Conclusions

The production of polyolefin fibre-reinforced self-compacting concrete has a high performance fresh-state behaviour when compared with steel-hooked fibres. In addition, it is possible to produce it without high powder content and admixtures even with fibre content up to 10 kg/m³.

The hardened properties of the self-compacting fibre-reinforced concrete obtained for the medium content of polyolefin fibres mixtures are analogous in compressive strength and elasticity modulus while the improvement of tensile strength was moderate. For high polyolefin fibre content mixtures, compressive strength slightly decreased and tensile strength increased 30% compared with a control plain self-compacting concrete, though it was 10% lower with a control steel fibre-reinforced self-compacting concrete.

The fracture energy obtained for all the polyolefin fibre-reinforced concrete mixtures is significantly higher when compared with the plain control mixture. Fracture toughness and ductility improvements are quite reliable even for the medium polyolefin fibre content mixtures. The shapes of the fracture curves in the notched three-point bending tests are smooth and have characteristic linear branches in the post-cracking behaviour. There are two characteristic turning points in the minimum load after a first softening branch and the maximum remaining load for larger deformations.

The dispersion obtained for the polyolefin fibre-reinforced self-compacting concrete with 4.5 kg/m³ and 6 kg/m³ was explained with the analysis of the fracture surfaces due to the lack of uniformity in the number and distribution of fibres. The minimum post-cracking load after the first softening branch (L_{MIN}) seems to have a linear relation with the number of fibres placed on the central third of the fracture surface. The remaining load-bearing capacity for large displacements has a maximum post-cracking load (L_{REM}) close to a 4.5 mm deflection. There seems to be a linear relationship with the total number of fibres in the fracture surface.

The value of f_{MIN} was analogous to f_{R1} because the deformations were similar; however, the value of f_{REM} should not be compared with f_{R3} since deflection was doubled for polyolefin fibre-reinforced concrete. The unloading trend of the fracture curves of steel fibre-reinforced reference concrete led to a smaller strength value for f_{R3} once the first fibre failed. For the polyolefin fibre-reinforced concrete, the load increased up to values of 4.5 mm of deflection and even for 8 mm the fibres still bore loads close to f_{MIN}.

Even for the mixture in the lowest threshold of fibre content (3 kg/m³ of polyolefin fibres added) the results of strength for large crack mouth openings of 2.5 mm in the notched three-point bending test (f_{R3}) were close to 20% of the stress on the limit of proportionality (f_{LOP}). Such a result complies with the ULS design standards. However, for structural reinforcement with the medium polyolefin fibre content FRC, a more extensive test campaign might be needed. The latter would increase the reliability of the results and clarify the influence of the flow and the casting procedure in the number and distribution of the fibres.

Concretes with high polyolefin fibre contents in which it is possible to reduce or even eliminate traditional steel reinforcement in structural applications is suitable in meeting with the principal standards and recommendation models. With the bond improver, the mixture with 10 kg/m³ exceeded the requirements of the EN-14651 (EN 14651:2007+A1,

2007), RILEM (RILEM- TC 162-TDF, 2000) and for the Spanish code for structural concrete EHE-08 (EHE-08, 2008).

For the SLS the values of crack mouth openings of 0.5 mm (f_{R1}), the values of the medium fibre content were not close to the requirements of 40% of the peak strength, though significant and reliable values were obtained. Furthermore, these values, even though they were not as high as for steel fibres, were stable for larger deformations.

Chapter 5

Comparison between polyolefin fibre-reinforced vibrated conventional concrete and self-compacting concrete

5.1 Introduction

Since VCC and SCC are the most commonly used types of concrete, the comparison between them was first assessed by means of mechanical testing of steel fibre reinforced concrete (SFRC), with there being significantly higher residual strengths in the case of SCC (Grünewald, 2004; Kooiman, et al., 2000). Furthermore, variations in the pouring method and mould dimensions or shapes imply changes in the distribution of fibres. This has been studied by analysing the position of the fibres and the fracture behaviour of concrete pieces obtained from slabs or specially shaped moulds (Zerbino, et al., 2012; Stähli, et al., 2008). In addition, it has been assessed by filling standard dimension moulds and using alternative methods (Torrijos, et al., 2010). Some studies have explained the results because of the differences in orientation and distribution of the fibres produced by the pouring and compaction procedures of concrete (Ferrara & Meda, 2006; Laranjeira, et al., 2012). The latter has provided significant information for the structural design of SFRC.

Macro-polymer fibres with improved mechanical properties provide PFRC analogous residual strengths as compared with SFRC although, at the time of writing, there remains hardly any published comparison between SCC and VCC using structural synthetic macro-fibres. Two main factors prevent the use of the same assumptions for polyolefin fibres: their remarkably lower density and their flexibility. Thus, this chapter aims to assess the differences in the behaviour of SCC and VCC reinforced with different dosages of polyolefin fibres by analysing the mechanical and fracture properties of eight concrete mixtures: two reference plain concretes (one VCC and one SCC) and three pairs of VCC and SCC reinforced respectively with 3, 4.5, and 10 kg/m³ of polyolefin fibres. The behaviour of each concrete was both assessed and justified by analysing the amount and position of fibres in the fracture surfaces generated.

The characterization of the mechanical properties and the good durability performance (shown by penetration of water under pressure testing), together with the flexural residual strengths and fibre positioning variations, have provided sound conclusions to be considered for the structural design of PFRC. In such a sense, it should be highlighted that the differences of fibre positioning in both types of concrete were more noticeable for the dosage of 10 kg/m³ which, on another note, amply exceeded the requirements of the standards to consider fibre contribution in structural design. The conclusions have shown that SCC distributed the fibres more homogeneously within the specimen, although the mould walls had more influence on the positioning of fibres for VCC specimens.

5.2 Concrete production: materials, design and manufacturing

Both VCC and SCC were produced by using the same materials described in subsection 4.2. Likewise, SCC mix proportioning was the same used in the previous Chapter 4. The changes in the fresh-state behaviour were achieved by minor modifications in the aggregates, proportioning and varying the amount of superplasticizer.

Regarding the VCC formulation, it is worth noting that it was a modification of the SCC mix proportioning. That is to say, a reduction of the amount of fine particles was carried out. This change was balanced by increasing the relative quantity of gravel and grit. It should be highlighted that the VCC mix design also meets the requirements of the standard EN-14845 (EN 14845-1, 2006; EN 14845-2, 2006; EN 14889-2, 2008), but for two considerations. On the one hand, the type of cement used was of 52.5 MPa of strength instead of 42.5 MPa because it was required to be as similar as possible to the SCC mixture. On the other hand, as such a standard requires drying of the aggregates and this research was required to follow procedures similar to those of real pouring and mixing.

Eight types of concrete were produced: two plain concretes, SCC and VCC, and six FRCs that were based on the same VCC and SCC formulations but adding 3, 4.5 and 10 kg/m³ of polyolefin fibres respectively. These mixtures were termed VCC3, SCC3, VCC4.5, SCC4.5, VCC10 and SCC10. In Table 5-1, the detailed mix proportioning of all the types of concrete that were produced can be seen. The fibres used, manufactured by Sika and called Sikafiber M-60 were the same shown in previous chapter in Figure 4-2 and with the same properties shown in Table 4-3.

Table 5-1: Concrete formulation per m³.

Concrete	Cement	LP	Water	Sand	Gravel	Grit	SP	Polyolefin fibres
	kg/m³	kg/m³	kg/m³	kg/m³	kg/m³	kg/m³	%cement weight	kg/m³
SCC	375	200	187.5	918	245	367	1.25	-
VCC	375	100	187.5	916	300	450	0.75	-
SCC3	375	200	187.5	918	245	367	1.25	3
VCC3	375	100	187.5	916	300	450	0.75	3
SCC4.5	375	200	187.5	918	245	367	1.25	4.5
VCC4.5	375	100	187.5	916	300	450	0.75	4.5
SCC10	375	200	187.5	918	245	367	1.25	10
VCC10	375	100	187.5	916	300	450	0.82	10

Using each type of concrete, two prismatic specimens of 600x150x150 mm and nine cylindrical specimens of 300 mm height and 150 mm of diameter were cast. All the specimens were stored at room temperature during the first 24 hours and then kept in a climatic chamber at 20ºC and 95% of relative humidity for 28 days until the age of testing.

Concerning the pouring methods, SCC mixes, all specimens were filled in a single pour from one of the sides of the mould and compacted and levelled off by the action of their own weight without any further compaction. Those specimens performed with VCC were compacted for 10 seconds by means of a vibratory table and filled following the procedure stated in the standards (EN 14651:2007+A1, 2007; RILEM TC-162-TDF, 2002). That is to say, they were filled initially in a central portion of approximately 90% of the height of the specimen and two portions in the half side of it. Then, the mould was topped and levelled while being compacted. Both consolidation processes might affect the distribution and orientation of the fibres and, as a consequence, the fracture behaviour of the specimens. These issues will be discussed in the following sections.

5.3 Fresh-state characterisation

The fresh-state behaviour of SCC mixes was previously assessed and can be seen in subsection 4.3.1. Regarding VCC mixes, their fresh-state properties were addressed by means of the slump test (EN 12350-2, 2002), whether they had fibres or not. In order to obtain similar results in the latter test, the amount of superplasticizer used was increased in VCC10 formulation from 0.75% to 0.82% with respect to cement weight. In consideration of such a modification, the results were around 15 cm of descent of the mass for all the formulations. The results of all the fresh-state tests can be seen in Table 5-2.

Table 5-2: Fresh-state tests results.

	Superplasticizer	Slump test
Parameter	%cement weight	*h* (cm)
VCC	0.75	15.0
VCC3	0.75	15.0
VCC4.5	0.75	15
VCC10	0.82	14.5

5.4 Mechanical behaviour and durability tests

The compressive strength, modulus of elasticity and indirect tensile strength tests were performed by using the cylindrical specimens. All these tests were carried out by following some of the most employed standards (EN 12390-3, 2009), (EN 12390-6, 2009), and (EN 12390-13, 2013). Each involved three specimens at 28 days of age. The mean values of all the tests and their coefficient of variation can be seen in Table 5-3. The results of the SCC mixes are similar to those shown in Chapter 4 and are shown with the aim of improving the comparison between the two types of concrete.

No major changes were noticed in the modulus of elasticity of the SCC mixes. However, it would seem that the addition of fibre contents above 3 kg/m^3 might worsen the compaction of the concrete in the moulds and thus reducing the test results. A similar phenomenon might also take place in the VCC mixes. It is worth noting that it was more evident for the fibre dosage of 10 kg/m^3 which would suggest that some of the increment in the scatter found ahead in the fracture results could be due to the same source. That is to say, such worse compaction of the concrete due to the presence of fibres could also have some influence on the fracture results.

When the values of the characteristic compressive strength (f_{ck}) and the indirect tensile strength *fct* were computed, no variations in the values obtained out of the boundaries of the typical experimental scatter were noted.

The durability performance of all the concretes manufactured was assessed by means of permeability tests according to the standard (EN 12390-8, 2000) with the results being shown in Table 5-3. According to those obtained, the presence of fibres did not influence the connected porosity network of concrete. The value of penetration of water under pressure of all the VCC mixes was greater than the equivalent formulation of SCC in all the mixes. Therefore, it could be argued that the coarser aggregate skeleton of the VCC mixes is responsible for the more permeable pore structure. In addition, due to the limited depth of penetration, below 20 mm, all the mixes performed with SCC are suitable for use in extremely harmful environments in accordance with (EHE-08, 2008). In contrast, VCC mixes (with depths of penetration below 30 mm) were apt for use in medium hazardous environments (according to EHE-08) due to a more permeable porous structure. Subsequently, it was concluded that the presence of the fibres had hardly any influence on the VCC and SCC results.

Table 5-3: Mechanical behaviour test results.

	E (GPa) (c.v.)	f_{ck} (MPa) (c.v.)	f_{ct} (MPa) (c.v.)	Depth of penetration of water under pressure (mm)
VCC	34 (0.04)	34 (0.04)	3.9 (0.10)	21.9
SCC	36 (0.03)	39 (0.01)	3.8 (0.14)	12.5
VCC3	30 (0.03)	31 (0.02)	3.6 (0.03)	25.9
SCC3	36 (0.06)	39 (0.01)	4.4 (0.09)	12.2
VCC4.5	31 (0.07)	31 (0.07)	4.2 (0.12)	14.8
SCC4.5	32 (0.01)	38 (0.06)	4.2 (0.20)	9.3
VCC10	28 (0.04)	28 (0.03)	4.1 (0.06)	23.7
SCC10	30 (0.02)	37 (0.02)	4.6 (0.09)	12.2

5.5 Fracture tests

Through using two notched prismatic specimens of 600x150x150 mm³ of each type of concrete, three-point bending tests were performed in accordance with the recommendation (EN 14651:2007+A1, 2007) and (RILEM- TC 162-TDF, 2000). The span of the test was 500 mm and the ligament length (h_{sp}) 125±1 mm in the fracture area. The test was performed under crack mouth opening displacement (CMOD) control until failure when the plain concrete specimens were tested. When the FRC was studied, the test was controlled with the CMOD gauge until an opening above 4 mm was reached. The deflection of the specimens was measured by means of two linear variable differential transducers (LVDT), one in each of the sides of the specimen Figure 5-1 offers a picture of a specimen while testing and a detailed view of the positioning of the CMOD gauge. The data acquisition system registered the position of the actuator, load, CMOD opening and LVDT values at both sides of the specimen. The configuration of the test can be seen in Figure 3-55.

Figure 5-1: Three-point bending tests: (a) specimen while testing; (b) detailed view of the CMOD gauge that controls the test.

In the post-peak cracking processes, the contribution of the fibres enabled the material to bear strains noticeably higher than those in plain concrete. In addition, the presence of fibres restrains the specimen from collapsing. Thus, although the tests were completed up to the limits established in the recommendations under CMOD control, they were continued to higher strain states. With that purpose, before the CMOD gauge reached its upper bound, the test control was changed to the position of the actuator. By doing this, it was possible to assess the behaviour of the FRC when bearing deflections noticeably higher than usual, span/40 (12.5 mm). At this stage the tests were considered ended.

It is worth noting that the especially meticulous manufacturing processes, being of key importance in this study, in addition to the accuracy of the equipment and measuring devices permitted the reduction of the scatter. The specimen positioning was carefully made by means of laser devices. The notch was machined with a water-cooled low-speed diamond cutting disc. The concrete beams rested on two rigid steel cylinders laid on two ground supports, which allowed free rotation out of the plane of the beam and guaranteed negligible friction rolling in the longitudinal direction of the beam. Thus, the results of the fracture tests on two beams showed a remarkably low degree of scatter. The latter is also supported with the results shown in Chapter 4.

5.6 Fracture results

In the plain concrete mixes, fracture behaviour of both SCC and VCC was considered analogous in accordance with the load-CMOD curves that appear in Figure 5-2. Both formulations behaved almost linearly up to their maximum load. After reaching this point, the unloading branch described the characteristic softening curve of all hardened concretes as having a practically exponential shape. When a CMOD value of 0.45 mm was reached the load borne by the specimens was less than 2 kN.

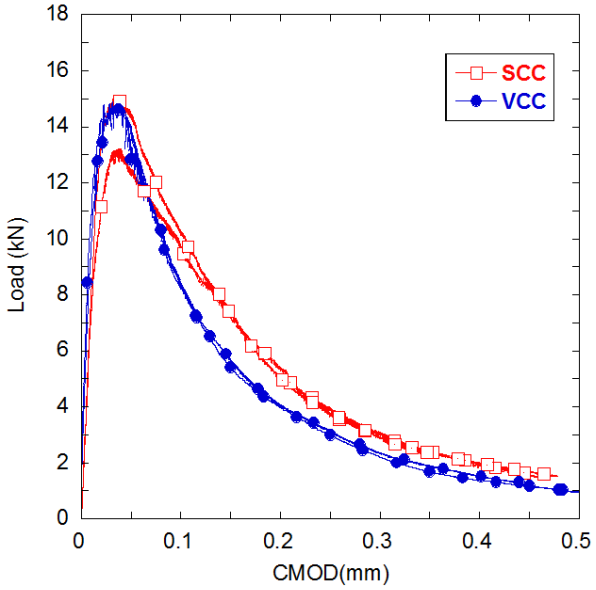

Figure 5-2: Load-CMOD curves of the reference SCC and VCC mixes.

When three-point bending tests of notched PFRC specimens were studied, the fracture curves resembled that represented in Figure 5-3. The typical curves showed three remarkable turning points (the description that follows examines the extraction of only a few parameters of each test). The first turning point took place when the loading-process reached the maximum value and very few inelastic processes were evident. Given that at such deformation the crack was still not perceptible to the naked eye, the turning point where the load reached the maximum is commonly known as the load at the limit of proportionality (L_{LOP}), with it being the overall maximum load in plain concrete. When load values beyond the limit of proportionality continue increasing, the behaviour of the material is denoted as hardening. Such behaviour is different from the softening behaviour that ruled the branch after f_{LOP}, as reported in many FRC types and especially for PFRC as was shown in Chapter 4. The softening behaviour is distinctive from plain concrete fracture and, in such a case, the steep unloading process leads to the specimen failing and collapsing. However, the polyolefin fibres absorb the energy released by the concrete in the fracture processes by so-called fibre bridging and changed the loading tendency. In such an instant, the curve reaches the minimum post-cracking load (L_{MIN}), represented in Figure 5-3. At this point, another loading process started again. Since polyolefin fibre anchorage was due to a rough surface, when enough fibres boasted sufficiently embedded length, load values retrieved as deformation grew. The end of the load-increasing-ramp was the third noticeable point of the described curve with the maximum post-cracking remaining load (L_{REM}) shown in Figure 5-3. The descending slope drawn after L_{REM} continues up to the end of the test. It should be mentioned that all the PFRC specimens showed this behaviour and none failed or collapsed, showing an improvement in ductility and toughness with respect to plain concrete.

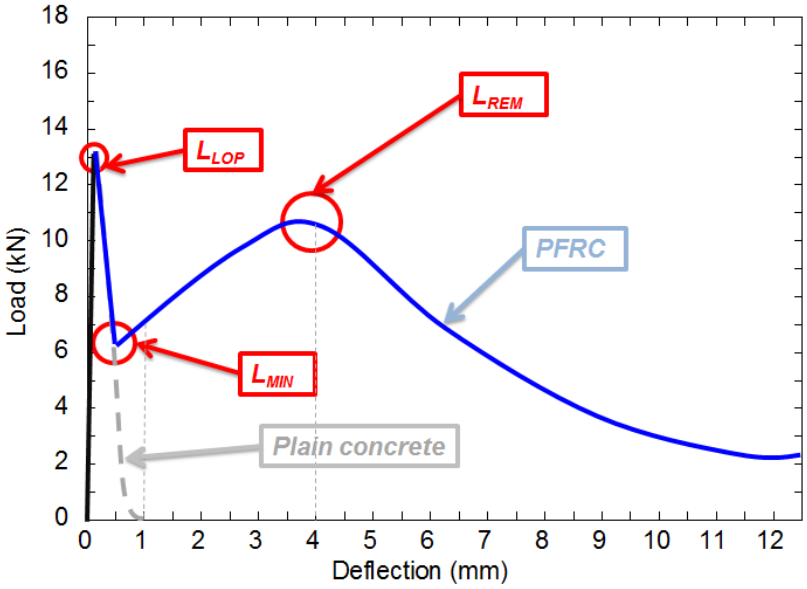

Figure 5-3: Schematic shape of the typical load-deflection curve obtained in a fracture test of PFRC.

The results of the fracture tests performed in SCC3 and VCC3 can be seen in Figure 5-4, where the load-deflection curves are shown. It is clear that although the scatter in both formulations was within the experimental scatter band, it was more limited in SCC3 and almost negligible. The maximum post-peak load was registered at similar values of deflection in SCC3 and VCC3. However, in the VCC3 formulation, one test showed a limited ability to restrain the unloading for L_{MIN}. In addition, the same test also showed a reduction of L_{REM}. Conversely, the unloading processes of SCC3 and VCC3 alike behaved in quite similar manners after 5 mm of deflection was reached. Moreover, for the final moments of the test, at 12 mm of deflection, the load values of all specimens were similar.

The results of the fracture tests performed in SCC4.5 and VCC4.5 can be seen in Figure 5-5, where the load-deflection curves are shown. It is clear that although the scatter in both formulations was within the experimental scatter band, it was more limited in SCC4.5. The maximum post-peak load was registered at almost the same values of deflection in SCC4.5, while in VCC4.5 there was 1 mm between the maximum post-peak loads (L_{REM}) of the two specimens tested. Moreover, the unloading processes of the SCC4.5 specimens showed a high degree of similarity, while in VCC4.5 the unloading branch of one of the specimens was above the values registered in the other specimen for equal deflection values. Then again, when a deflection of 12 mm was reached, the load values of the specimens were similar.

The fracture behaviour of SCC10 and VCC10 can be seen in Figure 5-6. Similarly to the previous comments regarding SCC4.5 and VCC4.5, the specimens produced with self-compacting concrete and 10 kg/m³ of fibres (SCC10) showed a more limited scatter than those made with vibrated concrete (VCC10). However, the differences found in VCC10 specimens occurred at the same deflection values. A 1 kN between the loads registered at L_{MIN}, grew as the tests progressed, differing L_{REM} from the two specimens 2 kN. Similarly to SCC4.5 and VCC4.5, when 12 mm of deflection was reached, the behaviour of the specimens was similar.

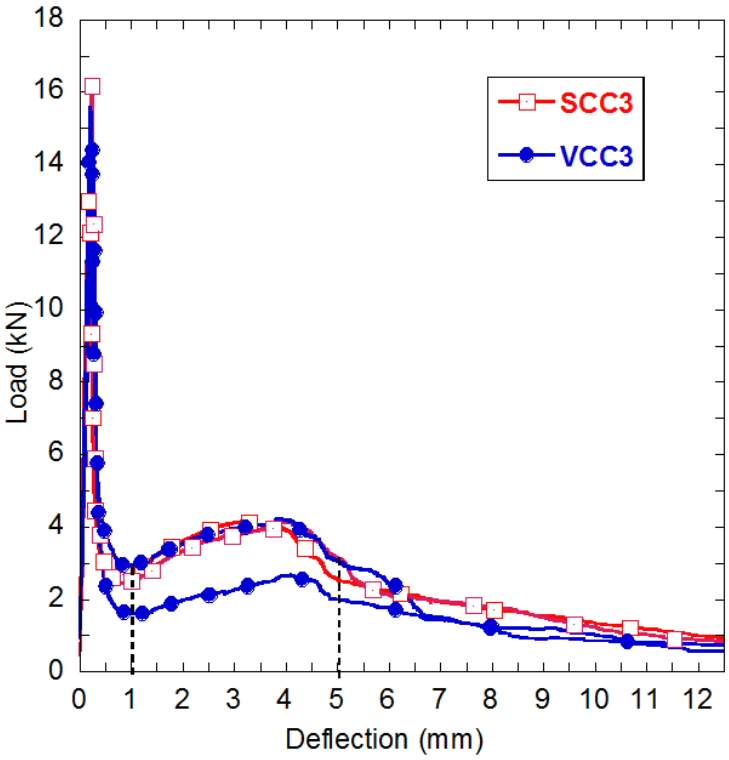

Figure 5-4: SCC3 and VCC3 load-deflection curves.

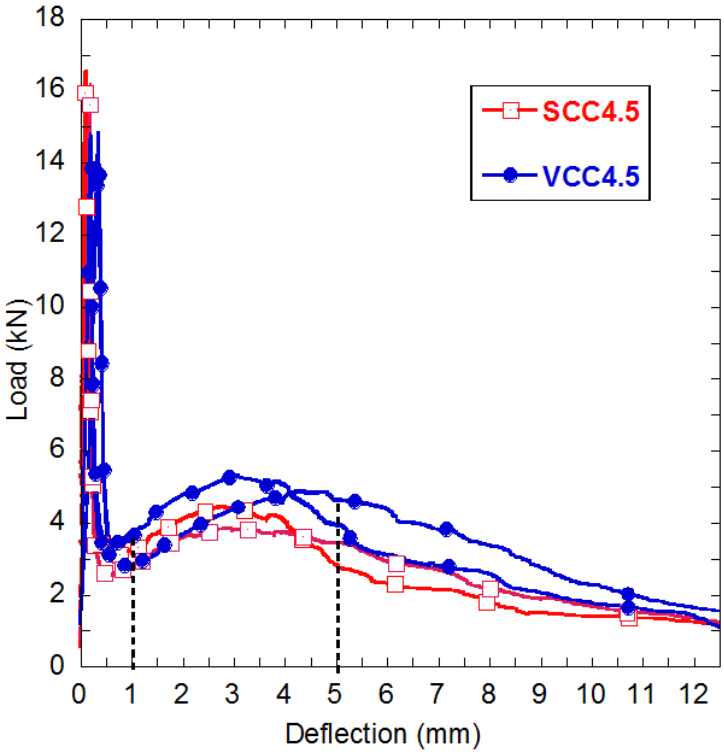

Figure 5-5: SCC4.5 and VCC4.5 Load-deflection curves.

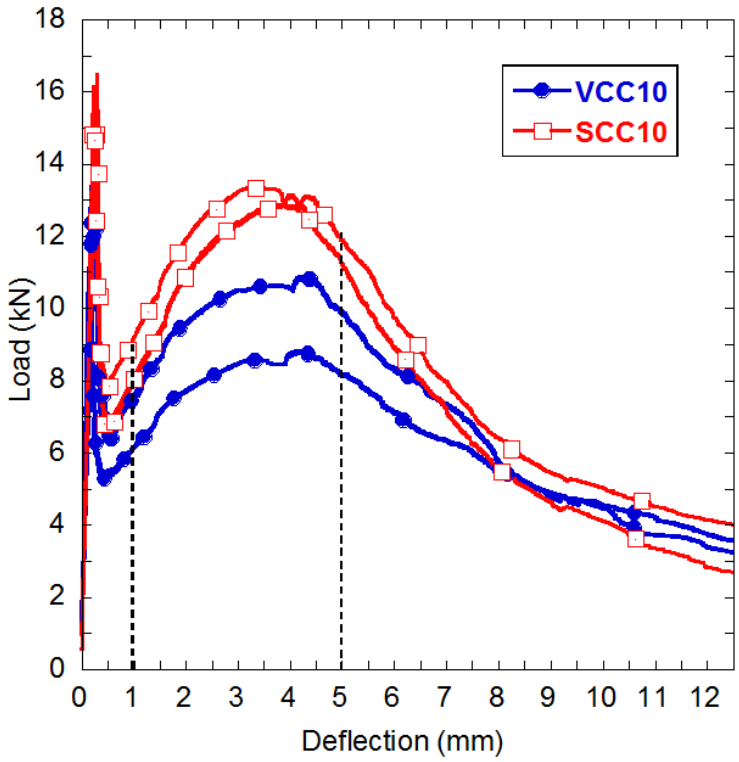

Figure 5-6: VCC10 and SCC10 load-deflection curves.

In order to quantify and compare the work of fracture for each type of concrete, the fracture energy (G_F) of all the mixes was analysed by means of the load-deflection curves of figures Figure 5-2, Figure 5-4, Figure 5-5 and Figure 5-6 and processed by using the formula of expression (5-1).

$$G_F = \frac{W_f}{b \cdot h_{sp}} = \frac{\int P \ d\delta}{B(D - a_0)} \qquad (5-1)$$

where W_f was the fracture work borne by the sample, b the width of the specimen and h_{sp} the length of the ligament. Expression (5-1) can also be found standing P stands for load, δ for the deflection, B for the width of the sample, D is the height and a_0 the depth of the notch. With the aim of offering a comparison at different strain states, the fracture energy was obtained at three deflections: at 1 mm of deflection, at 5 mm and at the end of the test (12.5 mm). All the values of the fracture energy obtained may be compared in Table 5-4. If such fracture energy values are analysed, it can be seen that the fracture energies of VCC and SCC showed a high degree of resemblance. This could be expected in accordance with the data shown in Figure 5-3. In such a sense, it could be concluded that the variations in fresh-state properties and the changes in the aggregate skeleton, did not influence the values obtained for such plain concrete elements.

When G_F was obtained at 1 mm of deflection, there were significant improvements of the fracture energy of all the formulations with fibres with respect to the plain concrete mixes. When analysing VCC3 and SCC3, it is clear that both formulations increased the fracture energy of the plain concretes up to 160%. Regarding the fracture energy obtained in VCC4.5, it almost doubled the plain concrete one, while the SCC4.5 fracture energy was around 160% of the former. Moreover, when the fracture energy of SCC10 was compared with the plain concrete, it was triple. In the case of VCC10 it was over 250% higher.

Table 5-4:Fracture energy.

	G_F (1 mm) (c.v.)	G_F (5 mm) (c.v.)	G_F (12.5 mm) (c.v.)
VCC (N/m)	153 (0.10)	-	-
SCC (N/m)	152 (0.10)	-	-
VCC3 (N/m)	257 (0.15)	881 (0.30)	1383 (0.22)
SCC3 (N/m)	249 (0.04)	1008 (0.01)	1651 (0.04)
VCC4.5 (N/m)	293 (0.04)	1239 (0.06)	2293 (0.06)
SCC4.5 (N/m)	244 (0.08)	1043 (0.07)	1820 (0.02)
VCC10 (N/m)	377 (0.14)	2296 (0.15)	4510 (0.11)
SCC10 (N/m)	454 (0.05)	2992 (0.04)	5420 (0.03)

When the fracture energies at a deflection of 5 mm were examined, both VCC3 and SCC3 were between 550% and 700% higher than that obtained in their respective plain concretes. While VCC4.5 showed a noticeable increment compared with VCC3, there was just a minor increment of the fracture energy of SCC4.5 with respect to SCC3. This might be a result of the position of the fibres in the fracture surface (this phenomenon will be studied in the following sections of the Chapter). Conversely, if VCC10 and SCC10 were analysed, it could be observed that the fracture energy of VCC10 was below the equivalent value obtained for SCC10. None of the two values are more than 15 times tougher than the plain concrete types studied. It is also out of note that there were noticeable differences between the fracture energy results obtained with VCC10 and SCC10. As the data presented in Table 5-4 merits further analysis, this will be carried out in the following sections.

As PFRC in many cases has been designed to benefit the performance of structures, it is necessary to meet the requirements established in the regulations and recommendations. In order to check the suitability of the mixes studied for such uses, it is necessary to transform the load obtained from the fracture tests performed into residual strength values. This task has been accomplished in accordance with EHE-08 (EHE-08, 2008) and the Model Code (fib Model Code, 2010) which provide the previously shown expression (4-1) that transforms load values into strength.

The residual strength values were obtained for the limit of proportionality and those corresponding to a CMOD opening of 0.5 mm (f_{R1}), 1.5 mm (f_{R2}), 2.5 mm (f_{R3}) and 3.5 mm (f_{R4}). The values of f_{R1} y f_{R3} are used to analyse the suitability of any FRC as a structural material in the referred standards. In order to examine the contribution of the fibres in the structural design, it is compulsory that f_{R1} be above 40% of $f_{ct,l}$ and f_{R3} exceed 20% of $f_{ct,l}$. These values were chosen to avoid brittleness in a typical steel fibre reinforced concrete where the load-bearing capacity of the material is higher at low strains than at higher strains.

As can be seen in Figure 5-3, Figure 5-4, Figure 5-5 and Figure 5-6, it is clear that the shapes of the curves are different from those represented in the standards (fib Model Code, 2010; EHE-08, 2008) which are clearly based on SFRC. All the fracture curves obtained in the PFRC mixes resemble that shown in Figure 5-3. Therefore, after reaching the minimum post-peak load value (L_{MIN}) the material is capable of sustaining higher loads and reaching a maximum post peak value (L_{REM}). Consequently, the brittleness limitation stated by the strength value at f_{R1} might be of relative significance when these regulations are used to assess the performance of PFRC. However, analysis of Table 6 reveals that SCC10 and VCC10 met the aforementioned requirements. In contrast, when VCC4.5 and SCC4.5 were

studied, although it is clear that these mixes did not fulfil the requirements, the lack of brittleness was evident. The latter is shown by the increment of the load that takes place in both mixes, VCC4.5 and SCC4.5, after reaching L_{MIN}. Regarding VCC3 and SCC3, although brittleness is avoided due to the increment of load that the material can bear at f_{R3}, there is only a 10% improvement of the strength between f_{R1} and f_{R3}. Therefore, its use should involve a careful study of the post-peak loading situations that can appear.

Table 5-5: Residual strength of concrete.

	$f_{ct,l}$ (MPa)	f_{R1}(MPa)	% $f_{ct,l}$	f_{R2} (MPa)	% $f_{ct,l}$	f_{R3} (MPa)	% $f_{ct,l}$	f_{R4} (MPa)	% $f_{ct,l}$
VCC3	4.81	0.93	19%	0.95	20%	0.91	29%	0.97	21%
SCC3	5.21	0.93	19%	0.93	19%	1.15	24%	1.27	26%
VCC4.5	4.74	1.06	22%	1.13	24%	1.40	29%	1.56	33%
SCC4.5	5.23	0.95	18%	1.03	20%	1.25	24%	1.32	25%
VCC10	4.21	1.98	47%	2.45	58%	2.87	68%	3.05	72%
SCC10	5.22	2.41	46%	3.16	61%	3.87	74%	4.16	80%

5.7 Fracture surface analysis

When the fracture surfaces were studied, it was evident that they were eminently flat and, therefore, the effect of the size of the aggregates in the fracture behaviour was negligible. Thus, the differences in the post-peak behaviour of all the PFRCs was analysed by counting the fibres in the fracture surfaces generated after the three-point bending tests. Figure 5-7 shows that the fibres in the fracture surface can be either broken or pulled out. It is worth noting that in the case of macro-polymer fibres, they can also be folded. In order to obtain accurate results, the pulled-out fibres were added to the broken fibres, obtaining the total number of polyolefin fibres in each fracture surface generated. The average results and total amount of fibres obtained can be seen in Table 5-6, as well as the coefficient of variation of the counts.

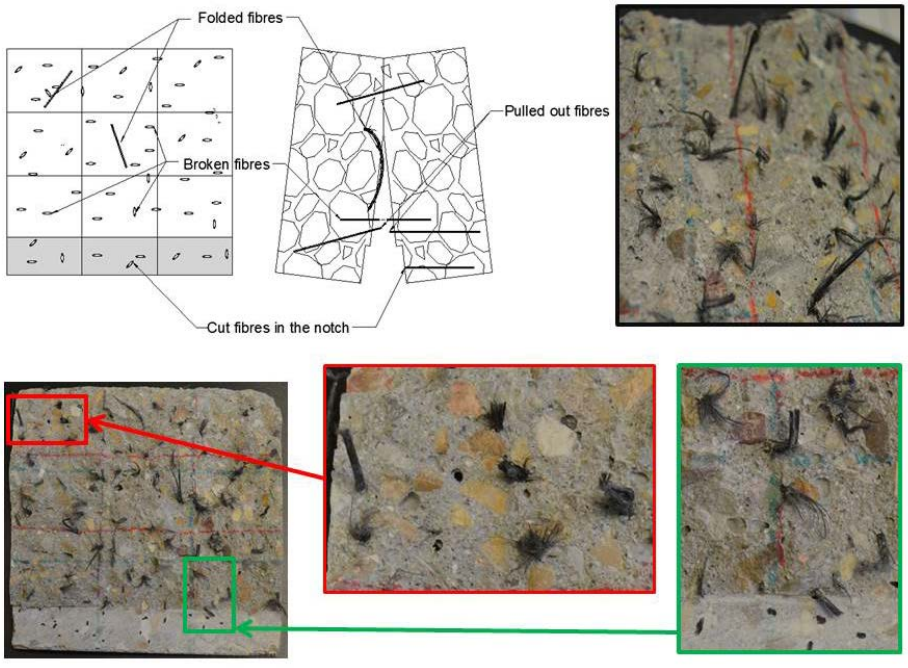

Figure 5-7: Fracture surface of a tested specimen with broken, cut, folded and pulled-out fibres.

In addition, the theoretical number of fibres in the fracture surface can be deduced by using expression (5-3), adapted from (Krenchel, 1975), (Soroushian & Lee, 1990) and (Dupont & Vandewalle, 2005).

$$\#th\ fibres = \frac{A \cdot V_f}{A_f} \qquad (5-3)$$

where V_f is the volumetric fraction computed with expression (3-1), A_f is the cross section of one fibre. By using these relations, the theoretical amount of fibres in the sections for the three amounts of fibres studied was found. The mixes with 3, 4.5 and 10 kg/m³ of fibres were expected to find in the fracture surfaces 111, 167 and 372 fibres respectively.

In order to compare the real amount of fibres and the theoretical number of fibres, a coefficient (θ), commonly known as orientation factor, that is calculated in accordance with expression (5-4) was obtained. This coefficient can be also seen in Table 5-6.

$$\theta = \frac{\#\ fibres\ counted}{\#\ fibres\ theoretical} \qquad (5-4)$$

Table 5-6: Data obtained in the counting of fibres and coefficient θ.

	# fibres th	*# fibres*	c.v. (%)	*θ*
VCC3	111	64	30.5%	0.58
SCC3	111	71	14.2%	0.64
VCC4.5	167	102	9.2%	0.61
SCC4.5	167	81	18.3%	0.49
VCC10	372	204	5.4%	0.55
SCC10	372	223	4.0%	0.60

The coefficient θ provides a comparison between the ideal disposition of the fibres and the real one. When θ is equal to one, the disposition of the fibres would be perpendicular to the fracture surface and, therefore, the amount of fibres counted and the theoretical would be the same. Conversely, if the fibres are parallel to the fracture surface, given that no fibre would be crossing the surface generated, the coefficient would be equal to zero. Consequently, the closer the value of θ to unity the better would be the orientation of the fibres for the case of the flexural tensile tests. As can be observed in Table 5-6, the highest orientation factor was obtained for SCC3. In addition, SCC10 and VCC4.5 and VCC3 showed similar values. The value of θ in SCC4.5 was noticeable lower than in the rest of formulations. It should also be noted that the mixes with higher amounts of fibres had more limited scatter. Moreover, as the amount of fibres decreases, as in VCC3, SCC3, VCC4.5 and SCC4.5, the scatter increased and was noticeably higher in VCC3 and SCC4.5 in comparison with their analogue formulations.

As shown by previous published studies, the existence of walls influences the orientation of the fibres within a piece of FRC (Kooiman, et al., 2000), (Stähli, et al., 2008), (Laranjeira, et al., 2012), (Dupont & Vandewalle, 2005), (Şanal & Özyurt Zihnioğlu, 2013), (Švec, et al., 2014), (Martinie & Roussel, 2011). In order to assess the influence of the walls of the mould in the disposition of the fibres, a more detailed counting process was performed. The latter was carried out by considering the recommendations of RILEM TC-162 placed in reference (Barr, et al., 2003). Here the fracture surface was divided in nine sectors equally spaced, with the notched surface being ignored. As Figure 5-8 shows, if the fibres were homogeneously distributed the percentage of fibres in each sector could be easily obtained. Moreover, an image of a real fracture surface has been also included in the figure where the

nine sectors are divided by red lines. The pouring direction of concrete is included too. The experimental results shown in Figure 5-9, Figure 5-10 and Figure 5-11 are the average values of fibres in each type of concrete.

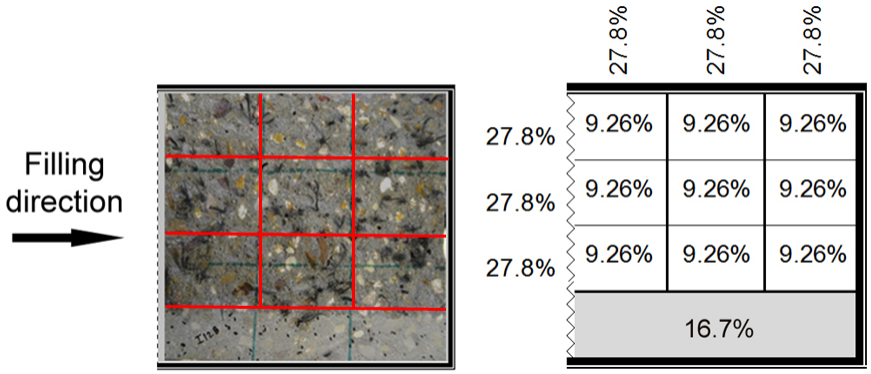

Figure 5-8: Theoretical distributions of fibres within the fracture surface.

The results obtained in the counting exercise performed in the mixes with 3 kg/m^3 of fibres can be seen in Figure 5-9. It also offers the percentage of the distribution of the fibres obtained which enables comparison with the theoretical distribution shown in Figure 5-8. Regarding VCC3, there was an almost uniform distribution of the fibres except for the central third of the fracture area generated, where there was a lack of fibres. Consequently, the amount of fibres that were not in the middle third seemed to be located in the top third, where 34.4% were placed. In addition, the percentage of fibres found in the notched area was above the theoretical values. As regards the distribution of fibres within the specimens manufactured with SCC3, there is a lack of fibres in the lower third of the fracture surface, especially in the central sector.

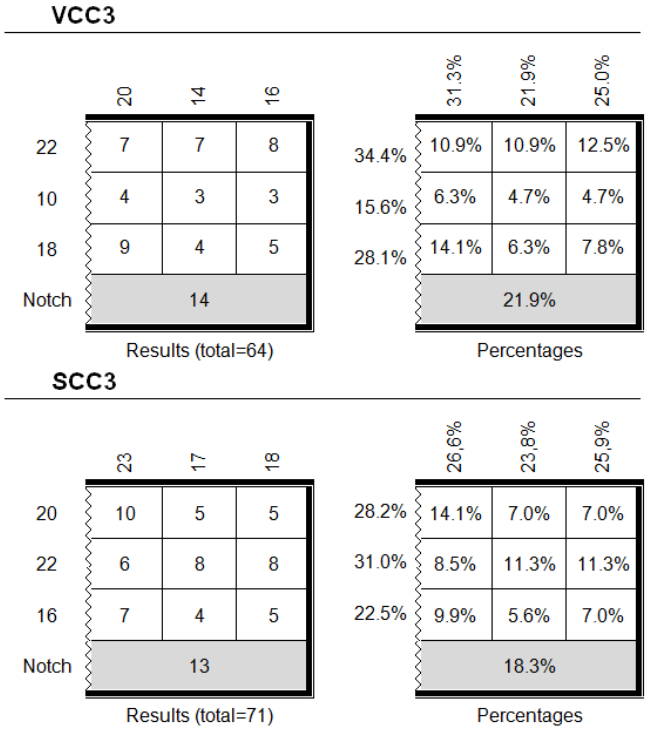

Figure 5-9: Fibre distribution in the fracture surfaces of a PFRC with 3 kg/m³ of fibres.

In the case of VCC4.5, Figure 5-10 reveals that the sectors that gathered higher amounts of fibres were those not near the lateral sides of the formwork. This might have been caused by the wall effect that has been previously detected in the aforementioned references. Consequently, the lower third and middle third of the fracture surface boasted fewer fibres than the theoretical prediction. As regards the distribution of fibres of SCC4.5 specimens, there was an anomalous distribution of fibres within the section. There was an extremely high amount of fibres in the upper third of the fracture surface that corresponds to one of the lateral sides of the mould. Nevertheless, the other lateral side, corresponding to the notched area, showed a lack of fibres that discarded the possibility of the wall effect being responsible for this tendency.

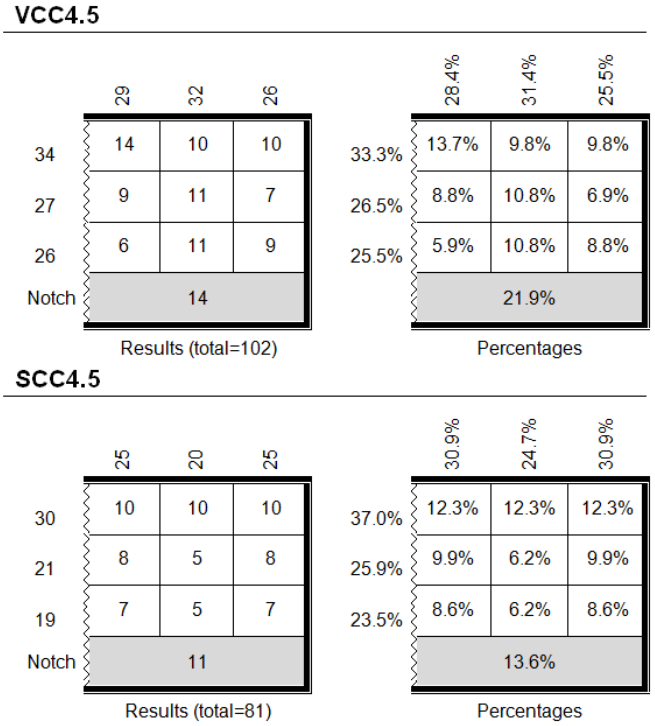

Figure 5-10: Fibre distribution in the fracture surfaces of a PFRC with 4.5 kg/m³ of fibres.

The specimens manufactured with VCC10 showed a clear tendency to gather higher amounts of fibres in the proximity of the lateral sides of the moulds, as Figure 5-11 shows. This can be observed by comparing the theoretical and real distribution of fibres in the upper third of the fracture area and in the notched area. Conversely, the specimens of SCC10 showed a homogeneous distribution of fibres. There is only a slight shift of fibres from the lower third of the fracture surface area towards the notched area.

If the nine equal sectors of the ligament area were considered, the homogeneity of the distribution of fibres could be evaluated by comparing the coefficient of variation of the number of fibres placed in each sector. In such a way, it would become a coefficient of distribution of the fibres (c.d.) in the respective surface. The lower the latter, the more uniform is the distribution. Consequently, a value of 0 would report an even distribution of fibres. The results are computed and summarised in Table 5-7, as well as the average number of fibres per sector of each concrete type. By analysing the table, for low contents of fibres slight differences can be found in the final distribution inside the fracture surface. In contrast, fibre positioning was remarkably improved in terms of distribution for 10 kg/m³ of polyolefin fibres in using self-compacting concrete. As can be seen, the differences in

the average number per sector are smaller than the differences in the value of the coefficient of distribution.

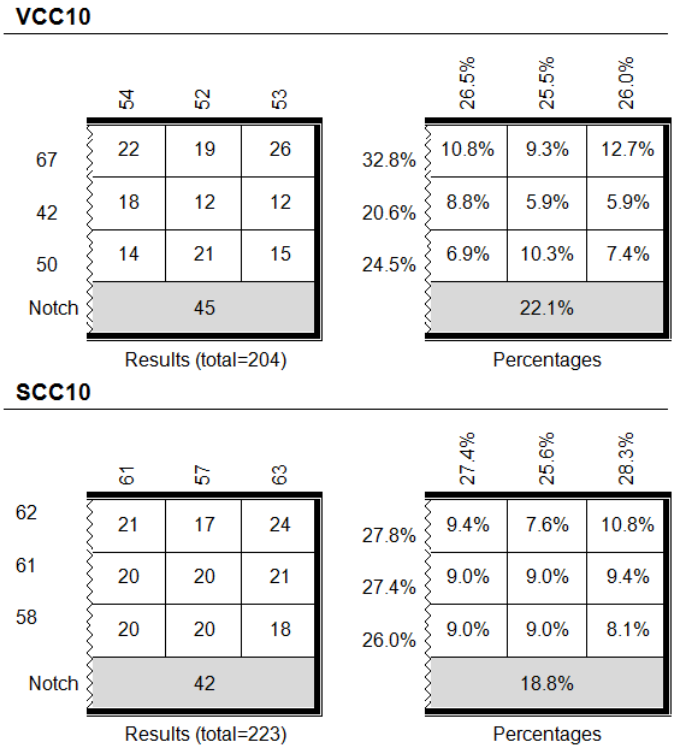

Figure 5-11: Fibre distribution in the fracture surfaces of a PFRC with 10 kg/m³ of fibres.

However, it remains unclear to what extent the distribution affected fracture results which are, at the end, the keystone in use of PFRC. The influence of the fresh state of the material in the post-peak behaviour cannot be clearly deduced when analysing Figure 5-9, Figure 5-10 and Figure 5-11 and Table 5-7.

Table 5-7: Average fibres per sector and the coefficient of distribution in the ligament surface.

Concrete	Average fibres per sector	Coefficient of distribution (c.d.)
VCC3	6	0.40
SCC3	7	0.39
VCC4.5	10	0.26
SCC4.5	8	0.26
VCC10	20	0.40
SCC10	22	0.32

With the aim of correlating the post-peak behaviour of the combinations tested with the counting process performed in the fracture surfaces, the total amount of fibres was divided in the three thirds of the ligament area. When the initial cracking is taking place, only the fibres placed in the lower part of the section are active. During the advance of the cracking process, more fibres could be considered to be bridging the crack. In this regard, when the crack sufficiently expands most of the fibres could be considered to be bearing stresses as shown in Figure 5-12.

This justified dividing the counting in sectors and thirds, in order to associate the residual loads with the active fibres in each crack opening or deformation state. The most important

parameters that determined the behaviour of concrete after reaching L_{PEAK} were the minimum load for small deflection values, L_{MIN}, and the maximum load after L_{MIN}, termed L_{REM}. These names have been previously used when explaining Figure 5-3.

The influence of the fibres in the upper two thirds of the ligament was considered negligible in the L_{MIN} values, In addition, a linear experimental correlation between the number of fibres and the value of L_{MIN} could be obtained. The latter can be better understood by examining Figure 5-12.

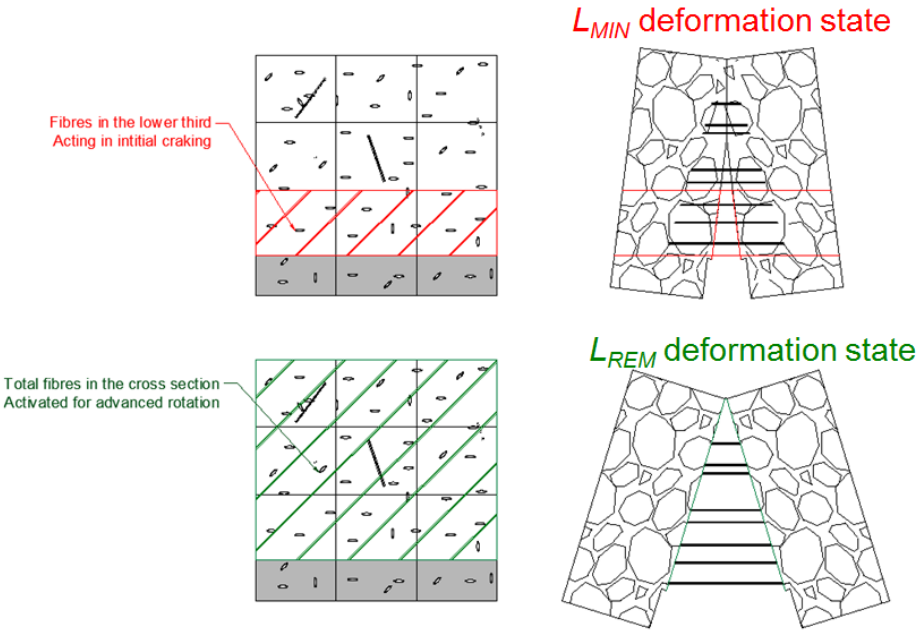

Figure 5-12: Division of the ligament area for relating the number of fibres with the post-cracking behaviour of PFRC.

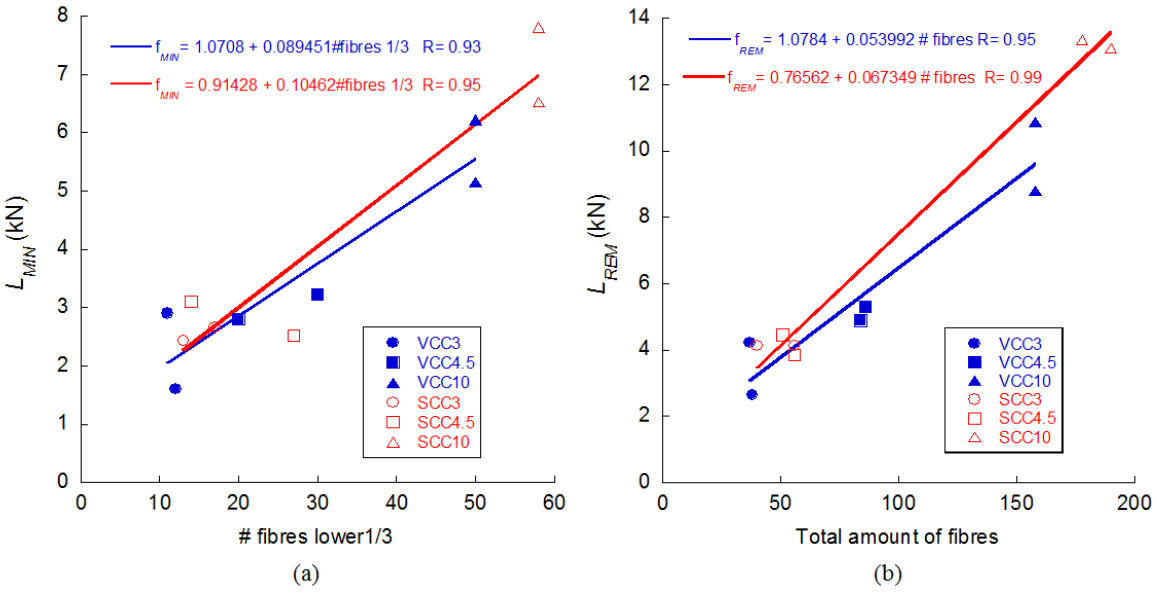

Figure 5-13: Relation between residual load and number of fibres: (a) L_{MIN} versus amount of fibres in the lower third of the fracture surface generated;(b) L_{REM} versus the total amount of fibres in the fracture surface generated.

The relation between the amounts of fibres located in the lower third of the fracture section and L_{MIN} values is shown Figure 5-13(a). In addition to the data gathered, a linear fitting for both VCC and SCC is computed. The two lines are close to each other, even though there was limited experimental data. Therefore, it seemed that there was no influence of the fresh-state properties of concrete on its fracture behaviour when laboratory specimens are studied. In addition, Figure 5-13(b) shows that when small dosages of fibres were used, there was a wider scatter in the results. Consequently, the circles that correspond to mixes SCC3 and VCC3 are close to some of the tests performed on SCC4.5 and VCC4.5.

When the relation between the maximum post-peak load (L_{REM}) and the total amount of fibres are analysed in a similar manner as in Figure 5-13(a), the similar behaviour of VCC and SCC observed was confirmed. Although the total amount of fibres in the sections was unequal, the maximum post-peak load borne by the specimen at high-strain states in the VCC and SCC mixes had a linear relation with the total number of fibres, as can be seen in the correlation coefficients in Figure 5-13(a). As in Figure 5-13(a), it can be seen in Figure 5-13(b) that in the SCC specimens there was a closer relation between the number of fibres and the specimen behaviour at high-strain states. Moreover, the correlation coefficients of SCC in both figures confirms that although there was no standardised procedure to fill the moulds when using SCC, the homogeneity of the material is better than in VCC. The slope of SCC linear fittings was higher in both figures, which may imply a better performance of an individual fibre in SCC than in VCC.

5.8 Conclusions

This Chapter has examined the influence of the fresh state of PFRC on its mechanical properties and durability. Fracture tests performed on VCC and SCC reinforced with 3, 4.5 and 10 kg/m^3 respectively of polyolefin fibres have shown similar behaviour, enabling a confident use of PFRC. In addition, the mixes with a 10 kg/m^3 dosage of fibres, VCC10 and SCC10, have met the requirements established in the standards that permit consideration of the contribution of the fibres in the structural design of a PFRC element.

The differences in fracture behaviour observed have been studied by analysing the fracture surfaces generated. This has been performed by means of a counting procedure that showed that SCC seems to distribute the fibres more homogeneously within the specimen length. Moreover, the effect of the walls of the moulds seemed to have a significant influence on the positioning of the fibres in VCC specimens. This phenomenon has been assessed by dividing the fracture surface generated in nine equal sectors and comparing the fibres found with an ideal disposition of the fibres within such a section.

A linear relation between the two main turning points of the fracture behaviour of PFRC, L_{MIN} and L_{REM}, and the amount of fibres in the lower third of the fracture surface and total amount of fibres in each surface has been established. According to the data assembled, it seems that the specimens manufactured with SCC had a more homogenous behaviour in spite of the absence of a standardised filling procedure of the moulds.

Regarding the other mechanical properties, it seems that f_{ct} and f_{ck} of the combinations of VCC and SCC studied were slightly influenced by the presence of fibres. On another note, the modulus of elasticity might decrease with significant amounts of fibres due to the worse compaction of the fresh concrete. In any case, all these results remain within the margins of a standard experimental scatter and should be handled carefully.

The durability performance of all the concretes manufactured has been assessed by means of permeability tests. According to the results obtained, it could be stated that the presence

of fibres do not influence the connected porosity network of concrete. The differences observed between the performance of VCC and SCC could be attributed to the changes induced by the different aggregate skeletons of the two types of concrete. In addition, all the mixes performed with SCC were suitable for use in extremely hazardous environments such as those in chemical industries or in the marine tidal range. In the case of VCC mixes, they were apt for use in medium hazardous environments, such as those in direct contact with marine water, erosive materials and in freeze-thaw conditions.

Additionally, with the results obtained some design considerations could be suggested, even though wider research on structural sizes would be useful. The relation between the number of fibres and the residual strengths of the material allows the designer to take advantage of the external vibration or the flux of SCC in order to improve their structural response of a certain element. In such a sense, as the fibre dosage was increased greater differences between VCC and SCC could be noticed. The most uniform distribution of the fibres was found for SCC specimens. And when producing elements with shapes that may be improved by taking advantage of wall effects, VCC was found to be the more influenced. An additional and sounder design consideration could be taken into account regarding durability, since the fibres did not increase the connected porosity of the concrete.

Chapter 6

Polyolefin fibre-reinforced concrete enhanced with steel-hooked fibres in low proportions

6.1 Introduction

Among the fibres used, the most common are made of steel due to their high modulus of elasticity and tensile strength. Concrete with steel fibres has been widely employed in the building industry for some time in applications such as industrial and airport pavements, reinforcement of projected concrete, and precast elements with reduced thickness, among others (Di Prisco, et al., 2008). These uses have been based on extensive studies of the mechanical behaviour of this type of concrete under tensile stresses, fatigue or even impact (Caverzan, et al., 2011; Lok & Zhao, 2004; Goel, et al., 2012). However, there are certain applications (such as tunnels and continuous slabs of high-speed railway) in which a concern about the effect of steel fibres on the magnetic and electric fields has led to the quantity of fibres used being reduced. Furthermore, the influence of the corrosion of steel fibres in the durability and performance of concrete remains a matter of study (Jean-Louis Granju, 2005; ACI Committee 544, Reapproved 2009).

One way of overcoming these problems is by adding several shapes and sizes of fibres made from the same material (Park, et al., 2012). The synergies that appear through using

this option have been previously studied (Vandewalle, 2007). Another way is adding fibres made from different materials and with dissimilar shapes (Abdulkadir Cüneyt Aydin, 2007; Yao, et al., 2003; Skazlic & Bjegovic, 2004; Vandewalle, 2006; Wang, et al., 2012). Some studies have analysed the synergies that appear when mixing different types of steel and polypropylene fibres (Qian & Stroeven, 2000a; Qian & Stroeven, 2000b). In such studies, the optimum proportions of fibres are established, as well as the contribution of the fibres to the mechanical properties of the composite material. In addition, the behaviour of this material was studied under repeated loading (Kooiman, et al., 2000). However, the newest technology in precast factories and for *in situ* applications, together with the improvements in concrete admixtures, enables production of SCC at a more competitive cost. This is achieved by reducing the cement content and by having a minimum amount of super-plasticizer (Sonebi, 2004), thus promoting the research of modifications of this type of concrete. The conjunction of SCC and fibre-reinforced concrete is one such option. The workability of concrete with a cocktail of steel fibres, the fibre anisotropy and the mechanical and fracture properties have been recently studied (Sahmaran, et al., 2005; Stähli, et al., 2007; Burcu Akcay, 2012; Pająk & Ponikiewski, 2013). Due to the problems previously mentioned, cocktails of synthetic and steel fibres added to SCC are analysed. Other studies have examined the effect of different proportions and fibre shapes, changes in the workability of the concrete (Ding, et al., 2008), and the respective mechanical properties (Ding, et al., 2009; Dawood & Ramli, 2012). In addition to these, some have viewed the contribution of two different types of fibres (steel and polypropylene) added to a standard reinforced concrete beam (You, et al., 2011). Nonetheless, almost all of these studies have been performed through using one type of fibre that is not structural, polypropylene fibre, and one fibre that can be considered structural, steel fibre.

Polyolefin fibres provide a twofold benefit: an alternative when a structural contribution of fibres is needed and use of steel fibres is unwise or inadmissible (Buratti, et al., 2011); and synergies in steel fibres and synthetic structural fibres (Oh, et al., 2007). One of the possible advantages over steel fibres could be improved performance in fresh state (which should be validated on a SCC). The weak point of synthetic fibres, probably caused by the low modulus of elasticity and the frictional adhesion with matrix, is the reduced load borne at small deformations when compared to a steel fibre-reinforced concrete (SFRC) (Zerbino, et al., 2012).

At the time of writing, given that a SCC with a cocktail of two types of structural fibres of different nature, polyolefin and steel fibres, is still a matter of study, there are both fresh and hardened characteristics of the concrete that merit analysis. Regarding SCC, there are subjects that might be of interest such as the improvement in self-compactability caused by the substitution of a certain amount of steel fibres for polyolefin ones and changes in the polyolefin fibre orientation that the presence of steel fibres may produce. Concerning the hardened properties, there are no analyses of the behaviour of a self-compacting hybrid fibre-reinforced concrete performed with polyolefin and steel fibres under tensile or compressive stresses. Furthermore, it could be of significant interest to study the fracture properties and toughness of a concrete with a cocktail of polyolefin and steel fibres with the aim of evaluating the possible use in structures instead of a standard reinforced concrete. Another way to focus research could be to improve a polyolefin fibre-reinforced concrete with a small quantity of steel fibres, enhancing the fracture behaviour on the very first deformations. With a low amount of short steel-hooked fibres it would be possible to reduce the load drop, due to its mechanical properties and the hooked shape. When they fail, the high deformations already reached would mobilize polyolefin fibres resistance

which would bear stresses up to much higher deformations. Additionally, this would allow a total traditional reinforcement substitution.

In order to achieve these objectives, an experimental campaign was performed by adding two amounts of polyolefin fibres, 4.5 and 6 kg/m³, to a reference SCC. This involved assessment of the fresh-state behaviour and the hardened and fracture properties, as well as the flexural and toughness improvements that the polyolefin fibres provide to the control SCC. To compare the influence of the types of fibres, two amounts of steel fibres (with volume fractions of 0.33% and 0.49%) were added to the same control SCC and the fresh and hardened properties studied. To study the synergies between the steel fibres and the new structural synthetic fibres in a SCC, manufacture of a SCC with polyolefin and steel fibres was attempted. This entailed two hybrid fibre-reinforced concretes being manufactured with the following amount of fibres: 25.88 kg/m³ and 4.5 kg/m³ of steel and polyolefin fibres respectively and 20 kg/m³ and 6 kg/m³ steel and polyolefin fibres respectively. These two hybrid concretes were characterized and their properties compared with those of the SCC reinforced only with one type of fibre.

Given that the contribution of fibres in the fracture process is strongly influenced by their distribution and orientation, if different mechanical behaviours are obtained, they may be explained due to an improved fibre positioning. To analyse this phenomenon a counting exercise was carried out in the fracture surfaces and related to the fracture tests.

6.2 Materials and mix proportioning

6.2.1 Materials

For the concrete production, the same materials described in Chapter 4 were used. In this case, two types of fibres were used: steel-hooked fibres with a smooth surface and 35 mm long, and polyolefin straight fibres with a rough surface and surface treatment and 60 mm long. Table 6-1 compares the main characteristics of the types of fibre, their material properties and their geometrical patterns. The concrete mix proportioning used was also described in subsection 4.2.2. A slight difference in the time schedule for the mixtures with the two types of fibres can be seen in Figure 6-1.

One plain concrete was manufactured in order to compare the influence of adding fibres and was named REF. To obtain a reasonable value of hybrid fibre proportions added to a SCC, values in the medium and lower threshold of their use were chosen for the two mixtures of steel fibres. However, regarding the polyolefin fibre contents, medium amounts were employed to reach as high a number of fibres as possible in the hybrid concretes. Two fibre contents of two fibre types had to be added to the hybrid FRC. In order to maintain the fresh properties close to the reference SCC exceeding 1% in volume fraction was avoided. All are summarized in Table 6-2.

Hence, a volume fraction of fibres of 0.49% was chosen to perform one mixture of both polyolefin and steel fibres separately. In the end, as it allowed a meaningful comparison of fresh and hardened properties a direct evaluation of the fracture behaviour of the two types could be carried out. For the SFRC, the volume fraction of 0.33% was also used in order to obtain a result in the lower threshold of their use. In terms of weight, this was equivalent to adding 25.88 kg/m³ of fibres. In the case of the volume fraction of 0.49%, this represented 38.82 kg/m³ of steel fibres. In that of polyolefin fibres, the same volume fraction was in terms of weight 4.5 kg/m³. One more mixture, with 0.66% or 6 kg/m³, was also manufactured for a subsequent comparison with hybrid mixtures. The two mixtures with

steel fibres were called S33 and S49 and the two mixtures with polyolefin fibres called P49 and P66.

Table 6-1: Properties of steel and polyolefin fibres.

PF SF 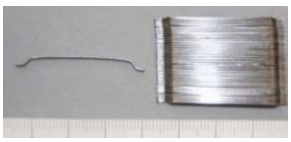

Fibre shape	Straight		Hooked	
Density	0.910	g/cm³	7.850	g/cm³
Length	60	mm	35	mm
Eq. diameter	0.903	mm	0.550	mm
Tensile strength	>500	MPa	1100	MPa
Modulus of elasticity	> 9	GPa	210	GPa
# Fibres per kg	27000		14500	
Surface structure	Rough		Smooth	

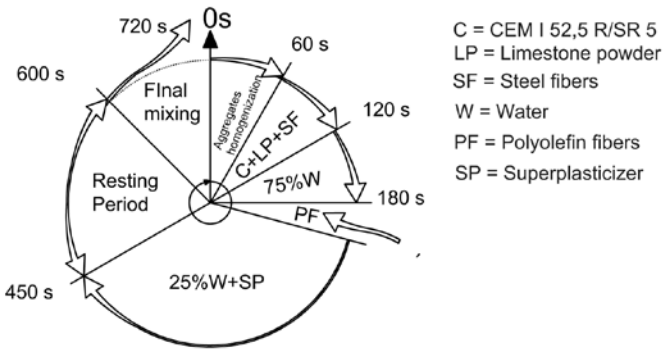

Figure 6-1: Mixing sequence.

The hybrid fibre proportions added to the mix were chosen with the aim of achieving an improved polyolefin fibre reinforced concrete (PFRC) with a small quantity of steel fibres. In that sense, the smaller fraction volume explained above of 0.33% was chosen to evaluate the synergies when a fibre cocktail with a 0.49% volume fraction of polyolefin fibres was added. This hybrid mixture was called H1, with a total fibre volume fraction of 0.82% having a total addition of 30.5 kg/m³ of fibres.

The research purpose was to produce a FRC with a combined use of both types of fibres that preserved the fresh properties and enhanced the concrete hardened behaviour of PFRC with a small amount of steel-hooked fibres. With that aim, one more hybrid mixture was produced in which the quantity of steel fibres was lessened to 20 kg/m³ (with a corresponding volume fraction of 0.25%) and mixed with up to 6 kg/m³ of polyolefin fibres completing the mix H2. While it is true that the total fibre volume fraction reached 0.91% (with it being higher than in H1), in terms of weight this entailed a total weight of fibres of 26 kg/m³ and reduction of 4.5 kg/m³. Furthermore, it allowed a comparison between two hybrid mixtures.

Table 6-2: Concrete mix proportions.

Cement (kg/m³)	LP (kg/m³)	SP (%Cement)	Water (kg/m³)	Sand (kg/m³)	Grit (kg/m³)	Gravel (kg/m³)
375	200	1.25	187.5	918	245	367

	SCC	PFRC		SFRC		Hybrid FRC	
Mixture	REF	P49	P66	S33	S49	H1	H2
Steel fibres (kg/m³)	-	-	-	25.9	38.8	25.9	20
Polyolefin fibres (kg/m³)	-	4.5	6	-	-	4.5	6

Based on the plain SCC mix design used as reference (REF), the six FRC mixtures were manufactured. In addition to the mentioned REF, FRC mixtures S33, S49, P49 and P66 were performed with only one type of fibres. Hybrid FRC mixtures H1 and H2 completed the research, as was previously stated, and is shown in Table 6-2. All were manufactured with a vertical axis concrete-mixer with 100 l of capacity. Nine cylindrical specimens with a diameter of 150 mm and height of 300 mm, and three prismatic specimens of dimension 430x100x100 mm³, were produced for each mixture. All the specimens were cured in a climatic chamber (20ºC and 95% humidity) until the age of testing.

6.3 Tests program and results

6.3.1 Assessment of fresh-state concrete properties

In order to characterize and compare the fresh-state behaviour of every concrete type, two tests were performed. The slump-flow test described in the standard EN: 12350-8 (EN 12350-8, 2010) and the V-funnel test in the standard EN: 12350-9 (EN 12350-9, 2010). The results of both tests on every concrete type are shown in Table 6-3.

It should be noted that all the results for REF and monotype FRC were among the limits of the most common standards which set a slump-flow spread (d_f) from 550 mm to 850 mm, a time for the slump-flow patty to reach 500 mm of diameter (T_{500}) lower than 8 s, and an emptying time of the V-funnel between four and 25 seconds (Walraven, 2003).

The slump-flow spread mean diameters showed a reduction, as expected, with the addition of fibres when compared with the results of plain concrete REF. As also anticipated, steel fibres had more influence on the flow properties with significant reduction of the patty. Times obtained for T_{500} remained at similar values for all the concrete types. In Figure 6-2 the slump-flow spread of the hybrid mixture H1 is portrayed to highlight the uniform distribution of fibres and the aggregates on the spread and also with no segregation signs.

As regards the V-funnel test results, it is important to mention that the hybrid mixtures had significantly higher fibre proportions which led to higher emptying times being obtained. Given that the test measures the fluidity and passing capacity, fibre addition increased the emptying times as the volume fraction rose. According to this, for hybrid mixtures, such emptying times were higher and for H2 mixture reached 25s which, while close to the upper limit, was still considered satisfactory.

Figure 6-2: Visual appearance of the slump-flow spread of H1.

Table 6-3: Test results for assessment of fresh concrete and mechanical properties.

Concrete	Slump flow test		V-funnel	f_{ck} (MPa)		E (GPa)	f_{ct} (MPa)	
	d_f (mm)	T_{500} (s)	t (s)	28d	c.v.	28d	28d	c.v.
REF	655	3.5	8	39.0	0.01	35.8	3.78	0.14
S33	570	3.5	10	41.7	0.01	33.7	5.32	0.15
S49	570	3.5	14	43.0	0.01	31.9	6.19	0.07
P49	600	3.5	11	38.5	0.06	31.2	4.18	0.20
P66	590	4.0	16	41.4	0.01	31.6	4.09	0.03
H1	565	4.0	14	36.5	0.03	33.0	5.41	0.04
H2	560	4.0	25	36.9	0.02	31.8	5.35	0.08

6.3.2 Assessment of mechanical properties

In order to obtain and compare the mechanical properties, the compressive strength, tensile splitting strength and modulus of elasticity were measured in accordance with the standards EN 12390-3 (EN 12390-3, 2009), EN 12390-6 (EN 12390-6, 2009) and ASTM C469-02e1 (ASTM C469-02e1, 2006). Three cylindrical specimens of each concrete type were tested for obtaining the compressive strength and tensile splitting strength. Modulus of elasticity was determined in one cylindrical specimen of each mixture. Table 6-3 shows the mean values and the coefficient of variation of the results. In Figure 6-3, a mechanical properties variation of each FRC on the basis of the plain REF mixture is performed.

Table 6-3 shows that for medium fibre contents of both types of fibres, compressive strength slightly increased as compared with the reference concrete. The compressive strength of P49 was similar to the reference concrete, while for P66, S33 and S49 it increased as may be seen in Figure 6-3. It should be pointed out that all the mono-fibre mixtures had very close results to the REF mixture, at around 39 MPa. It is also noticeable that the addition of fibres did not imply compaction problems and that the results were similar in that they also had low dispersions.

Figure 6-3 reveals that the compressive strength for hybrid mixtures decreased. As the fibre volume fraction added was approximately doubled and the self-compacting properties decreased, such a change may be attributed to a worse compaction. Through comparing hybrid fibre mixtures, it may be observed that the compressive strength was similar in both mixtures and close to 37 MPa which entailed a drop of 5%.

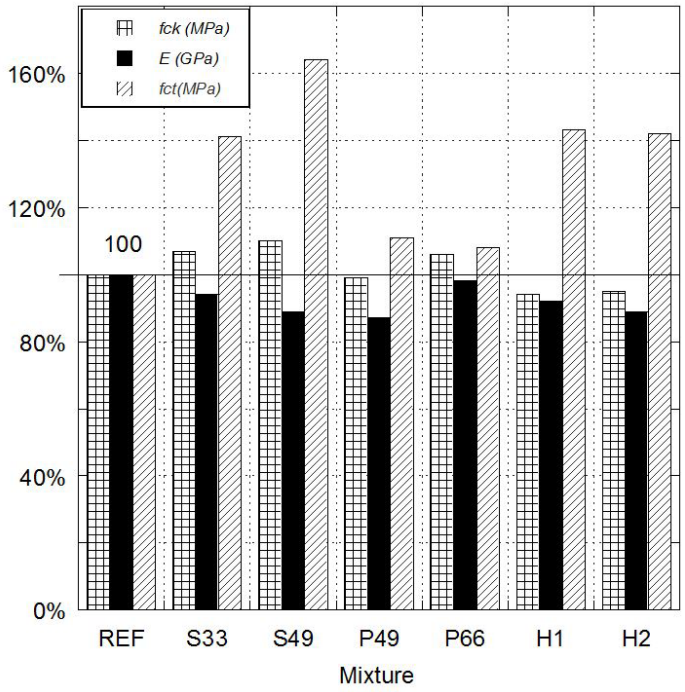

Figure 6-3: Mechanical properties.

Fibre addition increased indirect tensile strength in all concretes. For REF mixture the tensile strength obtained was in the order of magnitude expected. The best performance was obtained with the steel fibres that showed the best results, which was probably due to the anchorage of the fibres and the higher modulus of elasticity of the material itself. Moreover, the addition of polyolefin fibre also increased tensile strength.

Combination of the types of fibres provided similar results when both hybrid mixtures (H1 and H2) were compared. The result was 40% higher for the REF mixture and at values between the PFRC and SFRC (which was expected).

The reference concrete modulus of elasticity was close to 36GPa and decreased slightly for all concrete types with fibres. These results fitted those expected for PFRC, due to the lower modulus of elasticity of the fibres. In the case of steel fibres with a modulus of elasticity of six times higher when compared with concrete, some other reasons such as a worse compaction (the SCC compaction was under its own weight, without vibration) might have caused the lower results of the composite material. Hybrid mixtures had similar values and were also in the gap of the results obtained for the conventional mono-fibre FRC mixtures.

6.3.3 Flexural tensile strength

Test setup

The tests were performed in accordance with RILEM TC-187-SOC (RILEM TC-187-SOC, 2007) with the same configuration of the three-point bending tests that were carried out in Chapter 4. The scheme can be seen in Figure 4-4. Three prismatic specimens of each concrete type with dimensions 430x100x100 mm³ were tested. Thus, span was chosen as three times the depth and the notch height as one third of the depth in the centre of the span and the test was initially controlled by a clip-on gage CMOD device placed on the notch. Deflection was also measured by two LVDT devices on each side of the specimen. Time,

load and the machine actuator position data were also registered. Similarly to Chapter 4, when FRC deformations were higher than the upper limit of the CMOD device, the test control was changed to the actuator position until the end of the test.

Test results and discussion

In order to obtain the fracture energy of each concrete, load-deflection curves and load-CMOD curves were assembled. As previously mentioned, the load-CMOD curves registered values of only up to 4 mm. The comparable end of the test was defined at 8 mm of deflection. At that moment, no FRC specimens had collapsed. Three fracture tests were performed for every concrete mixture (Figure 6-4 and Figure 6-5 show the mean curves). Two main turning points of the curve shapes were also extracted (later discussed and shown in Table 6-4). The peak load (L_{PEAK}), defined as the first maximum load before the softening post-cracking branch and the minimum post-cracking load (L_{MIN}), were extracted. A summary of these values and the residual loads up to a CMOD of 0.5 mm, 1.5 mm, 2.5 mm and 3.5 mm extracted from load-CMOD curves, as well as the fracture energy results referring to deflection values of 1 mm, 5 mm and 8 mm determined from the load-deflection curves, are reported in Table 6-4.

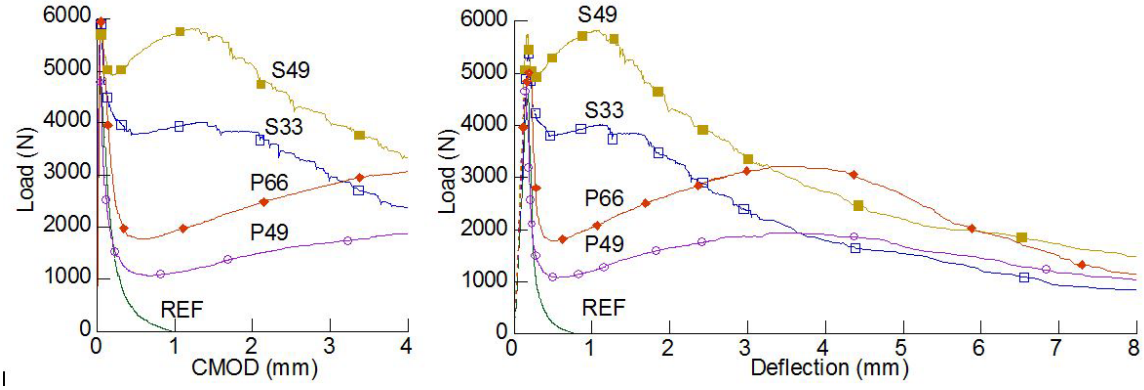

Figure 6-4: Mean load-CMOD and load-deflection curves for monotype FRC mixtures.

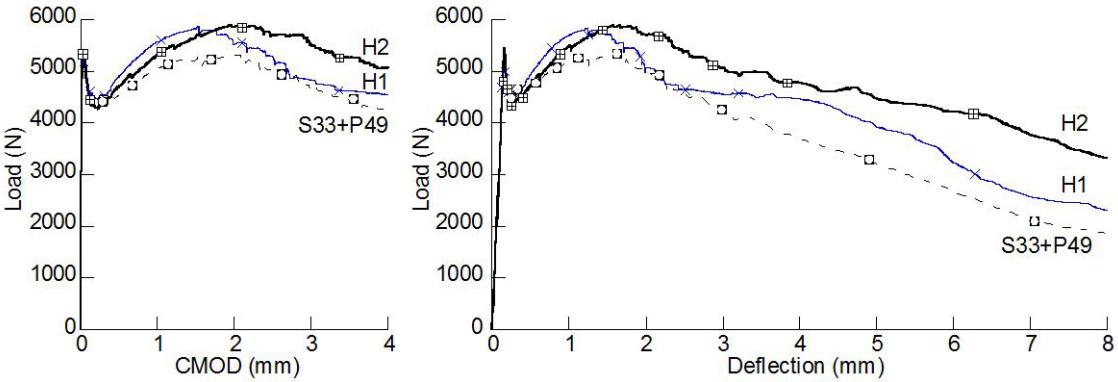

Figure 6-5: Mean load-CMOD and load-deflection curves for hybrid FRC.

A comparison of the experimental mean load-CMOD and load-deflection curves of the monotype FRC mixtures is shown in Figure 6-4. The behaviour of the reference concrete specimens was linear up to an elastic limit of about 50% of the peak load; from then on a deviation from linearity was observed due to the appearance and propagation of micro-cracks with the crack mouth width thus increasing faster. Once the peak load was reached, a clear softening branch followed until a quasi-brittle fracture occurred, dividing the specimens in two parts. The addition of a low fibre volume fraction of steel or polyolefin

fibres enabled a ductile behaviour. As the micro-cracks connected with each other and formed larger cracks, in addition to increasing the peak load, the fibres bridged more effectively both faces of the fracture surface which meant an improvement in the post-peak load bearing capacity and flexural toughness. When compared with the reference concrete specimens, as may be seen in Table 6-4, the higher the fibre volume content the better is the post-cracking response obtained.

Table 6-4: Mean values of load and fracture energy (G_F) of concrete mixtures

Concrete	L_{PEAK} (N)	*c.v.*	L_{MIN} (N)	*c.v.*	$L_{R0.5}$ (N)	*c.v.*	$L_{R1.5}$ (N)	*c.v.*	$L_{R2.5}$ (N)	*c.v.*	$L_{R3.5}$ (N)	*c.v.*	Fracture energy, G_F (N/m)		
													1mm	5mm	8mm
REF	4970	0.04	-	-	-	-	-	-	-	-	-	-	130	-	-
S33	5975	0.06	3733	0.06	3764	0.05	3943	0.03	3406	0.06	2689	0.06	570	2135	2621
S49	5766	0.07	4900	0.16	5303	0.06	5660	0.09	4443	0.05	3732	0.10	752	2935	3759
P49	5655	0.01	1064	0.33	1131	0.31	1301	0.37	1640	0.38	1810	0.40	254	1292	1846
P66	6120	0.06	1754	0.23	1775	0.20	2142	0.26	2632	0.27	2999	0.26	347	2065	2769
H1	5412	0.03	4454	0.11	4893	0.08	5827	0.10	5294	0.07	4627	0.08	709	3577	4931
H2	5515	0.07	4287	0.07	4708	0.07	5650	0.04	5700	0.11	5266	0.12	679	3707	5583

SFRC specimens S33 and S49 showed increases in peak load of 20% and 16% respectively when compared with the reference concrete. S33 had almost constant residual loads of about 65% of peak load across the CMOD range of 0.5-1.5 mm. S49 exhibited a pseudo-hardening response as the steel fibres began to pull out from the matrix with residual loads of 92% and 98% of peak load in the same CMOD range. Then, as the hooked-end fibres with short embedded length were pulled out, a slight softening and descending branch took place until the end of the test in both concretes.

PFRC specimens P49 and P66 showed an increment of the peak load of 14% and 23% respectively. In both concretes, after reaching the peak load, a steep descending branch began up to CMOD near 0.5 mm. At that point, P66 showed a load decay of about 71%, while the P49 load drop was 81% of peak load. The residual loads increased substantially afterwards and almost linearly, recovering more than 49% of the peak load in concrete P66 and 32% of the peak load in concrete P49 at CMOD 3.5 mm. However, the highest residual loads were obtained from the load-deflection curves at deflection near 4 mm with values of 55% and 34% of their peak loads for P66 and P49 respectively. This indicates that polyolefin fibres at the used volumes require a considerable crack opening within the small displacement range (suffering the consequence of abrupt load decay after peak load) to improve the after-cracking behaviour of the composite. The interlock between the fibre and the cracked matrix absorbs a considerable amount of energy in the large displacement range due to its moderate tensile strength and high elongation capacity.

If the results obtained from S49 and P49 (which had the same volume fraction content) are compared, the post-cracking strength and flexural toughness were higher in S49, due to steel fibre higher modulus and better anchorage with concrete matrix, as might have been expected. However, the absorption of energy performed by polyolefin fibres in large displacements was greater than that of steel fibres if fibres are compared weight for weight. For example, P66 with 6 kg/m^3 of polyolefin fibres had higher fracture energy than S33 with 26 kg/m^3 of steel fibres at a displacement value of 8 mm.

A comparison of mean load-CMOD and load-deflection curves between hybrid fibre-reinforced concretes H1 (0.33% SF + 0.49% PF) and H2 (0.25% SF + 0.66% PF) is shown in Figure 6-5. The addition of flexural responses of both concretes S33 and P49 (with one type of fibre) resulted in a lower analytical curve compared with that experimentally obtained from H1. Therefore, a synergy effect between short hooked-end steel fibres and macro plastic polyolefin fibres led to an improved flexural tensile response of the hybrid-fibre concretes. The mutual presence of the two types of fibres not only helped each fibre to mobilize more efficiently energy absorption capacity (obtaining residual loads in the first softening phase of 82% and 78% of the peak load in concrete H1 and H2 respectively), but also enabled a pronounced pseudo-hardening response and more stable post-cracking behaviour compared with monotype FRC mixtures. Concrete H2, which had a total volume fraction of 1.11 times that of concrete H1, with 5 kg/m^3 less steel fibre and 1.5 kg/m^3 more polyolefin fibre, exhibited a better post-cracking response from CMOD 1.5 mm until the end of the test, showing higher flexural toughness than concrete H1.

Figure 6-6 shows the relative residual loads in the specified CMOD values calculated as a percentage of the peak load of each mixture. The presence of two types of fibres in the hybrid concrete led to a more stable post-cracking behaviour and higher residual values when compared with mono-fibre-reinforced concretes. Figure 6-6 also shows the fracture energy of FRC mixtures in contrast to the fracture energy of the reference concrete in the specified deflection values. The fracture energy for a 5 mm and 8 mm deflection of hybrid composites is noticeably higher than for mono-fibre-reinforced concretes. Though the total fibre dosage of S49 (39 kg/m^3 of steel fibres) was higher than that of H1 (26 kg/m^3 SF + 4.5 kg/m^3 PF) and of H2 (20 kg/m^3 SF + 6 kg/m^3 PF), the residual loads of H1 and H2 were improved appreciably for CMOD greater than 1.5 mm.

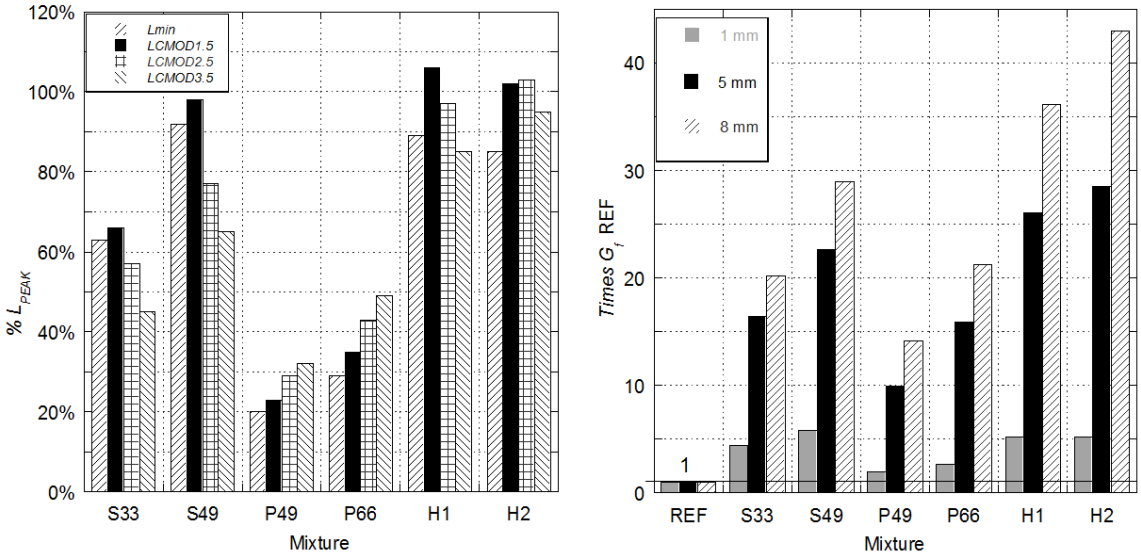

Figure 6-6: Residual strengths and fracture energy.

As may be seen in Figure 6-4, Figure 6-5 and Figure 6-6, the combination of small amounts of hooked-end steel fibres with low and moderate volume fractions of polyolefin fibres (0.49% and 0.66%) provide the reference concrete matrix with a significant degree of energy absorption ability. These synthetic macro-plastic fibres provide good energy absorption within the large displacement range, while the steel fibres improve residual load-bearing capacity in the small displacement range. Therefore, a material with a remarkable performance at low strains, which correlates with the serviceability limit state, was obtained. Moreover, this material showed stable post-cracking response and drastically improved fracture energy in the displacement values of 5 mm and 8 mm. These improvements were achieved, thus, using a low total content of fibres in weight.

Fracture surface analysis

The abovementioned synergy (shown in Figure 6-5), with a rise in fracture results of H1 if compared with the sum of S33 and P49, suggested that the types of fibres interacted with each other, with the result being an enhancement of the composite properties. The reasons for this obtained extra rise could be explained by means of a fracture surface analysis. As previously shown, the post-cracking concrete behaviour is closely linked with the number and distribution of fibres (Dawood & Ramli, 2012). In addition, it is known that steel fibres are rigid and tend to align with the flow of SCC, as previous research has shown, (Komloš, et al., 1995) though it should be noted that the low density and flexible nature of polyolefin fibres may cause a non-uniform distribution of the fibres.

In order to study the improvement achieved in the hybrid concretes, the fracture surfaces of all the concretes were analysed. Specimens with only polyolefin fibres showed deficient orientation of the fibres as some were curved or even folded, as may be seen in Figure 6-7(a). Furthermore, the distribution was not uniform on the fracture surface and contrary to what took place in the concretes with only steel fibres. Nonetheless, when hybrid FRC fracture surfaces were examined the orientation of both types of fibres seemed to be aligned with the same prevailing orientation, as may be seen in Figure 6-7(b) and Figure 6-7(c). The presence of the steel fibres may have oriented the polyolefin fibres, improving the fracture energy and load bearing capacities of H1 more than if the same amounts and types of fibres were added individually.

The theoretical number of fibres (*th*) placed in the fracture surface was obtained for each concrete by using expressions (3-1) or (5-3), considering that the fibres were uniformly distributed and perpendicular to the crack. The average total number of fibres obtained from the counting exercise and its coefficient of variation (c.v.) is shown in Table 6-5. Furthermore, the relation between the fibres counted in a given cross-section (*n*) and theoretical number of fibres (*th*) are shown in Table 6-5. This relation θ is the so-called "orientation factor" or "fibre efficiency factor" that assumes a homogeneous distribution of fibres in the section (Martinie & Roussel, 2011) and which may be computed with expression (6-1).

$$\theta = \frac{n}{th} = n\frac{A_f}{V_f A} \qquad (6-1)$$

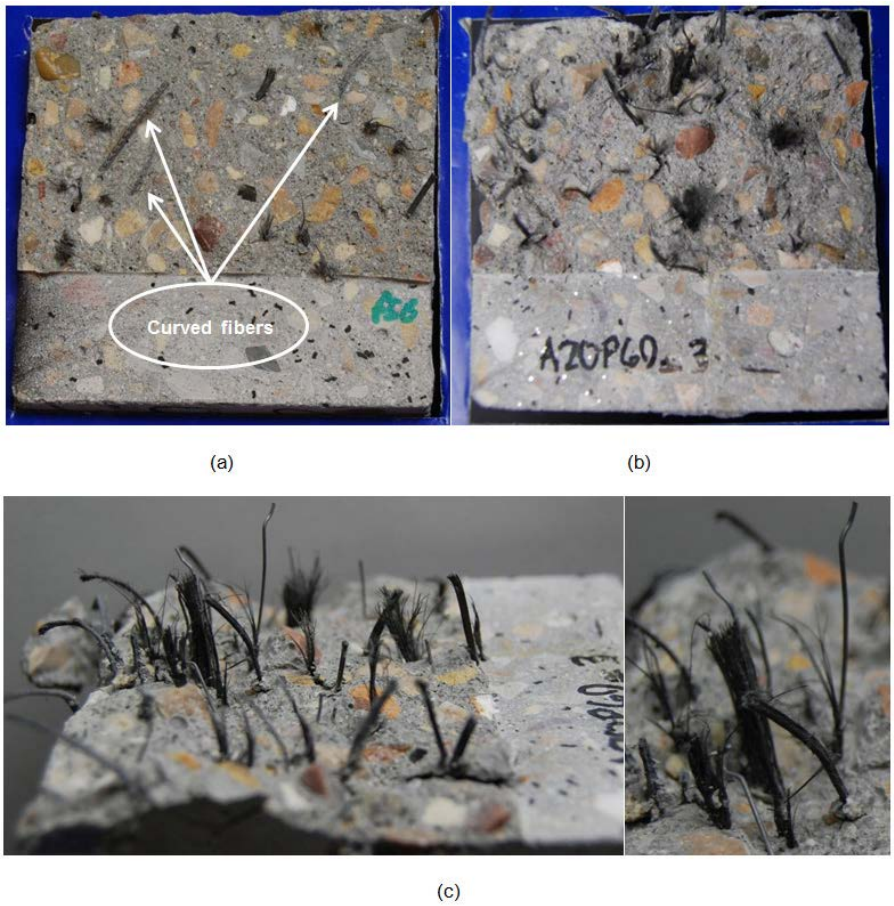

Figure 6-7: Hybrid FRC improved fibre orientation of polyolefin fibres: (a) Fracture surface of a P66 specimen; (b) Fracture surface of a H2 specimen; (c) Profile of a Hybrid FRC (H2).

Table 6-5: Number of fibres on the fracture surface.

Concrete	# theoretical		# average total		c.v. (%)		θ	
	SF	PF	SF	PF	SF	PF	SF	PF
S33	139	-	94	-	14%	-	0.68	-
S49	208	-	104	-	2%	-	0.50	-
P49	-	74	-	45	-	13%	-	0.61
P66	-	99	-	64	-	28%	-	0.65
H1	139	74	104	47	4%	7%	0.75	0.63
H2	107	99	83	75	10%	16%	0.78	0.76

In the fracture surface analysis shown in Table 6-5, some observations regarding the counting process should be made. First of all, the steel fibres that appear in each half of the tested sample should be added because all of them were pulled-out. In relation to the polyolefin fibres, 79% were clearly broken and only 21% were pulled-out on average. Consequently, the total number of polyolefin fibres was obtained, in each sample, by adding the broken and the pulled-out fibres of the two fracture surfaces generated.

Regarding the distribution of fibres along the specimen, the coefficient of variation showed less scattering in the distribution of the steel fibres. The SCC flow showed good performance in spreading evenly the metallic rigid fibres. However, when polyolefin fibres

were analysed, the coefficient of variation rose up to 28% for P66 concrete. The use of a combination of steel and polyolefin fibres led to a sound improvement in terms of scatter when compared with the mixes manufactured only with polyolefin fibres. The lowest dispersion was found for the H1 mixture with coefficients of variation of 4% and 7% for steel and polyolefin fibre respectively.

On another note, if fibres were perfectly aligned, the number of fibres counted would match the theoretical value and, therefore, the ratio θ would be the unity. Consequently, the counting process supplies a value that deals with the orientation of the fibres. The values obtained for θ were remarkably higher for hybrid mixtures, as can be seen when comparing H1 with S33 and P49 and H2 with S49 and P66.

6.4 Conclusions

The development of polyolefin fibres with improved mechanical properties, in addition to surface treatments which enhance adhesion with matrix, both allow production of high-performance concretes with good ductility and flexural toughness. The polyolefin fibres are light and show a significant deformation capacity. The addition of a low amount of fibres enables a stable and reliable post-cracking behaviour, maintaining fresh properties and with a lower weight of fibres.

It is possible to produce a hybrid fibre reinforced self-compacting concrete with a combination of hooked steel fibres and macro polyolefin fibres, preserving the high performance fresh properties within the most common self-compacting requirements. It should also be noted that the addition of fibres did not noticeably change the compressive strength, indirect tensile strength or modulus of elasticity of the reference SCC for any of the amounts, types or combination of fibres used.

It was possible to make a polyolefin fibre-reinforced concrete improved with the addition of low amounts (20-26 kg/m³) of hooked steel fibres. The fracture toughness and ductility, as well as residual strength, were increased if compared with the same proportions added separately and subsequently combined. This synergy in the fracture results led to a high-performance concrete capable of bearing loads close to the peak-load for deflections of L/60.

The weak point of polyolefin fibre-reinforced concrete for structural design, it could be argued, might be for small deflections. It is possible to produce a concrete with an almost constant post-cracking load bearing capacity by adding steel fibres to the fibre cocktail in the case of structural use being demanded. This Chapter suggests that it could be possible to produce a hybrid fibre-reinforced concrete with a fibre cocktail made of steel-hooked fibres and macro polyolefin fibres with a bilinear fracture load-deflection behaviour. The combination of the two types of anchorage chosen, it would seem, could offer a suitable joint action.

The combination of stiff and heavy fibre with a low density flexible synthetic macro fibre showed an additional advantage that enhances the orientation of the polyolefin fibres. The steel fibres enhanced the alignment of the polyolefin fibres, tending to place both types of fibres with the preferential orientation of the flow of self-compacting concrete. This improving effect was observed on the fracture surface of the specimens that showed the same preferential orientation for both types of fibres and a more uniform distribution of the polyolefin fibres.

Chapter 7

Pull-out behaviour and microstructural analysis

7.1 Introduction

Fibre bridging depends on the efficiency of the fibre-matrix interface property (Zollo, 1997). Regarding this inter-relationship, the shape of the fibre has been widely used in order to provide mechanical anchorages that increase the energy needed to extract the fibre from the matrix. However, the general effects that govern the process of pull-out are the bond adhesion and interfacial shear stress along the fibre-matrix interface. Some other significant effects are also needed to assess pull-out behaviour, such as the influence of the inclining angle and the achievement of the critical embedded length in which the fibre acts in all its tensile capacity (Li, et al., 1990; Laranjeira, et al., 2010a). Enhancement of fibre-pull-out has been at the centre of research, especially given that the possibilities to improve the post-cracking response of FRC are directly related. While research has encompassed a large variety of shapes and constituent materials of the fibres (Li, et al., 1997), it is possible to obtain relevant information by means of pull-out tests applied either to ease the selection of the fibre type or improve the fibre-performance and interface (Oh, et al., 2007). Moreover, with the data obtained from pull-out tests, even numerical models for the tensile

behaviour of the material have been developed (Naaman, 2003; Breitenbücher, et al., 2014). However, at the time of writing there is lack of research on the pull-out mechanisms of polyolefin based structural macro-polymer fibres.

In this study, two types of test configuration have been used with distinct purposes. The first one was performed with the aim of achieving the value of the critical length, placing polyolefin fibres inside a conventional mortar cube. The second line of work was performed by means of pull-out tests of polyolefin fibres embedded in several lengths and by varying the angle of incidence in a specimen made of self-compacting concrete (SCC) produced with the same mix as that examined in chapters 4, 5 and 6. This was carried out with digital image analysis (DIC) that allowed the initial elastic deformation of the fibre to be considered, in order to achieve the real pull-out curve once the displacement inside the matrix had started. Additionally, a qualitative analysis was completed by means of scanning electron microscopy (SEM) to analyse the microstructural composition of the interface fibre-matrix. The conclusions showed that the type of tests performed with digital analysis provide accurate results. The polyolefin fibre-matrix interactions were found to be especially suitable in terms of microstructure, with the pull-out results showing that polyolefin fibres outperformed steel straight fibres and had remarkable performance inside the cementitious matrix. It was found that performance was better when the fibre was embedded in the real concrete than in tests carried out with mortar. The inclining angle affects the pull-out behaviour. The peak load reached the maximum with an inclination of 45º and the maximum work to produce debonding occurred with 30º of inclining. The critical length is close to 20 mm of the embedded length.

7.2 Experimental details

7.2.1 Materials and specimens

The production methods of each mixture and configurations chosen are described in this subsection. Two types of cementitious matrixes were produced: mortar specimens and SCC specimens. Inside each piece, a polyolefin fibre was embedded (the properties are summarised in Table 4-3).

The mortar specimens were cubes of dimensions 40x40x40 mm³ with the fibre crossing them with an incidence angle of 90º at one of the faces. The mortar composition was performed according to the standard EN 196-1 (EN 196-1, 2005). A plastic cylinder sheath with the fibre inside was positioned across the mould from one side to the other. In order to assure the orientation and embedded length, the plastic sheaths were placed with only exposed the length designed for each case being left. The visual aspect of one specimen and the pouring procedure can be better understood after observing Figure 7-1 and Figure 7-2, where it can be noted that the specimens were painted in black for a better performance of the digital image analysis. The following five specimens with three embedded lengths were tested: 10, 20 and 30 mm. In such a sense, it is worth noting that 120 mm long fibres were provided by the manufacturer to assure that there was enough length inside the grip in order to avoid slip between the jaws and the fibre. The latter was additionally verified by processing the results of individual fibres tensile test with digital image analysis techniques.

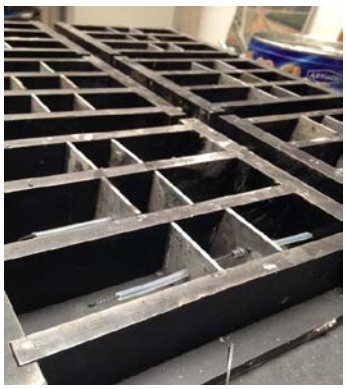

Figure 7-1: Empty moulds prepared for being poured with standardised mortar.

Figure 7-2: Visual aspect of the mortar specimens and the pouring of the moulds.

As regards the SCC specimens, the shape was cylindrical with a diameter of 90 mm. The height of the specimen was 60 mm. The details of the production of the concrete can be seen in Chapters 4, 5, and 6, with the mix proportioning being shown in Table 7-1 with a picture and the results of the slump flow test obtained in accordance with the standard EN-12350-8 (EN 12350-8, 2010).

Table 7-1: Concrete mix proportions, slump flow and characteristic strength.

Material		SCC
Cement (kg/m^3)		375
Limestone powder (kg/m^3)		200
Water (kg/m^3)		187.5
Sand (kg/m^3)		918
Grit (kg/m^3)		245
Gravel (kg/m^3)		367
w/c		0.50
Superplasticizer (kg/m^3)		4.7
	% cement weight	1.25
Slump-flow test	T_{500} (s)	3.25
	d_f (mm)	695
Characteristic strength, $f_{ck,28}$ (MPa)		39

Concerning the positioning of the fibres, cylindrical pieces of 50 mm thick made of expanded polystyrene were used as caps. In order to ensure that the incidence angle of the fibre and protruding length were the desired ones, the fibre was first fixed to the cap. Once the concrete was poured, the cap was carefully positioned in a manner that it covered the specimen. This can be seen in Figure 7-3. Before the test, the specimens were labelled and painted in black in the same manner and with the same aim as in the mortar specimens. Additionally, in both mortar and concrete specimens the surface in contact with the metallic frame was covered by Teflon tape to minimise the friction between the specimen and the metallic frame. Two specimens with 10 mm of embedded length and with 15 and 30 degrees of inclining angle are shown in Figure 7-4. The lengths produced were 5, 10, 15, 20, 25, 30 mm and the angles chosen 0º, 15º, 30º, 45º and 60º. This made a total number of 30 combinations tested. Three samples were produced from each combination of embedded length and incidence angle. To characterise the concrete properties, three 28-day cylindrical specimens with a diameter of 100 mm diameter and height of 150 mm were also manufactured and tested according to EN 12390-3 (EN 12390-3, 2009). The results showed a significant degree of resemblance with those produced in previous chapters (4, 5 and 6) with a characteristic compressive strength of 39 MPa.

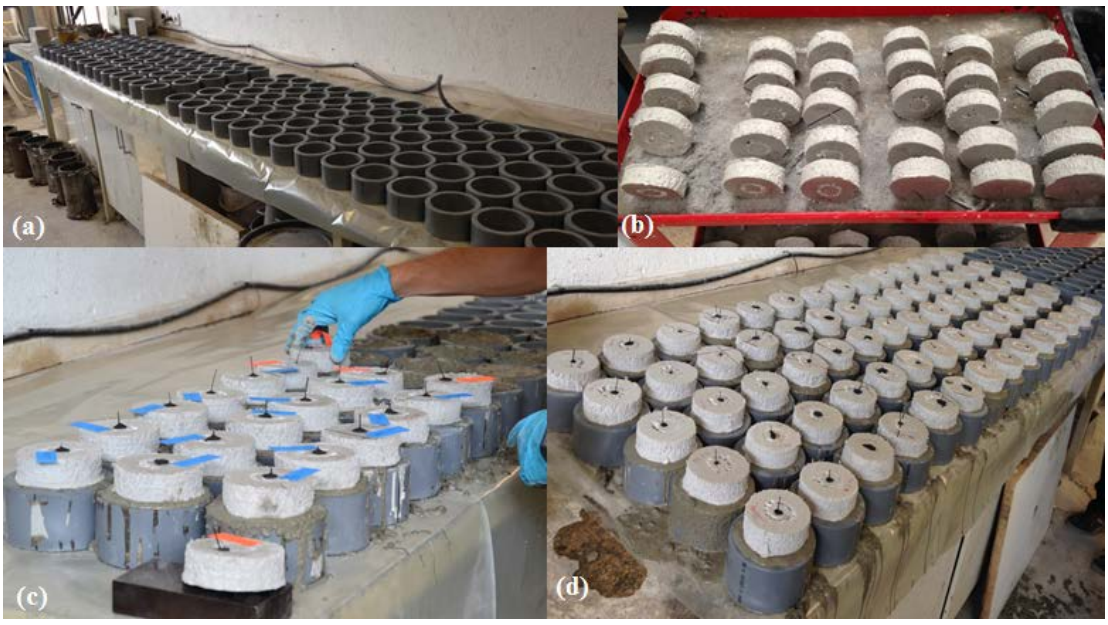

Figure 7-3: Manufacturing of the concrete samples, a) moulds, b)caps with the fibres inserted, c)positioning of the caps, d)setting of concrete with the fibres embedded.

Figure 7-4: Visual aspect before testing of two specimens with embedded length 10 mm long and incidence angle 15 and 30 degrees.

7.2.2 Test setup and procedures

The test setup comprised a metallic frame manufactured with two parallel aluminium plates fixed at a certain distance that stood on stainless steel bolts and washers. Both plates were 10 mm thick, with the top one having a slot cut. The latter enabled all the visible parts of the fibre to be recorded during the tests. As the fibre never crossed the concrete specimens, it was possible to fit the distance between the two plates equal to the height of the cylindrical piece. The schematic description of this test setup is depicted in Figure 7-5. The aluminium plate placed at the bottom slightly compressed the concrete piece. This eased the positioning and assured non-relative movements. It also allowed the use of commercially available 60 mm long fibres.

The video recorded one image per second by use of a high-definition IDS UI-1480SE camera. This device has a five-megapixel sensor with a resolution of 2560x1920 pixels. Such a sensor outperforms the conventional ones and obtains high-sensitivity and low-noise images that are appropriate for DIC.

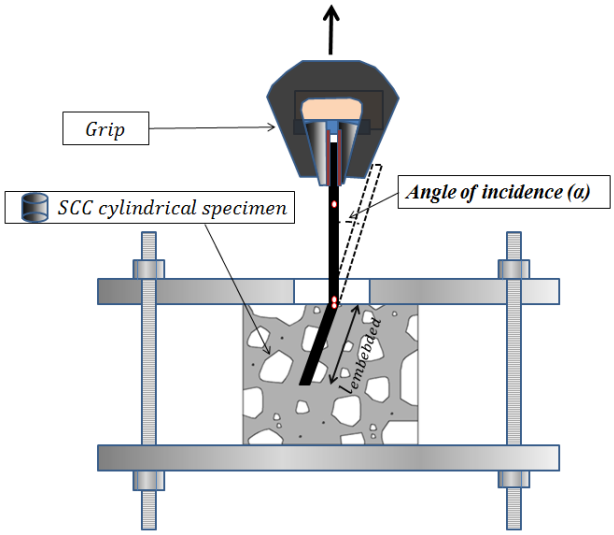

Figure 7-5: Sketch of the test configuration using concrete specimens.

The application of a two-dimensional image analysis can be achieved by synchronising mechanical testing and video recording. Given the availability of the frame rate and existence of the same time origin, the data from each source can be combined and load, strain and displacement related. While the load of the tests was obtained directly from the testing machine, the displacement, slip and strains had to be obtained from the recorded images. In order to do this, white spots were painted in various positions of the fibre, mortar or concrete block and the jaws that had been painted black. The aforementioned points can be seen in Figure 7-6. With the software *ImageJ* it was possible to determine the position of the gravity centre of each white point painted in all the images and, therefore, obtain the movement, displacement and strains.

Through processing these images, any non-desired displacement between the elements of the test setup would be detected. For instance, as the images would record any slip of fibre inside the grip this test would be ignored. This technique was used to obtain the minimum length that prevents the fibre inside the jaw from slipping when testing independent fibres. These tests were also used to tune the actuator displacement rate. In addition, the results assessed the mean ultimate stress of the fibres, which was 376 MPa.

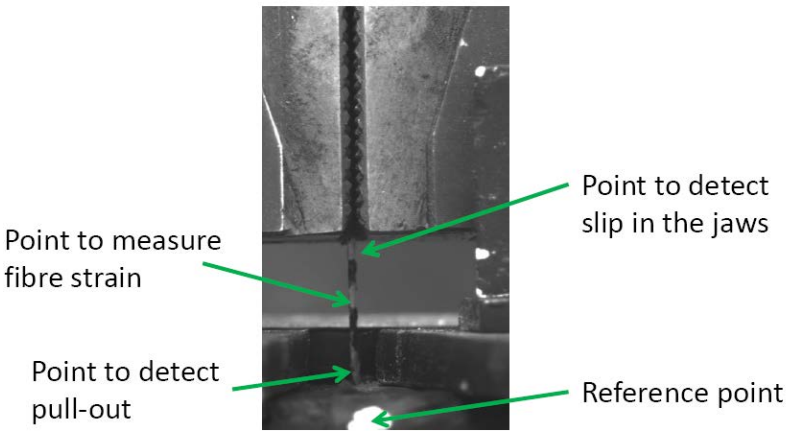

Figure 7-6: Points used to obtain slip, strain or fibre slip inside the jaws.

In the case of the mortar pieces, the tests concluded that fibres longer than the commercially available of 60 mm were required if measurement of the displacement of the fibres protruding in the opposite side of the mortar cube was required. Such displacement allowed assessment of when the frictional stage had started and when full debonding had taken place. Hence, during the tests the mortar piece was hanging from the fibre and held by the grip as shown in Figure 7-7. Since the upper aluminium plate impeded the ascension of the specimen, the only possible relative displacement between the plate and the grip was fibre pull-out. Similarly to the concrete tests, the position of the white dots (painted in analogous positions) permitted the study to attain the elastic strains of the fibres, the relative movements once bond adhesion had been surpassed, and the displacement of the fibres in any moment. In addition, the longer length of the fibres allowed measurement of the frictional adhesion of a fibre sliding inside the mortar beyond the samples performed with concrete and commercial fibres.

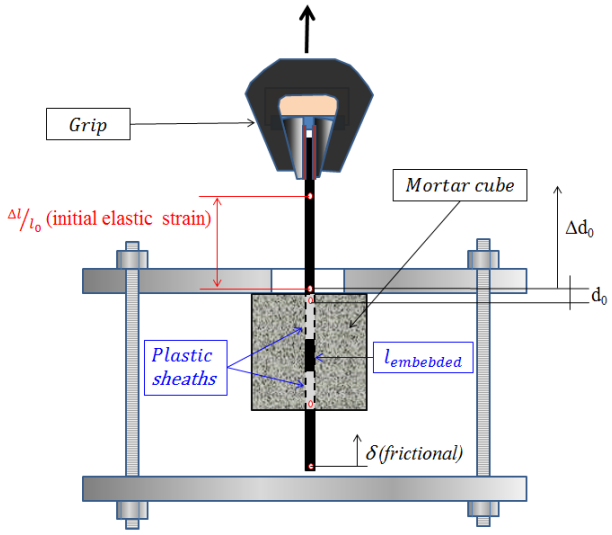

Figure 7-7: Sketch of the test configuration using mortar specimens.

The tests were controlled for both, mortar and concrete specimens, by the position of the actuator, which had a displacement rate of 0.02 mm/s.

7.3 Results and discussion

7.3.1 Representative curves and critical mean values

The typical scatter of fibre pull-out tests was obtained and can be seen in Figure 7-8 and Figure 7-9. In order to assess the representative curve, some curves were discarded and the representative one chosen from the other two. This procedure was chosen instead of averaging the curve, given that such a procedure produces a softening of the real shape of the curves. In the case of polyolefin fibres, this would represent a loss of information due to the typical squiggly line obtained that reflects their embossed surface. The information about the degree of scatter can still be evaluated by means of the coefficient of variation of the representative and critical values of the curves. Hence, it would be apparent that the procedure provides more useful visual information (the critical values are shown in tables with their corresponding coefficient of variation among the three specimens tested for each pull-out test configuration). It is worth noting that since the initial elastic strains were removed, the curves treated with digital image analysis start when the spot placed at the entrance of the fibres started moving and not at the initial load recorded by the load cell.

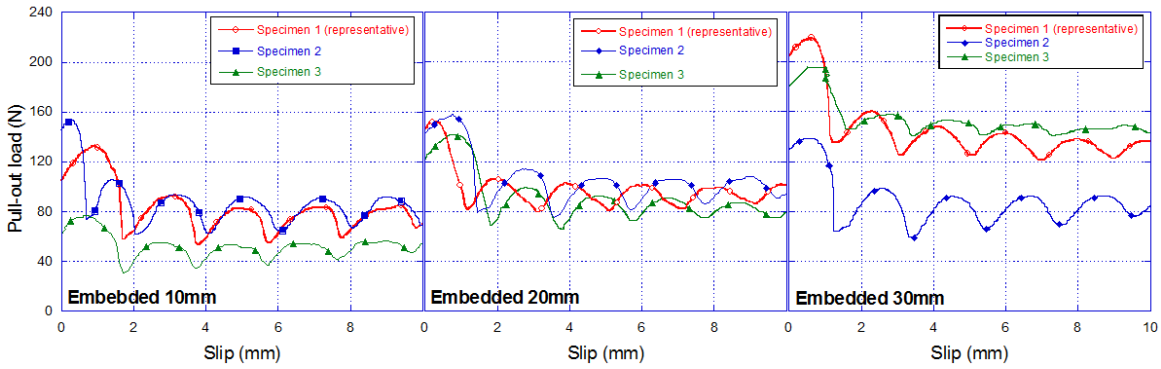

Figure 7-8: Scatter of the pull-out results of polyolefin fibres embedded in mortar matrix.

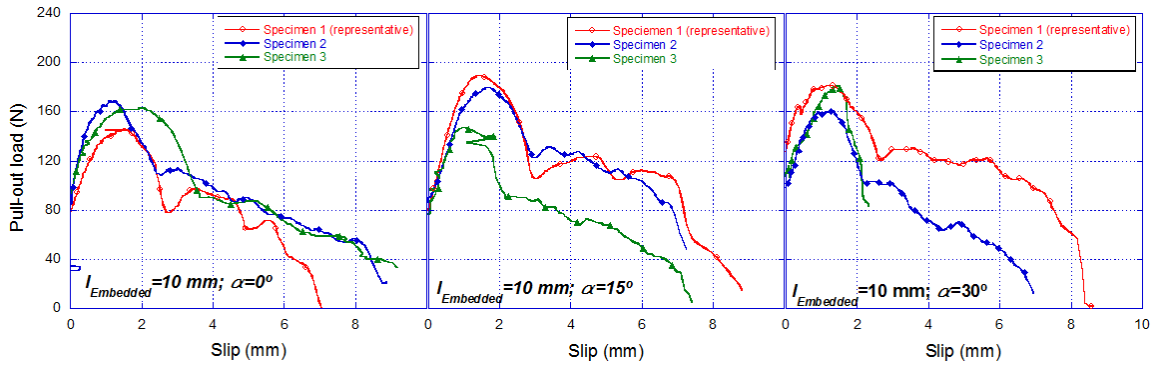

Figure 7-9: Scatter of the pull-out result of polyolefin fibres embedded 10 mm and varying angle in a self-compacting concrete matrix.

The final curves were prepared by subtracting the initial slope obtained from the elastic deformations with the aim of providing curves that show information only about the pull-out behaviour, as shown in Figure 7-10. This represents a sketch of pull-out tests on mortar and SCC specimens alike. In the figure, the representative values of load can be also identified: the maximum load named peak load (l_{peak}) and the load when only frictional adhesion opposed the extraction of the fibre $(l_{frictional})$. Moreover, the instant when the

fibre started sliding could be tracked in the video and, therefore, the load in which debonding took place ($l_{debonding}$). In such a sense, those values of load obtained the shear resistance by using expressions (7-1), (7-2) and (7-3). In these expressions, l stands for the embedded length and $\emptyset$ is the equivalent diameter of the fibres. In the tests, the debonding took place closely before reaching the peak load (a discussion about their values is later provided).

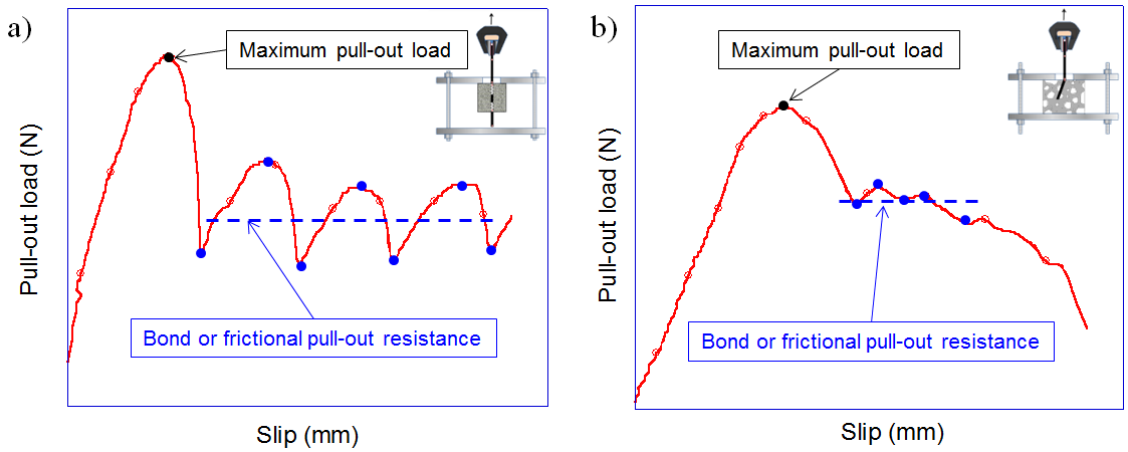

Figure 7-10: Sketch of the typical curves obtained in the pull-out tests with polyolefin fibres embedded in mortar (a) and self-compacting concrete (b).

$$\tau_{debonding} = \frac{l_{debonding}}{surface} = \frac{l_{debonding}}{\pi \cdot l \cdot \emptyset} \qquad (7-1)$$

$$\tau_{frictional} = \frac{l_{frictional}}{surface} = \frac{l_{frictional}}{\pi \cdot l \cdot \emptyset} \qquad (7-2)$$

$$\tau_{peak} = \frac{l_{peak}}{surface} = \frac{l_{peak}}{\pi \cdot l \cdot \emptyset} \qquad (7-3)$$

7.3.2 Polyolefin fibres pulled-out from normalized mortar

Two spots allowed the load-slip curves to be obtained once the fibres had initiated their relative movement inside the specimen, with one spot placed at the bottom of the fibre and the other painted at the entrance of the fibre in the mortar. As can be seen in Figure 7-11, given that the computed displacements of such points (shown in Figure 7-12) were analogous both spots could be used. In addition, it is important to highlight that the failure of the fibre-paste interface took place virtually at the same instant. This can be noted because the displacement of the two spots remained at zero until the debonding took place. The latter is understandable when referring to the spot painted at the end of the fibre.

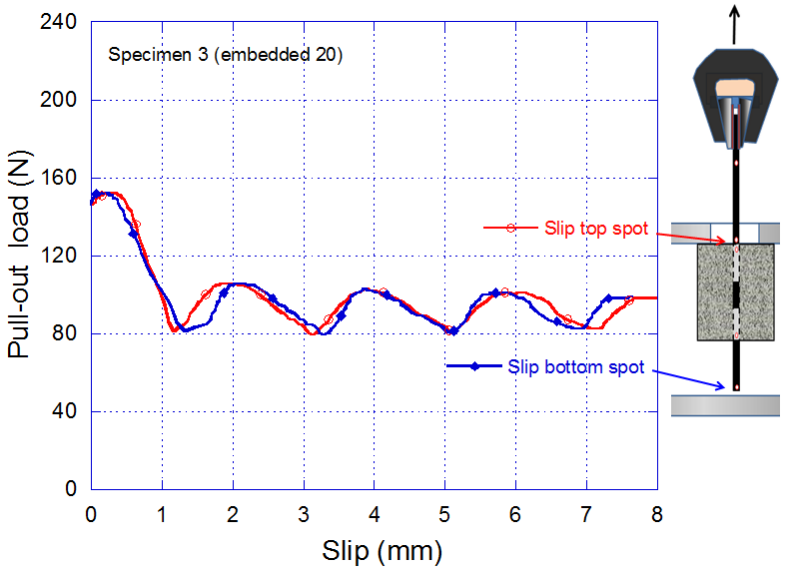

Figure 7-11: Sketch of the test configuration using concrete specimens.

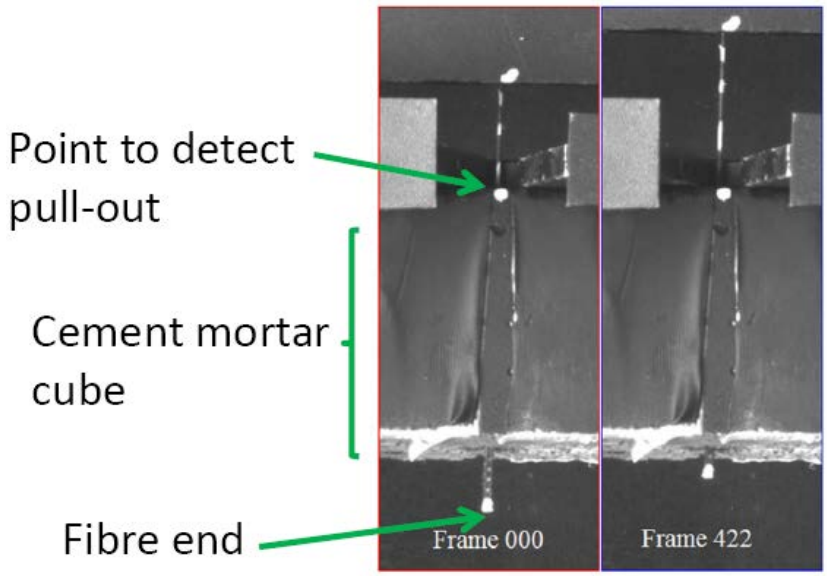

Figure 7-12: Points used to obtain slip, strain or fibre slip with mortar specimens.

In Figure 7-13, the representative pull-out curves of the three embedded lengths are shown. In the figure, it can be observed that the pull-out maximum load increases with the embedded length as well as the pull-out work. However, the mean values of $\tau_{frictional}$ are not directly related with the embedded length and are close among the three types of specimens, being slightly higher for the fibres only embedded 10 mm with respect to the 20 mm embedded ones. It should also be mentioned that none of the configurations exceeded the critical length in which the fibre would not have been pulled-out but broken. This is important because such a length is related with effectiveness of the fibres and the optimum length in this mortar matrix. Nevertheless, types of fibres designed to be fully mobilized by adherence and frictional adhesion were tested on real concrete to determine the effect of the matrix. In addition, it should be noted that the critical length changes with the incidence angle, as will be shown below in this study.

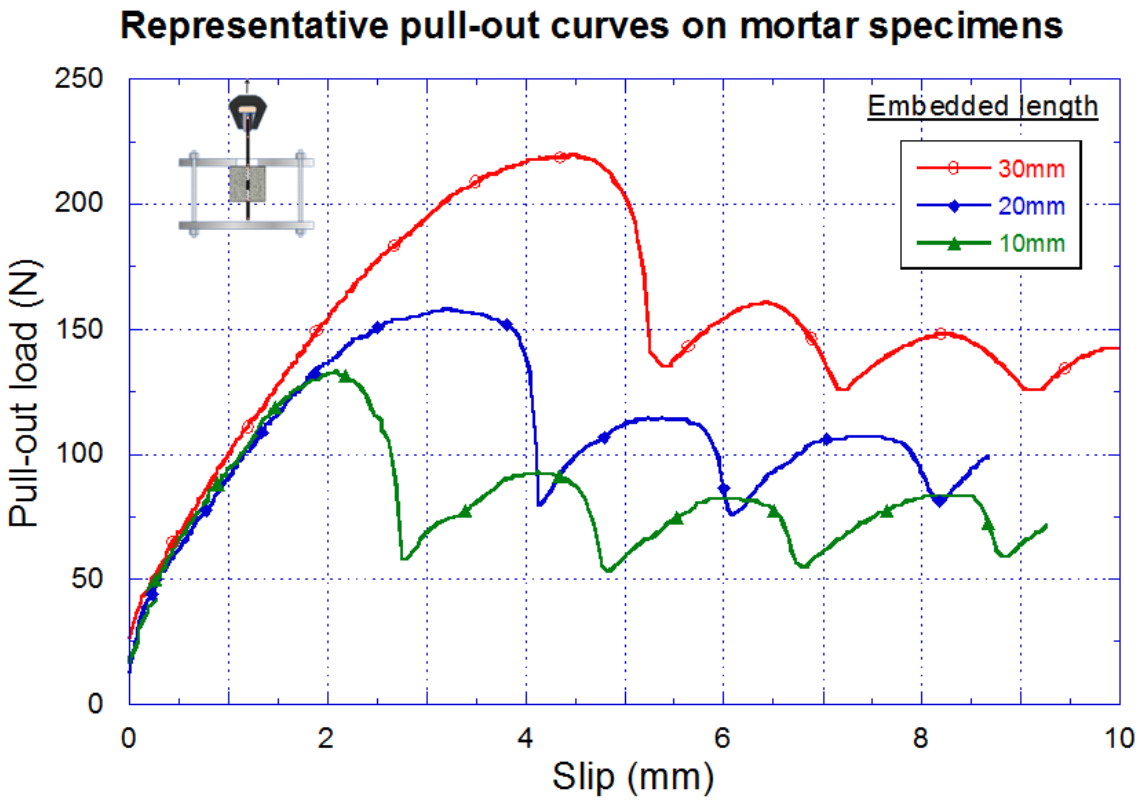

Figure 7-13: Representative pull-out curves of polyolefin fibres embedded 10, 20 and 30 mm in standard mortar specimens.

For a deeper analysis of the results and the degree of scatter, load, shear stresses and the coefficient of variation, have been computed in the three stages of behaviour: peak stage, debonding stage and frictional stage. These figures are placed in Table 7-2, which shows the limited scatter and the progressive increment of the peak load when the embedded length is increased. It is worth noting that the debonding stage shows that the stress for the first sliding was close in the 10 and 20 mm samples, even though the debonding load rose at a rate of 4.5 N/embedded mm. The mean load at the frictional stage also increased, though the shear stress did not show a clear tendency. If the effect on the load values of each embedded mm were analysed, it would be observed that for the specimens with 10 mm embedded in the matrix the values of load were remarkably higher than those with 20 and 30 mm embedded. Therefore, the load rates were 13.3, 11.6 and 6.7 N/ mm for the respective peak, debonding and frictional stages in the specimens with embedded length of 10 mm. In the same stages, the values for 20 mm embedded were 7.55, 6.65, 4.4 N/ mm and in the case of 30 mm embedded 6.97, 6.86, 4.73 N/ mm. The resemblance between the last two types and the differences with the first case should be noted. This could be explained by the small local effects and some boundary effects that took place at the beginning of the test that might have had more influence for shorter embedded lengths. This can be confirmed by computing the pull-out work up to the peak load, in which the results of work per millimetre were similar for all the embedded lengths and, in contrast, the total pull-out work showing the same tendency observed for the loads. All these values of energy consumed can be seen in Table 7-3. It is worth noting that for all the embedded lengths studied, the amount of energy consumed per mm of fibre length is almost constant at 20 N mm/ mm.

Table 7-2: Representative load and stress values of pull-out tests with polyolefin fibres in mortar specimens.

Mortar matrix	Peak stage				Debonding stage				Frictional stage			
Embedded length	Load			τ	Load			τ	Load			τ
(mm)	(N)	$\%\sigma_u$	c.v.	(MPa)	(N)	$\%\sigma_u$	c.v.	(MPa)	(N)	$\%\sigma_u$	c.v.	(MPa)
10	133	53%	0.01	4.59	116	46%	0.07	2.33	67	27%	0.08	2.33
20	151	60%	0.05	2.60	133	53%	0.18	2.30	88	35%	0.11	1.53
30	209	84%	0.07	2.41	206	82%	0.07	2.38	142	57%	0.06	1.63

Table 7-3: Representative pull-out work of polyolefin fibres in mortar specimens for debonding, reaching peak load and producing the entire pull-out.

Mortar matrix	Peak stage		Total	
Embedded length	Pull-out work		Pull-out work	
(mm)	(Nmm)	(Nmm)/mm	(Nmm)	(Nmm)/mm
10	200	20	755	76
20	394	20	947	47
30	579	19	1556	52

7.3.3 Self-compacting concrete specimens

Following the same rationale as in the case of the cement mortar samples test, some of the results of the pull-out tests on the concrete specimens have been plotted in Figure 7-14. These results were expected to be similar to the obtained in the cement mortar samples in qualitative terms. That is to say, the greater was the embedded length the more slip-displacement of the fibre took place. It was also expected that some increments regarding the maximum load as the inclining angle increased would be found. The former and latter can be observed in Figure 7-14. If the figure is analysed in detail, the peak load was maximum for 45º in the cases of embedded length 10 mm and 15 mm, and in the case of 5 mm of embedded length the incidence angle in which the test reached the highest peak load was 30º. It is worth mentioning at this point that in the case of fibres embedded at 20 mm, it was only possible to pull out the fibre with 0º of inclining angle. This provides a first sound conclusion of the study: any inclining angle for embedded length of 20 mm leads to the failure of the fibre, as does any longer embedded length.

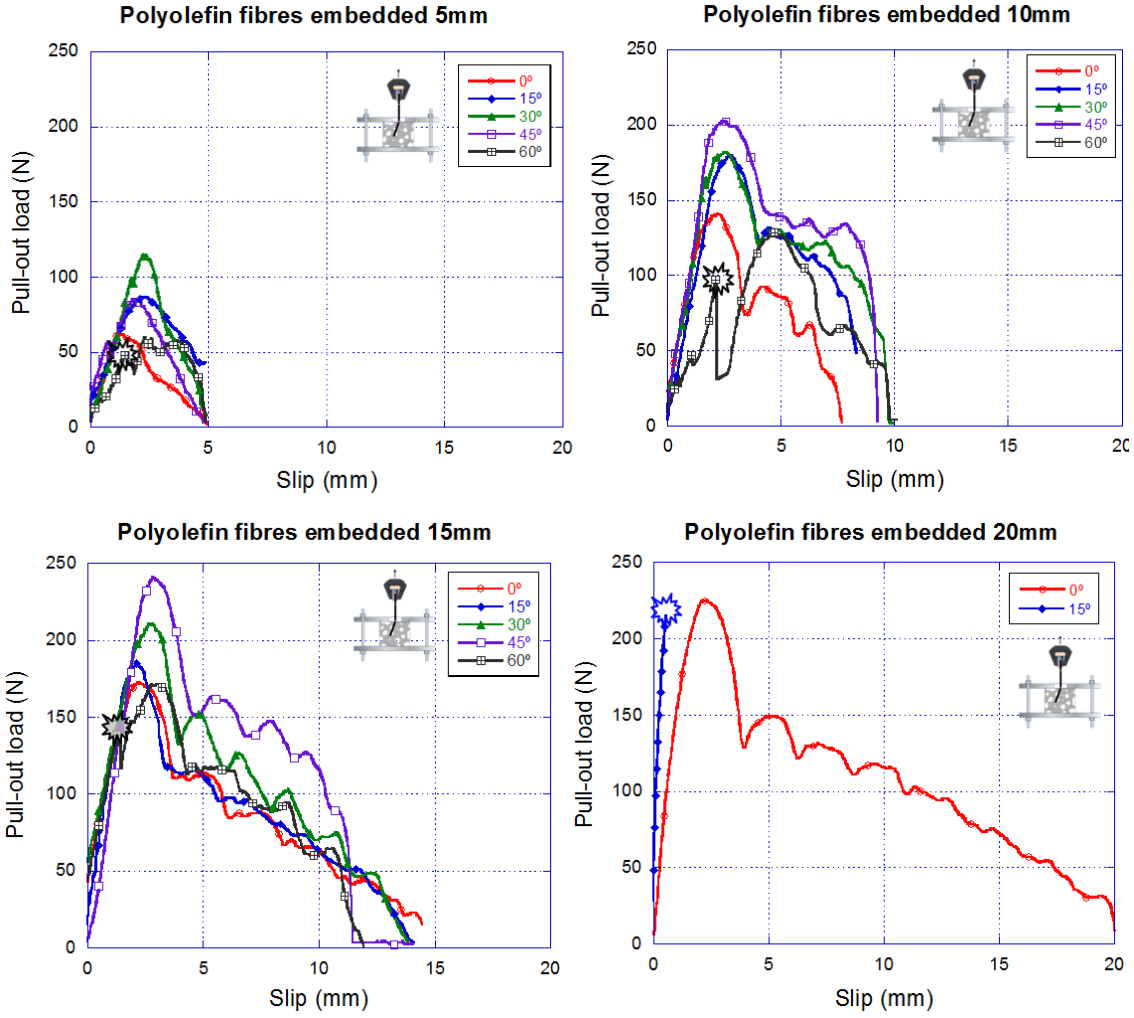

Figure 7-14: Influence of the inclining angle of polyolefin fibres embedded in a self-compacting concrete matrix.

The tests performed with embedded lengths of 25 mm and 30 mm finished with the rupture of the fibre. In such a case, the tests were close to uni-axial tensile tests of the fibres, as can be seen in Figure 7-15. Conversely, with an inclining angle of 60º, the concrete wedge placed between the fibre and the free surface failed due to the tensile stresses concentrating while pulling out the fibre. Such matrix failure was brittle. Nevertheless, the tests continued

up to the same fibre displacements of the rest of tests performed with the same embedded length and less inclination. This can be better understood by observing Figure 7-16.

Three failure modes were clearly seen: fibre pull-out, matrix spalling and fibre rupture. With the results of all the test combinations of embedded length and inclining angle, Table 7-4 has been built. This provides significant information for further analyses of fracture behaviour of polyolefin fibre reinforced concrete. In research done with steel fibres (Cunha, et al., 2010), some intermediate situations such as fibre pull-out with matrix spalling were described. However, in this study matrix spalling predominated over fibre pull-out. Matrix spalling took place in the tests with inclining angles of 60º, even for the specimens with only 5 mm of fibre embedded. On the contrary, fibres with embedded lengths that exceeded 20 mm were loaded up to tensile rupture with the angles studied. The frontier of fibre rupture and fibre pull-out was found for 20 mm embedded and inclined 15º.

Table 7-4: Summary of the pull-out failure mode of polyolefin fibres in a self-compacting concrete matrix and depending on the inclining angle and their embedded length.

Embedded length (mm)	Inclining angle (º)				
	0º	15º	30º	45º	60º
5	Pull-out	Pull-out	Pull-out	Pull-out	Matrix spalling
10	Pull-out	Pull-out	Pull-out	Pull-out	Matrix spalling
15	Pull-out	Pull-out	Pull-out	Pull-out	Matrix spalling
20	Pull-out	Rupture	Rupture	Rupture*	Rupture*
25	Rupture	Rupture	Rupture	Rupture	Rupture
30	Rupture	Rupture	Rupture	Rupture	Rupture

* One sample of the five tested failed due to matrix spalling and the rest reached the fibre rupture

It is worth mentioning that the DIC setup enabled stress-strain curves ($\sigma - \varepsilon$) of the fibres to be obtained. By means of the initial distance between two white spots and the progression of such a distance with load (synchronised through time with both machine and camera devices), fibre strain could be computed. Figure 7-15 shows the degree of resemblance among the curves of un-iaxial tests of the fibres and the pull-out tests with several geometrical configurations that led to the fibre rupture.

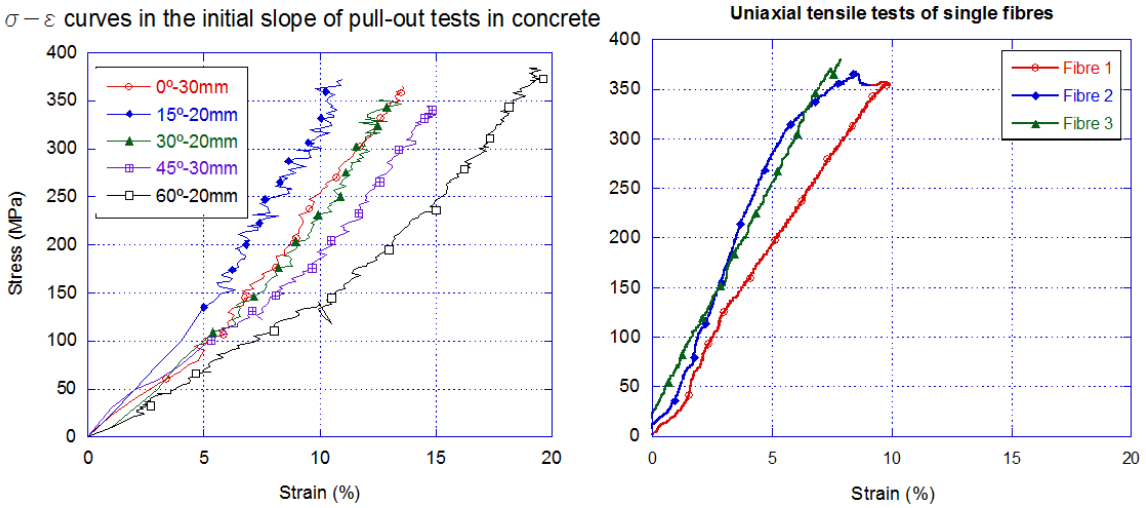

Figure 7-15: Stress- strain curves of fibres that failed by rupture during pull-out tests and uni-axial tensile tests on single fibres.

Concerning the influence of the embedded length, Figure 7-16 shows the comparative results for each inclining angle tested. The greater was the embedded length the more work had to be done to extract the fibre. The peak load was also clearly related, with it gradually increasing as the embedded length did. Nonetheless, in order to provide wider discussion it was necessary to compute the values in an analogous procedure such as that described for the tests with the fibres embedded in mortar pieces. For a more comprehensive analysis and discussion, the results of peak load are shown in Table 7-5, where it can be seen that the debonding shear stresses are close across the entire campaign. That is to say, if all the inclinations and embedded lengths in which the pull-out occurred were considered, the mean debonding shear stress would be 4.96 MPa and have a remarkably limited coefficient of variation of 0.20. Additionally, it should be highlighted that such a value doubled the debonding strength of the tests with mortar specimens placed in Table 7-2.

Table 7-5: Results of the pull-out tests of polyolefin fibres embedded in a self-compacting concrete matrix.

Specimen configuration		Peak load				Debonding	
$l_{embedded}$	Inclining angle	Load			τ	τ	
(mm)	°	(N)	$\%\sigma_u$	c.v.	(MPa)	(MPa)	c.v.
5	0	68	27%	0.20	4.70	4.34	0.15
5	15	87	35%	0.03	6.04	5.70	0.07
5	30	115	46%	0.08	7.93	7.60	0.07
5	45	88	35%	0.14	6.06	3.98	0.26
5	60	54	22%	0.43	3.75	MS*	-
10	0	149	60%	0.15	5.15	4.96	0.32
10	15	172	69%	0.13	5.95	5.12	0.15
10	30	172	69%	0.06	5.96	4.53	0.04
10	45	202	81%	0.17	6.99	5.81	0.17
10	60	138	55%	0.28	4.76	MS*	-
15	0	211	84%	0.18	4.87	4.55	0.14
15	15	216	86%	0.13	4.97	4.69	0.21
15	30	235	94%	0.14	5.41	4.52	0.01
15	45	242	97%	0.12	5.58	4.76	0.11
15	60	191	77%	0.13	4.42	MS	-
20	0	237	95%	0.08	4.11	3.89	0.09
20	15	263	105%	0.06	4.54	FR**	-
20	30	240	96%	0.04	4.15	FR**	-
20	45	257	103%	0.05	4.44	FR**	-
20	60	229	92%	0.05	3.97	FR**	-
25	0	245	98%	0.14	3.39	FR**	-
25	15	255	102%	0.09	3.53	FR**	-
25	30	247	99%	0.05	3.42	FR**	-
25	45	290	116%	0.14	4.01	FR**	-
25	60	196	78%	0.18	2.71	FR**	-
30	0	242	97%	0.12	2.79	FR**	-
30	15	258	103%	0.12	2.98	FR**	-
30	30	211	84%	0.05	2.43	FR**	-
30	45	243	97%	0.14	2.80	FR**	-
30	60	213	85%	0.13	2.46	FR**	-
Mean fibre rupture =		253	101%	0.10			

MS*: Matrix spalling ; FR**: Fibre rupture

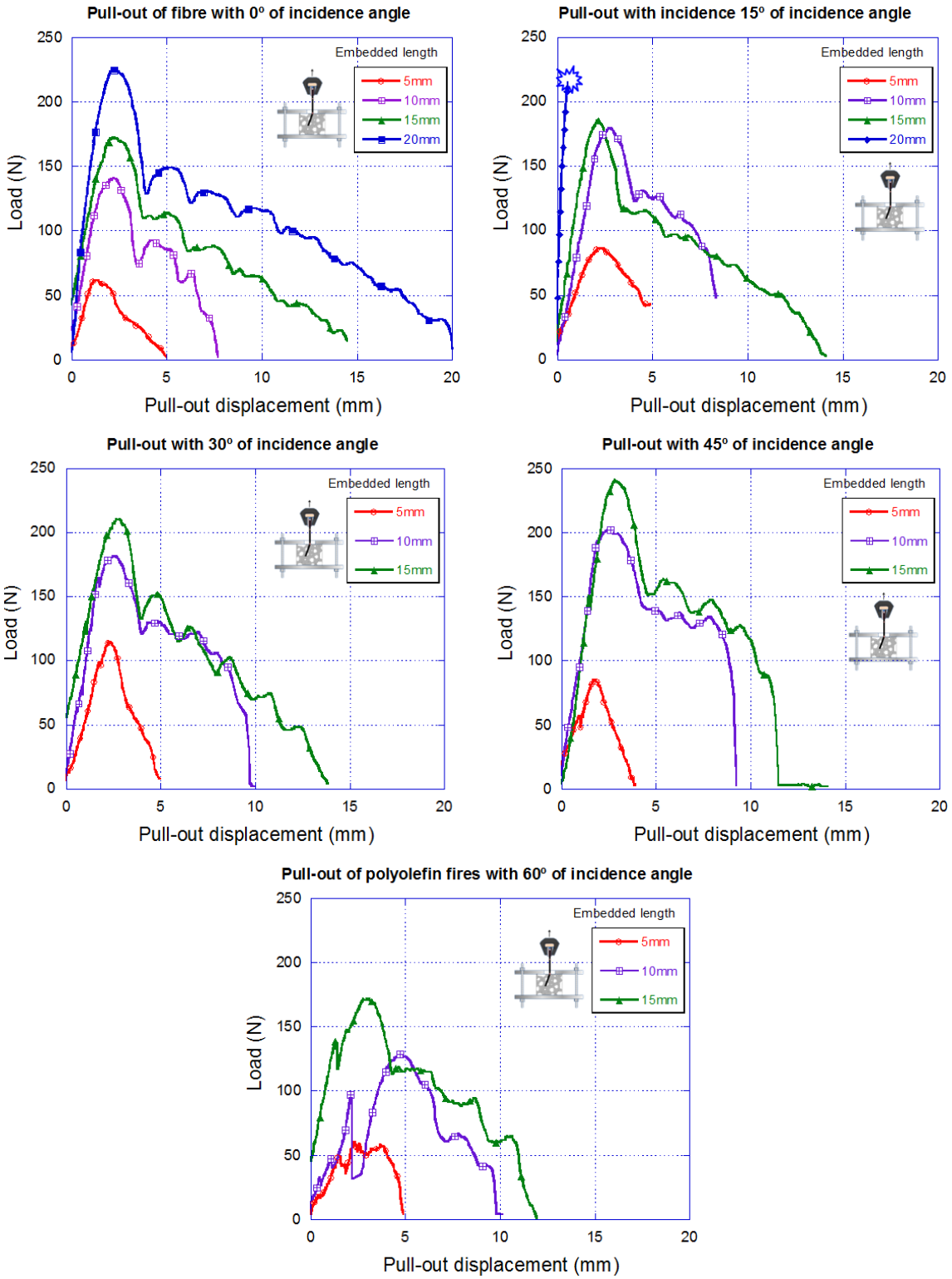

Figure 7-16: Influence of the embedded length of polyolefin fibres embedded in a self-compacting concrete matrix with several angles.

Figure 7-17 compares the peak load recorded in all tests with the results of pull-out tests performed on straight steel fibres in reference (Cunha, et al., 2010) embedded in SCC. If Figure 7-17 is observed, it can be seen that the peak load and inclining angle are two coupled parameters of the results. That is to say that the peak load increases with the embedded length but reaches its maximum value for 0º of inclining angle for an embedded length of 25 mm. However, for 15º degrees of inclining angle the highest values was found

for 20 mm of embedded length. In any event, the highest values of peak load tends to be close to that of 20 mm and the surrounding values with 15 or 25 mm of embedded length showed only small differences. The case of 15 mm embedded length shows how for 30º the value is close to the maximum one and it decreases for 0 or 60 degrees. As an overall conclusion, it could be stated that the best situation of the fibres in terms of reaching greater peak loads were in surroundings of 30º and 20 mm of inclining angle and embedded length. It is worth mentioning that in all the tests, the values surpassed or were very close to the reported in the abovementioned reference (Cunha, et al., 2010) for straight steel fibres.

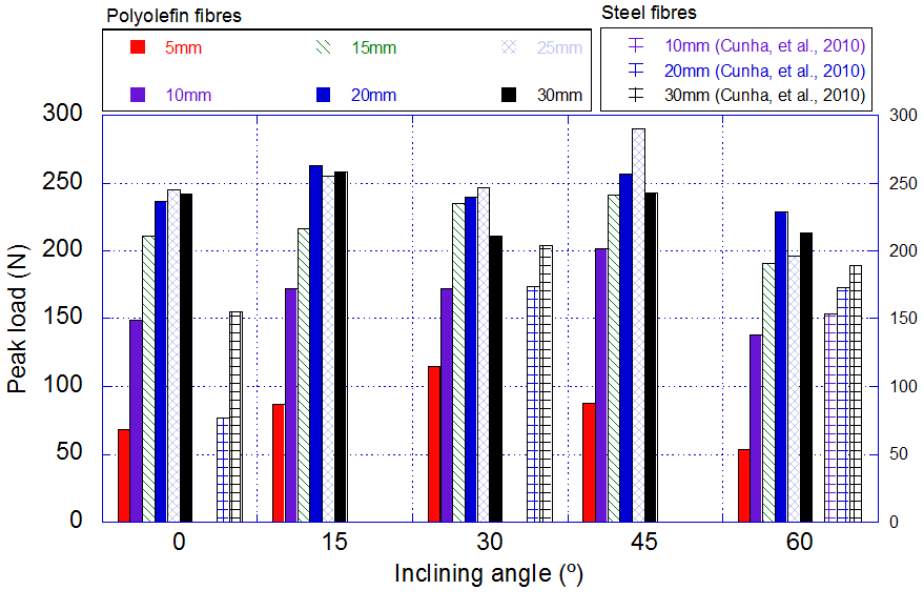

Figure 7-17: Peak load comparison of polyolefin fibres and straight steel fibres of reference (Cunha, et al., 2010) and depending on the inclining angle and the embedded length.

Figure 7-18 shows the evolution of pull-out work up to the peak load varying the embedded length and the incidence angle. It can be seen that for a 5 mm of embedded length the inclining angle is a key factor that increases the energy needed to pull-out the fibres at this stage. However for angles greater than 30º this effect seems to change its tendency. While in the tests performed with 10 mm embedded fibres the energy rose steadily with the inclining angle, in the case of 20 mm the pull-out energy slightly increase until 30º degrees diminishing for greater angles.

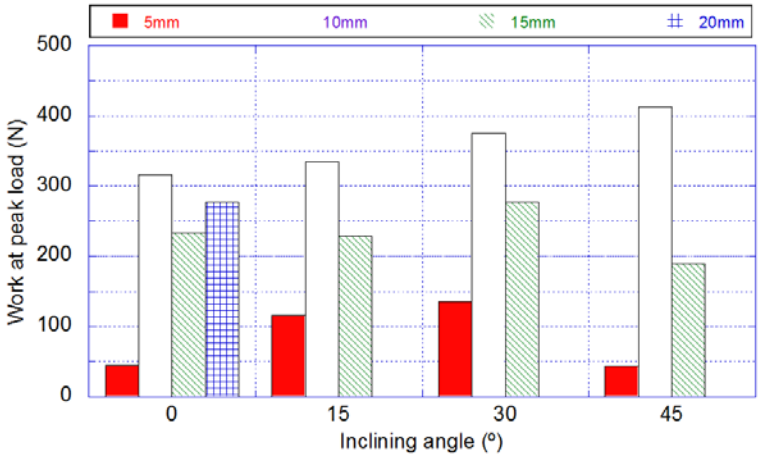

Figure 7-18: Work at peak load comparison of pull-out tests on polyolefin fibres embedded on self-compacting concrete.

Figure 7-19 compares the work at peak load of the tests. If the total work is analysed it can be concluded that the more inclined the more work is needed for all the configurations, which was expected. It is also worth comparing the results of peak load in mortar and self-compacting concrete matrixes with the same embedded length and without any inclination. Figure 7-20 compares the peak load of the analogue configurations. It can be concluded that the matrix has also a significant influence on the results and that concrete provided significantly greater values of peak load. If the tables and pull-out works are compared, such conclusion can be extended to the general pull-out behaviour of polyolefin fibres. In addition, in the case of mortar specimens with 30 mm of embedded length, the fibre pull-out loads were close to the one obtained when embedded in concrete for only 10 mm of embedded length. The results in self-compacting concrete with 30 mm of embedded length evidenced that the critical length in concrete was significantly exceeded with all the tests performed finished with fibre rupture.

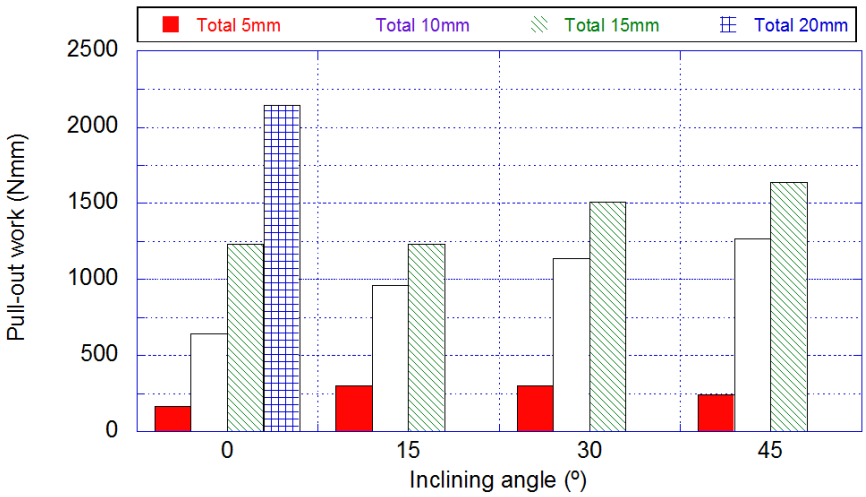

Figure 7-19: Pull-out work of polyolefin fibres embedded on self-compacting concrete.

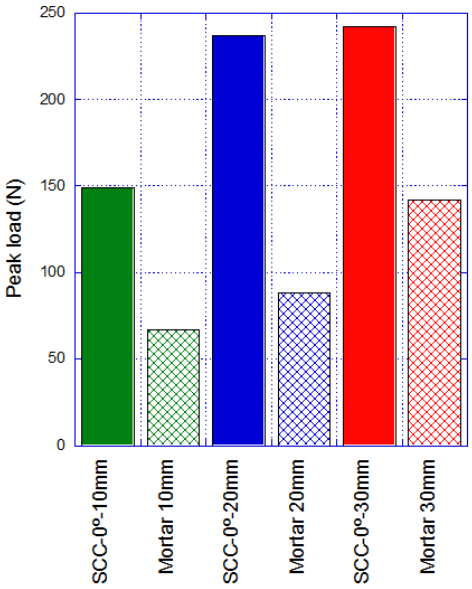

Figure 7-20: Peak load comparison of pull-out tests of polyolefin fibres embedded on self-compacting concrete and mortar matrixes.

7.4 Microstructural analysis

The bond improver admixture Sikatell 250 was added to the P10M mixture. As it has been previously shown, the adding of this admixture has improved the flexural behaviour and toughness of the PFRC. This sub-chapter shows the microstructural analysis of the interface between polyolefin fibre and cement paste. The study was made by using a scanning electron microscopy (SEM) JEOL JSM 6335F, at the Microscopy Centre of the Universidad Complutense Madrid. Several pieces from the mixture SCC10 extracted from the specimens tested on Chapter 4 were observed with this SEM.

Figure 7-21 shows the interface between polyolefin fibre and cement paste. Figure 7-22 shows the surface of a polyolefin fibre. Both figures show a sound interface between a polyolefin fibre and cement paste, without voids or discontinuities.

Figure 7-21: Interface between polyolefin fibre and cement paste.

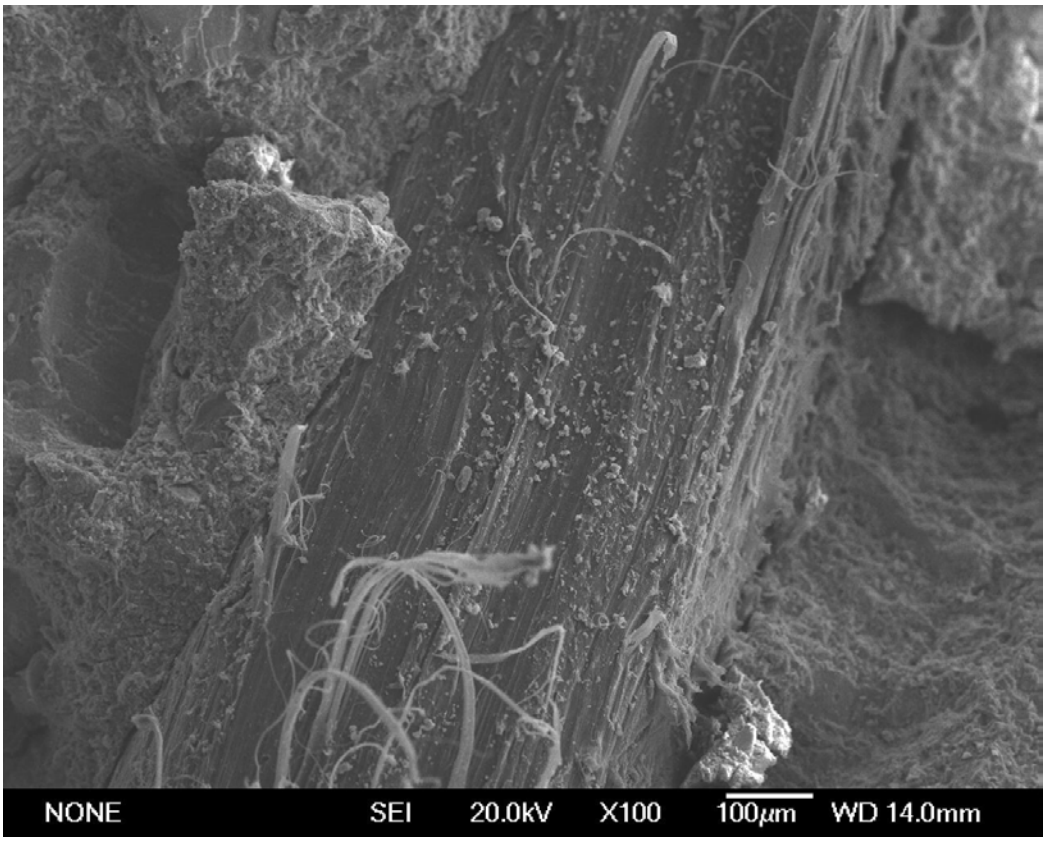

Figure 7-22: Surface of a polyolefin fibre.

Figure 7-23 shows a detailed view of the interface between polyolefin fibre and cement paste. Figure 7-24 shows the continuity between the C-H-S gel and polyolefin fibre. Once again both figures show a sound interface between polyolefin fibre and cement paste, without voids or discontinuities. In addition, Figure 7-25 shows the crib of cement paste when the polyolefin fibre was removed. Some parts of the filaments can be observed as being bonded on the crib. This result confirms the good bonding between polyolefin fibre and cement paste.

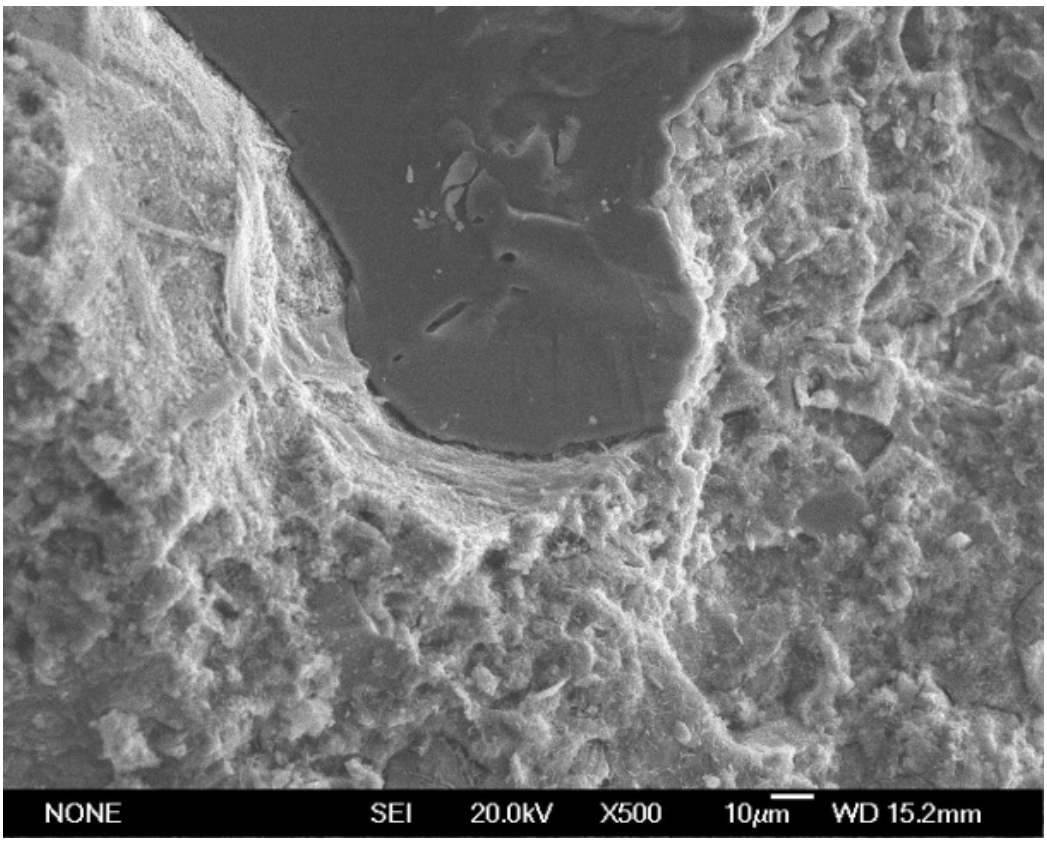

Figure 7-23: Interface between polyolefin fibre and cement paste.

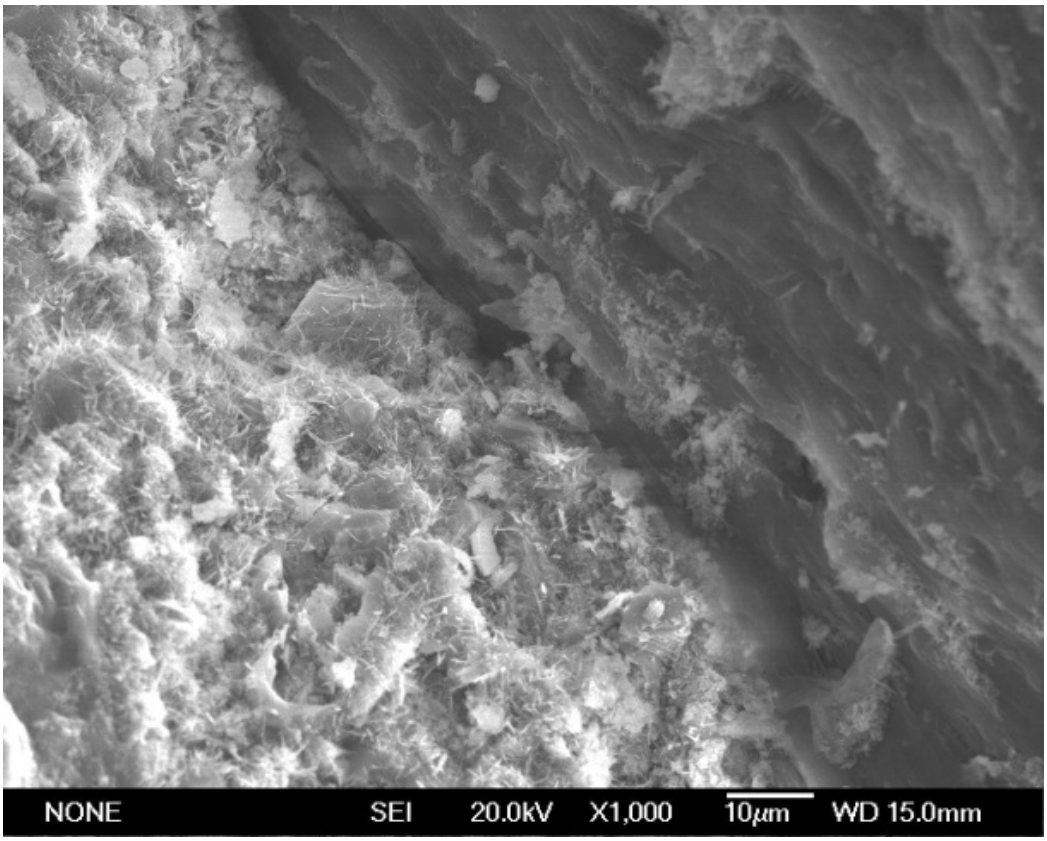

Figure 7-24: Continuity between C-H-S gel and polyolefin fibre.

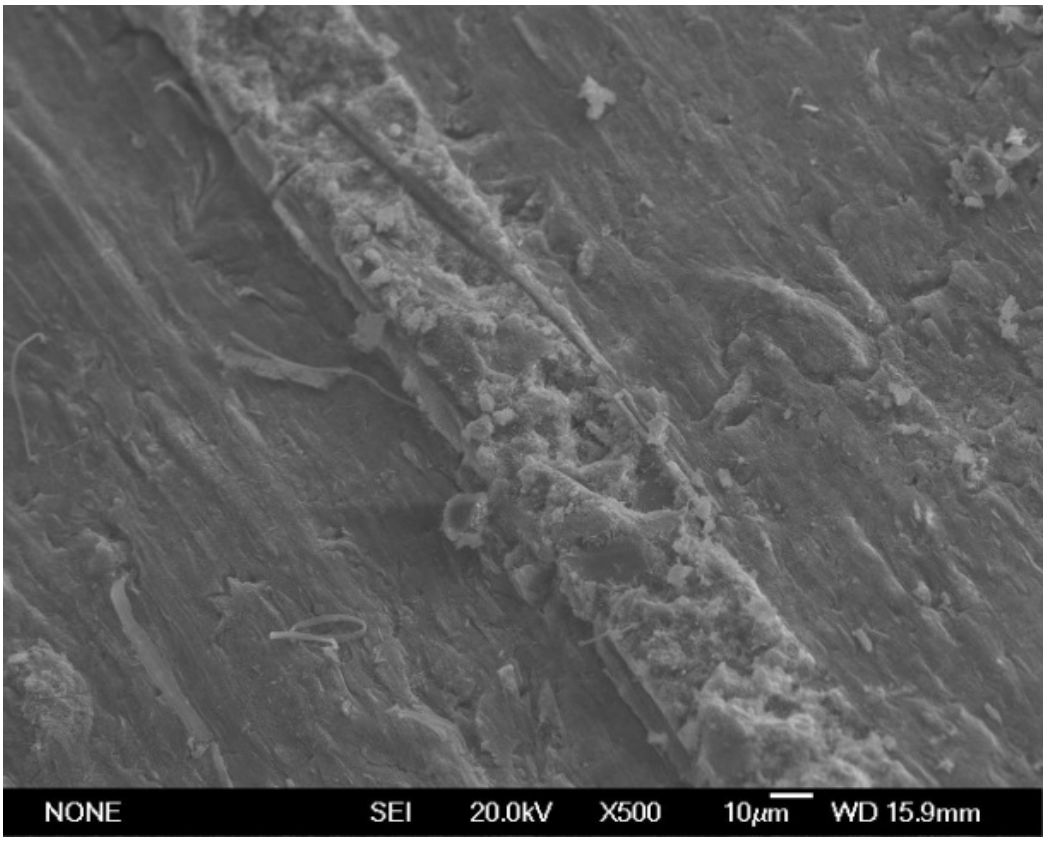

Figure 7-25: Crib of cement paste when polyolefin fibre was removed.

Additional photos (Figures 7-26 to 7-28) show the surface of the polyolefin fibre. Some particles on the fibre surface can be observed, apparently coming from the cement paste, which again indicates good bonding between fibre and cement paste.

According to the bond improver admixture Sikatell 250 supplier, this admixture reduces the air included in the bulk cement paste. This effect is beneficial for the bonding between fibre and cement paste because the contact area fibre-cement is larger. This hypothesis is ongoing research and is beyond the scope of this thesis.

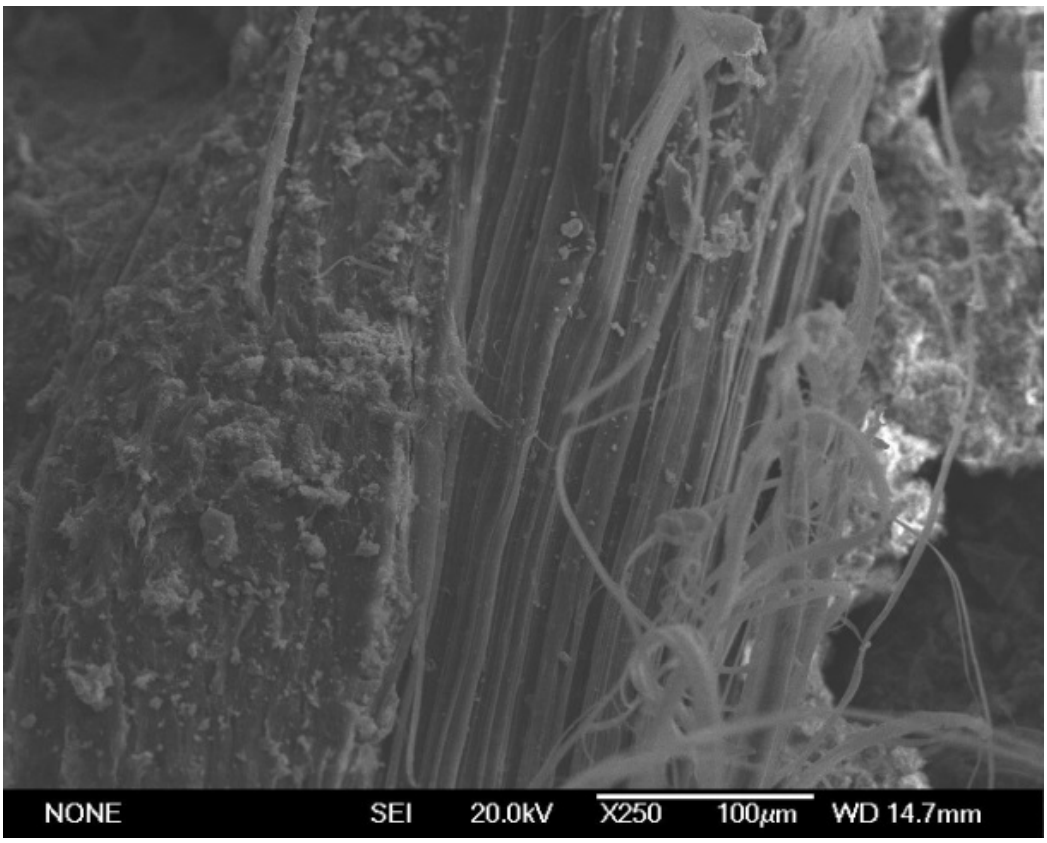

Figure 7-26: View of the Polyolefin fibre

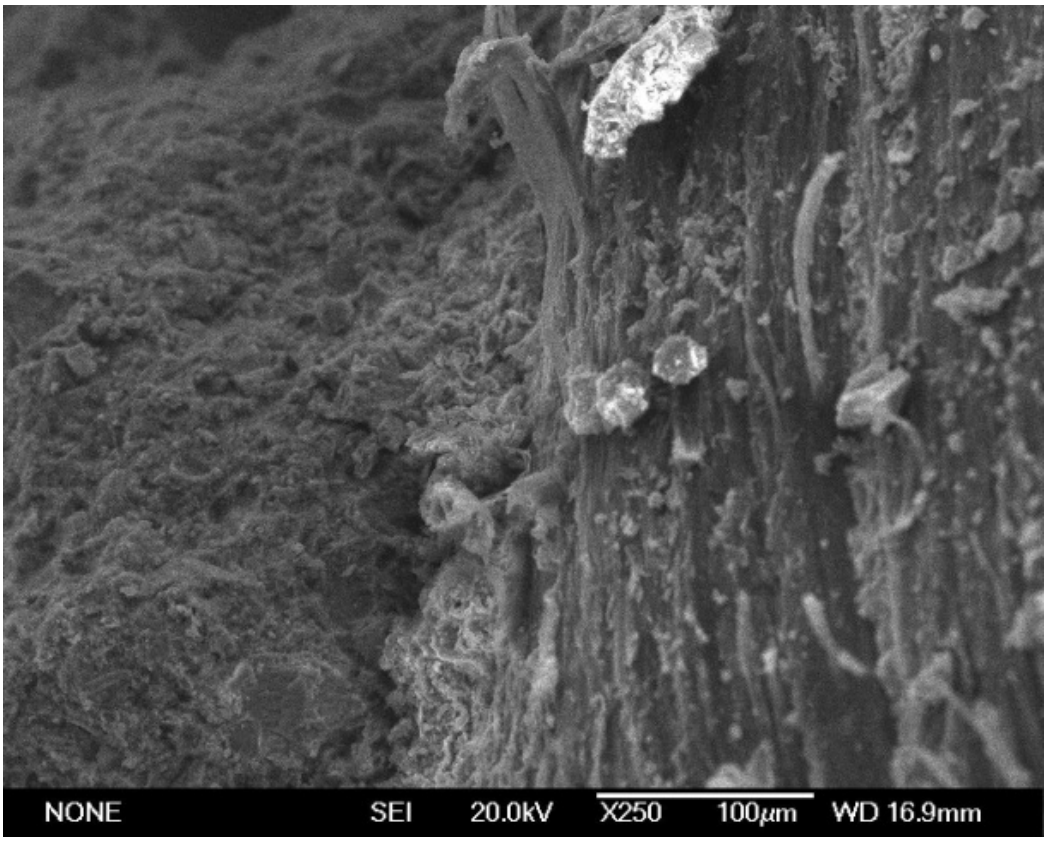

Figure 7-27: View of the Polyolefin fibre.

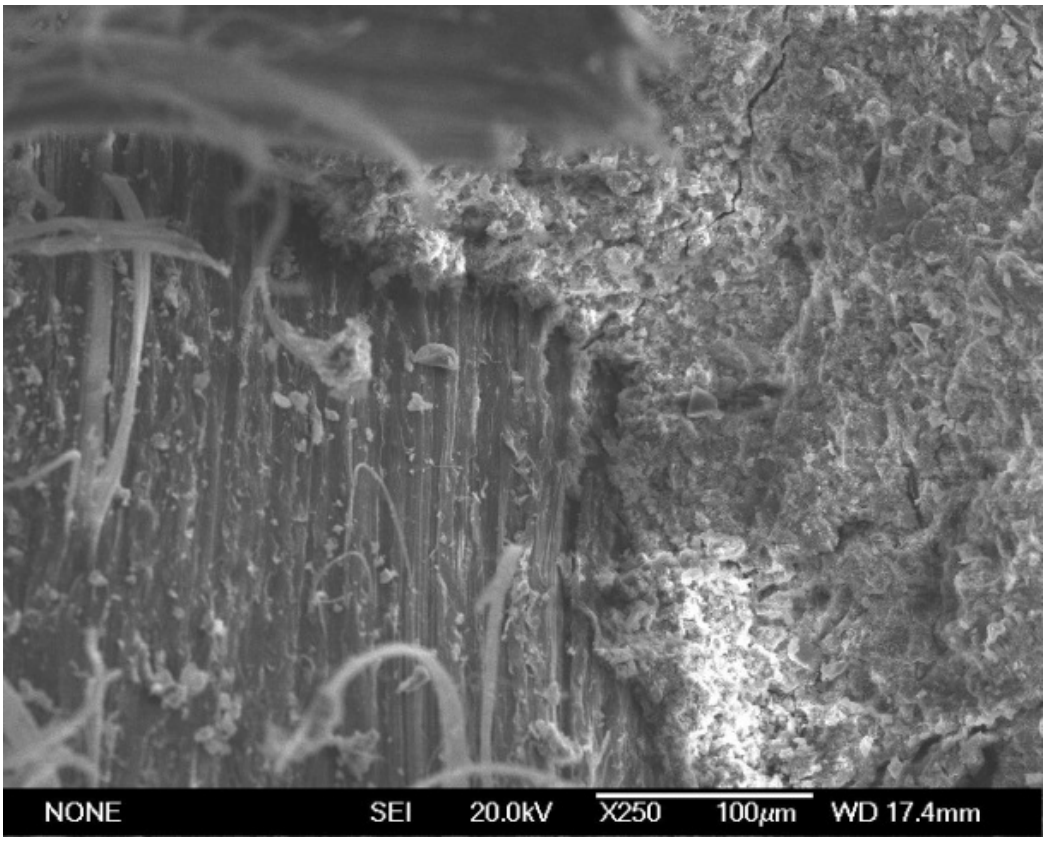

Figure 7-28: View of the Polyolefin fibre.

7.5 Conclusions

The pull-out tests performed with polyolefin fibres embedded in two types of cementitious matrixes showed a reliable performance with limited degrees of scatter. In this study, systematic procedures and tests provided information of significant importance in two of the most relevant cementitious matrixes. The results encompass the main parameters needed to characterise the pull-out behaviour when using macro-polymer polyolefin based fibres. While it is true that some portions of these conclusions could seem intuitive, it is should also be noted that at the time of writing there is a lack of research concerning the pull-out behaviour of this type of structural fibres. The results shown in this study, standing on a systematic and innovative campaign, support the noteworthy advantages of using PFRC in concrete elements with structural requirements. Hence, the results obtained provide interesting information for further numerical developments or design assumptions.

The pull-out tests designed have provided relevant information with help from video-extensometer and image analyses. This allowed strains and displacements to be obtained, which also assures the lack of non-desired relative displacements. In addition to this, it was possible to localise the instant at which the fibre starts sliding and correlate it with the debonding load at such a time.

The overall conclusions obtained for fibres pulled out from a SCC matrix could be summarized as the following:

- The pull-out tests confirmed that the inclining angle affects the pull-out behaviour. The peak load reached the maximum with an inclination of 45º and the maximum work to produce debonding occurred with 30º of inclining angle.
- Beyond 45º of inclination, matrix spalling is the most probable type of failure.
- The critical length of polyolefin fibres is close to 20 mm. Longer embedded lengths led to fibre rupture.
- With 15 mm of embedded length and any inclination (15º or more), the tests also ended when the fibre failed.
- The critical length, as well as the overall pull-out behaviour, are strongly influenced by the type of matrix in which the fibre is embedded with remarkably improved results being obtained when it is embedded in concrete rather than mortar.
- Peak load is related to the embedded length up to the critical length in which the results remain stable.
- The values obtained have shown that the pull-out work and load are comparable with those of steel fibres in other published work (Cunha, et al., 2010).
- Microstructural analyses have shown a detailed view of the interface between polyolefin fibre and cement paste. The continuity between C-H-S gel and polyolefin fibres exhibited a sound interface between polyolefin fibres and cement paste, without voids or discontinuities.

PART III: FIBRE POSITIONING: EXPERIMENTAL ASSESSMENT

Chapter 8

Influence of fresh concrete properties, compaction procedures and framework geometry on the mechanical response of PFRC

8.1 Introduction

The final positioning of fibres plays a major role in fibre reinforced concrete (FRC) performance, especially in fracture results used to evaluate the structural competence of the composite material. FRC post-cracking behaviour is related with the number of fibres acting in the cracked surface and their forming angle.

Following such rationale, numerous studies have sought to assess the parameters of the concrete formulation and production processes that may influence the performance of fibres in hardened SCC. Some authors have used a translucent fluid model to determine visually the position, density and orientation of steel fibres (Boulekbache, et al., 2010) with results being validated by testing concrete samples manufactured with a similar viscosity. The influence of the placing conditions, as well as the shape of formworks and casting procedures, have also been evaluated in other researchers using steel fibres. By analysing the distribution of steel fibres in samples filled in horizontal and vertical positions, both from the centre and from one side, it was found that the casting procedure had significant influence on the mechanical response of concrete (Torrijos, et al., 2010). Moreover, it was reported that a preferential orientation of the fibres in the proximities of the sides of the

samples, the so-called wall effect (Soroushian, et al., 1990), had a beneficial effect on the flexural response of the material. The impact of geometry and size of the formwork have also been measured by using U-shaped formworks and rectangular slabs (Stähli, et al., 2007; Zerbino, et al., 2012). The influence of the number of fibres was studied by means of a counting process in the fracture surfaces, in (Stähli, et al., 2007), and similarly in four sections of the samples in (Zerbino, et al., 2012). Both showed the noteworthy influence on the orientation of the fibres and, consequently the flexural response, of three parameters: the shape of the formwork, wall effect and viscosity. Furthermore, similar experimental studies have been carried out in concrete with two types of fibres (Stähli, et al., 2007; Burcu Akcay, 2012) in ultra-high-strength concrete (Kang, et al., 2011).

In order to widen knowledge in the field of steel fibre distribution in FRC, some authors have performed a deeper analysis of the results obtained in several experimental campaigns. Whereas a statistical approach showed that the orientation of fibres followed a Gaussian law, (Laranjeira, et al., 2011) a study by Dupont found an explanation for the inhomogeneous coefficient of orientation obtained in rectangular sections (Dupont, et al., 2005). In addition, some analytical models of the orientation of fibres in concrete that considered the complete production process have been recently offered (Laranjeira, et al., 2012) (Martinie, et al., 2011).

Hence, a significant advance has taken place in the relation between fibre orientation and mechanical properties of conventional concrete and SCC. Nevertheless, almost all the research carried out has dealt with steel fibres. One of the major areas that deals with polyolefin fibres is the reduced density of the polymer material of the fibres and its influence during the vibration process of the conventional concrete or the flow of the SCC. In addition to this, an equally important variable is the influence of the casting procedure when filling the laboratory samples.

As regards the influence of the length of the fibre on alignment in the case of steel fibres, previous research has shown it to be negligible (Vandewalle, et al., 2008). That is to say, fracture results should not be affected. However, for concrete reinforced with synthetic macro-fibres made of polyolefin, at the time of writing no data had been reported. Additionally, for rigid steel fibres, size recommendations that link aggregate size and mould size have been established in the standards. They recommended manufacture of specimen dimensions of at least 2.5 times greater than fibre length. Subsequently, for the use of fibres with a length of 60 mm the standardised size of the samples is strictly inside the requirements given that use of smaller moulds would increase wall effects which would, consequently, provide non-representative results.

In order to assess the influence of the fibre length and casting procedure, six samples of 150x150x600 mm^3 (depth-height-length) were manufactured. Four were manufactured with SCC by using 6 kg/m^3 of 48 mm long polyolefin fibres, and two were filled from one side while the other two were filled by pouring the concrete in the centre of the samples. The two remaining samples were produced with the same type of concrete though, instead of using 48 mm long fibres, 60 mm long fibres were used. The concrete was poured from one of the sides of the formwork.

Moreover, regarding the use of polyolefin fibres in vibrated conventional concrete (VCC), two more samples with standardised dimensions of 150x150x600 mm^3 (depth-height-length) were produced through use of the same 6 kg/m^3 of 60 mm long polyolefin fibres and following standard filling and consolidation processes. In contrast, three samples made with the same concrete and consolidation process, but with dimensions of 100x100x430

mm³ (depth-height-length), were cast. Given that the depth and height of the sample were lower than 2.5 times the fibre length, some of the aforementioned effects should be noted in both the fracture results and orientation of the fibres.

Assessment of the floatability of the fibres and the influence of the consolidation process in the distribution of fibres inside a tall concrete element is of significant interest. In order to address this question, four formworks of 150x450x600 mm³ (depth-height-length) were manufactured with a standard concrete with an addition of 6 kg/m³ of 60 mm long polyolefin fibres. These concrete elements were divided in three standard-size samples.

Concerning the influence of flow and the wall effect in SCC elements, a beam of 2200x250x150 mm³ was produced by using a SCC with 6 kg/m³ of 60 mm long polyolefin fibres. The zone near the lateral formwork was discarded to neglect the influence of the wall effect in the orientation of the fibres. This was performed by cutting a slice of 50 mm in both sides of the beam. Once this process ended, the beam was divided into four pieces with four 550x150x150 mm³ elements being obtained.

Hence, to assess the differences in behaviour in these combinations, two comparable types of plain concrete were produced with remarkably similar fracture energy. These were used as control formulations: VCC and SCC. The properties of the two types of concrete were assessed by means of mechanical tests. Two specimens of the standardised dimensions were also tested in order to obtain their fracture energy of both non-reinforced concrete types.

All the elements were tested to assess the influence of the following: concrete type, filling methods, compaction procedures, formwork shape and size, length of the fibre in relation with the specimen size and floating effects. With all the fracture results, a broader view of the fracture behaviour of PFRC was studied in order to provide reliability on its testing methods and applications.

8.2 Materials and mix proportioning

The component materials included were similar to those described in Chapter 4 in subsection 4.2. The polyolefin straight fibres with a rough surface and surface treatment were employed with two lengths of 60 and 48 mm. Apart from that, the characteristics of the fibres were the same shown in Table 4-3 and the visual aspect of Figure 4-2 (but for the shorter length).

Table 8-1: Concrete mix proportions (kg/m³).

Concrete type	Cement	LP	SP (%CEM)	Water	Sand	Grit	Gravel	48mm fibres	60mm fibres
SCC	375	200	1.25 %	187.5	918	245	367	---	---
SCC6-48(*)	375	200	1.25 %	187.5	918	245	367	6.00	---
SCC6-60	375	200	1.25 %	187.5	918	245	367	---	6.00
VCC	375	100	0.75 %	187.5	916	300	450	---	---
VCC6-60	375	100	0.75 %	187.5	916	300	450	---	6.00

(*) both SCC6-48S and SCC6-48C were manufactured with the same formulation

The proportions used in VCC and SCC are the correspondent to Chapter 4 and 5 and are shown in Table 8-1. The self-compacting formulation where 6 kg/m³ of 48 mm long fibres were used was named SCC6-48. Similarly, when 6 kg/m^3 of 60 mm long fibres were employed in the self-compacting formulation, the concrete was termed SCC6-60. Moreover, the conventional mix with 6 kg/m³ of fibres added was referenced as VCC6-60.

8.2.1 Concrete production

The mixing procedure shown in Figure 4-3 was followed for all the concretes with the aim of obtaining an optimum behaviour of concrete while in fresh state. A more detailed description of the process can be found in Chapter 4.

Figure 8-1: Pouring sketch of SCC: (a) poured from one side; (b) poured from the centre; (c) Method for casting the specimen following EN-14651 (EN 14651:2007+A1, 2007) or RILEM TC 162-TDF (RILEM- TC 162-TDF, 2000).

In order to analyse the influence of the fibre length, the same dosage of fibres was added to the same SCC formulation; whereas one formulation was performed with 48 mm long fibres (SCC6-48S), the other was manufactured with 60 mm long ones (SCC6-60S). In both cases the SCC was poured in the 600x150x150 mm³ formworks from one of the sides, as can be seen in Figure 8-1(a).

Furthermore, the effect of the casting procedure was assessed by comparing SCC6-48S with the same formulation poured from the centre of the sample SCC6-48C. This process can be seen in Figure 8-1(b). In all the processes mentioned above, the samples reached compaction due to their own weight.

The differences in the orientation and density of fibres caused by the vibration process when compared with the self-compaction of SCC were also studied. This was performed by manufacturing a vibrated conventional concrete with a 6 kg/m^3 dosage of 60 mm long fibres named VCC6-60. Two 600x150x150 mm³ samples were filled by following the standard process described in EN-14651 (EN 14651:2007+A1, 2007) and RILEM TC 162-TDF (RILEM TC-162-TDF, 2002) (a sketch of the method can be seen in Figure 8-1(c). The samples were later consolidated by means of a vibrating table for 10 seconds.

Furthermore, in order to analyse the effect of the flow, the pouring method and size of the specimens, a beam-shaped wooden mould 2200 mm long, 150 mm high and 250 mm deep was prepared. The formwork was filled with SCC6-60 from one of the sides, as can be seen in Figure 8-2 where the ease of filling achieved with this formulation - in spite of the 6 kg/m³ of polyolefin fibres used - is clear. The flowability of SCC permitted the flux to reach the end of the mould. When the bottom layer of SCC touched the final wall, the rest of the flux continued filling the mould layer-by- layer by means of gravity. In such a sense, the end of the mould was the last part to receive the desired level.

Figure 8-2: Long-beam formwork and pouring of SCC6-60.

The mould was removed after 24 hours and the concrete element shown in Figure 8-3a obtained. The total length of the element was chosen with the aim of obtaining four 550 mm long samples suitable for flexural tests. In Figure 8-3(a) the lines that divide the beam into four samples (L1, L2, L3 and L4) are shown in white and black ink. The samples were numbered from the casting point (L1) towards the end of the mould (L4). Moreover, the direction of the flow was also registered with white and black arrows sketched in all samples. In order to neglect the influence of the wall effect on the samples, a 50 mm thick lateral wall was removed from each side of the beam element. In Figure 8-3(b) the lateral surfaces removed can be perceived. Thus, the final dimensions of the samples were 550x150x150 mm^3 being suitable for flexural tests. Figure 8-3(c) shows the sample L1 obtained with the lateral sides removed to avoid the wall effect.

Figure 8-3: (a) Beam element after removing the mould; (b) sides removed from the concrete element to avoid the wall effect; (c) Sample L1 with the lateral sides removed.

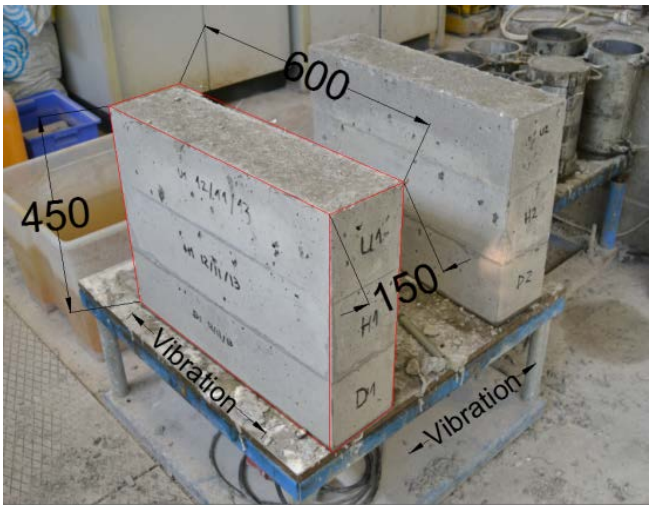

Figure 8-4: Vertical (UHD) concrete elements.

Finally, one more series of specimens based on VCC6 was manufactured and named UHD. These research series were produced with the aim of determining any possible floating of the fibre, due to its low density, after 30 seconds of consolidation on a vibrating table. The moulds had the same dimensions as the standard samples in both length and depth (EN 14651:2007+A1, 2007) (RILEM TC162-TDF, 2002). Nevertheless, the moulds were three times taller than the standardised moulds. Therefore, the dimensions were 600 mm length, 450 mm height and 150 mm depth. After 24 hours in the laboratory, the concrete was unmoulded and divided into three prismatic specimens of 600x150x150 mm³. The upper, central, and bottom ones were named U, H and D respectively. Figure 8-4 shows the appearance of the concrete elements before being cut in three regular specimens. In Figure 8-5 a summary of the elements manufactured can be seen.

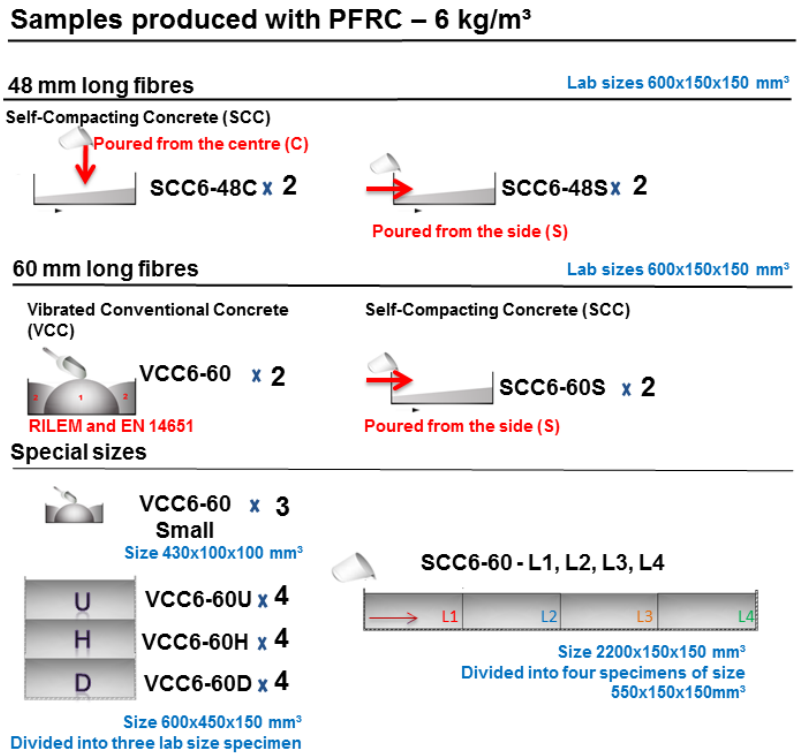

Figure 8-5: Concrete elements manufactured.

For the concrete types studied, eight cylindrical samples (150 mm diameter, 300 mm height) were cast. The latter were used to assess the compressive strength, modulus of elasticity and indirect tensile strength. The cylindrical samples and prismatic samples were stored in a climatic chamber at 20ºC and 95% of humidity until the age of testing.

8.3 Assessment of fresh-state concrete properties

Fresh properties of self-compacting concrete were assessed by means of the slump-flow test described in the standard EN: 12350-8 (EN 12350-8, 2010) and the V-funnel test in EN: 12350-9 (EN 12350-9, 2010). The tests were performed twice for the mixtures SCC (SCC6-48 and SCC6-60) and the results are shown in Table 8-2. All the results were among the limits of the most common standards which set a slump-flow spread (d_f) from 550 mm to 850 mm, a time for the slump-flow patty to reach 500 mm of diameter (T_{500}) lower than eight seconds, and an emptying time of the V-funnel between four and 25 seconds (Walraven, 2003).

The slump-flow spread mean diameters were as expected and similar to the references Chapter 4 and 5.The times obtained for T_{500} remained at similar values for all the concrete types. The uniform distribution of the fibres and aggregates on the spread was observed and had no signs of segregation. Insignificant differences were obtained with shorter fibres when SCC6-48 and SCC-60 were compared. Though a slight increase was obtained, values were very close in both cases, and T_{500} (as well as the emptying times of the V-funnel) remained at similar values.

8.4 Assessment of mechanical properties

The mechanical properties of the concretes were assessed by following standard procedures. The compressive strength was obtained in accordance with EN 12390-3 (EN 12390-3, 2009), whereas the tensile splitting strength was obtained as EN 12390-6 (EN 12390-6, 2009) states. In addition, the modulus of elasticity was assessed as EN 12390-13 (EN 12390-13, 2013) indicates. Three cylindrical specimens of each concrete type were tested for obtaining the compressive strength and tensile splitting strength. The modulus of elasticity was determined in one cylindrical specimen of each mixture. Table 8-2 shows the mean values and coefficient of variation of the results.

Table 8-2 shows that SCC compressive strength was higher than VCC. This increment in SCC might have been caused by the differences in the aggregate proportions used. The effect of the fibres in SCC is twofold, depending on the fibre length. When 48 mm long fibres were used there was a decrement of the compressive strength with respect to SCC. Nevertheless, when 60 mm long fibres were employed there were only slight differences identified in the compressive strength values. This phenomenon may have been caused by the higher number of fibres added when the shortest fibres were employed. A greater amount of fibres might be detrimental to the compaction of concrete in the sample mould. There were only insignificant differences between the compressive strength of VCC and VCC6-60. Regarding the elasticity modulus, in all the compositions manufactured with fibres lower values were obtained. As mentioned previously, the decrease may have been caused by worse compaction.

Table 8-2: Test results for assessment of fresh concrete and mechanical properties.

Concrete type	Slump flow test		V-funnel	*fck* (MPa)		*E* (GPa)	*fct* (MPa)	
	d_f (mm)	T_{500} (s)	t (s)	28d	c.v.	28d	28d	c.v.
SCC	655	3.5	8.0	39.3	0.01	35.8	3.78	0.14
SCC6-48	600	4.0	13.5	34.8	0.05	30.3	4.48	0.08
SCC6-60	590	4.0	16.0	41.4	0.01	31.6	4.09	0.03
	Slump test (mm)							
VCC	150.0		-	33.6	0.04	33.9	3.95	0.11
VCC6-60	142.5		-	32.9	0.04	29.9	3.75	0.07

The presence of fibres raised the indirect tensile strength of SCC within the order of magnitude expected (Martinie, et al., 2011). There was a greater increment when 48 mm long fibres were added which may have been caused by the greater amount of fibres added. In the case of VCC6-60, there was a reduction of 0.20 MPa when 6 kg/m^3 of 60 mm long fibres were added with respect to VCC. However, in all cases, the differences were inside the experimental scatter and no sound conclusions could be deduced.

8.5 Flexural tests

8.5.1 Testing methods

In this Chapter, the position of the notches performed before testing on the samples was important. In the concrete elements cast in standardised moulds, the position and direction of the notch was determined in accordance with the recommendations followed (EN 14651:2007+A1, 2007). These aforementioned relative positions of the notch were chosen in accordance with EN: 14651 (EN 14651:2007+A1, 2007) and RILEM TC 165-TDF (RILEM TC162-TDF, 2002) with the scheme shown in Figure 8-6.

The top surface during casting was also designated as a free surface. In such a way, the rest of the surfaces were in restrained conditions due to the walls of the moulds. Walls represent physical boundary conditions which entail a preferential orientation that affects increasing post-cracking response, given that such a preferential alignment is perpendicular to the cracked section in standard tests. In the centre of the cross-section the bulk should be in isotropic conditions. Nevertheless, if fibres were rigid it would not be geometrically possible to find a fibre perpendicular to a wall with a centre of gravity at a distance lower than half the length of the fibre (Martinie, et al., 2011). In such a sense, the so-called wall effect ensues from the tendency of the fibres to be positioned on a parallel plane to the wall. This is not related with casting procedures, but with fibre length and the geometry of the formwork. While polyolefin fibres might fold, the tendency to align due to the walls is considered to take place as soon the material is poured. The notch in these elements was performed in one of the lateral surfaces of the sample. Therefore, the free surface of the sample will be on one of the sides of the samples when testing. In Figure 8-7 a sketch of the mould, the sample and orientation of the notch can be seen. This orientation was used in all the standardised samples performed.

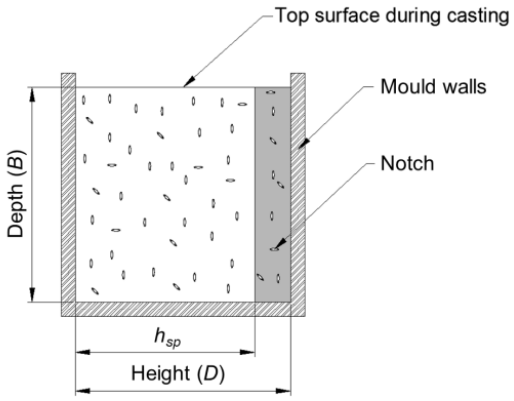

Figure 8-6: Relative position of the notch during casting used for standardized samples.

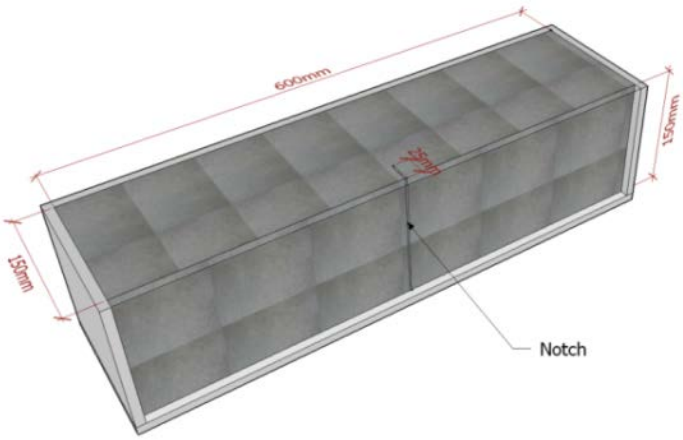

Figure 8-7: Notch sketch in a standardised sample.

In order to assess the floatability of the fibres when added to a standard concrete, a mould three times taller than a regular one was used. The dimensions of the latter and position of the notch can be seen in Figure 8-8 (which also shows the names of samples, given in accordance with their position in the concrete element). U stands for upper position, H for half position, and D for bottom position. As can be seen in Figure 8-8, the notches were sawn by following an analogue disposition as stated by EN 14651 (EN 14651:2007+A1, 2007) and RILEM TC-162 TDF (RILEM- TC 162-TDF, 2000).

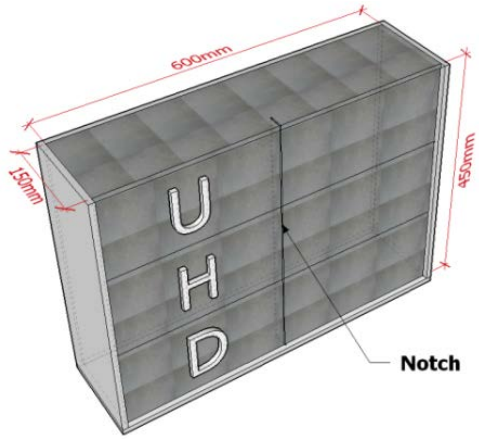

Figure 8-8: Vertical element filled with VCC6-60.

The influence of the flow in the distribution of the fibres along a beam element performed with SCC6-60 was ascertained by producing a beam of dimensions 2200x250x150 mm³. The beam was divided in four samples in accordance with the outline shown in Figure 8-9. Similarly to the orientation of standardised samples, the orientation of the notches was placed on one of the sides of the samples. It should be noted that in this element the effect of the proximity of the sides of the mould was neglected by crafting a mould 100 mm deeper than the usual concrete samples. The sides of the beam element, at 50 mm deep, were cut and discarded as can be seen in Figure 8-9. Only the subsequent four samples of 550x150x150 mm³ were stored in a climatic chamber until the age of testing.

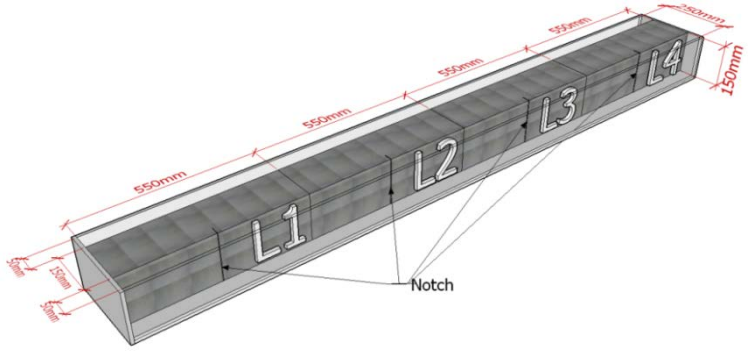

Figure 8-9: Beam element division; L1-L4 samples.

The flexural tensile tests were performed in accordance with one of the most common recommendations (EN 14651:2007+A1, 2007; RILEM TC162-TDF, 2002), used in both the construction industry and research. The tests were performed in 600x150x150 mm^3 samples, except those obtained from the beam element (L1-L4) which were 550x150x150 mm^3. However, the span between the bearings remained constant for the tests performed. The span was established in 500 mm. The tests procedure was similar to the described in subsection 5.5, but for the case of the smaller samples of dimensions 430x100x100 mm³ that were tested as described in subsection 4.2.3 in accordance with RILEM TC-187 SOC (RILEM TC-187-SOC, 2007) by using the three prismatic specimens with the same speed steps as the standard test. A comparison of the test geometry of the two specimen sizes is shown in Figure 8-10.

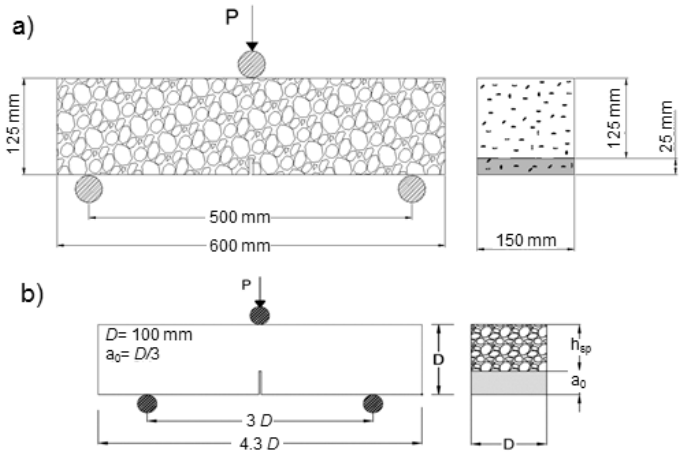

Figure 8-10: Fracture tests setup: (a) EN: 14651 and RILEM TC 162-TDF; (b) RILEM TC-187 SOC specimens.

Plain concrete fracture results

The quality of concrete has traditionally been assessed by means of compressive strength tests which are by far the most common carried out on concrete (Mindess, et al., 2003). Since concrete has low tensile strength, structural research, codes and practice have been based on compressive strength. Such compressive tests are relatively easy to perform and the variables affecting the results are consequently well known and detailed, showing accurately the main mechanical advantage of concrete. As the addition of fibres to concrete has hardly any influence on compressive strength, the main reason for using fibres lies in improving tensile response in post-cracking behaviour. In this sense, FRC has more regularly been defined by its residual post-cracking parameters from flexural tests in notched elements. In this study, the objective of using the two types of concrete design was not to achieve similar compressive strength but similar fracture energies. After the limit of proportionality is reached, the inelastic processes of plain concrete fracture barely contribute to preventing the collapse of the piece. Nonetheless, analysis should evaluate the energy added by fibres and the structural behaviour in the post-cracking region of the curves. In such a case, the fracture energy and residual load-bearing capacity of the plain concrete should be approximately the same.

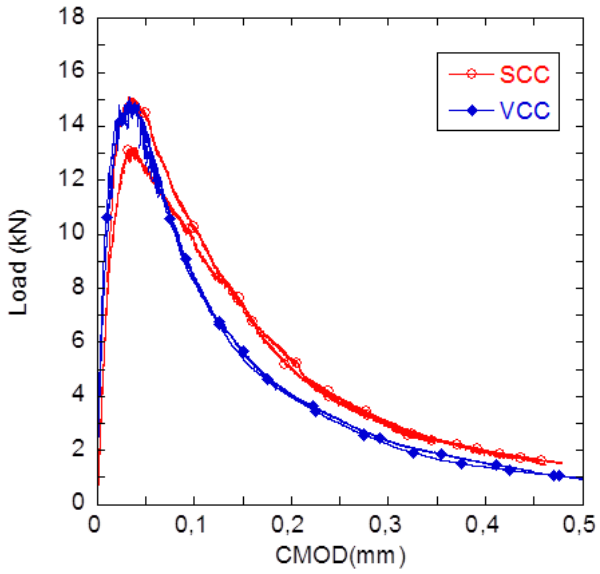

Figure 8-11: Plain concrete VCC and SCC fracture results obtained in 600x150x150 mm³ samples.

The results obtained in the fracture tests of plain VCC and SCC are shown in Figure 8-11, where the fracture energy obtained by expression (5-1) is placed in Table 8-3. The similarity of the concrete types should be noted. The abovementioned objectives were achieved. The fracture behaviour of both concrete types was analogous even at the maximum load. After it was reached, the typical exponential softening behaviour of concrete was evident. This results were previously analysed in Chapter 5.

Fracture results of polyolefin fibre reinforced concrete (PFRC)

Three-point bending tests of PFRC have been widely studied in Chapter 4 and 5. The typical curves showed three remarkable turning points and the description that follows

allowed discussion with the extraction of only a few parameters of each test. The first turning point took place when the loading-process reached the maximum value and only few inelastic processes were evident. Given that at such deformation the crack is still not perceptible to the naked eye, the turning point where the load reaches the maximum is commonly known as load at the limit of proportionality (L_{LOP}), with it being the overall maximum load in plain concrete. In the case of the post-cracking load values continuing and increasing after the limit of proportionality, the behaviour of the material would be denoted as hardening. Such behaviour is different from the softening behaviour that ruled the branch after L_{LOP}, as reported in many FRC types and especially for PFRC (see Chapter 4). The softening behaviour is distinctive of plain concrete fracture and, in such a case, the steep unloading process leads to the sample failing and collapsing. However, the polyolefin fibres absorb the energy released by the concrete in the fracture processes by so-called fibre bridging and change the loading tendency. In such an instant, the curve reaches the minimum post-cracking load (L_{MIN}), represented in Figure 5-3, while another up-loading process starts again. Since polyolefin fibre anchorage is due to a rough surface, when enough fibres boast sufficiently embedded length the load values retrieve as deformation grows. The end of the load-increasing-ramp is the third noticeable point of the described curve with the maximum post-cracking remaining load (L_{REM}) shown in Figure 5-3. The descending slope drawn after L_{REM} continues up to the end of the test. It should be mentioned that all the PFRC specimens showed this behaviour and none failed or collapsed, showing an improvement in ductility and toughness in plain concrete.

Fracture results of SCC specimens with two pouring methods

Figure 8-12 contains the load versus deflection and load versus CMOD curves obtained for mixtures SCC6-48S and SCC6-48C. In order to offer a more comprehensive comparison, the average behaviour is represented in a thicker width line. It can be observed that the shapes of the curves are similar, although the curves of the samples poured from the centre obtained higher load values. Nevertheless, the position of the three turning points, L_{LOP}, L_{MIN} and L_{REM}, were similar and occurred for the approximately the same deformation state. Therefore, it can be seen that L_{MIN} took place for CMOD values around 0.5 mm and, in the case of L_{REM}, the deflection value coincided between 2.5 and 3.0 mm. The small scatter obtained, which was even smaller for the specimens poured from the centre of the mould, should also be noted.

Although the manufacturing procedure described in EN: 14651 and RILEM TC-162 TDF states that the pouring position should be in the centre of the mould, most research with SCC has been performed by pouring it from the side. In addition, the way of filling the moulds highlighted by the codes (shown in Figure 8-1c) is considered suitable for relatively dry and externally vibrated concretes (Walraven, 2009). As previously stated, variations in the casting methods or compaction procedures might lead to significant differences in fibre orientation and, therefore, in fracture behaviour (as can be seen in Figure 8-12). Greater values of L_{REM} and L_{MIN} were obtained for SCC6-48C, which shows the influence of the filling procedure of the moulds. Thus, the real behaviour of FRC structural elements performed with fibre reinforced SCC may not be representative, as the filling procedure may not be reproduced in laboratory samples. This could be justified by the positioning and orientation of the fibres analysed in Chapter 9. Nonetheless, it cannot be overlooked that such differences might have been smoothed by the position of the notch which was performed in accordance with standards EN 14651 and RILEM TC 162-TDF.

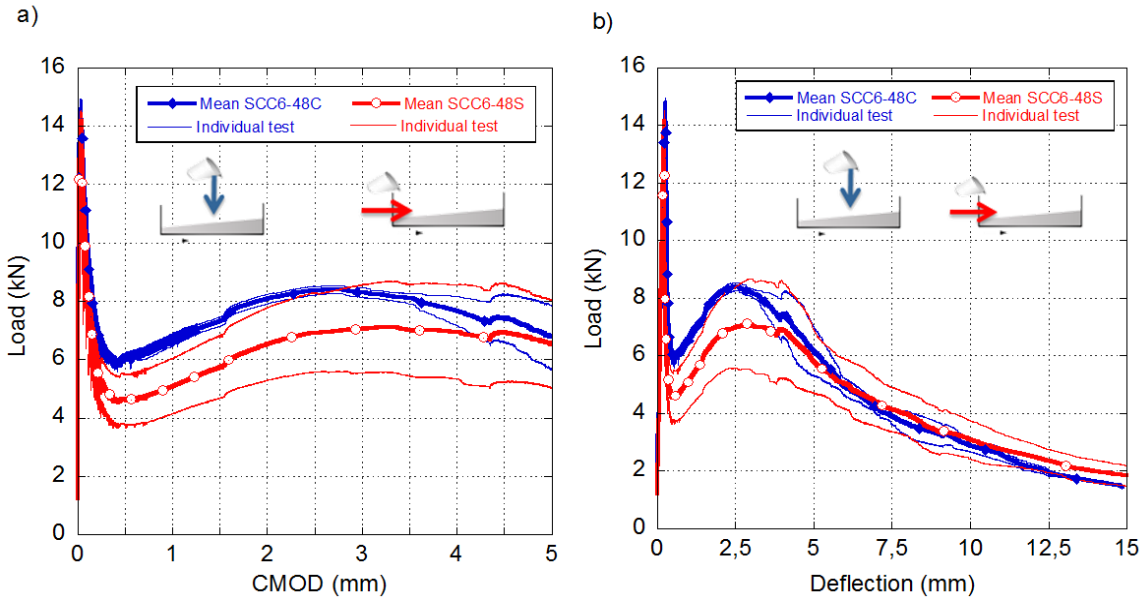

Figure 8-12: Mean fracture curves of SCC6-48C and SCC6-48S: (a) load versus CMOD; (b) load versus deflection.

Fracture results of SCC specimens with two fibre lengths

The load-deflection curves of SCC6-60S and the mean curve previously obtained for SCC6-48S are shown in Figure 8-13(a). Such mixtures were manufactured by adding the same weight of fibres but with a different fibre length. With the aim of highlighting any contrast between them, the mean load-CMOD curves of both types of concrete are shown in Figure 8-13(b). The scatter obtained was significantly small and the shapes of curves resembled those described in subsection 5.5. It should be noted that while the shapes of the curves are analogue, the deformations at L_{REM} were higher, probably, due to the longer fibres. This was not as noticeable as was expected. It could be argued, though, that any difference might be attributable to the statistically longer embedded length of the fibres in the cracked section. The 60 mm long fibres might be pulled out for deformations higher than the 48 mm long fibres.

The deformations where L_{REM} took place for the specimens reinforced with fibres and 60 mm long were in the approximate range of 3.5-4.0 mm which was appreciably higher than for SCC6-48 mixtures (about 3.0 mm). In SCC6-48S L_{REM} reached load values near 7 kN with a CMOD value of 3.0 mm, while SCC6-60S had similar load values when CMOD was around 4.0 mm. This is one noticeable effect in the behaviour of the samples caused by the larger length of the 60 mm long fibres. It should be mentioned that both mean curves could belong to the same concrete if an average experimental dispersion were considered. If Figure 8-13 is discussed in more detail, it can be clearly identified that the curves for 60 mm fibre length are displaced to the right of the drawing, with the mean curve of SCC6-48C being inside the shaded area. The slope of the uploading branch between L_{MIN} and L_{REM} was steeper for SCC6-48C, but the deformation at the L_{REM} point was smaller and remained inside the scatter band for conventionally used deformations.

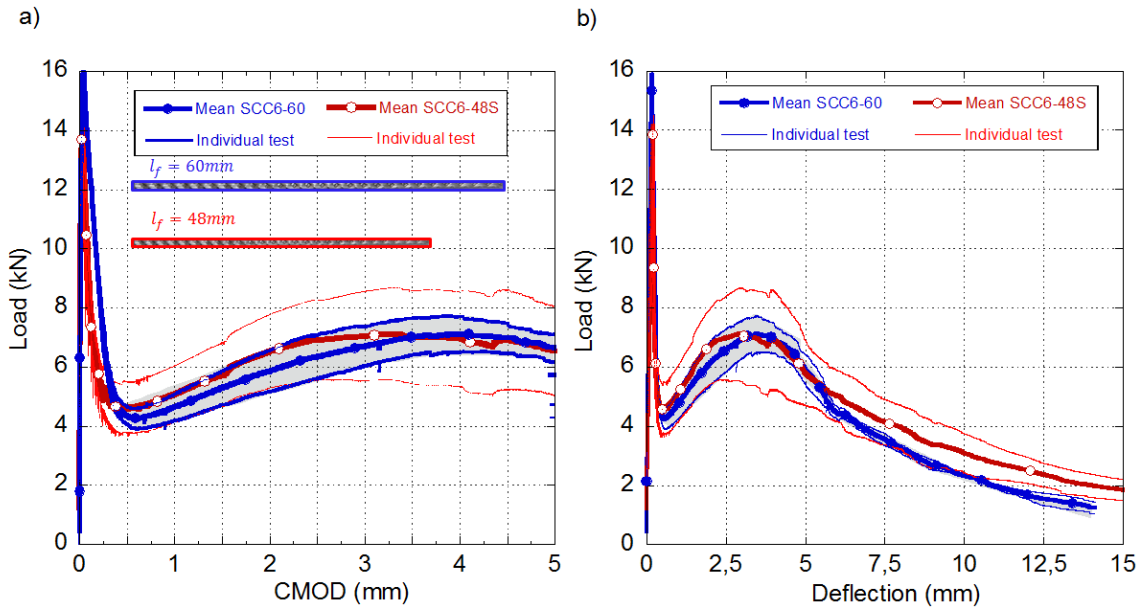

Figure 8-13: Fracture curves of SCC6-60S and mean curves of SCC6-48C: (a) load-CMOD; (b) load-deflection.

Fracture results of VCC specimens with standard and smaller sizes

It should be noted that in Figure 8-14(b) the vertical scale has been adapted to the loads obtained in the tests performed for the smaller beams, while the horizontal scale has been maintained. Nevertheless, scales for the specimens of 600x150x150 mm³ were the same as the previous shown figures.

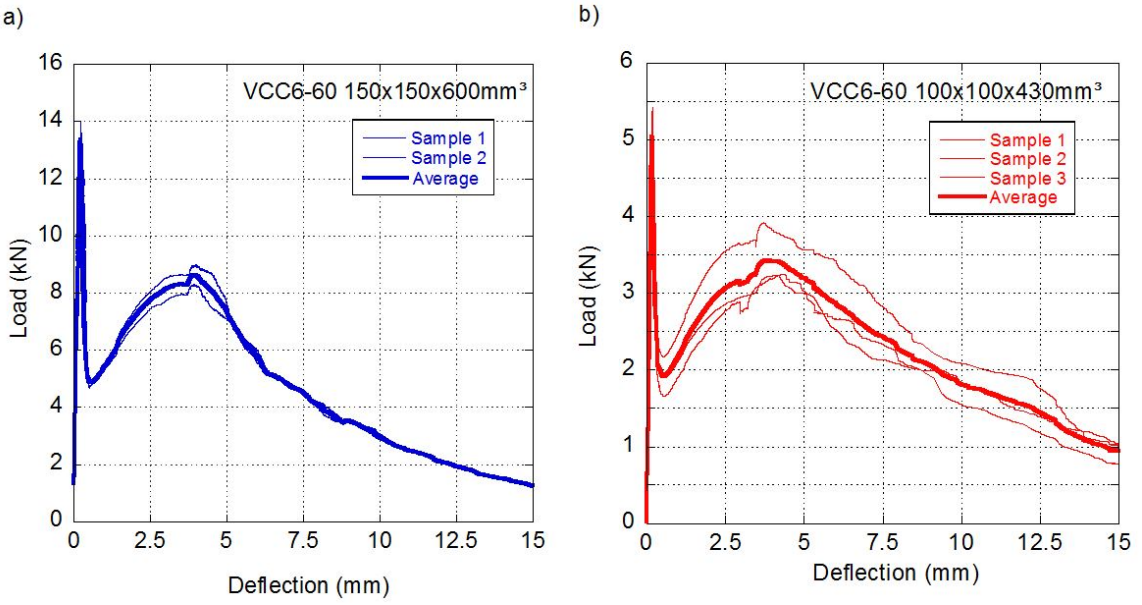

Figure 8-14: Load-deflection curves of VCC6-60: (a) mean and two specimens of dimensions 600x150x150 mm³; (b) mean and three specimens of dimensions 430x100x100 mm³.

The small scatter obtained was remarkable, as was the analogous position of deflection at the turning points. This easily appreciable event can be noted if Figure 8-14(a) is observed, the values of deflection for L_{REM} were similar to those obtained for SCC6-60S and around 4.0 mm. As the reason that justifies this is unclear, it will be examined in the later

discussion sections. If Figure 8-14(b) is observed, load values were clearly smaller but, in contrast, deformations for the turning points were alike. Moreover, given that the results provided such similar shapes they showed significantly smaller scatter for the standard size samples, which was probably due to the reduced influence of the wall effect when compared with the small beams. This will be discussed below and in Chapter 9 of the document by using the data obtained from counting the fibres on the fracture surfaces.

Long element: L series fracture results

When the long element was divided into four pieces and the sides removed, samples 550 mm long with a squared cross section of 150 mm sides were obtained. In such a way, these dimensions enabled the performance of fracture tests and extraction of comparable results. As mentioned previously, the samples were named L1, L2, L3 and L4 according to the flow direction. In Figure 8-15, the curves load-CMOD and load-deflection of the four samples are included. It should be noted that only one test for each position was performed. It can be observed that the first and second specimens, named L1 and L2, those close to the pouring point of concrete, had similar residual load values. In addition, such values were lower than those obtained for L3 and L4 which were close to the end of the beam.

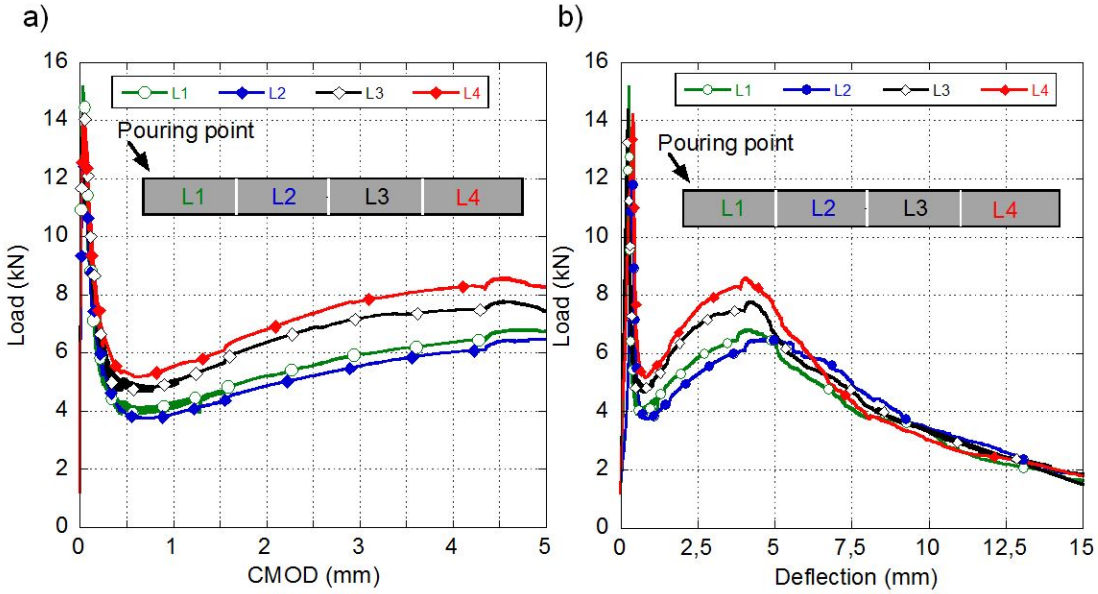

Figure 8-15: Fracture curves of L series: (a) versus CMOD; (b) load versus displacement.

L_{MIN} took place close to the CMOD values of 0.5 mm and L_{REM} was observed to be around 4.0 mm of deflection. It should also be noted that load values of L1 and L2 were similar to the results of the standard samples of SCC6-60S. However, such values in L3 and L4 were higher and closer to the values obtained on VCC6-60 standard specimens.

Vertical element: UHD series results

With the aim of comparing fracture results obtained for different heights in the UHD series, the mean load-deflection curves processed from the four samples of each type are placed in Figure 8-16. It may be noted that the lower beams named D showed better results than U and H (which were similar). The deformation states where the turning points occurred remained in similar positions as mentioned above. The results supported the idea of the

non-existence of any floating effect, at least in the lower sawn beam (D). It should be noted that, as expected, D had higher residual flexural results due to the existence of one more wall (the bottom one) that helped to align the fibres. The influence of such a wall in the orientation and position of the fibres will be assessed and reported in Chapter 8 of the thesis. In any case, at this point it should be noted that there was no noticeable scatter above the usual experimental dispersion.

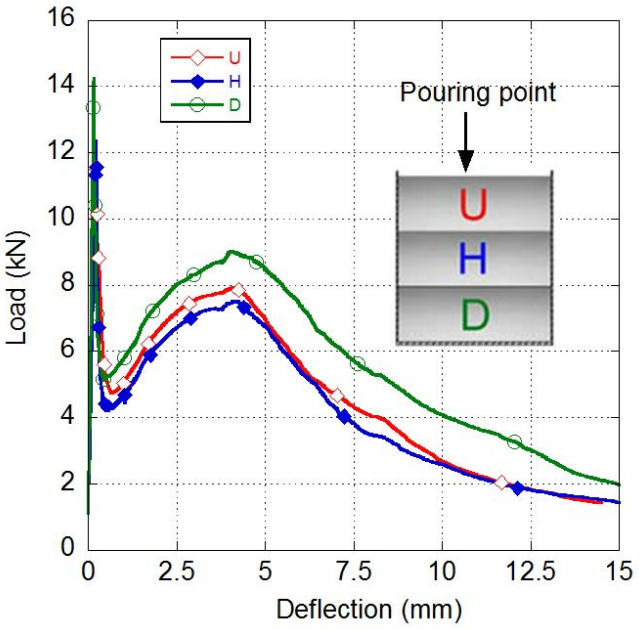

Figure 8-16: Mean load versus displacement curves of UHD series.

8.6 Discussion

8.6.1 Fracture energy and the turning points

Concrete fracture mechanics analyses have been typically conducted by means of the fracture energy. The latter relates the work of fracture (the area under load-deflection curve) and the fracture surface generated. Due to its brittleness, this parameter is useful when applied to concrete. In addition, it allows comparison of several concrete formulations. The fracture energy results obtained from plain concrete are shown in Table 8-3. It is important to note the similarity of the fracture energy between the two plain concrete types, VCC and SCC. Such behaviour shows that the variations of the fracture energy of the FRC did not depend on the plain concrete characteristics.

Even for small deformations, the contribution of the fibres increases the ductility and toughness of concrete. The fracture energy of all the PFRC formulations (SCC and VCC) with a deflection of 1 mm doubled that of plain concrete. For higher deflections of 12.5 mm, the fracture energy of PFRC was well over 20 times that of the same plain concrete. For this reason, for such PFRC mixtures fracture energy was obtained for three different deflection values. In order to assess the improvement at small deformations, fracture energy for a 1 mm deflection was obtained which corresponds to the failure deformation of plain concrete. In addition, as measurement and examination of the evolution of fracture energy close to L_{REM} was considered to be of relevance, this was also extracted for 5 mm of deflection. Moreover, fracture energy was obtained for 12.5 mm of the deflection which

would correspond to the final deformations. All these values, together with their coefficients of variation, can be observed in Table 8-3.

Table 8-3: Fracture energy of plain and fibre reinforced concrete.

	Concrete	Fracture energy, G_F (N/m)					
		1 mm	c.v.	5 mm	c.v.	12.5 mm	c.v.
Plain	VCC	152.8	0.10				
	SCC	152.4	0.10				
Standard Series	VCC6-60	337.8	0.01	1959.2	0.05	3457.1	0.04
	VCC6-60 Small	345.2	0.09	2180.4	0.12	4475.3	0.14
	SCC6-60S	329.6	0.04	1695.3	0.11	2888.0	0.09
	SCC6-48C	381.9	0.00	1999.7	0.06	3367.6	0.09
	SCC6-48S	310.4	0.16	1709.5	0.28	3132.2	0.28
UHD Series	VCC6-60U	336.5	0.16	1879.4	0.19	3490.4	0.20
	VCC6-60H	309.1	0.10	1718.0	0.13	3006.7	0.12
	VCC6-60D	350.6	0.11	2143.3	0.19	4215.6	0.17
	VCC6-60UHD	332.0	0.13	1913.6	0.19	3570.9	0.21
L Series	SCC6-60L1	313.6	-	1575.7	-	3034.3	-
	SCC6-60L2	270.3	-	1437.1	-	3096.2	-
	SCC6-60L3	357.5	-	1821.9	-	3508.3	-
	SCC6-60L4	386.8	-	1982.7	-	3519.6	-
	SCC6-60L	332.0	0.15	1704.4	0.14	3289.6	0.08
	Average PFRC6	335.7	0.10	1841.9	0.12	3432.6	0.14

In addition to the fracture energy, the loads taking place in the turning points previously described and their coefficient of variation have been extracted and are included in Table 8-3. Such loads, L_{LOP}, L_{MIN} and L_{REM} are a keystone of the flexural response of the material and should be used to complete a detailed analysis. However, L_{LOP}, did not seem to follow any trend or be affected by the addition of fibres or any of the factors employed in this research. This phenomenon was expected, as it had been previously stated in Chapters 4 and 5.

Small specimens of VCC6-60 had higher fracture energy than the rest of the mixtures or samples, being close to 4500 N/m for 12.5 mm of deflection. This could be attributable to the wall effect previously explained which may have helped to align the fibres. Apart from these samples, the narrow scatter was remarkable, especially in VCC6-60 standard samples, being the fracture energy similar for the rest of the mixtures at the deformation states considered.

Table 8-4: Mean values of load of all the concrete mixtures.

	Concrete type	L_{LOP} (kN)	c.v.	L_{MIN} (kN)	c.v.	L_{REM} (kN)	c.v.
Plain	VCC	14.87	0.02				
	SCC	14.15	0.09				
Standard Series	VCC6-60	13.78	0.03	4.82	0.02	8.60	0.05
	VCC6-60 Small	5.31	0.06	1.91	0.13	3.47	0.11
	SCC6-60S	15.92	0.06	4.10	0.08	7.13	0.12
	SCC6- 48C	15.02	0.01	5.60	0.01	8.51	0.02
	SCC6- 48S	14.27	0.03	4.58	0.27	7.13	0.30
UHD Series	VCC6-60U	14.07	0.06	4.63	0.22	8.06	0.19
	VCC6-60H	13.08	0.09	4.39	0.14	7.39	0.16
	VCC6-60D	14.21	0.08	5.48	0.15	9.44	0.21
	VCC6-60UHD	13.73	0.08	4.73	0.18	8.01	0.20
L Series	SCC6-60L1	14.94	-	4.02	-	6.81	-
	SCC6-60L2	12.74	-	3.76	-	6.52	-
	SCC6-60L3	14.29	-	4.74	-	7.75	-
	SCC6-60L4	14.06	-	5.16	-	8.52	-
	SCC6-60L	14.01	0.07	4.42	0.15	7.40	0.12
	Average PFRC6	14.22	0.07	4.66	0.13	7.81	0.11

In such a sense, the most notable results were obtained in D samples, VCC6-60 and SCC6-48C standard specimens. The external factors that affect the specimens might have improved the positioning of fibres. This phenomenon will be studied in Chapter 9. In the case of the D samples, which correspond to the bottom samples obtained from the vertical elements, the behaviour identified may be attributed to the absence of a floating effect, the existence of one more wall, and the probable plane orientation induced by the external vibration. This process also seemed to be efficient in VCC6-60 standard-size specimens. In the cases of L3 and L4, it should be noted that the action of the flux may have raised the fracture energy up to values similar to those obtained in VCC6-60. It is remarkable that the flux was capable of raising these values even in the absence of lateral walls which were removed after demoulding. Given that the best performance within the long element was identified at the end of the beam, it seems that once the flux had developed the fibres achieve a better orientation (Deeb, et al., 2014c). In this same regard, L_{MIN} and L_{REM} upper values took place for the same samples. Such loads for the referred cases were in the order of 5 kN for L_{MIN} and 8.5 kN for L_{REM}. Thus, the remaining load was approximately 70% higher than the minimum residual load.

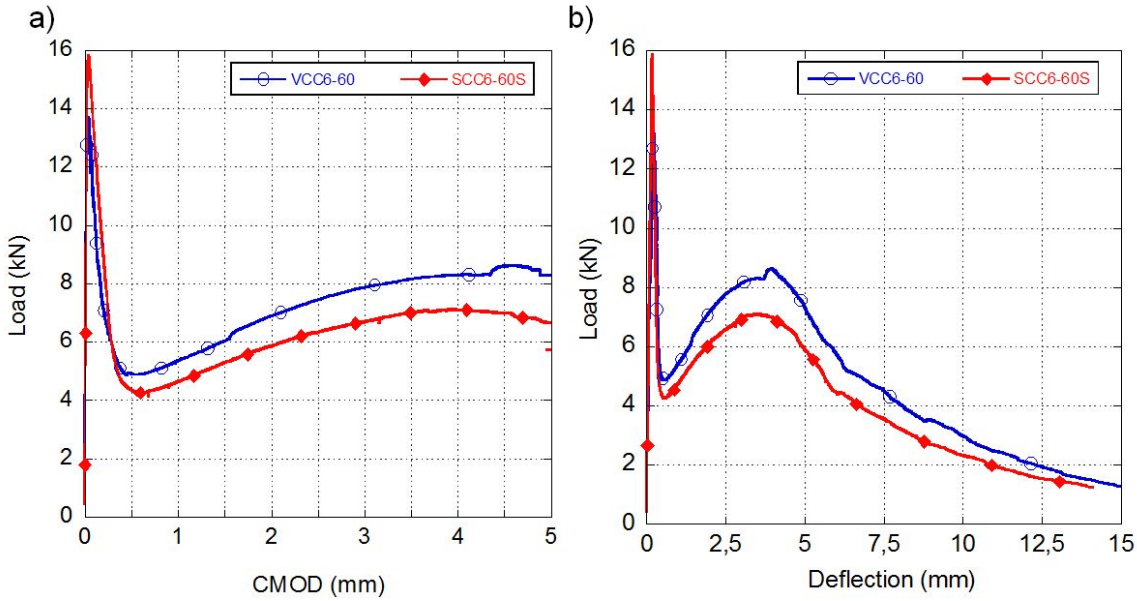

Figure 8-17: Fracture curves comparison of SCC6-60S and VCC60 laboratory beam tests: (a) versus CMOD; (b) load versus displacement.

The specimens were manufactured with two types of concrete, two fibre lengths, several sizes and pouring methods. All of them had some influencing factor compared with the reference standardised VCC. Note that the only common feature is that all had the same fibre dosage. With the aim of having an overall view of the behaviour of PFRC with 6 kg/m³ (PFRC6), the average results of all the concrete types were computed and are shown in the last row of Table 8-3. The fracture energy obtained was similar for all the deformations and the coefficient of variation remarkably limited. This means that PFRC6 behaved in a significantly similar manner even with the large variety of affecting factors. The latter was additionally confirmed by Figure 8-18. The reliable performance of PFRC6 should be highlighted as a sound conclusion, although the positioning of the notch may have had influence on the referred small scatter. The notch direction in the vertical and long elements was performed by following the standards as closely as possible. Although the positioning of the notch may have lessened the differences among the specimens, by averaging the variations on the positioning of the fibres, the reduced scatter found shows the robustness of the PFRC6 formulation. This is shown in the fracture curves obtained which did not show significant differences either in shapes or in post-peak loads. Figure 8-18 shows the confidence interval that would be obtained by keeping the fibre dosage and length steady. However, there should be positioning and orientation differences that might explain the differences among samples. The latter differences will be discussed in greater depth in Chapter 9 of the thesis.

Regardless of this reliable behaviour of PFRC6 that can be verified by the analysis of the turning points shown in Table 8-4, it is worth discussing the results of VCC compared to SCC ones. These two types of concrete are the most common found in construction. For rigid fibres, experimental evidence has been obtained that shows that the more is the external vibration energy the more the fibres tend to align in horizontal planes (Laranjeira, et al., 2012). For these rigid fibres, it has also been found that even in the absence of a boundary condition the fibres tend to align when SCC flows (Martinie, et al., 2011). For polyolefin fibres, these effects are still a matter of study. In such a sense, Figure 8-17 shows the mean curve of the referred mixtures. The results for the vibrated concrete were around 15% higher on average and the small degree of scatter even more relevant.

As there is a high resemblance of the fracture behaviour of the plain VCC and SCC, the better performance of the VCC6-60 compared with SCC6-60 in laboratory-standard specimens could only be caused by a better positioning of fibres. On the one hand, vibration for this size of specimens was clearly effective while on the other hand, compaction under its own weight, due to self-compacting properties, seemed to need more distance to improve the positioning of fibres (as pointed out in the results of L3 and L4). In such structural elements that have forms similar to the vertical or the long elements, a deeper analysis of the results based on the positioning and orientation of the fibres would provide highly valuable information. The intention of Chapter 9 of the research is to relate all the factors and so improving the knowledge of the behaviour of the polyolefin fibres inside the fresh VCC or SCC. It is also focused on identifying the final location of the fibres in structural members and so linking laboratory results not only to the material behaviour but also to structural members.

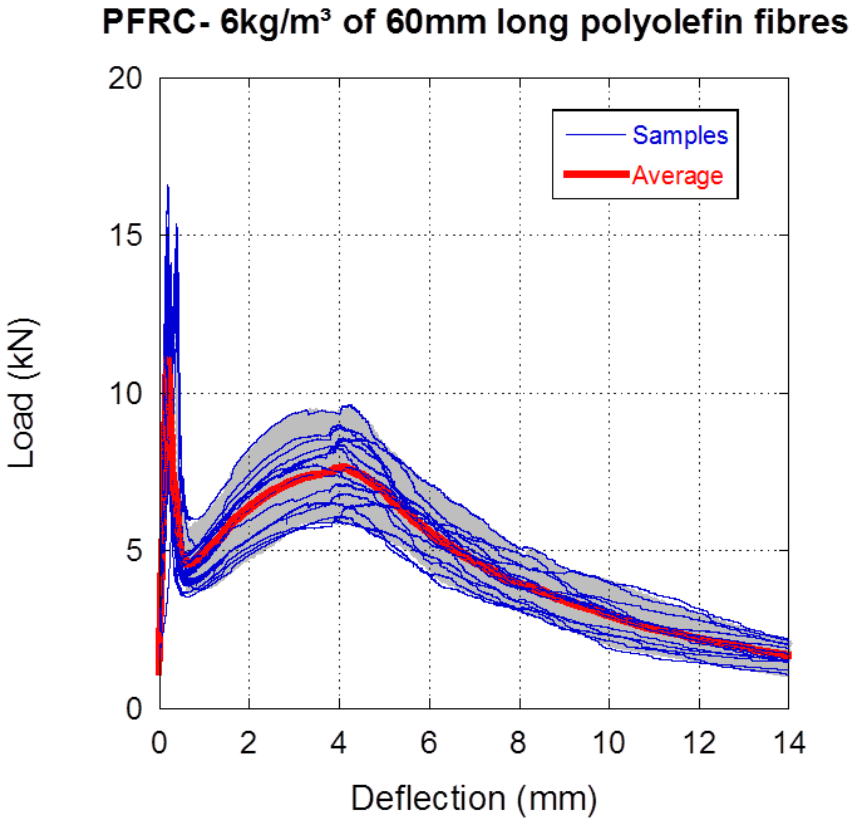

Figure 8-18: Load – deflection curves of the PFRC6 with 60 mm long fibres.

If Table 8-3 and Table 8-4 are observed, some difficulties may be identified when analysing the results obtained for the same concrete poured in two mould sizes. In order to address this, residual strength versus CMOD curves were plotted. Such residual flexural strength values were obtained by means of expression (2), which has also been included in test recommendations and standards (EN:14651, EHE-08, MC2010, RILEM TC 162-TDF). The standard EN: 14889-2 (EN 14889-2, 2008) defined this residual flexural strength as the theoretical stress at the tip of the notch which acts in the centre of an un-cracked section, involving linear distribution of force and subjected to a specified load in its correspondent CMOD. This is a convenient tool used to transform loads (F_j) to strength (f_{Rj}), enabling comparison of two sizes of sample as it also considers span (L), notch (a_0) or ligament (h_{sp}) and depth (b). Figure 8-19 shows the curves of residual strength-CMOD of the VCC6-60 samples for the beam sizes.

$$f_{Rj} = \frac{3}{2}\frac{F_j \cdot L}{b \cdot h_{sp}{}^2} \qquad (8-2)$$

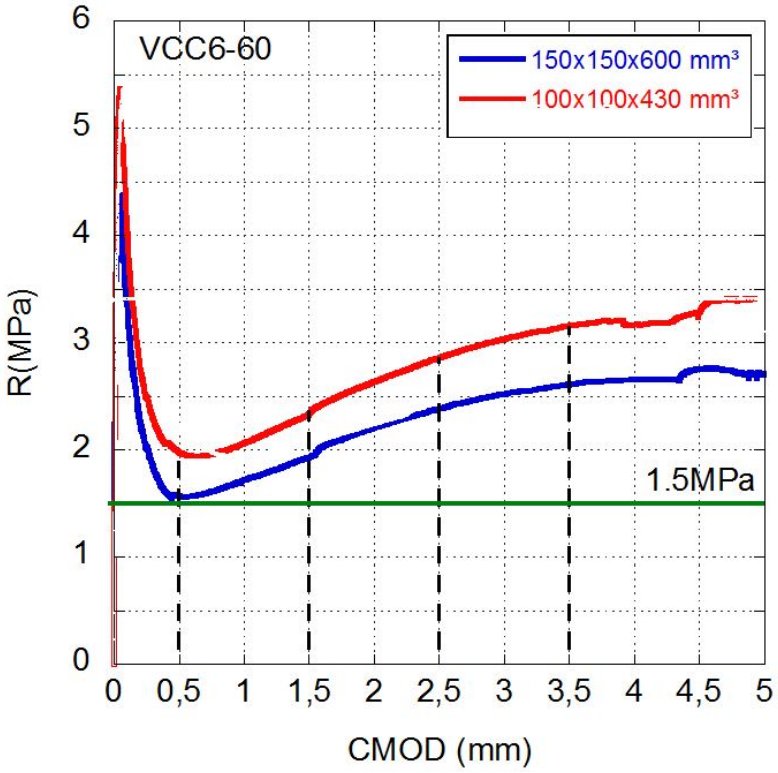

Figure 8-19: Residual flexural strength versus CMOD of VCC6-60 in the two beam sizes tested.

The shapes of the curves shown in Figure 8-19 appear to be comparable. The position of the turning points coincided despite the mean curve of the small beams being above that of the standard beam. A size effect is evident on concrete, which increases the fracture energy with the beam height and the opposite effect with the relative notch depth ($\alpha = a_0/D$) which affects it inversely (according to experimental evidence, Fracture energy increases for lower values of α) (Cifuentes Bulté, 2010; Duan, et al., 2003). In such a way, size effect might be considered of minor importance when compared with the wall effect. This would suggest that for FRC the size effect may be considered negligible in residual strengths (Di Prisco, et al., 2004). In such a sense, the results were expected due to the greater influence of the wall effect in smaller samples with the same fibre length. More detailed research on the size effect of PFRC is beyond the scope of this study.

8.6.2 Residual flexural strength

The standards relate the structural capacity of fibre reinforcement to residual flexural strengths obtained from the tests (EN 14651:2007+A1, 2007). Specifically, Model Code 2010 (fib Model Code, 2010) proposes relating Service Limits States (SLS) with stress values in a CMOD of 0.5 mm (f_{R1}) and also to relate Ultimate Limits States (ULS) with the stress values obtained from the test when CMOD is 2.5 mm (f_{R3}). Moreover, the standards (EHE-08, 2008; RILEM TC-162-TDF, 2002) have dealt with residual stress values in percentage values of the stress obtained for the limit of proportionality (f_{LOP}). f_{LOP} is defined in the standards as the maximum strength obtained for CMOD values lower than 0.05 mm. Additionally, the requirements for considering the contribution of fibres in

structural design have been set in the aforementioned recommendations in percentage terms of f_{LOP}. Both Model Code 2010 and Spanish structural code (EHE-08, 2008) require for structural use strengths of 40% of f_{LOP} for CMOD 0.5 mm and 20% of f_{LOP} for CMOD 2.5 mm (obtained with the test methods EN: 14651 or RILEM TC162-TDF). These limits are set to prevent brittleness (Di Prisco, et al., 2013) of the concrete piece. However, paradoxically it might be easier to meet these percentage requirements by using a poorer concrete. European Standard 14889 was approved in 2006 to regulate the use of fibres for concrete comprising two parts: first dealing with steel fibres and second one regarding polymer fibres. In such standards, not all the characteristics that may be relevant to the performance of FRC were addressed. However, those structural requirements at the same CMOD values were included but in terms of fixed stress values. That is to say that EN: 14889-2 specifies the volume of fibres that achieves a residual flexural strength of 1.5 MPa at 0.5 mm CMOD and 1.0 MPa at 2.5 mm CMOD obtained in specimens produced with a reference concrete enclosed in EN 14845 (EN 14845-1, 2006) and EN: 14651 test methods (EN 14651:2007+A1, 2007).

The suitability of all the combinations studied following (EN 14889-2, 2008) can be seen in Table 8-5. In it, the residual strength with its coefficient of variation and also the percent of f_{LOP} can be observed. Most of the results f_{R1} were slightly higher than the minimum strength previously stated in the standard. It is worth noting that L1, L2 specimens did not reach the strength f_{R1} of 1.5 MPa, though that was expected because of the removal of the two lateral walls. The same absence of one wall might explain the result of H specimens which also had results below 1.5 MPa for 0.5 mm of CMOD. H specimens were obtained sawing the upper and the bottom surfaces and the absence of the bottom wall may have lessened the number of fibres aligned in the cracked section. In an overall view of PFRC6, the strength at 0.5 mm of CMOD was 5% higher than 1.5 MPa. Similarly, it met the requirements at f_{R3} established in EN 14889 but also the required by EHE-08 or Model Code 2010. In the same line of argument previously followed for the discussion of fracture energy, such average values could be considered representative of the residual strengths of the material.

Furthermore, one more result should be highlighted: SCC6-60 specimens had the lowest results in laboratory standardised samples. Nevertheless, such results were only slightly higher than the result for L1 that was placed at the beginning of the long element. That suggested that the flux required some initial minimum length to be effective and align the fibres both in standardised samples (Deeb, et al., 2014c) and in the long element.

Regarding the differences that might have been introduced by using the shorter fibres with a length of 48 mm, this effect may have been smaller in SCC6-48S. The percentage limit set in Model Code 2010 at CMOD 0.5 mm was only complied with the samples SCC6-48C. The requirements at 0.5 mm of CMOD might have been achieved by using a concrete of lower f_{LOP} or by a small increment of the fibre dosage. Although the overall results for the two fibre lengths were similar, to reach the requirement in CMOD 0.5 mm the fibres 48 mm long had better behaviour. As expected, the requirements for CMOD 2.5 mm related to ULS were exceeded for all the specimens tested.

Table 8-5: Bending test results: residual flexural strength.

	Concrete	Residual flexural tensile strength (MPa)											
		f_{LOP}	f_{R1}	c.v.	$\%f_{LOP}$	f_{R2}	c.v.	$\%f_{LOP}$	f_{R3}	c.v.	$\%f_{LOP}$	f_{R4}	c.v.	$\%f_{LOP}$
	CMOD (mm)	<0.05	0.50			1.50			2.50			3.50		
Plain	VCC	4.76												
	SCC	4.53												
Standard Series	VCC6-60	4.41	1.57	0.03	36%	1.93	0.05	44%	2.38	0.06	54%	2.61	0.07	59%
	VCC6-60	5.38	1.98	0.13	37%	2.32	0.14	43%	2.85	0.15	53%	3.15	0.14	59%
	SCC6-60S	5.09	1.39	0.09	27%	1.69	0.15	33%	2.03	0.16	40%	2.25	0.12	44%
	SCC6- 48C	4.81	1.91	0.01	40%	2.34	0.03	49%	2.67	0.02	56%	2.59	0.03	54%
	SCC6- 48S	4.57	1.50	0.24	33%	1.83	0.26	40%	2.21	0.28	48%	2.24	0.32	49%
UHD Series	VCC6-60U	4.50	1.61	0.23	36%	2.02	0.26	45%	2.33	0.22	52%	2.42	0.20	54%
	VCC6-60H	4.19	1.41	0.13	34%	1.72	0.12	41%	2.10	0.14	50%	2.27	0.15	54%
	VCC6-60D	4.55	1.78	0.16	39%	2.18	0.23	48%	2.63	0.24	58%	2.81	0.22	62%
	VCC660-UHD	4.39	1.60	0.19	36%	1.97	0.22	45%	2.35	0.21	54%	2.50	0.21	57%
L Series	SCC6-60L1	4.78	1.30	-	27%	1.49	-	31%	1.78	-	37%	1.98	-	41%
	SCC6-60L2	4.08	1.22	-	30%	1.38	-	34%	1.66	-	41%	1.87	-	46%
	SCC6-60L3	4.57	1.59	-	35%	1.80	-	39%	2.19	-	48%	2.34	-	51%
	SCC6-60L4	4.50	1.69	-	37%	1.94	-	43%	2.35	-	52%	2.58	-	57%
	SCC6-60L	4.48	1.45	0.15	32%	1.65	0.16	37%	2.00	0.16	45%	2.20	0.15	49%
	Average	4.62	1.58	0.17	34%	1.89	0.20	41%	2.27	0.19	49%	2.43	0.18	52%

8.7 Conclusions

This chapter has examined the influence of a variety of factors on the fracture behaviour of PFRC. Modifications of fibre length, fresh-state properties, pouring processes, sample sizes, formwork geometries and consolidation procedures have been assessed. These factors have shown that there is a limited variation of the fracture behaviour regardless of the parameters chosen, enabling a confident and reliable use of PFRC. The results achieved for average values of residual flexural strength exceeded 1.5 MPa for CMOD 0.5 mm and 2.2 MPa in CMOD 2.5 mm. The small scatter between the results with two types of concrete and fibre lengths allowed a confidence band that provides good reliability for the use of this type of fibres to be obtained

Regarding the fibre length, the use of two lengths (48 mm and 60 mm), had minor effects on the fracture behaviour of PFRC. The strength values registered were significantly close in both formulations. Slight improvements with fibres 48 mm long were perceptible in the smaller openings of the CMOD gauge. The curves with such fibres shifted towards higher deformation, though the whole mean curve remained inside the scatter band of the curves obtained for the 60 mm long fibres reinforced mixtures.

The fracture tests performed on standard samples of vibrated conventional concrete (VCC6-60) and self-compacting concrete (SCC6-60), both reinforced with 6 kg/m³ 60 mm long polyolefin fibres, have shown that VCC6-60 reached higher values at the minimum post-cracking load (L_{MIN}) and the maximum post-cracking load (L_{REM}) when compared with the SCC6-60 formulation. Self-compacting fibre-reinforced concrete fracture behaviour seemed to need a critical initial distance greater than a standardised beam to improve the orientation with flux, especially for the 60 mm long polyolefin fibres.

In addition, an evaluation of the effects of the pouring process has been performed. When SCC6-60 concrete was poured into a standardised mould from the centre, the post-peak behaviour reached higher values than when it was poured from one of the sides of the mould.

Moreover, when samples of 430x100x100 mm³ were tested there was a strength increment with respect to the standardised specimens. This improvement might have appeared due to the greater wall effect that took place in the smaller samples. This could be of significant interest when slender PFRC elements are manufactured and might require a reduction of the standard size samples.

In order to correlate the results of the standard specimen size tests with structural applications of PFRC, two formworks were manufactured: a column element filled with VCC6-60 (vertical elements) and a beam element filled with SCC6-60 (long element). The following conclusions were extracted from the fracture tests:

- Fracture tests on H and U samples, the central and upper sawn specimens, showed that although the polyolefin fibre density was lower than the concrete paste it seems that there was no rise of the fibres towards the upper part of the column element. Furthermore, the fracture tests on D samples showed a better performance than U and H samples. This might have happened due to the presence of the wall effect caused by three walls of the formwork.

- Regarding the long element (L1-L4 samples) fracture tests it should be noted that the best behaviour was obtained for samples L3 and L4 which were at the end of the beam. This may have happened due to the presence of a greater amount of fibres or a better orientation of such fibres. Consequently, to obtain a better fracture behaviour using PFRC, the use of long formworks might enable the flux to develop properly and it seemed to help the fibres alignment and distribution, thus improving its fracture behaviour.

Chapter 9

Experimental assessment of fibre orientation and distribution

9.1 Introduction

Fracture behaviour of polyolefin fibre reinforced concrete (PFRC) affected by changing fibre length, pouring methods, specimen sizes and fresh-state rheology was analysed in previous Chapter 8. Given that the influence of these factors could be seen in fracture results, the following sections examine the positioning and orientation of the fibres. This was performed by counting the fibres located in the fracture surfaces. In addition, the samples were divided in portions in order to evaluate the orientation and distribution of the fibres in the elements tested.

Previous chapter has shown how the use of a medium amount of polyolefin fibres (6 kg/m^3) can provide an improvement in the ductility and flexural behaviour of a self-compacting concrete (SCC) and, similarly, in the use of a vibrated conventional concrete (VCC). A wide variety of possible situations and uses of a polyolefin fibre reinforced concrete (PFRC) subjected to fracture tests were studied by changing the fibre length, the fresh-state properties, pouring processes, sample sizes, formwork geometries and consolidation procedures. In such flexural tests, reported and discussed in Chapter 8 of the thesis, the fracture behaviour of the PFRC was assessed, obtaining such a noticeable improvement that

a reliable structural application of the material might be taken into account. However, there remains an underlying question about the influence of the aforementioned parameters on the variations of the distribution and orientation of the polyolefin fibres that deserves further study.

Accordingly, in order to obtain reliable results that enable this comparative analysis, this work is required not only to perform the same test but also to follow the same mixing procedure, using the same formwork and pouring the concrete in a similar way. The non-uniform orientation of the fibres should be considered when affected by the aforementioned variety of parameters, above all, when structural requirements are needed. The problem is that as most of such parameters are interlinked, they hinder the analysis. In such a sense, SCC introduces an extra factor due to the influence of the flux on the orientation of fibres and the relation with the casting direction and distance to the pouring position (Stähli, et al., 2008). Subsequently, the flexibility, density and length of the fibres affect their behaviour inside the flux, which is also related with the boundary conditions, casting direction and viscosity of concrete. Consequently, formwork geometries, concrete types and pouring procedures should be chosen in order to make some of the parameters negligible and thus highlight the influence of one of them.

The most commonly followed recommendations that deal with FRC, such as EN 14651 (EN 14651:2007+A1, 2007) and RILEM TC 162-TDF (RILEM TC-162-TDF, 2002), were prepared for use in conventional concrete and in steel fibre reinforced concrete. In these recommendations the moulds should be filled with conventional concrete, pouring it from its centre and with the sides being filled afterwards. After this process the element should be consolidated by means of external vibration. However, when working with SCC, the pouring process is commonly carried out from one of the sides of the mould, though no explicit procedure is stated. At the time of writing there is no published research that has considered the differences in behaviour and distribution of polyolefin fibres along the mould when filled either from one of the sides or the centre. This could be of importance because the casting procedure has been reported to cause significant affections in the properties of FRC (Torrijos, et al., 2010). Moreover, filling the moulds from the centre, as in conventional concrete, may lead to inadequate fracture results due to an unreal concentration of fibres on the fracture surfaces. In addition, the influence of the walls on the orientation of fibres in a hardened concrete element can be assessed by using different sizes of the moulds. Furthermore, the differences in the orientation of the fibres in a VCC and a SCC can also provide relevant information about the influence of the flux and the vibration process in the fibre distribution and orientation.

While research on the influence of such parameters by using laboratory-size specimens is of interest in itself, it is also a way to assess the characteristics of hardened concrete employed in structural elements. In order to fill the gap between in situ applications in real-size elements and the laboratory samples, some concrete elements of greater dimensions were analysed. Consequently, the influence of flux in the orientation of the fibres was evaluated in a beam element manufactured with PFRC. Furthermore, and due to the low density of polyolefin fibres, the vibration process might cause a floating of the fibres studied by comparing the positioning of fibres in standardised samples with vertical concrete elements after being produced.

These issues were analysed in this chapter with a thorough analysis of the positioning, distribution and orientation of 6 kg/m^3 of polyolefin fibres added to a variety of types of concrete. The evaluation was carried out in standard-size samples (600x150x150 mm^3) of vibrated concrete with 60 mm long fibres (VCC6-60). Similarly, this concrete was poured

in moulds of 430x100x100 mm^3, (VCC6-60 Small). In addition, this was assessed in SCC with 60 mm long fibres poured in standardised moulds from one side (SCC6-60S) and in SCC with 48 mm long fibres poured in standardised moulds both from one side (SCC6-48S) and the centre (SCC6-48C). Moreover, elements similar to real applications were evaluated by manufacturing vertical concrete elements of 600x150x450 mm^3 size divided in bottom, half and top standardised samples performed with vibrated concrete with 60 mm long fibres (named VCC6-60D, VCC6-60H and VCC6-60U, respectively). Finally, in a beam element of 2200x250x150 mm^3, where the 50 mm closer to the mould sides were discarded and the remaining element divided into four 550x150x150 mm^3 samples (SCC6-60L1 to SCC6-60L4 elements, with SCC6-60L1 being that closest to the pouring point) was analysed. The beam element was manufactured with-SCC with an addition of 60 mm long fibres. In order to provide more clarity on the variety of analysed specimens, the samples were shown in Figure 8-5.

9.2 Fibre orientation

With the aim of analysing fibre orientation, the same procedure and theoretical background considered in subsection 5.7 and the expressions (5-2), (5-3) and (5-4) were used. If the total length of one single fibre were known, with the same cross-sectional surface, and divided by the length of the beam, the fibres would cross the beam *th* times. If such an optimum fibre distribution took place, the number of fibres resulting from the counting exercise would be equal to *th*. When this value is compared with the number of fibres counted in one particular section (*n*), the denominated coefficient of orientation (θ) could be computed by using expression (3-8). Accordingly, if fibres were perfectly aligned, the number counted would match the theoretical value and, therefore, the ratio θ would be the unity. Consequently, the counting process supplies a value that deals with the orientation of the fibres, as Figure 9-1 shows.

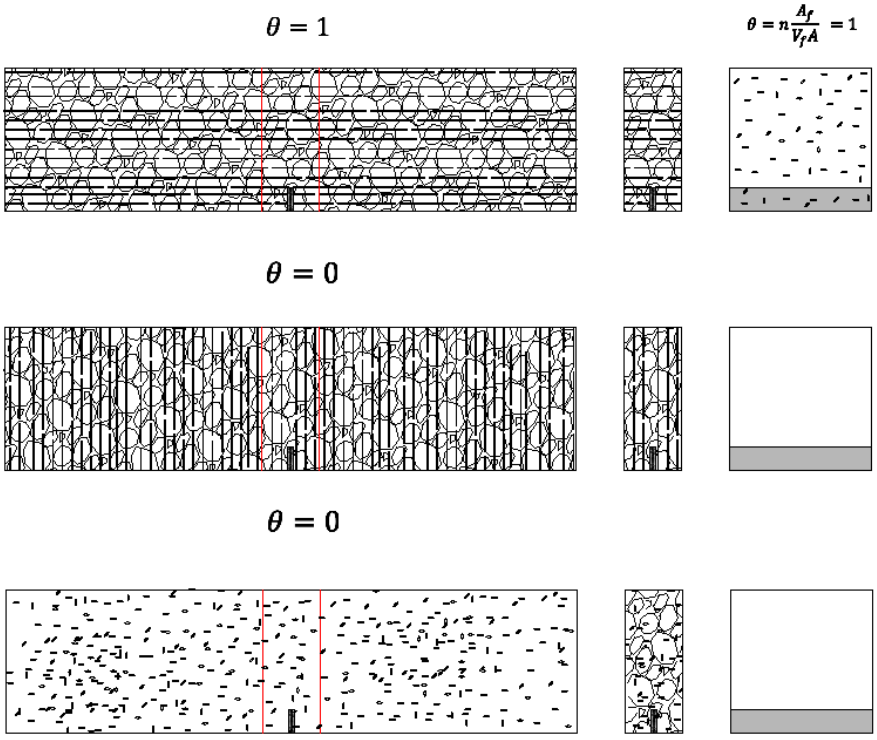

Figure 9-1: Orientation factor θ for different fibre orientations.

The prediction of the orientation factor θ has been assessed for rigid metallic fibres, obtaining values that range from 0.41 to 0.82 (Soroushian & Lee, 1990; Kang, et al., 2011). The emerging of polyolefin fibres has led to evaluation of such a factor for non-rigid fibres. Many factors under question remain after the results obtained in chapters 5 and 6 about the positioning of polyolefin fibres. Therefore, the present chapter provides a wider view about it and Chapter 10 has proposed a verified a model on this matter.

9.3 Fracture surfaces analysis

Previous research has shown that the differences found in fracture results may be explained by counting and locating fibres on the fracture surface of the divided piece (Soroushian, et al., 1990; Barr, et al., 2003; Boulekbache, et al., 2010). Additionally, the assumptions made about the positioning of fibres which may be affected by the variation of the put-in-place conditions can be verified. In conformity with this, and with the aim of studying the variations achieved while changing external conditions, the fracture surfaces of all the specimens tested were analysed. Moreover, Figure 5-7 revealed that it is easy to differentiate which fibres have been broken from those that have been pulled out. In order to obtain accurate results, the pulled-out fibres were added to the broken fibres, obtaining the total number of polyolefin fibres in each fracture surface generated.

A first approach that could provide relevant information involves ascertaining the proportions of broken and pulled-out fibres in all the manufactured concretes (Soroushian, et al., 1990; Barr, et al., 2003). This can be seen in Table 9-1. The first conclusion is that about 60% of the 60 mm long polyolefin fibres added to SCC were clearly broken, and therefore an average value of pulled-out fibres was around 40%. When comparing VCC6-60 and SCC6-60S it can be seen that fresh-state behaviour did not affect the amount of broken fibres. However, if the size of the samples were considered, the smaller the sample the smaller amount of pulled-out fibres. This might have happened as a result of a better orientation of the fibres. When comparing different fibre lengths used with the same type of concrete poured in the same moulds and following the same procedure (SCC6-60S versus SCC6-48S) the influence of the fibre length can be derived. Table 9-1 shows that in the case of 48 mm long fibres, the percentage of pulled-out fibres surpassed 50% while for SCC6-60 this value was lower than 40%. This might have occurred because when reducing fibre length there were fewer fibres embedded with at least the critical length needed to bear the maximum load that a fibre can sustain. However, when Figure 8-13 of the previous chapter is observed, it can be seen that there are only minor differences in the fracture behaviour of SCC6-60S and SCC6-48S, in spite of the different failure pattern of the fibres that bridge the cracks. While the higher amounts of fibres pulled out in the SCC6-48S samples cause an increment of the stiffness of the post-peak loading branch of the curve, they reduce the load bearing capacity of the samples for deflection values over 5.5 mm.

Similarly, there were no significant differences between the samples cut from the elements and those obtained in standard elements with conventional concrete, VCC6-60 in vertical elements and VCC6-60 in samples. Therefore, it would seem that the vibration process tends to affect the orientation of fibres in the same manner.

Conversely, if VCC6-60 small samples were compared with the same formulation of concrete poured in standard moulds, the influence of the sample size and wall effect could be assessed. There were almost 10% more pulled-out fibres in the small samples than in the standard ones. This might imply a better orientation and could be a consequence of the higher importance of the wall effect in the smaller samples.

This analysis can be extended by obtaining the orientation factor θ and its coefficient of variation (c.v.). Concerning the coefficient of variation, it may provide information regarding the homogeneity of the distribution of fibres in concrete elements. Table 9-1 shows the theoretical amount of fibres in each section: 223 fibres in the standardised samples and 99 in the 430x100x100 mm^3 samples. By comparing this theoretical number with the number of fibres counted, a first approach to the orientation factor, θ, can be obtained for all the variations considered.

Table 9-1 also shows the better orientation of the fibres that occurred in the VCC6-60 small samples when compared with the same concrete poured in standardised moulds. On the contrary, when VCC6-60 and SCC6-60 were compared with one another, only minor changes of θ were noticed. When adding the same dosage of fibres to a concrete with two different fibre lengths it was evident that when the shorter fibres were added a higher amount of fibres were included in the concrete. This might be appreciated when comparing SCC6-48S and SCC6-60S. It is also evident that a higher amount of fibres results in a greater value of θ, increasing from 0.50 to 0.65. In addition, the pouring procedure did not seem to have any influence on the amount of fibres that appeared in the fracture surface, as can be derived when contrasting SCC6-48C with SCC6-48S.

The comparison among the standard samples of VCC6-60 and those obtained from the vertical elements, VCC6-60U, VCC6-60H and VCC6-60D showed that the samples obtained from the middle and the upper part of the vertical element had similar θ values to the standard VCC6-60 samples. However, the samples from the bottom part of the vertical elements showed a better orientation factor than the standard samples.

When the elements from the long beam were studied, it became evident that the values obtained were slightly above those that occurred in the standard samples. One reason for this is because the sides of the beam element were cut to avoid taking into account the wall effect of the formwork. Therefore, the orientation of the fibres analysed was only affected by the bottom face of the mould and not by the sides of the mould. However, due to the limited data available from these results, this could not be considered a sound conclusion until more slides are counted and presented.

Hence, this enables an insight into the distribution and orientation of the fibres and provides the possibility to establish the connection between the fracture tests results shown in Chapter 8. That is to say, residual load-bearing capacity has to be related with the presence of fibres in the fracture surfaces. Given the brittle nature of concrete, it has negligible post-cracking residual strength and, as a result, the residual load-bearing capacity has to be caused by the existence of fibres on the fracture surfaces. As a consequence, post-cracking behaviour is closely associated with the number of fibres placed on the cracked surfaces. In such a way, the first approach to analyse fracture results entailed a counting exercise on the fracture surfaces. Other studies have suggested that the number of fibres has an influence on the fracture behaviour and that there is a strong dependence of the positioning of the fibres (Grünewald, et al., 2012; Lamanna & Scholer, 2002; Zerbino, et al., 2012).

Table 9-1: Analysis of the fracture surfaces.

	Concrete type	Surfaces	Fibre length	# theoretical	%Fibres pulled out	# average total	c.v. (%)	θ
	Number of fibres on the fracture surface							
Standard series	VCC6-60	4	60	223	37.5%	128	2.4%	0.57
	VCC6-60 Small	6	60	99	28.6%	73	6.8%	0.74
	SCC6-60S	4	60	223	38.0%	112	14.1%	0.50
	SCC6-48C	4	48	223	54.4%	142	3.5%	0.64
	SCC6-48S	4	48	223	52.1%	145	10.8%	0.65
Vertical elements	VCC6-60U	8	60	223	41.9%	129	7.4%	0.58
	VCC6-60H	8	60	223	43.8%	115	8.7%	0.51
	VCC6-60D	8	60	223	41.5%	144	12.3%	0.65
Long element	SCC6-60L1	2	60	223	43.5%	120	1.8%	0.54
	SCC6-60L2	2	60	223	46.3%	136	1.0%	0.61
	SCC6-60L3	2	60	223	45.7%	127	2.2%	0.57
	SCC6-60L4	2	60	223	41.4%	133	1.1%	0.60

Accordingly, with the aim of performing a deeper analysis, the fibre counting process was also carried out on the basis of RILEM TC 162-TDF (Barr, et al., 2003). In such a way, the counting process was performed by dividing the sample cross section in sectors so that any wall effects or non-homogenous distribution of fibres could be observed. Consequently, the broken surfaces of the beams were divided into nine equal areas in addition to the notch. In such a way, the dispersion of the fibres inside the fracture surface could be observed. A uniform distribution of fibres on the total surface would imply that the amount of fibres is proportional to the surface of the sector. The notched area was 16.7% of the total surface and the remaining nine sectors were equal with each one being 9.3%. The reference positioning of the figures in this section was rotated 90º in order to place the fracture surface in the relative position during the test (see also Figure 8-6. This leaves the free surface on the left of the scheme. The outline of this procedure is summarised in Figure 9-2(a) in contrast with Figure 9-2(b), showing the uniform distribution in a whole cut surface which is also used later. Figure 9-2(a) shows the abovementioned rotation of the samples prepared to perform the fracture tests.

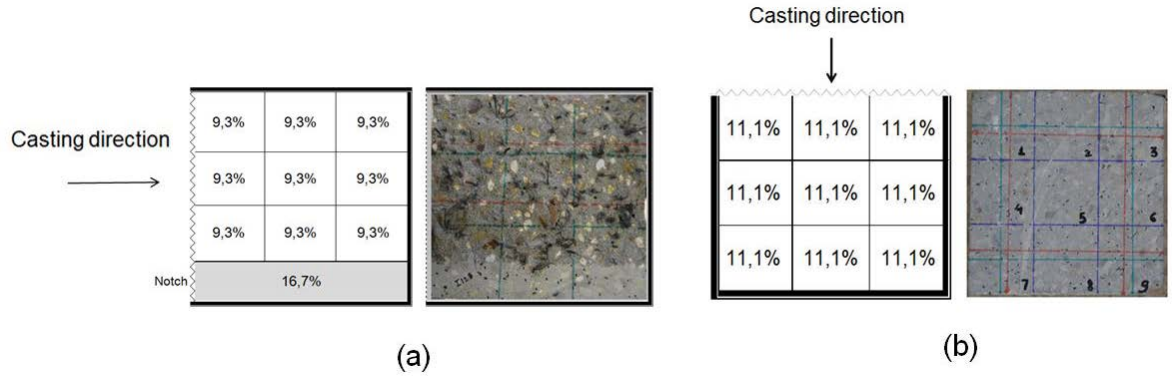

Figure 9-2: Uniform theoretical distribution of fibres: (a) in a notched standardised sample fracture surface; (b) in a complete sawn surface. The blue lines of the right image divide the concrete section in nine parts.

In Figure 9-3, Figure 9-4, Figure 9-5 and Figure 9-6 the results of the counting exercise made by sectors are placed in terms of average proportional distribution. This allows a comparison with the uniform distribution previously shown in Figure 9-2. The result in absolute numbers is placed in the Appendix A, as well as all the counting results.

If Figure 9-3, Figure 9-4 and Figure 9-5 are observed, some differences in the distribution of the fibres inside the fracture surface should be noted. On the one hand, for all the standard-size samples the amount of fibres in the notch is above the value obtained with a uniform distribution of fibres. This happened even for the SCC6-60L1-L4 samples, shown in Figure 9-5, which were not influenced by the presence of the two walls of the moulds. On the other hand, when smaller samples were used, with the VCC6-60 small samples, there were fewer fibres in the area of the notch.

When observing SCC6-48C in Figure 9-3, it could be seen that in the fracture section of the samples filled from the centre, most of the fibres were placed in the bottom of the surface (the right column in the sketches). This was not observed for the specimens cast from the side in which there was a reduction of the number of fibres positioned on the central sectors. This could be explained by the aforementioned increasing wall effect due to the fresh-state flux of SCC when moving from one side of the mould to the other. The specimens vibrated: VCC6-60 seemed to have a floating effect as the result shows in the left column that corresponds to the free surface had higher values. No wall effects were

noticeable, rather a more uniform distribution among sectors. SCC6-60S specimens also showed more evident wall effects instead of the possible floating that can be seen if VCC6-60 distribution is observed. Therefore, the results obtained for both types of SCC, when the standardised moulds were used, were alike in spite of the two lengths of fibres used.

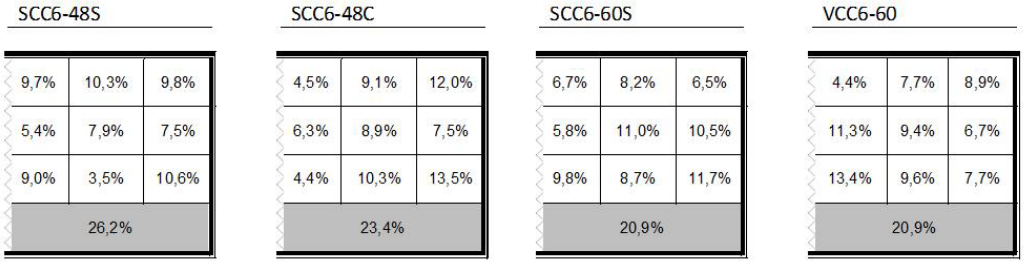

Figure 9-3: Average distribution of fibres in the fracture surfaces of SCC6-48S, SCC6-48C, SCC6-60S and VCC6-60.

Figure 9-4 shows that for the smaller beams of VCC6-60 the uniform distribution would mean 7.4% of the fibres in each sector of the fracture surface. This is caused because the depth of the notch is 33% of the total surface. If sectors placed on the upper third of the section are observed, the rising of the wall effects can be noted when compared with the standard VCC6-60 placed on Figure 9-3. In the percentage of fibres placed on the notch, it should be clarified that the wall effect was attenuated because the size of the notch was one third of the section for the small beams instead of one sixth.

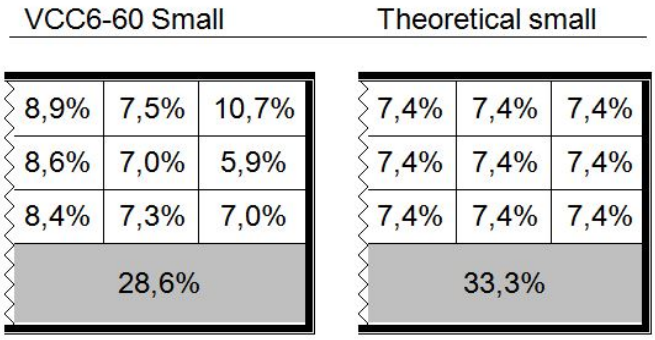

Figure 9-4: Average distribution of fibres in 100x100x430 mm^3 samples filled with VCC6-60.

In the case of the long beam (specimens L1, L2, L3 and L4), as Figure 9-5 shows, no tendencies were easily observed since only one specimen of each one was tested and counted. However, the positioning of the fibres along the beam will be analysed in the following sections.

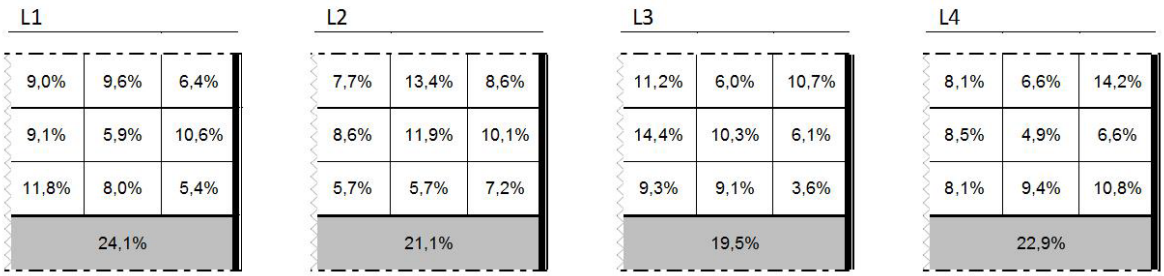

Figure 9-5: Average distribution of fibres in samples SCC6-60L1-L4.

As regards the vertical elements shown in Figure 9-6, D the sample fracture surfaces showed a quite uniform distribution. This might provide a hint of the limited floating effect of the fibres inside the vertical elements despite the vibration carried out after casting. Samples H and U did not register similar distributions of fibres, although no clear tendencies could be derived.

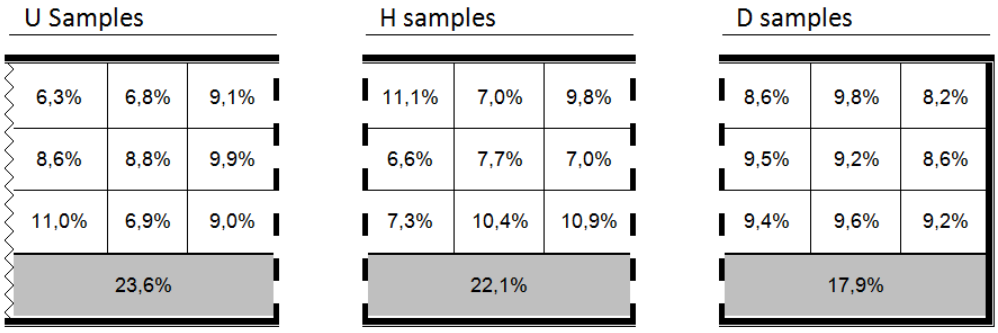

Figure 9-6: Average distribution of fibres in samples VCC60 elements.

In spite of all the data acquired in the counting process of the fracture surfaces, there were no evident effects of the differences induced by the effect of the flow of SCC or the vibration of VCC in the distribution of fibres within the nine sectors of the ligament area. However, if the nine equal sectors are taken into account, the homogeneity of the distribution of fibres can be evaluated by comparing the coefficient of variation of the number of fibres placed in each sector. In such a way it would become a coefficient of distribution of the fibres (c.d.). The lower the latter, the more uniform is the distribution. As Table 9-2 shows, the samples prepared with VCC registered, in almost all the cases, a more homogeneous distribution of fibres with respect to any of the formulations or pouring methods used. This is coherent with the aim of using a PF-SCC where the flux of the concrete is expected to distribute the fibres in layers with different locations.

Table 9-2: Coefficient of distribution of the fibres inside the fracture surfaces.

Concrete	Coefficient of distribution of the fibres in the cross section
VCC6-60	0.334
VCC6-60 Small	0.175
SCC6-60S	0.280
SCC6- 48C	0.356
SCC6- 48S	0.304
VCC6-60U	0.192
VCC6-60H	0.184
VCC6-60D	0.087
SCC6-60L1	0.314
SCC6-60L2	0.283
SCC6-60L3	0.373
SCC6-60L4	0.322

To correlate the post-peak behaviour of all the types of combinations tested with the counting process performed in the fracture surfaces, the total amount of fibres were divided in the three thirds of the ligament area, as explained in subsection 5.7 and Figure 5-7. When

the initial cracking is taking place, only the fibres placed in the lower part of the section are active. During the advance of the cracking process more fibres could be considered to be bridging the crack. In this regard, when the crack expands enough most of the fibres can be considered activated. This justified dividing the counting also in thirds, in order to correlate appropriately the residual loads with the active fibres in each crack in an opening or deformation state.

The most important parameters that determine the behaviour of the concrete after reaching L_{LOP} are the minimum load for small deflection values, $L_{MIN,}$ and the maximum load after L_{MIN}, which is usually termed as L_{REM}. These names have been previously used in Chapter 8 where their values may be checked. If it is considered that the influence of the fibres in the upper two thirds of the ligament is negligible, a linear experimental correlation between the number of fibres and the value of L_{MIN} can be obtained. This can be seen in Figure 9-7(a) where only the average values of L_{MIN} of each the samples of each type of combination is used.

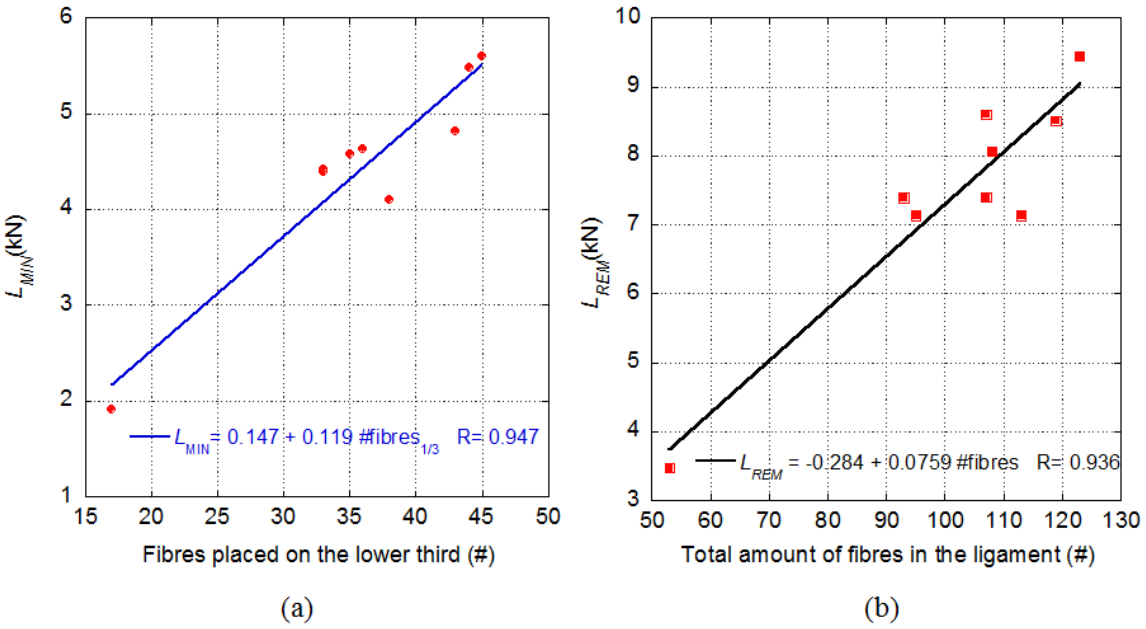

Figure 9-7: (a) Relation between f_{MIN} and the number of fibres in the lower third of the ligament area;(b) relation between f_{REM} and the total amount of fibres in the ligament area.

In such a way, L_{MIN} should be linked with the number of fibres that act in the initial cracks and, therefore, with the number of fibres placed in the lower third of the fracture surface. The experimental relation found can be also seen in Figure 9-7. The high correlation between the experimental results, no matter which fresh-state properties, pouring procedure or mould shape or size were used, is noticeable. This might be a consequence of the position of the notch in the concrete elements.

Regarding L_{REM}, it has been considered that when the sample reaches these deflection values all the fibres in the section bear a portion of the total load that the sample is supporting and, therefore, a correlation between the total amount of fibres in the section and L_{REM} has been performed. This can be seen in Figure 9-7(b) where the equation that relates the values is included.

These two experimental equations can serve as an approximation value of L_{MIN} and L_{REM} for every type of PFRC with 6 kg/m^3 of polyolefin fibres addition in both SCC and VCC. This was carried out by means of a counting process of the elements manufactured, which

is examined in the next section. Although these relations can be of great interest for structural design purposes, a further and deeper analysis can be performed. In any event, it should be noted that the linear fittings were also made in the case of steel fibres in previous studies (Zerbino, et al., 2012; Švec, et al., 2014; Di Prisco, et al., 2013; Barros, et al., 2005).

9.4 Cut surfaces: orientation factor affected by frameworks and concrete type

Analysis of the disposition of the fibres in concrete has been performed over the last decades (Stähli, et al., 2008; Soroushian & Lee, 1990; Dupont & Vandewalle, 2005; Laranjeira, et al., 2011; Barr, et al., 2003). As discussed in subsection 3.6, most of the research published has examined fibres made from steel. The disposition of the steel fibres has been studied by means of a wide variety of methods, such as visual inspection even in full-scale beams (Di Prisco, et al., 2013), electromagnetic methods, X-ray radiography and CT-scan (Robins, et al., 2003; Trainor, et al., 2013), among others. However, some of those methods are based on the magnetic properties of the materials and, consequently, cannot be applied when the fibres added are polymeric-based materials. Some published research has evaluated the positioning of polyolefin fibres by means of a CT-scan or X-rays (Kaufmann, et al., 2013). However, such studies have been performed in limited portions of PFRC with only one type of concrete in each study used. Due to the high cost of performing a CT-scan inspection of all the samples tested in this study, one that incurred lower costs and provided optimum results option was chosen.

After performing the fracture tests and analysing the fracture surfaces, each half of the samples was divided into five portions, as Figure 9-8 shows. The width of the portions was 60 mm in all the 600 mm long samples and 55 mm in the 550 mm long samples cut from the beam element. The amount of fibres in each surface was assessed by counting. This process provided information of the positioning of the fibres in the standardised size samples. Moreover, by processing the results of the samples obtained in the vertical and long elements, the disposition of the fibres in these real-size concrete pieces could be obtained.

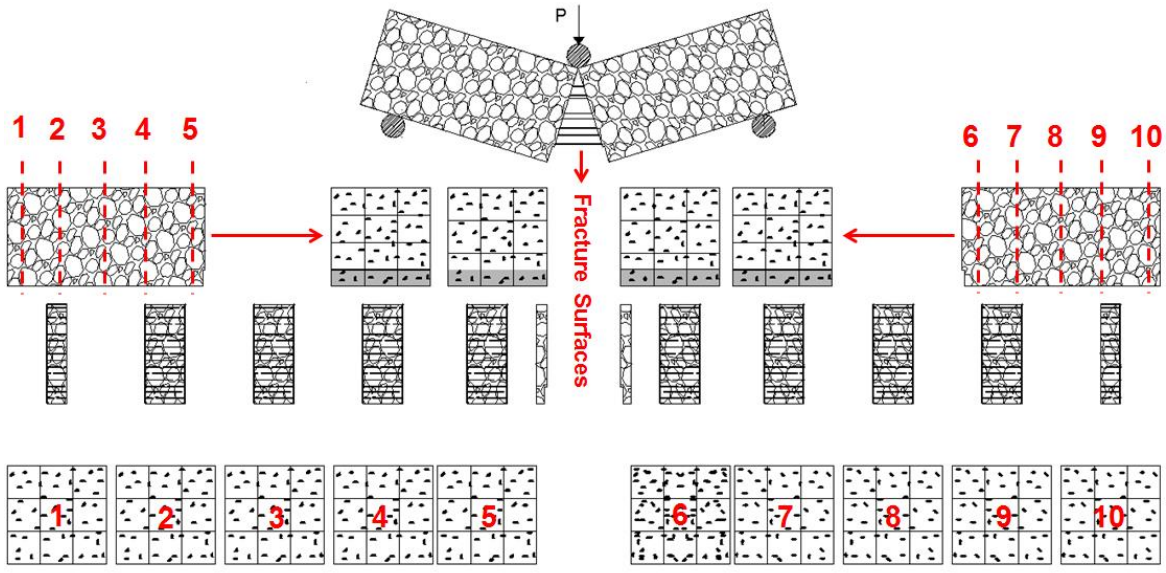

Figure 9-8: Portioning of the samples.

In order to address the problem, Table 9-3 uses data obtained from the counting process of all the sections. It summarises the positioning of the fibres along the main axis of the samples in the hardened concrete and widens the conclusions obtained if only the fracture surfaces is analysed. It should be highlighted that the values remained similar to those obtained for the fracture surfaces shown in Table 9-1. The small scatter with coefficients of variation around 15% in most of the cuts is also noticeable. This coefficient was obtained by comparing the theoretical amount of fibres in each section (# *th* cut) with the average value of the fibres counted in the cut section (#average cut).

After counting the sections, the orientation factor was obtained in accordance with that previously explained in expression (3-8). In addition to the orientation factor of the sections, $\theta section$, an average orientation factor of the samples was obtained, $\theta sample$. Table 9-3 shows that the sections of SCC6- 48C or SCC6-48S registered a value of θ *section* above the rest of the samples. This effect might have been caused by the greater amount of fibres added when the 48 mm long fibre was used. This increment of θ *section* is because the formulation of θ does not take into account the physical characteristics of the fibres, such as fibre length or equivalent diameter, and only considers the theoretical content of fibres. In the rest of the formulations similar values were obtained, ranging from 0.51 to 0.64. It should also be noted that the highest values were obtained for VCC6-60D samples and SCC6-60L3. In the case of VCC6-60D, this value might have been caused by the influence of the three walls of the mould. However, it should be pointed out that such a value of the orientation factor in the SCC6-60L3 samples was obtained by removing the sides of the beam element and, therefore, the influence of only one wall of the mould. Consequently, this remarkable value of θ *section* might be the result of the flux of the SCC.

When comparing the θ *section* values of SCC6-60S and the SCC6-60L1-L4, the influence of the flux of the SCC can be evaluated. The lower values of the SCC6-60S θ *section* value when compared with the SCC6-60L1-L4 values suggest that the limited length of the sample restrains the flux of concrete and, therefore, the change of orientation in the fibres. This effect can be also assessed in the final portions of the beam elements SCC6-60L1 and SCC6-60L4, where the lowest values of θ *section* inside the beam element were obtained.

The details of the experimental procedure performed that should not be overlooked were evaluated by calculating the θ *sample*. Such a value was computed by adding the partial counts of all the sections cut and dividing it by the theoretical number of fibres inside the sample in volume (th_{sample}). That is why for th_{sample} (as Table 9-3 shows) there should be more theoretical number fibres when shorter fibres where used. Moreover, it should be noted that in those samples where the width of the portions cut and the length of the fibres coincided with the values of θ *section* and θ *sample* were equal. However, θ *section* and θ *sample* of SCC6-48S and SCC6-48C are different, with θ *sample* being lower than θ *section*. This is because the width of the portions was 60 mm and more fibres were not counted as they did not appear in the surface of the portions and remained inside the portion. When the cuts were made at a distance smaller than the fibre length, some fibres were counted in two surfaces and the value of θ *sample* was higher than θ *section.* This was the case of the samples obtained from the beam element (from SCC6-60L1 to SCC6-60L4) that were cut into 55 mm thick slices.

In order to obtain an even more detailed evaluation of the positioning of the fibres, all the surfaces processed to obtain Table 9-3 were divided in nine sectors. A uniform distribution of fibres would lead to a proportional distribution of 11.1% of the fibres placed in each of the nine sectors, as Figure 9-2(b) shows. It should be noted that for this counting and also for the figures, casting direction is from top to bottom, leaving the free surface in the upper

side of the picture or figure. Due to the amount of data acquired in the whole process, the detailed results are placed in Appendix B and the average values shown in this section.

9.5 Orientation maps

Figure 9-9 shows the average results obtained for the cut surfaces of the samples made with SCC6-60S. In the top right part the average orientation factor of the samples, one line per sample, along the main dimension can be seen. The flux has been sketched in this plot with an arrow in the flux direction. According to the plot the orientation factor remains quite stable along the beam, although the pouring location was at one the sides of the mould. It is also important to highlight that at the pouring point the lowest values of the orientation factor were registered for the two samples. In the middle right picture of Figure 9-9, a sketch of the front view of a sample with the variation of the orientation factor along it can be seen. There are no values in the proximity of the walls of the mould because the data has been gathered and analysed as a uniform distribution of fibres placed in each sector of every portion of concrete. In addition, the data shown in the front view of the sample is the average of the orientation factor at every point studied, taking into account all the depth of the sample. Similarly, in the top view of the sample every point of the map has been obtained as the average orientation factor of all the height of the sample. The cross section shows the average value of the orientation factor across the length of the sample. The front view, top view, and the top cross section have been performed by taking as the extreme values of the orientation factor in the colour scale 0 and 1 which enables a direct comparison among all the parameters studied (including concrete type). In addition, the bottom cross section was performed by considering, as the extremes of the scale, the highest and lowest values of the orientation factor within the sample. This detects tendencies within the formulation studied. Furthermore, the distribution of fibres in terms of percentage of the total amount of fibres can be seen in the bottom left part of the Figure.

The front view of the average of the orientation factor of SCC6-60S shown in Figure 9-9 presents a quasi-homogeneous distribution. The central bottom part of the sample concentrated the best orientation of the fibres, while the left and right sides registered the worst orientation. This is consistent with the limited effect of the flux at the pouring point and the reflux of the concrete towards the centre of the sample after reaching the wall of the mould.

The top view shows a higher value of the orientation factor in the last part of the samples. This might also be a consequence of the reflux of concrete. When the cross section is analysed, it may be perceived that it is quite constant, with all the values being between 0.45 and 0.59. However, the highest values confirm the aforementioned wall effect. The distribution of fibres is nearly homogeneous within the section, though it displays higher amounts of fibres in the regions near the walls of the moulds.

Table 9-3: Number of fibres on the cut surfaces and the complete samples.

	Concrete type	Name	Surfaces	Fibre length	# th section	# average cut	c.v.	# th sample	# average sample	θ section	θ sample
Single series	VCC6-60	FC6-60	20	60	223	131	0.14	2232	1314	0.59	0.59
	SCC6-60S	SCC6-60	20	60	223	115	0.17	2232	1146	0.51	0.51
	SCC6-48C	SCC48	20	48	223	145	0.12	2790	1450	0.65	0.52
	SCC6-48S	SCC48	20	48	223	164	0.16	2790	1635	0.73	0.59
Vertical elements	VCC6-60U	U	40	60	223	133	0.13	2232	1329	0.60	0.60
	VCC6-60H	H	40	60	223	131	0.16	2232	1314	0.59	0.59
	VCC6-60D	D	40	60	223	143	0.14	2232	1428	0.64	0.64
	VCC6-60	Vertical element	120	60	223	136	0.15	6695	4072	0.61	0.61
Long element	SCC6-60L1	L1	10	60	223	119	0.28	2046	1190	0.53	0.58
	SCC6-60L2	L2	10	60	223	134	0.08	2046	1343	0.60	0.66
	SCC6-60L3	L3	10	60	223	143	0.14	2046	1433	0.64	0.70
	SCC6-60L4	L4	10	60	223	119	0.23	2046	1188	0.53	0.58
	SCC6	Long element	40	60	223	129	0.25	8183	5154	0.58	0.63

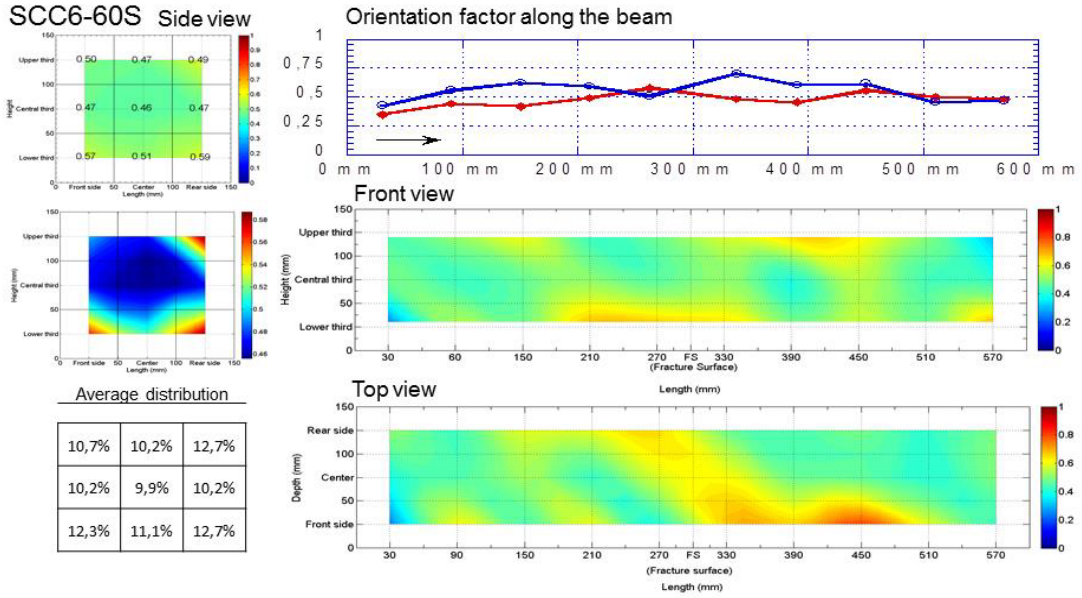

Figure 9-9: Summary of the orientation factor in SCC6-60S samples.

Figure 9-10 contains the results for VCC6-60 specimens which revealed higher values of the orientation factor in the vibrated concrete with the same dosage of fibres. Scatter along the beam was also small and the orientation factor also increased in the areas close to the corners, probably due to the existence of two boundaries. The central sector remained at a below-par percentage value of 10%. The lower third of the cross section also had more fibres counted. In all events, the vibration compaction procedure showed an increment of the orientation factor in the cut surfaces for the 60 mm long polyolefin fibres as compared with the results obtained for SCC6-60S. Since the upper third of the cross section had the lowest values, no floating effect could be clearly observed in the average distribution.

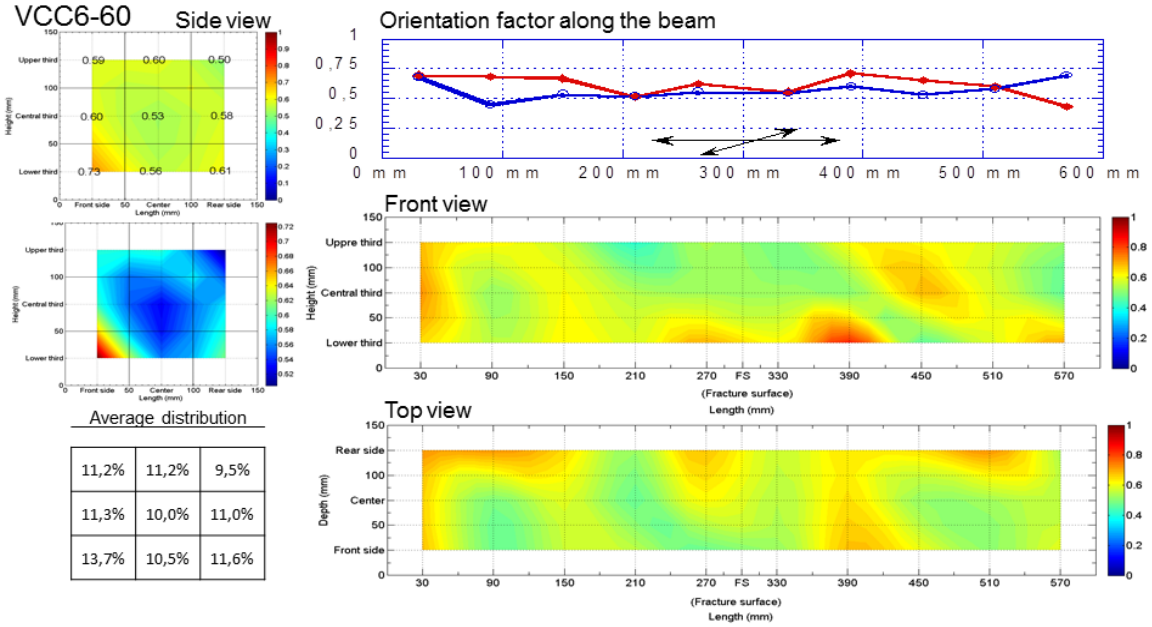

Figure 9-10: Summary of the orientation factor in VCC6-60 samples.

If Figure 9-11 is observed, a remarkable increment of the orientation factor when compared with SCC6-60S may be seen. The absence of almost any scatter between the orientation factors registered is also consistent with the similarity of the fracture results obtained in the fracture tests shown in Chapter 8. By observing both the front view and the top view, it is easy to locate a clear concentration of fibres in the whereabouts of the pouring point. The fibres were better oriented in the central sections from the bottom of the sample up to almost the top. It seems that many fibres stayed close to that position and the flux carried some fibres to the sides and flowed to the lower parts of the mould. This effect left more fibres in the centre, near to the fracture surface position and in the lower part of the beam. It should be noted that as there are more fibres in these areas, close to the fracture surfaces, this filling procedure might lead to higher fracture results. It can also be observed that the fibres tend to reach the sides of the moulds quite uniformly in the rest of the beam. When the orientation factor of the cross section is analysed, it can be seen that the orientation factor along the length is clearly influenced by the presence of the walls with the highest values being near to them. The distribution of fibres is consistent with this observation and gathers the highest amounts of fibres in the lowest two thirds of the sections. This distribution of fibres is consistent with the better fracture behaviour of these samples with respect to the SCC6-48S.

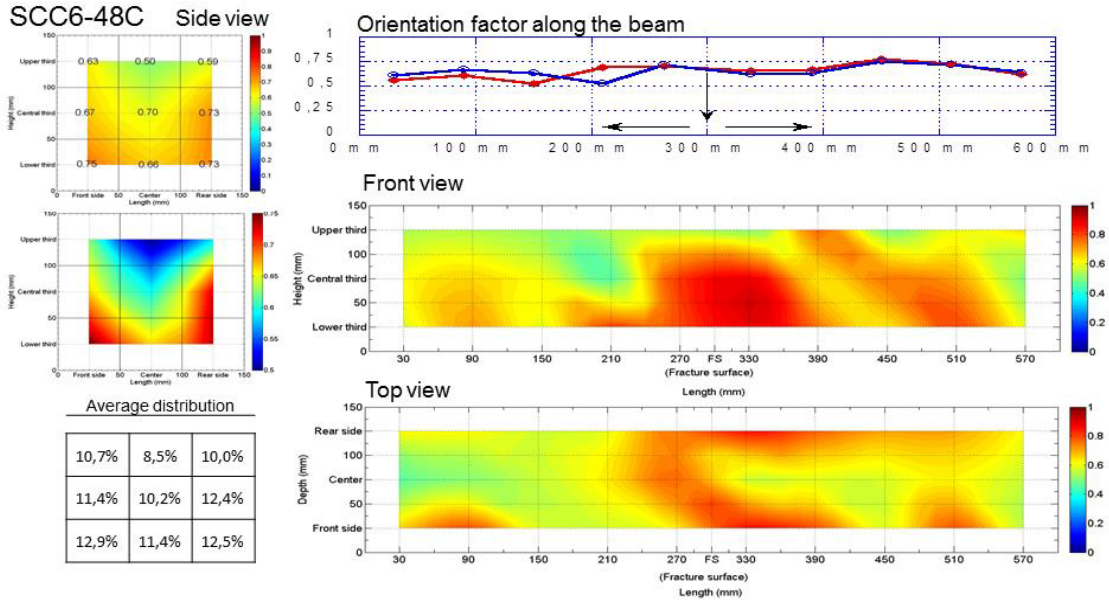

Figure 9-11: Summary of the orientation factor in SCC6-48C samples.

When the moulds were filled from one side to other by using 48 mm long fibres, SCC6-48S, the orientation factor was higher and more regular along the specimen with respect to the values of SCC6-60S or VCC6-60, with it being above 0.70 in most of the beam. This was expected, as explained above. The orientation of fibres also improved with respect to SCC6-48C. This can be seen by comparing Figure 9-11 with Figure 9-12. It is clear that SCC6-48S had more scatter than SCC48-60C. In accordance with this, the fracture behaviour shown in Chapter 8 registered more scatter, although within the normal experimental range. It is also remarkable that there was a high improvement of the orientation factor in the areas near the pouring point of the concrete, both in the front and top view, as happened in SCC6-48C. The lowest values of orientation factor were obtained for the central sectors, though they were still remarkably high values. According to this, the flux enabled the fibres to reach the end of the beam with high orientation factor values.

Only at the very beginning of the beam, a visible low value can be noticed. This area was probably behind the pouring point of the SCC and was finally filled. The front view placed in the figure shows the preferential positioning of the fibres in red. The fibres both reached the end of the beam and also became aligned with the direction of the flux. The improved preferential orientation due to the walls of the mould can also be observed in the bottom of the front view and the sides of the top view.

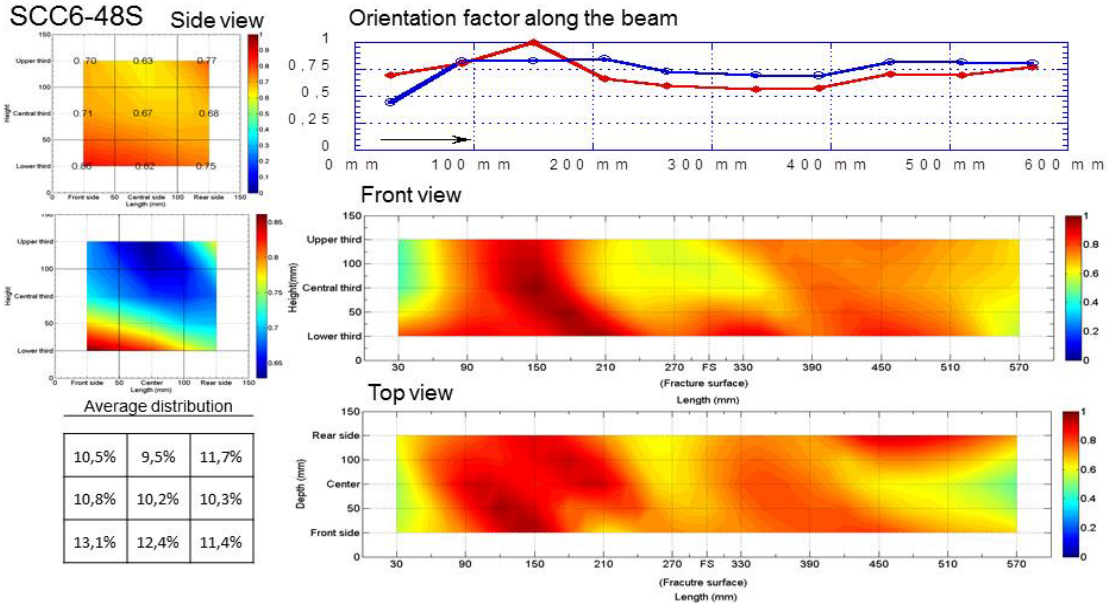

Figure 9-12: Summary of the orientation factor in SCC6-48S samples.

Figure 9-13 shows the orientation factor of the average of the four specimens of the same relative position. The scatter was small among them (U, H and D). In addition, there were no changes in tendency in the disposition of the fibres in the length of the samples along their main dimension which confirms that shown in Figure 9-10.

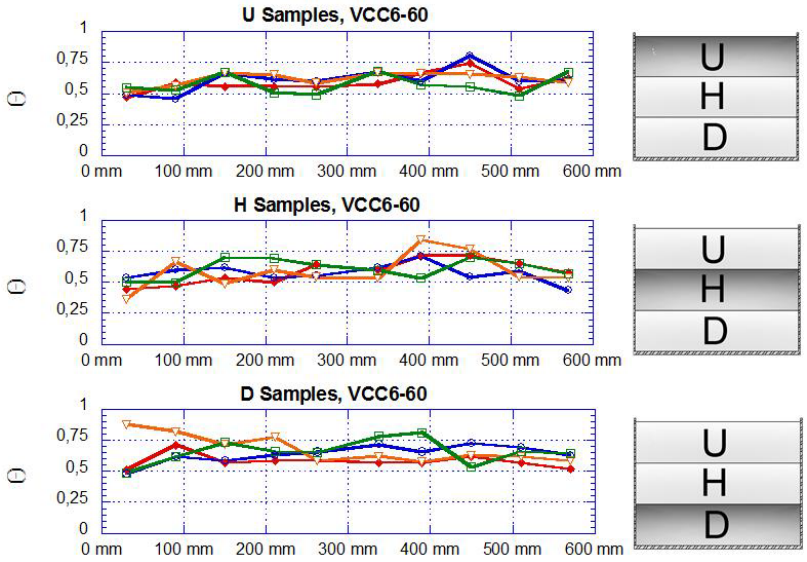

Figure 9-13: Orientation factor along the beams: (a) U specimens; (b) H specimens ; (c) D specimens.

Regarding the possible floating of the fibres caused by the consolidation process, the orientation factor in the three samples obtained by cutting the vertical elements was evaluated. The results of the four vertical elements are included in Figure 9-16. While the central portions of the samples located away from the sides of the moulds showed an almost negligible scatter, this value increased near the mould walls (possibly due to the boundary conditions). As Figure 9-14 highlights only slight differences in the orientation factor values within the same concrete element, it seems that there has been no displacement of the fibres towards the free surface. A further and deeper analysis was performed to confirm this tendency.

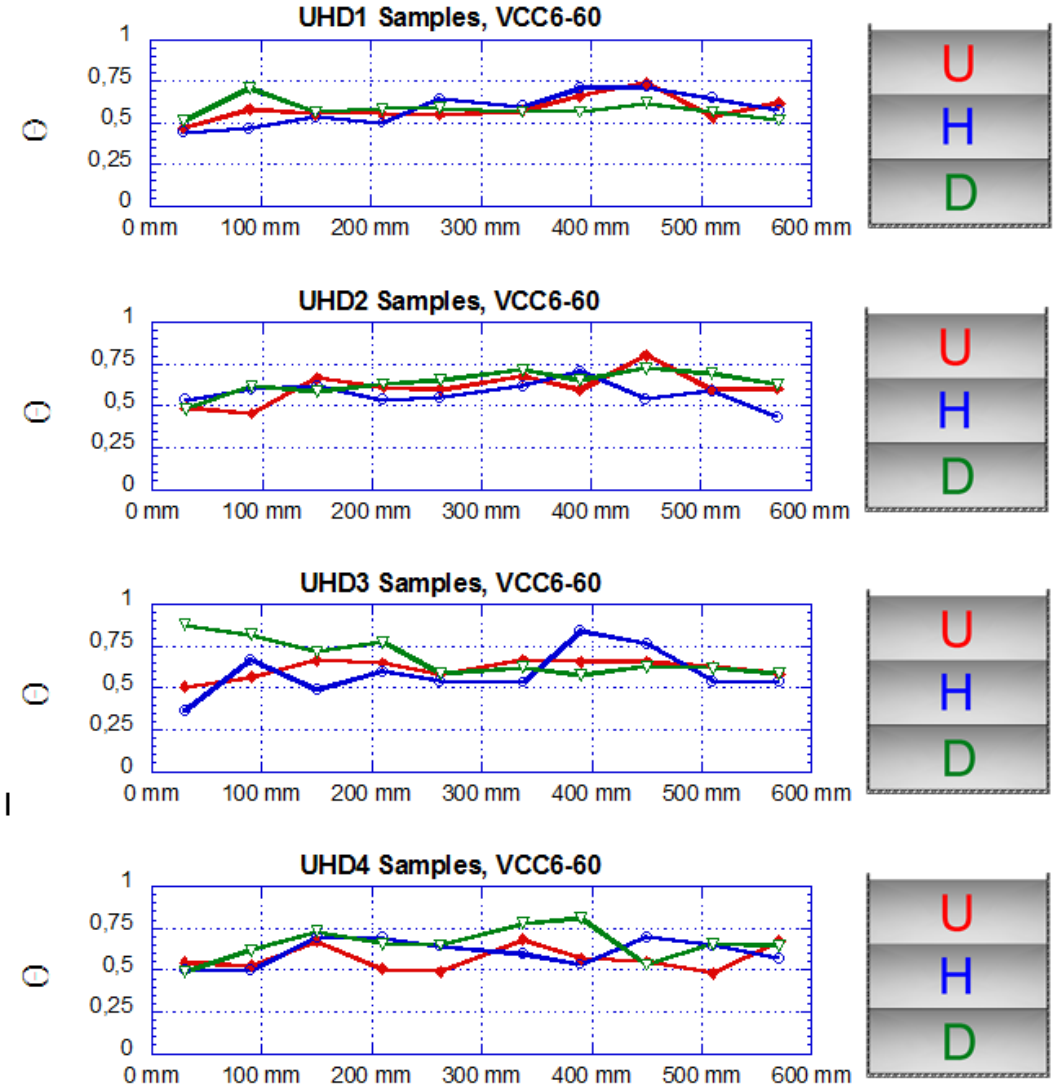

Figure 9-14: Evolution of the orientation factor in height in the tall concrete elements.

The orientation factors for each of the nine sectors, three of each sample were drawn in Figure 9-15. Each point of each vertical element is the average orientation factor of the element for that height according to Equations 9-1, 9-2 and 9-3. Figure 9-15 shows, by a black and dashed line, the average value of around 0.6 which is similar to those obtained in SCC with steel fibres. In addition, the orientation factor is quite stable within the height of the concrete element and, consequently, the floatation of the fibres can be discarded. It is also remarkable that near the bottom of the mould all the values of the orientation factor are close or above the average. This justifies the better behaviour of these samples in the fracture surfaces.

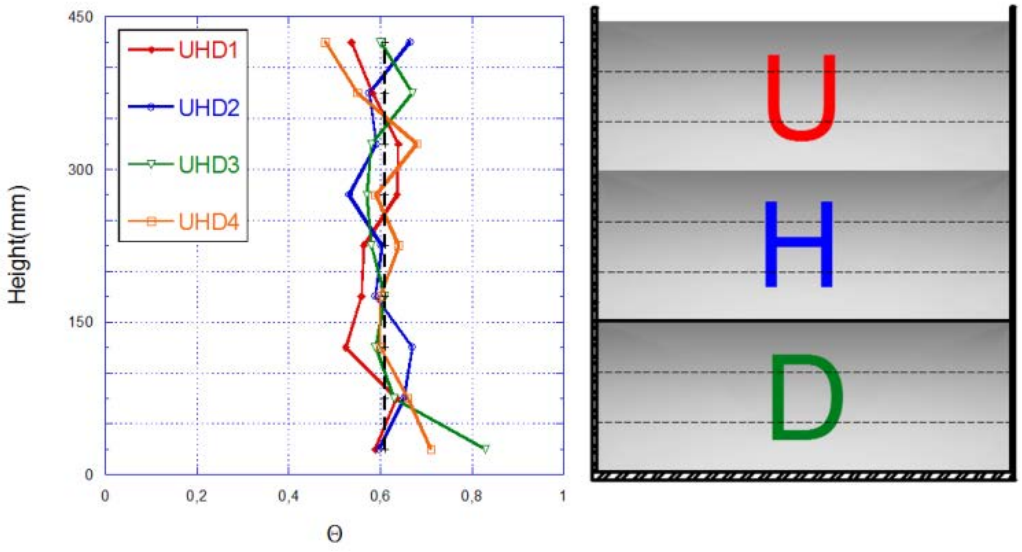

Figure 9-15: Average value of the orientation factor in height for the four vertical elements.

Figure 9-16 offers a panoramic view of the distribution of fibres and the variation of the orientation factor in the vertical elements. Similarly to Figure 9-9, Figure 9-10, Figure 9-11 and Figure 9-12, Figure 9-16 shows the average values of the orientation factor processed in the four concrete elements in top and front view and also in its cross section both in relative and absolute scale. In addition, the distribution of fibres within the three samples obtained can be seen in the right part. The top view shows that the orientation factor of the vertical element has been quite uniform along the main direction of the element. There are only slight changes at both extremes of the element and in one zone near to 450 mm. The front view of the vertical element is of remarkable interest, as it determines if there is any floatation of the fibres. According to this, it is clear that no vertical displacement of the fibres have occurred. There are greater concentrations of fibres in the lower part of the tall element and in the upper half of the element. If any floatation had taken place the distribution of fibres would be higher as the height increases and as it was observed that this phenomenon did not happen. This tendency can be more distinguishable in the cross section where the distribution of the orientation factor in the vertical element clearly displays a higher concentration of fibres, and therefore a higher orientation factor, in the lower half of the bottom sample cut from the mould. Above this zone there is a more uniform distribution of the orientation factor with subtle increments in the proximity of the walls of the mould. The increment of the orientation factor in the D samples is the main reason that justifies the better behaviour of the D samples in the fracture tests when compared with the H and U ones. The existence of corners with two boundary conditions may have caused this increment.

A similar analysis was performed in the samples obtained from the long horizontal element. However, it should be noted that as the sides of the beam element were removed, there was no influence of the lateral walls of the mould on the distribution of fibres. If the orientation factor along the beam element is evaluated, as Figure 9-17 shows, it is clear that at the beginning and at the end of the element the orientation of the fibres is worse than in the rest. This effect could be attributed to the reflux of the concrete when reaching the end of the mould and to the absence of flux in the proximity of the pouring point. Apart from these two areas, the orientation factor is quite stable and in most cases close to 0.6 which is similar to the experimental values obtained for SCC with a steel fibres addition (Laranjeira, et al., 2011). Furthermore, it is important to highlight that the positioning of the fibres

within the element was only influenced by the bottom wall of the mould. It should be emphasised that the central beams, L2 and L3, reached improved orientation factors even with only one wall at the bottom. The improvements achieved began at the first quarter of L1 and ended at the last quarter of L4, which supposes an improvement of around two meters. Therefore, once the flux developed, it helped the fibre to align with it for such a notable distance and reached values of orientation above 0.65.

If the cross section shown in Figure 9-17 is analysed, it is noticeable that it has more fibres in the lower third. It can be seen that the orientation factor in the lower third of the section reaches values up to 0.74. This value is a clear sign of the preferential orientation that the flux develops in the concrete element. In addition, in the rest of the element it seems that the orientation of the fibres is quite homogeneous.

Moreover, two aspects should not be overlooked. On the one hand, the orientation factor of these areas is slightly superior to 0.5 which is the one predicted for isotropic areas and in the other hand the areas near the free surface of the element do not show an increment with respect to the isotropic areas (Dupont, et al., 2005).

The top view of the orientation factor shows a remarkably homogeneous distribution of fibres at the same depth, although there were variations along the length. However, it can be seen how the greater values of the orientation factor gather in the central third of the concrete element. Conversely, in the front view it can be clearly observed that the fibre distribution in height was not uniform and that there was a higher value of the orientation factor in the lower surface of the end of L2 and in the middle of L3. It should also be mentioned that the influence of the bottom wall of the mould was clearly noticeable in great parts of the beam if the front view is considered. This tendency confirmed the analysis of the cross section of the beam where the greatest values of the orientation factor were located in the lower third, with the lowest values being at the upper third. Moreover, if the average distribution of fibres along the beam is considered, it is clear that there is a greater amount of fibres in the lower third than in the middle or upper third of the section

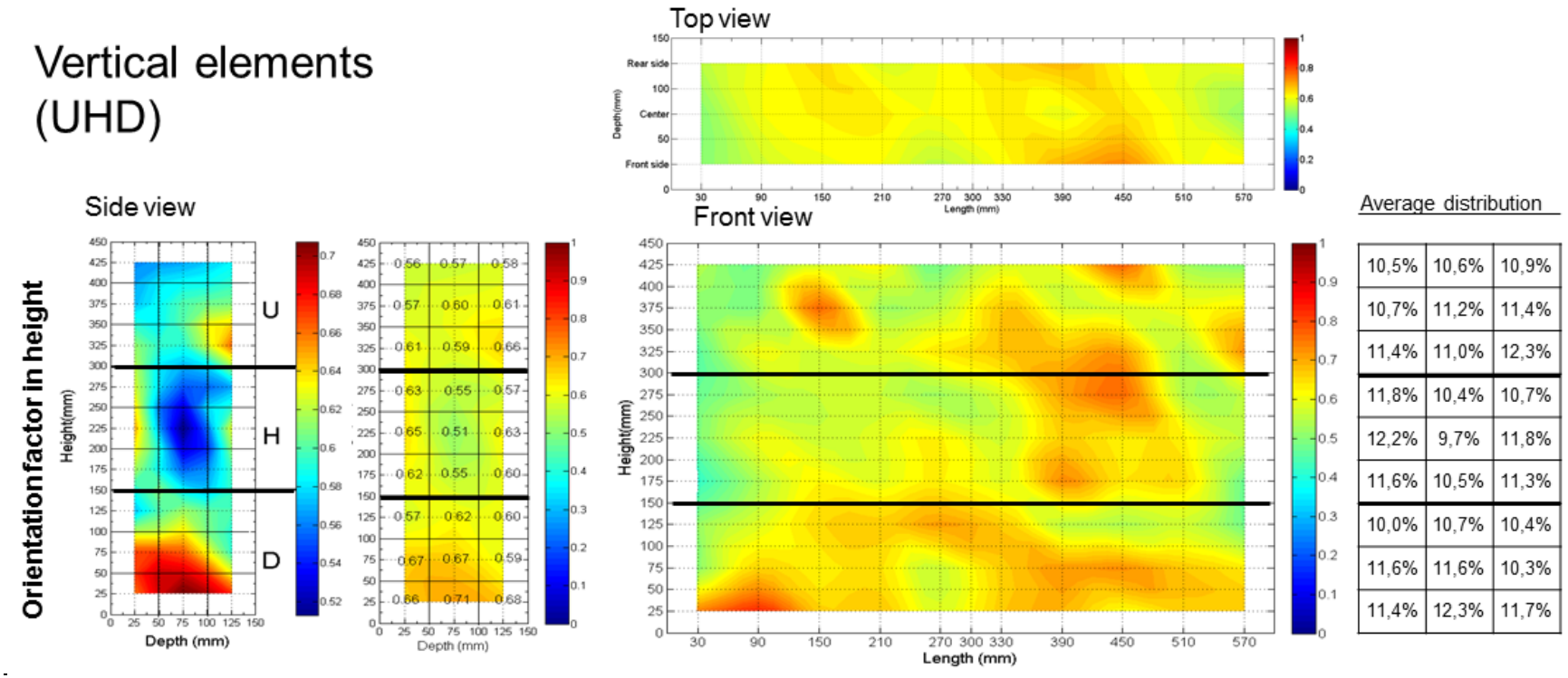

Figure 9-16: Summary of the orientation factor in VCC6-60 vertical elements.

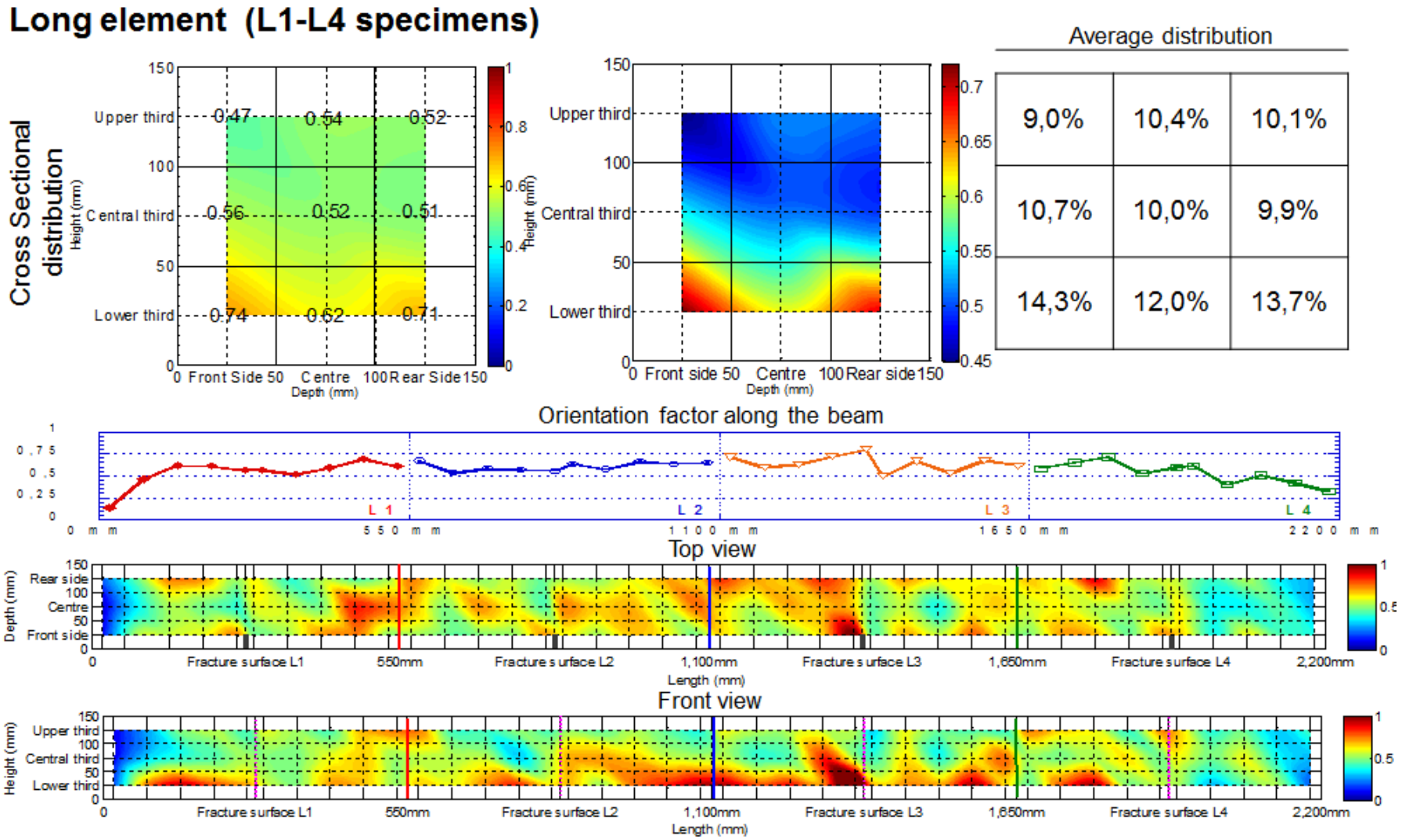

Figure 9-17: Summary of the orientation factor in SCC6-60 long element.

9.6 Conclusions

The analysis performed in the fracture surfaces of SCC reinforced with two different fibre lengths, 48 and 60 mm, has shown that the percentage of pulled-out fibres was greater for shorter fibres than longer ones. With the longer fibres, higher proportions of fibres were broken. Accordingly, it could be concluded that the loss due to the pulled-out fibres was compensated with a better orientation factor. This would explain that both types of fibres had at the end remarkably similar results in fracture, which would ratify the hypothesis, concluded in Chapter 8 by means of the counting exercise.

The minimum post-cracking load was proven to behave in a linear relation with the amounts of fibres located in the lower third of the fracture surface. Similarly, for high-strain states the maximum post-cracking load bearing capacity could be linearly linked with the total amount of fibres located in the ligament area. Both linear relations were clearly shown, although with only one fibre dosage of 6 kg/m^3.

The wall effect increased when the relation between fibre length and size of the formwork walls was higher, as concluded from the evaluation of the orientation factor of PFR-VCC by using the standardised samples compared with smaller specimens of 100x100x430 mm^3. It was evident that smaller beams had higher amount of fibres placed with a favourable orientation and close to the walls.

The absence of external consolidation energy of self-compacting concrete resulted in a more non-homogeneous distribution of fibres along the main direction of the standardised sample when it was poured from one of its sides.

On another note, when self-compacting concrete was poured in the centre of the samples or when a conventional concrete was used the distribution of fibres was more uniform. By analysing the maps of the coefficient of orientation in the samples manufactured with self-compacting concrete, it was clear that there is not a constant flux along the mould. This effect was shown by the high concentration of fibres in the proximity of the pouring point. Consequently, if the moulds are filled from its centre, the amount of fibres in this area is greater than in the rest of it. Nonetheless, it was concluded that SCC would lead to more reliable and comparative results by pouring the mould from the side.

There was no evidence of any floatation of the fibres towards the free surface of the mould when a taller mould was filled and vibrated, as was the case of vertical elements. This is of significant importance due to the already shown better behaviour of PFRC with respect to SFRC in foundations subjected to earthquake lateral loads. On the contrary, the presence of the walls of the mould in the lower parts of such specimens, D samples, induced higher concentrations of fibres. In the vertical elements it was found that the coefficient of orientation was quite stable, and around 0.6 both in length and height.

The analysis made in the long element, L1 to L-4 samples, showed that when a proper flux of self-compacting concrete developed, the orientation factor obtained had a preferential orientation and reached an orientation factor around 0.6. This value was considerably high, given that only one wall of the mould was affecting the orientation of the fibres.

The absence of external consolidation energy of self-compacting concrete resulted in a more non-homogeneous distribution of fibres along the main direction of the standardised sample when it was poured from one of its sides. On another note, when self-compacting

concrete was poured in the centre of the samples or when a conventional concrete was used the distribution of fibres was more uniform.

The analysis made in the horizontal element, similar to a beam, showed that when a flux of self-compacting concrete is developed, the orientation factor rises. The latter in the lower third of the section was even above the values obtained in previous studies for self-compacting concrete reinforced with steel fibres (Laranjeira, et al., 2012). This value was considerably high, given that only one wall of the mould was affecting the orientation of the fibres.

PART IV: MATERIAL MODELLING

Chapter 10

Analytical fibre orientation model

10.1 Introduction

Since fibres are by definition (EHE-08, 2008) randomly added to concrete during the mixing stage, the position and orientation of each isolated fibre depends on the pouring process, formwork geometry and rheological properties of concrete. The positioning of the fibres has been assessed by using stereological tools (Stroeven, 1986), statistical ones (Laranjeira, et al., 2011) and rheological studies (Martinie, et al., 2010; Stähli, et al., 2008). Regarding the orientation of fibres, it should be noted that some models are based on the angles that fibres take in the concrete bulk material. These seem to be appropriate when using methods such as CT-scan, X-Ray, optical methods, methodologies which seek to imitate concrete by using a translucent fluid, and others that exploit the electrical properties of concrete in measuring real angles (see Table 3-5).

Nevertheless, most of the works performed for this purpose have measured the number of fibres placed in a sawn surface or in the resulting surfaces after fracture tests (Gettu, et al., 2005). In such cases, the orientation factor proposed by Krenchel in 1975 (Krenchel, 1975) enables the use of a factor that offers a coupled value of the orientation and the distribution of the fibres. It provides a powerful comparative factor and allows a better understanding of fracture results. The ease of implementing counting procedures and developing models to

predict the amount of fibres that cross a certain vertical surface has boosted the use of this combination. With the use of the orientation factor (θ), it has been possible to assess the improvements in mechanical properties of SFRC by using self-compacting concrete (Laranjeira, et al., 2012) and the effects of several types of vibration on conventional concrete (Gettu, et al., 2005). In such a sense, research has confirmed that steel fibres, due to table vibration, tend to orientate along planes perpendicular to the casting direction.

However, there is still a lack of discussion about the orientation factor of PFRC, the effect of fibre-flexibility and length on the relation of the real number of fibres, and the theoretical expected amount of fibres that cross a certain vertical surface. In addition, as macro-synthetic fibres are remarkably different in the physical properties (especially due to lower density and flexibility) when compared with steel fibres, the models that deal with SFRC are questionable.

Moreover, post-cracking behaviour of the FRC has become the reference property. In order to provide trustworthy tools for designers, it is necessary to find predictive models that may allow the prediction of the number and positioning of the fibres placed in the critical sections of a structural piece (Torrijos, et al., 2010; Zerbino, et al., 2012; Laranjeira, et al., 2012; Rozière, et al., 2007).

With the aim of addressing this matter, a new model has been built for the theoretical prediction of the positioning of fibres as a reinforcement of concrete and which is adapted for rigid and non-rigid fibres alike. Indeed, the flexible nature of macro-synthetic fibres has been explicitly considered and has encompassed the calculation of the orientation factor of rigid and flexible fibres of different lengths. The model is based on understandable geometrical concepts, solved by numerical integration, and not only fits the most accepted values of the orientation factor but also improves the possibilities of applying counting methods to assess the homogeneity distribution of fibres in concrete elements.

10.2 Theoretical background: a review of theoretical models

10.2.1 The probability of random orientation

The random orientation of short linear elements and the geometrical probability problem is a longstanding question which was possibly first posed in the celebrated Buffon's needle problem (Buffon, 1777) that has also been shown to have a direct link with modern stereology and methodology and, therefore, with its applicability to modern concrete technology (Stroeven & Hu, 2006; Nemati & Stroeven, 2001). The initial problem required identification of the probability that a needle tossed at random on a horizontal plane ruled (a wooden floor with strips) with parallel straight lines, would come to rest by intersecting one of the lines. Several deductions achieved the solution that Laplace (marquis de Laplace, 1814) gave to the problem (Burton, 1985). The mathematical deduction used below introduces some of the geometrical concepts required to perform the model proposed in the following sections. It is clear that the probability sought is a function of the relation of the length of the element (l) and the distance between the lines (d), as depicted in Figure 10-1(a) where the total space of the probability would be defined with the bounds of two variables: the rotation angle (θ) and l/d. Consequently, the limits of the probability axes would be π (allowing all the possible angles) and the maximum distance (measured from the gravity point of the longitudinal element) that would be y equal to $d/2$, as may be better understood in Figure 10-1(b). In such a case, the lower is d the higher is the probability of

the needle crossing the line. Should the variables be independent, the probability would be the deduction shown in expression (10-1). However, in this case there is a limited distance $d - l\sin\theta$ where the needle could lie at its gravity point in which it would not cross the lines, as shown in Figure 10-1(a). This means that there is a clear relation with the probability function that could also help to solve the problem (Glaister, 1997). Given that the aforementioned distance y is equal to $l/2\sin\theta$, the probability of the needle crossing a line in a coupled probability distribution would be the area below such a function with values in the gap [0, π] over the total probability space. The mathematical process would then be the expression (10-2) and the geometrical explanation depicted in Figure 10-1(c). The previous statement refers to a two-dimensional situation for a fibre randomly distributed in a cell of dimension d equal to fibre length and thus resulting in a 2-D probability of $2/\pi$.

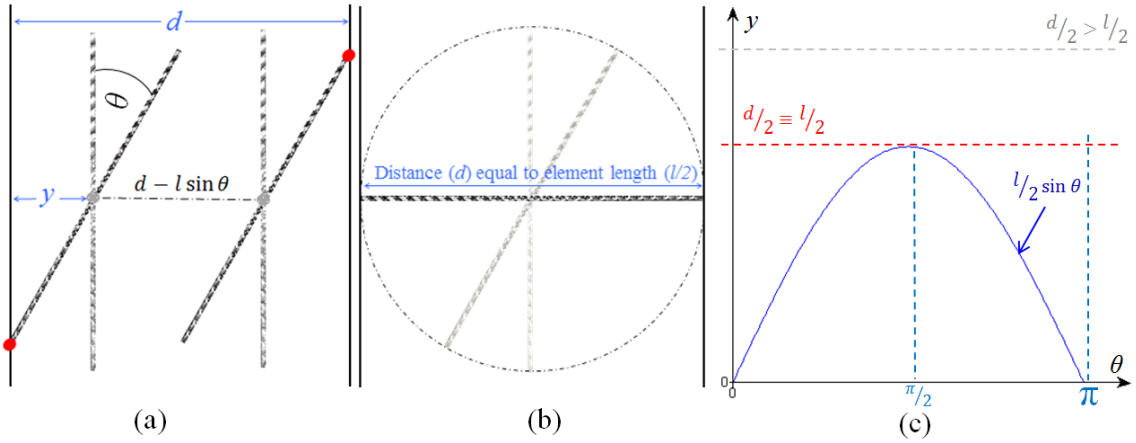

Figure 10-1: Buffon´s needle problem.

$$P(\theta) = \frac{1}{\pi};\ P(Y) = \frac{2}{d} \Longrightarrow P(\theta, Y) = \frac{2}{\pi d} \qquad (10-1)$$

$$P(\theta, Y) = \int_0^{\pi}\int_0^{l/2\,sin\,\theta} \frac{2}{\pi d}\, d\theta dy = \frac{2l}{\pi d};\ if\ \frac{l}{d} = 1 \Longrightarrow P(\theta, Y) = \frac{2}{\pi} \qquad (10-2)$$

Under perfect conditions, fibres would cross the crack perpendicularly to the fracture surface and prevent the division of the notched piece. Of course, in such a case all of the fibres would be aligned, uniformly spaced and suitably anchored with enough embedded length. Such a situation is that which would mark the best threshold of the behaviour of the composite material. If a factor to reduce this were to be used, it would take the value of one in the perfect orientation, distribution and anchorage features. Additionally, the desired factor is required to represent the loss of fibres in sectional cuts while the orientation changes.

It should be pointed out that for this situation, fibres could be idealized as a number with the same cross section and traverse the whole piece and complete the final volume fraction (V_f) that was added in the mixer. The theoretical number of fibres that cross any section would, at the end, be that obtained by means of expression (10-3). This number of fibres, which would enclose the theoretical number of fibres to be counted in any section, is termed in this research *th*. These long fibres would be placed in a straight manner and could be cut in a proportional number, being located at the end of the fibre length. Hence, the theoretical number of fibres to be counted in any sawn cross-section is not related with fibre

length but with volume fraction and the fibre-cross-sectional surface. Furthermore, such an idealized case would lead to the possibility of considering all the fibres as one fibre with the total section being placed on the gravity centre which would be equivalent to a reinforcing bar at the end.

Once the theoretical number of fibres in an idealistic positioning has been defined, the next step is to denominate the orientation factor (θ) as the relation of the number of fibres counted in a certain surface over its theoretical number. That is to say, it is possible to obtain the orientation factor once it has been counted by using the expression (10-4), with A being the cross section of the sample, A_f the section of one fibre and n the number of fibres actually counted in situ.

$$th = \frac{A \cdot V_f}{A_f} \qquad (10-3)$$

$$\theta = \frac{n}{th} = n\frac{A_f}{V_f A} \qquad (10-4)$$

Such an expression was introduced by Krenchel (Krenchel, 1975). Accordingly, if fibres were perfectly aligned, the number of fibres counted would match the theoretical value and, therefore, the ratio θ would be unity. Consequently, the counting process supplies a value that deals with the orientation of the fibres, though it should be noted that the orientation factor is not a measure of fibre efficiency. The evaluation of the orientation factor θ has been obtained for rigid metallic fibres, acquiring values that range from 0.41 to 0.82 (Soroushian & Lee, 1990).

In a general view, the three-dimensional situation could be described by measuring two angles which characterize the orientation of the fibre. Such angles are the rotation angles inside the planes that contain the fibres in its longitudinal axis. The third possible rotation would be possible in a plane located perpendicularly to the cross section, though rotation would not change the angle of the fibre axis with the fracture plane. That is to say, if fibres were assumed to be rigid cylinders the orientation of the fibres would be perfectly defined with a vector $\bar{f}$ with coordinates given as a function of two angles φ and β, as shown in Figure 10-2.

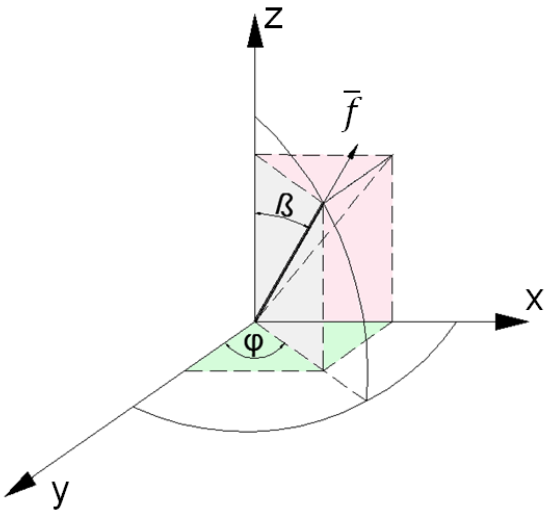

Figure 10-2: Possible rotation of an isolated fibre.

The description of the position of one isolated fibre could then be determined and extended with probabilistic concepts in order to approach a model of orientation of fibres. The probable orientation of the fibres, in an isotropic situation, has been considered as the relation between the projections in the x-y plane along all possible angles over the total area of the projected sphere that contains the fibre, as shown in Figure 10-3. If such an area were computed by turning around the x axis, and thus relating it with the total area, the probability obtained by expressions (10-5) and (10-6) would be 0.500, as shown in Figure 10-3. In any event, if this probability were considered for all the possible vertical planes, such a relation would be between the torus rotating along the vertical axis and the whole sphere of radius l_f, resulting in 0.589.

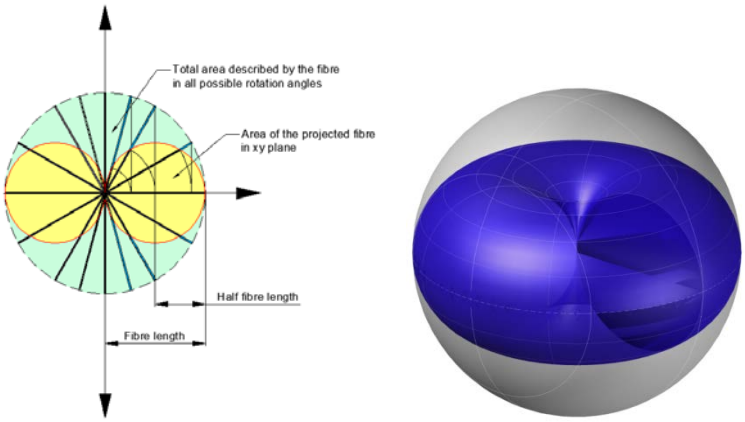

(a) (b)

Figure 10-3: Projected area of the fibre in all possible angles and the projected area of the sphere containing the fibre.

$$\theta = \frac{2 \cdot \pi \cdot \left(\frac{l_f}{2}\right)^2}{\pi \cdot {l_f}^2} = 0.500 \qquad (10-5)$$

$$\theta = \frac{2 \cdot \pi^2 \cdot \left(\frac{l_f}{2}\right)^3}{\frac{4}{3} \cdot \pi \cdot {l_f}^3} = 0.589 \qquad (10-6)$$

In the very first studies of the modern fibre reinforcement of concrete, Romualdi and Mandel (Romualdi & Mandel, 1964) set a value of θ extracted by means of expression (10-7) and showed that uniform probability of the randomly oriented fibres would become $4/\pi^2$.

$$\theta_{3D} = \frac{\int_0^{\frac{\pi}{2}} \int_0^{\frac{\pi}{2}} \frac{l_f}{2} \cdot sin\varphi \cdot sin\gamma \cdot d\varphi \cdot d\gamma}{\left(\frac{\pi}{2}\right)^2 \cdot l_f} = \frac{4}{\pi^2} \qquad (10-7)$$

The same value was obtained by Soroushian and Lee (Soroushian & Lee, 1990) from expressions (10-8) and (10-9) in 2-D and 3-D conditions of 0.637, 0.405 respectively when using rigid straight fibres. It should be noted that the value for the 2-D situation is equal to the solution of Buffon's needle problem. The one-dimensional situation would eventually lead in a value of θ equal to the unity.

$$\theta_{2D} = \frac{\int_0^{\frac{\pi}{2}} \frac{l_f}{2} \cdot cos\varphi d\varphi}{\int_0^{\frac{\pi}{2}} \frac{l_f}{2} d\varphi} = \frac{2}{\pi} = 0.637 \qquad (10-8)$$

$$\theta_{3D} = \frac{\int_0^{\frac{\pi}{2}} \int_0^{\frac{\pi}{2}} \frac{l_f}{2} \cdot cos\varphi \cdot cos\,\gamma \cdot d\varphi \cdot d\gamma}{\left(\frac{\pi}{2}\right)^2 \cdot l_f} = \left(\frac{2}{\pi}\right)^2 = 0.405 \qquad (10-9)$$

Some other research and analytical formulations have led to values in 2D being also equal to 2/π, though under most isotropic conditions in 3D this has been shown to be 0.500 (Dupont & Vandewalle, 2005). Such values were obtained by assuming that fibres could rotate freely around the gravity point, thus considering all orientations to be possible. That is to say, the end of the fibres would describe a sphere with radius half the length of the fibres as shown in Figure 10-4. The probability of occurrence on an angle related with the beam axis could hence be obtained by means of the expression (10-10) which relates the spherical cap surface with the sphere surface.

$$\theta_{3D} = \frac{\int_0^{\frac{\pi}{2}} cos(\vartheta) \cdot \frac{\pi \cdot {l_f}^2}{2} \cdot sen(\vartheta)\, d\vartheta}{2\pi \cdot \left(\frac{l_f}{2}\right)^2} = 0.500 \qquad (10-10)$$

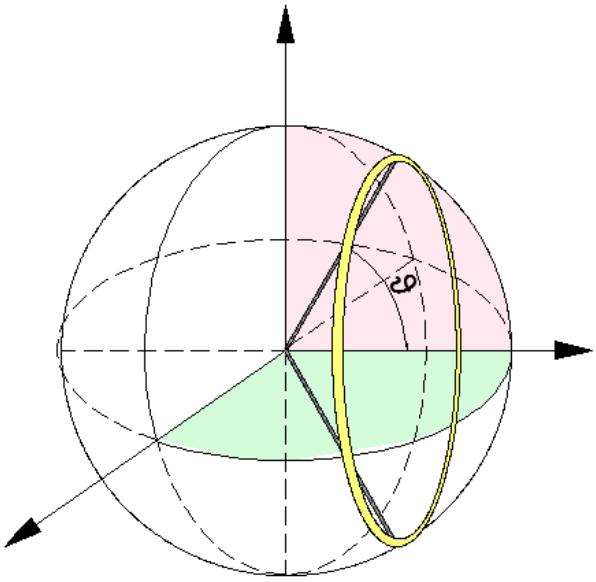

Figure 10-4: Ring described by the fibre on its possible rotational movements.

It is worth noting also that Stroeven (Stroeven & Shah, 1978; Kooiman, 2000) proposed a stereographical theory in which they showed that all fibre orientations would not have the same probability of concurrence by means of the calculation of the projected fibre length on the horizontal plane. The result proved that the contributions had a circular shape that depended on the angle of inclination and that it would not be independent from the fibre length, as can be seen in expression (10-11). Stroeven computed the average projected length and then followed the relation for the two-dimensional case proposed by Rao (Rao, 1979) and placed in expression (10-12).

$$L_{projected\,x,y} = \frac{\int_0^{\frac{\pi}{2}} l_f \cdot \sin\vartheta \cdot 2\pi \cdot \frac{l_f}{2} \cdot \sin\vartheta \; d\vartheta}{2\pi \cdot \left(\frac{l_f}{2}\right)} = \frac{\pi}{4} \cdot l_f \qquad (10-11)$$

$$\theta_{Rao} = \frac{\int_0^{\frac{\pi}{2}} \frac{\pi}{4} \cdot l_f \sin\vartheta \, d\vartheta}{\pi} = 0.500 \qquad (10-12)$$

10.2.2 The presence of boundaries and other sources of anisotropy

Isotropic conditions may only occur in an idealized situation in which use of concrete is not feasible. The general performance of concrete permits the production of an evolving material that provides the advantages of a fluid mass in the initial stages and strength in the hardened state. Thus, the presence of physical boundaries during the setting stages is needed in order to shape the final element as desired and is a key factor for the final positioning of fibres. Additionally, the rheological properties of the initial state make it necessary or not to use external compaction methods. In terms of the constituent materials of the composite, even gravity produces important affections on the final positioning of the aggregate that, of course, affects the fibre final positioning. Summarizing, anisotropy in concrete production can be shortened in the following significant lines: wall effects and pouring and compacting processes. The examination of the existing models has reviewed several of the most relevant research proposals that deal with such issues, with some research focussing on taking advantage of the framework for the design of SFRC (Laranjeira, et al., 2012; Orbe, et al., 2012).

One of the first assumptions that has provided sound result entails the presence of a wall that produces the effect of transferring the problem to a 2D situation. That is to say, the issue to be solved becomes even closer to Buffon's needle problem. The previously mentioned authors, Dupont and Vandewalle (Dupont & Vandewalle, 2005), estimated by numerical integration the values of the orientation factor in the lateral bands of a size of half the fibre length such as 0.600. Figure 10-5 shows the areas of the differential orientation factor that also included a square of size $(l_f/2)$ in the corners (which a value of orientation factor considered 0.84) due to two boundary conditions. Dupont and Vandewalle computed a final orientation factor, combining such values weighted in proportional terms to the corresponding fractional surface. Kooiman (Kooiman, 2000) addressed the vicinity of the boundaries with an abacus, varying the relative position of the fibre gravity point and the wall. It should be noted that the variation in the values of the orientation factor is related with the distance from the gravity point of the fibre and the fibre length, as the probability of crossing a line in the Buffon's problem is higher when the relation between the needle length and the distance between the parallel lines increases. However, even if it is assumed that in the closest position to the wall the problem is solved merely by reducing it into a two-dimensional situation, the intermediate increases do not seem to be linear. It could also be argued that gravity is only acting in the vertical direction. Subsequently, the influence of a vertical wall would differ from a horizontal one. What is clear is that one mould of an internal cross-sectional size of $(\mathrm{l_f}/2)^2$ would have a preferential orientation along its longitudinal axis. If the size is increased progressively, the orientation factor would descend to an asymptotic value of the isotropic value of 0.500.

Research into this matter has provided many functions that represent variations of the orientation factor as a function of the thickness of the piece (or the relation of fibre length with the thickness of the piece). Exponentially decreasing relations, such as those presented

in expressions (10-13) and (10-14) and published in references (Rosenbusch, 2004) and (Michels, et al., 2012), related the orientation factor with the specimen thickness (h). Nonetheless, Martinie (Rozière, et al., 2007) provided expressions and graphic descriptions that relate the orientation factor with the relation between fibre length and specimen thickness (l_{f_i}/h), as can be seen in expression (10-15). Laranjeira (Laranjeira, et al., 2012) proposed the use of a bilinear model to adjust the results of a theoretical model that can also be seen in expression (10-16). This provided one idealized model to be considered for the use of SCC that was to consider the flux of SCC taking place in virtual layers of thickness equal to the fibre length. Therefore, if such boundaries are considered, the value of the orientation factor in the bulk is the same as that assumed for the presence of one wall, close to 0.60. In such a sense, it should also be mentioned that the improvements of the orientation factor induced by shear during casting has been attributed to shear rate time and distance from the point of pouring (Rozière, et al., 2007). The shapes of the profiles of orientation factor based on these models are, in addition, comparable with the ones obtained by the abacus developed by Kooiman.

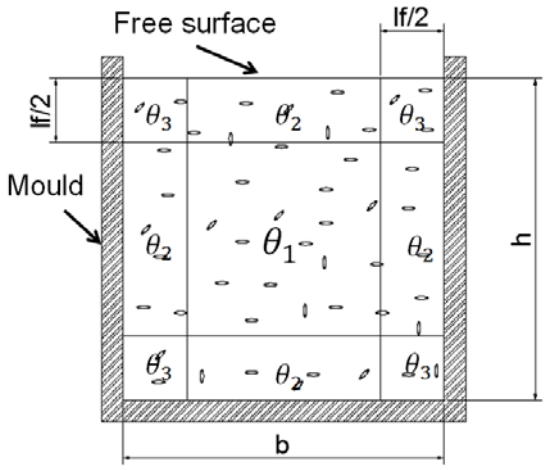

Figure 10-5: Cross-section of a beam divided into three different orientation zones, adapted from reference (Dupont & Vandewalle, 2005).

$$\theta = 0.382e^{-0.0033 \cdot h} + 0.37 \qquad Lin\ (1996)\ (10-13)$$

$$\theta = 0.699e^{-0.0024 \cdot h} \qquad Michels\ (2012)\ (10-14)$$

$$\theta = \theta_{isotropic} + {}^{l_f}/_{20h} \qquad Martinie\ (2011)\ (10-15)$$

$$\theta = \ 0.465 + 0.270 \cdot \theta_{isotropic} \quad \left(\geq \theta_{isotropic}\right) \qquad Laranjeira(2012)(10-16)$$

10.3 Simplified isotropic probability

Buffon's needle problem could also be solved by assuming that there are only a few positions for the gravity centre of the fibre that allow crossing of the lines in a given rotation angle. Those positions shown in Figure 10-1(a) would be all but those along the line of length $d - l\sin\theta$. Following such rationale, the same solution as that previously discussed (Glaister, 1997) may be obtained. Hence, the probability of crossing the line for

one given angle would involve the distance that the centre of the needle can land when crossing a crack over the total distance.

Built on the same logic, a simplified probability can provide a relatively close value for both the 3D and the 2D cases. That is to say, if fibres were placed with a given rotation angle, even if they were rigid and straight, it would be possible to count them in certain positions. For a given distance from the gravity point of the fibre to the counting surface, it would cross the surface for few rotations until it reached a critical angle in which it would not cross the referred plane. In an idealized case of the fibres being perpendicular to the sawn surface in a prismatic specimen cut in pieces of the same length of the fibre, all the fibres would be counted in one of the surface generated. Moreover, an average fibre with its centre equidistant to the two cut surfaces of one slide would disappear when 60º of rotation took place. Figure 10-6 shows this.

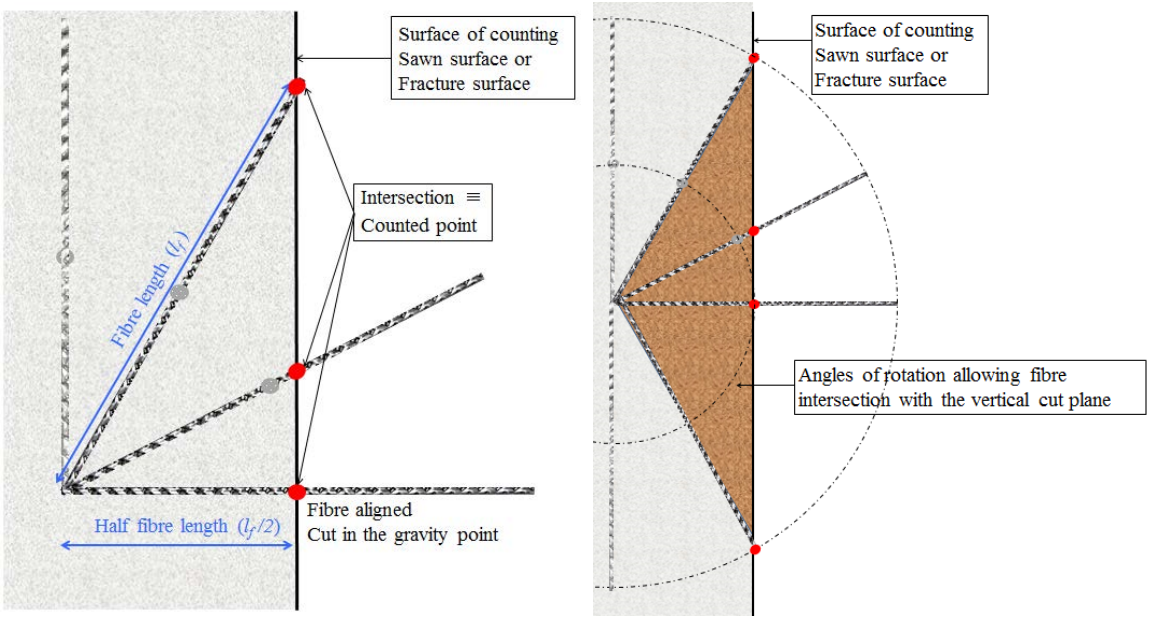

Figure 10-6: Cut surface with fibre oriented 60º and getting lost of the counting.

It is assumed that in an ideal positioning of a straight fibre it would be cut in its middle section (the most probable placement). Therefore, the rotation could be considered from its initial point, as shown in Figure 10-6. With this assumption, it can be noted that the fibre would be lost in the counting when it rotates 60º inside a vertical plane, because it would not reach the cut surface in which the counting exercise would be performed. The same would result if the rotation were taken into account inside a horizontal plane. This leads to a simple probabilistic value of 2/3 of the angles for 2D situation being counted in the plane which would be close to $2/\pi$. In the same way, for a three-dimensional situation the probability would be 4/9, given the two rotation planes. This would also be close to the models, and in between the Soroushian and Dupont values for 3D. Summarizing, the results of theoretical orientation factor for a straight shape in an infinite environment have taken, based on the previously mentioned models, the values summarized in Table 10-1.

Table 10-1: Values provided by the models and its main references.

Probabilistic boundaries	2-D	3-D
Buffon´s needle problem	$2/\pi = 0.637$	-
Soroushian (Soroushian & Lee, 1990; Romualdi & Mandel, 1964; Lee & Kim, 2010)	0.637	0.405
Dupont (Laranjeira, et al., 2012; Dupont & Vandewalle, 2005; Rao, 1979)	0.600	0.500
Simplified θ	0.667	0.444

These studies have been proved to be close to reality and have been considered before facing the model. Experimental evidence and models are close due to the small band of values that range between 0.42 and 0.82. However, it should be highlighted that while some of the reviewed values are accepted for most of the research none of the models agrees with all of them. Therefore, one model that gathers and fits the most relevant founding would provide reliability. In addition to this, some issues have arisen such as the assumption of the free surface showing the same behaviour as a boundary due to the finishing works of topping and levelling that are not in agreement with the maps shown in Chapter 9. Furthermore, the need of assessing the fitting of flexible and lower density fibres in the existing models also justified the development of the model presented in this chapter.

10.4 A new model to assess the orientation factor

10.4.1 Isotropic conditions: bulk area of the material

In the bulk zone, it could be considered that fibres are under isotropic conditions if the compaction is made with conventional times of vibration and no other of the previously summarized effects take place. In such conditions, the stereographical concept proposed in this study is to relate the sphere described by a single fibre that rotates around its gravity point and the intersection produced with a vertical plane. That plane would be the base of counting in a real specimen. The probability of a fibre intersecting a vertical plane would vary with the distance to the vertical plane as it is coupled with its rotation angle, as depicted in Figure 10-7. Thus, if the fibre is included in a cube cell of size l_f, the intersection with the plane that moves along its horizontal axis becomes a circumference that reaches its maximum surface of probability in an equatorial circumference of diameter equal to l_f. In such a sense, the intersection between the two spatial figures in the plane of counting represents for each distance the possible rotation angles that allow the fibre to cut the surface, which hence allows the fibre to be counted and act, preventing an idealized crack.

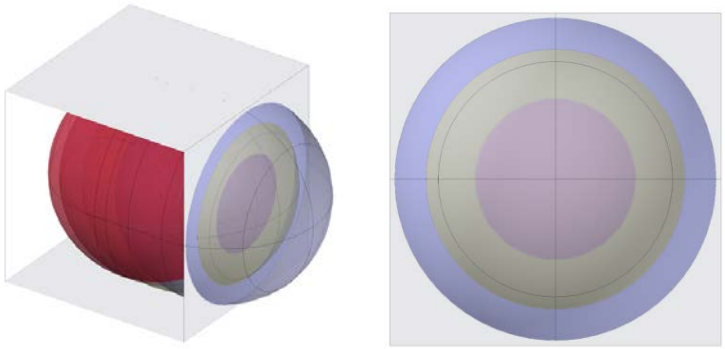

Figure 10-7: Sphere described by a fibre in all possible positions intersected with the vertical plane of counting.

An intermediate situation would describe a cone as having at its base the aforementioned circumference and a height of the distance between the plane and the fibre gravity point. With such an assumption, the probability of counting one fibre in a vertical plane could be given as a function of the two parameters: the fibre orientation angle (θ) and distance of the projected fibre to the cracked or cut surface. In such a sense, there is a critical orientation angle for each positioning of the fibre. At the end, such parameters draw a three-dimensional cone in each position. The cone-base surface is a circumference where all the possible positions of a fibre placed at that distance could cut in the referred counting plane. If a greater angle of orientation in the two perpendicular planes occurred, the fibre would be lost in the counting. This is shown in Figure 10-7. The extreme positions are an equatorial plane that contains fibres rotated 90º or at the cutting of a fibre in its extreme position by its last cross-section. The intermediate positions relate the probability of occurrence as a fraction of the base of the cone of such a position and the equatorial one with the fibre length as its radius, as shown in Figure 10-8.

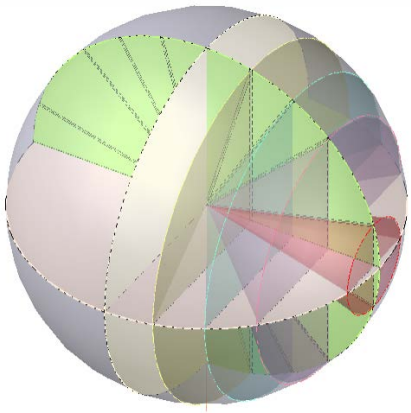

Figure 10-8: Graphical description of the cones formed by the probability situations.

Once the cone is defined, the graphical solution of the probability of occurrence of a single case would be the relation between the circumference described by the fibre in that case (A_S) and the base one of probability that would be the circumference (A_1). These are described in Figure 10-9.

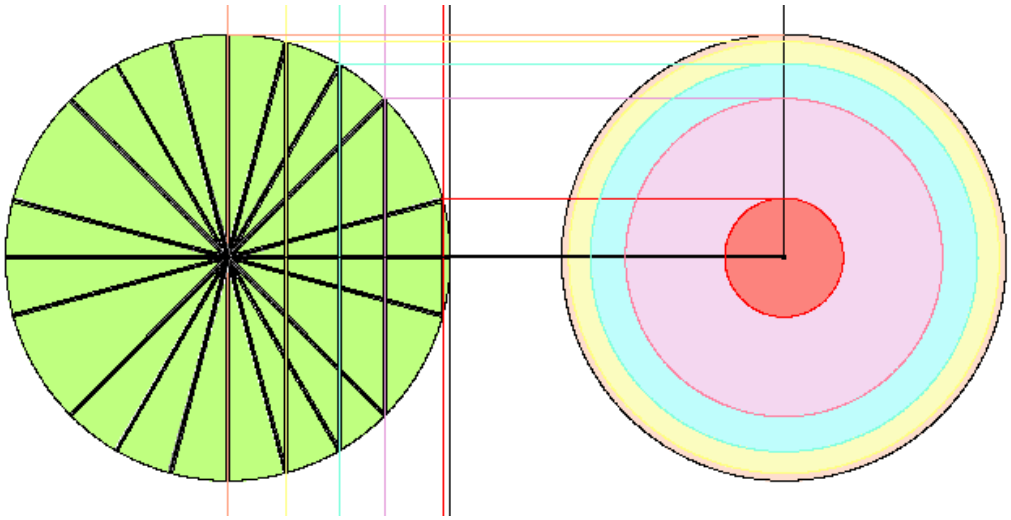

Figure 10-9: Surfaces of probability obtained as intersection of the vertical plane and the sphere described by the fibre.

If Figure 10-10 is observed, it may be seen that the values of such surfaces and the probability of occurrence in a given position could be computed by the expressions (10-17), (10-18) and (10-19). The probability situations can vary from values $\theta = \pi/2$, corresponding to the situation in which the fibre can describe the circumference with area A_1 , to $\theta = 0$ in which the fibre would be cut at its end and the circumference becomes a single point.

$$A_S = \pi \left(\frac{l_f}{2}\right)^2 sin\,(\theta)^2 \qquad (10-17)$$

$$A_1 = \pi \left(\frac{l_f}{2}\right)^2 \qquad (10-18)$$

$$P(\theta_i) = \frac{Base\ of\ the\ cone}{\pi \cdot \left(\frac{l_f}{2}\right)^2} = \frac{\pi \left(\frac{l_f}{2}\right)^2 sin\,(\theta)^2}{\pi \left(\frac{l_f}{2}\right)^2} = sin\,(\theta)^2\ for\ 0 < \theta < \frac{\pi}{2} \qquad (10-19)$$

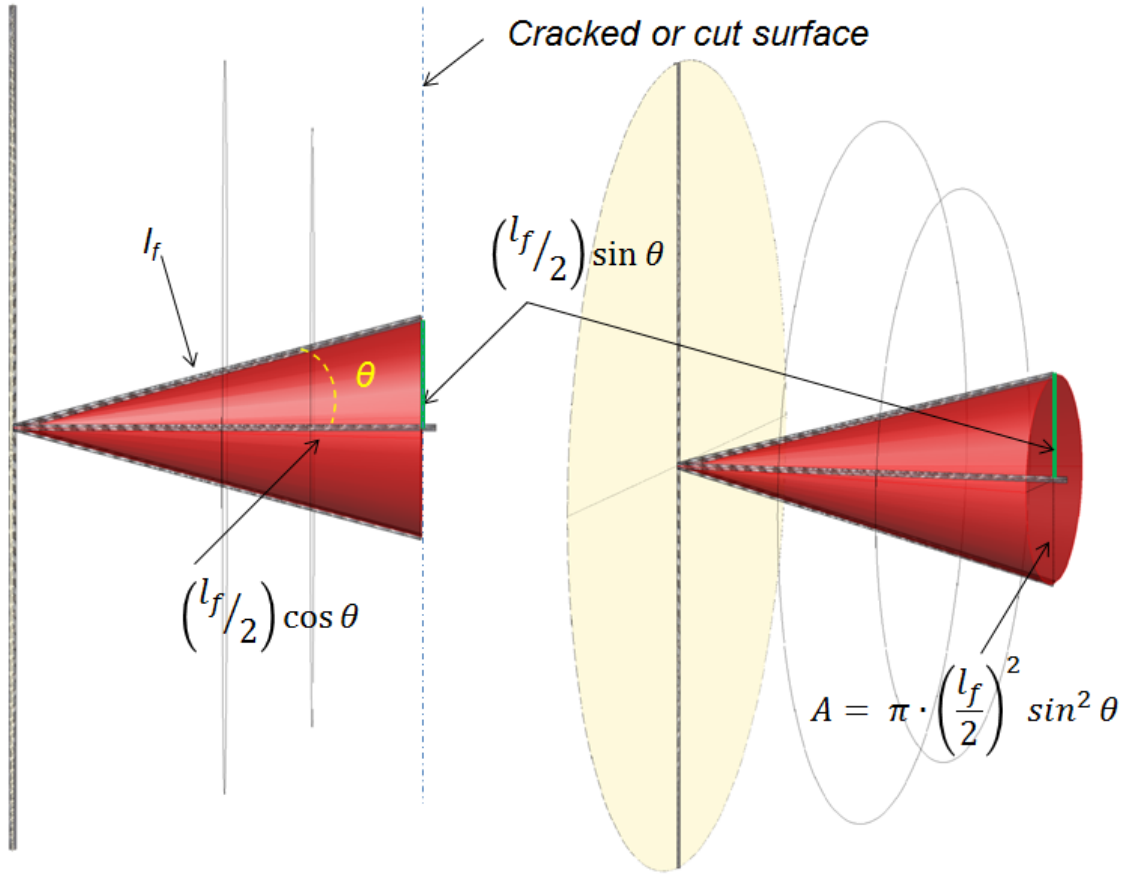

Figure 10-10: Graphical description of the model: the cone of a single position linked with its distance to the vertical plane and the reference circumference of probability one.

Therefore, the probability in a three-dimensional isotropic situation could involve the relation at a given distance of the surface drawn by the fibre that crosses the cut surface in all the angles of rotation and the total surface probability. If we consider the space probability as the average obtained in all the possible geometrical situations, expressions (10-20) would provide the solution. When graphically solved, the area under the probability curve can be an average in the space probability in the value of 0.500, as shown in Figure 10-11. This value could be considered as the mean orientation factor found in the bulk area.

$$P\left(\theta_{isotropic}\right) = \frac{\int_0^{\frac{\pi}{2}} sin\,(\theta)^2\ d\theta}{\frac{\pi}{2}} = 0.500 \qquad (10-20)$$

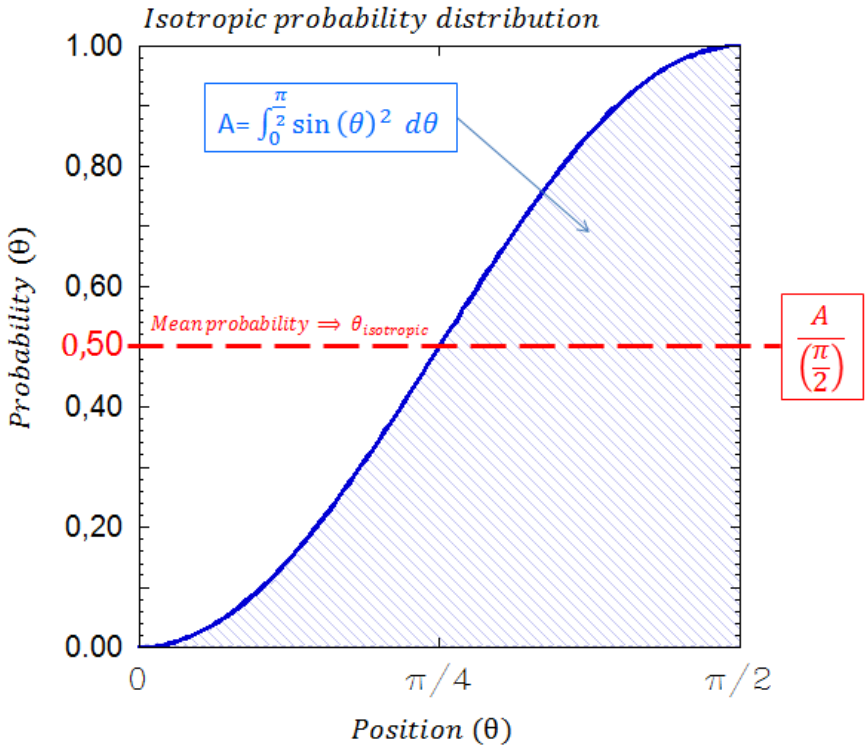

Figure 10-11: Isotropic probability distribution.

The value of 0.500 for isotropic conditions has been the most accepted, although some of the models and other considerations have led to lower values. As stated in the review, there is a wide range of assumptions that would lead to a model. However, one of the aims of the model presented in this thesis is to permit the already used data and assumptions when supported by experimental evidence. In such a sense, one other possibility (which has been discarded) would be to perform the analysis of the probability by mixing the average position computed and the probability of having at least the minimum length needed for such an angle of rotation $(1-\cos\theta)$. Such a probability would give the solution provided in expressions (10-21).

$$\theta = \frac{\int_0^{\frac{\pi}{2}} (1-cos\,\theta)\cdot \pi \cdot \left(\frac{l_f}{2}\right)^2 \cdot sin^2\,\theta\, d\theta}{\pi \cdot \left(\frac{l_f}{2}^2\right)} = 0.452 \qquad (10-21)$$

10.4.2 The presence of one wall

In order to address the presence of a wall, the graphical problem was firstly analysed. If Figure 10-12 is observed, it can be noted that the presence of a boundary condition impedes the fibre from taking certain positions. It should also be noted that if we consider the fibre distance to the wall from its gravity point, the symmetrical positions would not be reached. If the wall reaches the position of the centre of the sphere, in which the fibre would be located in the wall, given that the only possible rotations would be in the angle perpendicular to the paper the situation would be equal to a two-dimensional one.

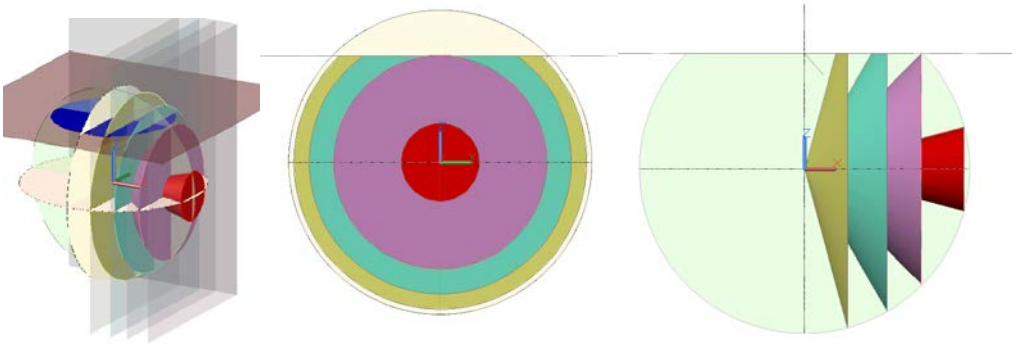

Figure 10-12: The presence of one wall.

If Figure 10-12 is analysed, two significant changes in the calculation emerge. The first is that the surface of probability one $(A_{1-1wall})$ is smaller than in the isotropic case, given that in the surface of the circumference two sectors have to be subtracted (one in the side of the wall and another in the symmetrical position). The second one is that there are two formulations for the drawing of the possible cut on the counting surface. In the positions of the cone not reaching a limit angle of rotation, the base of the cone remains as a circumference of similar dimensions. Once the distance allows rotation angles that would allow positions that are impeded by the existence of a boundary, the obstructed sector and its symmetrical position have to be subtracted. These can be seen in the description placed in Figure 10-13, Figure 10-14 and Figure 10-15. The area of the sectors of the positions not allowed could, therefore, be computed by expression (10-22). Subsequently, the resulting equations for computing the probability and thus the orientation factor for each relative distance to the wall are the expressions (10-23), (10-24), (10-25), (10-26), (10-27) and (10-28). It should be noted that the distance in terms of a fraction of the fibre length is needed in order to solve the numerical integration. It is logical that the relation of the two parameters, the distance and length of the element, influences the probability. According to such a claim, the models that show this profile in relative terms seem to the closest to those presented in this thesis.

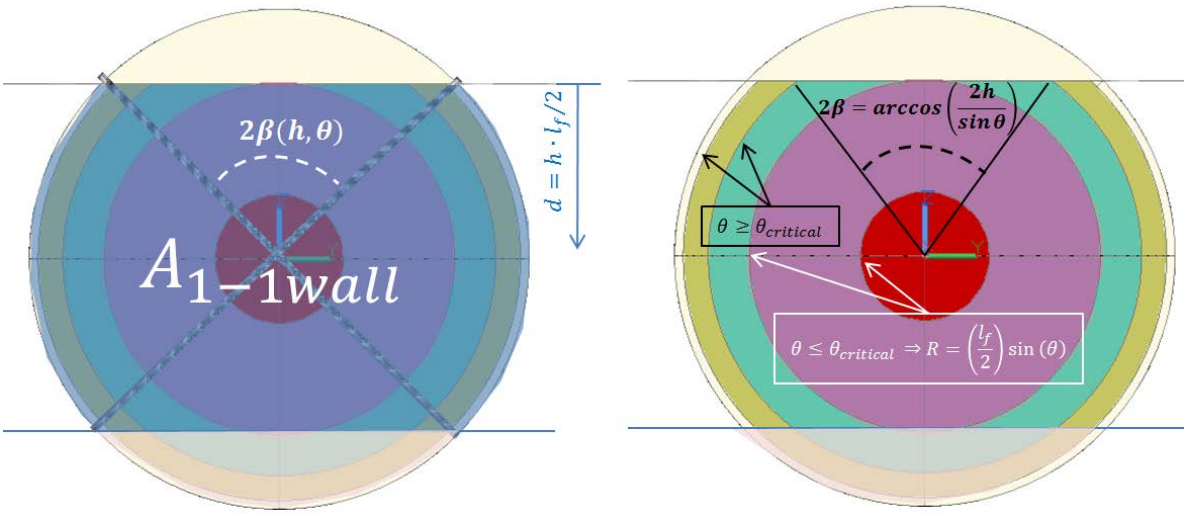

Figure 10-13: Description of the possible surfaces resulting of the possible rotation angle and distances to the wall.

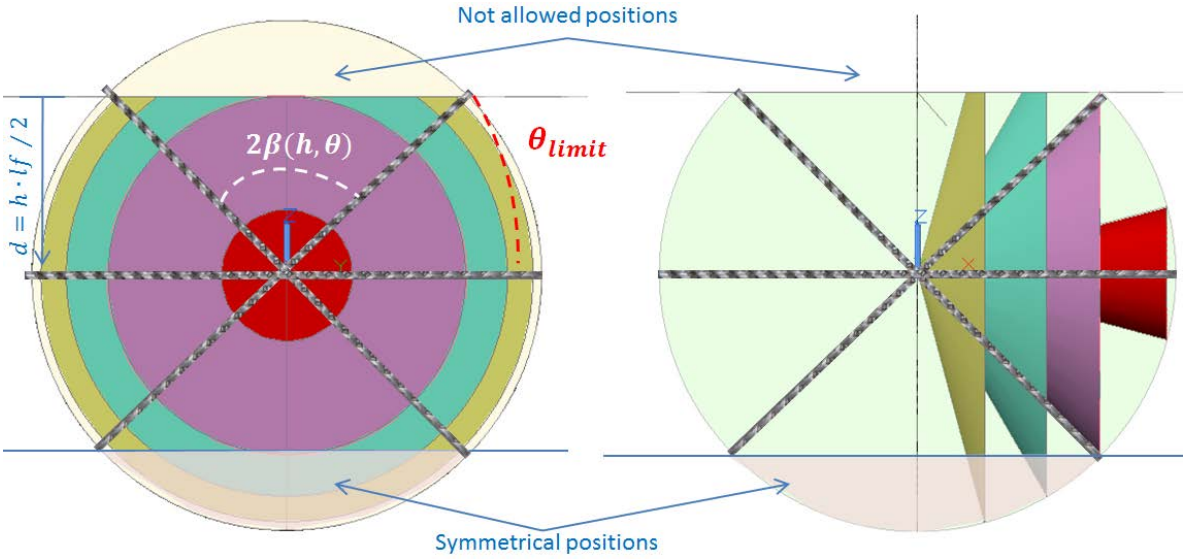

Figure 10-14: Description of the possible situations and resulting surfaces due to the presence of one wall.

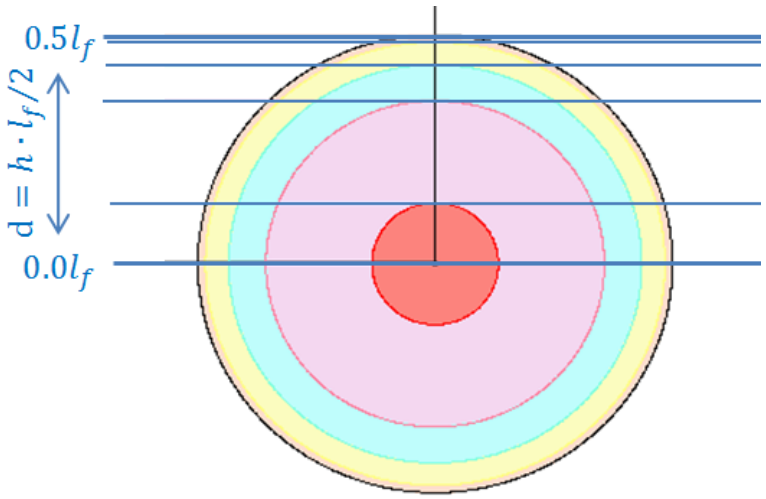

Figure 10-15: Distance to the wall as a fraction of half fibre length.

$$A_s = \frac{r^2}{2} \cdot (2\beta - sin\,2\beta) \qquad (10-22)$$

$$d = h \cdot \frac{l_f}{2} \qquad being\ 0 < h \leq 0.5 \qquad (10-23)$$

$$\theta_{limit} = arcsin\frac{2d}{l_f} \quad ; \quad \beta = arccos\frac{2d}{l_f} = arccos\,h \qquad (10-24)$$

$$A_{1-1wall} = \left(\frac{l_f}{2}\right)^2 \cdot \left[\pi - \frac{1}{2}(2\,arccos(h) - sin(2arccos(h)))\right] \qquad (10-25)$$

$$A_{i-1wall}\begin{cases} if\ \ \theta \leq \theta_{limit} \implies A_{i-1wall} = \pi\left(\frac{l_f}{2}\right)^2 sin\,(\theta)^2 \\ if\ \ \theta > \theta_{limit} \implies A_{i-1wall} = \left(\frac{l_f}{2}\right)^2 sin\,(\theta)^2 \cdot \left[\pi - \frac{1}{2}\left(2\,arccos\left(\frac{2h}{sin\,\theta}\right) - sin\left(2arccos\left(\frac{2h}{sin\,\theta}\right)\right)\right)\right] \end{cases} \qquad (10-26)$$

$$P(\theta_i) = \frac{A_{i-1wall}}{A_{1-1wall}} \qquad (10-27)$$

$$P(\theta_{1wall}(h)) = \frac{\int_0^{\theta_{critical}} \pi\,[sin\,(\theta)^2]\,d\theta + \int_{\theta_{critical}}^{\frac{\pi}{2}} sin\,(\theta)^2\left[\pi - \frac{1}{2}\left(2\,arccos\left(\frac{2h}{sin\,\theta}\right) - sin\left(2arccos\left(\frac{2h}{sin\,\theta}\right)\right)\right)\right]d\theta}{\left[\pi - \frac{1}{2}(2\,arccos(h) - sin(2arccos(h)))\right]} \qquad (10-28)$$

The numerical solution of this integral provides a value for each distance, varying from the case of a distance equal to half the fibre length to the one in which the fibre is in the wall plane. In such a sense, the probability distribution is unique for each distance and subsequently the mean value that is at the sought value. The area of probability when $h = 0.00\, l_f/2$ produces a mean value of probability of $2/\pi$, dividing the area under the red curve in Figure 10-16 by the length $\pi/2$ in order to average the value. It is worth noting that this value coincides with Buffon's solution, which could be considered the solution for a two-dimensional case.

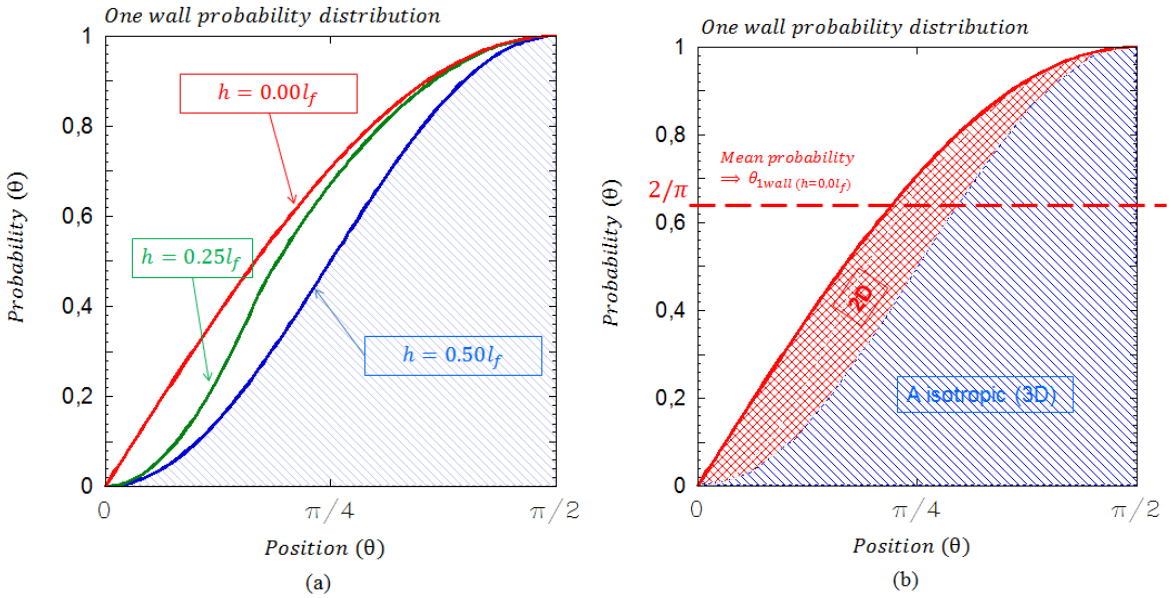

Figure 10-16: Probability distributions: (a) for several relative positions of the wall; (b) for the limit position $h = 0.00\, l_f/2$ and the computed average.

It is possible to build a profile of the orientation factor by giving values to h as a function of l_f. In doing so, the maximum value at the edge of the wall is $\theta_{1wall} = 2/\pi$, with the rest resulting in a continuously increasing curve from the value of the bulk up to what could be named as θ_{1wall}. Thus, the resulting profile is discussed below in the case of the presence of two walls. Table 10-2 offers the values of the orientation factor in several intermediate relative positions of the gravity point and the wall.

Table 10-2: Orientation factor as a function of the distance between fibre gravity point and one wall.

$\mathbf{h(l_f)}$	**θ**
0.500	**0.500**
0.400	**0.531**
0.250	**0.584**
0.100	**0.625**
0.000	**0.637**

10.4.3 The presence of two walls

Related to real specimens, the presence of two walls occurs in the corners of the moulds and would be merely an extension of the previous concept developed for one wall. If the position of the first wall is fixed in a position at a certain distance h defined as a fraction of $l_f/2$, the position of the new wall needs to define a new parameter in order to integrate the possible positions. That is to say, the distance with the second wall, named u in the study, can be defined as a fraction of $l_f/2$ and varies u from 0.0 to 0.5, as shown in expression (10-29) and as depicted in Figure 10-17. With this new parameter, it is possible to find the surfaces generated to compute the probability, since the position of the first wall remains fixed. Figure 10-17 shows some of the main points, surfaces and angles resulting from the existence of the walls and a singular situation in which the two planes would cut the circumference at a single point. In a general situation, a new limiting angle would appear that makes a distinction from the formulation. Such a second limit angle (θ_{limit2}) can be computed with expression (10-30).

$$d = u \cdot \frac{l_f}{2} \qquad being\ 0 < u \leq 0.5 \qquad (10-29)$$

$$\theta_{limit2} = arcsin\frac{2u}{l_f} \quad ; \quad \omega = arccos\frac{d_2}{l_f} = arccos\, u \qquad (10-30)$$

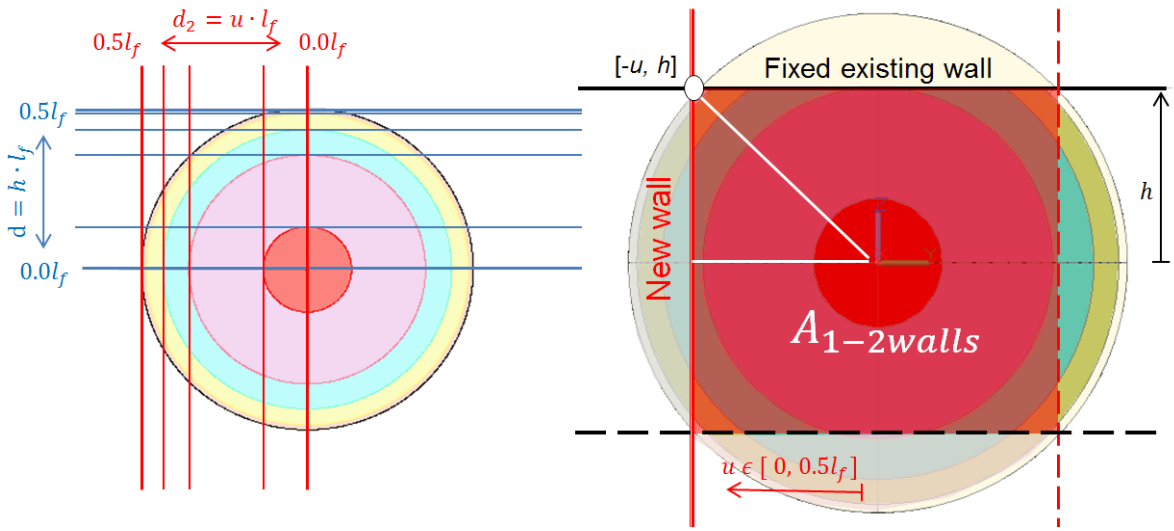

Figure 10-17: Position of the two walls defined by parameters h and u as a fraction of fibre length.

However, there is not only a new limit angle but also a key point for a general situation in which both planes intersect in a straight line idealized in a two-dimensional point. That point can be either outside or inside the circumference. Thus, the singular point in which such a key point belongs to the circle, border of the probability one circumference, is the limit between the two situations. Such a limit point (k) formulation can be obtained by means of expression (10-31). The latter situation is depicted in Figure 10-17 and the other two shown in Figure 10-18. It can be seen here that the reference surface of probability one ($A_{1-2walls}$) changes in shape and, therefore, should be computed in parts by the formulations placed in expression (10-32). For a better comprehension, Figure 10-19 shows the geometrical situation and the most important coordinates derived from it. It is worth

noting that as all the formulations were chosen as a function of $(l_f/2)$, most of the formulations relating the surfaces were not dependent on the fibre length.

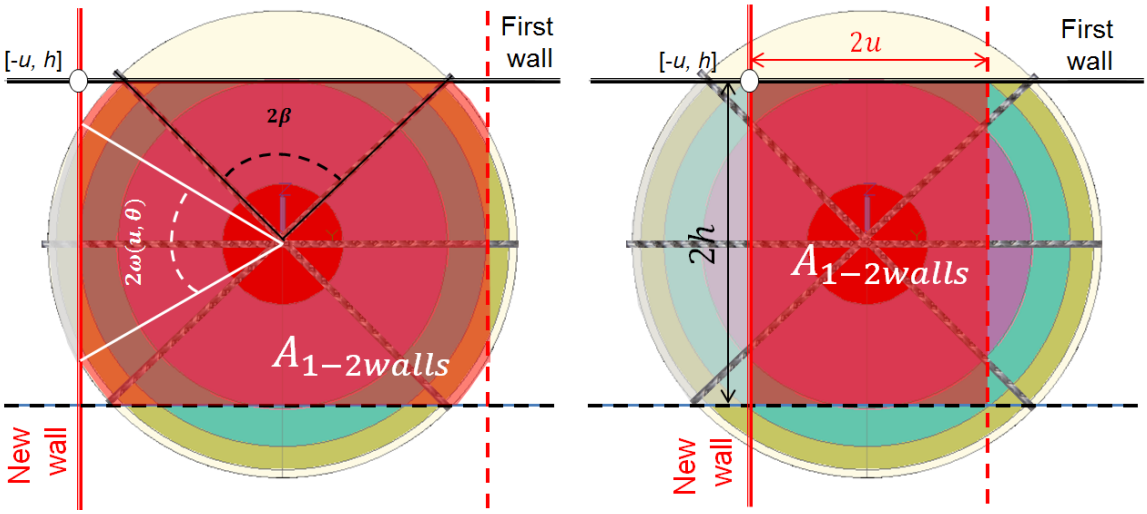

Figure 10-18: Description of the two possible situations for probability one reference surfaces due to the presence of two walls.

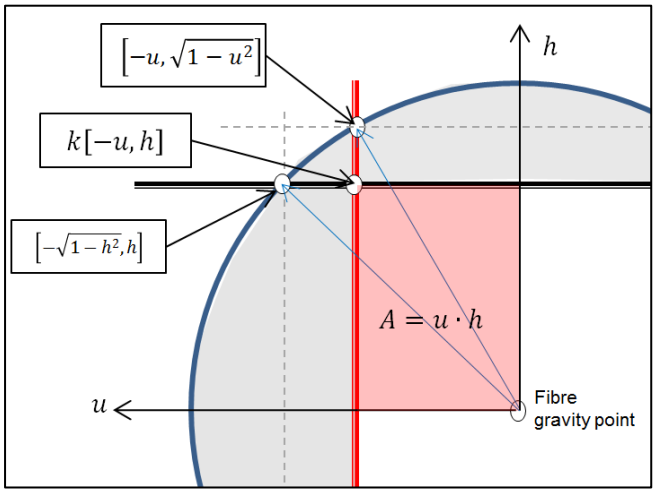

Figure 10-19: Geometrical situation and the most important coordinates derived from it.

For the first situation ($u \leq k$), regarding the probability for each distance to the second wall and varying the inclining angle of the fibre, the surfaces for specific cases take four possible formulations. The first one is a circumference of radius $(l_f/2)^2 \sin(\theta)^2$ and a surface analogous to expression (10-17) that varies from 0 to the two limit angles. It is evident at this point that when the distances of the planes (u, h) tend towards zero, the only possible orientation is aligned with the intersection line between the two planes, which subsequently takes the value one for the orientation factor. The second shape of a specific case would vary from one of the limit angles up to the value of the other angles (β, ω). That is to say, before the second of the limit angle is reached, only the sectors representing the area of not allowed positions of one of the wall have to be deducted. The third is when both limit angles have been surpassed, but the surface is still not a square because of the sectors in the corner. Finally, the shape described is a square for the singular positions. These situations are shown in Figure 10-20 in the same order described from (a) to (d). When ($u \geq k$), the last situation is not possible because the intersection line between the

two planes is outside the reference probability circumference and, subsequently, no case produces a square.

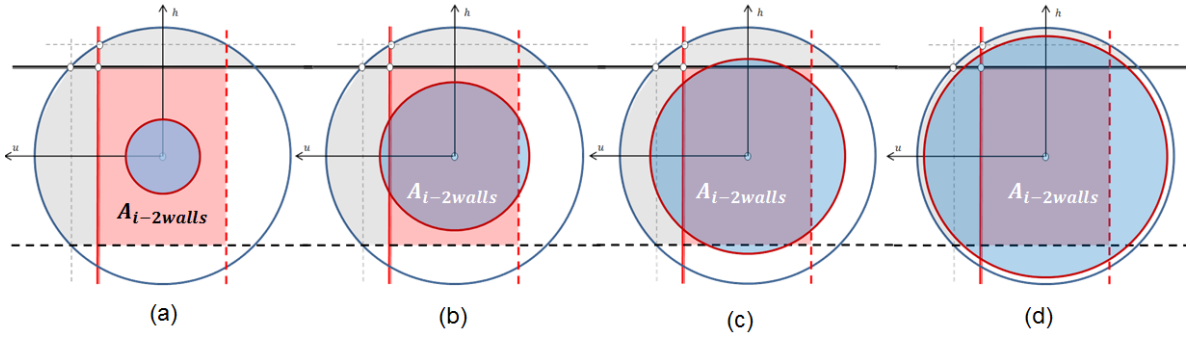

Figure 10-20: Shapes of the probability surfaces for specific when varying the inclining angle of the fibre for a given distance to the two walls.

As regards the formulation of the aforementioned shapes and obtaining of mean values of probability by numerical integration, the probability is defined with analogous processes to the previous probabilities in expression (10-33). The values of $A_{i-2walls}$ can be computed by means of the parametric expression (10-34), as previously explained, with the limit angles θ_{l1} and θ_{l2} being denominated. In the expression, there are five possibilities that consider that the limit angles can be greater than each other.

With such assumptions, limits and solving of the numerical integration, the probability surfaces and the mean values that vary the distance to the second wall (and for each fixed value of the first) would show a three-dimensional orientation factor map. It is evident that for the lowest values of (u, h), the mean orientation factor has to tend to one and for values of (u, h)close to 0.500, the orientation factor has to be close to 0.500. The latter can be seen in Figure 10-21.

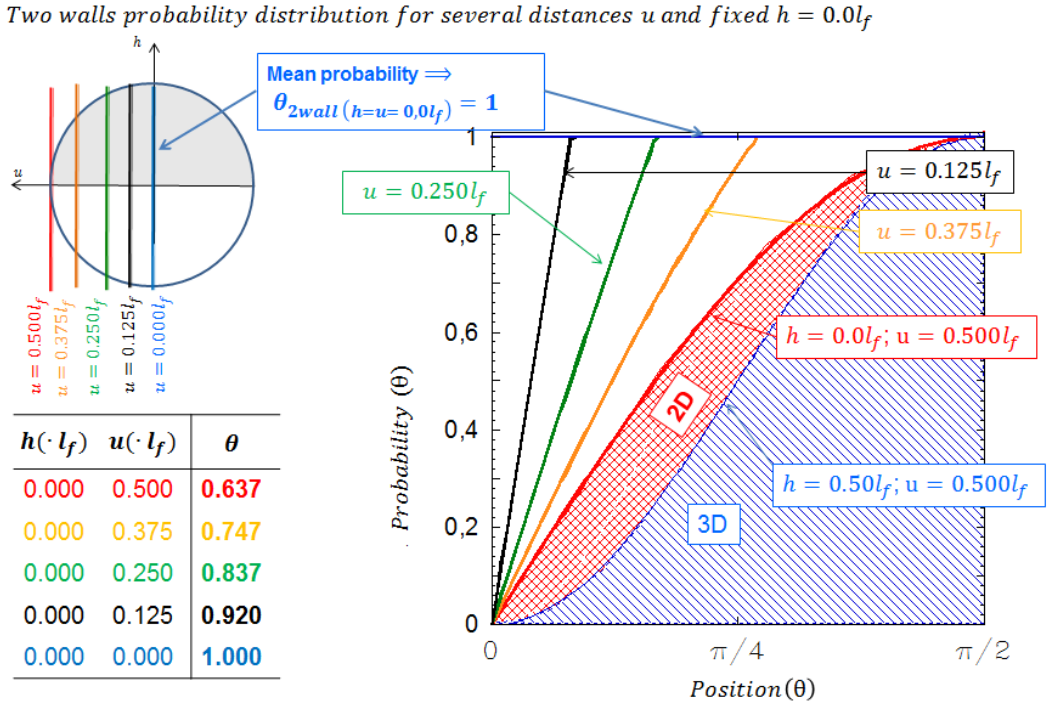

$h(\cdot l_f)$	$u(\cdot l_f)$	θ
0.000	0.500	**0.637**
0.000	0.375	**0.747**
0.000	0.250	**0.837**
0.000	0.125	**0.920**
0.000	0.000	**1.000**

Figure 10-21: Probability distributions varying u and h fixed in 0: one dimensional mean probability equal to one.

$$k = \sqrt{1-h^2} \tag{10-31}$$

$$A_{1-2walls}\begin{cases} if\ u > k \implies A_{1-2walls} = \left(\frac{l_f}{2}\right)^2 \cdot \left[\pi - \frac{1}{2}(2\,arccos(h) - sin(2arccos(h))) - \frac{1}{2}(2\,arccos(u) - sin(2arccos(u)))\right] \\ if\ u \le k \implies A_{1-2walls} = 2u \cdot 2h \end{cases} \tag{10-32}$$

$$P(\theta_i) = \frac{A_{i-2walls}}{A_{1-2walls}} \tag{10-33}$$

$$A_{i-2walls}\begin{cases} if\ \theta_i \le \theta_{l1} \le \theta_{l2} \implies A_{i-2wall} = \pi\left(\frac{l_f}{2}\right)^2 sin\,(\theta)^2 \\ if\ \theta_{l1} \le \theta_i \le \theta_{l2} \implies A_{i-2wall} = \pi\left(\frac{l_f}{2}\right)^2 sin\,(\theta)^2 \cdot \left[1 - \frac{1}{2}\left(2\,arccos\left(\frac{2h}{sin\,\theta}\right) - sin\left(2arccos\left(\frac{2h}{sin\,\theta}\right)\right)\right)\right] \\ if\ \theta_{l2} \le \theta_i \le \theta_{l1} \implies A_{i-2wall} = \pi\left(\frac{l_f}{2}\right)^2 sin\,(\theta)^2 \cdot \left[1 - \frac{1}{2}\left(2\,arccos\left(\frac{2u}{sin\,\theta}\right) - sin\left(2arccos\left(\frac{2u}{sin\,\theta}\right)\right)\right)\right] \\ if\ \theta_{l2} \le \theta_i \le \theta_{l1} \implies A_{i-2wall} = \pi\left(\frac{l_f}{2}\right)^2 sin\,(\theta)^2 \cdot \left[1 - \frac{1}{2}\left(2\,arccos\left(\frac{2u}{sin\,\theta}\right) - sin\left(2arccos\left(\frac{2u}{sin\,\theta}\right)\right)\right) - \frac{1}{2}\left(2\,arccos\left(\frac{2u}{sin\,\theta}\right) - sin\left(2arccos\left(\frac{2u}{sin\,\theta}\right)\right)\right)\right] \\ if\ \theta_{l2} \le \theta_{l1} \le \theta_i\ and\ u \le k \implies A_{i-2wall} = 2u \cdot 2h \end{cases} \tag{10-34}$$

If $h = 0.500$ and $u \to 0$, then the orientation factor takes the mean value of probability previously offered for the presence of one wall, $(2/\pi)$. In order to show the results and provide a better understanding, some of the intermediate situations have also been computed and the graphical solutions shown in Figure 10-22. With the aim of showing graphical solutions with significant visual information, the value of $h = 0.300 l_f$ was chosen. The reason was that in order to have the intersection point inside the reference circumference, there was a limit situation changing the sense of all those previously shown. That is to say, for the values of $u = h = \frac{1}{2\sqrt{2}}$, the intersection occurs in the circle described by the fibre. Subsequently, in order to provide better comprehension a lower value of h was chosen for the computed results and graphics of Figure 10-22.

Two walls probability distribution in several positions of the second and a fixed value $h = 0.300 l_f$

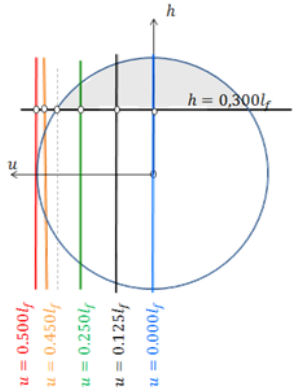

$h(\cdot\, l_f)$	$u(\cdot\, l_f)$	θ
0.300	0.500	**0.567**
0.300	0.375	**0.589**
0.300	0.250	**0.690**
0.300	0.125	**0.765**
0.300	0.000	**0.803**

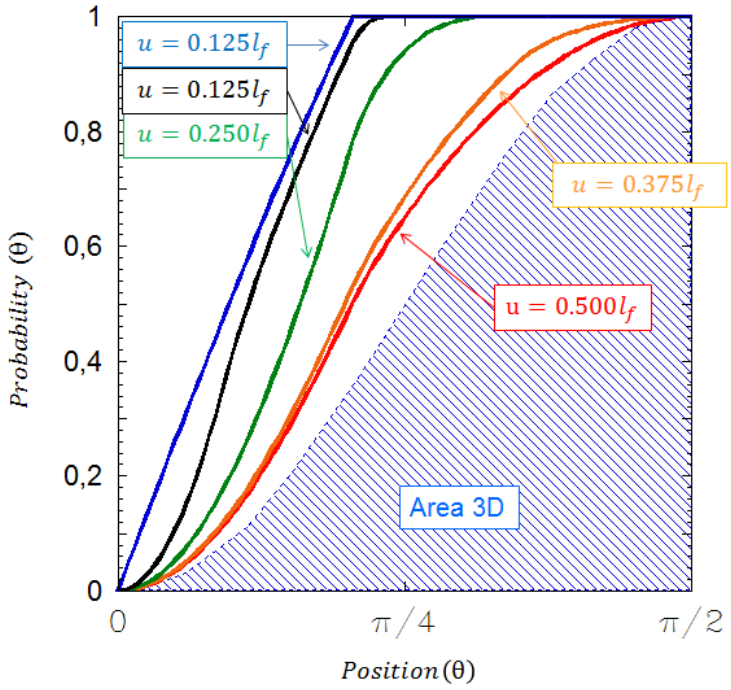

Figure 10-22: Probability distributions varying u and h fixed in 0.300 lf.

10.4.4 Orientation profile from the model

As may be observed in Figure 10-21, Figure 10-22 and Table 10-2, the values that the orientation factor take for a decreasing distance to the wall are continuously increasing up to the values obtained in the edges. That is to say, the profile of orientation factor that considers the presence of only one wall varies from 0.500 in the bulk to 0.637. In the case of the values of two walls when the first wall is considered in the edge, it would vary from 0.637 to 1.000. The reason for this is show the need of a curve in a certain position that provides the orientation factor. In order to fit the adequate function and develop predictive tools, performance of the graphical variation of the values is required. This is shown in Figure 10-23.

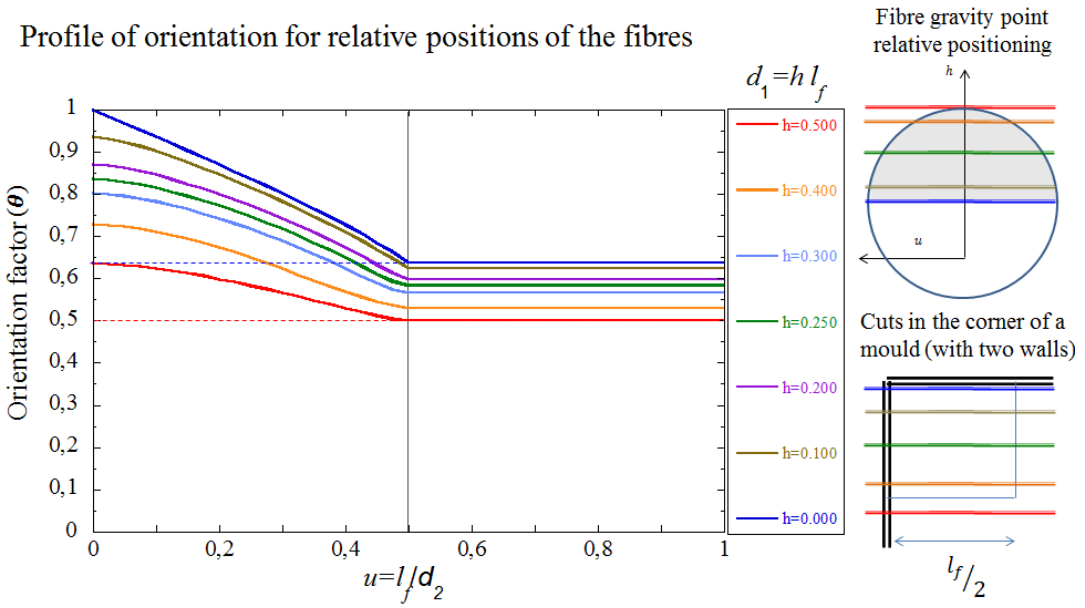

Figure 10-23: Profile of the value of the orientation factor as a function of the distance between fibre gravity point and the each of the two walls.

10.4.5 Non-rigid fibres: folding effect

The possible folding effects have been considered as a reduction of the sphere drawn by the fibre in the model. That is to say, the possible positions are the same but for a reduction of the projected fibres due to its own bending. In such a way, the expression needed has a geometrical relation with the cord (l_{fr}) of the circumference drawn by the fibre in each plane, as shown in Figure 10-19. The expression (10-35) relates the fibre length with the bend radius, with the probability of the reduction of the fibre being obtained for a maximum bending radius limited with half the fibre length. Expression (10-36) provides the projected length of the fibre for each curvature angle. The resulting reduction of probability is in the case of the average fibre having a length of 94.6% of the original length, as obtained by expression (10-37).

$$R = \frac{l_f}{2\varphi} \qquad (10-35)$$

$$l_{fr} = \frac{l_f}{\varphi} sin\,\varphi \qquad (10-36)$$

$$l_{fr} = \int_0^1 l_f \cdot \frac{1}{\varphi} \cdot sin\,\varphi \cdot d\varphi = 0.946 l_f \qquad (10-37)$$

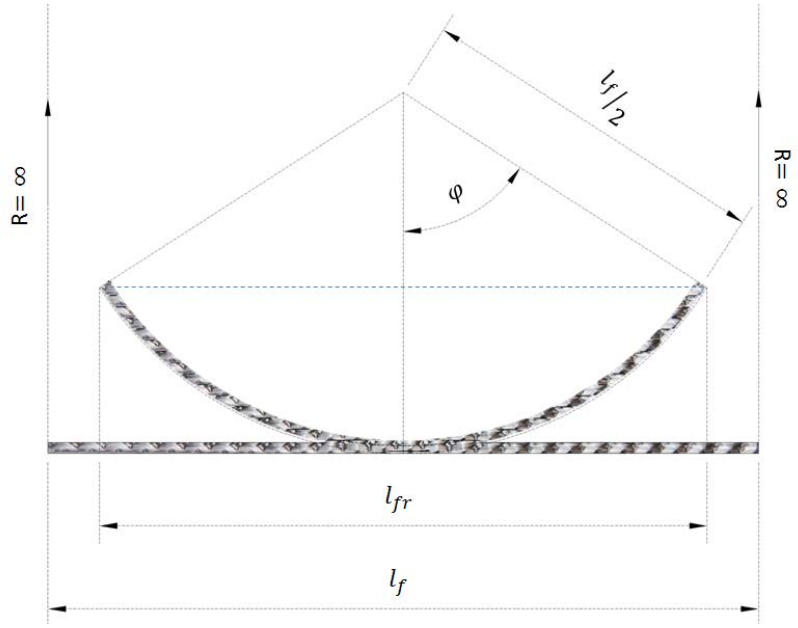

Figure 10-24: Fibre bending and reduction of its mean projection.

10.4.6 Fibres crossing a vertical plane and the influence of fibre length

One of the main purposes of this study has been to examine situations that may provide a number of fibres placed on a vertical plane of a prismatic laboratory sample made from fibre reinforced concrete. With such information, it would be possible to extrapolate results to structural sizes. The aim of the thesis is not only to provide a theoretical model but also to propose practical tools. This would allow assessment of the positioning of different fibre types of distinct materials or shapes. Thus, this model would predict the number of fibres that cross a vertical surface of the concrete element. In such a sense, it is worth noting that performing a counting exercise allows us not only to obtain the orientation factor but also to assess some other effects on the fibres. Such exercises can provide useful information, such as the fraction of fibres pulled out or broken, folded fibres or irregular accumulation, as shown in Figure 10-25 and Chapters 8 and 9.

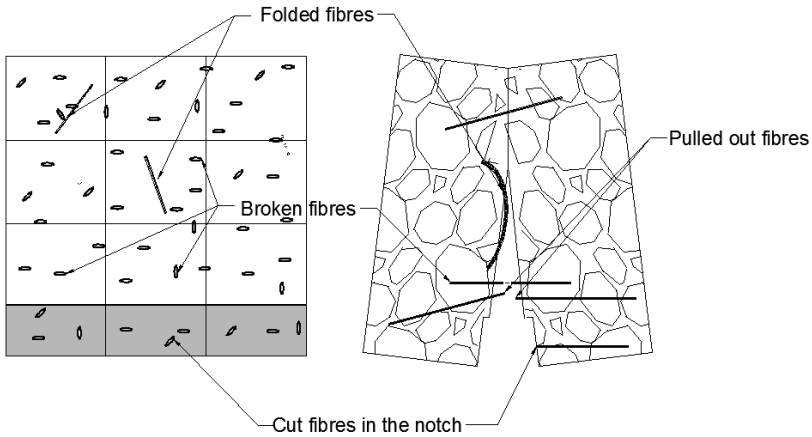

Figure 10-25: Other possibilities to be considered in a manual counting exercise.

Some of the most extensive counting methods have been reported due to the ease of performing them for steel and macro-polymer fibres (Di Prisco, et al., 2013; Barr, et al., 2003). In such a sense, the easiest way to perform the counting is to divide the fracture

surface after the mechanical tests in nine equal sectors apart from the notched area or, if the specimen has been divided into slices, the sawn surface into nine equal sectors. Since a wall effect influences the lateral bands closest to the moulds in a band of half the fibre length, the nine equal sectors are not always localized in a clear way. In any event, the corners and laterals would probably accommodate more fibres than the central part of the section.

Considering the surfaces of Figure 10-5 but not assuming the free surface as a wall, the resulting types of areas, $\theta_{isotropic}$ (θ_1), $\theta_{1wall}(\theta_2)$ or $\theta_{2wals}(\theta_3)$ are depicted in Figure 10-26(a). It should also be noted that if the free surface is not assumed as a wall, the concrete is not poured in the same position in which it is tested when hardened. It is rotated, as shown in Figure 10-26(b), with the position of the free surface being easy to localize if accurate results of the counting procedure are required.

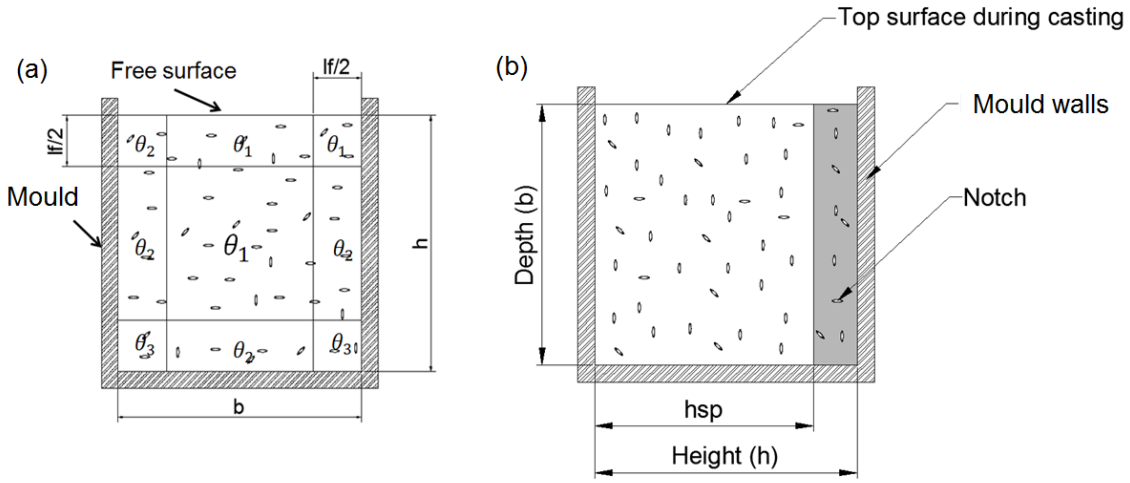

Figure 10-26: Sketch of the position of the free surface: (a) regarding the types of areas; (b) regarding the position of the notch for the mechanical tests.

Concerning the areas that Dupont and Vandewalle proposed in a previous reference (Dupont & Vandewalle, 2005), the computed results slightly vary and are close to the values proposed by Laranjeira (Laranjeira, et al., 2012). As can be seen in Figure 10-27, the theoretical values of the proposed model of the lateral bands of a width half of the fibre length are 0.578 instead of 0.600. In addition, for the corners affected by two walls, the model produces an average value of the square of size half the fibre length of 0.831 instead of 0.840. Aside from such differences, it should be noted that the experimental data reported in the references are also in accordance with the proposed model for steel fibres. This is important in terms of the validation of the model for such rigid fibres. With regard to polyolefin fibres, some additional experimental evidence is required in order to contrast the validity of the proposed factor.

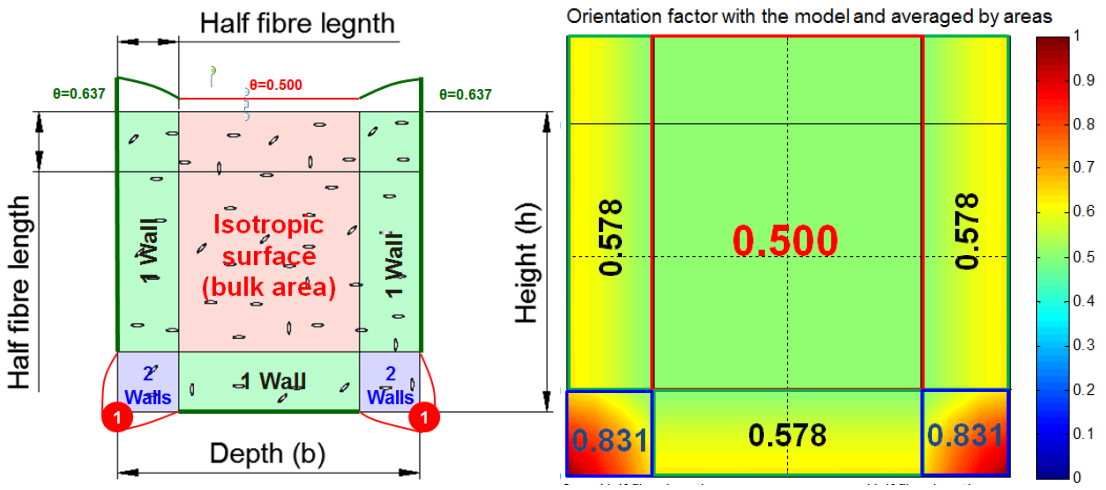

Figure 10-27: Theoretical areas of orientation factor: (a) Scheme of the sizes; (b) values obtained for the areas in the proposed model.

In order to provide practical tools, the two sizes of cross-sectional specimens placed on the test standards EN 14651, RILEM TC 162-TDF and ASTM C 1609 (ASTM C 1609/C 1690M-07, 2007) have been taken as an example. Those are the typical specimens for fracture tests with squared-cross-section sizes of 150 mm and 100 mm. In such a sense, one more evident factor should be chosen: the fibre length. The typical cases of 48 mm long and 60 mm long are polyolefin fibres and 35 mm long and 70 mm long are frequently used in steel fibres. In the case of specimens with 150x150 mm² squared-cross sections, a uniform distribution and orientation would lead to the results shown in Chapter 9 in Figure 9-2. In the case of the smaller beam of 100 mm² squared-cross sections and with one-third notches, the resulting percentage was shown also in Figure 9-4. These two sizes have been reported to enable assessment of the orientation factor in Chapters 4, 5, 6, 8 and 9.

An unnotched surface is that typically counted when the surface has been sawn. Hence, the division in nine equal sectors supplies a useful tool to assess the orientation factor. If Figure 10-29 and Figure 10-30 are analysed, it can be seen that the influence of the fibre length is clear, affecting the size of the areas that have improved orientation factors due to the existence of walls. Such boundary conditions, as previously stated, affect bands of half the fibre length, increasing its value of orientation factor. That is to say, the higher is the isotropic surface the lower is the overall orientation factor. As previously mentioned, the orientation factor is at the end of a non-linear continuously increasing function of the relation $l_f/specimen\ size$.This can be easily observed when comparing Figure 10-28 with Figure 10-29. The former represents a short fibre, 35 mm long, and a surface of 150x150 mm². With such dimensions, the isotropic surface is around 69% of the total surface. In the case of 60 mm long fibres and a smaller size of 100x100 mm², the isotropic area barely represents 28% of the total cross section as it can be seen in Figure 10-29. There is also some part of the isotropic surface in place in the notched surface that should be considered if the counting is carried out on a fracture surface.

Hence, the problem entails obtaining the orientation factor for each of the nine equal sectors that depend on the fibre length. In the unnotched surface, there are three general types of sectors: a central isotropic sector, corners affected by two walls and sides affected by one wall. The size of this area, either by one or by two walls, varies with the fibre length. The latter can be understood by analysing Figure 10-30.

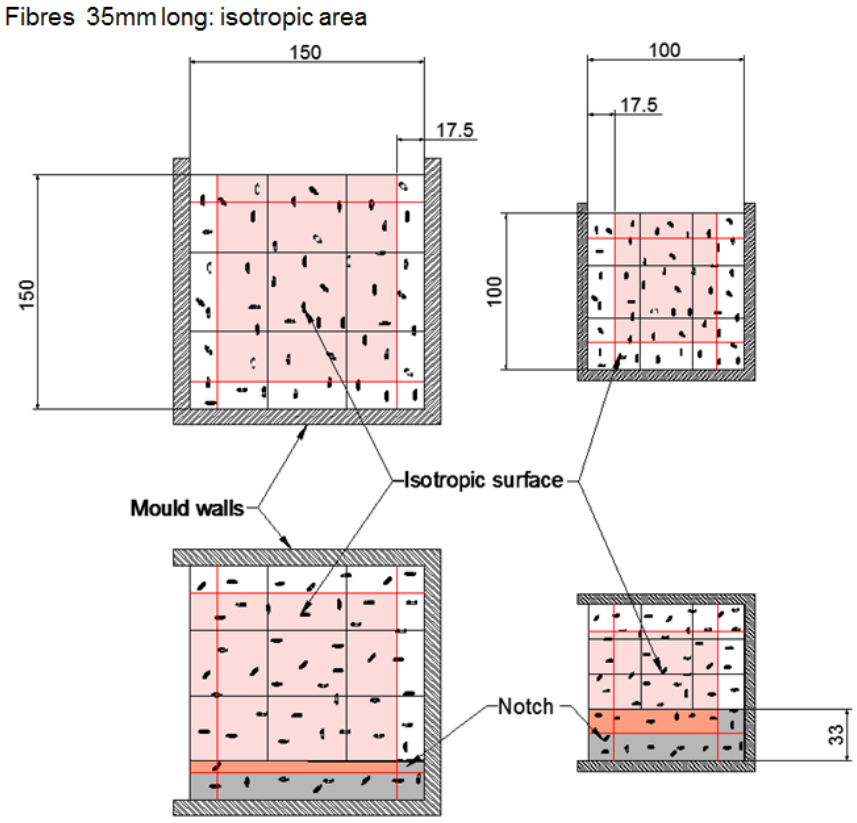

Figure 10-28: Isotropic surface in the surfaces of two specimen sizes for 35 mm long fibres.

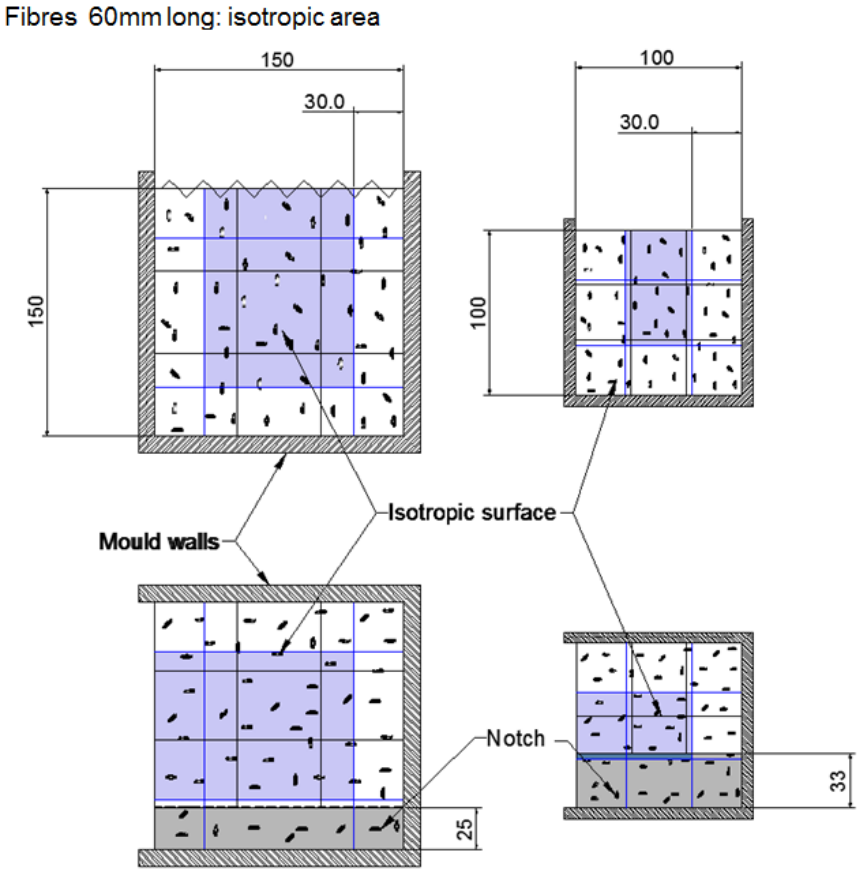

Figure 10-29: Isotropic surface in the surfaces of two specimen sizes for 60 mm long fibres.

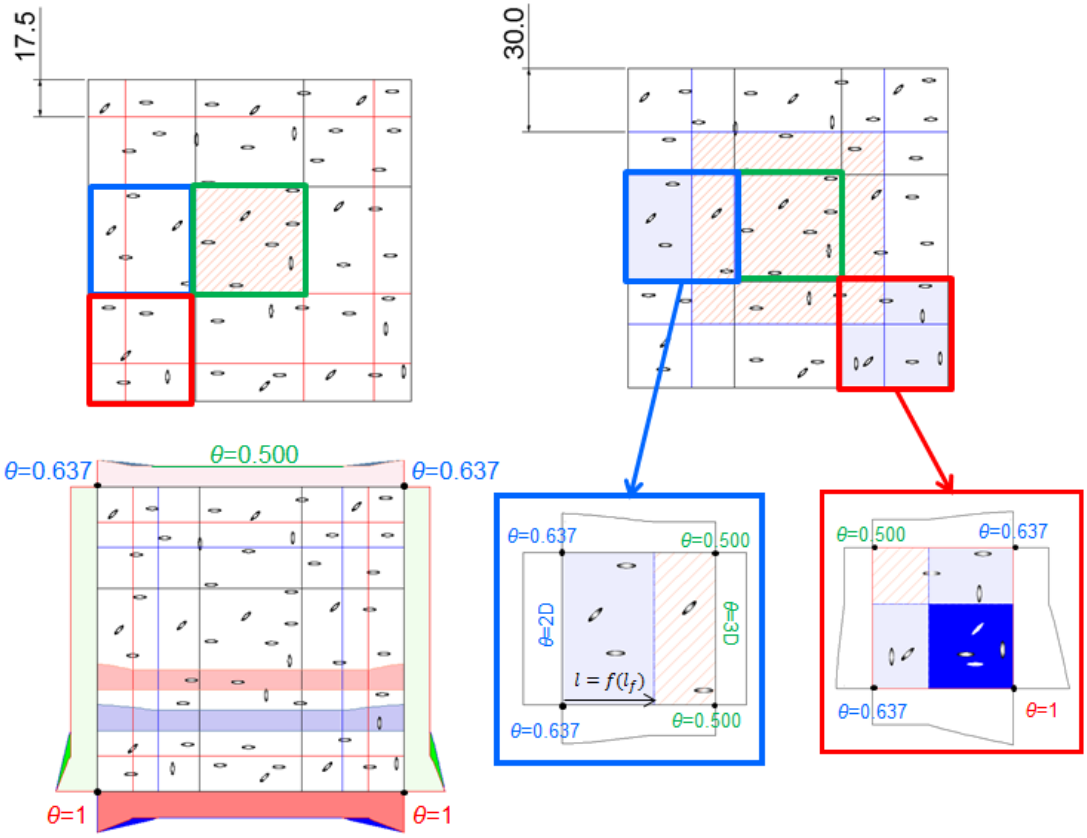

Figure 10-30: Scheme of the types of squares to be computed and the projection of the profile of the edges.

The computed results of the orientation factor in each of the nine equal sectors of a specimen with squared cross section of size of 150 mm² and for fibres 35, 48, 60 and 70 mm long are summarized in Figure 10-31. The overall orientation factor ranges from 0.532 to 0.574 for the longest fibres and show an increase of 7.8%. The differences are significantly more marked for the smaller size of 100 mm² of square-cross section, with the overall orientation factor varying from 0.552 for the shorter fibre to 0.627 of the longer one (13.7% higher). The latter can also be seen in Figure 10-32, as well as the more influence of the wall effect. It is worth noting that for 70 mm long fibres, even the central square is influenced by the surrounding walls, having a value of orientation factor up to 0.512. The same procedure can be used to achieve the orientation factor in the nine equal sectors of a notched beam, by considering the geometry to perform the limits of the numerical integrations and the average values. The results are placed in Figure 10-33 and Figure 10-34.

With the values of orientation computed, it is possible to achieve a number of fibres to be counted in each of the sector by fixing the fibre dosage and the cross-section surface of a single fibre. However, beyond such a simple and powerful possibility, a new concept appears that can be useful. Once the distribution of the orientation factor is not uniform, the number of fibres counted on similar surfaces would not be uniform either due to the orientation. That is to say, a uniform distribution would not lead to counting results such as those shown in Figure 9-2 and Figure 9-4 that are based on each proportional surface. In such a sense and for a sawn surface, the proportion of fibres in each of the equal squares if the distribution along and across the beam had been uniform would have had the

proportions shown in Figure 10-35 and Figure 10-36. These may be computed by means of expression (10-38).

$$\%Fibres_i = \frac{\theta_i}{9 \cdot \theta_{average}} \qquad (10-38)$$

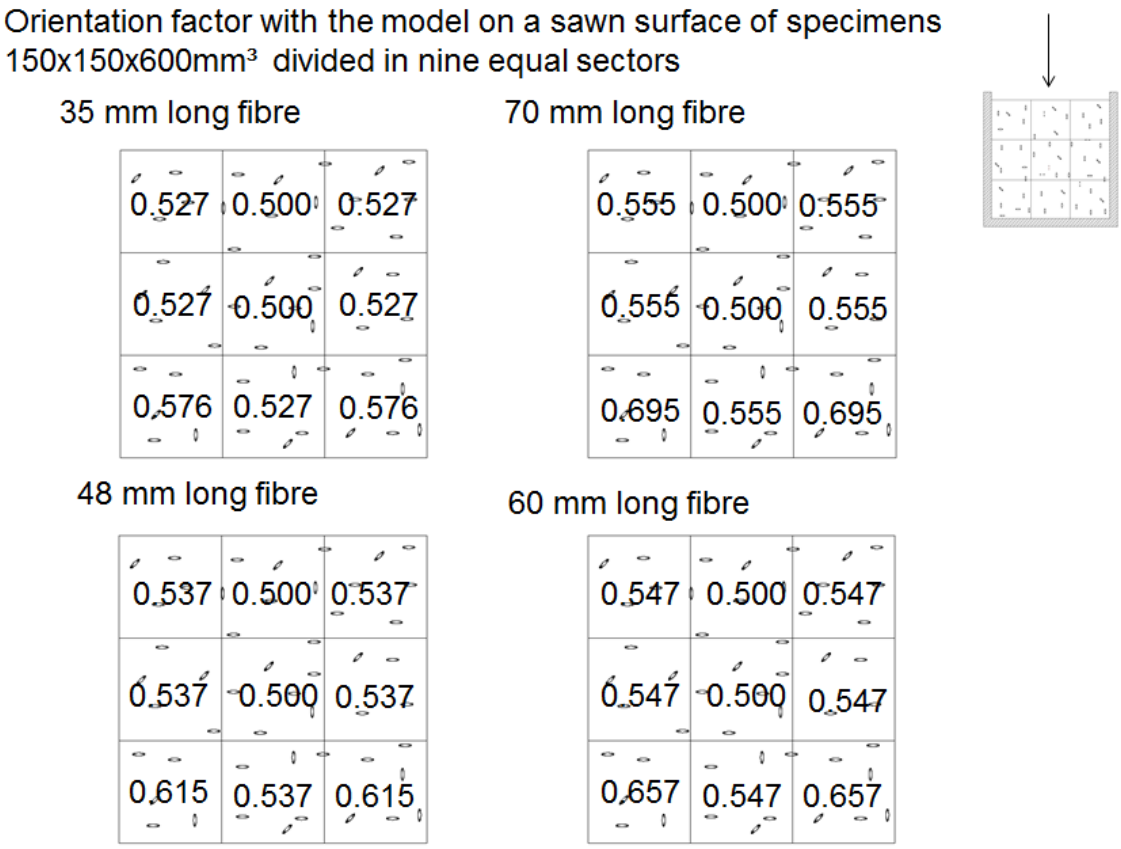

Figure 10-31: Theoretical orientation factor in each of the nine equal sectors of specimens of cross section size 150x150 mm².

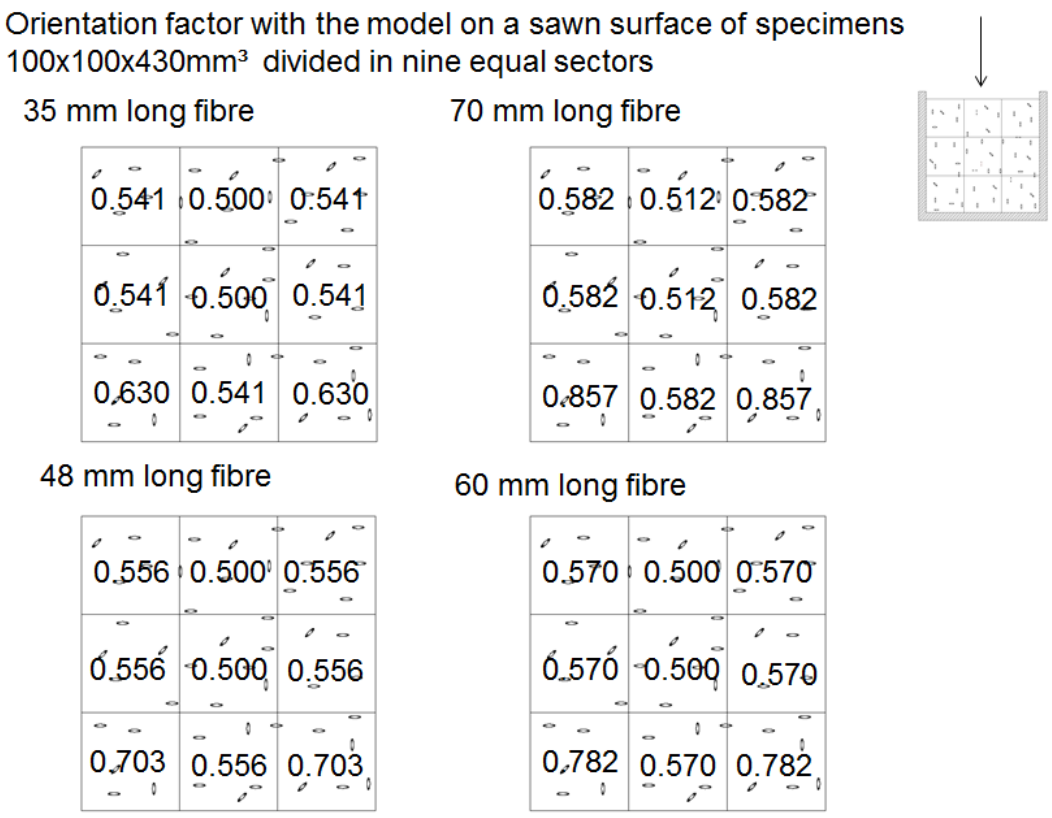

Figure 10-32: Theoretical orientation factor in each of the nine equal sectors of specimens of cross section size 100x100 mm².

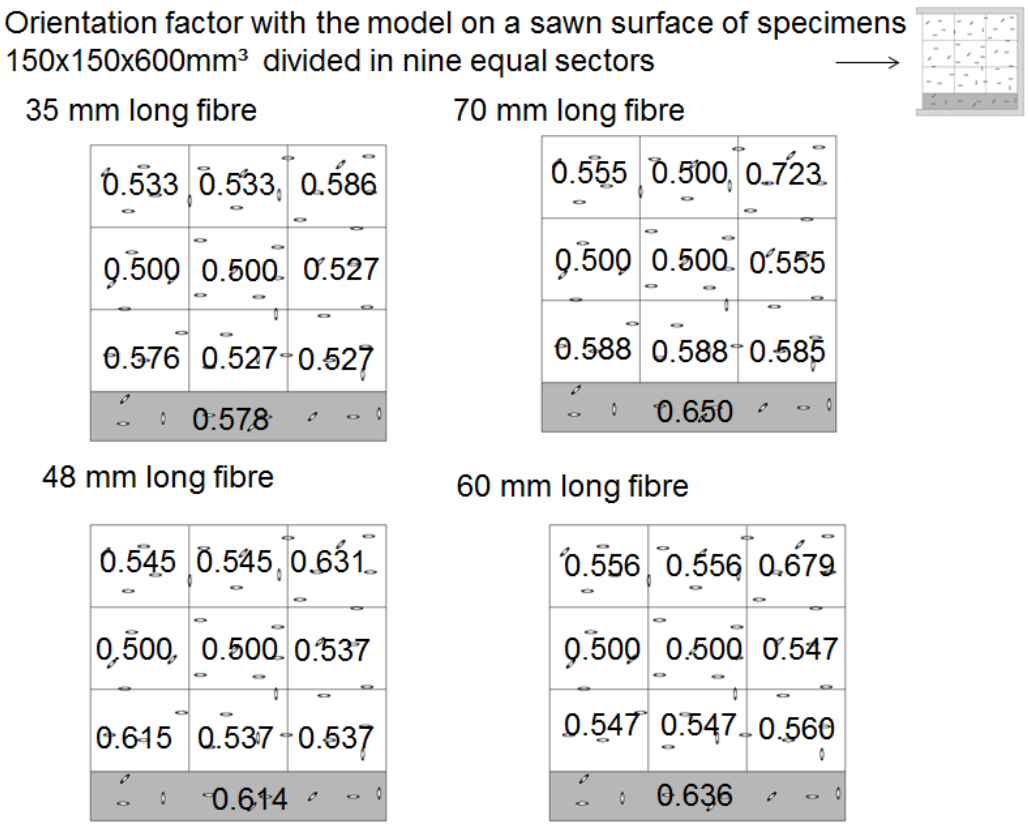

Figure 10-33: Theoretical orientation factor in each of the sectors of notched specimens of cross section size 150x150 mm².

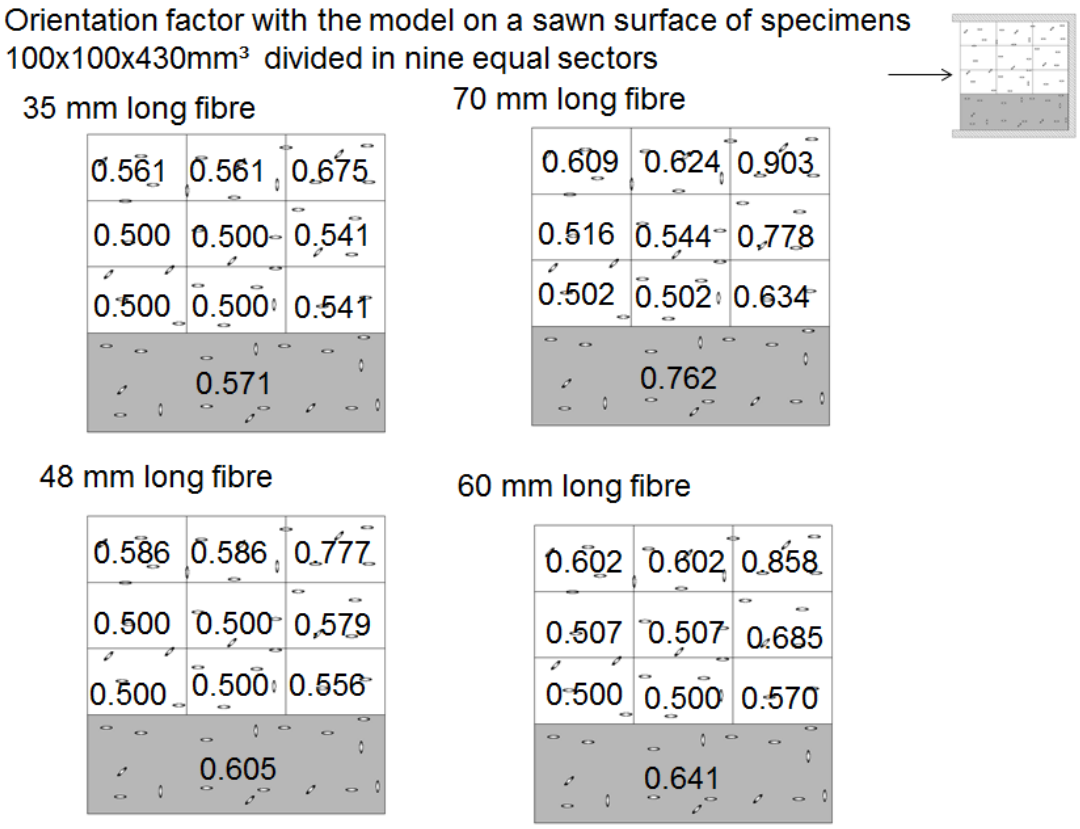

Figure 10-34: Theoretical orientation factor in each of the sectors of notched specimens of cross section size 100x100 mm².

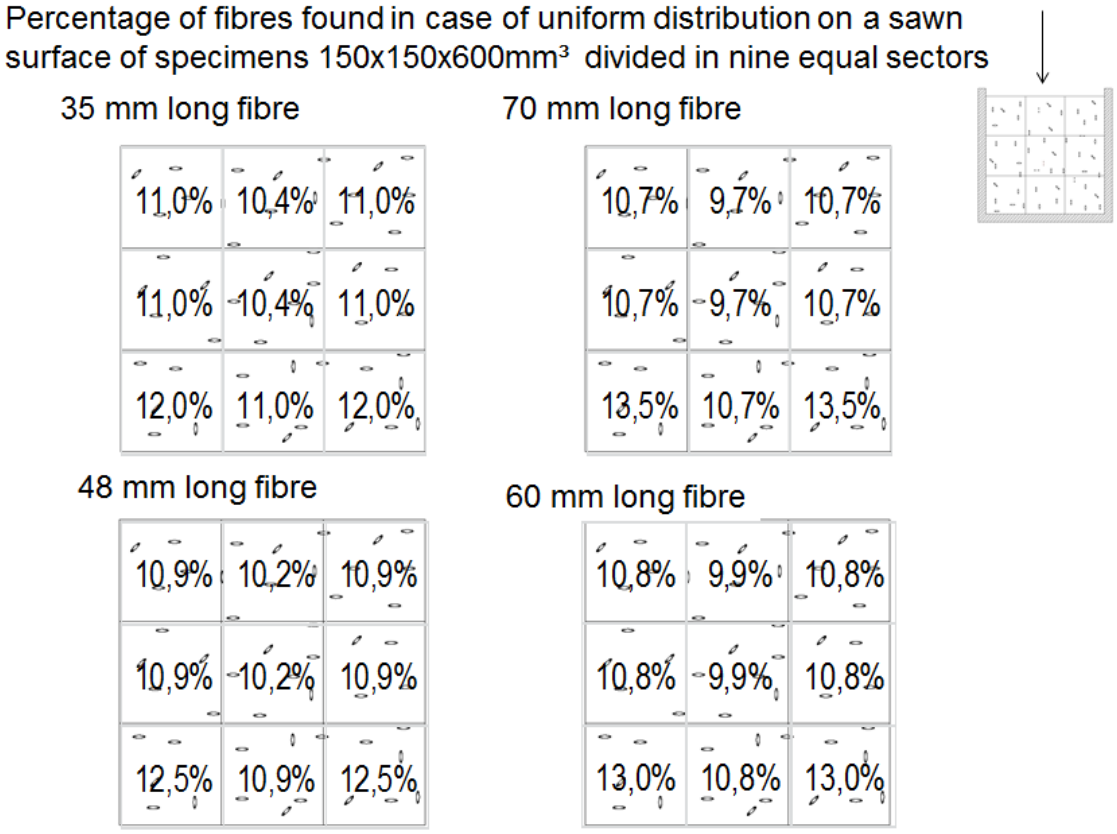

Figure 10-35: Percentage of fibres to be found in case of a uniform distribution and due to the orientation of the fibres on specimens of cross section size 150x150 mm².

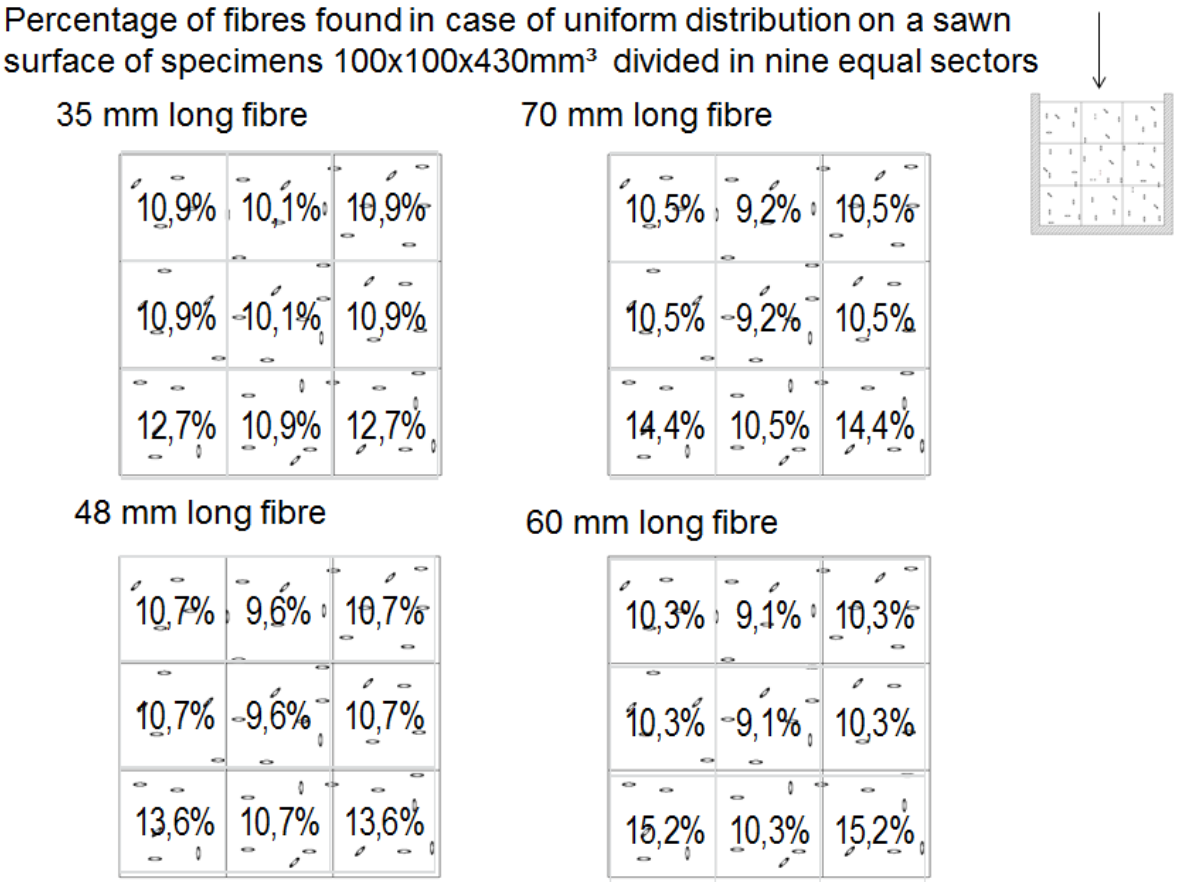

Figure 10-36: Percentage of fibres to be found in case of a uniform distribution and due to the orientation of the fibres on specimens of cross section size 100x100 mm².

In summary, a uniform distribution of the fibres across the cross-sectional surface and along the beam would lead to a non-proportional distribution of the fibres counted in equal squares, having an uneven percentage due to the distinct orientation of the sectors that are close to a wall or any other boundary condition. In addition to this, it is worth noting that the assumption of Laranjeira (Laranjeira, et al., 2012) establishes the value of the bulk in the case of SCC as being in the presence of one wall and thus idealizing the flux as taking place in a layer of fibre-length thickness.

10.5 Discussion and verification of the model

The variety of solutions, models and procedures to assess the orientation factor, makes it difficult to use reported experimental data to validate theoretical models. Even though this reveals the need of a standard procedure that would boost the possibility of sharing data, the values provided by using the presented model with regard to steel fibres can be validated with the data published in references (Dupont & Vandewalle, 2005; Di Prisco, et al., 2013; Barr, et al., 2003; Soroushian & Lee, 1990).

Dupont and Vandewalle (Dupont & Vandewalle, 2005) reported 107 examples, having an average value of the ratio calculated/experimental of 1.002. By using the presented model, all the 107 specimens were similarly computed and the results summarized in Table C-1 in

Appendix C. The ratio computed experimentally remained close, though on the conservative side at a value of 0.995 (and an analogous coefficient of variation of 35%).

With regard to the distribution of the fibres in a sawn surface, the results described by one reference (Barr, et al., 2003) provide percentage distributions that mark the main issues of Figure 10-32 and Figure 10-33, confirming that it is not advisable to consider the top surface during casting as a boundary. This is not so clear with the data reported by Soroushian and Lee (Soroushian & Lee, 1990), given that they divided the section into two columns instead of three which may reduce the effect. In any case, given that the top surface had a mean orientation factor of 0.608 and the bottom part of the section had 0.673, it may not be possible to assume the top surface as the existence of a wall. Moreover, the mean value of the experimental measurement of the orientation factor was 0.617. The model proposed by the above mentioned authors provided a theoretical orientation factor for the elements of 0.537, with it being clearly further from than the proposed model which would have a mean value would be 0.548 with a fibre 51 mm long.

The research reported by Di Prisco, Colombo and Dozio (Di Prisco, et al., 2013) provides an interesting evaluation of the model because of the significantly distinct conditions and sizes. They counted the fibres by dividing beams with a 300x300 mm² square cross-section into nine equal sectors. In such a size and fibre type (hooked-end steel fibres 60 mm long), the theoretical orientation factor would be according to the proposed model 0.527 and the experimental would be lower at 0.424. Nonetheless, the distributions of the fibres were not clear either. This leads to the conclusion that the models might not be reliable when fibre length is smaller than three or four times the size of the formwork. Larger structural sizes in which the distribution of the fibres are not clearly affected by a wall or a flux direction may have lower orientation factor than that assumed in the literature for an isotropic situation. In addition, for smaller sizes of 100x100 mm² square cross-section, and when using SCC with steel hooked-fibres 35 mm long, the experimental data in Chapter 6 provided an average orientation factor of 0.590. Computation of the orientation factor with the proposed model, with the assumption of the bulk zone, as having a boundary condition due to the flux (0.578 in the central sector) gives 0.593.

Regarding synthetic fibres, validation has been made in Chapters 4, 5, 8 and 9. In such a sense, the factor that affects the fibre length obtained by means of expression (10-37) was initially set on 0.946. With such a value, the ratio computed over experimental number of fibres counted takes a value 1.009. Since the value of the projected chord required verification, it was possible to pitch the limits of the integration placed in expression (10-37). The value of the projected folded fibre, $l_{fr,}$, that fits the model was 0.856, as shown in Appendix C with all the experimental data and computed values used for the validation of the model. Hence, with a slight change in the upper limit of the folding angle, the present model permits the use of a single factor to predict the number of fibres to be counted in a vertical surface of a beam made with fibre-reinforced concrete. The limit for a maximum curvature radius that fits the model was 0.895 radians. Therefore, this change in expression (10-40) would be that presented in expression (10-39).

$$l_{fr} = \int_0^{0.895} l_f \cdot \frac{1}{\varphi} \cdot sin\,\varphi \cdot d\varphi = 0.856 l_f \qquad (10-39)$$

One more validation may be of interest regarding synthetic fibres: the percentage of distribution in nine equal sectors counted. Figure 10-37 shows the results obtained in Chapter 9 for the sawn surface, which detailed counting results and which are also provided in the last two rows of Table C-2 of Appendix C. The table shows the mean experimental distributions of fibres in 20 surfaces with a 150x150 mm² square cross-section produced with PFRC with 6 kg/m³ polyolefin fibres 60 mm long. If compared with Figure 10-31, the theoretical approach and resemblance also confirm that the top surface, for synthetic fibres, does not behave as if a boundary existed.

PFRC with 6 kg/m³ of 60mm long polyolefin fibres

Mean distribution of fibres in VCC			Mean distribution of fibres in SCC			Theoretical distribution of fibres		
11,20%	11,20%	9,50%	10,70%	10,20%	12,70%	10,80%	9,90%	10,80%
11,30%	10,00%	11,00%	10,20%	9,90%	10,20%	10,80%	9,90%	10,80%
13,70%	10,50%	11,60%	12,30%	11,10%	12,70%	13,00%	10,80%	13,00%
(a)			(b)			(c)		

Figure 10-37: Mean experimental distributions of fibres in 20 surfaces with 150x150 mm² square cross-section produced with of PFRC with 6 kg/m³ polyolefin fibres 60 mm.

10.6 Conclusions

This chapter has reviewed the existing models and proposed a new calculation method to assess the orientation factor. The achievement of the orientation factor is useful in order to predict the number of fibres that cross a vertical section. In this regard, the review of the previous models has allowed an initial validation of the model for rigid fibres. Moreover, the most accepted values for the orientation factor in distinct positions of an isolated fibre inside the concrete were fully complied with by the results obtained by means of a numerical integration.

The model allowed the study to prepare curves with the profile of orientation when one and two walls affect the fibre positioning as a function of the relation of the fibre length and the distance to a wall. Additionally, with the shape of the curves obtained, it was possible to perform a curve fitting procedure a curve for such profile was proposed.

One additional proposal has been made with the aim of fitting the model for synthetic fibres that may fold. It should be noted that the use of such a type of fibres did not allow a direct use of the precedent models. In such a sense, this study proposed using a reduction factor based on the projected chord of a bent fibre. Although wider research on this matter would

provide reliability, due to the typical scatter of fibre reinforced concrete, the proposed concept of reducing the overall fibre length by a bending factor would appear to be suitable.

In order to provide tools that may enhance the use of fibre-reinforced concrete, tables and figures with the most common fibre lengths in practice have been built and validated. Since the fibre orientation varies within the relative position of the fibres across the section, it was found that a uniform distribution of the fibres did not match a proportional distribution that only considered the portion of surface. That is to say, a uniform distribution of the fibres on the cross-sectional surface and along the beam would lead to a non-proportional distribution of the fibres counted in equal squares, having an uneven percentage due to the distinct orientation of the sectors that are close to a wall or any other boundary condition. The values of such uniform distributions were computed and are also provided.

The model presented in this study permits comparison of the number of fibres predicted to cross a vertical plane with the most common structural fibres and lengths. Beyond such a possibility, it allows this to be done for non-rigid fibres. Moreover, it is a powerful tool gathered with the developed distribution tables also presented to evaluate the behaviour of new types of fibres or shapes in research. This also applies to the assessment of the influence of the placing conditions, pouring methods and rheological properties of the concrete in the final positioning of the fibres. In summary, this achieves not only a more reliable use of the fibres but also provides a valid and sound measurement base.

Chapter 11

Constitutive relations and numerical simulation of polyolefin fibre reinforced concrete

11.1 Introduction

Based on the post-cracking response of the experimental results of PFRC, it is possible to perform an inverse analysis and hence obtain the parameters that define the material behaviour. That is to say, it is possible to fit experimental data with an iterative method and numerical simulations by using either a smeared crack approach or cohesive crack approach. Should uni-axial tensile tests be used, the stress-crack width relation can be directly obtained. However, the three-point bending test is considered the standard test method and the residual strength obtained provides the reference values for structural design for both service and ultimate limit states. These issues have been discussed in previous chapters concerning structural requirements of codes and recommendations (CNR-DT 204, 2006; ACI Committee 544, Reapproved 2009; Fédération Internationale du Béton fib/International Federation for Structural Concrete, 2010; EHE-08, 2008; EN 14889-2, 2008) and their corresponding standardised tests methods (ASTM C 1609/C 1690M-07, 2007; EN 14651:2007+A1, 2007; RILEM TC-162-TDF, 2002). Inverse analysis approaches from bending tests have been previously performed to assess the constitutive relations of SFRC (Kooiman, et al., 2000), though there is a lack of published research on this matter for polyolefin macro-fibre reinforcement of concrete.

In this chapter, an inverse analysis is performed with the aim of fitting the constitutive relations from the experimental tests performed in Chapter 4. With such experimental data, it was possible to obtain the influence of fibre dosage in the constitutive relations. The numerical simulations were performed by using the finite element method (FEM) with a numerical procedure based on the cohesive model already tested for plain concrete or brickwork masonry (Sancho, et al., 2007; Reyes, et al., 2009).

With an assumed tri-linear constitutive diagram, it was possible to fit the numerical results with the mean experimental fracture curves of PFRC reinforced with contents of 3, 4.5, 6 and 10 kg/m³ of 60 mm long polyolefin fibres. The experimental curves used for the inverse analysis were those presented in Chapter 4. Moreover, the positions of the turning points of the constitutive relations have been explained from material parameters and some of the assumptions validated by means of additional experimental data for which procedure and significance are detailed below.

11.2 Numerical calculations

The use of the cohesive crack model proposed by Hillerborg (Hillerborg, et al., 1976) to approach the fracture behaviour of quasi-brittle materials has obtained successful results for concrete-like materials, as shown in (Cendón, et al., 2000). It requires the definition of a softening function as a material property that relates the stress across the crack σ with the crack opening w. Hillerborg later extended his proposal to fibre reinforced concrete (Hillerborg, 1980). It was also shown as a suitable model in assessing the fracture behaviour of anisotropic materials such as brickwork masonry (Reyes, et al., 2009; Gálvez, et al., 2013). In such a sense, the use of embedded crack models has allowed analysis to be performed in which the need of a tracking algorithm is avoided which permits the finite element to adapt itself in the stress field as long as crack opening remains under a small threshold (Sancho, et al., 2007). These elements have the crack embedded on them and FEM simulations have been performed. The main assumptions and the mathematical description of the model are described in detail in such published research.

In the case of the present work, the model previously described has been implemented in ABAQUS by using the subroutine UMAT and an auxiliary external file with the coordinates of the nodes and elements. When the crack remains null, $w = 0$, the element behaves elastically. Once the tensile strength is exceeded, the crack is introduced perpendicularly to the direction of the maximum principal stress. In such a situation, the computational procedure avoids the formation of quasi-orthogonal cracks and the crack adaptation at the element level fixes a crack direction with no further adaptation. Previous works have shown that these procedures bear resemblance to other work in avoiding crack locking (Reyes, et al., 2009).

11.3 Building a constitutive relation for PFRC

Hence, this chapter will adapt the already tested procedure with ABAQUS and the UMAT subroutine to the behaviour of PFRC. In such a sense, the non-linear fracture process zone emerges in the elements placed on the crack. The behaviour of the cohesive elements depends on a constitutive relation that needs to be iteratively fit. However, such softening curves need to be defined from a guessed initial shape. In this case, a tri-linear softening curve was chosen because there was a reloading branch in the fracture results, as explained in previous chapters. Figure 11-1 shows a finite element deformed mesh for modelling specimens of PFRC during a three-point bending test and after cracking.

The aim of this work was also to assess the building of the composite constitutive material model from the individual and separate contribution of concrete and fibres. The concept has been previously examined and can be better understood by observing Figure 3.54. In order to verify that some of the processes were actually taking place, one prismatic specimen of size 430x100x100 mm³ made with the same concrete as that examined in Chapter 4 and 10 kg/m³ (SCC-PFRC-10) was pre-cracked in the same configuration of the bending tests. After the crack had developed the sample was tested (the curve resulting is shown in green in Figure 11-2). The results obtained from plain concrete were added to those from the pre-cracked specimen. The figure shows an evident resemblance to the real test.

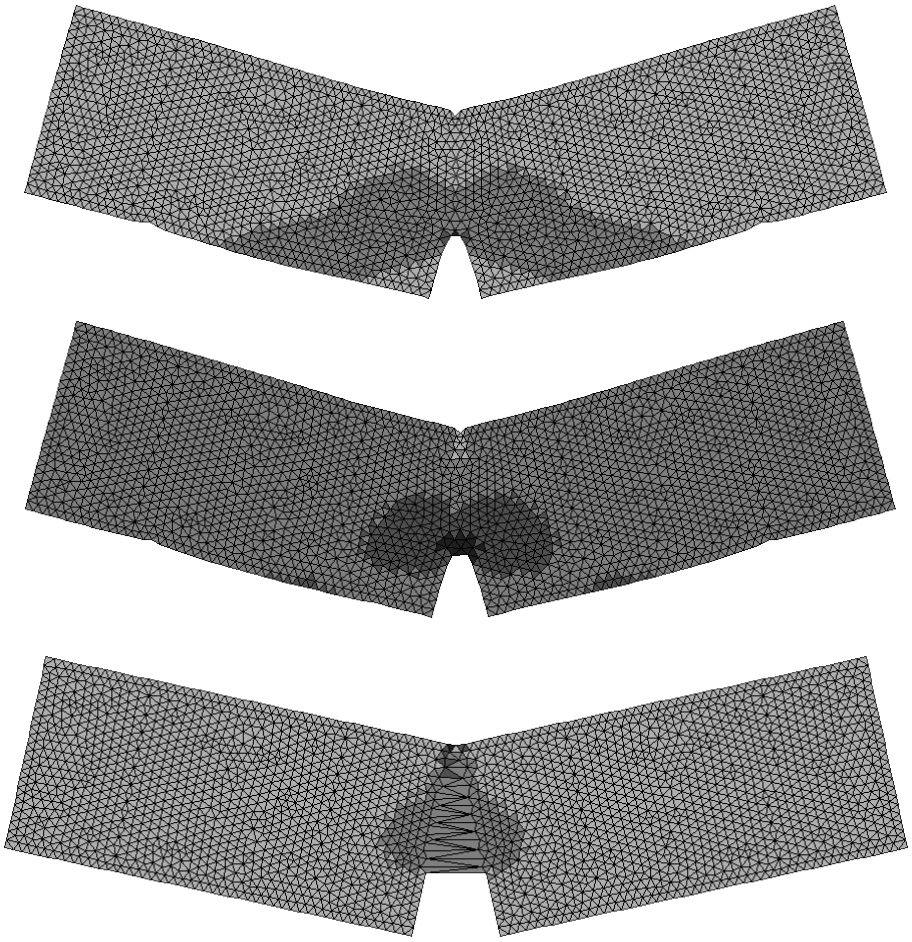

Figure 11-1: Finite element deformed mesh for modelling specimens of PFRC in three-point bending tests: three deformation stages.

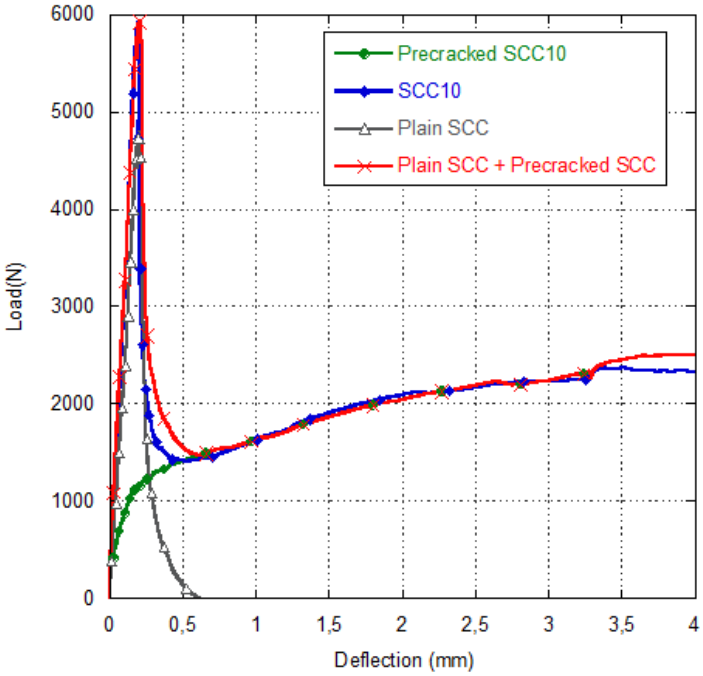

Figure 11-2: Individual contributions of concrete and fibres.

In order to obtain the stress-crack relation of the plain concrete, the classical material parameters were used in the numerical calculations. The modulus of elasticity (E) of the composite material is necessarily and directly related to the initial slope of the initial elastic branch. The tensile strength (f_{ct}) sets the stress in which the element cracks and hence defines the point at which the subroutine starts computing. These parameters were not significantly influenced by the presence of fibres and were kept constant for all the fibre dosages with the values shown in Table 11-1. An exponential softening curve of the plain concrete was assumed following expression (11-1) from (Bazant, et al., 1997)**.** Therefore, one additional material parameter of plain concrete was needed: fracture energy (G_F) which is also shown in Table 11-1.

$$\sigma = f_{ct}.e^{\left(-\frac{f_t \omega}{G_F}\right)} \qquad (11-1)$$

Table 11-1: Material properties used for the numerical simulations.

Material	Property	Unit	Value
Concrete	Modulus of elasticity (E)	GPa	30
	Tensile strength (f_{ct})	MPa	3.48
	Fracture energy (G_F)	N/m	130
Fibres	Tensile strength (σ_y)	MPa	376
	Orientation factor (θ)	-	0.60
	Pulled-out fibres at L_{REM}	%	42

Concerning the contribution of fibres, there were two key points to be considered and fitted with the test results. The first one was the minimum value reached by the softening curve after cracking, directly related to L_{min} of previous chapters and shown in Figure 11-3 as C_{min}. Following the same rational, the remaining strength of the material was related to L_{REM}. Hence, the turning point at which the post-cracking material behaviour reached its maximum strength was named C_{REM}. In order to compute the complete constitutive relation, it was necessary to mark an end to the strength and define point C_F. Figure 11-3 shows a schematic view of the points and the final shape of the softening curve.

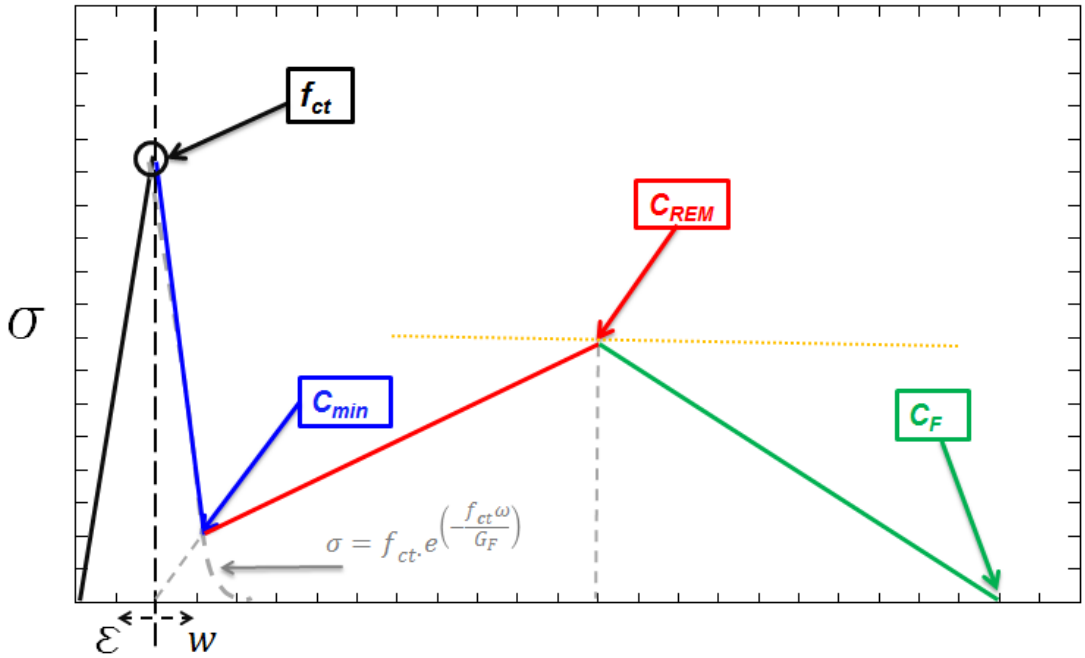

Figure 11-3: Sketch of the shape and position of the turning points of the constitutive relations for PFRC.

The coordinates of C_{min} were considered to be linked to the initial slope of the fibre contribution and fibre dosage. The intersection with the exponential softening curve of concrete, with a straight line passing through the origin of w and forming a certain angle function of the volume fraction, would define such a point. In the case of C_{REM}, the coordinates were linked to fibre dosage and the number of fibres pulled out at such a deformation or position, orientation factor and tensile strength of the fibres. The fibre properties considered in the numerical simulations were also included in previously shown Table 11-1.

11.4 Numerical results and discussion

The numerical calculations were performed by using the values of the singular points shown in Table 11-2. These values allowed the load-deflection curves to be obtained (the numerical simulations can be seen in Figure 11-4, Figure 11-5, Figure 11-6 and Figure 11-7). As can be observed, the results accurately reproduce the laboratory results of Chapter 4.

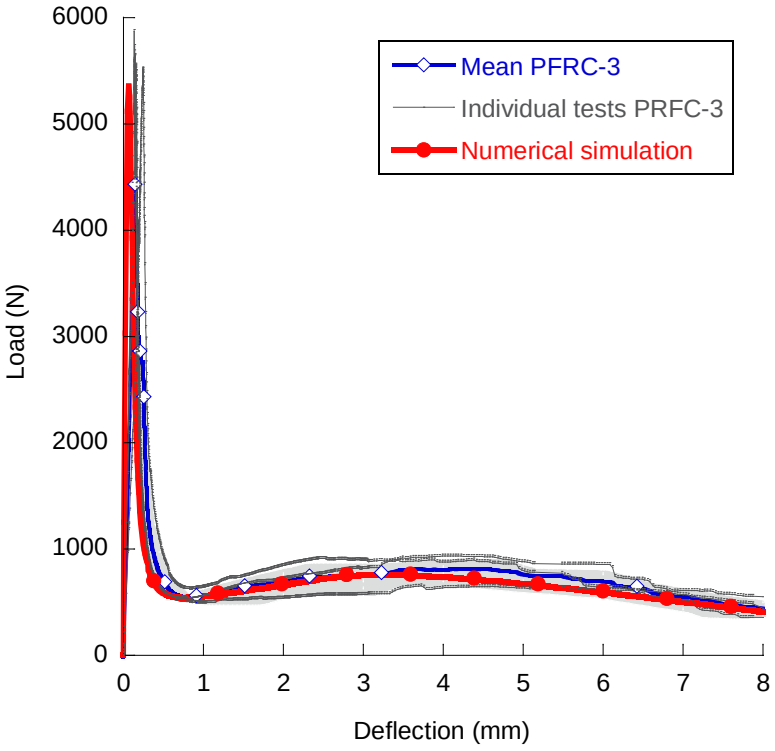

Figure 11-4: Envelope of the experimental records, mean fracture result curve and numerical simulation curve of PFRC with 3 kg/m³ of polyolefin fibres.

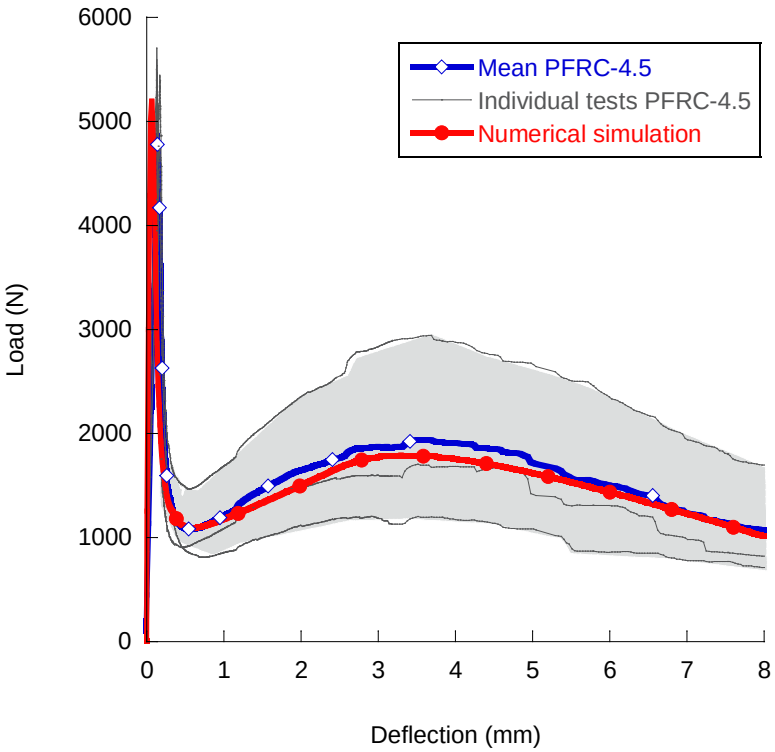

Figure 11-5: Envelope of the experimental records, mean fracture result curve and numerical simulation curve of PFRC with 4.5 kg/m³ of polyolefin fibres.

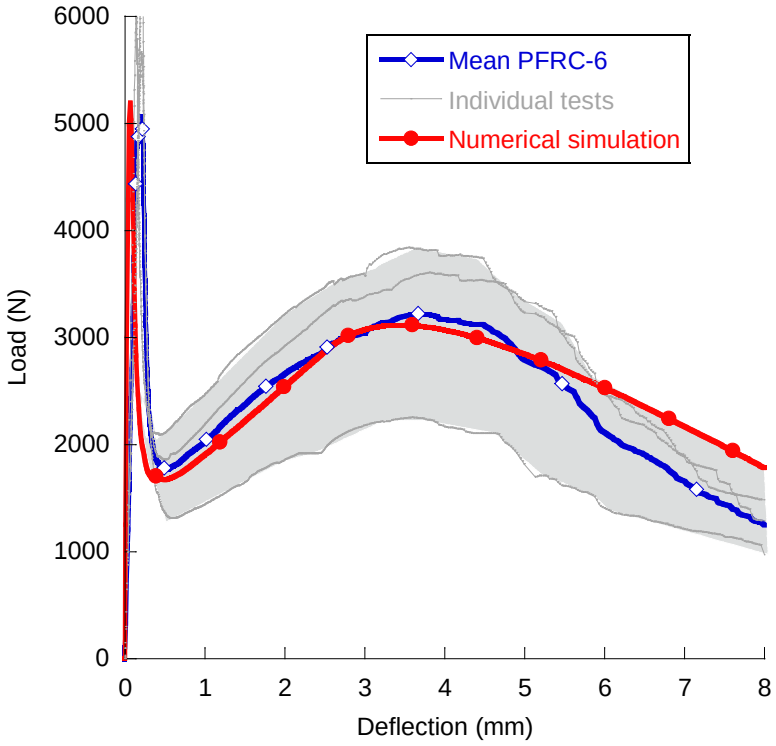

Figure 11-6: Envelope of the experimental records, mean fracture result curve and numerical simulation curve of PFRC with 6 kg/m³ of polyolefin fibres.

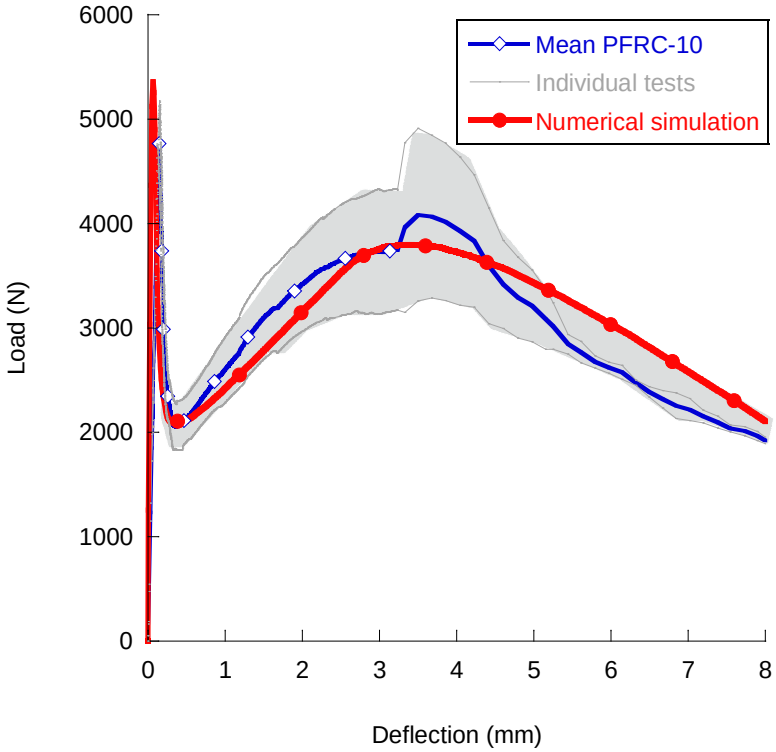

Figure 11-7: Envelope of the experimental records, mean fracture result curve and numerical simulation curve of PFRC with 10 kg/m³ of polyolefin fibres.

The values of the parameter for the numerical simulations can be seen in Table 11-2. Analysis shows that the angle of the initial slope increases with the fibre dosage, as can also be observed in Figure 11-8. However, both the figure and the table show that the crack opening for C_{REM} remains constant for all the PFRC content values. A stress-rise only took place with the increasing of volume fractions, reaching the maximum value for PFRC-10.

Table 11-2: Position of the turning points for the numerical simulation.

	C_{min}			C_{REM}		C_F (σ=0)
Concrete	w(mm)	σ(MPa)	Angle (rad)	w(mm)	σ(MPa)	w(mm)
PFRC-3	0.12	0.14	0.88	2.25	0.28	7.5
PFRC-4.5	0.09	0.28	1.25	2.25	0.68	7.5
PFRC-6	0.08	0.43	1.39	2.25	1.20	7.5
PFRC-10	0.07	0.57	1.45	2.25	1.45	7.5

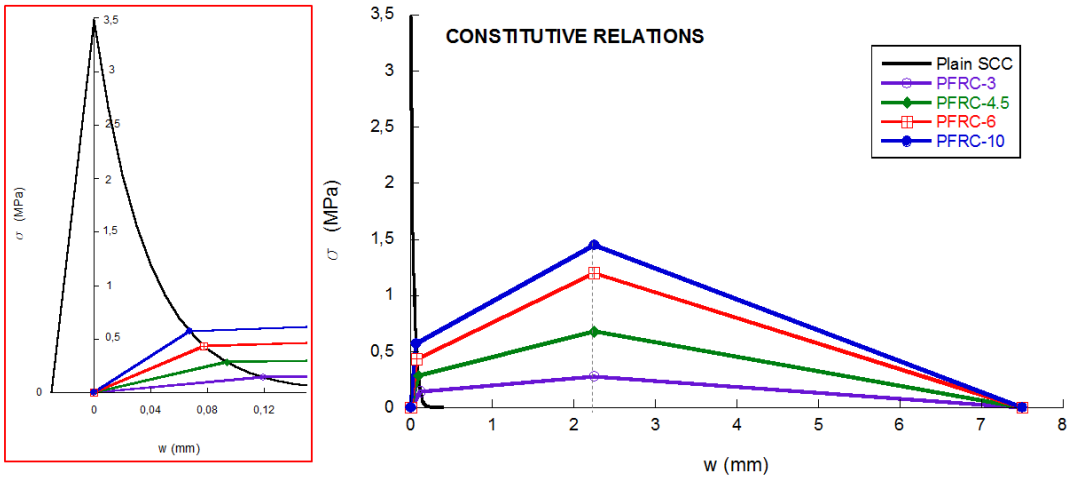

Figure 11-8: Constitutive relations for PFRC with fibre contents of 3, 4.5, 6 and 10 kg/m³.

With the values obtained of C_{min}, it is possible to fit the evolution of the angle with fibre dosage. In order to do so, the angles were plotted versus fibre dosage and the best fit was found for an exponential formulation shown in expression (11-2). The plot is shown in Figure 11-9. The linear fit could be adequate in terms of error (R^2 was equal to 0.87 for a linear fitting). Nevertheless, it was considered that such a type of linear function did not fully represent the physical phenomenon. The initial slope of the curve in Figure 11-9 indicates that a slight increase of volume fraction with small amounts of fibres means a significant increase in the angle of the straight line to assess C_{min}. For higher dosages of fibres, the increase in the slope was only slightly affected. This made sense, given that it is clear that the maximum angle that could result would be $\pi/2$ close to the value reached for 10 kg/m³ of polyolefin fibres (V_f=1.10%) of 1.45 radians. With this angle, it is possible to compute the intersection on the straight line with such a slope and the softening curve of plain concrete. The latter intersection is in the coordinates of C_{min}.

$$Angle = -3.6046 + 5.0625 \cdot (1 - e^{-6.55 \cdot Vf}) \implies R^2 = 0.99996 \qquad (11-2)$$

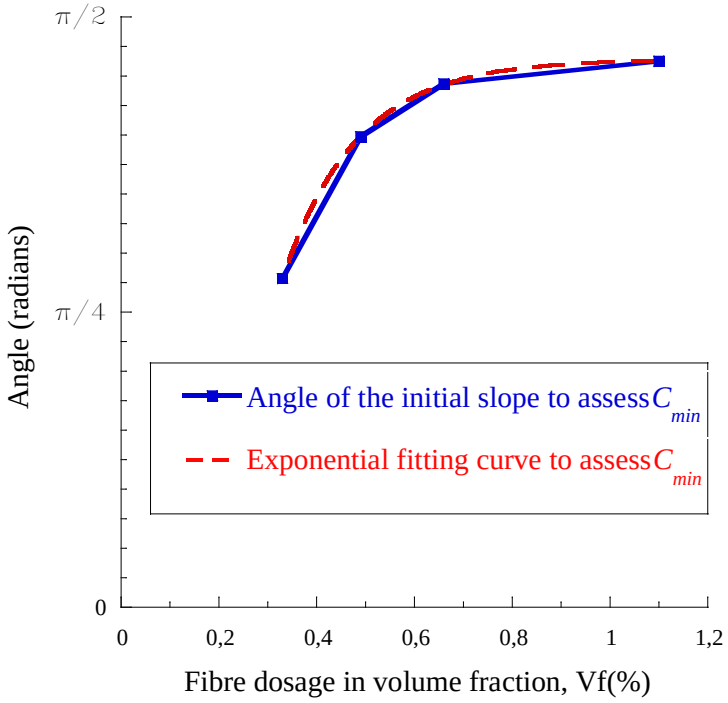

Figure 11-9: Angle of the line of initial fibre post-cracking contribution to assess the value of C_{min}.

Regarding the assessment of C_{REM} coordinates, the values of crack opening were equal to 2.25 for all the concrete formulations as mentioned above. Although the fibre dosage affected the stress values, the deformation state at which the fibre failure took place was constant. This was in accordance with the experimental results and conclusions of previous chapters. Furthermore, it also agrees with the assumption of fibres failing for certain equal deformations for a fixed fibre length. With these values it is possible to compute the reference length (l_{ref}), explained in Chapter 3, that relates the crack opening with the strains of the elastic branch by expression (11-3). In the expression (11-3), ε_u is the ultimate elastic deformation that was considered 0.012 and ε_{uf} is the ultimate elongation of the fibre set to 0.10 (10%). With such values and 2.25 mm of w, the reference length, l_{ref}, becomes 25.6 mm. This was in accordance with most of that reported in literature: approximately half fibre length (or the height of the ligament) or close to one third of the depth of the specimen (see sub section 3.7).

$$\varepsilon_{uf} = \varepsilon_u + \frac{w}{l_{ref}} \qquad (11-3)$$

The stress values were assumed as being related both with the fibre dosage and the number of fibres crossing the fracture surface. Therefore, a fibre orientation factor *(θ)* was introduced to reduce the volume fraction considered. The use of θ as a parameter, in order to consider the orientation factor, would allow fitting of the presented constitutive model to some other type of concrete or pouring method.

Before that reduction was made, the proportional number of fibres considered pulled out was also subtracted. This was done under the assumption that for the deformation state of the point C_{REM}, fibres would be pulled out. Assuming that fibre length has a significant influence on the number of fibres pulled out, as shown in Chapter 9, this factor can be used to fit some other fibre lengths.

Thus, if an increase in linear stress is assumed, the corresponding stress value of C_{REM} can be computed with expression (11-4), multiplying the coefficients by the ultimate tensile strength of the fibres (σ_y). If Figure 11-10 is observed, it can be seen that the linear fitting of the results obtained in the inverse analysis are similar to those ones assumed, with it being considered accurate when taking into account the experimental dispersion of concrete and PFRC. Expressions (11-5) and (11-6) can be used for linear fitting and exponential fitting respectively.

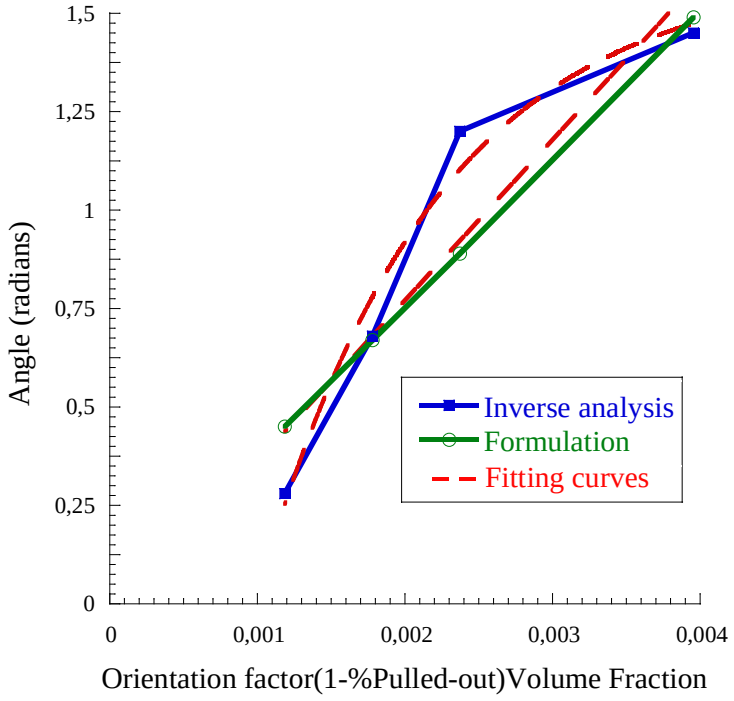

Figure 11-10: C_{REM}: Stress values from the inverse analysis (with linear and exponential fittings) and from the formulation proposed.

$$\sigma_{CREM} = (1 - \%Pulled - out) \cdot V_f \cdot \theta \cdot \sigma_u \qquad (11-4)$$

$$\sigma_{CREM(linear)} = -0.046414 + 408.28 \cdot \sigma \qquad \Longrightarrow R^2 = 0.85943 \qquad (11-5)$$

$$\sigma_{CREM(exponential)} = -2.0179 + 3.6296 \cdot \left(1 - e^{-827.7 \cdot (1 - \%Pulled - out) \cdot V_f \cdot \theta}\right)$$

$$\Longrightarrow R^2 = 0.97479 \quad (11-6)$$

11.5 Concluding remarks

The proposed procedure allowed verification of constitutive relations of PFRC, providing significant and useful information. The constitutive models have shown accurate reproduction of the behaviour of PFRC. The numerical calculations have provided results close to the mean results of the laboratory specimens in three-point bending test FEM simulations.

The numerical implementation, and use of ABAQUS with the subroutine UMAT with a cohesive embedded model, has shown its suitability in this type of material. The numerical model and experimental results presented emphasize that cohesive crack models are a helpful tool also for fibre reinforced concrete.

Regarding the inverse analysis, this allowed the fitting of constitutive models as a function of fibre dosage. The constitutive models have offered an accurate way of representing the fracture behaviour of the polyolefin fibre reinforced concrete, being within the scatter band of the results of fracture tests for all the PFRC types.

The constitutive models proposed provide a significant tool for structural designers in order to consider the mechanical contributions of the fibres in the post-cracking stages. Additional information can be obtained from the physical assumptions used in the discussion in case intermediate dosages.

The numerical simulations have shown that the tri-linear softening curves can reproduce the fracture behaviour of PFRC. Moreover, this has allowed accurate prediction of the constitutive relations from material properties and fibre dosage characterized in previous chapters.

PART V: CASE STUDY

Chapter 12

Case study: Structural cast-in-place application of polyolefin fibre reinforced concrete in a water pipeline supporting elements

12.1 Introduction

Previous chapters have shown that polyolefin-based macro-fibres can meet the requirements of the standards to consider their post-cracking contribution in the structural design of fibre reinforced concrete. Long synthetic fibres have also revealed a very good performance in comparison with steel fibres in fresh state and with significant deformations (see Chapter 4). The combination of the types of structural fibres has shown their capacities and synergies (Chapter 6). Although these properties have enabled the use of these types of fibres, there remain a few cast-in-place applications, which may boost their use and make FRC more reliable for structural designers. Therefore, the main drawback of such material is the lack of experience and the dependence on a suitable fibre distribution along the pieces.

In this chapter, a real application of polyolefin fibre reinforced concrete is reported. Its use enabled a reduction of the overall material cost and a total substitution of the customary steel-bar reinforcement. Moreover, it allowed an improvement in the concrete pouring rate and completion deadlines along the pipeline. In order to assure that structural requirements

were fulfilled with reliability, quality control was a key point in the construction works and, therefore, is also described. The conclusions revealed a noteworthy reliable performance of the polyolefin fibre reinforced concrete, with there being a remarkably limited scatter of the residual strengths and this provided of trustworthiness for its use in possible future structural applications.

The possibility of its use in structural elements relies on the capacity to produce the concrete with procedures that ensure the adequate fibre volume in each position. In such a sense, for in-situ applications, not only achieving the satisfactory mix proportioning but also testing a put-in-place process that ensures a good fibre distribution are needed. Moreover, the quality assurance of concrete during the execution works is critically important in preventing disparity. In order to show the suitability in cast-in-place applications of a PFRC with 5 kg/m^3 of polyolefin fibres used in the construction of the foundations of a pipeline, a detailed quality control procedure has been performed. This was done by determining the amounts of fibres used and assuring the concrete properties by testing the flexural behaviour of standard specimens in the following stages of production: in the first 100 m^3, and in the following 200 m^3, 600 m^3 and 800 m^3 of concrete produced. The mechanical results showed how this type of PFRC is suitable for this application, thus saving time and consequently reducing the final cost of the project.

12.2 Project description: the contribution of polyolefin fibres

The pipeline was planned to connect two villages in the Madrid region located 7.4km apart. The pipeline was made of steel and had a circular cross section with a diameter of 1016 mm. The mechanical characteristics of the reinforced concrete foundations were f_{ck} above 25 MPa. As the most used recommendations establish, in certain cases when the flexural response of FRC meet the requirements set, the contribution of the fibres can be considered in the structural design. The requirements that are commonly set deal with the contribution of the fibres at certain crack-mouth opening displacement (CMOD) values, specifically when the CMOD is 0.5 mm and 2.5 mm (Di Prisco, et al., 2013). These two reference values are termed as f_{R1}, and f_{R3}, and the load borne by the specimen should be at least 40% of f_{LOP} and 20% of f_{LOP} respectively. In the latter occasions, f_{LOP} stands for the maximum load registered during the flexural test of the specimen with the CMOD being less than 0.05 mm. These requirements have been customarily met with the addition of steel fibres to concrete, but the recent development of plastic fibres has raised the question about their suitability. Previous studies have shown that certain amounts of fibres can affect the flexural behaviour of concrete positively, allowing compliance with the requirements set in the applicable regulations (FIB, 2010; EHE-08, 2008). Regarding the project analysis, if the requirements of (FIB, 2010; EHE-08, 2008) are met, the traditional reinforcement of the concrete of the pipeline foundations made by steel bars shown in Figure 12-1 could be totally substituted by PFRC. In such a case, the cross section of the pipeline in the natural soil would change, as shown in Figure 12-2a) and Figure 12-2b).

The stresses introduced in the foundations by the internal pressure of 1.21 MPa were the main load that the PFRC foundations had to bear. The most loaded parts of the pipeline were the elbows, in particular that sketched with a red line in Figure 12-3a) that is also shown in Figure 12-3b). This section was calculated by using a finite element program which provided the stress field shown in Figure 12-3c). In Figure 12-3c), the dark blue colours stand for the maximum tensile stresses, with the area being 0.67 MPa. The red colour that appears in the same figure shows the lateral compressive stresses which were far from the compressive strength of the concrete designed.

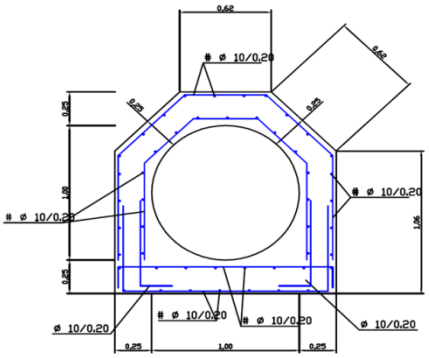

Figure 12-1: Detail of steel bar reinforcement of the foundation performed with conventional concrete and steel rebars.

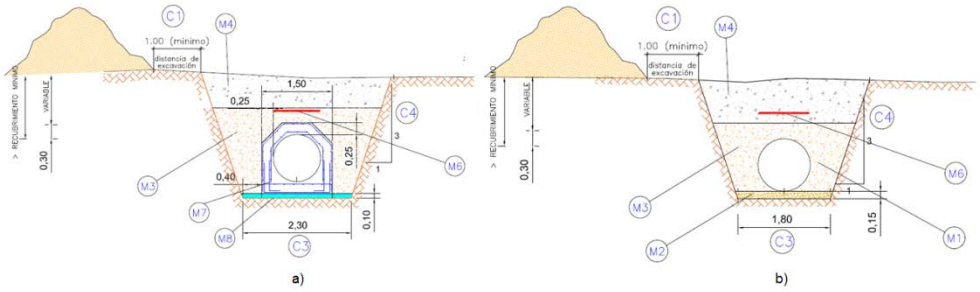

Figure 12-2: Pipeline and terrain cross section a) by using customary reinforced concrete, b) by using PFRC.

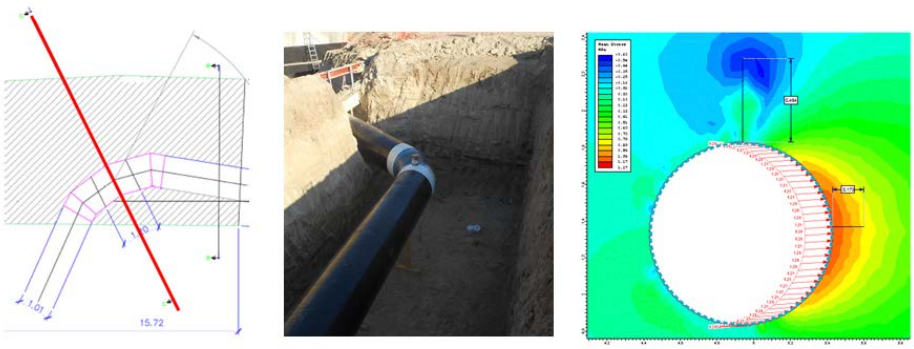

Figure 12-3: a) Sketch of the pipeline elbow subjected to the greatest stresses; b) image of the elbow ready to be stabilised with PFRC; c) numerical simulation of the interaction between the pipeline and the concrete foundations.

Based on the structural calculations performed, a decision was taken to substitute the reinforced concrete option with a PFRC with a compressive strength above 30 MPa and with a residual flexural strength above at 1.4 MPa in f_{R1} and f_{R3}.

12.3 Materials and mixing

Based on the mechanical requirements of the concrete, a decision was taken to employ 5 kg/m^3 Barchip48 fibres in order to eliminate the steel bars firstly planned. An image of the fibres used and their properties may be seen in Table 12-1.

Table 12-1: Barchip48 fibres properties.

Base Resin	Modified Olefin	Outlook of the fibres used
Length	48 mm	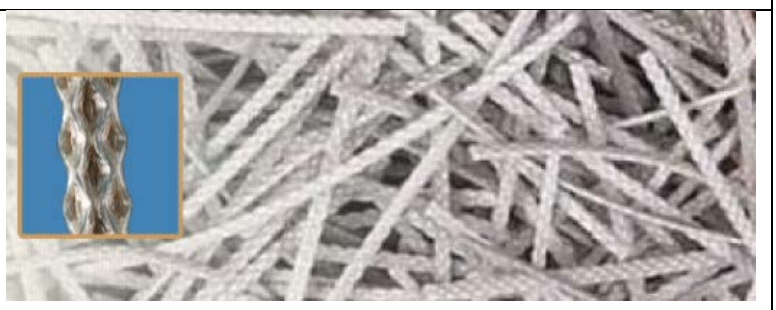
Tensile Strength	640 MPa	
No. Fibres per kg	59,500	
Specific Gravity	0.90-0.92	
Modulus of elasticity	10 GPa	

The fibres were added to a concrete manufacture with the proportions shown in Table 12-2. The aggregates used were siliceous and the grading of mix of the two may be seen in Figure 12-4. The cement used had between 6% and 20% of silica fly ash and a strength at 28 days above 42.5 MPa. The superplasticizer used was Sikament 175 with a 1.19 kg/l density. The fluidificant used was Sikament T-1405. The percentages shown in Table 12-2 refer to the amount of cement used.

Table 12-2: Concrete mix proportions per m^3.

Aggregates		Cement	Superplasticizer	Fluidificant	Water
Coarse	Fine				
815 kg	1,045 kg	325 kg	2.6 kg (0.8%)	4.55 kg (1.4%)	115 l

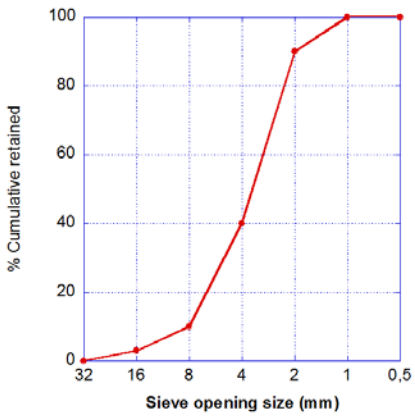

Figure 12-4: Grading of the used aggregates.

The concrete used was manufactured in an industrial plant by using a procedure similar to that applied in standard concrete. The fibres were manually added with the fine aggregate.

This procedure can be seen in Figure 12-5. Once it was manufactured, the concrete was transported to the construction site in volumetric concrete mixers. Once at the construction site, the concrete was cast in place by means of pumping, as can be seen in Figure 12-6. This type of casting in place and the absence of any steel reinforcing bar enabled production of an average of 70 linear metres of foundations of the pipeline each working day. In addition, the outstanding outlook of the concrete element once hardened can be also seen if Figure 12-6. The consolidation process was performed by means of manual vibrators.

Figure 12-5: Manual fibre addition.

Figure 12-6: Concrete pumping and result.

12.4 Material quality control at the construction site and of the concrete fresh properties

The experimental programme carried out examines the mechanical response of the PFRC employed at the construction site by sampling concrete from the same material used in the real structure. The quality control of the material was performed by casting at the site in both cylindrical samples, with a 300 mm height and 150 mm diameter, and prismatic samples of 600x150x150 mm^3. The filling process of the prismatic samples is shown in Figure 12-7. All these samples, once hardened, were de-moulded and stored in a climatic chamber at 20ºC and with a relative humidity above 95% until the age of testing.

It is important to highlight that at the beginning of the construction process the quality control of the material poured was stricter than in the subsequent stages. That meant that sampling was more frequent in the first stages than the later ones. This could be done due to the positive mechanical response of the samples taken from the mixed material.

Consequently samples were taken from the first 100 m^3, and afterwards from the following 200 m^3, 600 m^3 and 800 m^3.

Figure 12-7: Filling of the moulds and levelling of the surface of the prismatic samples.

The fresh properties of concrete were determined by means of Abrams slump test, one of the most common regulations (EN 12350-2, 2002). The test results showed only slight differences between the formulations manufactured, as shown in Table 12-3.

Table 12-3: Fresh-state properties, fibre contents and compressive strength results.

Type of concrete	Volume controlled (m^3)	Slump test (cm)	Fibre content (kg/m^3)	Δfibre content	Compressive strength (MPa)
PFRC-1	100	8.0	4.68	-6.4%	30.67
PFRC-2	100	7.0	5.68	13.6%	32.31
PFRC-3	200	7.1	--	--	32.42
PFRC-4	200	7.5	5.22	4.5%	31.93
PFRC-5	600	9.0	5.59	11.8%	33.05
PFRC-6	600	7.5	7.05	41.0%	32.19
PFRC-7	800	8.7	6.66	33.2%	31.80
PFRC-8	800	--	6.12	22.5%	--

As can be seen in Table 12-4, the viscosity of the concretes manufactured in the concrete batching plant is quite stable and is in all cases near 8 cm. This viscosity enabled the pumping of the PFRC, as can be seen in Figure 12-6.

One factor that determines the post-peak behaviour of PFRC is the fibre content. It was important to determine the content of fibres and check that the amounts of fibres added were steady in all the volumes of concrete manufactured. It is worth noting that the design of the PFRC set that the amount of fibres added should be 5 kg/m^3. The volume of fibres was determined following this recommendation (UNE 83512-1, 2005) with the results obtained shown in Table 12-4. It is clear that in all cases the amount of fibres added was close or above the design quantity. Even in certain cases the amount of fibres added was more than 40% higher than that designed. Based on this data, if the distribution of fibres is uniform within the mix, the results of the flexural behaviour of PFRC should comply with the requirements established.

12.5 Mechanical properties assessment

The mechanical properties of all the concretes were assessed following standard procedures. The compressive strength was obtained in accordance with EN 12390-3. As Table 12-4 shows, all formulations had a compressive strength above the 30 MPa needed in the construction project. In addition, if the coefficient of variation of the compressive strength is considered, which is 2.23%, it could be said that there is scarcely any variation of the strength in spite of the existing differences in the fibre dosage observed.

12.5.1 Fracture tests

The tests were performed in accordance with EN: 14651 (EN 14651:2007+A1, 2007), with the scheme being shown in Figure 12-8. Figure 12-9 shows the relative position of the notch. A span distance of 500 mm and a notch in the centre of the span of 25 mm±1 mm were chosen with the loading cylinder located in the centre of the span. As stated in the regulations, the tests were performed with the displacement control and setting two different stages, as may be seen in Figure 12-10. In all cases, when the test speed increased the CMOD was above the recommended values in the regulations. The fibres absorb energy and control the crack growth during the fracture process (see Chapter 4). Irrespective of if this is due to fibre rupture, fibre bridging, fibre pull-out, fibre debonding or matrix cracking, these mechanisms prompt significantly higher deformations than with regular concrete. The CMOD values almost reached their upper bound and in all cases were above 4.5 mm. An image of one of the samples while testing can be seen in Figure 12-8b). With the aim of reducing the scatter non-attributable to the material, the testing setup and the placing of the sample in the bearings were carefully performed with a laser leveller. The sample rested on two rigid steel cylinders laid on two ground supports, which allowed free rotation out of the plane of the beam and guaranteed negligible friction rolling in the longitudinal direction of the beam. In addition, to minimise the influence of the variation of the dimension of the ligament area, all samples were notched with a water-cooled low-speed diamond cutting disc.

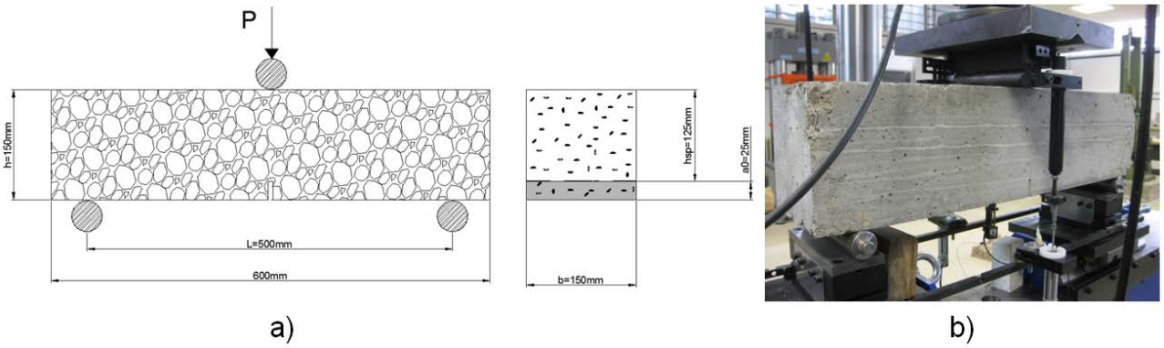

Figure 12-8: Fracture tests: a) sketch of the three-point bending tests; b) sample while testing.

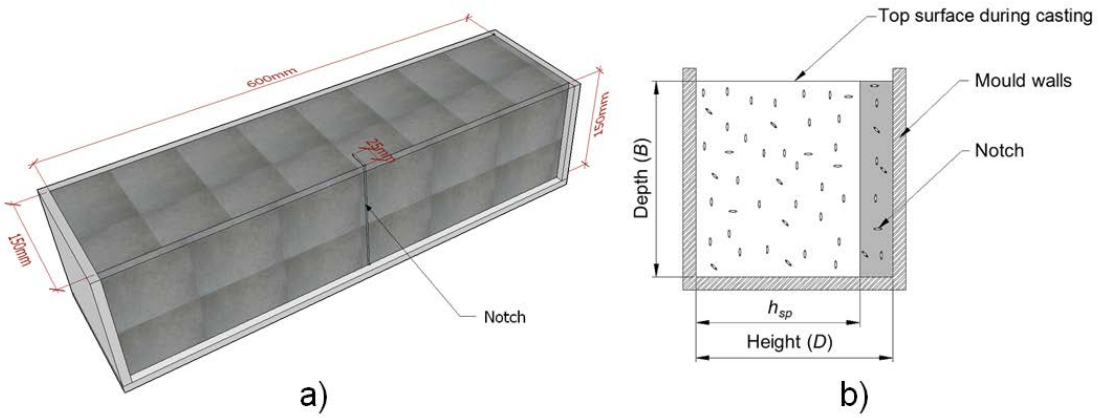

Figure 12-9: Position of the notch in the sample.

Figure 12-11 shows the results of the fracture tests from the samples manufactured with concrete from the batch first 100 m^3 pumped. In Figure 12-11a) it may be seen that there is quite a low scatter among the three samples tested. The peak load of the three tests is quite similar, but the minimum post-peak load, commonly termed as f_{MIN}, is not particularly stable. One of the three samples had a post-peak behaviour below the other two curves. This might be the result of a degree of inhomogeneity in the distribution of fibres in all the concrete mixed or due to a bad distribution of fibres within the sample tested.

In Figure 12-11b), it can be noted that the tendency observed in Figure 12-11a) is repeated. There are two samples capable of bearing greater post-peak loads than the other. On this occasion, the tendency is even more pronounced than in the previous tests. It is also noticeable that the behaviour of one of the samples is clearly different from the other two.

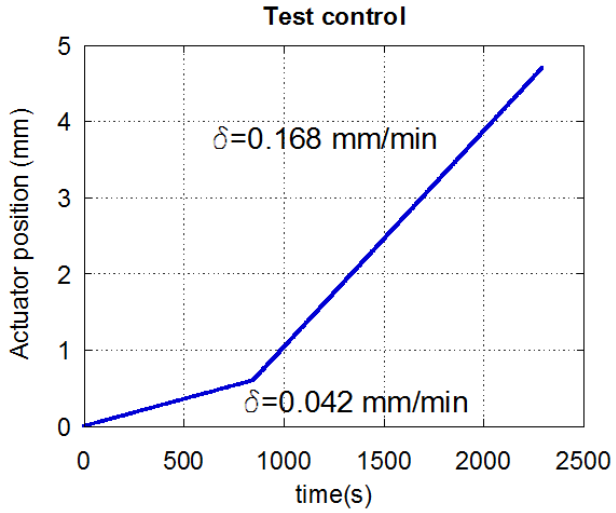

Figure 12-10: Actuator position displacement used as test control.

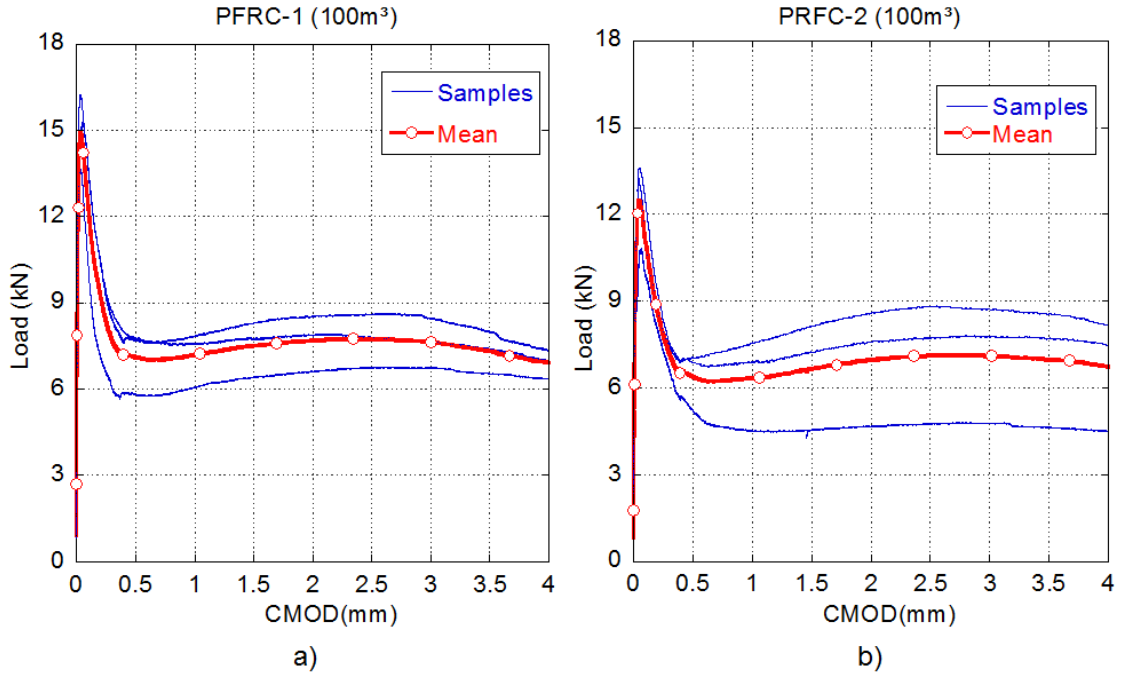

Figure 12-11: Fracture results of samples from the first batch 100 m³ pumped.

The samples of Figure 12-12a) showed a similar behaviour in all the fracture parameters. Two of the samples showed a close resemblance and had similar curves. The third sample had lower peak load and lower strengths during the residual stages of the test.

Regarding the behaviour of the samples shown in Figure 12-12b) it can be said that the shapes of the curves obtained resemble the typical behaviour of PFRC in a fracture test. The three typical turning points, that is to say the peak-load, minimum post-peak load, and maximum post-peak load, can be clearly distinguished. In addition, there were two samples that behaved quite similarly, while the other sustained higher loads throughout the test.

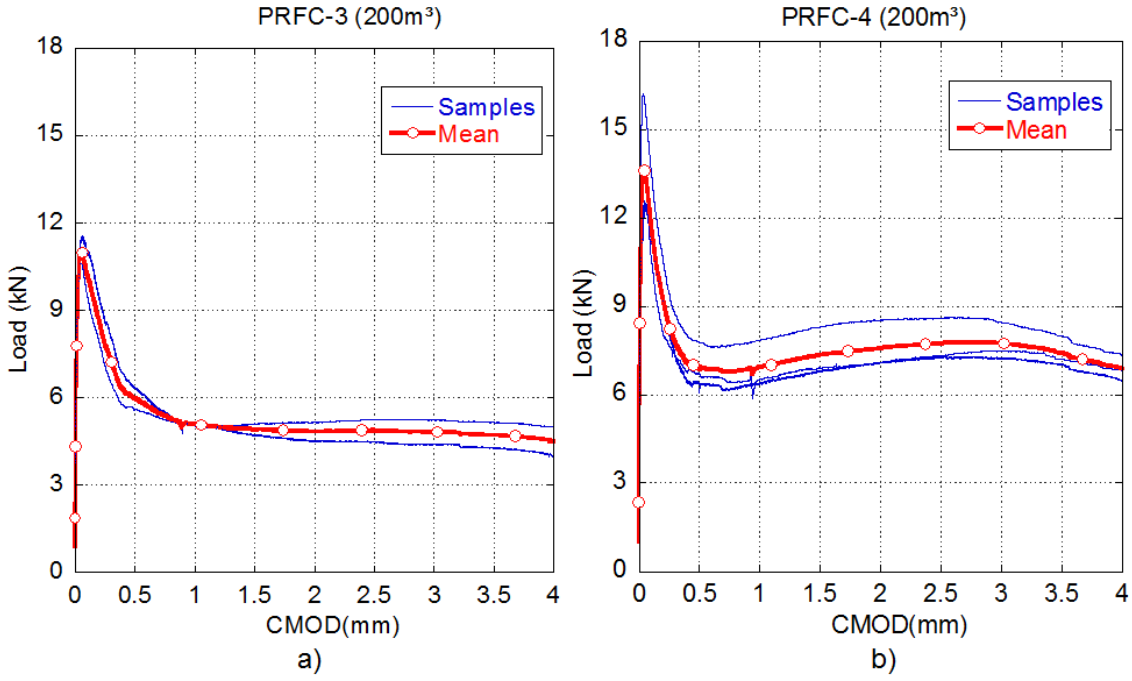

Figure 12-12: Fracture results of samples from a batch of 200 m³ pumped.

When the batch of the concrete pumped increased up to 600 m³, six samples were cast in standardised moulds. The behaviour of those samples when tested under fracture conditions can be seen both in Figure 12-13a) and in Figure 12-13b). In both figures, it can be seen that the scatter was more pronounced than in almost all the samples obtained from smaller batches of concrete. In the case of Figure 12-13a), although the peak value of the test was quite similar in all samples, the unloading part of the curve showed a different slope in one of the samples tested. In addition, the minimum post-peak load changes noticeably for the three samples. Moreover, it is clear that there is no clear trend in the post-peak loading part of the curve. Whereas there is one of the samples with almost no increment of the load bearing capacity, there is another that withstood more load after f_{MIN}. However, the curves shown in Figure 12-13b) resembled some of the patterns previously observed in Figure 12-11 and Figure 12-12: two of the curves were very close while the third sample had lower values of both peak load and residual strengths. It is worth noting that the CMOD values for the turning points are alike in the three tests.

When analysing curves Figure 12-14a) and Figure 12-14b) it is easy to perceive that, as in Figure 12-13, there were two tendencies. While the curves shown in Figure 12-14a) had a dissimilar behaviour, those shown in Figure 12-14b) behaved with almost no noticeable scatter. In Figure 12-14a) it can be observed that except in the case of the peak load, the rest of turning point of the curves did not register comparable load values. This might be the reflection of an inhomogeneous content of fibres or the result of a non-uniform distribution of fibres within the fracture section. In Figure 12-14b) it can be seen how the three tests had a quite similar behaviour. In all the turning points the load values obtained are quite similar and even the slopes after them were alike. Similarly to Figure 12-12a) the three samples tested were only capable of maintaining the minimum post-peak load, with there being no increment of the load bearing capacity in any of the three samples.

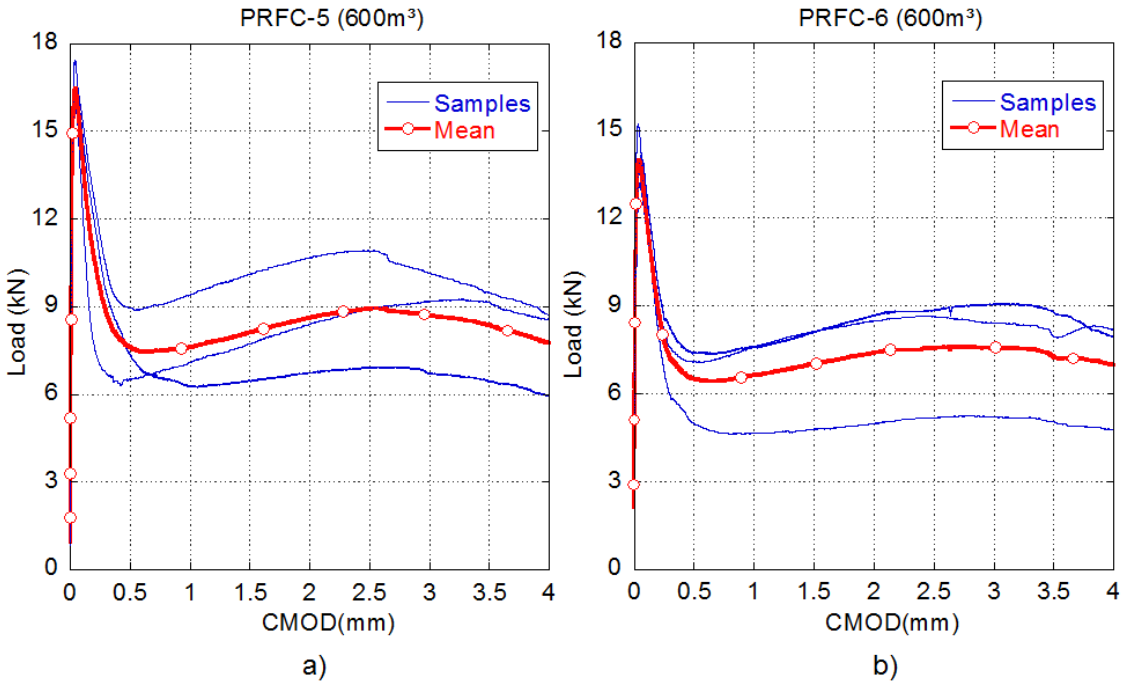

Figure 12-13: Fracture results of samples from a batch of 600 m³ pumped.

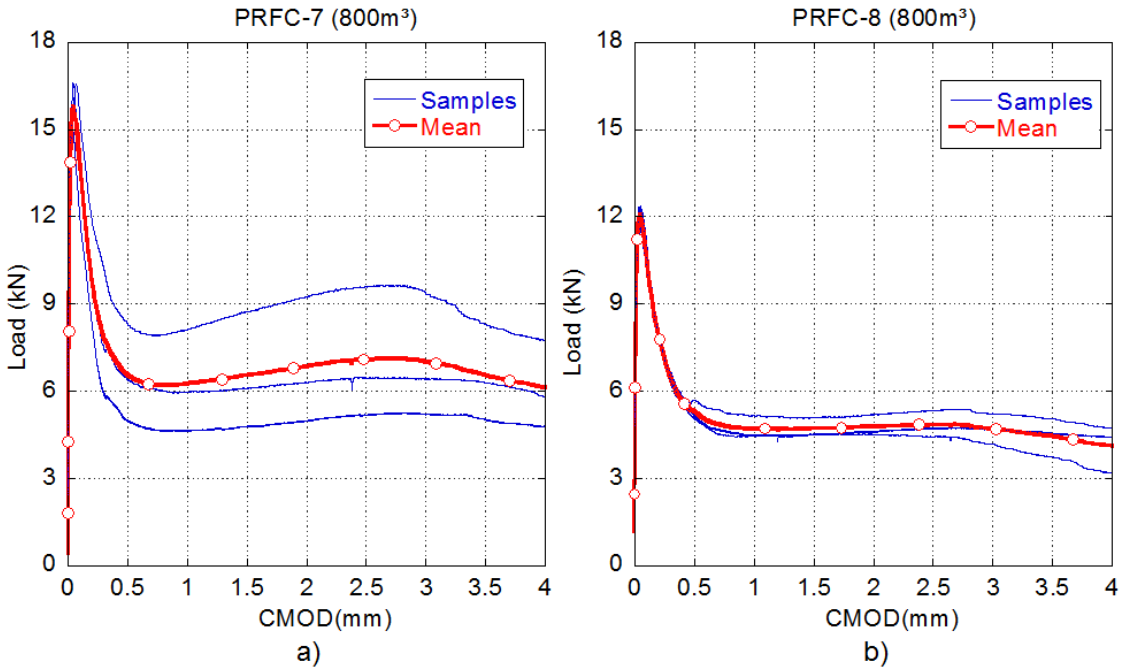

Figure 12-14: Fracture results of samples from 800 m³ pumped.

Figure 12-15 offers a summary of all the curves previously shown. In this figure, the mean of the fracture curves of each of the concrete volumes of each batch sampled can be seen, that is to say, 100 m³, 200 m³, 600 m³ and 800 m³. In addition, the mean of all the samples tested has been also included. As can be seen, although there might have been variations in the concrete production and in the sampling procedures throughout the construction period, the scatter in the fracture results is limited. The area where all the mean results are located clearly shows that a reliable use of this type of PFRC can be guaranteed. In addition, the three typical turning points for similar CMOD values enable its use for the structural design in the state of service limit (SLS) and ultimate limit state (ULS). It is also worth noting that the mean curves that are at the borders of the mean behaviour area, which are shadowed in the figure, correspond to the highest volumes of the batches controlled, 600 m³ and 800 m³. In this respect, the reduced scatter of these two curves with respect to those obtained in the samples taken from the controlled concrete with batches of 100 m³ and 200 m³ is also notable. Regarding this matter, it is important to highlight that the behaviour of PFRC is not only influenced by the amount of fibres added but also by the positioning of the fibres within the fracture section, as shown in previous chapters 4, 5 and 6. This can be seen comparing PFRC1 and PFRC2 in Figure 12-11 and Table 12-4. Although an analysis of the fracture surfaces of the samples tested might provide useful information in justifying the curves that appear in Figure 12-15, such a question is beyond the scope of this chapter.

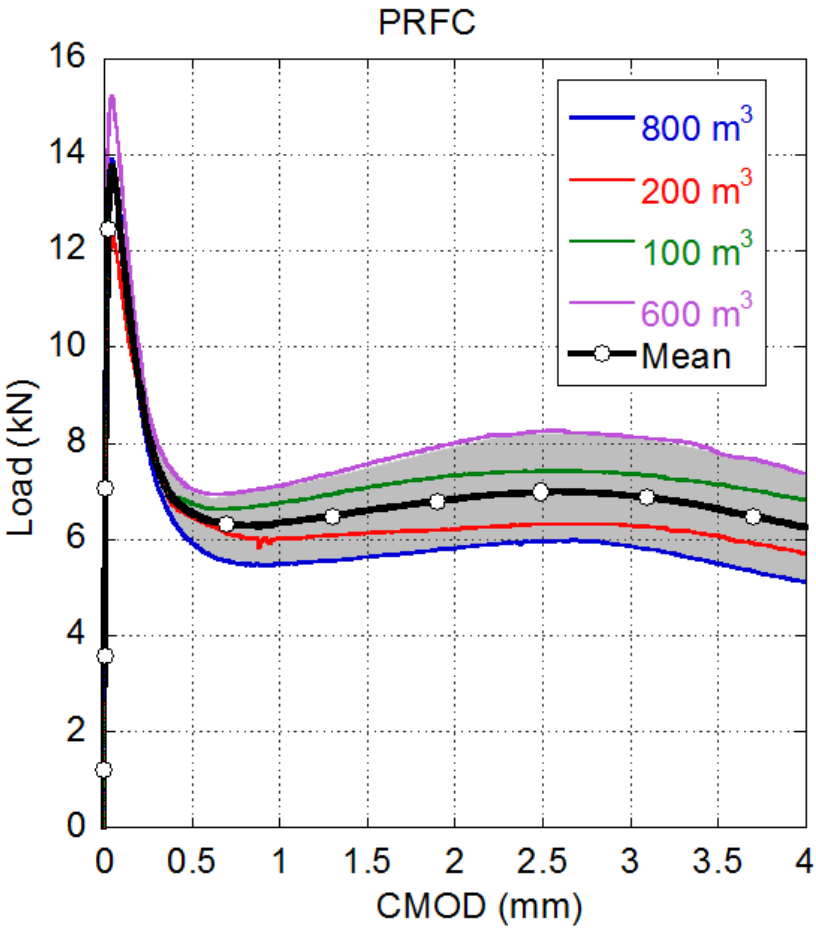

Figure 12-15: Mean fracture results.

12.5.2 Fracture characteristic values

Despite the discussion of the results performed in the previous section, and which shows that the suitability of this type of PFRC in real applications is beyond doubt, it is necessary to check how it meets the requirements of the most common standards. The standards relate the structural capacity of fibre reinforcement to residual flexural strengths obtained from the tests (EHE-08, 2008). Specifically, Model Code 2010 (FIB, 2010) proposes relating the SLS with stress values in a CMOD of 0.5 mm (f_{R1}) and the ULS with the stress values obtained from the test when CMOD is 2.5 mm (f_{R3}). Moreover, the standards (FIB, 2010) (EHE-08, 2008) have dealt with residual stress values in percentage values of the stress obtained for the limit of proportionality (f_{LOP}). The latter is defined in the standards as the maximum strength obtained for CMOD values lower than 0.05 mm. Additionally, the requirements for considering the contribution of fibres in structural design have been set in the aforementioned recommendations in percentage terms of $f_{LOP.}$ The Model Code 2010 (FIB, 2010) requires for structural use strengths of 40% of f_{LOP} for CMOD 0.5 mm and 20% of f_{LOP} for CMOD 2.5 mm (obtained with the test methods EN: 14651 (EN 14651:2007+A1, 2007) or RILEM TC162-TDF (RILEM TC162-TDF, 2002)). European Standard 14889 (EN 14889-2, 2008) was approved in 2006 to regulate the use of fibres for concrete and comprised two parts: the first dealt with steel fibres and the second with polymer fibres. In such standards not all the characteristics that may be relevant to the performance of FRC were addressed. However, those structural requirements at the same CMOD values were included but in terms of fixed stress values. That is to say, EN: 14889-

2 (EN 14889-2, 2008) specifies the volume of fibres that achieves a residual flexural strength of 1.5 MPa at 0.5 mm CMOD and 1.0 MPa at 2.5 mm CMOD obtained in specimens produced with a reference concrete enclosed in EN 14845 (EN 14845-1, 2006) and EN: 14651 test methods (EN 14651:2007+A1, 2007).

Moreover, it should be remembered that in this project the maximum stress that the PFRC should bear was 1.40 MPa both at f_{R1} and f_{R3}. In order to obtain the residual stresses of the fracture section, the values of load at certain values of CMOD were obtained by means of expression (12-1), which has also been included in test recommendations and standards (RILEM TC162-TDF, 2002) (EN 14651:2007+A1, 2007). In this expression F_j stands for loads, f_{Rj} for strength, L for span, h_{sp} is the ligament height and b is the depth of the specimen. The standard EN: 14889-2 (EN 14889-2, 2008) defined this residual flexural strength as the theoretical stress at the tip of the notch which acts in the centre of an uncracked section, involving linear distribution of force and subjected to a specified load in its correspondent CMOD.

As may be seen in Table 12-4, the values of the residual strength at a CMOD of 0.5 mm exceeded the design structural tensile requirements of PFRC set at 1.40 MPa. Regarding the requirements established in The Model Code 2010, for f_{R1} all the values are above the 40% limitation stated. In addition, the residual strength set in the European Standard 14889 is surpassed by all the values registered in the tests. Similarly, the residual strength value f_{R3} set in the European Standard 14889 is clearly below all the values obtained in the tests. Moreover, those values also comply with the mechanical requirements set in the structural design of the concrete bed of the pipeline. Likewise, when the residual strength at f_{R3} are examined it may be noted that all specimens exceeded 20% of f_{LOP} which is the requirement established by EN-14651. All the requirements established by any of the three recommendations studied are also complied with if the mean values of all samples are obtained as can be seen in Table 12-4.

$$f_{ct,j} = \frac{3}{2}\frac{F_j \cdot L}{b \cdot {h_{sp}}^2} \qquad (12-1)$$

Table 12-4: Concrete residual strength at f_{R1} and f_{R3}.

	PFRC-1			PFRC-2			PFRC-3		PFRC-4			PFRC-5			PFRC-6			PFRC-7			PFRC-8			Mean
f_{LOP} *(MPa)*	5.19	4.39	4.89	3.46	4.37	4.24	3.42	3.70	4.04	4.02	5.19	5.57	5.27	5.08	4.53	4.25	4.92	5.36	4.26	5.36	3.73	3.85	3.97	4.48
f_{R1} *(MPa)*	2.49	1.87	2.46	1.64	2.20	2.25	1.79	2.05	2.05	2.15	2.49	2.34	2.87	2.1	2.38	2.27	1.58	2.67	2.42	2.04	1.66	1.61	1.81	2.14
$\%f_{LOP}$	48	43	50	47	50	53	52	55	51	54	48	42	54	41	53	53	32	50	57	38	44	42	45	48
f_{R3} *(MPa)*	2.75	2.16	2.50	1.52	2.47	2.83	1.68	1.43	2.32	2.36	2.75	2.22	3.5	2.87	2.84	2.77	1.66	3.06	2.48	2.07	1.51	1.43	1.71	2.30
$\%f_{LOP}$	53	49	51	44	57	67	49	39	58	59	53	40	66	57	63	65	34	57	58	39	41	37	43	51%

12.6 Conclusions

This chapter presents the use of a type of PFRC as an alternative to a conventional reinforced concrete. Based on the structural design, the limits of mechanical properties of the material were established in 30 MPa under compressive stress and 1.4 MPa in tensile stresses. The latter value had to be maintained in f_{R1} and f_{R3} alike.

The absence of reinforcement bars, as well as the ease of the pumping of concrete into the moulds, enabled construction of an average of 70 linear meters of pipeline per day. As this production rate permitted savings in both time and money, it provided an advantage with respect to the customary steel bar reinforced concrete option.

The concrete production control process was divided in four production stages, where volumes of 100 m^3, 200 m^3, 600 m^3 and 800 m^3 batches were selected. From each of these batches, samples were taken for hardened and fresh-state tests.

The slump test results showed that a regular viscosity of concrete may be obtained with PFRC, even though there was a high volume of concrete produced. In addition, this enabled pumping of concrete without major difficulties which subsequently enhanced the production rate of the pipeline. Regarding the tests that checked the amount of fibres added, in all but one case the content of fibres exceeded the theoretical design addition.

Concerning the compressive strength tests, all the results were above the design limits established by the structural design requirements. The fracture behaviour of the samples showed reliable behaviour of PFRC with a 5 kg/m^3 addition of polyolefin fibres in spite of the large volume of concrete produced. Fracture test results met the requirements set on the design project, 1.40 MPa at f_{R1}, and f_{R3}, as well as those stated in EN: 14651 (EN 14651:2007+A1, 2007). In the case of the requirements set in EN 14651, the mean behaviour of the samples permitted the contribution of the fibres in the structural design to be considered.

PART VI: CONCLUDING REMARKS

Chapter 13

Concluding remarks

The characterization of polyolefin fibre-reinforced concrete has shown that fracture behaviour had a narrow degree of scatter in relative terms when dealing with FRC, even with notable intentional variations of the production conditions and concrete types. In addition to this, fresh-state and hardened properties were suitable for structural uses and the presence of fibres did not influence the results of permeability, meaning that the quality of the concrete in terms of durability was unaffected. Moreover, the case study showed that it is possible to produce this type of concrete with reliability and obtain results that exceed the requirements of the regulations in real applications.

As stated in the introduction of this thesis and even in its title, the sought objectives are considered at three levels: material properties, modelling and design practical considerations. Consequently, the final overall conclusions are organised under the same scheme. Moreover, a new line with promising results by combining polyolefin and steel fibres has provided sound conclusions that are summarised at the end of the chapter.

13.1 Material properties

The production of polyolefin fibre-reinforced self-compacting concrete (PFR-SCC) has a superior performance fresh-state behaviour when compared with steel-hooked fibres, even with a fibre content of 10 kg/m³.

The hardened properties obtained in PFR-SCC for the medium fibre content mixtures (with 3, 4.5 and 6 kg/m³), regardless of the amount of fibres used, were analogous in compressive strength and elasticity modulus, while the improvement of tensile strength was moderate. All these results had plain concrete as a reference. For high-fibre content (10 kg/m³), compressive strength slightly decreased and tensile strength increased by 30% compared with a plain self-compacting concrete, though it was 10% lower compared with a reference steel fibre-reinforced self-compacting concrete.

Modifications of consolidation procedures, fibre length, formwork geometries, fresh-state properties, pouring processes and specimen sizes have also been assessed. These factors have shown that there is a limited variation of the fracture behaviour regardless of the parameters chosen, enabling a confident and reliable use of PFRC.

The scatter obtained in PFR-SCC with 4.5 kg/m³ and 6 kg/m³ is consistent with the lack of uniformity in the number and distribution of fibres in the fracture surfaces. The remaining load-bearing capacity for considerable strain states has a maximum post-cracking load (L_{REM}) close to a 4.5 mm deflection for all dosages.

The permeability test results obtained by using both types of concrete, VCC and SCC (reinforced with polyolefin fibres) showed that the presence of fibres does not influence the connected porosity network of concrete.

SCC mixes have a more uniform distribution of fibres as compared with VCC. The difference is enhanced when increasing fibre dosage in standardised specimens.

Furthermore, the positioning of the fibres in the specimens and how this affects the material performance has been examined. This was performed by counting the fibres located in the fracture surfaces as well as determining their orientation and distribution. It was concluded that fibres did not show any tendency to float.

Shorter fibres (48 mm long) showed a higher percentage of pulled-out fibres and the longer fibres (60 mm long) appeared to be broken in higher proportions. The fracture results obtained in concretes manufactured with both fibre lengths were similar. It was concluded that the better orientation factor of the shorter fibres was balanced by the increasing of the number of fibres with an insufficient embedded length.

Experimental evidence presented in this thesis has shown that PFRC has a reliable fracture behaviour. Self-compacting PFRC, when applied to other sizes of structural elements, seems to behave noticeably better than laboratory specimens due to a significantly improved orientation of the fibres. Likewise, in real structures, the effect of vibration seems to be remarkably suitable, having consistent fracture results and homogeneous distributions of the fibres. Both VCC and SCC reinforced with polyolefin fibres encompass the main compaction procedures and pouring methods in the construction industry.

Hence, the results obtained provide interesting information that could lead designers to a reliable use of PFRC because of the limited scatter observed, notwithstanding the various shapes and varied placing conditions.

The results of pull-out tests provided significant information about the pull-out maximum strength, the frictional shear stress and the energy absorbed in the process. Pull-out tests were designed and performed with polyolefin fibres embedded in mortar and self-compacting concrete specimens. Six embedded lengths and variable inclinations from 0º to 60º were tested. The maximum peak load occurs with 45º inclination, whereas the maximum debonding energy is at 30º. At beyond 45º the failure pattern type becomes matrix spalling. The critical embedded fibre length was found to be 20 mm, although it is strongly influenced by the matrix type.

Microstructural analyses have shown a detailed view of the interface between polyolefin fibre and cement paste. The continuity between C-H-S gel and polyolefin fibres exhibited a sound interface between polyolefin fibres and cement paste, without voids or discontinuities.

13.2 Numerical tools

A new analytical model capable of assessing the orientation factor is proposed. The achievement of the orientation factor is significantly useful in predicting the number of fibres crossing a vertical section. The review of the previous studies has allowed an initial validation for rigid fibres. The most accepted values for the orientation factor in distinct positions of an isolated fibre inside the concrete complied with the results obtained by means of a numerical integration.

The model allows curves to be prepared with the profile of orientation when one and two walls are affecting the fibre positioning as a function of the ratio of the fibre length and the distance to a wall. It also supports the case of synthetic fibres that can bend. The use of such a type of fibres did not allow direct application in previous models.

In order to provide tools that may facilitate the use of polyolefin fibre-reinforced concrete, tables and figures with the most common commercial fibre lengths have been built and validated. The distinct orientation of the sectors that are close to a wall or any other boundary condition has been accounted for in the model.

Inverse analysis has allowed the constitutive models of PFRC in tension to be proposed and verified. The relations have been discussed as a function of fibre dosage. The latter allows designers to perform calculations to assess the residual load-bearing capacity of PFRC with the most commonly used volume fractions of fibres.

The trilinear softening curves verified by the inverse analysis represent the behaviour of the composite material. The three turning points were related with the material properties of concrete and polyolefin fibres. The tensile strength of concrete was the maximum strength reached in the first linear branch. An exponential softening curve followed that maximum strength value up to the strength at which the fibres absorb the energy released in the fracture processes. At such a point, a reloading branch took place up to values that were related not only with the volume fraction of fibres but also with the orientation factor. The latter allows modifications to be performed when the matrix properties and placing conditions vary.

13.3 Design considerations

Fracture tests performed on VCC and SCC reinforced with 3, 4.5, 6 and 10 kg/m³ respectively of polyolefin fibres have shown similar behaviour, enabling a confident use of

PFRC. Mixes with a 10 kg/m³ dosage of fibres have met the requirements established in the standards that permit consideration of the contribution of the fibres in the structural design of a PFRC element using VCC and SCC alike.

Even for the lowest fibre content (3 kg/m³ of polyolefin fibres), the results of PRF-SCC stress for crack mouth openings of 2.5 mm (f_{R3}) were close to 20% of the stress on the limit of proportionality. Such a result complies with the ULS design standards. However, it should be noted that for structural reinforcement with medium polyolefin fibre content (4.5 and 6 kg/m³), an extensive test campaign might be needed to increase the reliability of the results and clarify the influence of the flow and casting procedure in the number and distribution of the fibres.

It is possible to reduce or even eliminate traditional steel reinforcement in structural applications with PFR-SCC. That is to say, PFR-SCC mixes with high polyolefin fibre content (10 kg/m³) met the requirements of the principal standards and recommendations in considering the contribution of the fibres in the structural design. Through using the bond improver, the mixture with 10 kg/m³ improved the fracture results and exceeded the requirements of the EN-14651, Model Code, RILEM and of the Spanish code EHE-08 (EHE-08, 2008).

For the SLS the values of crack mouth openings of 0.5 mm (f_{R1}) and values of the medium fibre content of PFR-SCC were not close to the commonly required 40% of the peak strength. However, stable, significant and reliable values were obtained.

The mixes performed with SCC were suitable for use in extremely hazardous environments, such as those located near to chemical industries or those influenced by maritime tidal conditions. In the case of VCC mixes, it was found that they were apt for use in medium-level hazardous environments, such as those in direct contact with marine water and erosive materials, and under freeze-thaw conditions.

The effects of the pouring process and size have also been examined. When PFR-SCC with 6 kg/m³ of polyolefin fibres was poured into a standardised mould from the centre, the post-peak behaviour reached higher values than when it was poured from one of the sides of the mould. In addition, a significant strength increase was found due to the greater wall effect that took place in the smaller samples. This could be of major interest when slender PFRC elements are manufactured.

Structural-size elements of PFRC with two formworks were manufactured: a column element filled with vibrated PFRC and a long-beam element filled with self-compacting PFRC.

It was found that although the polyolefin fibre density is lower than the concrete paste, there was no rise of the fibres towards the upper part of the column element. Distribution of the fibres on vertical elements is shown to be adequate. This is of significant importance due to the aforementioned better behaviour of PFRC with respect to SFRC in foundations subjected to earthquake lateral loads. Vibrated conventional concrete reinforced with polyolefin fibres performs adequately and shows no noticeable ascension or sinking effects.

The use of long formworks enables the flux to develop properly and helps fibre alignment and distribution, thus improving fracture behaviour. In the examination of the positioning and orientation of the fibres, it was shown that with adequate flux and vibration orientation factors as high as 0.6 may be reached. The maps of fibre positioning enabled sound and useful tools in future designing of PFRC to be provided.

The proposed orientation model allows comparison of the number of fibres predicted to cross a vertical plane with the most common structural fibres and lengths. This is a powerful tool, along with the developed distribution tables, in evaluating the behaviour of new types of fibres or shapes in research. In addition, the assessment of the influence of the placing conditions, pouring methods and rheological properties of the concrete in the final positioning of the fibres is included in the model.

In order to address a lack of experience when using PFRC in real applications, PFRC was applied in the supporting elements of a water pipeline. A significant reduction of the overall material cost and total substitution of the customary steel-bar reinforcement was achieved. This also allowed an improvement in the concrete pouring rate and completion deadlines.

In the construction of the pipeline, supporting elements that pump PFRC (5 kg/m³ addition) showed no difficulties. The viscosity was relatively stable in spite of the high volume of concrete produced. Fracture test results met the requirements set in the design project, 1.40 MPa at f_{R1}, and f_{R3}, as well as those stated in EN: 14651, making it possible to qualify the fibre.

13.4 Enhancing the performance with a combination of fibres

It is possible to produce a hybrid fibre reinforced self-compacting concrete with a combination of hooked steel fibres and macro polyolefin fibres, preserving the high-performance fresh properties within the most common self-compacting requirements. It should also be noted that the addition of fibres did not noticeably change the compressive strength, indirect tensile strength or modulus of elasticity of a reference SCC for any of the amounts, types or combination of fibres used. The fracture behaviour with the combination of the two types of fibres was remarkably stable and met the structural requirements of the standards. The fracture toughness and ductility, as well as residual strength, were increased if compared with the same proportions added separately and subsequently combined.

Moreover, a synergy effect was detected with it being concluded that there is a large field of research for future applications. This synergy in the fracture results led to a high-performance concrete capable of bearing loads close to the peak-load for deflections of Span/60. This effect was observed on the fracture surface of the specimens that showed the same preferential orientation for both types of fibres and an improved orientation and distribution of the polyolefin fibres.

Chapter 14

Future works

The overall conclusions have shown that polyolefin fibre-reinforced concrete has an excellent behaviour in both fresh and hardened states. The permeability tests performed in this work had notable results. The fracture behaviour met the requirements of the standards in order to consider the residual contribution of the fibres in structural design and the case study provided reliable results in real applications.

However, in the context of modern technologies of concrete and the future possible requirements that structural design encompasses, there is still a lack of research in PFRC. Starting with the material properties, uni-axial tensile tests and square panel tests would provide important information for potential applications of PFRC. Furthermore, the evaluation of the behaviour of PFRC combined with steel bar reinforcements would also allow new possibilities in the use of polyolefin fibres to reduce the amount of reinforcing bars.

In such a sense, the combination with various types of fibres opens a promising field for new research that may provide significant results. Future design of FRC could be focussed on selecting the optimum combination of fibre types and contents. The results of this thesis support such a future research line with worthy perspectives.

The shear capacity of PFRC may also provide designers with more information about the contributions of the polyolefin fibres that would enhance their use in structural applications. Given that polyolefin fibres outperform steel fibres in terms of chemical stability and that significant FRC structural applications are applied under water or in tunnelling applications, advanced research in PFRC durability would boost their use. If the results confirm the expected, this would permit substitution of steel fibres in those environments in which the latter might be corroded. Other interesting design situations are those related with fatigue loading, fire events and freeze-thaw cycles.

The chemical admixture used in this thesis to enhance the adhesion between the fibre and the matrix presents notable possibilities for potential research. Microstructural analysis may provide information about the changes in hydrated compounds that could produce improvements in fracture. Moreover, pull-out tests performed with analogous configurations, such as the ones presented in this thesis, would also provide remarkable information.

Regarding the numerical models, deeper research could be performed in order to link FEM calculations and sectional analysis. Those types of calculations would provide tools similar to those conventionally used by engineers in design tasks. In addition, with the results obtained in the pull-out tests, the development of possible direct approaches to connect them with the orientation results could enhance the proposed constitutive models with new assumptions.

Bibliography

Abdulkadir Cüneyt Aydin. (2007). Self compactability of high volume hybrid fiber reinforced concrete. Construction and Building Materials, 21(6), 1149-1154.

Abrishambaf, A., Barros, J. A., & Cunha, V. M. (2013). Relation between fibre distribution and post-cracking behaviour in steel fibre reinforced self-compacting concrete panels. Cement and Concrete Research, 51, 57-66.

ACHE. (2000). Monografía M-2. Manual de tecnología del hormigón reforzado con fibras de acero.

ACHE. (2008). Monografía M-13: Hormigón autocompactante: Diseño y aplicación.

ACI. (2007). Self-Consolidating Concrete. ACI 237R-07. American Concrete Institute (ACI).

ACI Committee 544. (2008). ACI 544.3R-08.Guide for specifying, proportioning, and production of fiber reinforced concrete. Farmington Hills: American Concrete Institute.

ACI Committee 544. (Reapproved 2009). ACI 544. 1R-96.State-of-the-Art Report on Fiber Reinforced Concrete.

AENOR (2005). UNE 83512-1. Hormigones con fibras : determinación del contenido de fibras de acero.

AENOR. (2003). UNE-EN 12620 Áridos para hormigón.

AENOR. (2006). UNE-EN 1097. Ensayos para determinar las propiedades mecánicas y físicas de los áridos.

AENOR. (2008). EN 14651:2005+A1:2007. Método de ensayo para hormigón con fibras metálicas. Determinación de la resistencia a la tracción por flexión (límite de Proporcionalidad (LOP), resistencia residual).

AENOR. (2009). UNE-EN 12390-3. Resistencia a compresión de probetas.

AENOR. (2010). UNE-EN 12390-6. Resistencia a tracción indirecta de probetas.

AENOR. (2010). UNE-EN 12390-8. Ensayo de Penetración de agua bajo presión.

AENOR. (2011). UNE-EN 12350-8. Hormigón autocompactante. Ensayo del Escurrimiento.

AENOR. (2011). UNE-EN 12350-9. Hormigón autocompactante. Ensayo del embudo en V.

AENOR. (2011). UNE-EN 12350-10. Hormigón autocompactante. Caracterización de la fluidez en presencia de barras. Método de la caja en L.

AENOR. (2012). UNE-EN 933-1. Ensayos para determinar las propiedades geométricas de los áridos. Parte 1: Determinación de la granulometría de las partículas.

Aguado, A., & Laranjeira, F. (2007). Presentación del Anejo de hormigón con fibras de la EHE y ecuación constitutiva del hormigón con fibras. Aplicaciones estructurales de hormigón con fibras, 2007-JT-02, (pp. 1-12). Barcelona.

Aiello, M., Leuzzi, F., Centonze, G., & Maffezzoli, A. (2009). Use of steel fibres recovered from waste tyres as reinforcement in concrete: pull-out behaviour, compressive and flexural strength. Waste Management, 29(6), 1960–70.

Akers, S., Kaufmann, J., Lübben, J., & Schwitter, E. (2009). Reinforcement of Concrete and Shotcrete using Bi-Component Polyolefin Fibres. Concrete Solutions 2009 Conference. Sydney.

Alani, A. M., & Beckett, D. (2013). Mechanical properties of a large scale synthetic fibre reinforced concrete ground slab. Construction and Building Materials, 41, 335-344.

Alberti, M. G. (2013). Respuesta mecánica de un hormigón autocompactante reforzado con fibras de poliolefina. Madrid: TFM, ETSICCP Universidad Politécnica de Madrid.

Ali, M., Majumdar, A., & Rayment, D. (1972). Carbon fibre reinforcement of cement. Cement and Concrete Research , 201-212.

Al-Mattarneh, H. (2014). Electromagnetic quality control of steel fiber concrete. Construction and Building Materials, 73, 350-356.

Almeida Filho, F. M., Barragán, B. E., Casas, J. R., & El Debs, A. L. (2010). Hardened properties of self-compacting concrete — A statistical approach. Construction and Building Materials, 24(9), 1608–1615.

Altoubat, S. A., Roesler, J. R., Lange, D. A., & Rieder, K. A. (2008). Simplified method for concrete pavement design with discrete structural fibers. Construction and Building Materials, 22(3), 384-393.

Altun, F., Haktanir, T., & Ari, K. (2007). Effects of steel fiber addition on mechanical properties of concrete and RC beams. Construction and Building Materials, 21(3), 654–661.

Aly, T., Sanjayan, J., & Collins, F. (2008). Effect of polypropylene on shrinkage and cracking of concretes. Materials and Structures , 41(10), 1741-1753.

Armelin, H. S., & Banthia, N. (1997). Predicting the flexural postcracking performance of steel fiber reinforced concrete from the pullout of single fibers. ACI Materials Journal, 94(1).

ASTM C 1609/C 1690M-07. (2007). Standard test method for flexural performance of fiber reinforced concrete (using beam with third-point loading). (A. S. Materials, Ed.) 1–8.

ASTM C469-02e1. (2006). Standard test method for static modulus of elasticity and Poisson´s ratio of concrete in compresion.

ASTM International. (2009). ASTM C 29/C 29M -09. Standard Test Method for Bulk Density (Unit Weight) and Voids in Aggregate. West Conshohocken: ASTM International.

Atis, C., & Karahan, O. (2009). Properties of steel fiber reinforced fly ash concrete. Construction and Building Materials, 23(1), 392-399.

Aveston, J., Cooper, G., A, & Kelly, A. (1971). In the properties of fiber composites. Conference proceedings, IPC Science and Technology (pp. 15-24). Guildford, UK.

Baeza, F. J. (2011). Función de percepción de la deformación en matrices cementicias conductoras mediante adición de fibras de carbono . Tesis Doctoral, Universidad de Alicante.

Bakhshi, M., & Nasri, V. (2014). Developments in design for fiber reinforced concrete tunnel. 2nd FRC International Workshop Fiber Reinforced Concrete: from design to Structural Applications, 1st ACI-FIB Joint Workshop. Montreal, Canada.

Balouch, S., Forth, J., & Granju, J. (2010). Surface corrosion of steel fibre reinforced concrete. Cement and Concrete Research , 40(3), 410-414.

Banholzer, B., Brameshuber, W., & Jung, W. (2005). Analytical simulation of pull-out tests—the direct problem. Cement and Concrete Composites, 27(1), 93-101.

Banholzer, B., Brameshuber, W., & Jung, W. (2006). Analytical evaluation of pull-out tests—the inverse problem. Cement and Concrete Composites, 28(6), 564-571.

Bannister, D. J., Andrews, M. C., Cervenka, A. J., & Young, R. J. (1995). Analysis of the single-fibre pull-out test by means of Raman spectroscopy: Part II. Micromechanics of deformation for an aramid/epoxy system. Composites science and technology, 53(4), 411-421.

Banthia, N., & Gupta, R. (2006). Influence of polypropylene fiber geometry on plastic shrinkage cracking in concrete. Cement and Concrete Research, 36(7), 1263-1267.

Banthia, N., & Sappakittipakorn, M. (2007). Toughness enhancement in steel fiber reinforced concrete through fiber hybridization. Cement and Concrete Research, 37(9), 1366–1372.

Banthia, N., & Sheng, J. (1996). Fracture toughness of micro-fiber reinforced cement composites. Cement & Concrete Composites, 18(4), 251-269.

Banthia, N., & Trottier, J. F. (1992). Micromechanics of steel fiber pull-out: rate sensitivity at very low temperatures. Cement and Concrete Composites, 14(2), 119-130.

Baran, E., Akis, T., & Yesilmen, S. (2012). Pull-out behavior of prestressing strands in steel fiber reinforced concrete. Construction and Building Materials, 28(1), 362-371.

Barr, B. I. G., Lee, M. K., de Place Hansen, E. J., Dupont, D., Erdem, E., Schaerlaekens, S., & Vandewalle, L. (2003). Round-robin analysis of the RILEM TC 162-TDF beam-bending test: Part 3—Fibre distribution. Materials and Structures, 36(9), 631-635.

Barragán, B. (2002). Failure and toughness of steel fiber reinforced concrete under tension and shear. PhD Thesis: Universitat Politècnica de Catalunya.

Barragán, B. E., Gettu, R., Martín, M. A., & Zerbino, R. L. (2003). Uniaxial tension test for steel fibre reinforced concrete—a parametric study. Cement and Concrete Composites, 25(7), 767-777.

Barros, J. &. (2001). Fracture energy of steel fiber-reinforced concrete. Mechanics of Advanced Materials and Structures 8(1), 29-45.

Barros, J. A., Cunha, V. M., Ribeiro, A. F., & Antunes, J. A. (2005). Post-cracking behaviour of steel fibre reinforced concrete. Materials and Structures, 38(1), 47-56.

Barros, J., & Figueiras, J. (1999). Flexural behavior of SFRC: testing and modeling. Journal of Materials in Civil Engineering, 11 (4), 331-339.

Basheer, P., Chidiact, S., & Long, A. (1996). Predictive models for deterioration of concrete structures. Construction and Building Materials, 10(1), 27-37.

Bazant, Z. P. (1984). Size effect in blunt fracture: concrete, rock, metal. Journal of Engineering Mechanics, 110(4), 518-535.

Bazant, Z. P., & Planas, J. (1997). Fracture and size effect in concrete and other quasibrittle materials. CRC press.

Bazant, Z. P., Ozbolt, J., & Eligehausen, R. (1994). Fracture size effect: review of evidence for concrete structures. Journal of structural Engineering, 120(8), 2377-2398.

Bazant, Z., & Oh, B. (1983). Crack band theory for fracture of concrete. Materials and Structures, 2(1), 155-177.

Beckert, W., & Lauke, B. (1998). Critical discussion of the single-fibre pull-out test: does it measure adhesion? Composites Science and Technology, 57(12), 1689-1706.

Behfarnia, K., & Behravan, A. (2014). Application of high performance polypropylene fibers in concrete lining of water tunnels. Materials & Design, 55, 274-279.

Bencardino, F., Rizzuti, L., Spadea, G., & Swamy, R. N. (2008). Stress-strain behavior of steel fiber-reinforced concrete in compression. Journal of Materials in Civil Engineering, 20(3), 255-263.

Bentur, A., & Mindess, S. (1985). Cracking processes in steel fiber reinforced cement paste. Cement and Concrete Research, 15(2), 331-342.

Bentur, A., & Mindess, S. (2006). Fibre reinforced cementitious composites. Taylor & Francis.

Bentur, A., Mindess, S., & Diamond, S. (1985). Pull-out processes in steel fibre reinforced cement. International. Journal of Cement Composites and Lightweight Concrete, 7(1), 29-37.

Berard, A. (1874, December 15). Patent No. U.S. Patent No. 157,903.

Bermejo Nuñez, E. (2009). Dosificación, propiedades y durabilidad en hormigón autocompactanate para edificación. Tesis Doctoral. Madrid: Universidad Politécnica de Madrid.

Bermejo, E. B., Moragues, A., Gálvez, J. C., & Fernández Cánovas, M. (2010). Permeability and pore size distribution in medium strength self-compacting concrete. Materiales de Construcción, 60(299), 37-51.

Bernard, E. S. (2004). Durability of cracked fibre reinforced shotcrete. Shotcrete: More Engineering Developments: Proceedings of the Second International Conference on Engineering Developments in Shotcrete, (pp. 59-65). Cairns, Queensland, Australia: Taylor & Francis.

Bernard, E. S. (2009). Design of fibre reinforced shotcrete linings with macro-synthetic fibres. Shotcrete for Underground Support XI. P11. ECI Symposium Series.

Bernasconi, A., Cosmi, F., & Hine, P. J. (2012). Analysis of fibre orientation distribution in short fibre reinforced polymers: A comparison between optical and tomographic methods. Composites Science and Technology, 72(16), 2002-2008.

Bertolini, L., Bolzoni, F., Pastore, T., & Pedeferri, P. (2004). Effectiveness of a conductive cementitious mortar anode for cathodic protection of steel in concrete. Cement and Concrete Research , 34(4), 681-694 .

Bischoff, P. H. (2003). Tension stiffening and cracking of steel fiber-reinforced concrete. Journal of Materials in Civil Engineering, 15(2), 174-182.

Bissonnette, B., Pierre, P., & Pigeon, M. (1999). Influence of key parameters on drying shrinkage of cementitious materials. Cement and Concrete Research, 29(10), 1655–1662.

Blanc, R., Germain, C., Baylou, P., & Cataldi, M. (2006). Fiber orientation measurements in composite materials. Composites Part A: Applied Science and Manufacturing, 37(2), 197-206.

Blanco, A. (2013). Characterization and modelling of SFRC elements. Doctoral Thesis, Universitat Politècnica de Catalunya.

Blanco, A., Pujadas, P., de la Fuente, A., Cavalaro, S., & Aguado, A. (2013). Application of constitutive models in European codes to RC–FRC. Construction and Building Materials, 40, 246-259.

Blanco, A., Pujadas, P., Fuente, A. d., & Aguado, A. (2010). Comparative analysis of constitutive models of fibre reinforced concrete. Hormigón y Acero , 61(256), 83-100.

Boulekbache, B., Hamrat, M., Chemrouk, M., & Amziane, S. (2010). Flowability of fibre-reinforced concrete and its effect on the mechanical properties of the material. Construction and Building Materials, 24(9), 1664-1671.

Brandt, A. (2008). Fibre reinforced cement-based (FRC) composites after over 40 years of development in building and civil engineering. Composite Structures, 86 (1-3), 3-9.

Breitenbücher, R., Meschke, G., Song, F., & Zhan, Y. (2014). Experimental, analytical and numerical analysis of the pullout behaviour of steel fibres considering different fibre types, inclinations and concrete strengths. Structural Concrete, 15(2), 126-135.

Brühwiler, E., & Denarié, E. (2013). Rehabilitation and strengthening of concrete structures using Ultra-High Performance Fibre Reinforced Concrete. Structural Engineering International, 23(4), 450-457.

Buffon, G. L. (1777). Essai d'arithmétique morale. Histoire naturelle, générale er particulière, Supplément 4, 46-123.

Buratti, N., Mazzotti, C., & Savoia, M. (2011). Post-cracking behaviour of steel and macro-synthetic fibre-reinforced concretes. Construction and Building Materials, 25(5), 2713-2722.

Burcu Akcay, M. A. (2012, March). Mechanical behaviour and fibre dispersion of hybrid steel fibre reinforced self-compacting concrete. Construction and Building Materials, 28(1), 287-293.

Burón, M. F. (2006). Hormigón autocompactante. Criterios para su utilización. In M. F. Burón, Hormigón (pp. 52-64).

Burton, D. M. (1985). The history of mathematics: An introduction, Senventh edition. McGraw-Hill.

Caratelli, A., Meda, A., Rinaldi, Z., & Romualdi, P. (2011). Structural behaviour of precast tunnel segments in fiber reinforced concrete. Tunnelling and Underground Space Technology, 26(2), 284-291.

Carballosa de Miguel, P., & Pacios Alvarez, A. (2011). Diseño optimizado de un hormigón autocompactante reforzado con fibra de polipropileno con función estructural, para el empleo en rehabilitación. V Congreso de ACHE. Barcelona, España.

Cavalaro, S. H., López, R., Torrents, J. M., & Aguado, A. (2014). Improved assessment of fibre content and orientation with inductive method in SFRC. Materials and Structures, 1-15.

Caverzan, A., Cadoni, E., & Di Prisco, M. (2011). Dynamic tensile behavior of self-compacting steel fibre reinforced concrete. Appl. Mechs. And Mats., 82, 220-225.

Cendón, D. A., Gálvez, J. C., Elices, M., & Planas, J. (2000). Modelling the fracture of concrete under mixed loading. International Journal of Fracture, 293–310.

Cengiz, O., & Turanli, L. (2004). Comparative evaluation of steel mesh, steel fibre and high-performance polypropylene fibre reinforced shotcrete in panel test. Cement and Concrete Research, 34(8), 1357-1364.

Chen, B., Wu, K., & Yao, W. (2004). Conductivity of carbon fiber reinforced cement-based composites. Cement and Concrete Composites, 26(4), 291-297 .

Chen, B., Wu, K., & Yao, W. (2004). Conductivity of carbon fiber reinforced cement-based composites. Cement and Concrete Composites, 26(4), 291-297 .

Chen, P., & Chung, D. (1995). Improving the electrical conductivity of composites comprised of short conducting fibers in a nonconducting matrix: the addition of a nonconducting particulate filler. Journal of Electronic Materials, 24(1), 47-51.

Chiarello, M. Z. (2005). Electrical conductivity of self-monitoring CFRC. Cement and Concrete Composites, 27, 463-469.

Chopin, D., Francy, O. L., S., & Rougeau, P. (2003). Creep and shrinkage of heat-cured self-compacting concrete (SCC). Proceedings of the Third International Symposium on Self- Compacting Concrete, RILEM, (pp. 672-683).

Chung, D. (2003). Multifunctional cement-based materials. New York, NY, USA: Marcel Dekker Inc., ISBN 0824746104.

Cifuentes Bulté, H. (2010). Análisis del Comportamiento en Fractura y del Efecto de Borde en Hormigones de Altas Prestaciones Reforzados con Fibras de Polipropileno. Tesis Doctoral, Universidad de Sevilla.

CNR-DT 204. (2006). Guide for the design and construction of fiber-reinforced concrete structures. Roma: Consiglio Nazionale delle Riserche.

Cunha Victor, M., Sena-Cruz José, M., & Barros Joaquim, A. (2007). Pullout behaviour of hooked-end steel fibres in self-compacting concrete. Report 07-DEC/E06.

Cunha, V. M., Barros, J. A., & Sena-Cruz, J. M. (2010). Pullout behavior of steel fibers in self-compacting concrete. Journal of Materials in Civil Engineering, 22(1), 1-9.

Dawood, E. T., & Ramli, M. (2012). Mechanical properties of high strength flowing concrete with hybrid fibers. Construction and Building Materials, 28(1), 193-200.

DBV . (2001). Merkblatt Stahlfaserbeton. Deutsche Beton Vereins.

DBV. (1992). Technologie des Stahlfaser-betons und Stahlfaserprit.

De la Fuente, A., Escariz, R. C., de Figueiredo, A. D., & Aguado, A. (2013). Design of macro-synthetic fibre reinforced concrete pipes. Construction and Building Materials, 43, 523-532.

De la Fuente, A., Lin, L., Cavalaro, S., & Aguado, A. (2014). Design of FRC tunnel segments considering the ductilityrequirements of the MC-2010 – Application to the BarcelonaMetro Line 9. 2nd FRC International Workshop Fiber Reinforced Concrete: from design to Structural Applications, 1st ACI-FIB Joint Workshop. Montral, Canada.

De Larrard, F. (1997). A new rheometer for soft-to-fluid fresh concrete. ACI Materials Journal, 94(3), 234-243.

De Larrard, F., & Belloc, A. (1997). The Influence of Aggregate on the Compressive Strength on Normal and High-Strength Concrete. ACI Materials Journal, 94(5), 417-426.

De Larrard, F., Ferraris, F., C., & Sedran, T. (1998). Fresh concrete : A HerscheI-Bulkley material. Materials and Structures, 31, 494–498.

De Montaignac, R., Massicotte, B., & Charron, J. P. (2012). Design of SFRC structural elements: flexural behaviour prediction. Materials and Structures, 45(4), 623-636.

De Oliveira e Sousa, J. L., & Gettu, R. (2006). Determining the tensile stress-crack opening curve of concrete by inverse analysis. Journal of Engineering Mechanics, 132(2), 141-148.

Deeb, R., Kulasegaram, S., & Karihaloo, B. L. (2014a). 3D modelling of the flow of self-compacting concrete with or without steel fibres. Part I: slump flow test. Computational Particle Mechanics, 1-17.

Deeb, R., Kulasegaram, S., & Karihaloo, B. L. (2014b). 3D modelling of the flow of self-compacting concrete with or without steel fibres. Part II: L-box test and the assessment of fibre reorientation during the flow. Computational Particle Mechanics, 1-18.

Deeb, R., Karihaloo, B. L., & Kulasegaram, S. (2014c). Reorientation of short steel fibres during the flow of self-compacting concrete mix and determination of the fibre orientation factor. Cement and Concrete Research, 56, 112-120.

Denarié, E., Habel, K., & Brühwiler, E. (2003). Structural behavior of hybrid elements with Advanced Cementitious Materials (HPFRCC). In R. Publications (Ed.), PRO 30: 4th International RILEM Workshop on High Performance Fiber Reinforced Cement Composites (HPFRCC 4), 1, pp. 301-312. Ann Arbor, Michigan, USA.

Di Prisco, M., Colombo, M., & Dozio, D. (2013). Fibre-reinforced concrete in fib Model Code 2010: principles, models and test validation. Structural Concrete, 14(4), 342-361.

Di Prisco, M., Felicetti, R., Lamperti, M., & Menotti, G. (2004). On size effect in tension of SFRC thin plates. Fracture Mechanics of concrete Structures, 1075-1082.

Di Prisco, M., Ferrara, L., Colombo, M., & Mauri, M. (2004). On the identification of SFRC constitutive law in uniaxial tension. 6th International RILEM Symposium on Fibre Reinforced Concretes (pp. 72).

Di Prisco, M., Lamperti, M., Lapolla, S., & Khurana, R. (2008). HPFRCC thin plates for precast roofing. Proceedings of second international symposium on ultra high performance concrete (pp. 675–682). Kassel, Germany.

Di Prisco, M., Plizzari, G., & Vandewalle, L. (2009). Fibre reinforced concrete: new design perspectives. Materials and Structures, 42(9), 1261–1281.

Diamond, S., & Huang, J. (2001). The ITZ in concrete - a different view based on image analysis and SEM observations. Cement & Concrete Composites, 23(2), 179–188.

DiFrancia, C., Ward, T. C., & Claus, R. O. (1996). The single-fibre pull-out test. 1: Review and interpretation. Composites Part A: Applied Science and Manufacturing, 27(8), 597-612.

Dinakar, P., Babu, K., & Santhanam, M. (2007). Mechanical properties of high volume fly ash self-compacting concretes. Proceeding of Fifth International RILEM Symposium on Self-Compacting Concrete, (pp. 651-658).

Ding, Y., Liu, S., Zhang, Y., & Thomas, A. (2008, July). The investigation on the workability of fibre cocktail reinforced self-compacting high performance concrete. Construction and Building Materials, 22(7), 1462-1470.

Ding, Y., Zhang, Y., & Thomas, A. (2009, January). The investigation on strength and flexural toughness of fibre cocktail reinforced self-compacting high performance concrete. Construction and Building Materials, 23(1), 448-452.

Domingo, A., Serna, P., & Lázaro, C. (2003). Construcción de la JCHYPAR, una lámina delgada de hormigón reforzado con fibras de acero, en el oceanográfico de Valencia. Hormigón y Acero, 228, 177-186.

Domone, P. (1998). The slump flow test for high-workability concrete. Cement and Concrete Research, 28(2), 177-182.

Domone, P. (2006). Self-compacting concrete: An analysis of 11 years of cases studies. Cement and Concrete Composites, 28(2), 197-208.

Domone, P. L. (2007). A review of the hardened mechanical properties of self-compacting concrete. Cement and Concrete Composites, 29(1), 1-12.

Døssland, Å. L. (2008). Fibre reinforcement in load carrying concrete structures. Doctoral dissertation, PhD thesis, The Norwegian Inst. of Technology.

Dozio D.Ò. (2008). SFRC structures: Identification of the uniaxial tension characteristic constitutive law. In PhD Thesis, Politecnico de Milano.

Duan, K., Hu, X., & F.H. Wittmann. (2003). Boundary effect on concrete fracture and non-constant fracture energy distribution. Engineering Fracture Mechanics, 70(16), 2257-2268.

Dubey, R., & Kumar, P. (2012). Effect of superplasticizer dosages on compressive strength of self compacting concrete. International Journal of Civil and Structural Engineering, 3(2), 360-365.

Dupont, D. (2003). Modelling and experimental validation of the constitutive law and cracking behavior of steel fibre reinforced concrete. In PhD Thesis, Katholieke Universiteit Leuven.

Dupont, D., & Vandewalle, L. (2005). Distribution of steel fibres in rectangular sections. Cement and Concrete Composites, 27(3), 391-398.

DYWIDAG-SYSTEMS INTERNATIONAL. (2004). Hormigón de alta resistencia-Primera aplicación de pilares HH.

Easley, T. C., Faber, K. T., & Shah, S. P. (1999). Use of aCrack -Bridging S
Pullout Test to Study Steel Fiber/Cementitious Matrix Composites. Journal of the American Ceramic Society, 82(12), 3513-3520.

Edington, J., & Hannant, D. (1972). Steel fibre reinforced concrete. The effect on fibre orientation of compaction by vibration. Materials and Structures, 5(1), 41-44.

EFNARC. (2002). Specifications and guidelines for SCC, UK .

EHE-08. (2008). Spanish Structural Concrete Code. Spanish Minister of Public Works.

El-Dieb, A. S. (2009). Mechanical, durability and microstructural characteristics of ultra-high-strength self-compacting concrete incorporating steel fibers. Materials & Design, 30(10), 4286-4292.

El-Dieb, A., & Reda Taha, M. (2012). Flow characteristics and acceptance criteria of fiber-reinforced self-compacted concrete (FR-SCC). Construction and Building Materials, 27(1), pp., 585–596.

Elices, M., & Planas, J. (1996). Fracture mechanics parameters of concrete: An overview. Advanced Cement Based Materials, 4, 116-127.

Elices, M., Guinea, G. V., Gomez, J., & Planas, J. (2002). The cohesive zone model: advantages, limitations and challenges. Engineering Fracture Mechanics, 69(2), 137-163.

Elser, M., Tschegg, E., & Stanzl-Tschegg, S. (1996). Fracture behaviour of polypropylene-fibre-reinforced concrete under biaxial loading: An experimental investigation. Composites Science and Technology(56), 933-945.

EN 12350-10. (2010). Testing fresh concrete. Part 10: Self-compacting concrete. L-box test.

EN 12350-2. (2002). Testing fresh concrete-Part 2: Slump test. European Committee for Standardization.

EN 12350-3. (2009). Testing fresh concrete. Part III: Vebe test.

EN 12350-8. (2010). Testing fresh concrete. Part 8: Self-compacting concrete. Slump-flow test.

EN 12350-9. (2010). In Testing fresh concrete. Part 9: Self-compacting concrete. V-funnel test.

EN 12390-13. (2013). Testing hardened concrete - Part 13: Determination of secant modulus of elasticity in compression.

EN 12390-3. (2009). Testing hardened concrete. Part 3: Compressive strength of test specimens.

EN 12390-6. (2009). Testing hardened concrete. Part 6. Tensile spliting strength of test specimens.

EN 12390-8. (2000). Testing hardened concrete. Depth of penetration of water under pressure.

EN 14651:2007+A1. (2007). Test method for metallic fibre concrete. Measuring the flexural tensile strength (limit of proportionality (LOP), residual).

EN 14845-1. (2006). Test methods for fibres in concrete. PartI: Reference concretes.

EN 14845-2. (2006). Test methods for fibres in concrete. Part II: Effect on concrete.

EN 14889-2.(2008). Fibres for concrete.Polymer fibres. Definitions, specifications and conformity.

EN 196-1.(2005). Methods of testing cement–Part 1: determination of strength. European Committee for Standardization.

Enfedaque Diaz, A. (2008). Resistencia a impacto de morteros de cemento reforzados con fibra de vidrio (GRC). Doctoral dissertation, Universidad Politécnica de Madrid, ETSICCP.

Enfedaque, A., Molina-Aldareguía, J. M., Gálvez, F., González, C., & LLorca, J. (2010). Effect of glass fiber hybridization on the behavior under impact of woven carbon fiber/epoxy laminates. Journal of Composite Materials, 44(25), 3051-3068.

Enfedaque, A., Paradela, L., & Sánchez-Gálvez, V. (2012). An alternative methodology to predict aging effects on the mechanical properties of glass fiber reinforced cements (GRC). Construction and Building Materials, 27(1), 425–431.

European Committee for Standardization. (2004). Eurocode 2: design of concrete structures—part 1-1: general rules and rules for buildings.

Exodus 5:6-7. The Holy Bible. English Standard Version Copyright © 2001 by Crossway Bibles, a division of Good News Publishers.

Faifer, M., Ottoboni, R., Toscani, S., & Ferrara, L. (2011). Nondestructive testing of steel-fiber-reinforced concrete using a magnetic approach. Instrumentation and Measurement, IEEE Transactions on, 60(5), 1709-1717.

Fanella, D., & Naaman, A. (1985). Stress-strain properties of fiber reinforced mortar in compression ACI Journal. 82 (4), 475–483.

Fantilli, A. P., & Vallini, P. (2007). A cohesive interface model for the pullout of inclined steel fibers in cementitious matrixes. Journal of Advanced Concrete Technology, 5(2), 247-258.

Fantilli, A. P., Vallini, P., & Chiaia, B. (2011). Ductility of fiber-reinforced self-consolidating concrete under multi-axial compression. Cement and Concrete Composites, 33(4), 520-527.

Fathy, A. M., Sanz, B., Sancho, J. M., & Planas, J. (2008). Determination of the bilinear stress-crack opening curve for normal and high-strength concrete. Fatigue & Fracture of Engineering Materials & Structures, 31(7), 539-548.

Fava, C., Bergol, L., Fornasier, G., G. F., & Rocco, C. (2003). Comportamiento en fractura de hormigones autocompactantes. Anales de Mecánica de la fractura, 20(1), 338–343. Benicassim, España.

Fava, C., L., Bergol, G.Fornasier, Giangrasso, F., & C.Rocco. (2003). Fracture behaviour of self-compacting concrete. Proceedings of the 3rd international RILEM symposium on self-compacting concrete (pp. 628-636). Reykjavik: O. Wallevik, I. Nielsson.

Felekoğlu, B., Tosun, K., & Baradan, B. (2009). Effects of fibre type and matrix structure on the mechanical performance of self-compacting micro-concrete composites. Cement and Concrete Research, 39(11), 1023-1032.

Ferguson, R., & Shum, S. B. (2012). Social learning analytics: five approaches. Proceedings of the 2nd international conference on learning analytics and knowledge, (pp. 23-33).

Fernández Cánovas, M. (2007). Hormigón. Colegio de Ingenieros de Caminos, Canales y Puertos.

Ferrara, L. P.-D. (2007). A method for mix-design of fiber-reinforced self-compacting concrete. Cement and Concrete Research, 7(6), 957–971.

Ferrara, L., & Meda, A. (2006). Relationships between fibre distribution, workability and the mechanical properties of SFRC applied to precast roof elements. Materials and Structures, 39(4), 411-420.

Ferrara, L., Faifer, M., & Toscani, S. (2012). A magnetic method for non destructive monitoring of fiber dispersion and orientation in steel fiber reinforced cementitious composites—part 1: method calibration. Materials and Structures, 45(4), 575-589.

Ferrara, L., Faifer, M., Muhaxheri, M., & Toscani, S. (2012). A magnetic method for non destructive monitoring of fiber dispersion and orientation in steel fiber reinforced cementitious composites. Part 2: Correlation to tensile fracture toughness. Materials and Structures, 45(4), 591-598.

Ferrara, L., Ozyurt, N., & di Prisco, M. (2011). High mechanical performance of fibre reinforced cementitious composites: the role of “casting-flow induced” fibre orientation. Materials and Structures, 44(1), 109-128.

Ferrara, L., Park, Y. D., & Shah, S. P. (2008). Correlation among fresh state behavior, fiber dispersion, and toughness properties of SFRCs. Journal of Materials in Civil Engineering, 20(7), 493-501.

Ferrara, L., Park, Y. D., & Shah, S. P. (2007). A method for mix-design of fiber-reinforced self-compacting concrete. Cement and Concrete Research, 7(6), 957–971.

fib Model Code. (2010). Model Code. Paris: Fédération Internationale du Béton fib/International Federation for Structural Concrete.

Filho, R., Scrivener, K., England, G., & Ghavami, K. (2000). Durability of alkali-sensitive sisal and coconut fibres in cement mortar composites. Cement and Concrete Composites, 22(2), 127–143.

Foster, S. J., Voo, Y. L., & Chong, K. T. (2006). FE analysis of steel fiber reinforced concrete beams failing in shear: variable engagement model. ACI Special Publication (237).

Fu, S. Y., & Lauke, B. (1996). Effects of fiber length and fiber orientation distributions on the tensile strength of short-fiber-reinforced polymers. Composites Science and Technology, 56(10), 1179-1190.

Galao, O., Zornoza, E., Baeza, F. J., Bernabeu, a., & Garcés, P. (2012). Efecto de la adición de nanofibras de carbono en las propiedades mecánicas y de durabilidad de materiales cementantes. Materiales de Construcción, 62(307), 343–357.

Gálvez, J. C., Cendon, D. A., & Saouma, V. (2002). A discrete crack approach to normal/shear cracking of concrete. Cement and concrete research, 32(10), 1567-1585.

Gálvez, J. C., Enfedaque, A., & Alberti, M. G. (2014). Materialesde construcción II: Apuntes de hormigón reforzado con fibras. ETSICCP, UPM, Unidad Docente de Materiales de Construcción.

Garcés, P., Zornoza, E., Andión, L. G., Baeza, F., & Galao, Ó. (2010). Hormigones conductores multifuncionales. Alicante, España, ISBN 978-84-9948-080-0: Editorial Club Universitario ECU.

Garcia, T., Agulló, L., Aguado, A., & Canals, G. (2004). Evaluacion de la tenacidad en el hormigón proyectado reforzado con fibras poliméricas de alto módulo. Boletín de la Sociedad Española de Cerámica y Vidrio, 43(2), 552–555.

Gent, A. N., & Wang, C. (1992). Matrix cracking initiated by fibre breaks in model composites. Journal of materials science, 27(9), 2539-2548.

Georgiadis, A., Anagnostopoulos, N., & Sideris, K. (2007). Mechanical characteristics of self-compacting concretes produced with different filler material. In RILEM (Ed.), Proceeding of Fifth International RILEM Symposium on Self-Compacting Concrete, (pp. 611).

Gerstle, W., & Ingraffea, A. R. (1991). Does bond-slip exist? Concrete International, 13(1), 44-48.

Gettu, R., & Agulló, L. (2004). Estado del arte del hormigón autocompactable y su caracterización (Parte I). Cemento y Hormigón, 861, 50–67.

Gettu, R., & Agulló, L. (2004). Estado del arte del hormigón autocompactable y su caracterización (Parte II). Cemento y Hormigón, 862, 32–55.

Gettu, R., Aguado, A., Zangelmi, E., Carmona, S., & Carbonari, G. (1998). Recientes avances en lacaracterización del comportamiento mecánico de hormigones de altas prestaciones. 1er Symp. Nacional de Hormigón de Altas Prestaciones, (pp. 41-51). Madrid, ETSICCP, Univ. Politécnica de Madrid.

Gettu, R., Gardner, D. R., Saldivar, H., & Barragán, B. E. (2005). Study of the distribution and orientation of fibers in SFRC specimens. Materials and Structures , 38(1), 31-37.

Giaccio, G., Tobes, J., & Zerbino, R. (2008). Use of small beams to obtain design parameters of fibre reinforced concrete. Cement and Concrete Composites, 30(4), 297-306.

Glaister, P. (1997). Playing cards with Buffon. Mathematical Spectrum , 30(1), 8-9.

Goel, S., Singh, S., & Singh, P. (2012). Flexural fatigue strength and failure probability of Self Compacting Fibre Reinforced Concrete beams. Engineering Structures, 40, 131–140.

Goldfein, S. (1963). Plastic fibrous reinforcement for Portland Cement. Technical Report No. 1757-TR, US Army Engineering Research and Development Laboratories, Fort Belvoir.

Gomes, P. G. (2001). Experimental Optimization of High-Strength Self-Compacting Concrete. Proceedings Second International Symposium on Self-Compacting Concrete, (pp. 377-386).

Gómez, J. F., & Maestro, M. B. (2005). Guía práctica para la utilización del hormigón autocompactante. Instituto Español del Cemento y sus Aplicaciones.

Granju, J.-L., & Balouch, S. U. (2005). Corrosion of steel fibre reinforced concrete from the cracks. Cement and Concrete Research, 35(3), 572-577.

Groth, P. (2000). Fibre reinforced concrete – Fracture mechanics methods applied on self-compaction concrete and energetically modified binders. PhD Thesis, Luleå University of Technology.

Grünewald, S. (2004). Performance-based design of self-compacting fibre reinforced concrete. Delft, The Netherlands: Delft University Press.

Grünewald, S., & Walraven, J. (2000). Self-compacting fiber reinforced concrete - Test methods and properties of the fresh state. Ibausil, 14. Int. Baustofftagung, Weimar, (pp. 51-66).

Grünewald, S., & Walraven, J. C. (2001). Parameter-study on the influence of steel fibers and coarse aggregate content on the fresh properties of self-compacting concrete. Cement and Concrete Research, 31(12), 1793-1798.

Grünewald, S., & Walraven, J. C. (2002). High strength self-compacting fibre reinforced concrete: behaviour in the fresh and hardened state. 6th International Symposium on HSC/HPC, Vol. 2, (pp. 977-89).

Grünewald, S., & Walraven, J. C. (2003). Rheological measurements on self-compacting fibre reinforced concrete. PRO 33: 3rd International RILEM Symposium on Self-Compacting Concrete (pp. 49-58). RILEM Publications.

Grünewald, S., Laranjeira, F., Walraven, J., Aguado, A., & Molins, C. (2012). Improved Tensile Performance with Fiber Reinforced Self-compacting Concrete. In High Performance Fiber Reinforced Cement Composites 6 (pp. 51-58). Netherlands: Springer.

Grupo Español del Hormigón. (1996). Durabilidad de estructuras de hormigón. Guía de diseño CEB, boletín GEHO 12.

Guinea, G. V., Planas, J., & Elices, M. (1994). A general bilinear fit for the softening curve of concrete. Materials and Structures, 27(2), 99-105.

Gul, M., Bashir, A., & Naqash, J. A. (2014). Study of Modulus of elasticity of Steel Fiber Reinforced Concrete. International Journal of Engineering and Advanced Technology, 3(4), 304-309.

Gupta, P., Banthia, N., & Yan, C. (2000). Fiber Reinforced Wet-Mix Shotcrete under Impact. Journal of Materials in Civil Engineering, 12(1), 81–90.

Habel, K. (2004). Structural behaviour of elements combining ultra-high performance fibre reinforced concretes (UHPFRC). Tesis Doctoral. Lausanne, Suiza: Ecole Polytechnique Federale de Lausanne.

Habel, K. E., & Brühwiler, E. (2006). Structural response of elements combining ultrahigh-performance fiber-reinforced concretes and reinforced concrete. Journal of Structural Engineering, 132(11), 1793-1800.

Habel, K., Viviani, M., Denarié, E., & Brühwiler, E. (2006). Development of the mechanical properties of an Ultra-High Performance Fiber Reinforced Concrete (UHPFRC). Cement and Concrete Research, 36(7), 1362–1370.

Han, T.-Y., Lin, W.-T., An Cheng, R. H., & Huang, C.-C. (2012). Influence of polyolefin fibers on the engineering properties of cement-based composites containing silica fume. Materials & Design, 37, 569-576.

Hillerborg, A. (1980). Analysis of fracture by means of the fictitious crack model, particularly for fibre reinforced concrete. The International Journal of Cement Composites.

Hillerborg, A., Modéer, M., & Petersson, P. E. (1976). Analysis of crack formation and crack growth in concrete by means of fracture mechanics and finite elements. Cement and Concrete Research, 6(6), 773-78.

Hine, P. J., Davidson, N., Duckett, R. A., & Ward, I. M. (1995). Measuring the fibre orientation and modelling the elastic properties of injection-moulded long-glass-fibre-reinforced nylon. Composites Science and Technology , 53(2), 125-131.

Hine, P., Parveen, B., Brands, D., & Caton-Rose, F. (2014). Validation of the modified rule of mixtures using a combination of fibre orientation and fibre length measurements. Composites Part A: Applied Science and Manufacturing, 64, 70-78.

Hoy, C. W. (1998). Mixing and mix proportioning of fibre reinforced concrete. University of Paisley.

Ivorra, S., Garcés, P., Catalá, G., Andión, L. G., & Zornoza, E. (2010). Effect of silica fume particle size on mechanical properties of short carbon fiber reinforced concrete. Materials & Design, 31(3), 1553-1558.

Janotka, I., Krajci, L., Komlos, K., Frt'alová, M., & Halás, P. (1992). Investigations on the relationship between phase composition and chloride corrosion of steel fiber reinforcement in cement mortar. ACI Materials Journal, 89(3), 223-229.

Japan Road Association. (2002). Japanese specifications for highway bridges, part V: seismic Design.

Jean-Louis Granju, S. U. (2005, March). Corrosion of steel fibre reinforced concrete from the cracks. Cement and Concrete Research, 35(3), 572-577.

Jerrett, D., & Cuddington, J. T. (2008). Broadening the statistical search for metal price super cycles to steel and related metals. Resources Policy, 33(4), 188-195.

Jo, B.-W., Shon, Y.-H., & Kim, Y.-J. (2001). The evaluation of elastic modulus for steel fiber reinforced concrete. Russian Journal of Nondestructive Testing, 37(2), 152-161.

Johnston, D. (1996). Proportioning, mixing and placement of fibre-reinforced cements and concretes, Production Methods and Workability of Concrete. In M. a. Bartos (Ed.). E & FN Spon, London.

Jones, P., Austin, S., & Robins, P. (2008). Predicting the flexural load-deflection response of steel fibre reinforced concrete from strain, crack-width, fibre pull-out and distribution data. Materials and Structures, 41(3), 449-463..

Kakooei, S., Akil, H. M., Jamshidi, M., & Rouhi, J. (2012). The effects of polypropylene fibers on the properties of reinforced concrete structures. Construction and Building Materials, 27(1), 73-77.

Kameswara Rao, C. V. (1979). Effectiveness of random fibres in composites. Cement and Concrete Research, 9(6), 685-693.

Kang, S. T., & Kim, J. K. (2011). The relation between fiber orientation and tensile behavior in an Ultra High Performance Fiber Reinforced Cementitious Composites (UHPFRCC). Cement and Concrete Research, 41(10), 1001-1014.

Kang, S. T., Lee, B. Y., Kim, J. K., & Kim, Y. Y. (2011). The effect of fibre distribution characteristics on the flexural strength of steel fibre-reinforced ultra high strength concrete. Construction and Building Materials, 25(5), 2450-2457.

Kaufmann, J., Frech, K., Schuetz, P., & Münch, B. (2013). Rebound and orientation of fibers in wet sprayed concrete applications. Construction and Building Materials, 49, 15-22.

Kaufmann, J., Lübben, J., & Schwitter, E. (2007). Mechanical reinforcement of concrete with bi-component fibers. Composites Part A: Applied Science And Manufacturing, 38(9), 1975-1984.

Kawashima, K., Zafra, R., Sasaki, T., Kajiwara, K., & Nakayama, M. (2011). Effect of Polypropylene Fiber Reinforced Cement Composite and Steel Fiber Reinforced Concrete for Enhancing the Seismic Performance of Bridge Columns. Journal of Earthquake Engineering, 15(8), 1194–1211.

Kazemi, M., Fazileh, F., & Ebrahiminezhad, M. (2008). Cohesive Crack Model and Fracture Energy of Steel-Fiber-Reinforced-Concrete Notched. Journal of Material in Civil Engineering, 19(10), 884–890.

Khayat, K. H., A., T.-H., Tamboue, B. T., & Petrov, N. (1996). Réfection du quai No 45 du Port de Montréal, Final report. Université de Sherbrooke, Sherbrooke, QC, Canada.

Kim, D. J., Naaman, A. E., & El-Tawil, S. (2008). Comparative flexural behavior of four fiber reinforced cementitious composites. Cement & Concrete Composites, 30(10), 917-928.

Kim, J.-K., Zhou, L., & Mai, Y. -W. (1993). Stress transfer in the fibre fragmentation test. Journal of Materials Science, 28(22), 6233–6245.

Klug, Y., & Holschemacher, H. (2003). Comparison of the hardened properties of selfcompacting and normal vibrated concrete. Proceedings of the Third International Symposium on Self-Compacting Concrete.

Köksal, F., Altun, F., Yigit, I., & Sahin, Y. (2008). Combined effect of silica fume and steel fiber on the mechanical properties of high strength concretes. Construction and Building Materials, 22(8), 1874-1880.

Komloš, K., Babál, B., & Nürnbergerová, T. (1995, June). Hybrid fibre-reinforced concrete under repeated loading. Nuclear Engineering and Design, 156(1-2), 195-200.

Kooiman, A. G. (2000). Modelling Steel Fibre Reinforced Concrete for Structural Design. TU Delft, Delft University of Technology.

Kooiman, A. G., Van Der Veen, C., & Walraven, J. C. (2000). Modelling the post-cracking behaviour of steel fibre reinforced concrete for structural design purposes. Heron, 45(4), 275-308.

Krenchel, H. (1975). Fibre spacing and specific fibre surface. In Fibre reinforced cement and concrete (pp. 69-79). UK: The Construction Press.

Krenchel, H., & Shah, S. P. (1986). Synthetic fibres for tough and durable concrete. Developments in Fiber Reinforced Cement and Concrete, RILEM Symposium, (pp. 333-338).

Lamanna, A. J., & Scholer, C. F. (2002). Design of Durable Concrete Railroad Crossings. Final Report, FHWA/IN/JTRP.

Lancha, J. C. (2014). FRC wind Towers. 2nd FRC International Workshop Fiber Reinforced Concrete: from design to Structural Applications, 1st ACI-FIB Joint Workshop. Montreal, Canada.

Lappa, L. (2007). High strength fibre reinforced concrete: static and fatigue behavior in bending. PhD Thesis, Delft University of Technology.

Laranjeira, F. (2010). Design oriented constitutive model for steel fiber reinforced concrete. Tesis doctoral, Universidad Politécnica de Cataluña.

Laranjeira, F., Aguado, A., & Molins, C. (2010a). Predicting the pullout response of inclined straight steel fibers. Materials and Structures, 43(6), 875-895.

Laranjeira, F., Aguado, A., Molins, C., Grünewald, S., Walraven, J., & Cavalaro, S. (2012). Framework to predict the orientation of fibers in FRC: a novel philosophy. Cement and Concrete Research, 42(6), 752-768.

Laranjeira, F., Grünewald, S., Walraven, J., Blom, C., Molins, C., & Aguado, A. (2011). Characterization of the orientation profile of steel fiber reinforced concrete. Materials and Structures, 44(6), 1093-1111.

Laranjeira, F., Molins, C., & Aguado, A. (2010b). Predicting the pullout response of inclined hooked steel fibers. Cement and Concrete Research, 40(10), 1471-1487.

Lataste, J. F., Behloul, M., & Breysse, D. (2008). Characterisation of fibres distribution in a steel fibre reinforced concrete with electrical resistivity measurements. NDT & E International, 41(8), 638-647.

Lawrence, P. (1972). Some theoretical considerations of fibre pull-out from an elastic matrix. Journal of Materials Science, 7(1), 1-6.

Lee, C., & Kim, H. (2010). Orientation factor and number of fibers at failure plane in ring-type steel fiber reinforced concrete. Cement and Concrete Research, 40(5), 810-819.

Lee, M. K., & Barr, B. I. G. (2004). An overview of the fatigue behaviour of plain and fibre reinforced concrete. Cement and Concrete Composites, 26(4), 299-305.

Leemann, A. B., & Gasser P. & Holzer, L. (2006). Influence of compaction on the interfacial transition zone and the perebility of concrete. Cement and Concrete Research, 36(8), 1425-1433.

Leung, C. K., & Li, V. (1992). Effect of fiber inclination on crack bridging stress in brittle fiber reinforced brittle matrix composites. Journal of Mechanics and Physics of Solids, 40(6), 1333-1362.

Leung, C., & Li, V. (1991). New strength-based model for the debonding of discontinuous fibres in an elastic matrix. Journal of Materials Science, 26(22), 5996–6010.

Li, V. C. (1992). A simplified micromechanical model of compressive strength of fiber-reinforced cementitious composites. Cement and Concrete Composites, 14(2), 131-141.

Li, V. C., & Stang, H. (1997). Interface property characterization and strengthening mechanisms in fiber reinforced cement based composites. Advanced Cement Based Materials, 6(1), 1-20.

Li, V. C., Wang, Y., & Backer, S. (1990). Effect of inclining angle, bundling and surface treatment on synthetic fibre pull-out from a cement matrix. Composites, 21(2), 132-140.

Li, V. C., Ward, R., & Hmaza, A. M. (1992). Steel and synthetic fibers as shear reinforcement. ACI Materials Journal, 89(4), 499-508.

Li, V., Stang, H., & Krenchel, H. (1993). Micromechanics of crack bridging in fiber reinforced concrete. Materials and Structures, 26(162), 486-494.

Li, Y., Mai, Y.-W., & Ye, L. (2000). Sisal fibre and its composites: a review of recent developments. Composites Science and Technology, 60(11), 2037–2055.

Lim, T., Paramsivam, P., & Lee, S. (1987). Bending Behaviour of Steel-Fiber Concrete Beams. ACI Journal, 286-298.

Liu, M. (2010). Self-compacting concrete with different levels of pulverized fuel ash. Construction and Building Materials, 24(7), 1245-1252.

Liu, X., Ye, G., De Schutter, G., Yuan, Y., & Taerwe, L. (2008). On the mechanism of polypropylene fibres in preventing fire spalling in self-compacting and high-performance cement paste. Cement and Concrete Research, 38(4), 487–499.

Lok, T. S., & Zhao, P. J. (2004). Impact Response of Steel Fiber-Reinforced Concrete Using a Split Hopkinson Pressure Bar. Journal of Materials in Civil Engineering, 54–59.

Lok, T., & Xiao, L. (1998). Tensile behavior and moment-curvature relationship of steel fibr reinforced concrete. Magazine of Concrete Research, 50(4):359-36.

López, J. A., Serna, P., Camacho, E., Coll, H., & Navarro-Gregori, J. (2014). First Ultra-High-Performance Fibre-Reinforced Concrete Footbridge in Spain: Design and Construction. Structural Engineering International, 24(1), 101-104.

Malhotra, V. M., & Mehta, P. K. (2005). High-performance, high-volume fly ash concrete : materials, mixture proportioning, properties, construction practice, and case histories (Second Edition). Ottawa, Canada: Suppementary Cementing Materials for Sustainable Development.

Mangat, P., & Gurusamy, K. (1988). Corrosion resistance of steel fibres in concrete under marine exposure. Cement and Concrete Research, 18(1), 44-54.

Markeset, G. (1993). Failure of concrete under compressive strain gradients. PhD Thesis, Norwegian Institute of Technology, Trondheim.

Markovich, I., Van Mier, J. G., & Walraven, J. C. (2001). Single fiber pullout from hybrid fiber reinforced concrete. Heron, 46(3), 191-200.

Marquis de Laplace, P. S. (1814). Essai philosophique sur les probabilités.

Martinie, L., & Roussel, N. (2011). Simple tools for fiber orientation prediction in industrial practice. Cement and Concrete Research, 41(10), 993–1000.

Martinie, L., Rossi, P., & Roussel, N. (2010). Rheology of fiber reinforced cementitious materials: classification and prediction. Cement and Concrete Research, 40(2), 226-234.

Mas, P. B. (2012). Criterios de selección del aditivo superplastificante en HAC. 3º Congreso Iberoamericano sobre hormigón autocompactante. Avances y Oportunidades, (pp. 55-66). Madrid.

Maya, F. L. (2011). Estudio de estructuras aporticadas prefabricadas con uniones basadas en hormigones con fibras. Doctoral dissertation, PhD Thesis, ETSICCP-Universidad Politécnica de Madrid.

McIntyre, J. E. (2004). Synthetic fibres: nylon, polyester, acrylic, polyolefin. Elsevier.

Meda, A., & Rinaldi, Z. (2014). Steel fibers reinforcement for precast lining in tunnels with different diameters. 2nd FRC International Workshop Fiber Reinforced Concrete: from design to Structural Applications, 1st ACI-FIB Joint Workshop. Montreal, Canada.

Melián, G., Barluenga, G., & Hernández-Olivares, F. (2010). Aumento de la tenacidad de hormigones autocompactables reforzados con fibras cortas de polipropileno. Materiales de Construcción, 60(300), 83–97.

Michels, J., Waldmann, D., Maas, S., & Zürbes, A. (2012). Steel fibers as only reinforcement for flat slab construction–Experimental investigation and design. Construction and Building Materials, 26(1), 145-155.

Mindess, S., Wang, N., Rich, L., & Morgan, D. (1998). Impact Resistance of Polyolefin Fibre Reinforced Precast Units. Cement and Concrete Composites, 20(5), 387-392.

Mindess, S., Young, J., & Darwin, D. (2003). Concrete (Second Edition). Pearson Education, Upper Saddle River, NJ.

Mlekusch, B. (1999). Fibre orientation in short-fibre-reinforced thermoplastics II. Quantitative measurements by image analysis. Composites Science and Technology, 59(4), 547-560.

Mobasher, B. (2014). Design based approaches for fiber reinforced concrete - An overview of ACI committee 544 activities. 2nd FRC International Workshop Fiber Reinforced Concrete: from design to Structural Applications, 1st ACI-FIB Joint Workshop. Montreal, Canada.

Monteagudo, S. (2014). Estudio microestructural y de los procesos de hidratación de cementos con adiciones. Tesis Doctoral, ETSICCP, Universidad Politécnica de Madrid.

Mu, R., Miao, C., Luo, X., & Sun, W. (2002). Interaction between loading, freeze–thaw cycles, and chloride salt attack of concrete with and without steel fiber reinforcement. Cement and Concrete Research, 32(7), 1061–1066.

Naaman, A. E. (2003). Engineered steel fibers with optimal properties for reinforcement of cement composites. Journal of Advanced Concrete Technology, 1(3), 241-252.

Naaman, A., & Najm, H. (1991). Bond-slip mechanisms of steel fibers in concrete. ACI Materials Journal, 88(2), 135-145.

Nanni, A. (1991). Fatigue behaviour of steel fiber reinforced concrete. Cement and Concrete Composites, 13(4), 239–245.

Narayanan, R., & Darwish, I. (1987). Shear in prestressed concrete beams containing steel fibres. International Journal of Cement Composites and Lightweight Concrete, 9(2), 81–90.

Navarro Ferrer, F., & Estaban García, M. (2003). Empleo del hormigón autocompactable en la prefabricación. Hormigón y Acero, 228-229, 161-166.

Nawy, E. (2008). Construction Engineering Handbook. 2ed. FL, USA: Taylor & Francis group.

NCSP-07. (2007). Spanish Earthquake Resistant Code: Bridges. Ministerio de Fomento, Madrid.

Nemati, K. M., & Stroeven, P. (2001). Stereological analysis of micromechanical behavior of concrete. Materials and Structures, 34(8), 486-494.

Neville, A. M. (1981). Properties of concrete (Third Edition ed.). London: Pitman.

Newman, J., & Choo, B. S (2003). Advanced Concrete Technology 3: Processes. Butterworth-Heinemann.

Níelsson, I., & Wallevik, Ó. H. (2003). Rheological Evaluation of Some Empirical Test Methods – Preliminary Results. PRO 33: 3rd International RILEM Symposium on Self-Compacting Concrete, 33, 59-68. RILEM publications.

Oh, B. H., Kim, J. C., & Choi, Y. C. (2007). Fracture behavior of concrete members reinforced with structural synthetic fibers. Engineering Fracture Mechanics, 74(1-2), 243-257.

Okamura, H. &. (1999). Self-compacting concrete development, present and future. Proceedings of first international rilemsymposiumonself-compacting concrete (PRO 7), pp. 3–14. Stockholm: RILEM Publications.

Okamura, H. O. (1998). A rational mix-design method for mortar in sel-compacting concrete. The 6th East Asia-Pacific Conference on Structural Engineering & Construction.

Orbe, A., Cuadrado, J., Losada, R., & Rojí, E. (2012). Framework for the design and analysis of steel fiber reinforced self-compacting concrete structures. Construction and Building Materials, 35, 676-686.

Ozawa, K., & Ouchi, M. (1999). Proceedings of the International Workshop on Self-Compacting Concrete. Kochi.

Ozyurt, N., Mason, T. O., & Shah, S. P. (2006). Non-destructive monitoring of fiber orientation using AC-IS: An industrial-scale application. Cement and Concrete Research, 36(9), 1653-1660.

Pacios Alvarez, A., Tanner, P., & Márquez Zárate, J. M. (2012). Prototipo de la fabricación de una bóveda con hormigón autocompactante con fibras poliméricas. Lecciones aprendidas. 3º Congreso Iberoamericano sobre hormigón autocompactante. Avances y Oportunidades, (pp. 447-455). Madrid.

Pacios, A., Miguel, C. d., Gutiérrez-Jiménez, J., & Tanner, P. (2011). Polypropylene fiber-reinforced self-compactin concrete for the reconstruction of the cathedral of La Laguna, Canary Island, Spain. Proceedings of the 9th Symposium on High Performance Concrete. Design, Verification and Utilization. Rotorua: Nueva Zelanda.

Pająk, M., & Ponikiewski, T. (2013). Flexural behavior of self-compacting concrete reinforced with different types of steel fibers . Construction and Building Materials, 47, 397-408.

Park, K., Paulino, G. H., & Roesler, J. (2010). Cohesive fracture model for functionally graded fiber reinforced concrete. . Cement and Concrete Research, 40(6), 956–965.

Park, S. H., Kim, D. J., Ryu, G. S., & Koh, K. T. (2012). Tensile behavior of Ultra High Performance Hybrid Fiber Reinforced Concrete. Cement and Concrete Composites, 34(2), 172–184.

Parra, C. V. (2007). Mechanical properties of selfcompacting concrete. Proceedings of the Fifth International RILEM Symposium on SCC, RILEM, pp. 645–650.

Parra, C., Valcuende, M., & Gómez, F. (2011). Splitting tensile strength and modulus of elasticity of self-compacting concrete. Construction and Building Materials, 25(1), 201-207.

Pastoriza, A., Andion, L. G., & Nuñez, A. (1970). Elementos de elasticidad. E.T.S.I.C.C.P. MADRID.

Pérez, A., Climent, M., & Garcés, P. (2010). Electrochemical extraction of chlorides from reinforced concrete using a conductive cement paste as an anode. Corrosion Science , 52(5), 1576-1581.

Persson, B. (2005). Shrinkage and creep of high performance self-compacting concrete (HPSCC). ACI Special Publication, (pp. 155–179).

Petersson, Ö., & Billberg, P. (1996). A model for Self Compacting Concrete. RILEM Conference Production Methods an Workabiliy of Concrete. Scotland.

Petersson, Ö., & Billberg, P. (1999). Investigation on blocking of self- compacting concrete with different maximum aggregate size and use of viscosity agent instead filler. RILEM Symposium Stockholm, (pp. 333-344).

Petroski, H. (2006). Success through failure: The paradox of design. Princeton University Press.

Pigeon, M., & Pleu, R. (1995). Durability of concrete in cold climates.First Edition. Great Britain.

Planas, J., & Elices, M. (1992). Shrinkage eigenstresses and structural size-effect. Fracture Mechanics of Concrete Structures, Elsevier Applied Science, London, 939-950.

Planas, J., Elices, M., Guinea, G. V., Gómez, F. J., Cendón, D. A., & Arbilla, I. (2003). Generalizations and specializations of cohesive crack models. Engineering Fracture Mechanics, 70(14), 1759-1776.

Polanco-Loria, M. (1997). Numerical modelling of plain and reinforced concrete by damage mechanics. Trondheim : Department of Structural Engineering, Norwegian University of Science and Technology .

Pompo, A., Stupak, P. R., Nicolais, L., & Marchese, B. (1996). Analysis of steel fibre pull-out from a cement matrix using video photography. Cement and Concrete Composites, 18(1), 3-8.

Ponikiewski, T. (2010). The workability of steel fibre reinforced self-compacting concrete. Modern buildind materials, structures and techniques, (pp. 264-269). Vilnius Gediminas Technical University.

Ponikiewski, T., Gołaszewski, J., Rudzki, M., & Bugdol, M. (2014). Determination of steel fibres distribution in self-compacting concrete beams using X-ray computed tomography. Archives of Civil and Mechanical Engineering.

Pons, G., Proust, E., & Assié, S. (2003). Creep and Shrinkage of self compacting concrete: A Different Behaviour compared with Vibrated Concrete? Proceedings of the Third International Symposium on Self-Compacting Concrete, RILEM, (pp. 645-654).

Poppe, A. &. (2005). Creep and shrinkage of self-compacting concrete. First International Symposium on Design, Performance and Use of Selfconsolidating Concrete, pp. 329–336.

Prisco, M. d., Lamperti, M., Lapolla, S., & R. Khurana. (2008). HPFRCC thin plates for precast roofing. Proceedings of second international symposium on ultra high performance concrete. Kassel.

Pujadas, P. (2013). Caracterización y diseño del homigón reforzado con fibras plásticas. Tesis Doctoral, Universidad Politécnica de Cataluña.

Pujadas, P., Blanco, A., Cavalaro, S. H., Aguado, A., Grünewald, S., Blom, K., & Walraven, J. C. (2014). Plastic fibres as the only reinforcement for flat suspended slabs: Parametric study and design considerations. Construction and Building Materials, 70, 88-96.

Pujadas, P., Blanco, A., Cavalaro, S., & Aguado, A. (2014). Plastic fibres as the only reinforcement for flat suspended slabs: Experimental investigation and numerical simulation. Construction and Building Materials, 57, 92-104.

Pujadas, P., Blanco, A., Cavalaro, S., de la Fuente, A., & Aguado, A. (2014). Fibre distribution in macro-plastic fibre reinforced concrete slab-panels. Construction and Building Materials, 64, 496-503.

Purnell, P., & Beddows, J. (2005). Durability and simulated ageing of new matrix glass fibre reinforced concrete. Cement and Concrete Composites, 27(9), 875-884.

Purnell, P., Short, N. R., Page, C. L., Majumdar, A. J., & Walton, P. L. (1998). Durability of GRC made with new cementitious matrices. GRC Proceedings 1998.

Purnell, P., Short, N., & Page, C. (1999). Accelerated ageing characteristics of glass-fibre reinforced cement made with new cementitious matrices. Composites Part A: Applied Science and Manufacturing, 30(9), 1073–1080.

Purnell, P., Short, N., Page, C., & Majumdar, A. (2000). Microstructural observations in new matrix glass fibre reinforced cement. Cement and concrete Research, 30(11), 1747–1753.

Qian, C., & Stroeven, P. (2000a). Fracture properties of concrete reinforced with steel–polypropylene hybrid fibres. Cement and Concrete Composites, 22(5), 343-351.

Qian, C., & Stroeven, P. (2000b, January). Development of hybrid polypropylene-steel fibre-reinforced concrete. Cement and Concrete Research, 30(1), 63-69.

Radtke, F. K., Simone, A., & Sluys, L. J. (2010). A computational model for failure analysis of fibre reinforced concrete with discrete treatment of fibres. Engineering Fracture Mechanics, 77(4), 597-620.

Ramakrinshnan, V. (1999). Structural Application of Polyolefin Fiber Reinforced Concrete. ACI , Special Publication 183(13), 235-253.

Ramakrishnan, V., & MacDonald, C. N. (1997). Durability evaluations and performance histories of projects using polyolefin fiber reinforced concrete. ACI Special Publication170. 4th Internaitonal Conference indurability of concrete, pp. 665-680.

Ramakrishnan, V., & Sivakumar, C. (1999). Performance of Polyolefin Fiber Reinforced Concrete Under Cycling Loading. ACI SP, Special Publication 186, 161-182.

Rao, C. K. (1979). Effectiveness of random fibres in composites. Cement and Concrete Research, 9(6), 685-693.

Ravindrarajah, R., & Tam, C. (1984). Flexural strength of steel fibre reinforced concrete beams. International Journal of Cement Composites and Lightweight Concrete, 6(4), pp. 273-278.

Redon, C., Chermant, L., Chermant, J. L., & Coster, M. (1998). Assessment of fibre orientation in reinforced concrete using Fourier image transform. Journal of Microscopy, 191, 258-265.

Redon, C., Chermant, L., Chermant, J. L., & Coster, M. (1999). Automatic image analysis and morphology of fibre reinforced concrete. Cement and Concrete Composites, 21(5), 403-412.

RILEM- TC 162-TDF. (2000). Test and design methods for steel fibre reinforced concrete. Materials and Structures, 33, 75-81.

RILEM TC-162-TDF. (2002). Bending test: Final recommendations.

RILEM TC162-TDF. (2002). Test and Design methods for Steel Fibre Reinforced Concrete: Bending test (final recommendation). Materials and Structures, 35, 579-582.

RILEM TC-187-SOC. (2007). Indirect test for stress-crack opening curve.

Robins, P. J., Austin, S. A., & Jones, P. A. (2003). Spatial distribution of steel fibres in sprayed and cast concrete. Magazine of Concrete Research, 55(3), 225-235.

Robins, P., Austin, S., & Jones, P. (2002). Pull-out behaviour of hooked steel fibres. Materials and Structures, 35(August), 434–442.

Rocco, C., Guinea, G. V., Planas, J., & Elices, M. (1999). Size effect and boundary conditions in the Brazilian test: experimental verification. Materials and Structures, 32(3), 210-217.

Roelfstra, P. E., & Wittmann, F. H. (1986). Numerical methods to link strain softening with failure of concrete. Fracture Toughness and Fracture Energy , 163-175.

ROM 4.1-94. (1994). Recomendaciones para proyectar y construir Pavimentos Portuarios. Ministerio de Fomento.

Romero Mendoza, H. (2011). Tesis Doctoral: Deterioro del hormigón sometido a ensayos acelerados de hielo-deshielo en presencia de cloruros. ETSICCP-Universidad Politécnica de Madrid.

Romualdi, J. P., & Batson, G. B. (1963). Behavior of reinforced concrete beams with closely spaced reinforcement. ACI. ACI Journal Proceedings, 60(6).

Romualdi, J. P., & Mandel, J. A. (1964). Tensile Strength of concrete Affected by Unigormly Distributed and Closely Spaced Short Lengths of wire Reinforcement . ACI Journal Proceedings , 61(6).

Romualdi, J., & J., M. (1964). Tensiles strength of concrete affected by uniformly distributed and closely spaced short lengths of wire reinforcement. ACI Journal Proceedings, (pp. 657-672).

Roqueta, G., Jofre, L., Romeu, J., & Blanch, S. (2011). Microwave Time-Domain Reflection Imaging of Steel Fiber Distribution on Reinforced Concrete. Instrumentation and Measurement, IEEE Transactions on, 60(12), 3913-3922.

Rosenbusch, J. (2004). Einfluss der Faserorientierung auf die Beanspruchbarkeit von Bauteilen aus Stahlfaserbeton. Beton und Stahlbetonbau, 99(5), 372-377.

Rozière, E., Grange, S., Turcry, P., & Loukil, i. A. (2007). Influence of paste volume on shrinkage cracking and fracture properties of self-compacting concrete. Cement and Concrete Composites, 29(8), 626-636.

Sahmaran, M., Li, V., & Andrade, C. (2008). Corrosion Resistance Performance of Steel-Reinforced Engineered Cementitious Composite Beams. ACI Materials Journal, 105(3), 243-250.

Sahmaran, M., Yurtseven, A., & Yaman, I. O. (2005, December). Workability of hybrid fiber reinforced self-compacting concrete. Building and Environment, 40(2), 1672-1677.

Şanal, İ., & Özyurt Zihnioğlu, N. (2013). To what extent does the fiber orientation affect mechanical performance? Construction and Building Materials, 44, 671-681.

Santaló, L. A. (2004). Integral geometry and geometric probability. Cambridge University Press.

Schumacher, P. (2006). Rotation capacity of self-compacting steel fiber reinforced concrete. PhD Thesis, Delft University of Technology.

Sebaibi, N. B. (2014). Influence of the distribution and orientation of fibres in a reinforced concrete with waste fibres and powders. Construction and Building Materials, 65, 254-263.

Sedran, T. D. (1996). Mix design of self-compacting concrete. In D. M. P.J.M.Bartos, Production Methods and Workability of Concrete (pp. 439-450). London, England: Eds E&FN Spon.

Sedran, T., & De Larrard, F. (1999). Optimisation of self-compacting concrete thanks to packing model. RILEM Symposium, (pp. 321-332).

Seng, V. &. (2005). Creep and shrinkage of self-compacting concrete with different limestone powder contents. Proceedings of the Fourth International RILEM Symposium on Self-Compacting Concrete, pp. 981–987.

Serna, P. (2007). Recientes ejemplos estructurales de aplicación de hormigón de fibras. Aplicaciones estructurales de hormigón con fibras, Universitat Politècnica de Catalunya. Departament d'Enginyeria de la Construcció (EC), pp. 33-47.

Serna, P., Arango, S., Ribeiro, T., Núñez, a. M., & Garcia-Taengua, E. (2009). Structural cast-in-place SFRC: technology, control criteria and recent applications in Spain. Materials and Structures, 42(9), 1233–1246.

Shah, S. P., & Ouyang, C. (1991). Mechanical Behavior of Fiber-Reinforced Cement-Based Composites. Journal of the American Ceramic Society, 74(11), 2727-2953.

Shah, S. P., & Rangan, B. V. (1971). Fiber reinforced concrete properties. ACI Journal Proceedings, 68(2), pp. 126–135.

Sharama, A. K. (1986). Shear strength of steel fiber reinforced concrete beams. ACI Journal Proceedings, 83(4).

Sharma, A. (2004). Numerical simulations of blast-impact problems using the direct simulation Monte Carlo method. Doctoral dissertation, The Pennsylvania State University.

Silva, F., Filho, R., Filho, F., & Fairbairn, E. (2010). Physical and mechanical properties of durable sisal fiber–cement composites. Construction and Building Materials, 24(5), 777–785.

Sivakumar, A., & Santhanam, M. (2007). A quantitative study on the plastic shrinkage cracking in high strength hybrid fibre reinforced concrete. Cement and Concrete Composites, 29(7), 575-581.

Skarendahl, A., & and Petersson, O. (2000). Self-Compacting Concrete, State of the Art Report of RILEM Technical Committee 174-SSC, Cachan Cedex, France: RILEM Publications S.A.R.L.

Skarendahl, A., & Petersson, O. (2000). Self-Compacting Concrete, State of the Art Report of RILEM Technical Committee 174-SSC. Cachan Cedex, France: RILEM Publications S.A.R.L.

Skazlic, M., & Bjegovic, D. (2004). Effects of hybrid fibres on the properties of fiber-reinforced concrete. In R. F. M. di Prisco (Ed.), 6th International RILEM Symposium on Fibre Reinforced Concretes (pp. 1381-1390). RILEM Publications SARL.

Slowik, V., Villmann, B., Bretschneider, N., & Villmann, T. (2006). Computational aspects of inverse analyses for determining softening curves of concrete. Computer Methods in Applied Mechanics and Engineering, 195(52), 7223–7236.

Soetens, T., Van Gysel, A., Matthys, S., & Taerwe, L. (2013). A semi-analytical model to predict the pull-out behaviour of inclined hooked-end steel fibres. Construction and Building Materials, 43, 253-265.

Solomon, H. (1978). Geometric Probability. Philadelphia: PA: SIAM.

Sonebi, M. (2004). Medium strength self-compacting concrete containing fly ash: Modelling using factorial experimental plans. Cement and Concrete Research, 34(7), 1199–1208.

Song, H. B. (2001). Early-age creep and shrinkagein self-compacting concrete incorporating GGBFS. Proceedings of the Second International Symposium on SCC, pp. 413-21.

Song, P. S., & Hwang, S. (2004). Mechanical properties of high-strength steel fiber-reinforced concrete. Construction and Building Materials, 18, 669–673.

Song, P. S., Hwang, S., & Sheu, B. C. (2005). Strength properties of nylon- and polypropylene-fiber-reinforced concretes. Cement and Concrete Research, 35(8), 1546–1550.

Sorensen, C., Berge, E., & Nikolaisen, E. B. (2014). Investigation of Fiber Distribution in Concrete Batches Discharged from Ready-Mix Truck. International Journal of Concrete Structures and Materials, 8(4), 279-287.

Soroushian, P., & Lee, C. D. (1990). Distribution and orientation of fibers in steel fiber reinforced concrete. ACI Materials Journal, 87(5), 433-439.

Soroushian, P., Nagi, M., & Okwegbu, A. (1992). Freeze-thaw durability of lightweight carbon-fiber reinforced cement composite. ACI Materials Journal, 89(5), 491-494.

Soutsos, M. N., Le, T. T., & Lampropoulos, A. P. (2012). Flexural performance of fibre reinforced concrete made with steel and synthetic fibres. Construction and Building Materials, 36, 704-710.

Spiratos, N., Pagé, M., Mailvaganam, N. P., Malhotra, V. M., & Jolicoeur, C. (2003). Superplasticizers for Concrete: fundamentals, technology, and practice. Supplementary Cementing Materials for Sustainable Development, Incorporated, 2003.

Stähli, P., & van Mier, J. G. (2007). Manufacturing, fibre anisotropy and fracture of hybrid fibre concrete. Engineering Fracture Mechanics, 74 (1–2), 223-242.

Stähli, P., Custer, R., & Mier, J. G. (2007). On flow properties, fibre distribution, fibre orientation and flexural behaviour of FRC. Materials and Structures, 41(1), 189–196.

Stang, H., & Shah, S. P. (1986). Failure of fibre-reinforced composites by pull-out fracture. Journal of Materials Science, 21(3), 953-957.

Stroeven, P. (1978). Morphometry of fibre reinforced cementitious materials. Matériaux et Construction, 11(1), 31-38.

Stroeven, P. (1986). Stereology of concrete reinforced with short steel fibres. Heron, 31(2), 15-28.

Stroeven, P., & Hu, J. (2006). Effectiveness near boundaries of fibre reinforcement in concrete. Materials and Structures, 39(10), 1001-1013.

Stroeven, P., & Hu, J. (2006). Review paper–stereology: Historical perspective and applicability to concrete technology. Materials and Structures, 39(1), 127-135.

Stroeven, P., & Shah, S. P. (1978). Use of radiography-image analysis for steel fiber reinforced concrete. Testing and Test Methods of Fiber Cement Composites, 345-353.

Švec, O., Žirgulis, G., Bolander, J. E., & Stang, H. (2014). Influence of formwork surface on the orientation of steel fibres within self-compacting concrete and on the mechanical properties of cast structural elements. Cement and Concrete Composites, 50, 60-72.

Swamy, R. N., & Mangat, P. S. (1974). Influence of fibre-aggregate interaction on some properties of steel fibre reinforced concrete. Matériaux et Construction, 7(5), 307-314.

Szwabowski, J., & Ponikiewski, T. (2002). Rheological properties of fresh concrete with polypropylene fibres. 3rd International Conference: Concrete & Concrete Structures, (pp. 24-25). Žilina, Slovakia.

Tagnit-Hamou, A., Vanhove, Y., & Petrov, N. (2005). Microstructural analysis of the bond mechanism between polyolefin fibers and cement pastes. Cement and Concrete Research, 35(2), 364-370.

Tan, K., Murugappan, K., & Paramasivam, P. (1994). Constitutive relation for steel fibre concrete under biaxial compression. Cement and Concrete Composites, 16(1), 9–14.

Taylor, H. F. (1990). Cement chemistry. Thomas Telford.

Thomas, J., & Ramaswamy, A. (2007). Mechanical Properties of Steel Fiber-Reinforced Concrete. Journal of Materials in Civil Engineering, 19(5), 385–392.

Thorenfeldt, E. (2003). Theoretical tensile strength after cracking. Fibre orientation and average stress in fibres. Proceedings of the Nordic Concrete Federeation Workshop on Design Rules for Steel Fibre Reinforced Concrete Structures, (pp. 43-60).

Tiberti, G., Minelli, F., & Plizzari, G. (2014). Reinforcement optimization of fiber reinforced concrete linings for conventional tunnels. Composites Part B: Engineering, 58, 199-207.

Toledo, R., Ghavami, K., Sanjuan, M., & England, G. (2005). Free, restrained and drying shrinkage of cement mortar composites reinforced with vegetable fibres. Cement & Concrete Composites, 27(5), 537-546.

Torrents, J. M., Blanco, A., Pujadas, P., Aguado, A., Juan-García, P., & Sánchez-Moragues, M. Á. (2012). Inductive method for assessing the amount and orientation of steel fibers in concrete. Materials and Structures, 45(10), 1577-1592.

Torrents, J., Juan-García, P., Patau, O., & Aguado, A. (2009). Surveillance of steel fibre reinforced concrete slabs measured with an open-ended coaxial probe. Proceedings of the XIX IMEKO World Congress: Fundamental and Applied Mtrology. Lisbon, Portugal.

Torrijos, M. C., Barragán, B. E., & Zerbino, R. L. (2010). Placing conditions, mesostructural characteristics and post-cracking response of fibre reinforced self-compacting concretes. Construction and Building Materials, 24(6), 1078–1085.

Torroja Miret, E. (1956). Razón y ser de los tipos estructurales (4ª Edición 1976 ed.). Instituto de Ciencias de la Construcción Eduardo Torroja, Madrid.

Trainor, K. J., Foust, B. W., & Landis, E. N. (2012). Measurement of energy dissipation mechanisms in fracture of fiber-reinforced ultrahigh-strength cement-based composites. Journal of Engineering Mechanics, 139(7), 771-779.

TRB. (2006). Control of cracking in concrete: State of the art (Vols. Circular No.E-C107,). Washington, D.C.

Trottier, B. Y., Mahoney, M., & Forgeron, D. (2002). Can Synthetic fibers Replace in Slabs-on-Ground ? Concrete International, 24(11), 59–68.

Trottier, J. F., & Mahoney, M. (2001). Innovative Synthetic Fibers. Concrete International, 23(06), 23-28.

Uchida, Y., Kunieda, M., & Rokugo, K. (2014). FRCC - Design and application in Japan. 2nd FRC International Workshop Fiber Reinforced Concrete: from design to Structural Applications, 1st ACI-FIB Joint Workshop. Montreal, Canada.

Ugbolue, S. C. (2009). Polyolefin fibres: industrial and medical applications. CRC Press.

Van Gysel, A. (2000). Studie van het uittrekgedrag van staalvezels ingebed in een cementgebonden matrix met toepassing op staalvezelbeton onderworpen aan buiging. Doctoral Thesis, Ghent University.

Vandewalle, L. (2006). Hybrid fiber reinforced concrete. Measuring, Monitoring and Modeling Concrete Properties, 77-82.

Vandewalle, L. (2007). Hybrid fibre concrete: is there a synergetic effect? Advances in Construction Materials 2007, 219-228.

Vandewalle, L., Heirman, G., & Van Rickstal, F. (2008). Fibre orientation in self-compacting fibre reinforced concrete. Proc. of the 7th Int. RILEM Symp. on Fibre Reinforced Concrete: Design and Applications (BEFIB2008), (pp. 719-728).

Viacava, I., Sensale, G., Cavalaro, S., & Aguado, A. (2012). Directrices de dosificación para hormigones autocompactantes de baja y media resistencia. 3º Congreso Iberoamericano sobre hormigón autocompactante. Avances y oportunidades., (pp. 35-44). Madrid.

Vieira, M., & Bettencourt, A. (2003). Deformability of hardened SCC. International RILEM Symposium on Self-Compacting Concrete, (pp. 637–644).

Voo, Y. L., Poon, W. K., & Foster, S. J. (2010). Shear strength of steel fiber-reinforced ultrahigh-performance concrete beams without stirrups. Journal of structural engineering, 136(11), 1393-1400.

Wafa, F. F., & Ashour, S. A. (1992). Mechanical properties of high-strength fiber reinforced concrete. ACI Materials Journal, 89(5), 449-455.

Wallevik, O. (2003). Rheologiy – A Scientific Approach to Develop Self-Compacting Concrete. 3rd Internacional Symposium on Self-Compacting Concrete, (pp. 23-31). Iceland.

Walraven, J. (2003). Structural application of self compacting concrete. Proceedings of 3rd RILEM international Symposium on Self Compacting concrete. Reykjvic, Icelnd: RILEM Publications PRO 33, August 2003.

Walraven, J. (2003). Structural aspects of self compacting concrete. Proceedings of the 3 rd international RILEM Symposium on SCC, (pp. 15-22).

Walraven, J. C. (2009). High performance fiber reinforced concrete: progress in knowledge and design codes. Materials and Structures, 42(9), 1247-1260.

Wang, A. L., & Kicey, C. J. (2011). On the accuracy of Buffon's Needle: a simulation output analysis. Proceedings of the 49th ACM Southeast Conference, (pp. 233-236).

Wang, N., Mindess, S., & Ko, K. (1996). Fiber reinforced concrete beams under impact loading. Cement and Concrete Research, 26(3), 373-376.

Wang, P., Huang, Z., Jiang, J., & Wu, Y. (2012). Performances of hybrid fiber reinforced concrete with steel fibers and polypropylene fibers. (ASCE, Ed.) Civil Engineering and Urban Planning, 458-461.

Wang, Y., Backer, S., & Li, V. C. (1987). An experimental study of synthetic fibre reinforced cementitious composites. Journal of Materials Science, 22(12), 4281-4291.

Wang, Y., C.Li, V., & Baker, S. (1988). Modelling of fibre pull-out from a cement matrix. The International Journal of Cement Composites and Lightweight Concrete, 10(3), 143–149.

Wei, S., Mandel, J., & Said, S. (1986). Study of the Interface Strength of Steel Fibre Reinforced. Cement Based Composites, ACI Journal, 83, 597-605.

Wen, S., & Chung, D. (2003). A comparative study of steel- and carbon- fibre cement paste as piezoresistive strain sensors. Advances in Cement Research, 15(3), 119-128 .

Wimpenny, D., Angerer, W., Cooper, T., & Bernard, S. (2009). The use of Steel and Synthetic Fibres in Concrete under Extreme Conditions. 24th Biennial Conference of the Concrete Institute of Australia. Sydney, Australia.

Won, J. P., Lim, D. H., & Park, C. G. (2006). Bond behaviour and flexural performance of structural synthetic fibre-reinforced concrete. Magazine of Concrete Research, 58(6), 401-410.

Wu, J., & Chung, D. (2005). Pastes for electromagnetic interference shielding. Journal of Electronic Materials, 34(9).

Wuest, J. (2004). Etude Exploratoire des Propriétés Mécaniques de Bétons de Fibres Ultra Performants de Structures. Diploma thesis MCS, Swiss Federal Institute of Technology(EPFL), Lausanne, Switzerland.

Xu, B. W., & Shi, H. S. (2009). Correlations among mechanical properties of steel fiber reinforced concrete. Construction and Building Materials, 23(12), 3468-3474.

Yan, L., Jenkins, C., & Pendleton, R. (2000). Polyolefin fiber-reinforced concrete composites: Part I. Damping and frequency characteristics. Cement and Concrete Research, 30(3), 391-401.

Yan, L., Jenkins, C., & Pendleton, R. (2000). Polyolefin fiber-reinforced concrete composites: Part II. Damping and interface debonding. Cement and Concrete Research, 30(3), 403-410.

Yan, L., Pendleton, R. L., & Jenkins, C. H. (1998). Interface morphologies in polyolefin fiber reinforced concrete composites. Composites Part A: Applied Science and Manufacturing. Cement and Concete Research, 29(5-6), 643–650.

Yang, Q. S., Qin, Q. H., & Peng, X. R. (2003). Size effects in the fiber pullout test. Composite structures, 61(3), 193-198.

Yao, W., Li, J., & Keru Wu. (2003, January). Mechanical properties of hybrid fiber-reinforced concrete at low fiber volume fraction. Cement and Concrete Research, 33(1), 27-30.

Yardimci, M. Y., Baradan, B., & Tasdemir, M. A. (2008). Studies on the relation between fiber orientation and flexural performance of SFRSCC. BEFIB 2008: 7th RILEM International Symposium on Fibre Reinforced Concrete, pp. 711-718.

Yazici, S., Inan, G., & Tabak, V. (2007). Effect of aspect ratio and volume fraction of steel fiber on the mechanical properties of SFRC. Construction and Building Materials, 21(6), 1250-1253.

Yehia, S., & Tuan, C. (1999). Conductive concrete overlay for bridge deck deicing. ACI Materials Journal , 96(3), 382-391 .

You, Z., Chen, X., & Dong, S. (2011). Ductility and strength of hybrid fiber reinforced self-consolidating concrete beam with low reinforcement ratios. Systems Engineering Procedia, 1, 28-34.

Zandi, Y., Husem, M., & Pul, S. (2011). Effect of distribution and orientation of steel fiber reinforced concrete. Proceedings of the 4th WSEAS international conference on Energy and development-environment-biomedicine, (pp. 260-264).

Zerbino, R., Barragán, B., Agulló, L., García, T., & Gettu, R. (2006). Reología de hormigones autocompactables. Ciencia y Tecnología del Hormigón, 51-64.

Zerbino, R., Tobes, J. M., Bossio, M. E., & Giaccio, G. (2012). On the orientation of fibres in structural members fabricated with self compacting fibre reinforced concrete. Cement and Concrete Composites, 34(2), 191–200.

Zhan, Y., & Meschke, G. (2014). Analytical Model for the Pullout Behavior of Straight and Hooked-End Steel Fibers. Journal of Engineering Mechanics.

Zhao, X., He, X. J., Yan, S., & Anh, N. P. (2014). Computational and Simulation Analysis of Pull-Out Fiber Reinforced Concrete. Advances in Materials Science and Engineering.

Zheng, Z., & Feldman, D. (1995). Synthetic fibre-reinforced concrete. Progress in Polymer Science, 20(2), 185-210.

Zīle, E., & Zīle, O. (2013). Effect of the fiber geometry on the pullout response of mechanically deformed steel fibers. Cement and Concrete Research, 44, 18-24.

Zollo, R. (1997). Fiber-reinforced concrete: an overview after 30 years of development. Cement & Concrete Composites, 19, 107-122.

Zonsveld, J. J. (1975). Properties and testing of concrete containing fibres other than steel. RILEM Symposium 1975 on fibre reinforced cement and concrete, pp. 217-226.

Publications derived from this thesis

Journal papers published

- M.G. Alberti, A. Enfedaque, J.C. Gálvez, Comparison between polyolefin fibre reinforced vibrated conventional concrete and self-compacting concrete, Construction and Building Materials, Volume 85(15), 2015, Pages 182-194, ISSN 0950-0618, http://dx.doi.org/10.1016/j.conbuildmat.2015.03.007.

- M.G. Alberti, A. Enfedaque, J.C. Gálvez, M.F. Cánovas, I.R. Osorio, Polyolefin fiber-reinforced concrete enhanced with steel-hooked fibers in low proportions, Materials & Design, Volume 60, August 2014, Pages 57-65, ISSN 0261-3069, http://dx.doi.org/10.1016/j.matdes.2014.03.050.

- M.G. Alberti, A. Enfedaque, J.C. Gálvez, On the mechanical properties and fracture behavior of polyolefin fiber-reinforced self-compacting concrete, Construction and Building Materials, Volume 55, 31 March 2014, Pages 274-288, ISSN 0950-0618, http://dx.doi.org/10.1016/j.conbuildmat.2014.01.024.

- M.G. Alberti, A. Enfedaque, J.C. Gálvez, Hormigón autocompactante reforzado simultáneamente con fibras estructurales de poliolefina y conformadas de acero, Cemento y Hormigón, (963), Pages 8-15, ISSN: 0008-8919, 2014.

Contributions to workshops and conferences

- M.G. Alberti, A. Enfedaque, J.C. Gálvez and A. Ferreras, "Pull-out" de fibras de poliolefina: Influencia de la inclinación y la longitud embebida en la resistencia al arrancamiento de las fibras. Anales de Mecánica de la Fractura, 32, Pages 267-272, ISSN 0213-3725, 2015.

- M.G. Alberti, A. Enfedaque and J.C. Gálvez, On the fracture behavior and mechanical properties of polyolefin fiber-reinforced self-compacting concrete, 2nd FRC International Workshop Fiber Reinforced Concrete: from design to Structural Applications, 1st ACI-FIB Joint Workshop, 2014, Montreal, Canadá.

- M. G. Alberti, V. Agrawal, A. Enfedaque and J. C. Gálvez, Hormigón reforzado con alto contenido de fibras de poliolefina, Anales de Mecánica de la Fractura 31, Vol. 1, pp. 213-218, ISSN 0213-3725, 2014.

- M.G. Alberti, I.R. Osorio, A. Enfedaque and J.C. Gálvez, Propiedades mecánicas de hormigones reforzados con una combinación de fibras de poliolefina y acero, VI Congreso de ACHE, Madrid, 3-5 Junio, 2014.

- M. G. Alberti, A. Enfedaque y J. C. Gálvez, Hormigón reforzado con fibras de poliolefina estructurales: comparación de un hormigón autocompactante y un hormigón vibrado, VI Congreso de ACHE, Madrid, 3-5 Junio, 2014.

- M. G. Alberti, A. Enfedaque y J. C. Gálvez, Estudio del comportamiento mecánico y en fractura de un hormigón autocompactante con fibras de poliolefina, Anales de Mecánica de Fractura, 30, Vol. 1, Pages 73-78, ISSN: 0213-3725, 2013.

Appendix A: CE Mark SikaFiber M60.

BUREAU VERITAS
Certification

CERTIFICADO DE CONFORMIDAD CE

Certificado nº: 1035-CPD- ES024048-C

En virtud del Real Decreto 1630/1992, de 29 de diciembre, modificado por el Real Decreto 1328/1995, de 28 de julio, por el que se dictan disposiciones para la aplicación de la Directiva 89/106/CEE del Consejo de las Comunidades Europeas, de 21 de diciembre de 1988, relativa a la aproximación de las disposiciones legales, reglamentarias y administrativas de los Estados Miembros sobre los productos de construcción, se ha verificado que los productos:

FIBRA POLIMÉRICA PARA USO ESTRUCTURAL EN HORMIGONES, MORTEROS Y PASTAS.

Marca: Sika Fiber T-60 y Sika Fiber M-60

Tipo: Macrofibra de Polipropileno, homopolímero y polietileno

Clase: II

Densidad: 0'9 gramos/cm^3

Longitud: 60 mm

Diámetro: 0'92 mm

Forma: Monofilamento plano y franulado

Resistencia tracción: 560 N/mm^2

Módulo elasticidad: 20.5 kN/mm^2

Fabricado por: Nº de asunto 5439772

Comercializado por: **SIKA, S.A.U.**

Crta. Fuencarral, 72. P.I. Alcobendas

28108 Alcobendas (Madrid)

Norma: **UNE EN 14889-2:2008**

está sometido por el fabricante a un control de producción en fábrica y al ensayo posterior de las muestras tomadas en la fábrica de acuerdo con un plan de ensayo preestablecido, y que el organismo notificado BUREAU VERITAS CERTIFICATION, S.A. ha llevado a cabo los ensayos de tipo inicial del producto, la inspección inicial de la fábrica y del control de la producción en fábrica, y que realiza el seguimiento periódico, la evaluación y la aprobación del control de producción en fábrica. Este certificado indica que se han aplicado todas las disposiciones relativas a la evaluación de la conformidad descritas en el Anexo ZA de las normas armonizadas mencionadas y que el producto cumple todos los requisitos exigibles.

Este certificado faculta al fabricante para fijar el marcado CE sobre los productos y será válido salvo anulación o retirada por BUREAU VERITAS CERTIFICATION, S.A.

Este certificado permanece válido mientras las condiciones establecidas en las normas armonizadas correspondientes, las características técnicas del producto, las condiciones de fabricación de la planta, o el sistema de CPF, no hayan cambiado significativamente hasta el 12 de abril de 2016.

Fecha de entrada en vigor inicial: Madrid, 19 de junio de 2013

Firmado:

Manuel Medina Fernández-Regatillo
Director General

Bureau Veritas Certification S.A.
Edificio Caoba, C/ Valportillo Primera 22-24
Polígono Industrial La Granja
28108 – Alcobendas (MADRID)
Organismo Notificado 1035
Organismo de control con acreditación ENAC: OC-P/005

Appendix B: Results of the counting exercises.

Legend

Free surface

Mould wall

Cut Surface

Comments:

- The values represented in the present appendix are in average values of fibres in natural numbers.
- Fracture surfaces were counted in twice: once with nine equal sectors and once with nine equal sectors including the notch.
- Fracture surfaces are represented on the fracture test position, with free surface on the left and the notch in the bottom.
- Cut surfaces are represented with the free surface on the top as they were cast.

B.1.-Fibres counted on the fracture surfaces

VCC6-60 average fracture surfaces counted

Size (mm)	Broken			Pulled-out			Total		
	50	50	50	50	50	50	50	50	50
50	5	7	8	2	3	2	9	12	13
50	10	8	5	4	3	2	18	14	9
50	18	10	10	4	2	2	25	14	14
42	3	6	7	2	3	2	6	11	12
42	9	7	5	3	3	2	15	13	9
42	8	8	6	6	2	2	20	12	10
25	NOTCH			NOTCH			21		

SCC6-60S average fracture surfaces counted

Size (mm)	Broken			Pulled-out			Total		
	50	50	50	50	50	50	50	50	50
50	5	7	5	2	3	3	9	14	10
50	6	7	8	2	2	4	10	11	16
50	11	6	14	2	2	2	15	10	18
42	5	5	4	2	3	2	8	10	7
42	4	7	7	1	4	2	6	14	12
42	6	5	6	3	3	5	12	11	15
25	NOTCH			NOTCH			17		

SCC6-48C average fracture surfaces counted

Size (mm)	Broken			Pulled-out			Total		
	50	50	50	50	50	50	50	50	50
50	2	7	8	4	5	6	9	16	20
50	2	8	5	4	4	5	11	16	16
50	7	11	14	3	4	5	14	20	23
42	2	6	7	3	4	6	8	14	18
42	2	7	5	5	3	3	11	12	11
42	2	5	7	3	6	7	8	17	21
25	NOTCH			NOTCH			25		

SCC6-48S average fracture surfaces counted

Size (mm)	Broken			Pulled-out			Total		
	50	50	50	50	50	50	50	50	50
50	7	6	5	5	7	7	17	19	20
50	6	4	5	3	3	5	12	11	15
50	10	13	12	3	1	2	15	15	16
42	6	4	5	5	6	6	15	17	16
42	4	5	3	2	3	5	8	11	13
42	5	2	7	5	2	4	15	6	15
25	NOTCH			NOTCH			27		

U Specimens average fracture surfaces counted

Size (mm)	Broken			Pulled-out			Total		
	50	50	50	50	50	50	50	50	50
50	4	7	7	4	3	5	11	12	16
50	8	8	8	3	3	4	14	14	15
50	9	11	13	2	1	3	14	14	19
42	3	6	6	3	2	4	10	9	14
42	5	7	7	2	3	4	10	13	15
42	7	5	6	4	2	4	14	9	13
25	NOTCH			NOTCH			23		

H Specimens average fracture surfaces counted

Size (mm)	Broken			Pulled-out			Total		
	50	50	50	50	50	50	50	50	50
50	7	4	6	4	3	3	14	10	13
50	4	6	6	3	3	4	11	11	14
50	8	13	11	2	1	2	12	15	14
42	6	4	6	4	3	3	13	9	12
42	3	5	4	3	2	3	8	9	9
42	4	7	7	3	2	3	10	11	13
25	NOTCH			NOTCH			20		

D Specimens average fracture surfaces counted

Size (mm)	Broken			Pulled-out			Total		
	50	50	50	50	50	50	50	50	50
50	9	9	8	3	4	4	15	17	15
50	9	8	9	5	5	3	19	18	15
50	11	11	11	3	2	2	17	15	14
42	7	8	7	3	4	3	13	15	12
42	8	7	7	3	4	3	14	14	12
42	7	7	8	5	4	3	16	15	14
25	NOTCH			NOTCH			21		

L specimen average fracture surfaces counted

Size (mm)	Broken			Pulled-out			Total		
	50	50	50	50	50	50	50	50	50
50	7	8	7	4	3	4	15	15	16
50	6	5	7	5	3	4	15	12	14
50	13	10	9	3	2	1	19	14	11
42	6	7	7	3	2	3	12	11	13
42	6	6	5	5	3	3	15	11	12
42	5	5	5	4	3	2	12	11	9
25	NOTCH			NOTCH			22		

L1 average fracture surfaces counted

Size (mm)	Broken			Pulled-out			Total		
	50	50	50	50	50	50	50	50	50
50	7	7	5	4	3	3	15	13	11
50	5	6	7	6	3	3	16	11	13
50	13	12	9	4	1	1	21	13	10
42	6	7	4	3	3	2	12	12	8
42	4	4	7	5	2	3	13	7	13
42	5	6	4	6	2	2	17	10	7
25	NOTCH			NOTCH			23		

L2 average fracture surfaces counted

Size (mm)	Broken			Pulled-out			Total		
	50	50	50	50	50	50	50	50	50
50	7	14	6	4	6	4	15	25	14
50	3	7	10	5	4	5	12	14	19
50	13	10	6	3	1	2	19	12	9
42	6	10	6	3	4	4	11	18	13
42	4	9	7	6	4	4	15	17	15
42	4	4	5	3	2	3	9	8	10
25	NOTCH			NOTCH			23		

L3 average fracture surfaces counted

Size (mm)	Broken			Pulled-out			Total		
	50	50	50	50	50	50	50	50	50
50	6	7	9	6	3	3	17	13	14
50	9	6	5	7	4	3	22	13	10
50	14	9	7	4	1	1	21	11	9
42	6	4	9	6	2	2	17	8	13
42	8	8	4	6	2	2	20	12	8
42	5	6	2	4	4	2	13	13	6
25	NOTCH			NOTCH			19		

L4 average fracture surfaces counted

Size (mm)	Broken			Pulled-out			Total		
	50	50	50	50	50	50	50	50	50
50	8	7	10	3	1	7	13	9	24
50	9	2	7	2	4	4	12	9	15
50	11	11	14	3	4	2	16	19	17
42	7	6	10	2	1	6	11	8	21
42	7	2	3	2	3	4	11	8	11
42	6	6	9	3	5	3	11	15	15
25	NOTCH			NOTCH			24		

B.2.- Laboratory series cut surfaces counting exercise

VCC6-60	Cut#		1	2	3	4	5	6	7	8	9	10
Average #fibres		Position (mm)	30	90	150	210	262.5	337.5	390	450	510	570
15 15 13	**FRONT VIEW**	125	51	46	42	31	40	37	46	46	44	39
15 13 14		75	54	39	46	41	40	39	38	51	44	35
18 14 15		25	49	41	47	44	52	46	63	35	44	52
	TOP VIEW	125	54	54	49	39	51	42	48	48	54	40
		75	49	37	44	35	46	41	48	39	39	41
		25	51	36	42	41	35	39	51	45	38	44

SCC6-60S	Cut#		1	2	3	4	5	6	7	8	9	10
Average #fibres		Position (mm)	30	90	150	210	262.5	337.5	390	450	510	570
12 12 15	**FRONT VIEW**	125	34	39	45	32	35	45	51	47	38	22
12 11 12		75	36	32	35	38	34	38	30	41	33	31
14 13 15		25	17	40	36	52	52	49	38	43	36	53
	TOP VIEW	125	38	32	44	45	49	35	33	36	32	37
		75	29	33	39	32	43	45	36	35	31	37
		25	18	46	33	45	29	52	50	60	44	32

SCC6-48C

Cut#		1	2	3	4	5	6	7	8	9	10
Average #fibres	Position (mm)	30	90	150	210	262.5	337.5	390	450	510	570
16 12 15	FRONT VIEW 125	40	41	39	41	41	38	57	37	45	49
17 15 18	75	46	49	46	34	60	66	48	56	53	37
19 16 18	25	44	53	45	61	58	67	56	48	60	44
	TOP VIEW 125	46	46	43	45	55	64	58	53	53	46
	75	34	38	42	48	57	42	44	44	47	42
	25	50	59	44	43	46	64	59	44	59	41

SCC6-48S

Cut #		1	2	3	4	5	6	7	8	9	10
Average #fibres	Position (mm)	30	90	150	210	262.5	337.5	390	450	510	570
17 16 19	FRONT VIEW 125	34	58	67	49	44	56	55	57	53	49
18 17 17	75	33	57	73	48	47	45	58	55	51	48
21 20 19	25	60	66	63	72	57	68	56	64	58	41
	TOP VIEW 125	45	58	67	54	46	55	53	69	65	53
	75	39	67	64	68	48	59	57	46	44	35
	25	43	56	72	47	55	55	59	61	53	49

B.3.- Vertical elements

Average #fibres in cut					Cut	1	2	3	4	5	6	7	8	9	10
					Position (mm)	30	90	150	210	262.5	337.5	390	450	510	570
14	14	14	FRONT VIEW	U	425	41	36	43	46	36	44	45	58	40	38
14	15	15			375	38	37	57	39	41	51	43	43	45	47
15	15	16			325	34	45	43	44	47	51	51	53	41	54
16	14	14		H	275	35	40	42	42	39	44	53	57	41	41
16	13	16			225	37	45	42	44	47	43	49	47	47	42
15	14	15			175	31	40	47	44	47	44	54	48	49	35
14	15	15		D	125	39	44	49	50	53	50	41	40	43	36
17	17	15			75	38	49	47	48	42	50	53	54	50	48
16	18	17			25	55	62	50	50	44	51	51	46	49	50
			TOP VIEW		125	123	135	144	131	136	146	153	138	133	135
					75	112	136	140	141	136	141	133	144	134	114
					25	112	127	135	136	124	139	154	163	136	141

B.4.- Long element

L1	Cut	1	2	3	4	5	6	7	8	9	10
Average #fibres in cuts	Position (mm)	20	80	140	200	260	290	350	410	470	530
10 14 13	FRONT VIEW 125	8	21	37	41	32	44	39	33	52	57
11 12 11	75	8	25	31	34	40	38	37	45	50	39
18 12 18	25	15	56	70	60	53	44	38	53	51	39
	TOP VIEW 125	16	35	56	54	39	46	32	40	34	40
	75	6	27	40	36	31	44	43	37	63	57
	25	9	40	42	45	55	36	40	54	56	38

L2	Cut	1	2	3	4	5	6	7	8	9	10
Average #fibres in cuts	Position (mm)	570	630	690	750	810	840	900	960	1020	1080
11 15 11	FRONT VIEW 125	56	32	32	38	33	38	34	40	34	30
14 15 14	75	42	41	42	25	42	52	53	50	43	41
19 18 17	25	50	45	55	63	48	51	40	57	64	72
	TOP VIEW 125	56	45	38	42	36	40	38	45	52	49
	75	52	38	54	46	34	55	49	52	42	57
	25	40	36	37	38	53	46	40	50	47	37

L3

Average #fibres in cuts		
12	11	15
17	14	12
22	19	22

	Cut	1	2	3	4	5	6	7	8	9	10
	Position (mm)	1120	1180	1240	1300	1360	1390	1450	1510	1570	1630
FRONT VIEW	125	45	41	41	42	40	25	45	35	33	31
	75	42	32	34	63	39	32	48	30	46	57
	25	72	60	65	55	98	53	55	53	72	49
TOP VIEW	125	62	53	50	62	51	39	54	47	46	46
	75	49	41	52	50	49	35	42	29	47	49
	25	49	39	38	48	77	36	52	42	58	42

L4

Average #fibres in cuts		
13	14	13
14	11	14
14	12	14

	Cut	1	2	3	4	5	6	7	8	9	10
	Position (mm)	1670	1730	1790	1850	1910	1940	2000	2060	2120	2180
FRONT VIEW	125	56	49	46	31	55	51	30	35	24	33
	75	39	37	41	48	36	46	36	45	29	23
	25	35	59	72	38	42	40	23	34	40	16
TOP VIEW	125	50	46	67	42	43	41	32	40	27	21
	75	43	46	41	40	36	46	28	29	33	22
	25	37	53	51	36	54	50	29	45	33	29

Appendix C: Tables for the verification of the analytical fibre orientation model.

Table C-1: Experimental data and results used for verification of the model using steel fibres.

Dupont and Vandewalle data [75]									Presented model in this thesis		
No. (#)	Fibre dosage (kg/m³)	Fibre type	*lf* (mm)	*df* (mm)	α	Exp. (#)	calc. (#)	Ratio calc./exp.	θ	Computed #	comp/ exp.
1	20	RC 65/60 BN	60	0.92	0.58	92	41	0.45	0.57	41	0.45
2	20	RC 65/60 BN	60	0.92	0.58	68	41	0.61	0.57	41	0.61
3	20	RC 65/60 BN	60	0.92	0.58	77	41	0.54	0.57	41	0.54
4	20	RC 65/60 BN	60	0.92	0.58	74	41	0.56	0.57	41	0.56
5	20	RC 65/60 BN	60	0.92	0.58	127	41	0.32	0.57	41	0.32
6	20	RC 65/60 BN	60	0.92	0.58	38	41	1.09	0.57	41	1.09
7	20	RC 65/60 BN	60	0.92	0.58	66	41	0.63	0.57	41	0.62
8	20	RC 65/60 BN	60	0.92	0.58	55	41	0.75	0.57	41	0.75
9	20	RC 65/60 BN	60	0.92	0.58	84	41	0.49	0.57	41	0.49
10	20	RC 65/60 BN	60	0.92	0.58	44	41	0.94	0.57	41	0.94
11	20	RC 65/60 BN	60	0.92	0.58	57	41	0.72	0.57	41	0.72
12	20	RC 65/60 BN	60	0.92	0.58	30	41	1.38	0.57	41	1.37
13	20	RC 65/60 BN	60	0.92	0.58	50	41	0.83	0.57	41	0.82
14	20	RC 65/60 BN	60	0.92	0.58	35	41	1.18	0.57	41	1.18
15	20	RC 65/60 BN	60	0.92	0.58	48	41	0.86	0.57	41	0.86
16	20	RC 65/60 BN	60	0.92	0.58	45	41	0.92	0.57	41	0.92
17	20	RC 65/60 BN	60	0.92	0.58	36	41	1.15	0.57	41	1.15
18	60	RC 65/60 BN	60	0.92	0.58	224	124	0.55	0.57	124	0.55
19	60	RC 65/60 BN	60	0.92	0.58	324	124	0.38	0.57	124	0.38

Dupont and Vandewalle data [75]									Presented model in this thesis		
No. (#)	Fibre dosage (kg/m³)	Fibre type	*lf* (mm)	*df* (mm)	α	Exp. (#)	calc. (#)	Ratio calc./exp.	θ	Computed #	comp/ exp.
20	60	RC 65/60 BN	60	0.92	0.58	326	124	0.38	0.57	124	0.38
21	60	RC 65/60 BN	60	0.92	0.58	246	124	0.5	0.57	124	0.50
22	60	RC 65/60 BN	60	0.92	0.58	237	124	0.52	0.57	124	0.52
23	60	RC 65/60 BN	60	0.92	0.58	294	124	0.42	0.57	124	0.42
24	60	RC 65/60 BN	60	0.92	0.58	222	124	0.56	0.57	124	0.56
25	60	RC 65/60 BN	60	0.92	0.58	159	124	0.78	0.57	124	0.78
26	60	RC 65/60 BN	60	0.92	0.58	183	124	0.68	0.57	124	0.68
27	60	RC 65/60 BN	60	0.92	0.58	237	124	0.52	0.57	124	0.52
28	60	RC 65/60 BN	60	0.92	0.58	171	124	0.72	0.57	124	0.72
29	60	RC 65/60 BN	60	0.92	0.58	270	124	0.46	0.57	124	0.46
30	60	RC 65/60 BN	60	0.92	0.58	175	124	0.71	0.57	124	0.71
31	60	RC 65/60 BN	60	0.92	0.58	110	124	1.13	0.57	124	1.12
32	60	RC 65/60 BN	60	0.92	0.58	159	124	0.78	0.57	124	0.78
33	60	RC 65/60 BN	60	0.92	0.58	166	124	0.75	0.57	124	0.75
34	60	RC 65/60 BN	60	0.92	0.58	179	124	0.69	0.57	124	0.69
35	60	RC 65/60 BN	60	0.92	0.58	175	124	0.71	0.57	124	0.71
36	40	RC 65/60 BN	60	0.92	0.58	72	83	1.15	0.57	82	1.15
37	40	RC 65/60 BN	60	0.92	0.58	94	83	0.88	0.57	82	0.88
38	40	RC 65/60 BN	60	0.92	0.58	91	83	0.91	0.57	82	0.91
39	40	RC 65/60 BN	60	0.92	0.58	70	83	1.18	0.57	82	1.18
40	40	RC 65/60 BN	60	0.92	0.58	81	83	1.02	0.57	82	1.02
41	40	RC 65/60 BN	60	0.92	0.58	43	83	1.92	0.57	82	1.92
42	40	RC 65/60 BN	60	0.92	0.58	85	83	0.97	0.57	82	0.97
43	40	RC 65/60 BN	60	0.92	0.58	79	83	1.04	0.57	82	1.04
44	40	RC 65/60 BN	60	0.92	0.58	72	83	1.15	0.57	82	1.15
45	40	RC 65/60 BN	60	0.92	0.58	73	83	1.13	0.57	82	1.13
46	40	RC 65/60 BN	60	0.92	0.58	67	83	1.23	0.57	82	1.23
47	40	RC 80/35 BN	35	0.44	0.54	264	344	1.30	0.53	336	1.27
48	40	RC 80/35 BN	35	0.44	0.54	249	344	1.38	0.53	336	1.35
49	40	RC 80/35 BN	35	0.44	0.54	250	344	1.37	0.53	336	1.34
50	40	RC 80/35 BN	35	0.44	0.54	273	344	1.26	0.53	336	1.23

Dupont and Vandewalle data [75]									Presented model in this thesis		
No. (#)	Fibre dosage (kg/m³)	Fibre type	*lf* (mm)	*df* (mm)	α	Exp. (#)	calc. (#)	Ratio calc./exp.	θ	Computed #	comp/ exp.
51	40	RC 80/35 BN	35	0.44	0.54	304	344	1.13	0.53	336	1.10
52	40	RC 80/35 BN	35	0.44	0.54	294	344	1.17	0.53	336	1.14
53	60	RC 80/35 BN	35	0.44	0.54	382	516	1.35	0.53	503	1.32
54	60	RC 80/35 BN	35	0.44	0.54	329	516	1.57	0.53	503	1.53
55	60	RC 80/35 BN	35	0.44	0.54	278	516	1.85	0.53	503	1.81
56	60	RC 80/35 BN	35	0.44	0.54	375	516	1.37	0.53	503	1.34
57	60	RC 80/35 BN	35	0.44	0.54	314	516	1.64	0.53	503	1.60
58	60	RC 80/35 BN	35	0.44	0.54	327	516	1.58	0.53	503	1.54
59	50	RC 80/60 BN	60	0.75	0.58	145	156	1.08	0.57	155	1.07
60	50	RC 80/60 BN	60	0.75	0.58	144	156	1.09	0.57	155	1.08
61	50	RC 80/60 BN	60	0.75	0.58	189	156	0.83	0.57	155	0.82
62	50	RC 80/60 BN	60	0.75	0.58	200	156	0.78	0.57	155	0.78
63	50	RC 80/60 BN	60	0.75	0.58	107	156	1.46	0.57	155	1.45
64	50	RC 80/60 BN	60	0.75	0.58	185	156	0.84	0.57	155	0.84
65	50	RC 80/60 BN	60	0.75	0.58	135	156	1.16	0.57	155	1.15
66	50	RC 80/60 BN	60	0.75	0.58	158	156	0.99	0.57	155	0.98
67	25	RC 65/60 BN	60	0.92	0.58	19	52	2.71	0.57	52	2.71
68	25	RC 65/60 BN	60	0.92	0.58	47	52	1.1	0.57	52	1.10
69	25	RC 80/60 BP	60	0.75	0.58	84	78	0.93	0.57	78	0.92
70	25	RC 65/60 BN	60	0.92	0.58	40	52	1.29	0.57	52	1.29
71	75	RC 65/60 BN	60	0.92	0.58	184	155	0.84	0.57	155	0.84
72	75	RC 65/60 BN	60	0.92	0.58	171	155	0.9	0.57	155	0.90
73	75	RC 65/60 BN	60	0.92	0.58	138	155	1.12	0.57	155	1.12
74	25	RC 80/60 BP	60	0.75	0.58	89	78	0.88	0.57	78	0.87
75	25	RC 80/60 BP	60	0.75	0.58	96	78	0.81	0.57	78	0.81
76	25	RC 80/60 BP	60	0.75	0.58	79	78	0.99	0.57	78	0.98
77	25	RC 80/60 BP	60	0.75	0.58	83	78	0.94	0.57	78	0.93
78	25	RC 80/60 BP	60	0.75	0.58	67	78	1.17	0.57	78	1.16
79	25	RC 80/60 BP	60	0.75	0.58	67	78	1.17	0.57	78	1.16
80	25	RC 80/60 BP	60	0.75	0.58	76	78	1.03	0.57	78	1.02
81	25	RC 80/60 BP	60	0.75	0.58	110	78	0.71	0.57	78	0.71

Dupont and Vandewalle data [75]									Presented model in this thesis		
No. (#)	Fibre dosage (kg/m³)	Fibre type	*lf* (mm)	*df* (mm)	α	Exp. (#)	calc. (#)	Ratio calc./exp.	θ	Computed #	comp/ exp.
82	25	RC 80/60 BP	60	0.75	0.58	64	78	1.22	0.57	78	1.21
83	25	RC 65/60 BN	60	0.92	0.58	51	52	1.01	0.57	52	1.01
84	25	RC 65/60 BN	60	0.92	0.58	60	52	0.86	0.57	52	0.86
85	25	RC 65/60 BN	60	0.92	0.58	60	52	0.86	0.57	52	0.86
86	25	RC 65/60 BN	60	0.92	0.58	47	52	1.1	0.57	52	1.10
87	25	RC 65/60 BN	60	0.92	0.58	59	52	0.87	0.57	52	0.87
88	25	RC 65/60 BN	60	0.92	0.58	61	52	0.85	0.57	52	0.85
89	25	RC 65/60 BN	60	0.92	0.58	29	52	1.78	0.57	52	1.78
90	25	RC 65/60 BN	60	0.92	0.58	45	52	1.15	0.57	52	1.15
91	50	RC 80/60 BN	60	0.75	0.58	172	156	0.91	0.57	155	0.90
92	50	RC 80/60 BN	60	0.75	0.58	153	156	1.02	0.57	155	1.01
93	75	RC 65/60 BN	60	0.92	0.58	199	155	0.78	0.57	155	0.78
94	75	RC 65/60 BN	60	0.92	0.58	137	155	1.13	0.57	155	1.13
95	75	RC 65/60 BN	60	0.92	0.58	158	155	0.98	0.57	155	0.98
96	75	RC 65/60 BN	60	0.92	0.58	168	155	0.92	0.57	155	0.92
97	75	RC 65/60 BN	60	0.92	0.58	182	155	0.85	0.57	155	0.85
98	75	RC 65/60 BN	60	0.92	0.58	136	155	1.14	0.57	155	1.14
99	35	RC 65/40 BN	40	0.62	0.55	146	154	1.05	0.54	150	1.02
100	35	RC 65/40 BN	40	0.62	0.55	124	154	1.24	0.54	150	1.21
101	35	RC 65/40 BN	40	0.62	0.55	143	154	1.08	0.54	150	1.05
102	60	RC 65/40 BN	40	0.62	0.55	197	264	1.34	0.54	256	1.30
103	60	RC 65/40 BN	40	0.62	0.55	216	264	1.22	0.54	256	1.19
104	60	RC 65/40 BN	40	0.62	0.55	213	264	1.24	0.54	256	1.20
105	60	RC 65/60 BN	60	0.92	0.58	98	124	1.26	0.57	124	1.26
106	60	RC 65/60 BN	60	0.92	0.58	127	124	0.97	0.57	124	0.97
107	60	RC 65/60 BN	60	0.92	0.58	89	124	1.39	0.57	124	1.39
					Average of all 107 beams=			1.002	Average of all 107 beams=		0.995
					Coefficient of variation=			36%	Coefficient of variation=		36%

Table C-2: Experimental data and results used for verification of the model using macro-synthetic fibres.

Chapter	Fibre dosage (kg/m³)	#sections counted	type of section	Concrete type	Surface size	*lf* (mm)	Factor *lfr* = 0.856 lfr	exp. (#)	θ exp	θ	$\theta(lfr)$	#th	# *lfr*	comp./exp. *lfr*	comp./exp. *lf*
6	4.5	4	Fracture surface	SCC	0.1	60	51.4	45	0.605	0.624	0.612	74	46	1.01	1.032
6	6	4	Fracture surface	SCC	0.1	60	51.4	64	0.645	0.624	0.612	99	61	0.95	0.967
5	3	4	Fracture surface	VCC	0.15	60	51.4	64	0.574	0.561	0.550	112	61	0.96	0.978
5	4.5	4	Fracture surface	VCC	0.15	60	51.4	102	0.609	0.561	0.550	167	92	0.90	0.921
5	10	4	Fracture surface	VCC	0.15	60	51.4	204	0.548	0.561	0.550	372	205	1.00	1.023
5	3	4	Fracture surface	SCC	0.15	60	51.4	71	0.636	0.598	0.593	112	66	0.93	0.940
5	4.5	4	Fracture surface	SCC	0.15	60	51.4	81	0.484	0.598	0.593	167	99	1.23	1.236
5	10	4	Fracture surface	SCC	0.15	60	51.4	223	0.600	0.598	0.593	372	221	0.99	0.997
9	6	4	Fracture surface	VCC	0.15	60	51.4	128	0.574	0.561	0.550	223	123	0.96	0.978
9	6	6	Fracture surface	VCC	0.1	60	51.4	73	0.736	0.602	0.584	99	58	0.79	0.818
9	6	4	Fracture surface	SCC	0.15	60	51.4	112	0.502	0.598	0.593	223	132	1.18	1.192
9	6	20	Sawn surface	VCC	0.15	60	51.4	131	0.587	0.561	0.550	223	123	0.94	0.956
9	6	20	Sawn surface	SCC	0.15	60	51.4	115	0.515	0.598	0.593	223	132	1.15	1.160
# Sections counted		86											Mean ratio experimental / computed =	1.0000	1.0151
													coefficient of variation=	12%	12%